# Facies analysis, source rock geochemistry, tectonic evolution, and sequence stratigraphy of the Greymouth Basin, South Island, New Zealand.

by

**Mrinmoy Maitra**

Department of Geological Sciences
School of Earth and Environment

A thesis submitted in fulfilment of the requirements for the
Degree of Doctor of Philosophy

**Supervisors**

Dr. Kari Bassett
Dr. Andy Nicol
Dr. Rob Boyd

**University of Canterbury**

**August, 2020**

# Abstract

The Greymouth Rift Basin is part of the Late Cretaceous to Early Palaeocene West Coast-Taranaki Rift System in New Zealand that includes the petroleum producing deeply buried Taranaki Basin. The Greymouth Basin comprises alternating fluvial and lacustrine deposits with an abundance of high-quality coals and coaly mudstones. These sedimentary rocks, unlike most parts of the rift which are deeply buried and only available via seismic analysis, are accessible in outcrops and through extensive drill cores. This research aims to develop tectonic-sedimentary models and sequence stratigraphic framework to understand the evolution of the Greymouth Rift Basin from Late Cretaceous to Early Palaeocene as well as to infer the petroleum potential of the lacustrine deposits. The results can be used as an analogue for deeply buried Late Cretaceous sedimentary basins in New Zealand, including hydrocarbon producing Taranaki Basin.

The sedimentary facies analyses of the Greymouth Basin indicate that the north-western side of the basin was dominated by alluvial fans alternating with fan deltas whereas the southern and eastern sides of the basin were dominated by meandering rivers and floodplains alternating with muddy low gradient deltas. Deep, organic-rich, thick lacustrine facies were deposited in the centre of the basin commonly replaced by thick, low ash, mires during alluvial phases. The overall facies distribution suggests a half-graben geometry for the Greymouth Basin with the primary basin-bounding fault located to the north-west. This contradicts with previous tectonic models of the Greymouth Basin where a basin bounding fault was postulated on the eastern side of the basin based on isopach maps of the coal-bearing strata from drill cores.

Better mapping of shoreline and shallow subaqueous facies has led to revised isopach maps and cross-sections allowing interpretation of the basin's tectonic development through time. The Greymouth Rift Basin widened through time as indicated by westward stepping of the basin bounding fault and younger basal bounding surface with ever younger sediments sitting directly on the basement. The basin's sedimentary fill also thickened through time as indicated by the thickening of the conglomerates and lacustrine mudstones up-section. Results show that the oldest alluvial-lacustrine phase of the Jay and Ford members records small isolated lakes separated by alluvial fan-fan delta conglomerate facies marking the locations of small, discontinuous normal faults. As the basin widened and deepened through time, new faults formed to the west, small intra-basinal faults became inactive or amalgamated to form a major basin bounding fault. This major border fault controlled the subsidence of the late syn-rift phase of the basin. Applying the information about the evolution of the Greymouth Basin, it can be concluded that the West Coast-Taranaki Rift basins experienced the same basin development history initiating from small sub-basins that widened and deepened through time from the amalgamation of active normal fault segments.

Sequence stratigraphic analysis of the Greymouth Basin indicates that a complete depositional sequence likely records episodes of increased subsidence rates relative to sediment supply that increases the accommodation condition. This was followed by a longer period of tectonic quiescence when decreased subsidence rates in the basin permitted deltaic systems to prograde into the lake eventually completely infilling it and transitioning to alluvial systems across the basin. The onset of each phase of more rapid subsidence in the Greymouth Basin was marked by a sequence boundary. The sequence boundaries correlate with subaerial unconformities as the basin widened due to the progressive creation of new faults to the northwest. The results indicate that the cyclic variation of the alluvial-lacustrine deposits was associated with the rift basin development where the primary driving force was episodic tectonic activity through time compared to other dominant factors like climate variation or outflow of streams.

# Table of Contents

# List of Figures

**Chapter 1:**

**Chapter 2:**

**Chapter 3:**

**Chapter 4:**

**Chapter 5:**

# List of Tables

# Acknowledgments

First and foremost, I would like to thank my supervisor and mentor, Dr. Kari Bassett, for her continuous support from the beginning of my thesis, especially during the final months and during the Christchurch mosque attack in March 2019. I would like to thank her for lending her knowledge and the time, and the effort she spent on this research. I would like to acknowledge her support during the interruption of my study because of the multiple moves of the office and the labs of the Geological Science Department to the temporary location and then to the new building. Without her supports, it was not possible to complete this thesis.

My gratitude goes to Dr. Andy Nicol for inspiring me throughout my Ph.D. and to support me every time I stepped into his office for asking help. I would also like to thank Dr. Rob Boyd for sending valuable information and lending his knowledge about the Greymouth Coalfield.

This project was funded by the Ministry of Business, Innovation, and Employment of New Zealand (MBIE) through GNS Science-led research program on New Zealand petroleum source rocks, fluids, and plumbing systems (contract C05X1507), Research Aim 1.4: Discovering our lacustrine source rock potential. I would like to acknowledge MBIE for supporting my research. My special thanks to Dr. Daniel Mohnhoff, a former geochemist from the GNS (Geological and Nuclear Science), for giving me the opportunities to visit Slaty Creek on West Coast with him. I would also like to thank him for accompanying me during sampling the lacustrine mudstones and describing the cores at National Core Store in Featherston, Wellington. My gratitude goes to GNS scientists Mr. Richard Sykes and Dr. Sebastian Naeher for lending their academic and technical knowledge, and expertise throughout my Ph.D.

I would like to thank 'Mason Trust Fund' in the Department of Geological Sciences at the University of Canterbury for funding several field trips at Greymouth and for visiting at National Core Store in Featherston. I must mention one name, Mr. Daniel Willmott, manager of the National Core Store. He was always ready (with a smile on his face) for finding the particular core boxes for me during my visit at the core storage in Featherston. I am also grateful to John Southward for his technical and IT support throughout my study in the Department of Geological Sciences.

Finally, I would like to thank my wife Pallabi for her supports and motivation from the beginning of the day we arrived in Christchurch together. To my daughter lovely Tonika, thanks a lot for being the reason to smile at the beginning and the end of every da

# Chapter 1: Introduction, geological background and previous works

## 1.1 Introduction

The Late Cretaceous to Early Palaeocene Greymouth Basin is a part of the West Coast-Taranaki Rift System in New Zealand (Strogen et al. 2017). Unlike most parts of the rift system which are deeply buried and only available via seismic analysis, the Greymouth Basin sedimentary rocks are accessible in outcrop and through extensive drill cores. The basin has been extensively mined for coal and oil seep discoveries suggest it may also be a petroleum prospect (Gage 1952; Wellman 1971; Suggate and Waight 1998). The basin is filled with braided river conglomerates, raised mire coals, meandering river sandstones and lacustrine mudstones (Nathan et al. 1986; Newman 1985; Sherwood et al. 1992; Boyd and Lewis 1995; Ward 1997). Most previous studies of the Greymouth Basin have primarily focused on the characterization of coal and not the non-coal bearing deposits except where they directly affected the coal (Bowman et al. 1984; Newman 1985; Newman and Newman 1992; Ward 1997). In particular, thick conglomerate deposits as well as fine grained alluvial and lacustrine sediments in the basin have been relatively less studied.

The previous models of the Greymouth Basin indicate a half-graben geometry with a basin-bounding fault located in the east (Bowman et al. 1984; Ward 1997). Most of the previous researches have not studied the conglomerate in the northwest side of the basin in detail and therefore the conglomerates have not been used to evaluate the tectonic setting of the Greymouth Basin. The previous studies mostly focused on coals and associated coaly sediments (Gage 1952; Newman 1985; Ward 1997). The other non-coal-bearing fine-grained deposits (meandering fluvial and lacustrine mudstones) were less studied (not with a focus to differentiate the various subaerial deposits from shoreline and subaqueous deposits) to identify various organic sediments of the basin and to understand the palaeogeography of the basin. Therefore the main purposes for conducting this research are multifold and address: i) the importance of the conglomerates for identifying the main basin bounding fault, ii) the importance of the architecture of the lithofacies across the basin for developing palaeogeographic maps leading to a better understanding of petroleum potential units, iii) the importance of lithofacies architecture for determining basin evolution, and iv) the application of lacustrine sequence stratigraphy to understand the fundamental controls on lake development in the basin

## 1.2 Location and Formation of the Greymouth Basin

The Greymouth Basin is located at the southern end of the Paparoa Range in the West Coast region of South Island in New Zealand. The basin is bounded by the modern day coastline along the West Coast and the Montgomerie-Mount Davy Fault System in the east (Figure 1.1A, 1.1B, 1.1C). The Greymouth Coalfield is an important part of this basin which is extensively drilled for low ash, low sulphur bituminous coal (Morgan 1911; Gage 1952; Newman 1985; Barry et al. 1994; Boyd and Lewis 1995; Ward 1997; Cody 2015). The primary data sources for this research have been taken from the borehole descriptions, drill cores and geophysical logs (gamma ray and density) of the Greymouth Coalfield.

The Cretaceous break-up of Gondwana and the formation of a series of extensional basins in New Zealand have been previously documented by many authors (Figure 1.2; e.g. Laird 1981, 1993, 1994; Nathan et al. 1986; Bishop 1992; Turnbull et al. 1993; King and Thrasher 1996; Gaina et al. 1998; Cook et al. 1999; Laird and Bradshaw 2003, 2004; King et al. 2011; Strogen et.al. 2017; Mortimer et al. 2017). Extension began as early as ca. 130 Ma with widespread extension and rifting between Australia and Antarctica as part of the fragmentation of Gondwana in the SW Pacific (Laird and Bradshaw 2004). During that time, the

New Zealand subcontinent was still undergoing convergent margin tectonics which abruptly switched to extension at approximately 105±5 Ma leading to separation of New Zealand from Gondwana at ~82 Ma (Laird 1993, 1994). The change from convergence to rifting is represented by a major angular unconformity throughout most of New Zealand, separating older, subduction related rocks from younger, less deformed strata. The onset of extension resulted in the widespread development of NW-WNW trending fault-controlled grabens and half-grabens (overlying core complex low angle detachment faults) filled with the non-marine deposits of the mid-Cretaceous Pororari Group in Westland (Tulloch and Kimbrough 1989; Laird 1993, 1994; Laird and Bradshaw 2004). Syntectonic basin sediments were primarily derived from local fault scarps above core complex detachment faults and strongly reflect the geology of small local drainage systems (Nathan 1978).

During the time of drifting as a passive continental block/plateau between 85 Ma to 53 Ma (Gaina et. al., 1998), conventional basin tectonic theory predicts that New Zealand's continental margin should have been passively accumulating sediments in a subsiding wedge driven by sediment loading (Ingersoll and Busby 1995). However, this is clearly not the case for the West Coast, where a series of NNE-trending extensional to transtensional basins, termed the West Coast-Taranaki Rift System, were formed during the Late Cretaceous and remained active until the Early Palaeocene (Laird 1993, 1994; King and Thrasher 1996). The onset of the 2$^{nd}$ phase of rifting did not occur until after ~1700 km of separation had taken place between Australia and New Zealand and after approximately 15 million years of quiescent passive margin behaviour (Laird 1994; Gaina et. al. 1998).

A recent study of the timing of rifting in the Taranaki Basin from Strogen et al. (2017) shows two temporally distinct phases of rifting recording Gondwana break-up (Figure 1.2). The first phase (Zealandia Rift Phase) produced half-grabens trending NW to WNW during the mid-Cretaceous (c. 105 – 83 Ma). The second phase (West Coast–Taranaki Rift Phase produced N to NE-trending extensional half-grabens in the shelfal Taranaki Basin during the latest Cretaceous (c. 80– 55 Ma). These two phases were separated by a short period (c. 83 – 80 Ma) of uplift and erosion representing a break-up unconformity. The Greymouth Basin is a product of the second rifting phase.

## 1.3 Structure and lithostratigraphy of the Greymouth Basin

The faults that formed the Greymouth Basin are oriented in a NNE-SSW direction and have been reactivated as reverse faults in the modern compressional tectonic regime of New Zealand during the late Cenozoic (<15 Ma) to present day (Bishop, 1992; Bishop and Buchanan, 1995; Ghisetti and Sibson, 2006; Sibson and Ghisetti, 2010; Barnes and Ghisetti 2013; Stahl 2014). Geophysical and geological studies of the West Coast region identify a number of large historical earthquakes in this region associated with these reverse faults (Berryman 1980; Nathan et al. 1986; Anderson et al. 1993, 1994; Stirling et al. 2012; Barnes and Ghisetti 2013; Figure 1.3). The sedimentary strata of the Greymouth Basin have been folded and cross-cut by the younger, oblique-slip Montgomerie-Mt Davy Fault Systems (Figure 1.1C).

The Greymouth Basin is filled by the Late Cretaceous to Early Palaeocene terrestrial sediments of the Paparoa Formation, the formally defined name replacing the older name of Paparoa Coal Measures (Nathan 1978; Laird and Bradshaw 2004). Over the past hundred years, the nomenclature of the Paparoa Formation has been redefined numerous times due to the complexity of laterally correlative lithologies (Table 1.1). The stratigraphy published by Nathan (1978) has been used in this thesis.

The Paparoa Formation unconformably overlies basement of highly deformed, Cambrian-Ordovician Greenland Group turbidite successions (Gage 1952; Nathan 1978; Laird 1992, 1994; Laird and Bradshaw

2004; Mortimer et al. 2013). Deposition was entirely non-marine through the Early Palaeocene, comprising conglomerates, sandstones, and mudstones associated with thick coal deposits. The formation has been the target of drilling in two large commercial bituminous coalfields, the Greymouth and Pike River coalfields. The Paparoa Formation is overlain by the Eocene Brunner Formation followed by the deposition of the Island Sandstone and Kaiata formations, the result of passive margin subsidence and marine transgression in the Eocene (Nathan et al. 1986; Newman and Newman 1992; Rattenbury et al. 1998).

The Paparoa Formation is divided into five members according to their diverse range of lithologies and sedimentary facies (Figure 1.4; Nathan et al. 2002). On the eastern margin of the Paparoa Basin, coal deposits are associated with sandstone facies with interbeds of carbonaceous mudstone (Jay, Rewanui and Dunollie members); these are interpreted as peat mire and meandering river/overbank deposits (Gage 1952; Newman 1985; Ward 1997). Correlative conglomerates on the western side of the basin (Jay, Rewanui and Dunollie Members) are interpreted as alluvial fan/braided river deposits (Newman 1998; Ward 1997; Cody 2015). Dark grey, well bedded to massive, carbonaceous siltstones and mudstones with thin-bedded normally graded sandstones (Ford, Waiomo and Goldlight members) are interpreted as lacustrine deposition in the centre of the basin (Newman 1985; Newman and Newman 1992; Cody 2015).

### 1.3.1 Jay Member

The oldest member of the Paparoa Formation, the Jay Member is composed of breccia, breccia-conglomerates, sandstones, mudstones and coal-seams (Gage 1952; Newman 1985). The member is further divided into three units which are Jay (i), Jay (ii), and Jay (iii) (Gage 1952). Jay (i) is the lowermost unit of the Jay Member which is composed of angular to subangular greywacke breccia and breccia-conglomerates with less sandy matrix (Gage 1952). Greywacke and argillite clasts from the Greenland Group basement are predominant and quartz is fairly common, whereas granite and schist clasts are absent (Gage 1952; Newman 1985). Jay (i) is interpreted as fanglomerate or talus-breccia (Gage 1952). The absence of rounded clasts and lack of sorting were the primary reasons cited indicating the minor role of water during their transportation and deposition. Jay (ii) is the middle unit comprising clast-supported conglomerates with rare sandstone lenses with clasts of predominantly Greenland Group derived greywacke and argillite with minor vein quartz and hornfels clasts (Gage 1952). Jay (ii) is interpreted as alluvial fan conglomerate but more dominated by stream flow processes as indicated by rounded clasts and moderate sorting (Gage 1952; Newman 1985; Ward 1997). The uppermost unit is Jay (iii) which mainly contains much finer sandstones and siltstones with numerous thin coal-seams and carbonaceous mudstones (Gage 1952). Coal seams are often dirty and thus not considered to be economically viable (Newman 1985). The Jay (iii) sandstones and coals are interpreted to have been deposited in a lower energy flood plain adjacent to a meandering river environment (Gage 1952; Newman 1985; Ward 1997). As economic coals are not found in the Jay Member, it has not been targeted by the coal companies and most drillholes do not fully penetrate the member. Therefore, lateral correlation between drillholes is poor. The approximate age of the Jay Member is estimated to be around 71 Ma (Laird 1994) which coincides with the beginning of sea floor spreading in the Tasman Sea (Gaina et al. 1998).

### 1.3.2 Ford Member

The Ford Member is the oldest lacustrine mudstone member of the Paparoa Formation and composed of dark grey to brown grey mudstones and siltstones with thin sandy lenses (Newman 1985; Ward 1997). Numerous leaf impressions, plant debris, and freshwater molluscs and snails are found in Ford Member mudstones (Gage 1952). The presence of freshwater fossils indicates deposition took place in a lacustrine

environment (Gage 1952). The Ford Member is restricted to the eastern side of the Greymouth Basin. Ward (1997) reclassified mudstones from the northwest side of the basin, particularly at Twelve Mile Beach and nearby drillholes, as belonging to the Ford Member based on the revision of several drillholes data (unpublished). However, detailed correlation work by Cody (2015) rejected this reassignment and the mudstone at Twelve Mile Beach is still classified as the Waiomo Member after Nathan (1978).

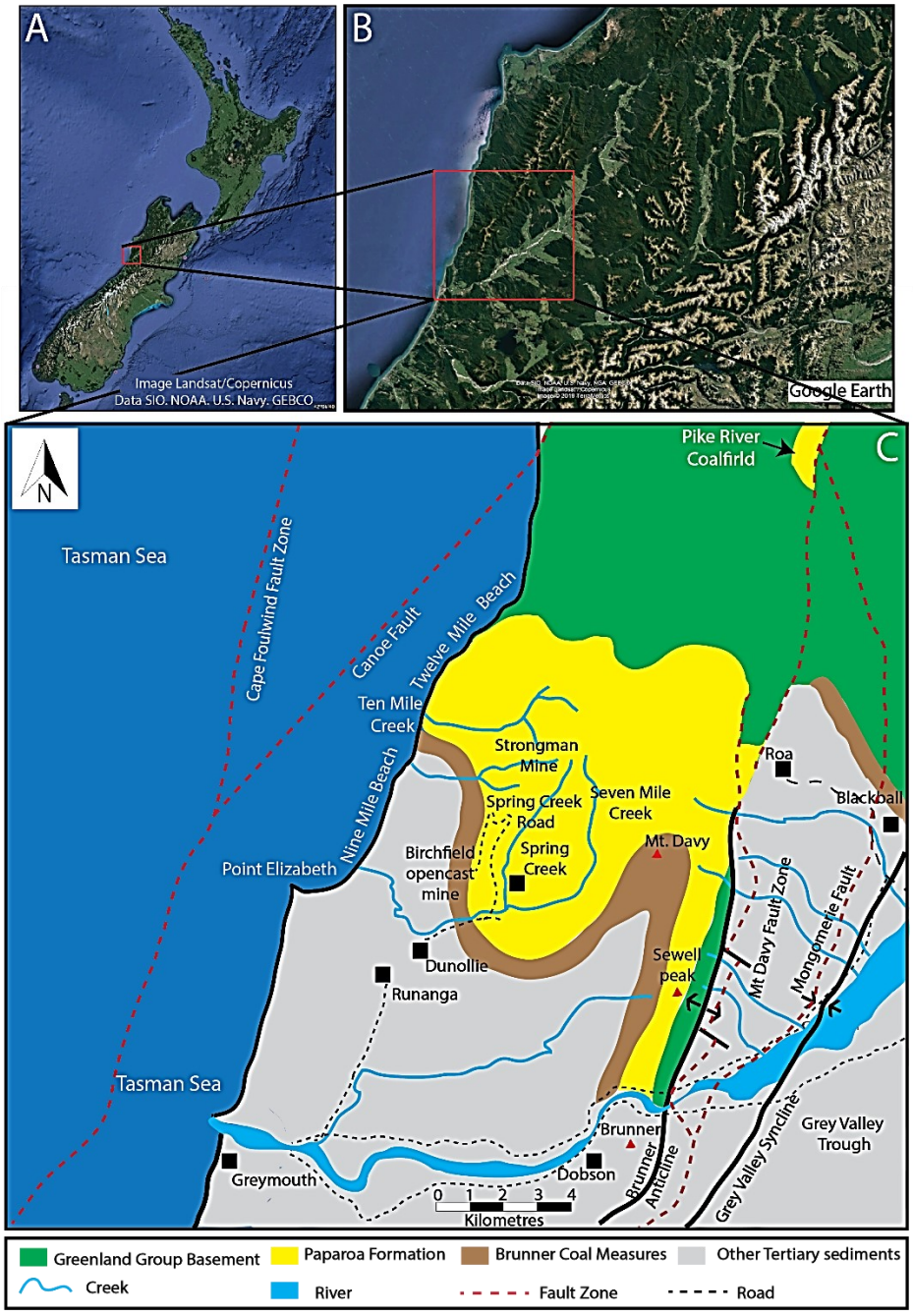


Figure 1. 1: A) and B) google earth image showing the location of the Greymouth Basin, South Island, New Zealand, and C) geological and structural map of the study area (modification based on the information from Gage 1952; Newman 1985; Suggate 2014; Nathan 1986; Nathan et al. 2002; Rattenbury and Isaac 2012). Red triangle on the map represents mountain peak and black square shows important cities.

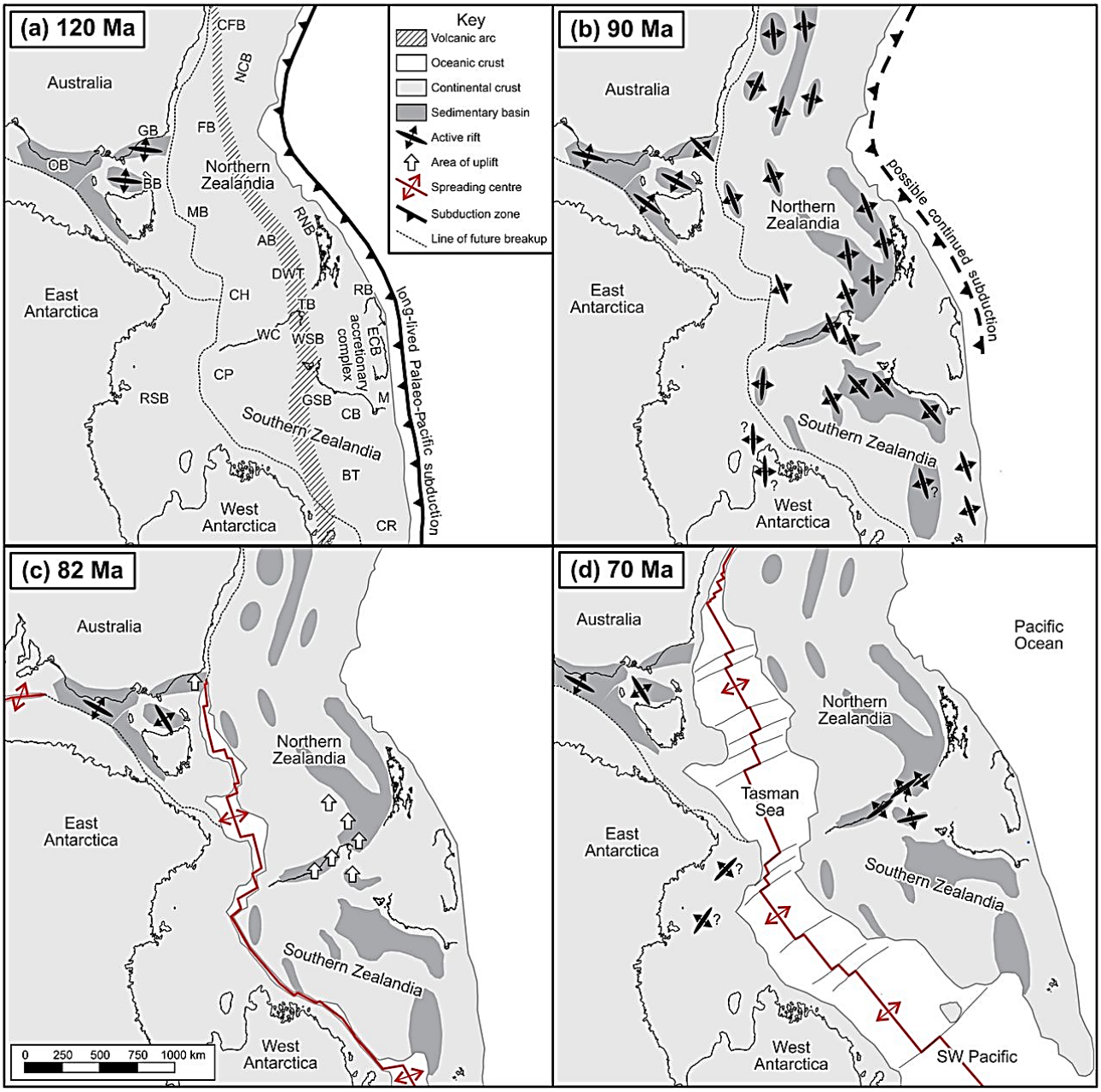


Figure 1. 2: Tectonic reconstruction for the Zealandia–Australia–Antarctica region from 120 Ma to 70 Ma (Strogen et. al. 2017), A) the active convergent plate boundary system at the eastern margin of Gondwana; B) first phase of rifting (Zealandia rift phase) with NW to WNW trending half-grabens; C) Initiation of separation of New Zealand from Australia by sea floor spreading in the west and a short period of uplift and erosion to the east from the spreading centre, and D) second phase of rifting (West Coast–Taranaki rift phase) with N to NE trending half-grabens; the red dot is the location of the Greymouth Basin. Basin abbreviations in (a): AB, Aotea; BB, Bass basins; BT, Bounty Trough; CB, Canterbury; CFB, Capel–Faust; CH, Challenger; CP, Campbell; CR, Chatham Rise; DWT, Deepwater Taranaki; ECB, East Coast; FB, Fairway; GB, Gippsland; GSB, Great South; M, Marlborough; MB, Monwai; NCB, New Caledonia; OB, Otway; RB, Raukumara; RNB, Reinga–Northland; RSB, Ross Sea; TB, Taranaki; WC, West Coast; WSB, Western Southland.

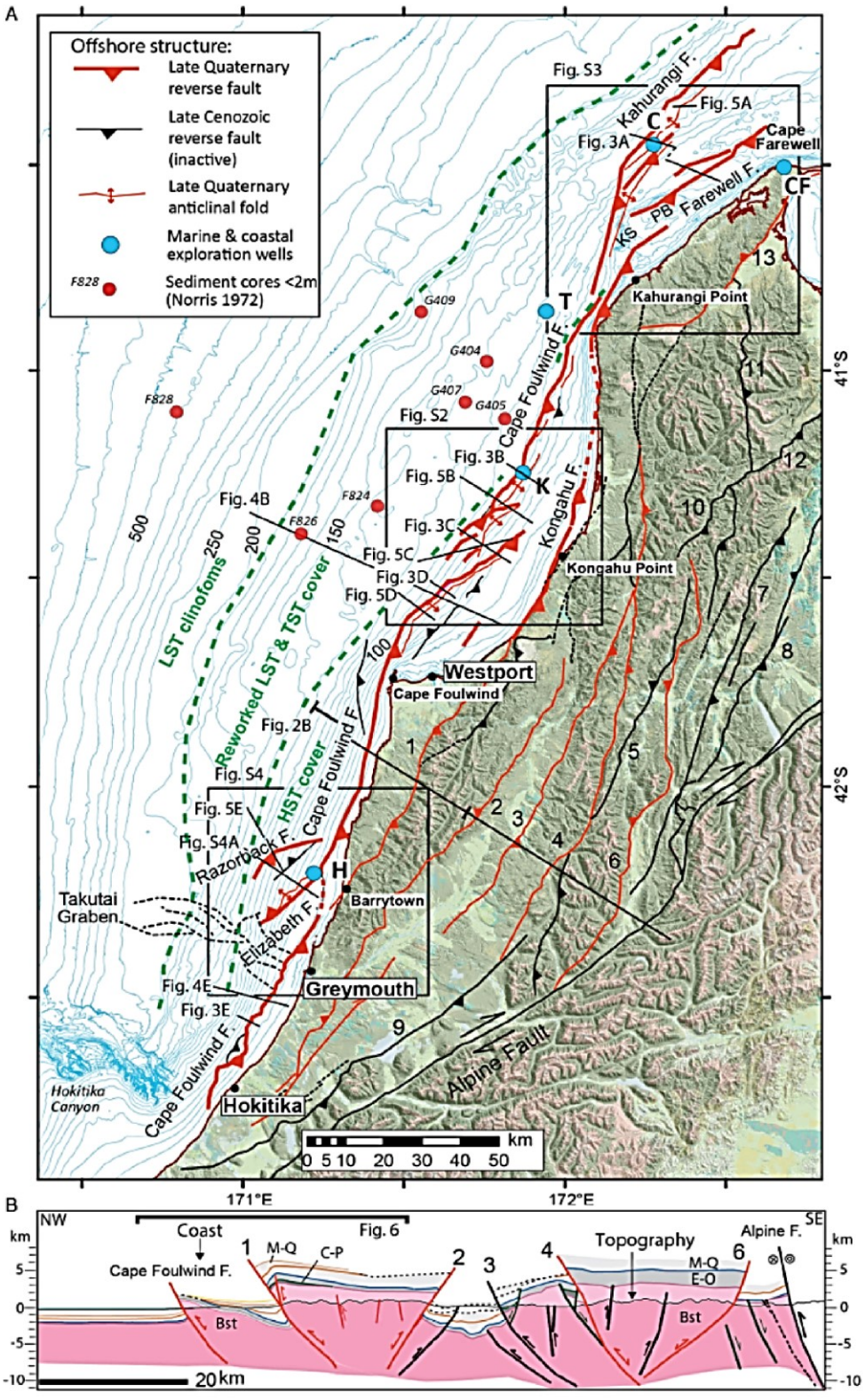


Figure 1. 3: Active faults offshore identified from the high-resolution seismic survey (A) with a cross-section (B) in offshore West Coast where red lines represent compressionally reactivated Late Quaternary normal faults. No evidence of reactivation exists for the reverse faults in black. (Barnes and Ghisetti 2013).

Table 1. 1: Different nomenclature of the Paparoa Formation

<table>
<tr><th colspan="5">Nomenclature of the Paparoa Coal measures</th></tr>
<tr><th>Gage 1952</th><th colspan="2">Nathan 1978</th><th colspan="2">Ward 1997</th></tr>
<tr><td>Dunollie Formation</td><td rowspan="8">Paparoa Formation</td><td>Dunollie Coal Measures Member</td><td colspan="2">Dunollie Formation</td></tr>
<tr><td>Goldlight Formation</td><td>Goldlight Mudstone Member</td><td colspan="2">Goldlight Formation</td></tr>
<tr><td>Rewanui Formation</td><td>Rewanui Coal Measures Member</td><td rowspan="3">Rewanui Formation</td><td>Rewanui Coal Measures Member</td></tr>
<tr><td>Waiomo Formation</td><td>Waiomo Mudstone Member</td><td>Waiomo Mudstone Member</td></tr>
<tr><td>Morgan Formation</td><td>Morgan Coal Measures Member</td><td>Morgan Coal Measures Member</td></tr>
<tr><td>Ford Formation</td><td>Ford Mudstone Member</td><td>Ford Formation</td><td>Ford Mudstone Member</td></tr>
<tr><td rowspan="2">Jay Formation</td><td rowspan="2">Jay Coal Measures Member</td><td></td><td>Ford Transitional Member</td></tr>
<tr><td colspan="2">Jay Formation</td></tr>
</table>

### 1.3.3 Morgan Member

The Morgan Member is divided into igneous-clast conglomerates and greywacke-clast conglomerates with correlative sandstones and coals (Gage 1952; Newman 1985). The igneous-clast conglomerate unit also included basaltic lava flows and pillow lavas which are restricted to the east near Roa Mine (Gage 1952). Gage (1952) inferred that a volcano erupted in this area, flowing to the west where lava formed pillows when they reached the Ford Lake system. The greywacke clast conglomerate with correlative sandstones and coals is almost indistinguishable from the Jay (ii) unit of the Jay Member. Conglomerate lithofacies are found in the east and the northwest of the Greymouth Basin. Greywacke clast conglomerates are interpreted to have been deposited from erosion of the Greenland Group basement and possible reworking of the Jay Member (Newman 1985), whereas the fine-grained materials are likely a result of advancing fans and deltas which eventually infilled the Ford Lake (Gage 1952). When lakes did not exist, an alluvial environment with low lying meandering rivers, oxbow lakes and low energy swamps and mires developed, as indicated by the sandstone with crossbeds and ripples, and thick coal mire units in the eastern side of the basin (Newman 1985; Boyd and Lewis 1995; Ward 1997). Coal seams found in the Morgan Member are thick, low ash, and low sulphur in content, and economically viable (Newman 1985; Ward 1997). Dating of igneous clasts and basalts of the Morgan Member indicate an approximate age of 68 Ma (Laird 1994).

### 1.3.4 Waiomo Member

The Waiomo Member is composed of massive dark-brown or brown grey mudstones containing abundant very fine micaceous and thin, normally graded sandstone beds (Gage 1952; Newman 1985; Cody 2015).

Numerous fragmented plant fossils with occasional freshwater molluscs and snails are found in the member indicating deposition took place in a lacustrine environment (Gage 1952; Ward 1997). The published map of the Greymouth region shows that the Waiomo Member extends from the northwest at Twelve Mile Beach eastward to the Roa mine in the northeast where it is truncated by the Montgomerie-Mount Davy Fault Systems (Nathan 1978). The contacts with the underlying Morgan Member and the overlying Rewanui Member are gradational over several metres (Gage 1952).

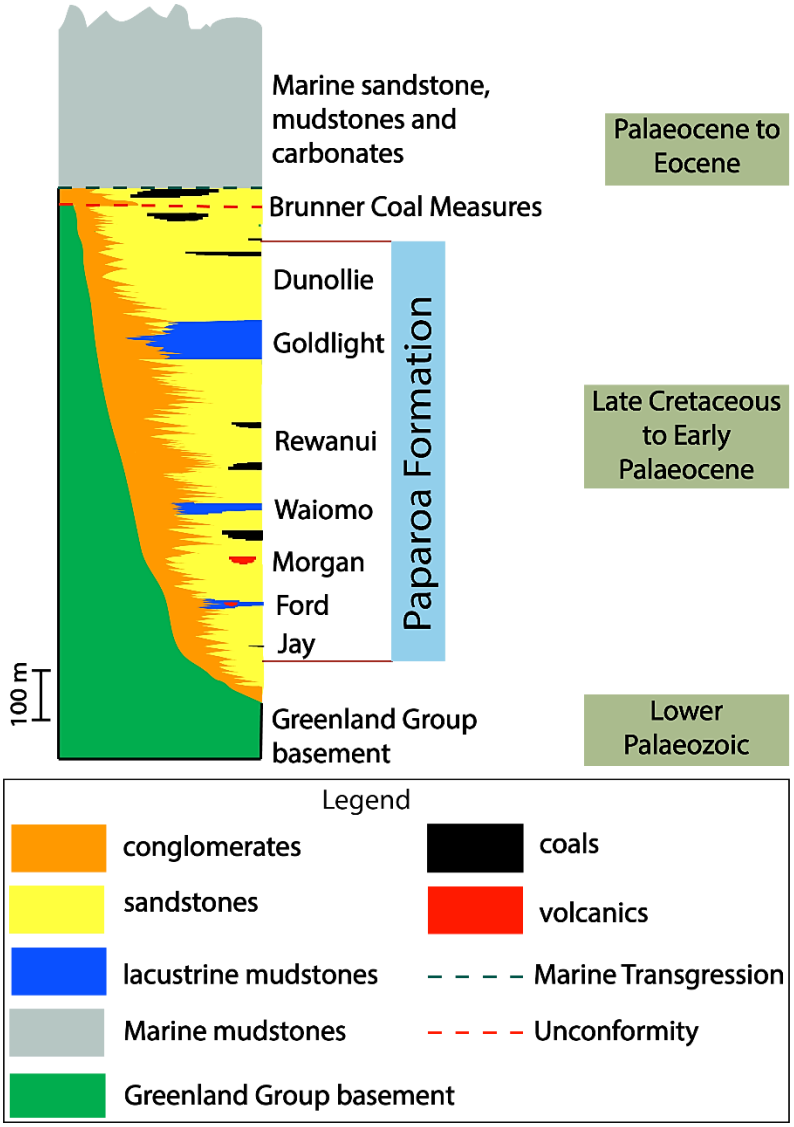


Figure 1. 4: Generalized stratigraphy of the Paparoa Formation modified from Boyd and Lewis 1995.

### 1.3.5 Rewanui Member

The Rewani Member is the thickest of all the coal bearing members of the Paparoa Formation and has been extensively drilled for economic coals (Gage 1952; Newman 1985). The Rewanui Member is divided into two compositional suites; the Eastern and the Western Compositional Suites (Gage 1952; Ward 1997). The Western Compositional Suite is composed of thick and extensive conglomerates which become finer towards the basin centre and is interpreted to have been deposited in high energy alluvial fan environments as evident from the boulder to cobble clast conglomerates at Twelve Mile Beach (Ward 1997). Unlike the

previous Jay and Morgan members, granite clasts are common in the Rewanui Member along with greywacke and argillite clasts derived from the Greenland Group basement (Newman 1985; Steadman 2017). The Eastern Compositional Suite is composed of mostly quartz sandstones and rare granule to pebble conglomerates associated with thick coal seams and carbonaceous horizons (Gage 1952; Ward 1997). The Eastern Compositional Suite was deposited in a alluvial environment with low lying meandering rivers, oxbow lakes and low energy swamps and mires as indicated by the sandstone with crossbeds and ripples, and thick coal mire units (Newman 1985; Ward 1997). Palynological evidence has placed the Cretaceous-Tertiary boundary near the top of the Rewanui Member and the approximate age of the Rewanui Member is estimated to be 65 Ma (Ward 1997).

### 1.3.6 Goldlight Member

The Goldlight Member is the thickest lacustrine member of the Paparoa Formation and comprises massive grey to dark grey mudstone (Gage 1952). Siderite bands are common in this mudstone and leaf and plant fossils are found in some areas. The Goldlight Transitional Member is a subdivision proposed by Ward (1997) where the non-massive sandstones and minor conglomerates found on the northwestern side of the Greymouth Basin were included in this transitional member. Overall deposition was interpreted to have taken place in a lacustrine environment as evident from the lack of marine fossils and the presence of siderite bands (Gage 1952; Bowman et al. 1984; Newman 1985; Cody 2015) The Goldlight Member is extensive and can be found across the basin before it is truncated by the Montgomerie-Mount Davy fault zones in the east (Nathan 1978). It was deposited in the Early Palaeocene and gradationally overlies Late Cretaceous Rewanui Member.

### 1.3.7 Dunollie Member

The Dunollie Member is the youngest member of the Paparoa Formation and primarily composed of conglomerates, sandstones, siltstones, coals and carbonaceous mudstones (Gage 1952; Ward 1997; Nunweek 2001). The conglomerates are found on the northwestern side of the basin where they are indistinguishable from the Rewanui Member conglomerates at Twelve Mile Beach (Gage 1952). However, the top of the conglomerates is white, highly bleached, and the sandstones are more quartzose and uniformly bedded in the northwest (Gage 1952; Nunweek 2001). Granite clasts are common in the Dunollie Member (Newman 1985). However, Greenland Group derived greywacke and argillite clasts are the most dominant. The clast-supported, pebble to cobble sized conglomerates are interpreted to have been deposited in alluvial fan and braided river environments as indicated by the presence of imbrication and crossbeds (Gage 1952; Ward 1997). The fine sandstones, siltstones, and coals are thought to have been deposited in an alluvial environment where meandering river and the floodplain processes were dominant. Coals are not particularly extensive and are often split, indicating they are not economically viable (Gage 1952).

### 1.3.8 Brunner Formation

The Brunner Formation overlies the highly bleached, uppermost section of the Dunollie Member in the northwest and consists of conglomerates with minor sandstone lenses, whereas in the centre where the basin was still topographically low, mostly quartz-rich sandstones with occasional thick coal seams are found (Gage 1952; Nathan et al. 1986). The bleaching is thought to represent a significant unconformity between the deposition of the tectonically confined Paparoa Formation and the onset of extensive regional depositional system during the Eocene (Nathan 1978). However, the Brunner Formation is suggested to be older in the northwest part than in the central and eastern part of the Greymouth basin, and is termed as Brunner P Member (Palaeocene Brunner) (Nunweek 2001; Monteith 2015). Deposition mostly took place

in alluvial environments in a topographic lowland area bounded by encroaching marine depositional systems (Gage 1952; Nathan 1978).

### 1.3.9 Island Sandstone and Kaiata Mudstone

A sequence of Eocene marginal marine and marine sediments overlies the Brunner Formation comprising the Island Sandstone and Kaiata Mudstone of the Kaiata Formation (Gage 1952; Nathan 1978). The Island Sandstone conformably overlies the Brunner Formation and is composed of brownish grey, fossiliferous, muddy fine to very fine sandstone which was deposited in a shallow marine, inner shelf environment (Lever 1999). The Kaiata Mudstone conformably overlies the Island Sandstone and consists of dark grey, glauconitic, calcareous, sandy mudstone (Gage 1952; Nathan 1978; Lever 1999). The deposition took place in marine environment (Gage 1952; Lever 1999).

## 1.4 Previous studies of the Greymouth Basin

Previous studies of the Greymouth Basin have tended to focus on the characterization of the economic coals with minor palynological studies, provenance analysis of conglomerates and sandstones, isopach maps, basin tectonic models, and petroleum potential.

### 1.4.1 Characterization of coals

The previous studies of the Greymouth Basin have primarily focused on the characterization of coals. These studies are broadly discussed by many authors and will be briefly summarized here (Morgan 1911; Gage 1952; Nathan 1978, 1996; Newman 1981, 1985; Bowman et al 1984; Newman and Newman 1992; Boyd and Lewis 1995; Ward 1997; Kemp et al. 1999). Exploration of the Greymouth Basin coals commenced in 1938 (Gage 1952) and continued until 1978, due to the interest of Strongman and Liverpool State Mine and Japanese mining industries (Newman 1985; Ward 1997). These studies included topographic surveying, geologic mapping, stratigraphy, structural geology, and analysis of coal properties and resources. Renewed investigation of the Greymouth Coalfield took place between 1979 and 1984 undertaken by the Mines Division, Ministry of Energy during the Coal Resources Survey (CRS) programme (Bowman 1984; Bowman et al. 1984). The aims of the CRS were to define the remaining coal resources and to identify mining targets for possible future development (Bowman et al. 1984).

Academic interest led to more detailed study of the coal seams of the Paparoa Formation, particularly of coal petrology, palaeoenvironmental analysis, coal geochemistry and maturation of coal in the basin (Newman 1985; Newman 1988). The main investigation was to define coal rank as well as the petroleum potential of the basin using vitrinite reflection, and it was established that New Zealand coals with similar ranks can vary in geochemistry and properties. The studies concluded that additional coal deposits were likely to exist onshore at greater burial depths to the south of the Greymouth Coalfield. These studies made a great contribution to the understanding of the geology of the Greymouth Basin.

### 1.4.2 Provenance analysis of the Paparoa Formation

Conglomerates of the older Paparoa Formation, (Jay, Ford and Morgan Members) contain predominantly quartz and greywacke sandstone clasts and appear to consistently lack alkali feldspar and granite rock fragments (Newman 1985; Figure 1.5A). In contrast, conglomerates of the younger Rewanui and Dunollie members have a granite source in addition to the greywacke source (Figure 1.5B). The sandstones of the Jay and Morgan members are predominantly quartz-rich, whereas those of the Rewanui and Dunollie members are largely composed quartz and feldspar (Gage 1952; Newman 1985; Ward 1997). This change

in composition reflects different source areas during deposition of the older versus younger Paparoa Formation. Gage (1952) believed that the Greenland Group basement was the source in the east and a granitic basement (either Rahu or Karamea Suite granites) was the source in the west. However, Newman (1985) and Ward (1997) thought that the sources were the opposite of what Gage (1952) had interpreted. A recent MSc study examined the provenance of the Paparoa Formation with the help of geochemical analyses of clasts (Steadman 2017). The Steadman study contradicts both previous interpretations, suggesting that the granite clast compositions are inconsistent with Rahu and Karamea Suite granites, and best fits a new A-type granite which has low barium and strontium content and is likely located somewhere offshore to the west. Provenance analysis of fine-grained sandstones using the scanning electron microscope-cathodoluminescence (SEM-CL) technique (Bernet and Bassett, 2005) was conducted by Ettmuller (2003) (published in Bassett et al., 2006). The results show that the older sediments from both the western and eastern parts of the basin were derived mainly from low-grade metamorphic Greenland Group rocks with only a 15-20% contribution from granites. This continued in the younger sediments from the western side of the basin, those from the eastern side of the basin, however, were derived from metasediments of the Greenland Group with a possible upward increase in a high-grade metamorphic source.

### 1.4.3 Tectonic models of the Greymouth Basin

The tectonic setting of the Greymouth Basin has been variably modelled as a complex full graben (Bowman et al. 1984), a half-graben rift basin (Newman 1981, 1985; Ward 1997), a transtensional rift basin (Ettmuller et al. 2006), and a sag basin (Suggate 2014). Most of the Greymouth basin models have been developed from the interpretation of the isopach maps of different members of the Paparoa Formation.

Early isopach maps of the different members were interpreted to indicate lateral vs longitudinal change in basin orientation during the deposition of the Paparoa Formation (Gage 1952; Bowman et al. 1984; Newman 1985; Ward 1997). The isopach maps of the older Jay and Ford members suggest that deposition was in a NW-WNW trending basin (Figure 1.6A, 1.6B), whereas the maps of the younger Rewanui and Dunollie members suggest deposition in a NNE-SSW trending basin (Figure 1.6E, 1.6F). The Morgan and Waiomo members were interpreted as the transition of basin change (Figure 1.6C, 1.6D). This change in basin orientation was interpreted to be the result of a shift in the orientation of extension during the break-up of Gondwana. However, a recent interpretation of the lacustrine mudstone isopach maps of the Paparoa Formation shows that the older Ford Member and the younger Waiomo Member have the same NNE-SSW orientation, indicating the basin orientation was probably not changed (Cody 2015).

The Greymouth Basin was first modelled as a complex full-graben rift basin with two primary depocentres which were separated by a stable palaeo-high zone in the middle of the basin (Bowman 1984; Figure 1.7). The Strongman-Ten Mile Depocentre, the full graben to the west, was bounded by an active fault along its western margin and a mid-basin tectonic hinge zone along its eastern margin. The Eastern Basin Depocentre, the full graben to the east, was bounded by a minor tectonic hinge zone along its western margin and a 2$^{nd}$ minor hinge zone along its eastern margin. The model illustrates that the subsidence, as well as the sediment thicknesses and the distribution of the Late Cretaceous to Early Palaeocene sediments in the Greymouth Basin, were largely controlled by these NNE-SSW-oriented, deep seated, syn-depositional faults.

Newman (1981, 1985) introduced a complex structural model modifying the Bowman (1984) paired graben model with both NNE-SSW and WNW-ESE structural trends (Figure 1.8). The author interpreted an active, basin-bounding fault on the eastern margin as controlling the majority of basin subsidence. The author also

concluded that a progressive increase in conglomerate thickness in the northwest suggested a palaeoslope from northwest to southeast but interpreted it as being less active during the majority of deposition in the Greymouth Basin.

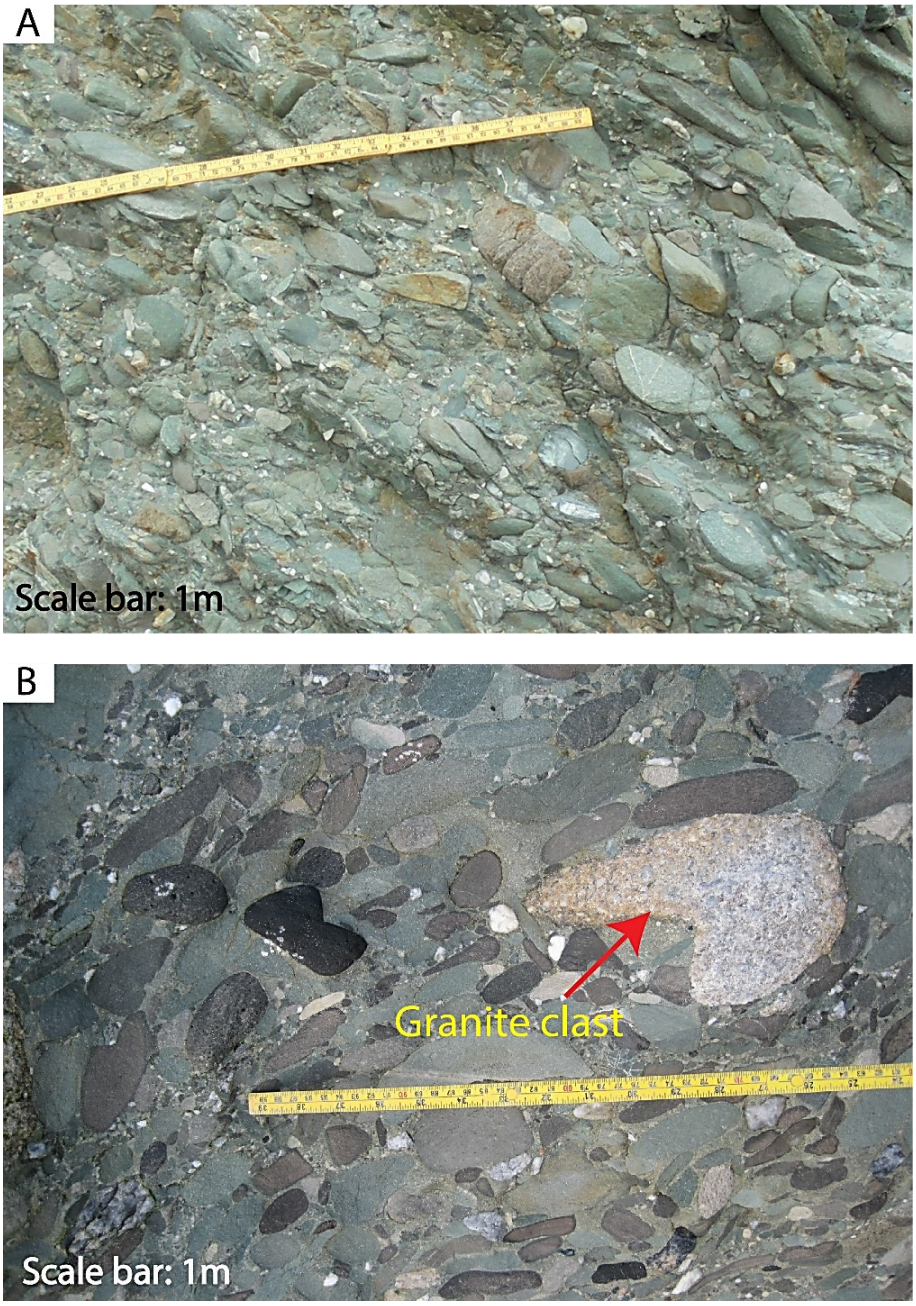


Figure 1. 5: A) Absence of granite clasts in Morgan member (older) of Paparoa Formation at Twelve Mile Beach, and B) Presence of granite clasts in Rewanui member (younger) of Paparoa Formation at Twelve Mile Beach.

A comprehensive study by Ward (1997) broadly focused on the lithostratigraphy, tectonostratigraphy and palynostratigraphy of the Paparoa Formation. The author proposed a model which is best characterised as an eastward deepening half-graben with a master fault on the eastern margin (Figure 1.9). The model also

describes a western margin area along which relatively minor local faulting occurred with conglomerates sourced from that side of the basin. However, the author concluded that the eastern margin fault was responsible for the overall subsidence of the Greymouth Basin. Therefore, in most cases where a fault was postulated it was located on the eastern side of the basin. The result was primarily based on the presence of the Montgomerie - Mt Davy fault zones marking the eastern boundary of the Paparoa Formation.

The Greymouth Basin is interpreted as a downwarping sag basin by Suggate (2014). The sag basin concept was introduced as a result of reinterpretation of the timing of the faults on the eastern side of the basin. Suggate discussed one of the oldest sedimentary cross-sections produced by Gage (1952) which showed no active faulting in the eastern part of the Greymouth Basin during the entire Late Cretaceous and Early Palaeocene depositional phase. Gage (1952) interpreted this structure as a downfold in which Late Cretaceous and Palaeocene sediments were deposited. This sag basin structure resembles the structure of the Mawhera Basin in the West Coast (Suggate and Waight 1999; Suggate 2013).

Other alternative basin models suggested that extension may have been accommodated as a result of oblique movement on the NNE–SSW oriented faults in a transform setting (Bishop 1992; Laird 1994). These palaeo-reconstruction models and the interpretations about the changes in the primary extension directions of the basin lead to the possibility of the Greymouth Basin having formed as a transtensional basin. This could account for the enduring narrowness of the basin with its thick sediment accumulation. Strike-slip fault movement was also suggested based on provenance analysis of quartz grains in Paparoa Formation sandstones (Bassett et al. 2006).

## 1.5 Scope of this thesis

Various aspects of the Greymouth Basin had not been studied in detail, and thus were unclear or unrecognised. These opportunities led to the present research.

### 1.5.1 Tectonic setting of the Greymouth Basin

Most previous studies of the Greymouth Basin have primarily focused on the characterization of coal and not on the non-coal bearing deposits except where they directly affected the coal (Bowman et al. 1984; Newman 1985; Newman and Newman 1992 and Ward 1997). Although tectonic models have been developed using analysis of the borehole lithologies and outcrop sediments, the thick conglomerate deposits on the western margin of the basin had not been thoroughly studied or considered for characterising its tectonic setting. The conglomerates were often not included in isopach maps because they were not targeted for drilling by the coal companies. My research on the non-coal bearing lithologies has highlighted the importance of the conglomerate facies during deposition of the latest Cretaceous Rewanui and Dunollie members. At Twelve Mile Beach, the combined thickness of Rewanui and Dunollie conglomerates is almost 400 m thick. The study of this thick conglomerate section improved the understanding of the tectonic development of the Greymouth Basin, the location of the primary basin bounding faults and their effects on basin geometry and subsidence.

In most cases, the tectonic models of the Greymouth Basin show a fault on the eastern side of the basin (Montgomerie - Mt Davy fault zones) based on isopach maps of the coal-bearing strata from drill cores. However, a recent study by Suggate (2014) showed that the Montgomerie - Mt Davy Fault Systems was not active until very late in the basin's history and thus could not have been the primary basin bounding fault for the majority of the basin's subsidence history. More recent work suggests that thick conglomerate

deposits indicate high relief on the west and therefore the basin bounding fault could have been located in the northwest (Bassett et al. 2014).

This discrepancy has led to the following research questions for this thesis:

- In what environments did the conglomerate deposition of the Greymouth basin take place?
- What is the significance of the conglomerate deposits at Twelve Mile Beach?
- What is the tectonic setting of the Greymouth Basin?

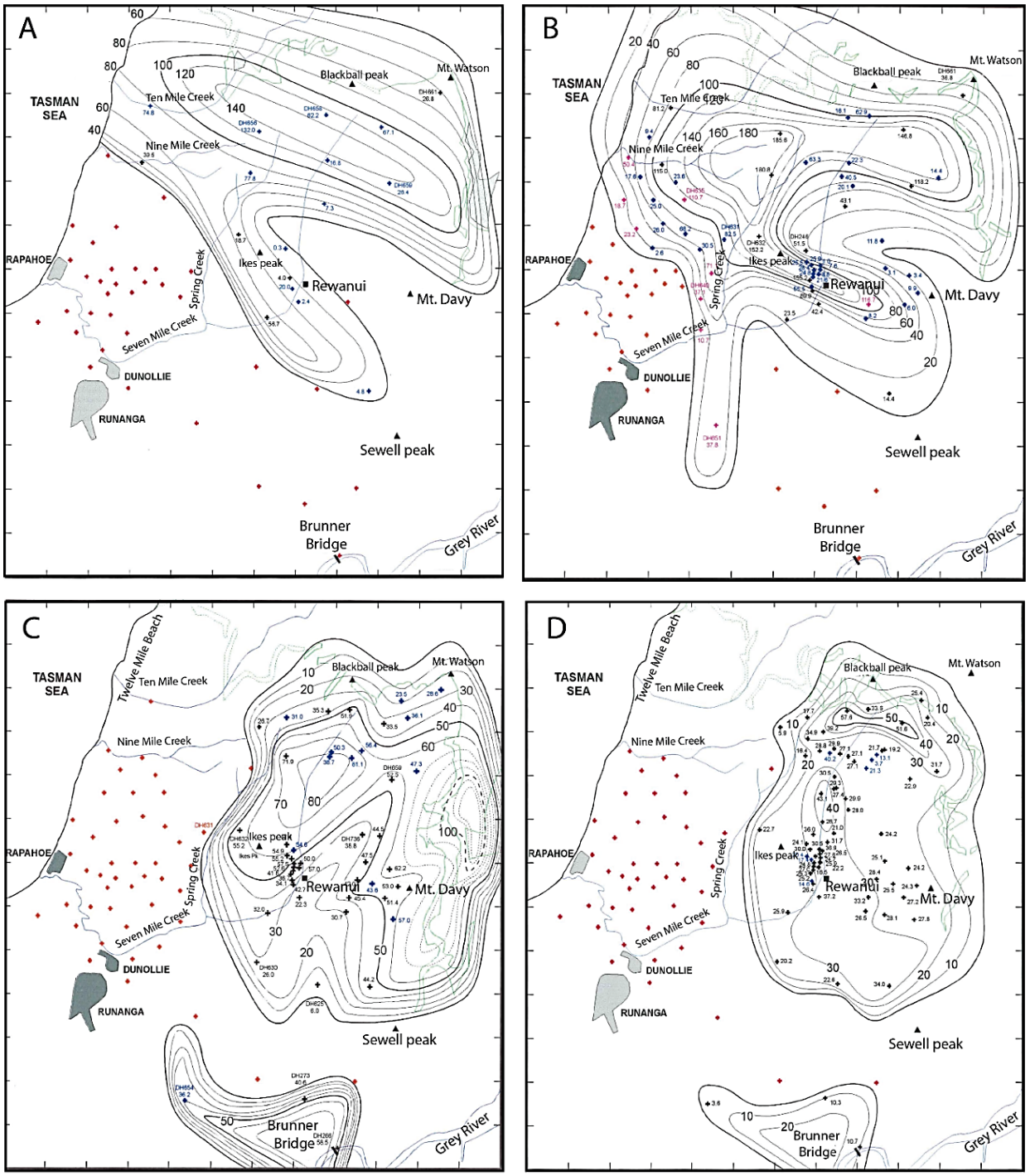

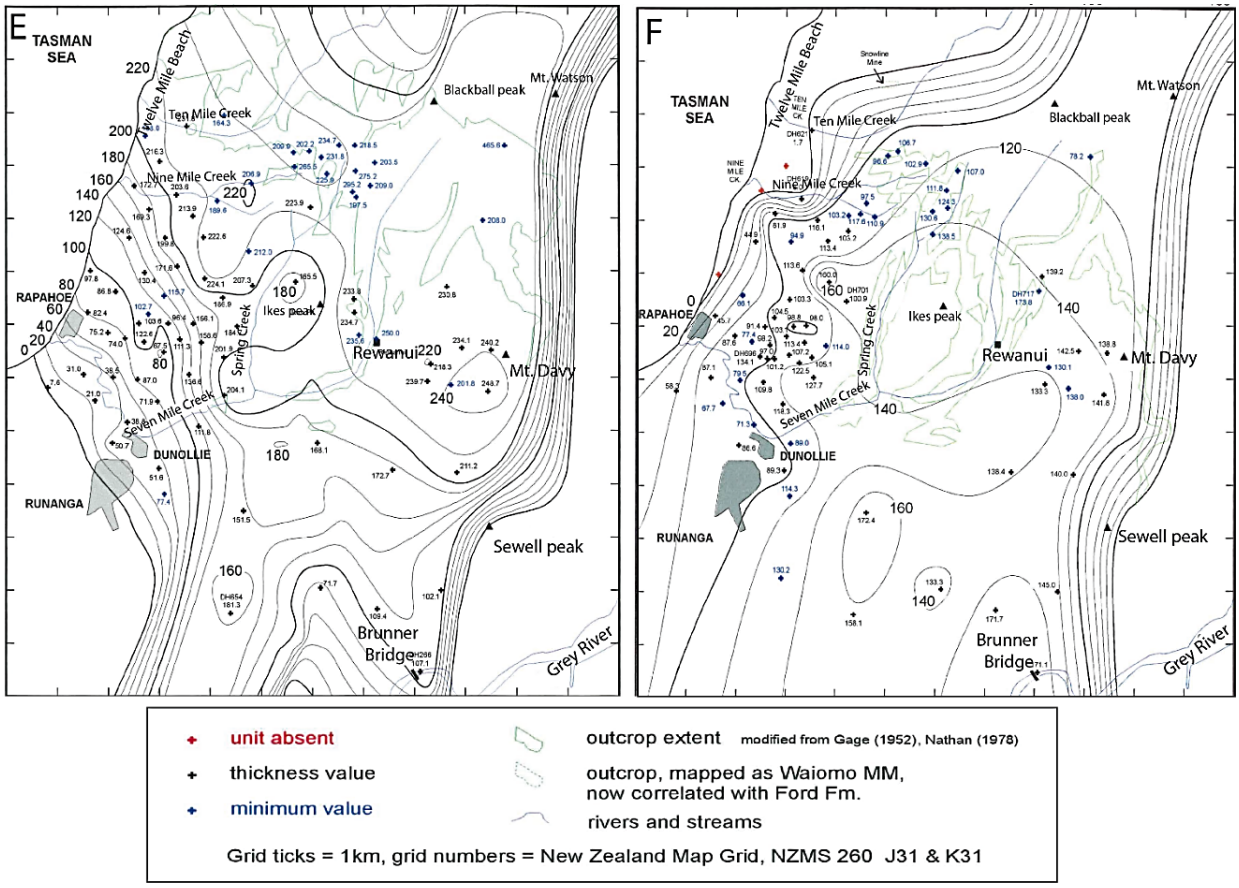


Figure 1. 6: Isopach maps of six members of the Paparoa Formation showing the change in basin orientation from NNW-SSE to NNE-SSW, developed by Ward (1997); A) Jay Member isopach map showing NNW-SSE basin orientation, isopach interval 20 m; B) Ford Member isopach map showing NNW-SSE basin orientation, isopach interval 20 m; C) Morgan Member isopach map showing the transition to NNW-SSE from NNE-SSW, isopach interval 10 m; D) Waiomo Member isopach map showing the transition to NNW-SSE from NNE-SSW, isopach interval 10 m; E) Rewanui Member isopach map showing NNE-SSW basin orientation; isopach interval 20 m; and F) Goldlight Member isopach map showing NNE-SSW basin orientation, isopach interval 20 m.

Chapter 2 deals with the sedimentary facies analysis of the conglomerates which help to understand the overall depositional processes of conglomerates and their associated tectonic setting.

Previous studies on the Paparoa Formation have introduced two quite distinct orientations for basin bounding faults based on isopach maps of the alluvial and lacustrine deposits; NW-WNW and NNE-SSW (Gage 1952; Newman 1985; Ward 1997). The revised Ford and Waiomo member isopach maps by Cody (2015) led to the argument that no dramatic change occurred in basin orientation, and the Paparoa Formation was deposited in a single structural basin type during its life span.

The questions framing the research from the above review include:

- Did the Greymouth basin change its orientation from WNW to NNE during Late Cretaceous to Early Palaeocene?

- Did the Greymouth Basin form in a pure extensional setting? How was the extension accommodated in Greymouth Basin?
- How did the Greymouth Basin evolve through time?

Chapter 4 deals with these research questions which help to interpret the tectonic evolution of the Greymouth Basin. The Greymouth Basin evolution will eventually contribute more information to the context of the formation of the West Coast–Taranaki Rift System.

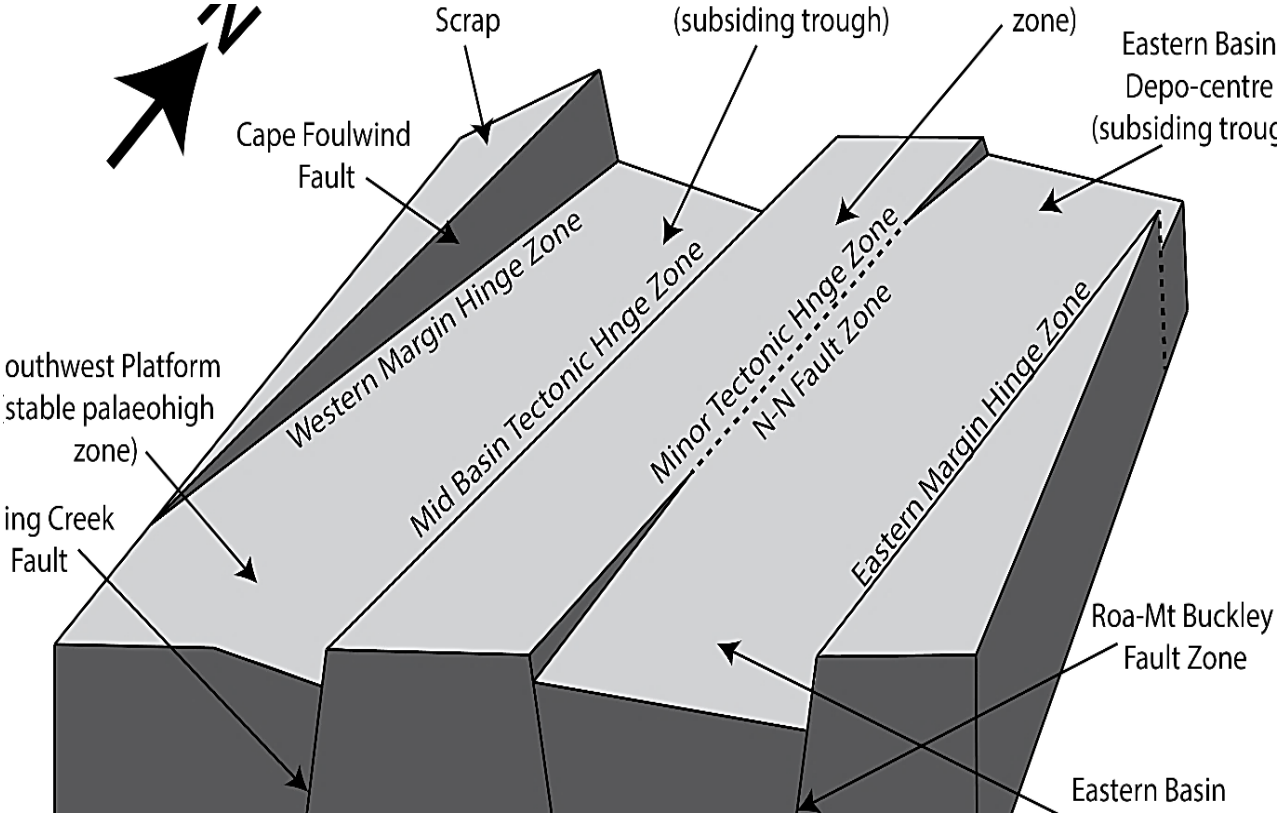


Figure 1. 7: Schematic tectonic model of the Greymouth Basin, Bowman et al. (1984), showing multiple depocentres and basin high.

### 1.5.2 Petroleum potential of the Greymouth Basin

The Greymouth Basin is a small part of the Late Cretaceous West Coast-Taranaki Rift System of which one part, the Taranaki Basin, is currently the only petroleum producing basin in New Zealand. Cretaceous-Cenozoic coals and coaly mudstones have already proven to be source rocks for the Taranaki Basin and are interpreted to have sourced large volumes of petroleum derived from terrestrial woody gymnosperm and/or angiosperm-dominated organic matter (Noble et al, 1991; Moore et al., 1992; Curry et al., 1994; Sykes et.al., 2013). Late Cretaceous lacustrine mudstones have also been suggested to be potential source rocks in the Taranaki Basin and other offshore basins in New Zealand although there is no direct geochemical evidence to date (Killops 1994, 2010). Most parts of the West Coast-Taranaki-Rift System, including the petroleum producing Taranaki Basin, are deeply buried and can only be interpreted via seismic analysis and drillholes.

The Greymouth Basin, however, is highly accessible. It is known for its high quality, low ash coal deposits and has been extensively drilled for mining exploration as well as having accessible outcrops. It is filled

with the Late Cretaceous to Early Palaeocene non-marine Paparoa Formation which contains lacustrine, peat mires, and organic-rich meandering alluvial units (Morgan 1911; Gage 1952; Nathan et al. 1986; Newman 1985; Sherwood et al. 1992; Boyd and Lewis 1995; Ward 1997). However, available nomenclature is inadequate to understand the complex lateral and vertical facies relationships between coaly, alluvial and lacustrine units of the Greymouth Basin. The separation of coal bearing alluvial members Conglomerates from lacustrine mudstone members of the Paparoa Formation is not always simple, particularly across the 'transitional' shoreline facies (Ward 1997) which also contain a significant amount of organic matter. Understanding the "transitional lithosomes", may change the estimated volume of potential lacustrine source rocks.

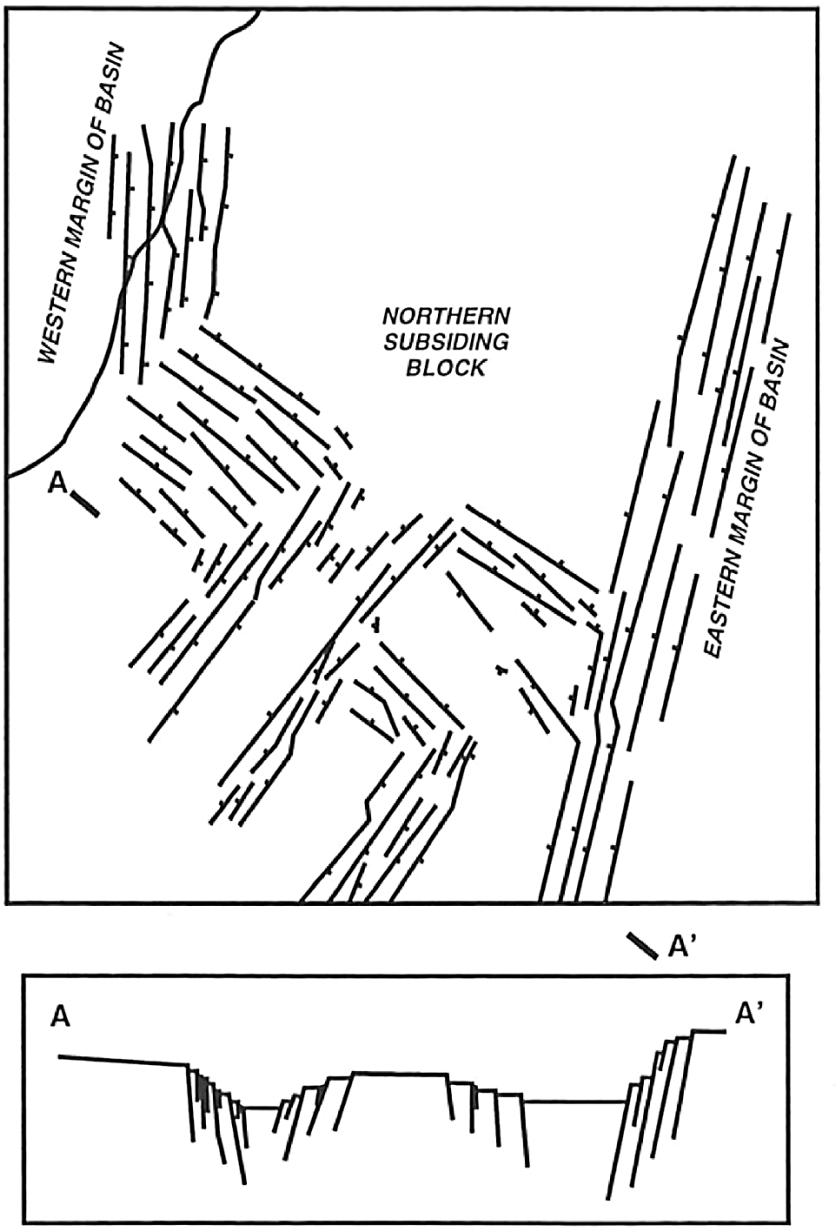


Figure 1. 8: Schematic structural model of the Greymouth Basin, Newman (1981), showing master basin bounding fault located to the east.

The Paparoa Formation also shows promising petroleum potential evidenced by the existence of oil and gas seeps in the area (Morgan 1911; Nathan et al. 1986, 2002). A recent MSc study on the lacustrine mudstones (Cody 2015) indicates that they show potential as petroleum generating source rocks and having a shale gas potential in addition to the already identified coal and coaly mudstone source rock potential. A detailed study of the accessible source rock facies from the Greymouth Basin could be used as an analogue for inaccessible frontier basins in offshore New Zealand.

Important research questions that have come out of this review include:

- What are the types of potential source rock facies in Greymouth basin?
- How does it increase the volume of potential source rock facies?
- What is the lateral extent and variability of different potential source rocks of the Greymouth basin?

Chapter 3 details the sedimentary analysis and geochemistry of the hydrocarbon source rocks. This will help to evaluate which type of fine-grained sediments are the potential source rock facies of the Greymouth Basin and whether the Greymouth Basin can act as an analogue for the other deeply buried Late Cretaceous basins in New Zealand.

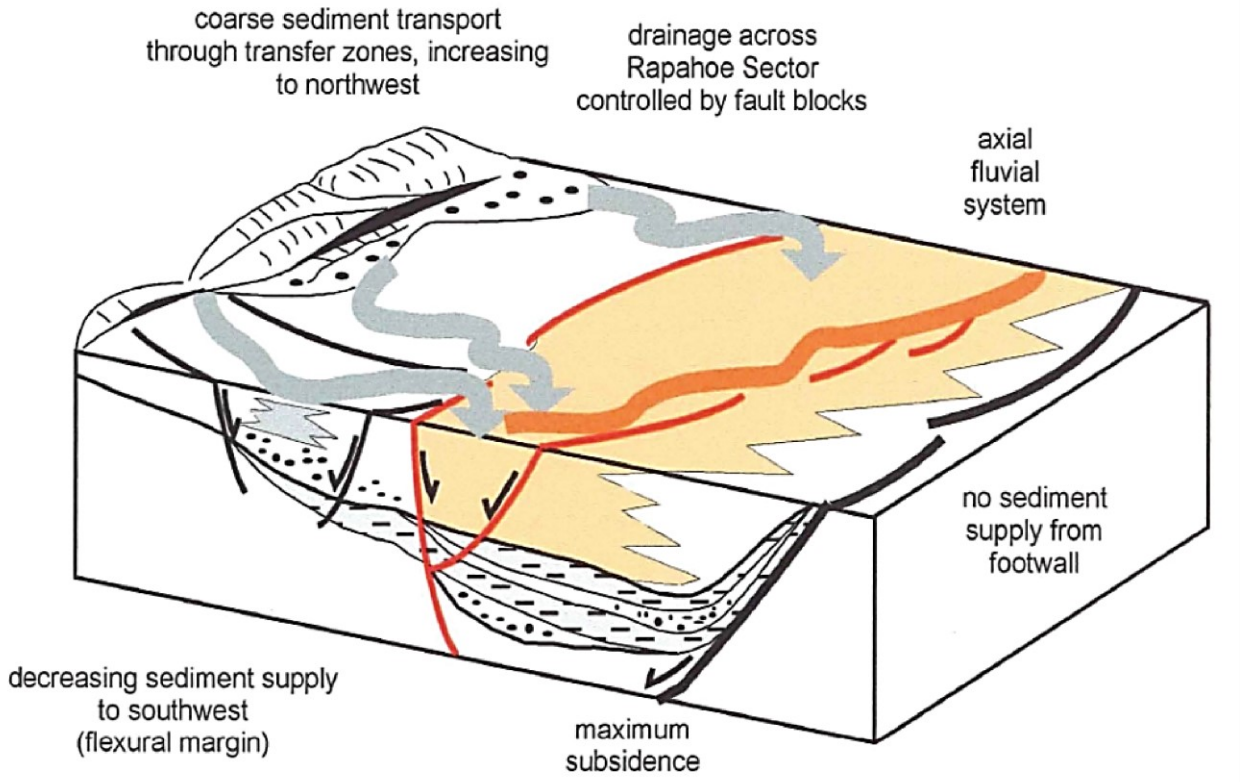


Figure 1. 9: Greymouth Basin Subsidence model from Ward (1997), showing the master basin bounding fault to the east.

### 1.5.3 Lacustrine sequence stratigraphy of the Greymouth Basin

The deposition of terrestrial rift basins account for a growing segment of current petroleum exploration because of the presence of both coaly sediments and lacustrine mudstones which might act as gas and oil generating source rocks (Carroll and Bohacs 2001). Lacustrine sequence stratigraphic analysis improves

correlation and can be used to predict the lateral extent and variability of these source rocks. In addition, lacustrine sequence stratigraphy provides a useful framework to understand the primary controlling factors of the cyclic alluvial-lacustrine deposition in terrestrial rift basins.

The lithostratigraphy of the Greymouth Basin indicates cyclic alternation between alluvial and lacustrine sediments in the centre of the basin. In addition, previous interpretations on geochemical and maturation properties of the coals and lacustrine mudstones of the Paparoa Formation indicate they are good source rocks for hydrocarbon generation (Newman 1985; Nathan et al. 1986; Cody 2015).

The background of the Greymouth Basin requires a lacustrine sequence stratigraphic analysis to understand the following questions:

- What were the factors/driving forces that controlled the overall cyclic fluvio-lacustrine rocks of the Paparoa Formation of the Greymouth Basin?
- Did the Greymouth Basin experience a single driving force or more than one?
- How does a lacustrine sequence stratigraphic analysis correlate different sequences of the Paparoa Formation?

Chapter 5 deals with above questions which help to understand the lacustrine sequence stratigraphic analysis of the Greymouth Basin.

## 1.6 Chapter design

There are six chapters in this thesis. Each chapter is designed as publishable journal paper except Chapter 1 and Chapter 6 which represent the introduction and the conclusions of this thesis, respectively. Therefore, some repetition is necessary.

## 1.7 Co-authorship and the contributions of the co-authors

I wrote all publishable the chapters in this thesis. My supervisor, Dr. Kari N. Bassett, helped me revise and commented on the science of each chapter. The data collection as well as the analysis of data were done by me except for Chapter 3. For Chapter 3, the lacustrine mudstone samples were collected by me and Dr. Daniel Mohnhoff, a former geochemist from the Geological and Nuclear Science (GNS) in New Zealand. However, the geochemical analysis of these samples was conducted by Dr. Sebastian Naeher from the GNS and Dr. Daniel Mohnhoff.

# Chapter 2: Alluvial fans and fan deltas in the Paparoa Formation, Greymouth Basin: A new rift model.


## Abstract

A detailed sedimentary facies analysis of the conglomerates and interbedded fine grained sediments found on the northwestern side of the Greymouth Rift Basin has identified the presence of fan deltas alternating with alluvial fans. The presence of a lake in the centre of the basin is established by the lacustrine facies association. From the conglomeratic sedimentary facies, eight lithofacies have been identified and grouped into three facies associations defining the fan deltas and alluvial fans. The gravelly turbidites facies comprises mostly grey to yellowish brown sandstones with occasional conglomerate lenses and dropstones. The associated sandy turbidites facies contains normally graded coarse to fine sandstones. The gravelly delta slope facies comprises interbedded conglomerates and sandstones with abundant soft sediment deformation and load casts. These three lithofacies are grouped into the prodelta facies association where sedimentation processes were mostly dominated by high density turbidity currents, hyperpycnal flows, subaqueous debris flows, and soft sediment deformation. The gravelly mouthbar facies comprises conglomerate channels with enigmatic fitted clast fabrics present. The interdistributary bay facies is primarily composed of carbonaceous sandstones and coaly stringers. These two lithofacies are grouped into the fan delta front facies association where sedimentation processes were mostly dominated by river flow, channel avulsion, and shallow bays between avulsing river mouths. Thick clast-supported conglomerate deposits are categorized as gravelly braided river facies whereas matrix supported, poorly sorted conglomerates are interpreted as debris flow facies. Overbank floodplain facies comprise laminated sandstones, siltstones, and carbonaceous mudstones with abundant coaly rootlets. These three facies are grouped into the alluvial fan/fan delta plain facies association where the common sedimentary processes are high energy stream flows, subaerial debris flows, and low energy floodplain processes on the lower slopes of fan deltas.

The facies interpretations suggest that most deposition took place in gravelly fan-delta environments with subaerial, shoreline, and subaqueous parts. The lack of steeply dipping foresets, with little differentiation from adjacent topsets and bottomsets, suggests the fan deltas were low angle Hjulström-types. These alternated with short-lived stream flow-dominated alluvial fans deposited during times when no lake was present in the basin's centre. Facies distribution indicates that the alluvial fan/fan delta facies are restricted to the northwestern side of the basin. The thickness of the conglomeratic facies decreases from the northwest to the southeast suggesting that the primary basin-bounding fault of the Greymouth Rift Basin is currently located offshore to the northwest.


## 2.1 Introduction

The presence of lakes and associated fan-delta deposits are limited in aerial extent and are found in a wide range of tectonic, climatic and geographical settings (Wells 1984; Killick 1988; Fernandez et al., 1988; Flint and Turner 1988; McPherson et al., 1988). For example, rift basins with rapid subsidence and high relief from extensional faults have lakes in the basin centre with fan-deltas and alluvial fans adjacent to the basin bounding faults (Leeder and Gawthorpe 1987; Ingersoll and Busby 1995; Gawthorpe and Leeder 2000). The deposition of conglomerates and their associated sediments in fan-delta environments has been documented by many researchers who focussed on both recognizing types of fan-deltas and characterizing

their associated subaerial, shoreline and subaqueous deposits (Wescott and Ethridge 1980; Postma 1983, 1984, 1991; Postma and Roep 1985; Postma et al., 1988; Nemec and Steel 1984; Higgs 1990; McConnico and Bassett 2007;). Identification of fan delta type and components is important for inferring palaeogeographic and tectonic settings of a basin as well as interpreting alluvial sediment supply (Nemec and Steel 1984; Kochel and Johnson 1984; Harvey 1984; McPherson et al., 1988; Orton 1988). To be more specific, sedimentary deposits like fan delta conglomerates may serve as a primary means of dating movement on basin-margin faults, particularly those which are syn-tectonic in origin (Colombo 1994). All above goals require detailed facies analysis of conglomerates and associated finer grained lithologies.

Greymouth Basin is part of the Late Cretaceous West Coast- Taranaki Rift Systems in New Zealand; it has accessible outcrops along the coast and has been extensively explored with respect to economic coal deposits and their associated fine grained lithofacies (Figure 2.1A; Gage 1952; Bowman 1984; Newman 1985; Boyd and Lewis 1995; Ward 1995, 1996, 1997; Kamp et al 1999; Bassett et al. 2006). The most recent published interpretation of the tectonic setting of the Greymouth Basin modelled it as a rift basin with a basin bounding fault on the eastern side (Ward 1997) with basin axis lacustrine mudstones alternating with meandering alluvial sandstones and raised mires (Figure 1.10; Newman and Newman 1992; Sherwood et al., 1992; Boyd and Lewis 1995; Ward 1997; Maitra and Bassett 2017). However, more recent work has suggested that the eastern margin faults (Montgomerie - Mt Davy Fault System) were not active until very late in the basin's history and thus could not have been a primary basin bounding fault for the majority of the basin's subsidence history (Suggate 2014).

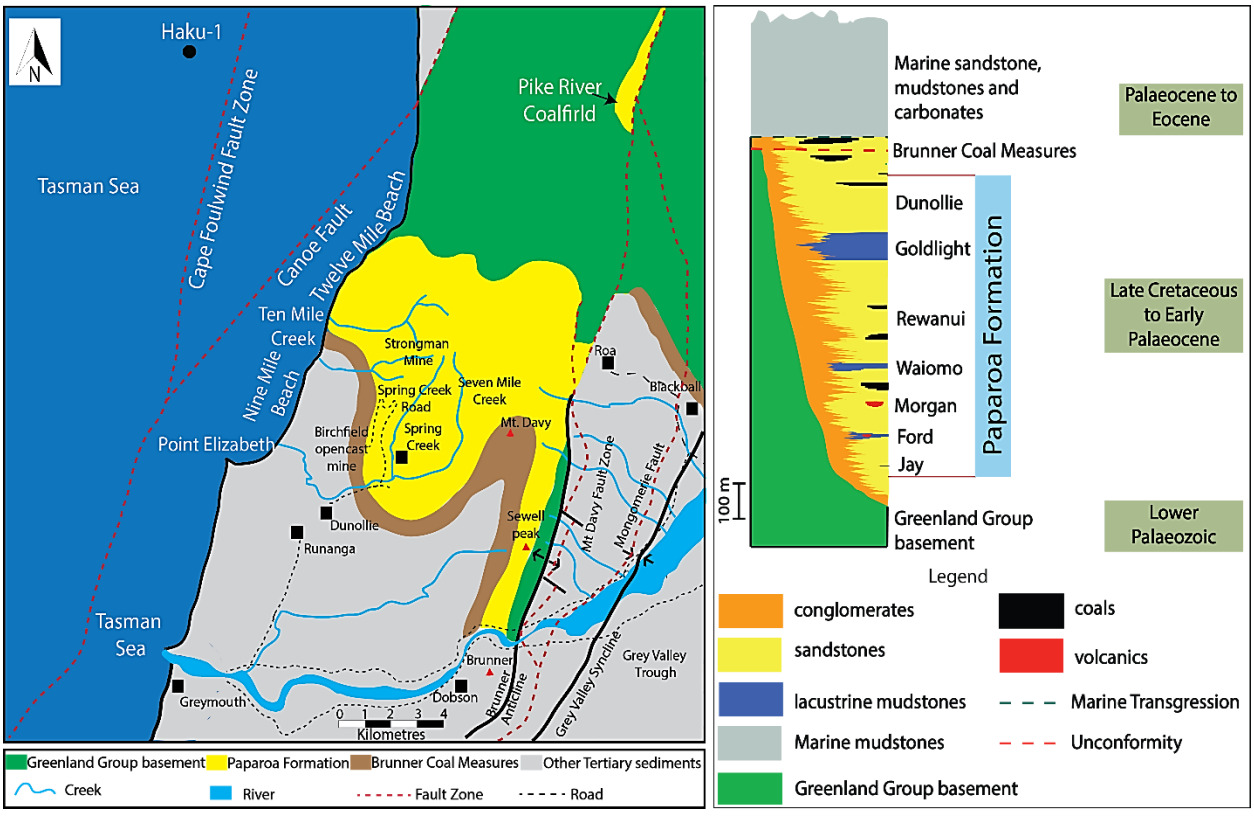


Figure 2. 1: A) Geological and structural map of the study area (modification based on the information from Gage 1952; Newman 1985; Suggate 2014; Nathan 1986, Nathan et al. 2002; Rattenbury and Isaac 2012), and B) Generalized stratigraphy of Paparoa Formation, modified from Boyd and Lewis 1995.

A thick conglomerate sequence exists on the northwestern margin of the basin along the modern day coast. The large grain size (up to boulders) and overall thickness (>400 m) indicates high palaeo-relief and therefore suggests the basin bounding fault should be located to the northwest (Bassett et al. 2014). In addition, the presence of lacustrine turbidites, debris flows, and soft sediment deformation of variable scales suggests subaqueous deposition. Both observations led to the realization that a detailed sedimentary facies analysis of the conglomerates is required in order to understand the palaeogeographic and tectonic setting of the basin. Our new research identifies extensive fan deltas and alluvial fans along the northwestern margin of the Greymouth Basin leading to a new interpretation of the basin's tectonic evolution.

**2.2 Alluvial fans and fan deltas**

Alluvial fans develop at the foot of fault-bounded mountains where high energy streams reach the valley floor and are mostly composed of gravel sized grains of subaerial origin (McPherson et al., 1988; Blair 2002; Blair and McPherson 1994, 2009; Horton and DeCelles 2001; Weissmann et al. 2010). As a consequence of their high-relief catchments, alluvial fans mostly tend to aggrade through catastrophic sedimentary processes associated with occasional flash flood events of relatively short duration and debris flows with higher sediment to water ratios (Ventra and Clarke 2018). Braided river fans are also composed of gravel - rich sediments formed on a purely braided alluvial plain where stream flows are the dominant process. Channel gravels are the most abundant facies and are commonly unstratified (massive), matrix-supported gravel beds or horizontally stratified, imbricated, clast-supported gravel beds (McPherson et al., 1988). Debris flow dominated alluvial fans are mostly higher in gradient, i.e., Karlskaret fan in Norway, Spring Canyon alluvial fan at Death Valley in California etc. (Larsen and Steel 1978; Blair 2002) whereas stream flow dominated braided river fans exhibit relatively lower gradient, i.e., alluvial fans in the Canterbury Plains and Kosi river fan in the Indogangetic plains (Agarwal and Bhoj 1992: Singh et al. 1993).

When alluvial fans prograde into water such as a lake, a fjord or an arm of the sea it is termed a "fan delta" where the depositional processes switch from subaerial to shoreline at the water's edge and shoreline to subaqueous under the water (Nemec and Steel 1984; Harvey et. al., 2005). By definition, fan deltas are gravel-rich deltas formed where steep gradient fans prograde directly into a standing body of water (McPherson et al. 1988; Rees et al., 2018). In fan deltas, subaerial processes are similar to those developed in an alluvial fan and are either debris flow or streamflow dominated. Shoreline components are primarily developed from channel processes and avulsion with some modification by lacustrine or ocean processes and fossil content (Bhattacharya 2010). Subaqueous components involve deposition from debris flow, sliding/slumping (mass flow processes) and high-density turbidity currents (high bed load channel processes) due to either delta front failure or by heavy input from high energy rivers originating in highland mountains (Sohn 1997; Falk and Dorsey 1998; Sohn et al., 1999).

The degree of sorting and the organisation of depositional facies in a fan delta depend on the steepness of slope and feeder systems. When the feeder system is acting as a line source, two types of fan deltas with highly unstable channels are commonly developed (Postma 1990, 2003). Gilbert-type fan deltas form on steep slopes and thus have steeply dipping sandy and/or gravelly foresets with fine-grained gently inclined bottomsets, and horizontal to subhorizontal sandy and/or gravelly topsets (Colella 1988; Dorsey et al. 1995; Falk and Dorsey 1998; Sohn et al., 1997; Sohn et al., 1999; Bassett and Orlowski 2004; McConnico and Bassett 2007; Rohais et al. 2008; Rees et al., 2018). Subaqueous high concentration debris flows and turbidity currents from alluvial bedloads are responsible for the generation of the foresets (Galloway and Hobday 1996; Gobo et al. 2014) with bottomsets influenced by the tails of debris flows and turbidity currents generated at the delta front (Rees et al., 2018). Hjulstr*ö*m-type fan deltas, on the other hand, do

not have steep slopes and therefore do not develop inclined foresets and exhibit less differentiation of topset, foreset and bottomset deposits (Postma 1990, 2003). The subaqueous foresets found in the Hjulström type of fan delta have a similar gradient to its delta plain (Kereszturi et al. 2015). The depositional processes are almost similar in both types of fan deltas (Postma 1990). The presence of soft sediment deformation structures are common in both Gilbert-style fan deltas and Hjulström type fan deltas, both types of fan deltas are dominantly composed of gravel-rich sediments delivered from an adjacent high, and both types are found in a wide range of tectonic, climatic and geographical settings (Nemec and Steel 1984; McPherson et al., 1988; Killick 1988; Fernandez et al., 1988; Flint and Turner 1988; Postma and Cruickshank 1988; Prior et al. 1984; Rhine and Smith 1988).

## 2.3 Greymouth Basin

The Greymouth Basin is located in the West Coast region of the South Island of New Zealand. It is bounded by the Cape-Foulwind Fault Zone in the west and the Montgomerie-Mt Davy fault zone in the east (Suggate 2014; Figure 2.1A). The basin was infilled with Late Cretaceous to Early Palaeocene terrestrial sediments named the Paparoa Formation (commonly known as the Paparoa Coal Measures) (Laird and Bradshaw 2004). The Paparoa Formation is further divided into four alluvial members (Jay, Morgan, Rewanui and Dunollie) which are separated by three lacustrine mudstone members (Ford, Waiomo and Goldlight) (Figure 2.1B; Gage 1952; Nathan et al. 1986; Newman and Newman 1992; Boyd and Lewis 1995). The Paparoa Formation unconformably overlies Greenland Group basement rocks of Early Ordovician age and underlies the transgressive sequence of Palaeocene-Eocene Brunner Formation to calcareous Island Sandstone, Kaiata Mudstone and Oligocene Cobden Limestone of the Haerenga Super Group (Gage 1952; Nathan et al. 1986, 2002; Newman and Newman 1992; Boyd and Lewis 1995; Ward 1997; Mortimer et al. 2014; Cody 2015; Figure 2.1B).

Conglomerates are found in each of the alluvial members and are well exposed in outcrops along the coast (Twelve Mile Beach and Ten Mile Creek) and penetrated in several drillholes on the western margin of the Greymouth Basin. The textural study of conglomerates in the Rewanui and Dunollie members of the Paparoa Formation shows pronounced lateral changes across the basin, particularly towards the west and northwest where conglomerates rapidly increase in abundance (Newman 1985). Part of the conglomerate section at Twelve Mile Beach and Ten Mile Creek was described by Emma Cody (2015) in order to define the sedimentary facies of conglomerates associated with the lacustrine deposits. She concluded that the conglomerates were deposited as debris flows in gravelly delta front environments and braided river deposits in gravelly delta plain environments.

The more typical lithologies of the Jay, Morgan, Rewanui, and Dunollie members includes meandering river channel sandstones often in distinct lensoidal shapes with strong basal scour (e.g. Miall 2010; Toonen et al., 2012). Coarse coaly fragments and other plant material are present in channel sandstones along with cross-bedding structures. Lateral to the channels are often inversely to normally graded crevasse splay sandstones interbedded with floodplain mudstones (e.g. Elliott 1974; Guion 1985; Bridge 1984). These contain abundant plant detritus along with downward branching roots. Channel sandstones commonly fine upward to oxbow lake carbonaceous mudstones fining further to high ash coal beds (e.g. Toonen et al., 2012). Both the carbonaceous mudstones and the muddy coals contain abundant detrital plant material and common rootlets. The sandy meandering alluvial deposits are mainly found in the central, eastern and southwestern parts of the Greymouth Basin but interfinger with the conglomeratic facies to the northwest.

Newman (1981, 1985), as part of her analysis of the coal facies, introduced a rift model for the Greymouth Basin with both NNE-SSW (for the older members) and WNW-ESE (for the younger members) structural trends, and an active basin bounding fault controlling the majority of basin subsidence located on the eastern margin. She concluded that a progressive increase in conglomerate thickness to the northwest suggested a palaeoslope from northwest to southeast but interpreted it as being the less active side of the basin (rate of fault offset) during the majority of deposition. A wide and comprehensive study by Ward (1997) broadly focused on the coal-bearing lithostratigraphy and palynostratigraphy of the Paparoa Formation and proposed a tectonic model which is best characterized as an eastward deepening half-graben with a master fault along the eastern margin. He also concluded that the eastern margin fault was responsible for the overall subsidence of the Greymouth Basin.

## 2.4 Methods

Sedimentary facies analysis of conglomerate deposits has been done mostly by studying outcrops. Key field techniques for outcrops include 1) measuring bed thickness and geometry, 2) describing clast size, shape, composition and sorting, 3) identifying sedimentary structures, 4) measuring bedding strike and dip, 5) measuring palaeocurrent direction from cross-beds and clast imbrication, and 6) indentifying trace fossils/plant remain. Interesting features were documented by taking photographs and were located using a hand held GPS. A number of faults were identified in the sections and beds were correlated as best as possible according to the nature of the fault and the amount of offset visible.

Discriminating different conglomerate facies in cores was not easy or convincing. The sedimentary facies of conglomerates and their associated deposits found in drill holes has been compared with outcrops and then correlated in order to get a better understanding of the lateral distribution of facies (Figure 2.2; Appendix 1; Appendix 2). Lithologies in drill holes have been described from existing drill cores and washed samples during several drilling programs since 1980. Core descriptions were taken from the original logs downloaded from NZPM (New Zealand Petroleum and Minerals) website and modified after inspection of the actual cores. However, the core diameters are too small to describe the large clasts or to recognize several diagnostic characters such as soft sediment deformation, large cross beds, etc. Geophysical logs (gamma ray log and density log) are not available for the most of the drill holes located in the northwest as the drill holes of this region didn't penetrate the economic coal deposits. Seismic lines present in this area are not convincing for the interpretation of sedimentary facies due to poor resolutions. Therefore, the most reliable source for detailed sedimentary facies description of the conglomeratic lithofacies is the Twelve Mile Beach outcrop. Stratigraphic columns have been constructed for drill holes and outcrops which are used to correlate the drill holes and develop a fence diagram of the northwestern part of the basin.

## 2.5 Sedimentary facies analysis

Sedimentary facies analysis of conglomerates and their associated deposits have been grouped into four facies associations i) lacustrine ii) prodelta, iii) fan delta front and iv) alluvial fan/fan delta plain (Table 1). The lacustrine facies association is made up of two lacustrine lithofacies of 1) lacustrine massive mudstone and 2) lacustrine mudstones with minor thin sandstones. The prodelta facies association is composed of the gravelly turbidites facies and the gravelly delta slope facies. The fan delta front facies association is made of the gravelly mouthbar facies and the interdistributary bay facies. The alluvial fan/fan delta plain association includes the debris flow facies, the gravelly braided river facies and the overbank floodplain

facies. The alluvial fan/fan delta facies association are found in both the fan delta setting when there was a lake in the centre of the basin, as well as in the alluvial fan setting when there was no lake in the basin.

### 2.5.1 Lacustrine mudstones of the Waiomo and Goldlight members

The lacustrine mudstones consist of laminated, carbonaceous mudstones and siltstones identified as lacustrine by the presence of freshwater molluscs from Hyridella species and pollen from Nothofagus (southern beech) species (Gage 1952; Ward 1997). In some areas, the lacustrine mudstones are interbedded with thin, normally graded, turbidite sandstones, some carrying conspicuous plant debris. In both outcrops and drill holes, lacustrine mudstones are easy to identify. These mudstones have been interpreted to have been deposited in the distal parts of a fresh water lake occasionally reached by small scale turbidity currents (e.g. Renaut and Gierlowski-Kordesch 2010). Detail facies analysis of the lacustrine mudstones are shown in Chapter 3.

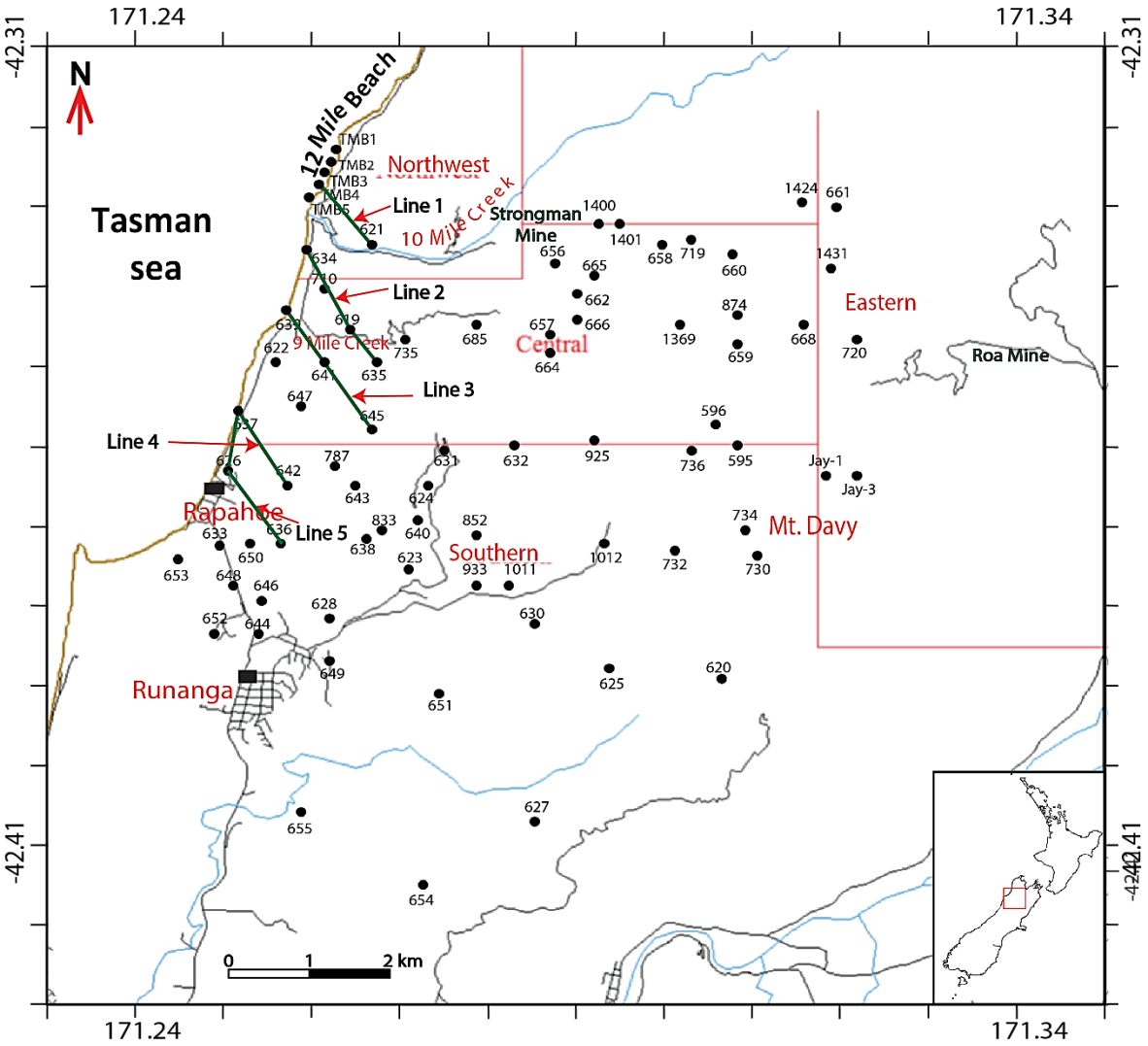


Figure 2. 2: Map of the Greymouth Basin showing the drillholes that have been used to study detailed sedimentary facies of the Paparoa Formation. Inset shows location in New Zealand. The green lines show the lines used to create cross-sections in order to develop a NW-SE fence diagram of the conglomeratic lithofacies.

Table 2. 1: Lists of facies associations and related lithofacies of conglomerates of the Paparoa Formation in the Greymouth Basin

| Facies association | Lithofacies |
|---|---|
| Lacustrine | Massive mudstones facies<br>Mudstones and minor thin sandstones facies |
| Prodelta | Gravelly turbidite facies<br>Gravelly delta slope facies |
| Fan delta front | Gravelly mouthbar facies<br>Interdistributary bay facies |
| Alluvial fan/fan delta plain | Debris flow facies<br>Gravelly braided river facies<br>Overbank floodplain facies |

### 2.5.2 Prodelta facies association

The gravelly turbidites facies, and the gravelly delta slope facies are grouped into the prodelta facies association.

#### *2.5.2.1 Gravelly turbidite facies*

*Description:* The gravelly turbidite facies (Figure 2.3A, 2.3B) is characterized by mostly grey to light grey siltstones (60%) with common sandstone beds (30%) and occasional conglomerate lenses (10%). Siltstones are grey to light grey and laminated. Siltstone beds are up to 1 meter thick but more commonly range between 10 cm and 50 cm in thickness. Sandstone beds are normally graded and composed of grey to light grey, fine to medium sandstone (Figure 2.3C). The basal part of the sandstone beds sometimes comprises a lag of pebbles a single clast thick. Sandstone beds are often interbedded with siltstones. Occasional coarse sandstones are present in some places. Sandstone beds are commonly 20-30 cm thick. Conglomerate lenses are mostly clast-supported, pebble in size, subangular to subrounded, and occur in lenticular beds (Figure 2.3B). The matrix supported, poorly sorted, angular to subangular conglomerates are found in some places. The clasts are dominantly Greenland Group metasandstones with little quartz in them. The lenses are mostly 30 cm-50 cm (up to 90 cm) thick and 80 cm-1 m wide. Isolated pebble or cobble clasts can be found in some places scattered in the sandstone beds with a maximum diameter of 1.5 cm (Figure 2.3D). Bioturbation is absent. This facies is common in outcrops and some drill holes located in the northwestern corner of the basin and is easy to distinguish.

*Interpretations:* The gravelly turbidites facies is interpreted to have been deposited in a lacustrine setting from high energy turbidity currents where the source is a gravel rich fan delta. High density turbidity currents, grain flows and debris flows commonly occur from rapid increases in sediment delivery and over-steepening on delta fronts resulting in a mixing of sediments as they travel down slope (e.g. Boggs 2006; Renaut and Gierlowski-Kordesch 2010). Normal grading of the clasts in the conglomerate lenses and an erosional lower contact suggests that turbulent flow during transport resulted in mixing within the flow and differential settling of the clasts (e.g. Rees et al., 2018). The matrix supported, poorly sorted, angular to

subangular conglomerates are interpreted as debris flows. These are likely to be subaqueous in origin and are more concentrated than turbidites leading to the lack of grading and sorting during deposition (e.g. Blair 1999). A debris flow, when passing into water, may considerably reduce its thickness and travel further by splitting into small lobes which leave thin gravel lenses and become enveloped by finer grained lacustrine deposits (Nemec and Steel 1984). Some of the conglomerate lenses found in this facies could have been deposited in this way. Normally graded sandstone beds are the indication of turbidity currents. The siltstone beds resulted from settling of finer sediment out of suspension once the turbidity current moved through (e.g. Stow et al 1996). Isolated conglomerate clasts that indent underlying layers are interpreted as dropstones which can form from the release of a clast transported by a melting iceberg (Gilbert 1990; Bennett et al. 1996). However, recent leaf fossil and beech tree pollen studies indicate that the climate was too warm to support major bodies of ice (Ward 1997; Kennedy 2003; Raine et al. 2017). Therefore, other modes of transport such as vegetation rafting are likely to be responsible for the presence of dropstones. For example, clasts in tree roots are usually ripped out of the soil proximal to the shoreline and may have been deposited either by being shaken free or when the wood raft sinks (Emery 1955, 1965; Bennett et al. 1996). Clasts could also have been transported by reeds and grass mats found close to the shoreline where debris flows overtopped the shoreline mats (Postma et al. 1988).

#### *2.5.2.2 Gravelly delta slope facies*

*Description:* The gravelly delta slope facies consists primarily of grey to white conglomerates with minor sandstones. These are primarily interbedded and are commonly deformed by load casts. Large cross-beds (~1-2 m height) are found in conglomerates in some locations (Figure 2.4A). In some places, sandier cross-beds are found lining with conglomerates (Figure 2.4B). The relative percentages of conglomerates and sandstones are 85% and 15% respectively. Bed thickness ranges between 3 and 7 metres in the outcrops and the facies is thick and multi-storeyed. Conglomerates are composed of quartz and Greenland Group sandstones, pebble to cobble in size, primarily clast but sometimes matrix supported, subangular to subrounded and moderately sorted. Occasional outsized clasts greater than cobbles exist in some locations. Conglomerates show reverse grading in some locations (Figure 2.4C). The matrix comprises fine to medium grained sandstone. Sandstone beds are grey, mostly medium grained, moderately sorted, and preserved as lenses (Figure 2.4A). The facies contains abundant soft sediment deformation including load casts and convolute bedding in both the conglomerate and sandstone beds (Figure 2.4D). Sandstones mostly contain flame structures and fluid escape features. Bioturbation and roots are absent in this facies. The gravelly delta slope facies is identified at Twelve Mile Beach and in several drill holes on the northwestern side of the basin. This facies is difficult to distinguish in outcrops and nearly impossible to identify in drill cores.

*Interpretation:* This facies is interpreted to have been deposited in a subaqueous, delta slope environment. The facies would have been dominated by hyperpycnal stream flows in the upper part of the delta slope as indicated by clast-supported textures in conglomerates, reverse graded conglomerates and cross-beds infill of the most of the small subaqueous channels. Hyperpycnal stream flow is a sediment-water mixture having a bulk density greater than the receiving water body and when this flow enters a lake it plunges and move basinward as a land–derived underflow (Bates 1953, Zavala and Pan 2018). Episodic hyperpycnal flows commonly develop in fan-delta settings with steep gradients and small catchment areas. The presence of a high percentage of conglomerates indicates the source was proximal to the lake and transferred during exceptional river discharges (e.g. Zavala and Pan 2018).

The other possible subordinate process in the upper delta slope region could be periodic gravity driven mass transport by the stream channel during flood events or by delta front failure as indicated by the presence of

high percentage of conglomerate deposits with occasional sandstone beds (e.g. Postma 1984, 1990; Nemec 1990). Deposition from a high bed load stream would result in progressive over-steepening of the delta front ensuring delta front failure or sediment loading on steep subaqueous slumps leading to slope failure (e.g. Nemec and Steel 1984; Boggs 2006). The relatively high percentage of conglomerates alternating with sandstone beds indicates a continuous source of gravel rich sediments through subaerial channel bedloads composed of pebble to cobble size clasts. The sandstone beds are most likely deposited from the tail of debris flows of high-density turbidity currents (e.g. Makaske et al. 2002; Jones and Hajek 2007).

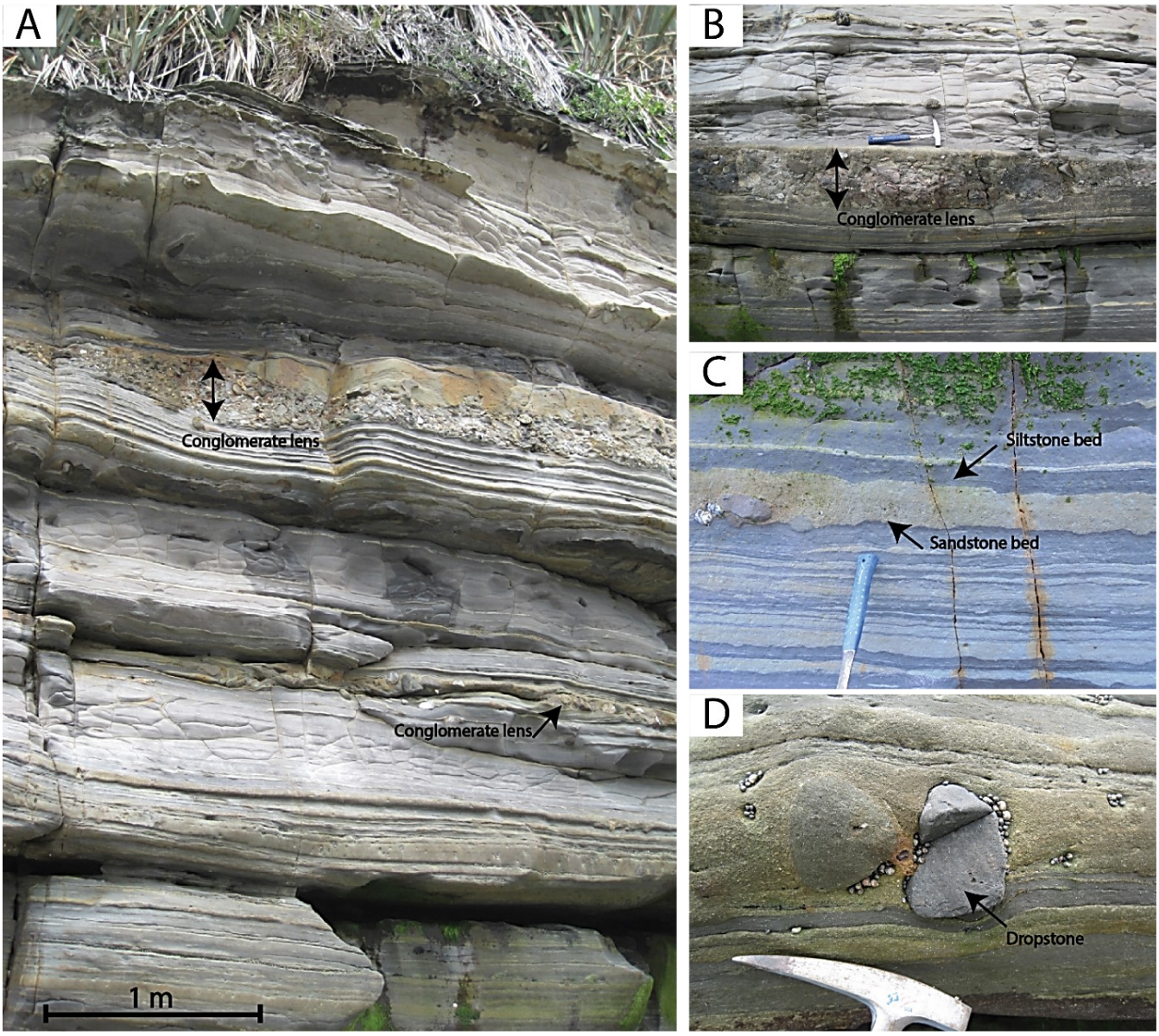


Figure 2. 3: Gravelly turbidite facies at Twelve Mile Beach outcrop, A) thick gravelly turbidites facies; B) conglomerate lens in gravelly turbidite lens; C) Sandstone turbidite beds showing erosional and wavy base with the lower silty mudstone and lamination in silty mudstone at the upper contact, and D) Dropstone indents and disrupts the laminated siltstone and sandstone layer.

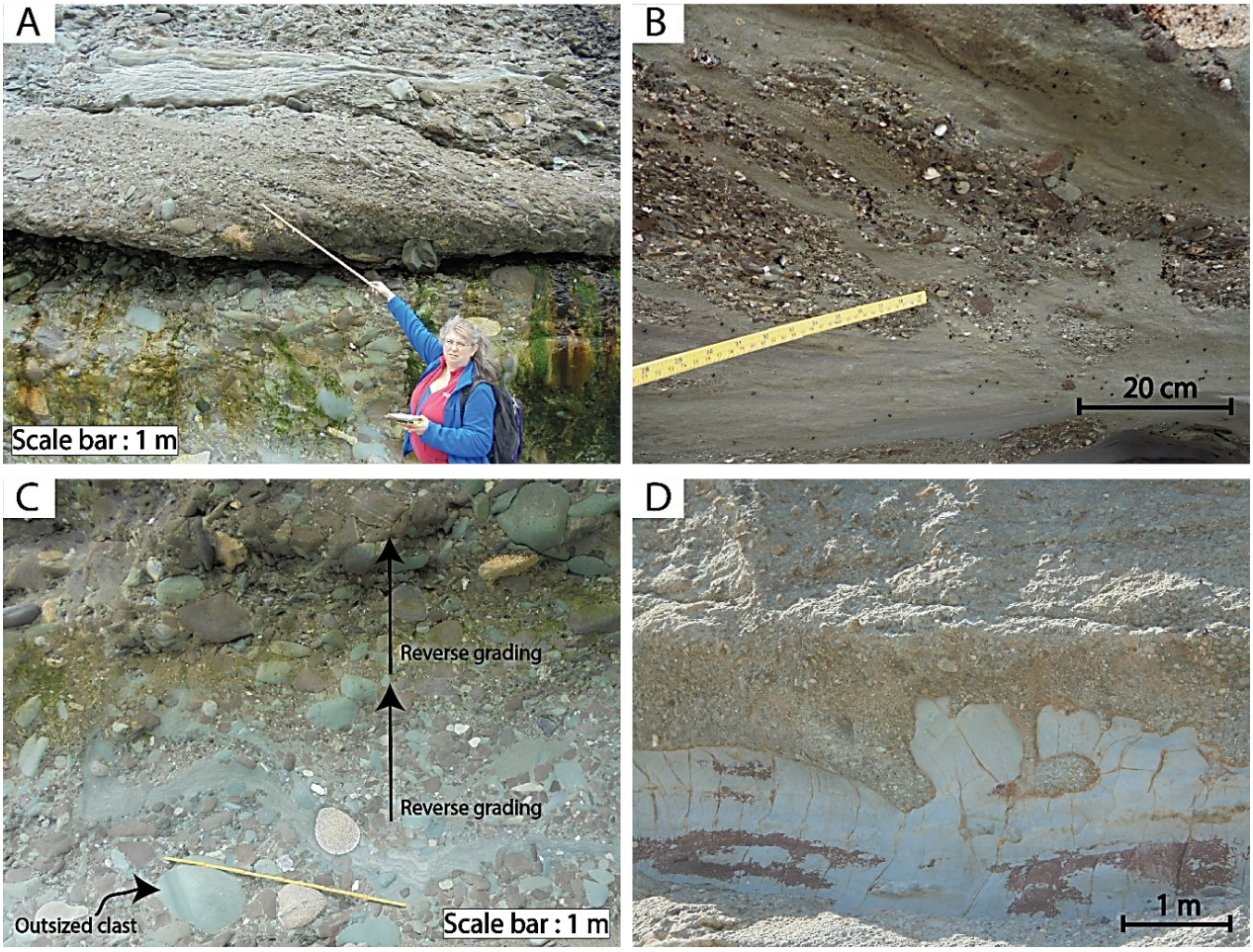


Figure 2. 4: Gravelly delta slope facies at Twelve Mile Beach outcrop shows A) large crossbeds in conglomerates, B) crossbedded conglomerates and sandstones, C) reverse grading in conglomerate, D) load casts and deformed sandstone lens.

The presence of abundant soft sediment deformation suggests that deposition was subaqueous and likely more proximal where slope gradient was higher. Soft-sediment deformation structures document the physical processes which take place in a depositional environment when sediments are unconsolidated: generally, these structures have a diagnostic value in the interpretation of hydrodynamic conditions, the palaeoslope orientation of a sedimentary environment and the presence of syndepositional seismic and/or tectonic activity (Mills 1983; Van Loon and Brodzikowski, 1987; Van Loon 1992; Maltman and Bolton 2003). Deformation occurs in unconsolidated sediments when they are in a liquid-like state brought about by liquefaction and/or fluidization processes (sensu Allen, 1977). The main potential trigger agents for liquefaction are overloading, unequal loading, wave-induced cyclical and/or impulsive stresses, earthquakes and sudden changes in groundwater levels (e.g. Owen 1996; Owen and Moretti 2011). Some kinds of soft-sediment deformation structures (sandstone-mud load cast structures, ball-and-pillow structures, convolute lamination, water escape structures, etc.) are very common in turbiditic successions (Sanders 1956, 1965; Sultwold 1959; Ricci Lucchi 1968; Hein 1982; Guy 1992; Stromberg and Bluck 1998) and they are basically interpreted as indicators of liquefaction and/or fluidization processes induced by rapid sedimentation (Lowe 1975; Allen 1982; Stromberg and Bluck 1998). Regarding the deformed sandstones at Twelve Mile Beach in the present study, the deformation probably originated mainly from

rapid sedimentation with occasional destabilization of the delta slope due to high bed- load channel migration into the lake which impacted soft fine-grained lacustrine deposit at high speed.

Regarding the examination of the clast-supported, reverse graded conglomerates with abundant soft sediment deformation at Twelve Mile Beach, it can be concluded that deposition probably occurred in fan delta with a steep gradient, perhaps fed directly from a river mouth, along with hyperpycnal flow and occasional slope failure.

### 2.5.3 Fan delta front facies association

The gravelly mouthbar facies and the interdistributary bay facies are grouped into the fan delta front facies association.

#### *2.5.3.1 Gravelly mouthbar facies*

*Description:* The gravelly mouthbar facies mainly consists of thick conglomerate beds, ranging from 1 m to 6 m thick, with cobble-sized clasts that are clast-supported, subangular to subrounded and moderately sorted (Figure 2.5A). Little or no matrix is present in this facies. The conglomerate beds exhibit scour at the base that may be progressively infilled by downstream accretion cross-beds (Figure 2.5B). Conglomerates are pebble to cobble in size and primarily clast-supported. Clasts are composed of quartz and Greenland Group sandstones. Hints of clast imbrication suggest the palaeotransport direction was towards the southeast during deposition (Figure 2.5C). In some locations, conglomerate beds start with erosional scour at the base infilled with crossbeds/foresets that grade upward into parallel bedded topsets with sheet like geometry (Figure 2.5B). Conglomerates are mostly clast-supported and pebble in size. The foreset orientations also suggest the palaeotransport direction was towards the southeast during deposition. Some clasts show jigsaw-like fitted edges with sharp contacts and angular indentations on clast interfaces (Figure 2.5D). The clast contacts are highly variable in shape and size. The metasedimentary clasts are fitted tightly together regardless of the relative hardness of argillite vs metasandstone with examples of either lithology indenting the other. Fitted clasts occur in lenses which are approximately 5-7 m wide and 1-2 m thick. Bioturbation and roots are absent in this facies. The gravelly mouthbar facies is found at Twelve Mile Beach and in several drill holes in the northwestern part of the basin.

*Interpretation:* This facies is interpreted to have been deposited in a delta front environment where a high bed load distributary channel enters a standing body of water (e.g. a lake) and dumps the bed load at the mouth of the channel forming a coarsening upward mouthbar sequence (e.g. Reading 1996; Bhattacharya 2010). High velocity flow and high deposition rate explain the lack of bioturbation and roots. The presence of scours suggests the channel incises the underlying beds. The infilling of the channel, first by foresets changing upward to parallel topset beds suggests subaqueous high concentration flows from alluvial bedloads in the delta front which are responsible for the generation of the foresets and topsets (Galloway and Hobday 1996; Gobo et al. 2014).

The fitted clast textures are interpreted to have been formed in a channel mouth bar in the fan delta front setting. There is little understanding of the processes that produce such fitted clast textures. Some spectacular fitted clast textures have recently been described from the rocky shore platform near Reglan in New Zealand by Nelson and Hood (2016). The study shows intricately fitted beach boulders where clast-to-clast contacts mutually interpenetrate each other. Some contacts are more complex which tightly interdigitate and interlock with little or no intervening void spaces whereas others are subtle and weakly developed. These occur on a modern cliff-backed rocky shoreline on a promontory with large waves. The

authors interpret a process that involves in situ abrasion by microseisms from wave impacts on the cliffs causing jostling and abrasion of the clasts until the intricately fitted contacts form. There is no evidence of large waves in the Greymouth Basin lacustrine members so such a process would be inappropriate for the fitted clast textures here. Instead, we interpret in situ abrasion in an alluvial channel environment following the work of Schumm and Stevens (1973). They suggest the role of microvibrations from clast collisions and winnowing of fines from the streamflow as being the most likely reason for the formation of fitted clast textures in mouthbars. According to Schumm and Stevens (1973), when the effect of combined lift and drag forces act on a submerged cobble, it vibrates in place without net downstream movement. Another experimental study by Brewer et al. (1992) has concluded the same, demonstrating that clasts can be subject to abrasion by over-passing bedload.

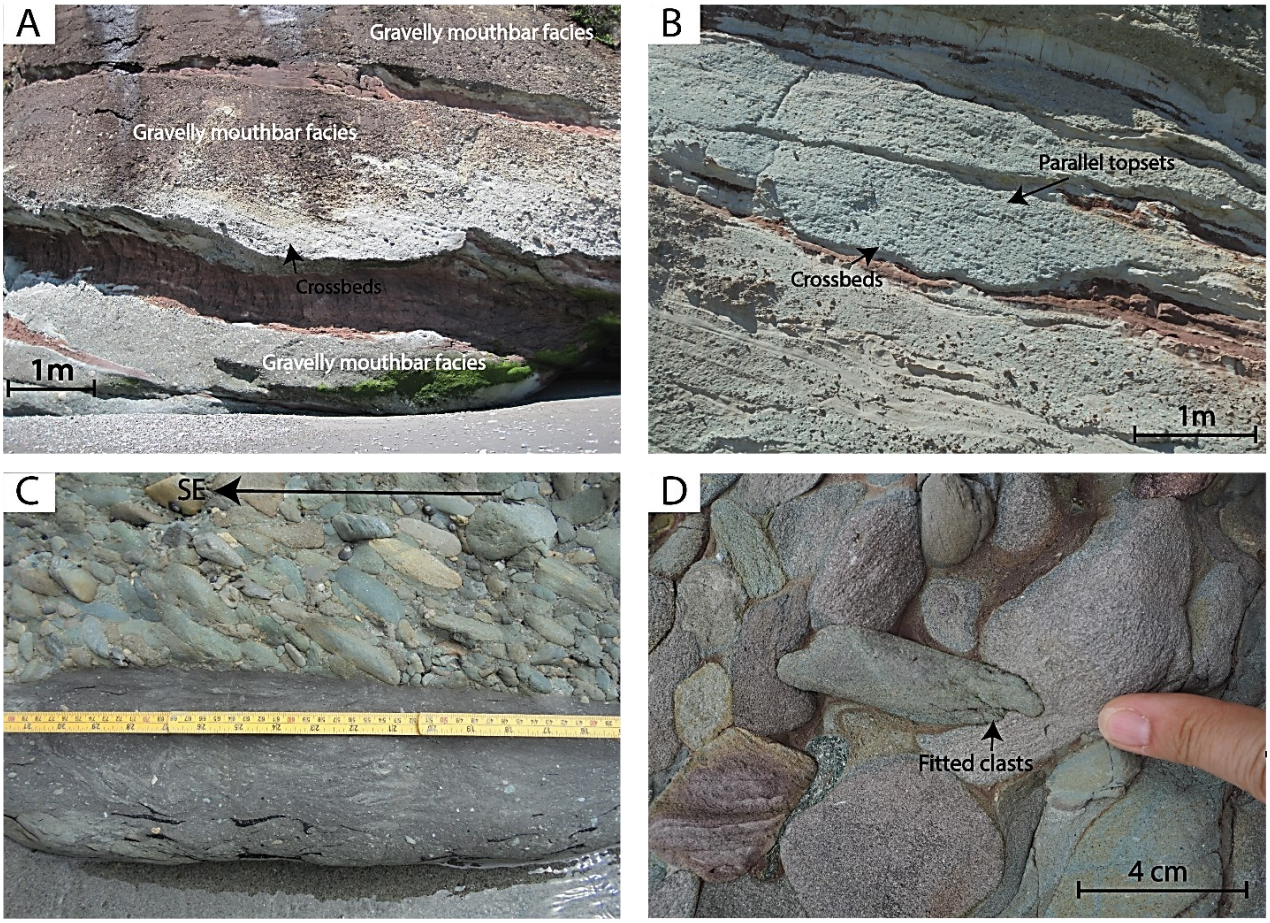


Figure 2. 5: Gravelly mouthbar facies at Twelve Mile Beach shows A) interbedded gravelly mouthbar channels with crossbeds and interdistributary bay sandstones, B) mouthbar channel with infilling crossbeds at the base and planar beds at the top, C) Clast imbrication in gravelly mouthbar channel showing palaeocurrent orientation towards southeast, and D) angular indentations on clast interfaces showing fitted clast texture.

We suggest that the long term in situ abrasion of clasts in the gravelly mouthbar facies could explain both the winnowing of the fine sediments from the gravel dominated area and the intricate nature of the clast-to-clast contacts. The association of the interlocking clasts with the coarsening upward beds indicates that the jostling and abrasion likely took place at the mouth of the channel as it entered the lake.

### *2.5.3.2 Interdistributary bay facies*

*Description:* The interdistributary bay facies are carbonaceous sandstones interbedded with gravelly mouthbar facies. Carbonaceous sandstones are grey to dark grey in colour, medium to fine grained, moderately sorted, and highly bioturbated (Figure 2.6A). In some locations, sandstones become highly carbonaceous siltstones grading to mudstones (Figure 2.6B). Sandstones are interlaminated with coaly material in places (Figure 2.6C). Rootlets are absent but plant materials are present (Figure 2.6D). Plant materials are black, scattered or in small lenses (less than 1 cm) (Figure 2.6D). The thickness of the facies ranges between 30 cm to 1 metre.

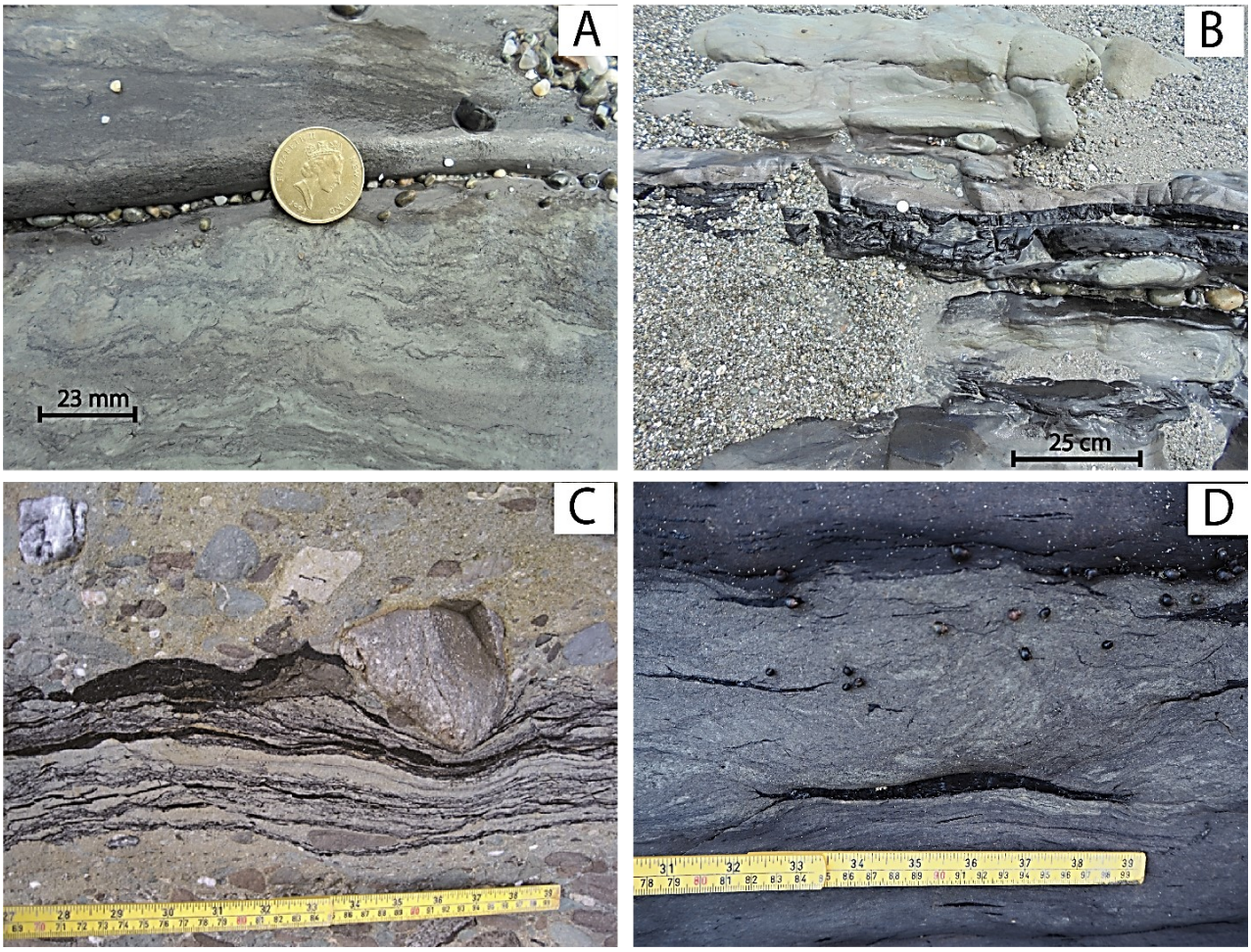


Figure 2. 6: Interdistributary bay facies at Twelve Mile Beach shows A) highly bioturbated sandstones, B) highly carbonaceous sandstones with carbonaceous siltstones and muddy high ash coals, C) interlaminated sandstones and plant materials, and D) carbonaceous sandstone with plant materials.

*Interpretation:* This facies is interpreted to have been deposited in subaqueous, relatively low energy environments. The association of this facies with the gravelly mouthbar facies indicates the facies was deposited in interdistributary bays adjacent to an active channel mouth where channel avulsion is a dominating process. Coaly stringers associated with clastic particles are occasionally present in this facies due to the relative abundance of floodplain vegetation or the abundant shoreline plants of a marsh which can be carried out as leaf mats during floods. The absence of rootlets indicates the deposition is subaqueous

in origin. The presence of bioturbation suggests that deposition occurs in shallow water where the conditions favour substrate colonization by burrowing organisms (e.g. Jones et al., 2008).

### 2.5.4 Alluvial fan/fan delta plain facies association

The debris flow facies, the gravelly braided river facies and the overbank floodplain facies are grouped into the braided alluvial fan/fan delta plain facies association. This facies association represents subaerial deposition on either an alluvial fan when no lake was present or on the delta plain of a fan delta when a lake was present.

#### *2.5.4.1 Debris flow facies*

*Description:* The debris flow dominated fan facies is characterized by matrix supported, subangular to subrounded, poorly sorted conglomerates that generally lack an erosional base (Figure 2.7A). Conglomerates are composed of quartz and Greenland Group sandstones, aplites, granites and basalts. Clasts vary from pebble to cobble in size. The matrix is coarse-grained sandstones and granules. This facies is commonly interbedded with the gravelly braided river facies. The thickness of the facies commonly ranges between 60 cm to 5 m and is easily identified in outcrop. This facies is found only in one drillhole in the west where the thickness reaches about 17.7 m (Figure 2.7B).

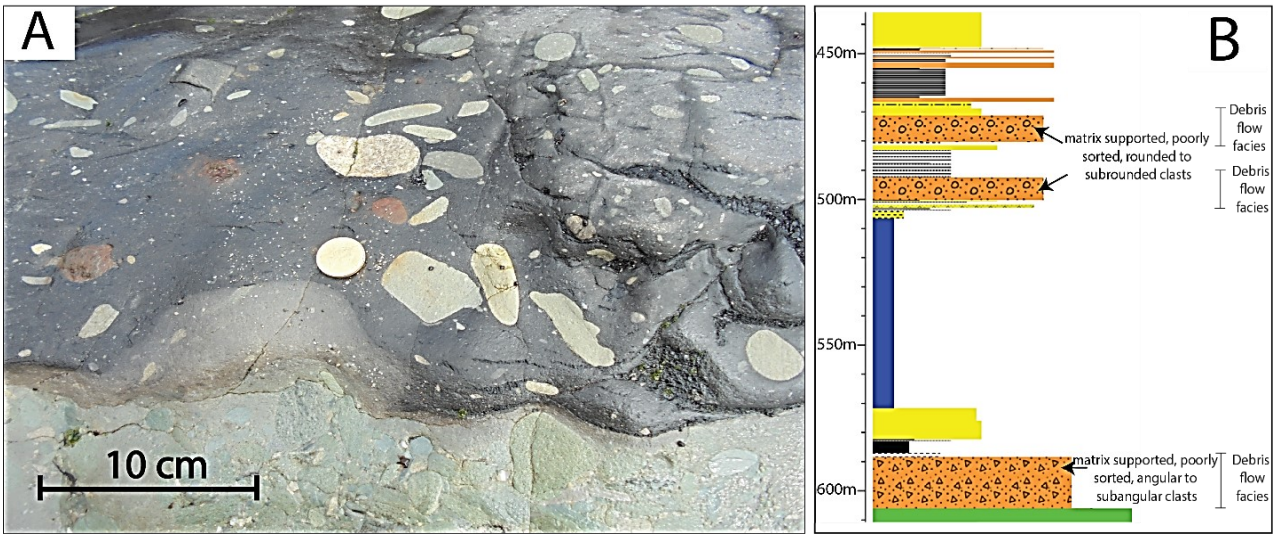


Figure 2. 7: Alluvial fan/fan delta plain facies association; A) debris flow facies at Twelve Mile Beach, and B) debris flow facies in borehole DH-619.

*Interpretation:* This facies is interpreted to have been deposited by debris flows in an alluvial fan where a small percentage of entrained water and air move the particles downslope under the force of gravity (e.g., Tanaka and Maejima 1995). Debris flows are more concentrated than turbidites with higher yield strength leading to the lack of grading and sorting during deposition as indicated by the matrix supported, poorly sorted texture lacking an erosional base (e.g., Nemec and Steel 1984; Blair 1999). The mixture of different grain sizes and clasts with no structure and no well-developed grading suggests the deposition may have taken place in a subaerial environment (e.g. Maejima 1988; Tanaka and Maejima 1995) as landslide, typically at times of heavy rainfall on bare slopes (Miall 2010). However, the debris flows are also common in a subaqueous setting when large masses of loose sediments are mobilized by failure and liquefaction on a sloping surface (Miall 2010). The presence of angular to subangular clasts indicates that the debris flows

probably travelled only a short distance from where they originated and were therefore deposited proximal to a fault.

### *2.5.4.2 Gravelly braided river facies*

*Description:* The gravelly braided river facies comprises clast-supported, cobble to boulder sized, rounded to subangular, moderate to poorly sorted conglomerate with thin sandstone lenses (Figure 2.8A. 2.8B). Conglomerates are composed of quartz and Greenland Group sandstones, aplites, granites and basalts. The gravel sand ratio for this facies is approximately 95:5. The facies is thick and multi-storeyed with variable bedding thickness ranging from a minimum of one metre to a maximum of 10 metres in outcrop and drill cores. In some locations, the conglomerate beds are not well defined and show indistinct stratification. Clasts show imbrication. The average clast diameter ranges between 5 cm (pebble) and 8 cm (cobble) whereas the larger clasts are 15-20 cm (cobble) in diameter. A few outsized granite clasts are boulder size (>30 cm) (Figure 2.8A). The bases of the conglomerate sections are commonly sharp and erosional. Sandstone lenses are usually 1 metre to 2 metres wide and up to 20 cm thick. Sandstones are grey to light grey, medium to coarse sand sized, moderately sorted and occasionally show channel shape geometry. There is no trace of bioturbation or roots in this facies and no soft sediment deformation. The gravelly braided river facies is commonly found in outcrops located at the northwestern side of the Greymouth Basin, particularly at Twelve Mile Beach and Ten Mile Creek. Drill cores on the northwestern side of the basin commonly have this facies.

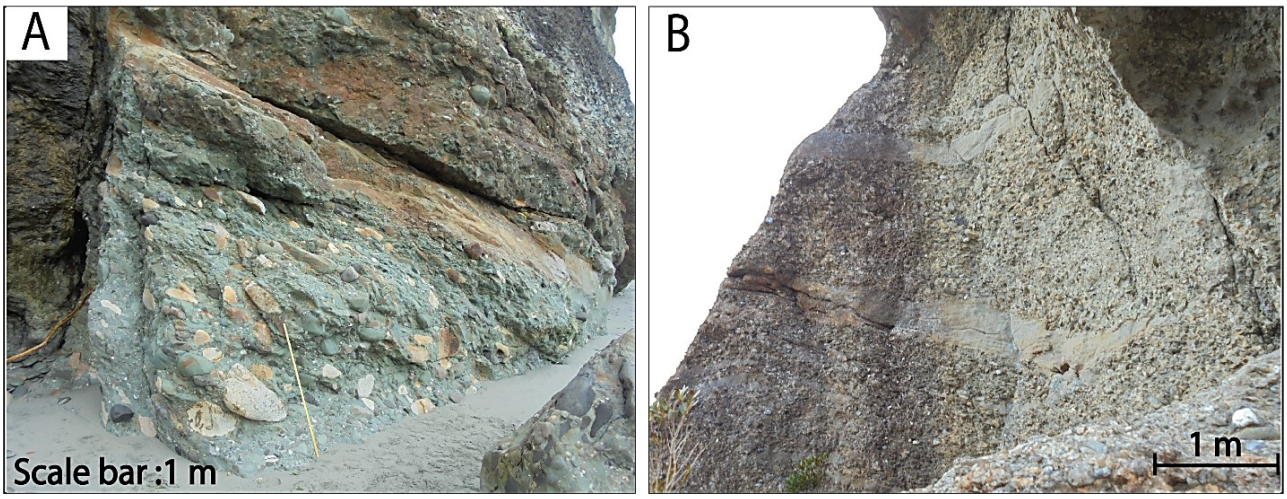


Figure 2. 8: Alluvial fan/fan delta plain facies association at Twelve Mile Beach; A) gravelly braided river facies at Twelve Mile Beach shows out sized clasts in conglomerate with imbricated clasts, and B) pebble to cobble conglomerate with sandstone lenses in gravelly braided river facies.

*Interpretation:* The facies is interpreted to have been deposited in a braided river environment where the dominant process of deposition is bedload dominated high energy stream flow. Conglomerate beds were deposited as longitudinal gravel bars with lenticular bodies in a shallow river setting while sandstone lenses occurred as bar top channel deposition during lower flows (e.g. Kazanci 1990; Miall 1996; Collinson 1996; Miall 2010). Sharp and erosional bases of conglomerates are evidence of stronger channelized transportation. The presence of subangular clasts, indistinct stratification and lack of well-defined beds indicate that the conglomerates likely travelled a relatively short distance before deposition (e.g. Kazanci 1988; Turkmen et al. 2007). Sandstones were deposited in conglomerate beds from waning flow in bar-top

channels. There is no direct evidence as to whether the braided rivers were part of a streamflow dominated alluvial fan or the delta plain topset facies of a gravelly fan delta other than association of subaqueous gravelly facies. It is also difficult to correlate lacustrine phases in the basin into the adjacent alluvial fans.

### *2.5.4.3 Overbank floodplain facies*

*Description:* The overbank floodplain facies consists primarily of less carbonaceous silty mudstones and sandstones with abundant roots (Figure 2.9A). This facies includes rare pebbles in some places. Sandstones are fine grained, moderately sorted and only slightly carbonaceous. Silty mudstones are grey in colour and slightly clayey. Coaly roots are vertical and downward branching in the facies. Bioturbation from burrows often disrupts the rootlets. (Figure 2.9A). Pyrites are found in some places (Figure 2.9B). The thickness of the facies ranges between 60 cm and 1m.

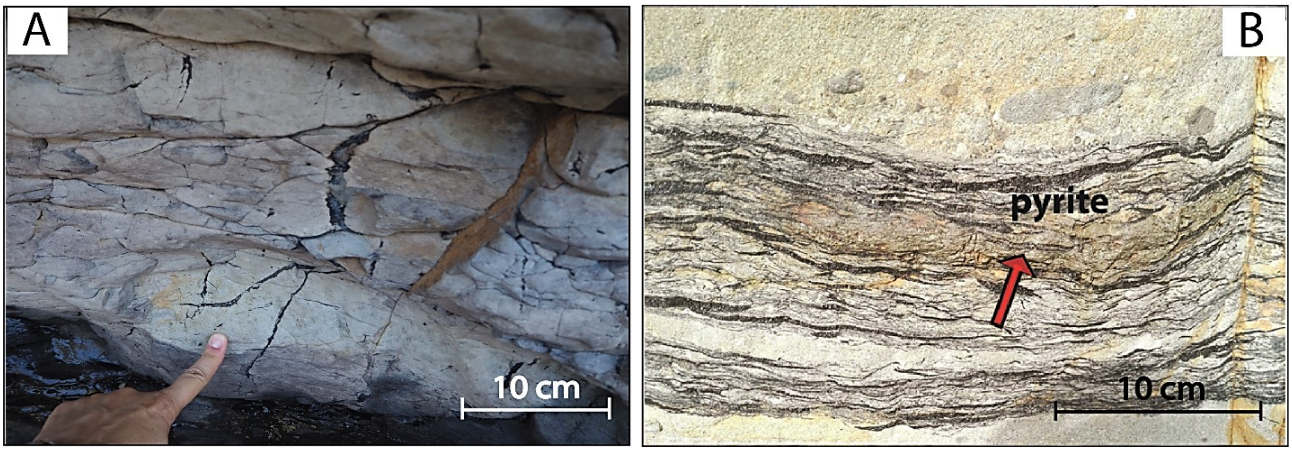


Figure 2. 9: Alluvial fan/fan delta plain facies association at Twelve Mile Beach; A) overbank floodplain facies showing clayey mudstone and coaly roots branching downward, and B) laminated sandstones and carbonaceous materials with pyrite in overbank floodplain facies.

*Interpretation:* This facies is interpreted to have been deposited in a low energy environment on the delta plain or in the streamflow alluvial fan environment as overbank deposits. The lamination of coals and fine sandstone indicates a low energy environment with episodic flooding from overflowing rivers (Reading 1996). The presence of mudstones indicates deposition occurred from the settlement of suspended fine-grained clastic materials. Rootlets indicate the facies was subaerial in origin. Disrupted and bioturbated laminations indicate that the sediment was exposed to surface processes shortly after deposition (MacEachern et al. 2010). The presence of pyrite indicates that deposition took place in anoxic environments.

## 2.6 Stratigraphic analysis of the sedimentary facies

The conglomerates are best exposed in the approximately 2 km long cliffs along the coast on the northwest side of the Greymouth Basin but also extend inland. A number of drill holes from the northwestern part of the basin have been used to map the distribution of the conglomerate facies and to interpret the geometry of the proposed fan deltas. The large clast diameters as well as large soft sediment deformation features are not easily identified in cores because of the small diameter (~5 cm). Therefore, most of the facies are described at Twelve Mile Beach and are used as a reference to identify similar sedimentary facies in nearby cores.

### 2.6.1 Twelve Mile Beach outcrops

Twelve Mile Beach has a large exposed section of the conglomeratic lithofacies of the Paparoa Formation cropping out on the shore platform as well as in the cliff face (Figure 2.1). Access to this outcrop is relatively easy, although it depends on the tides and weather. The quality of the outcrop is superb and this allowed the recording of a detailed stratigraphic log of the conglomeratic lithofacies (Appendix 1; Figure 2.10-2.14).

The basal contact with underlying Greenland Group basement rocks is visible in the shore platform. It is sharp, wavy and clearly an angular unconformity. The overlying stratigraphy is interpreted as alluvial fan/fan delta plain facies association and is assigned to the Morgan Member of the Paparoa Formation (~1-10 m, Column 1, Figure 2.11). The majority of the conglomerate beds are clast-supported, sub-angular to sub-rounded, moderately sorted, imbricated, cobble conglomerates with occasional interbedded medium-grained to laminated fine-grained sandstone beds. These are interpreted as braided river facies. Interbedded with the clast-supported conglomerates are a few matrix-supported, poorly sorted, cobble conglomerates interpreted as debris flow facies. Laminated sandstones with bioturbation and plant material are identified as overbank floodplain facies. The southeast direction of palaeocurrent flow from imbricated clasts indicates the origin of the braided river systems was adjacent highland areas probably originated somewhere in the northwest. The presence of interspersed debris flows suggests that the highlands were nearby.

The next ~24 m of overlying interbedded conglomerate and sandstone beds are interpreted as belonging to the delta front facies association consisting of alternating gravelly mouthbar facies and interdistributary bay facies (~10-34 m, Column 1, Figure 2.11). The gravelly mouthbar facies is composed of clast-supported, moderately sorted, cobble conglomerate beds. A 60 cm bed of matrix- supported, pebble conglomerates of the debris flow facies is also present. The interbedded laminated, carbonaceous, bioturbated, very fine-grained sandstone beds with coaly stringers are interpreted as interdistributary bay facies. The matrix supported pebble conglomerates were deposited by debris flows in a subaqueous setting. The presence of ripples and small-scale soft sediment deformation structures also indicate that deposition took place in a subaqueous environment. The presence of a 30 cm thick carbonaceous siltstones and muddy high ash coal bed of the overbank floodplain facies indicates deposition took place in a subaerial floodplain environment near the delta front. Deposits show multiple coarsening upward sequences. The overall deposition indicates that the sedimentation was occurred in a delta front environment but variously slightly subaerial to slightly subaqueous. The interbedded nature of the facies is probably due to repeated channel avulsion typical of a fan delta.

The overlying fining upward sequence of interbedded conglomerates and sandstones of the gravelly turbidites facies is interpreted as part of the prodelta facies association and marks the transition to the lacustrine Waiomo Member. The gravelly turbidites comprise normally graded, cobble to pebble conglomerate beds interbedded with normally graded sandstone beds with partial Bouma sequences in a roughly 50:50 ratio (~34-37 m, Columns 1-2, Figure 2.11). We interpret the conglomerates as deposited by high energy turbidity currents sourced from the nearby river mouth with the fine sandstones deposited by smaller turbidity current events. Grain size continues to fine to poorly sorted, mud-rich, intensely bioturbated, thinly interbedded, fine grained sandstones and siltstones with hints of flaser bedding (~37-39.5 m, Column 2, Figure 2.10). These may be the result of turbidity currents modified by bioturbation and slope parallel bottom currents, common in many lakes (Rebesco 2014).

The transition to deposition of the lacustrine facies association is relatively abrupt. Grain size decreases to laminated very fine sandstones and siltstones (~39.5-41.5 m) to laminated mudstones and siltstones (~41.5-

49 m) and coarsens up again to laminated very fine sandstones and silty mudstones (~49-52 m) (Column 2, Figure 2.11). These are interpreted as deposited in a distal lacustrine environment with minor turbidity currents. The abrupt change in facies association is probably due to the rapid subsidence of the basin when available accommodation space exceeds the amount of sediment supply. The distal part of the Waiomo Lake was sediment starved and, therefore, the deposition occurred mainly from suspension settlings from the tails of turbidity currents and hyperpycnal flows.

The overlying deposits are of the prodelta facies association (~ 52-59 m, Column 2, Figure 2.11). These are mostly gravelly turbidite facies composed of normally graded sandstone beds with lenses of normally graded conglomerate beds with erosional basal contacts and presence of occasional matrix supported, poorly sorted, angular to subangular conglomerates. Isolated conglomerate clasts and scattered dropstones indent and disrupt the sandstone layers in ~ 10% of the beds (Figure 2.3D). The normally graded conglomerates are interpreted as deposited by high energy turbidity currents sourced from a nearby river mouth whereas the fine sandstones are interpreted as deposited by smaller turbidity current events. The matrix supported, poorly sorted, angular to subangular conglomerates are interpreted as subaqueous debris flows. Dropstones were likely carried in vegetation mats or logs during floods from the nearby river mouth of the fan delta. These facies record the infilling of the lake and progradation of the fan delta. This may indicate a decrease in the rate of subsidence in the basin or an increase in sediment supply.

The transition to deposition of the delta front facies association is marked by a sharp and deeply erosional contact with a basal <1 m thick lens of matrix supported conglomerate composed of clasts of laminated, deformed grey to dark grey mudstone and siltstone (~95%) (~59 m, column 2, Figure 2.11). The contact represents the Waiomo-Rewanui contact. The clasts are interpreted as lacustrine mudstone rip-up clasts as thin section analysis shows striking similarities to the lacustrine massive mudstone facies of the Waiomo Member (Cody 2015; Figure 2.15A and B). The deeply erosional contact represents a channel cutting into the underlying soft and partially consolidated lacustrine mudstones of the Waiomo Member, and which were then preserved as lag deposits at the base of the overlying gravelly mouthbar channel (Figure 2.15A and B). This also suggests decreasing accommodation and subsidence rate of the basin. Sediments source from adjacent highlands was most likely relatively constant, therefore sediment bypassing and valley incision probably occurred during periods of reduced accommodation which eroded the underlying soft and partially consolidated lacustrine mudstones.

The overlying section are at least 52 m thick, representing gravelly mouthbar facies alternate with interdistributary bay facies, gravelly turbidite facies and gravelly delta slope facies (~63-115 m, columns 2-5, Figure 2.10; Figure 2.11). The interbedded conglomerates and sandstones show multiple coarsening upward sequences. Conglomerates are clast-supported, cobble in size and have sharp, erosional bases. Cross-beds (~1 m in height) can be found infilling subtle channel forms in some locations (Figure 2.4A). Sandstones are fine to medium grained and exhibit faintly wavy laminations, bioturbation, and small load cast structures (Figure 2.16). The coarsening and thickening upward sequences of mouthbar conglomerates to interdistributary bay sandstones indicates repeated channel avulsion typical of fan deltas. The presence of gravelly turbidite facies and gravelly delta slope facies indicate high density hyperpycnal and turbidity flows travelling down from delta front to delta slope due to rapid increase in sedimentation rate. The overall thickness suggests a relatively high subsidence rate in order to keep the fan delta front at a single location.

A short-lived change to subaerial settings is indicated by the overlying deposits of alluvial fan/fan delta plain facies association (~115-120 m, Column 4, Figure 2.12). The channelized conglomerate bed is assigned to the gravelly braided river facies. It is overlain by laminated sandstone to muddy siltstone beds

with abundant vertical rootlets of the overbank floodplain facies indicating subaerial deposition. This may correlate with axial alluvial systems in the centre of the Greymouth Basin, suggesting that the rate of subsidence decreased to its minimum at this stage in the basin history. The relatively constant supply of coarser sediments from adjacent highlands gradually infilled the lake, resulting in the end of a lacustrine phase and the onset of an alluvial phase.

The overlying, very thick deposits consist of mostly gravelly mouthbar facies of the fan delta front facies association alternating with gravelly delta slope facies of the prodelta facies association (~120-378 m, columns 4-11, Figure 2.11; Figure 2.12; Figure 2.13; Figure 2.14). The interbedded conglomerates and sandstones show sharp and deformed contacts with each other. Conglomerates are clast-supported, rounded to subrounded, and pebble to cobble in size. They often contain lenses with jigsaw fitted clast textures in channels filled with lateral accretion foresets. Sandstone lenses are deformed and may have the occasional conglomerate lens. Channels start with erosional scour at the base infilled with lateral accretion foresets that grade upward into parallel beds indicating scour at the channel mouth with progressive infilling. These indicate high sediment concentration bedloads from hyperpycnal flows from the channel mouth at the fan delta front. The presence of fitted clast textures indicates the jostling and abrasion of clasts at the mouth of the channel as it entered the lake. Soft sediment deformation structures such as load casts and convolute bedding are abundant indicating a subaqueous setting on a steep fan delta slope with ongoing basin subsidence. The deposition was likely to have been the result of channel avulsions in a high bed load setting in a prograding fan delta environment. The alternation between fan delta front and prodelta facies may be due to simple channel switching controlling sediment supply or may record subtle changes in subsidence rate with a fairly constant sediment supply; our data isn't able to differentiate between the two models. However, such a great thickness of continuous deposition of gravelly facies indicates that the creation of accommodation in the basin was huge and mostly likely due to a very high subsidence rate controlled by a basin-bounding fault. The amount of sediment supply was high enough to fill the available accommodation space and to keep the shoreline in the same location for a long time. The continuous supply of conglomerates indicates adjacent highlands with active faults which probably controlled the overall subsidence and deposition of the basin. In the basinward direction, this great thickness of fan delta conglomerates correlates with the >200 m thick lacustrine mudstones of the Goldlight Member.

The overlying ~12 m of alternating conglomerate and sandstone deposits represents gravelly mouthbar and interdistributary bay facies of the delta front facies association. Conglomerates are clast-supported, rounded to subrounded, and pebble to cobble in size with occasional fitted clast textures. Sandstones are fine to medium grained and birturbated. Layers of organic matter are present in sandstones. The interbedded conglomerates and sandstones show sharp and erosional contacts with each other. This deposition of fan delta front association suggests a relatively slow subsidence rate with constant sediment supply probably in a retreating fan delta environment.

The overlying conglomerates and sandstones are clast-supported, pebble to cobble in size with no fitted clast textures or soft sediment deformation present (~378m-400m, columns 11-12, Figure 2.14). The interbedded minor sandstone lenses are not normally graded and not deformed. These conglomerates are interpreted as the gravelly braided river facies and probably mark the transition from a fan delta setting to a subaerial alluvial fan setting during a time when there was no lake present in the centre of the basin. This suggests that subsidence rate decreased in the basin yet remained high. These conglomerates are the uppermost conglomerates in the stratigraphy of the Paparoa Formation and are assigned to the Dunollie Member.

The outcrop of the upper Dunollie Member conglomerates is bleached nearly white yet is the same composition as all underlying conglomerates. It is overlain by a local unconformity before deposition of the glauconitic, fossiliferous, calcareous Island Sandstone. The gradual decrease in basin subsidence rate was relatively constant at this stage, however, the influx of the ocean suggests the accommodation was still quite high. Further towards the basin centre, the Dunollie Member is overlain by the coals and conglomerates of the Brunner Formation representing peat bogs and fluvial deposition. The highly bleached section at Twelve Mile Beach is interpreted as a bleached weathered surface below a thick coastal coal swamp. Unfortunately, the unconformity removed the overlying coals so this is somewhat speculative although it matches the stratigraphy elsewhere of a deep weathering profile beneath coals (Monteith, 2014). The unconformity at the top of the bleached weathered section represents the onset of the marine transgression and was mostly likely formed by wave erosion along a transgressive surface.

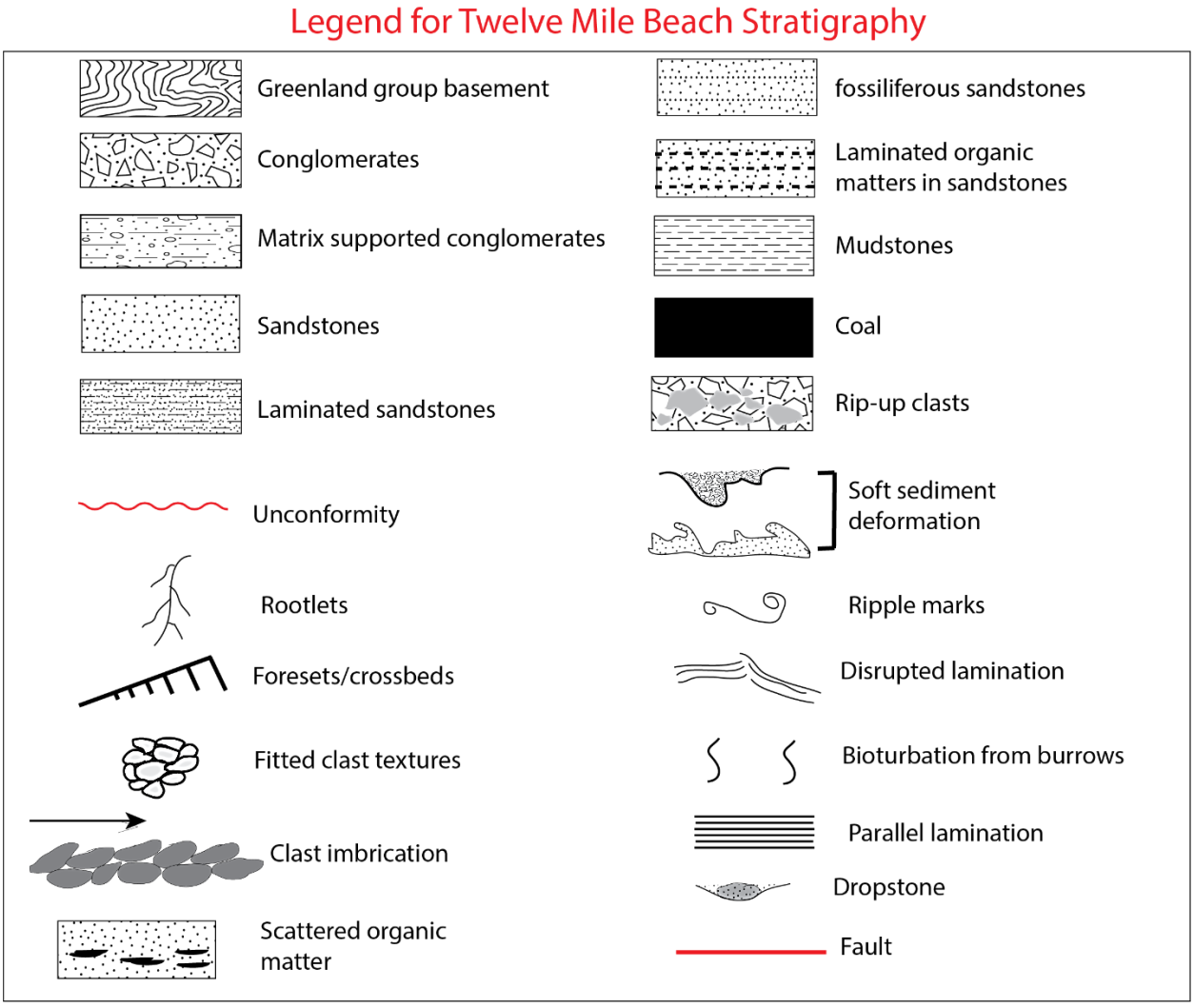


Figure 2. 10: Legends show for Twelve Mile Beach stratigraphy.

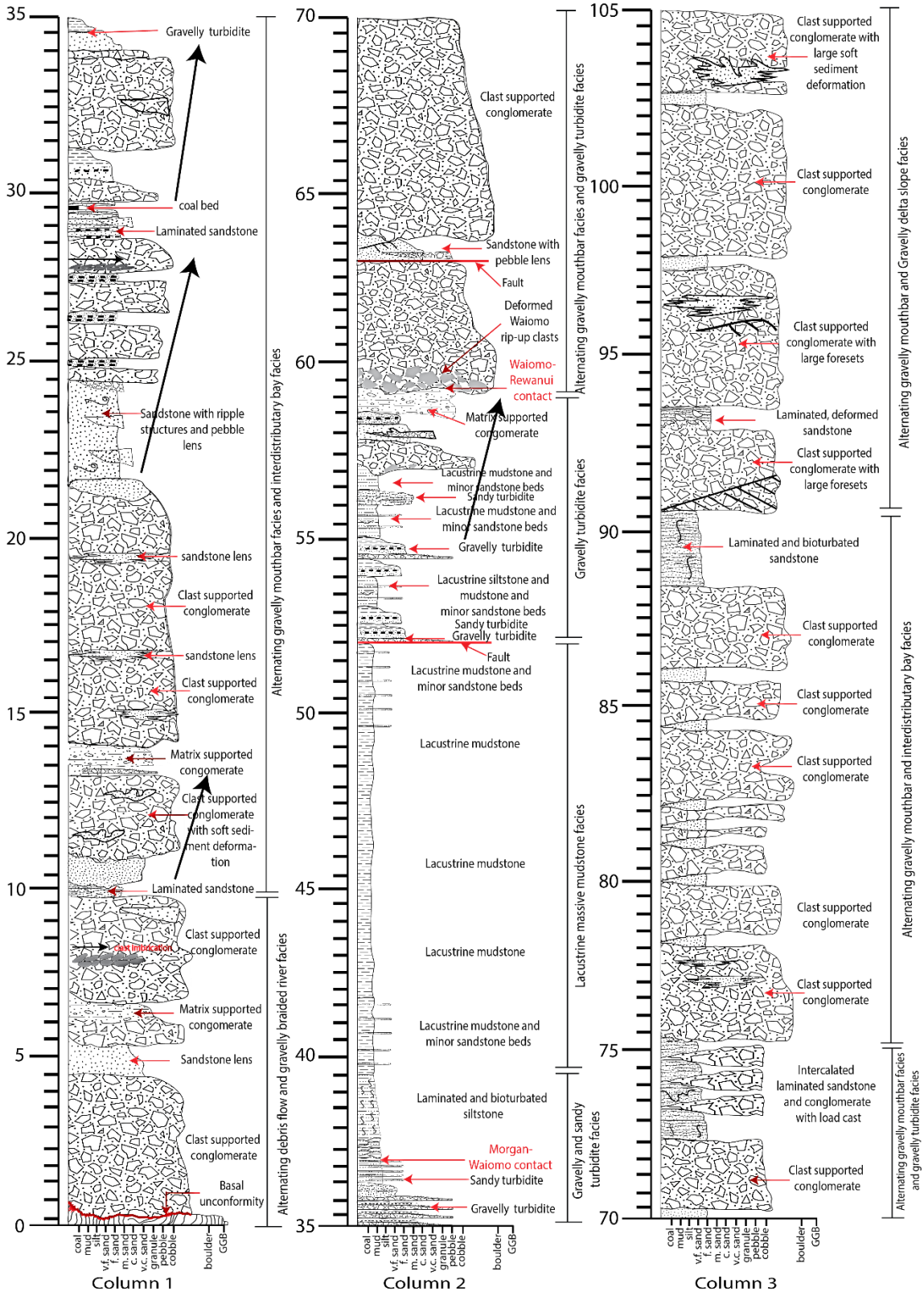


Figure 2. 11: Twelve Mile Beach stratigraphic columns (column 1-column 3). Depths are in meters with 50 cm divisions.

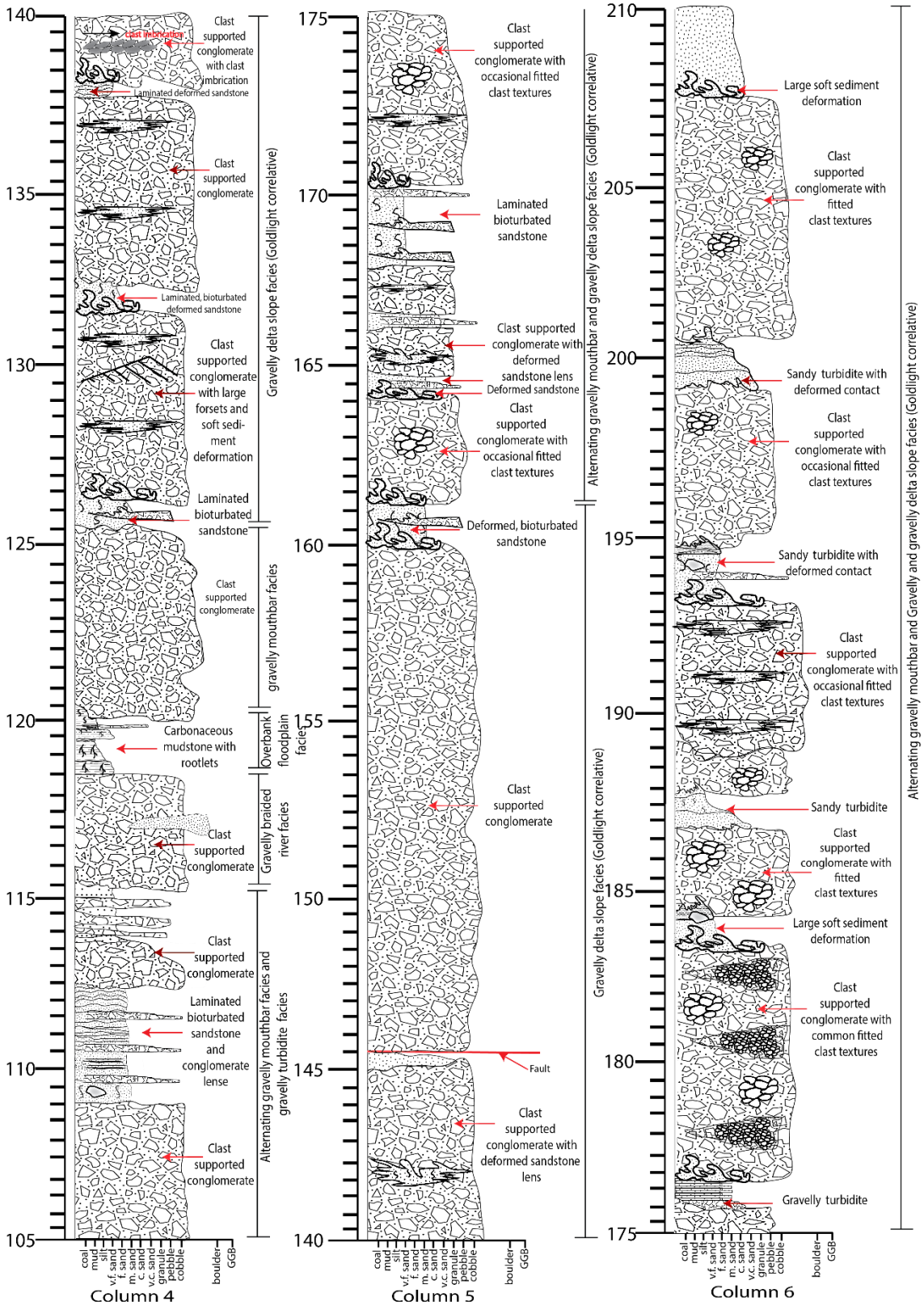


Figure 2. 12: Twelve Mile Beach stratigraphic columns (column 4-column 6). Depths are in meters with 50 cm divisions.

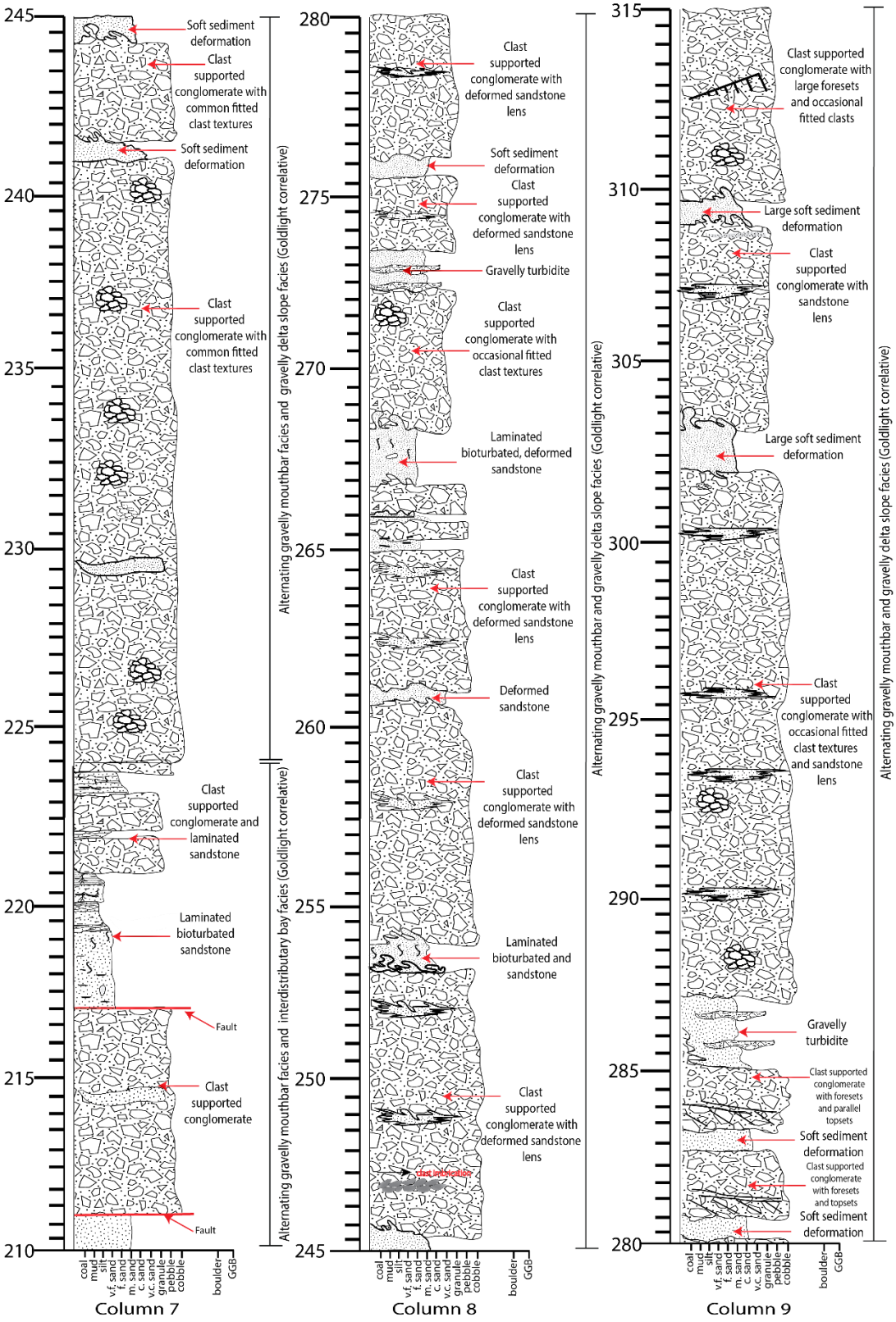


Figure 2. 13: Twelve Mile Beach stratigraphic columns (column 7-column 9). Depths are in meters with 50 cm divisions.

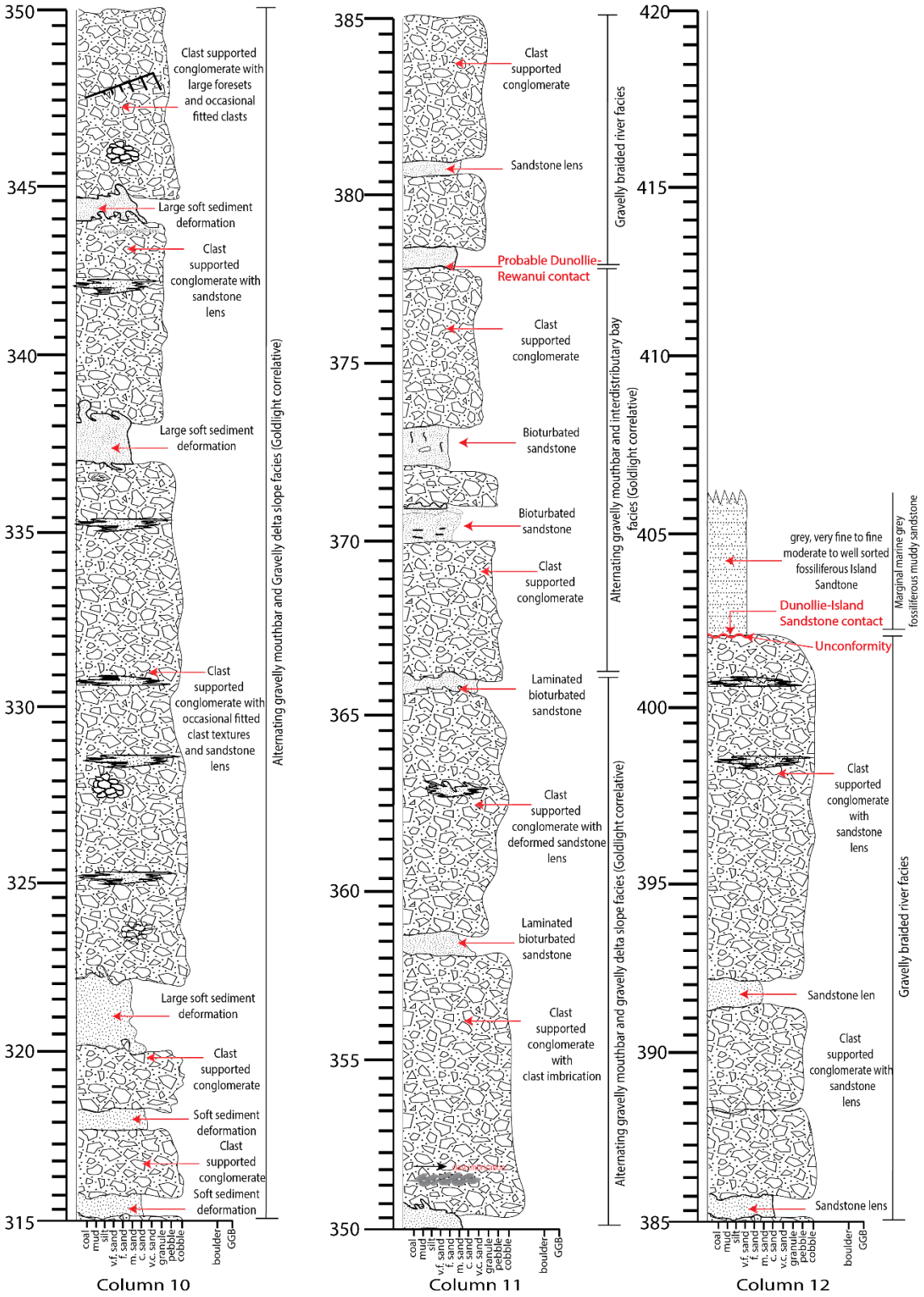


Figure 2. 14: Twelve Mile Beach stratigraphic columns (column 10-column 12). Depths are in meters with 50 cm divisions.

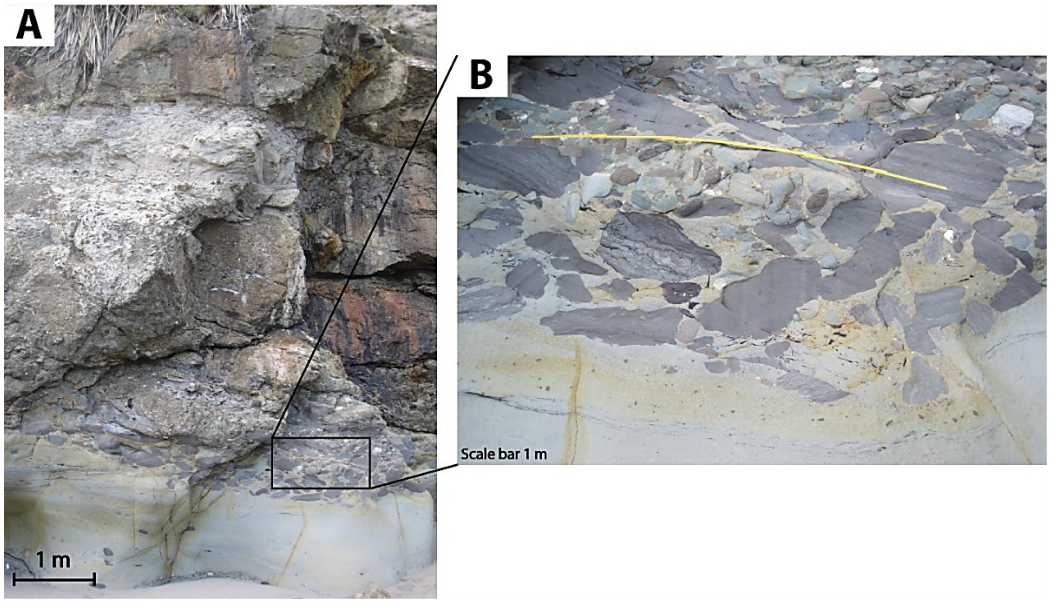


Figure 2. 15: Waiomo mudstone rip-up clasts, A) a layer of Waiomo rip-up clasts at the contact of the Waiomo Member and the Rewanui Member at Twelve Mile Beach, B) a close up view of the Waiomo mudstone rip-up clasts.


Figure 2. 16: Alternating gravelly mouthbar facies and interdistributary bay facies with small load cast structures at Twelve Mile Beach.

### 2.6.2 Drill holes

Twelve Mile Beach stratigraphy is correlated with several drill holes located in the northwestern part of the basin (Figure 2.2). Among these, eleven (DH-619, DH-621, DH-626, DH-634, DH-635, DH-636, DH-637,

DH-639, DH-641, DH-642 and DH-645) contain conglomerate lithologies and are important for interpreting the palaeogeography. Drill hole thicknesses are corrected for dip. In cases where dips are too low, corrected thicknesses remain more or less same as the original thicknesses. Drill holes are presented from northwest to southeast in order to understand the lateral changes in facies perpendicular to the interpreted highland area (Appendix 2; Figure 2.17). Five correlation panels oriented NW-SE have been drawn to examine facies perpendicular to the highlands to the northwest (Figure 2.2; Figure 2.17).

The drill holes on the northwestern corner (DH-634 and DH639) encounter conglomerates of the basal Morgan Member before encountering the Greenland Group basement rocks (Figures 2.2, Figure 2.13; Line 2 and 3). To the south, the basal Morgan Member in the drill holes (DH-621) becomes mostly sandy before encountering the basement (Figure 2.13, Line 1). DH-645 doesn't penetrate to the Greenland Group basement. In borehole DH-637, the Rewanui Member sits directly on basement (Figure 2.17, Line 3 and 4).

The alluvial fan/fan delta plain facies association is found in almost every borehole in the Morgan Member. Debris flow facies are mostly poorly sorted, rounded to subrounded, pebble to cobble, matrix supported conglomerates; angular to subangular, brecciated debris flow facies are only found in borehole DH-619 (Figure 2.17, Line 2). Gravelly braided river facies are mostly moderately to poorly sorted, rounded to subangular, pebble to cobble sized, clast-supported conglomerates with thin sandstone lenses. Conglomerates of the subaqueous prodelta facies association are too difficult to identify in core since the diameter is too small to see the diagnostic large soft sediment deformation features and thus may be included in the gravelly braided river facies.

Lacustrine mudstones assigned to the Waiomo Member are found in both DH-621 and DH-645 as indicated by the presence of thick, laminated, carbonaceous mudstones and siltstones with leaf and fresh water fossils ((Figure 2.17, Line 1 and 3). Laterally, the fan delta front facies conglomerates associated with the Waiomo Lake can be identified in DH-621, DH-634 and DH-645 by their coarsening upward sequences from sandy and gravelly mouthbar facies to carbonaceous mudstones of interdistributary bay facies (Figure 2.17, Line 1, 2 and 3).

The overlying Rewanui Member comprises thick alluvial fan/fan delta plain facies association in almost every borehole (Figure 2.17, Line 1-5). The thickness decreases from northwest to southeast. Clast-supported, pebble to cobble sized, rounded to subangular, moderately to poorly sorted conglomerates interbedded with thin sandstone lenses of the gravelly braided river facies are the most abundant facies in all drill holes. These are occasionally interbedded with matrix supported, poorly sorted, rounded to subrounded, pebble to cobble conglomerates of debris flow facies in some drill holes. Overbank floodplain facies are associated with gravelly braided river facies as indicated by interlaminated sandstone and carbonaceous siltstone with rootlets. Similar to the Morgan Member, the core diameter is too small to recognize the prodelta facies association and thus these are probably misidentified as gravelly braided river facies.

The lacustrine facies association of the Goldlight Member is mostly found to the southeast. To the northwest, laterally correlative fan delta front facies association is the most abundant. An overall coarsening upward sequence is found in drill holes located in the northwest. The sequence includes interbedded Clast-supported, rounded to subrounded, pebble to cobble conglomerates of gravelly mouthbar facies and carbonaceous sandstone and siltstones of interdistributary bay facies (Figure 2.17, Line 1-5).

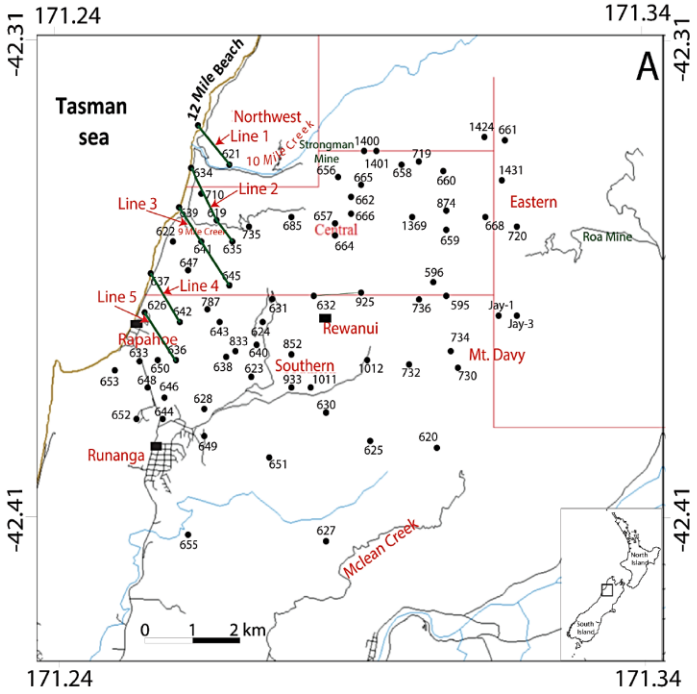
171.24
171.34
-42.31
-42.41
A
Tasman sea
12 Mile Beach
Northwest
Line 1
10 Mile Creek
Strongman Mine
Line 2
Line 3
9 Mile Creek
Central
Eastern
Roa Mine
Line 4
Line 5
Rapahoe
Rewanui
Mt. Davy
Southern
Runanga
Mclean Creek
North Island
South Island
0 1 2 km

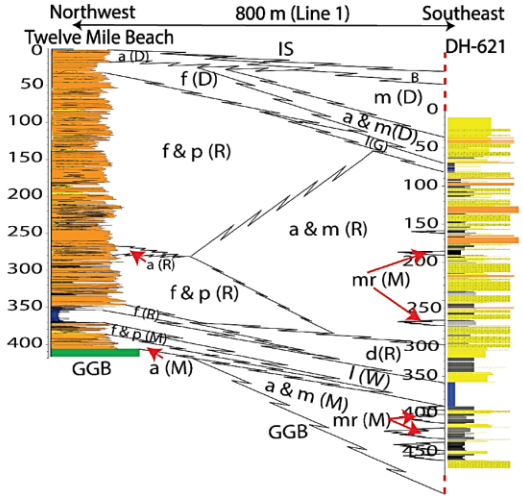
Northwest
800 m (Line 1)
Southeast
Twelve Mile Beach
DH-621
IS
B
a (D)
f (D)
m (D)
a & m(D)
l(G)
f & p (R)
a & m (R)
a (R)
mr (M)
f & p (R)
f (R)
f & p (M)
d(R)
l (W)
GGB
a (M)
a & m (M)
mr (M)
GGB


Legend
Greenland Group basement
Conglomerate
Sandy conglomerate
Sandstone
Muddy sandstone
Lacustrine mudstone
Carbonaceous mudstone
High carbonaceous mudstone
Coal
Brunner Formation
Island Sandstone
Kaiata Mudstone
Correlation
Tentative correlation
IS-Island Sandstone
KM-Kaiata Mudstone
B-Brunner Formation
a-alluvial fan facies association
a&m-alternating alluvial fan and meandering alluvial/delta plain facies association
m-meandering alluvial/delta plain facies association
d-delta front facies association
mr-mire facies association
f & p- alternating fan delta front and prodelta facies association
f-fan delta front facies association
p-prodelta facies association
l-lacustrine facies association
(D)-Dunollie Member
(R)-Rewanui Member
(M)-Morgan Member
(G)-Goldlight Member
(W)-Waiomo Member

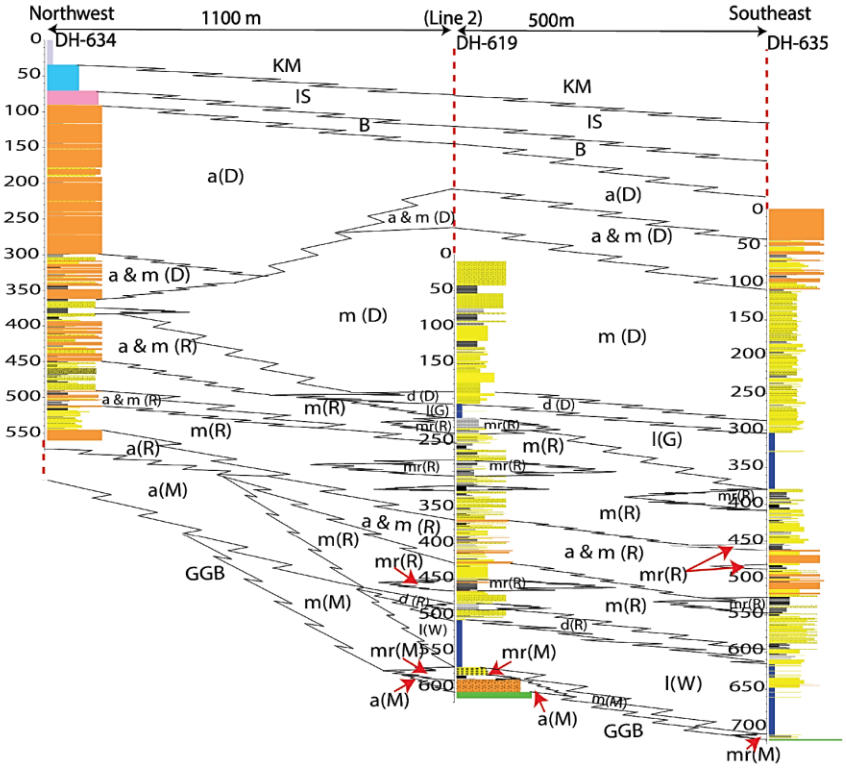
Northwest
1100 m
(Line 2)
500m
Southeast
DH-634
DH-619
DH-635
KM
IS
B
a(D)
a & m (D)
m (D)
a & m (R)
m(R)
a(R)
a(M)
GGB
d (D)
l(G)
mr(R)
d(R)
l(W)
mr(M)

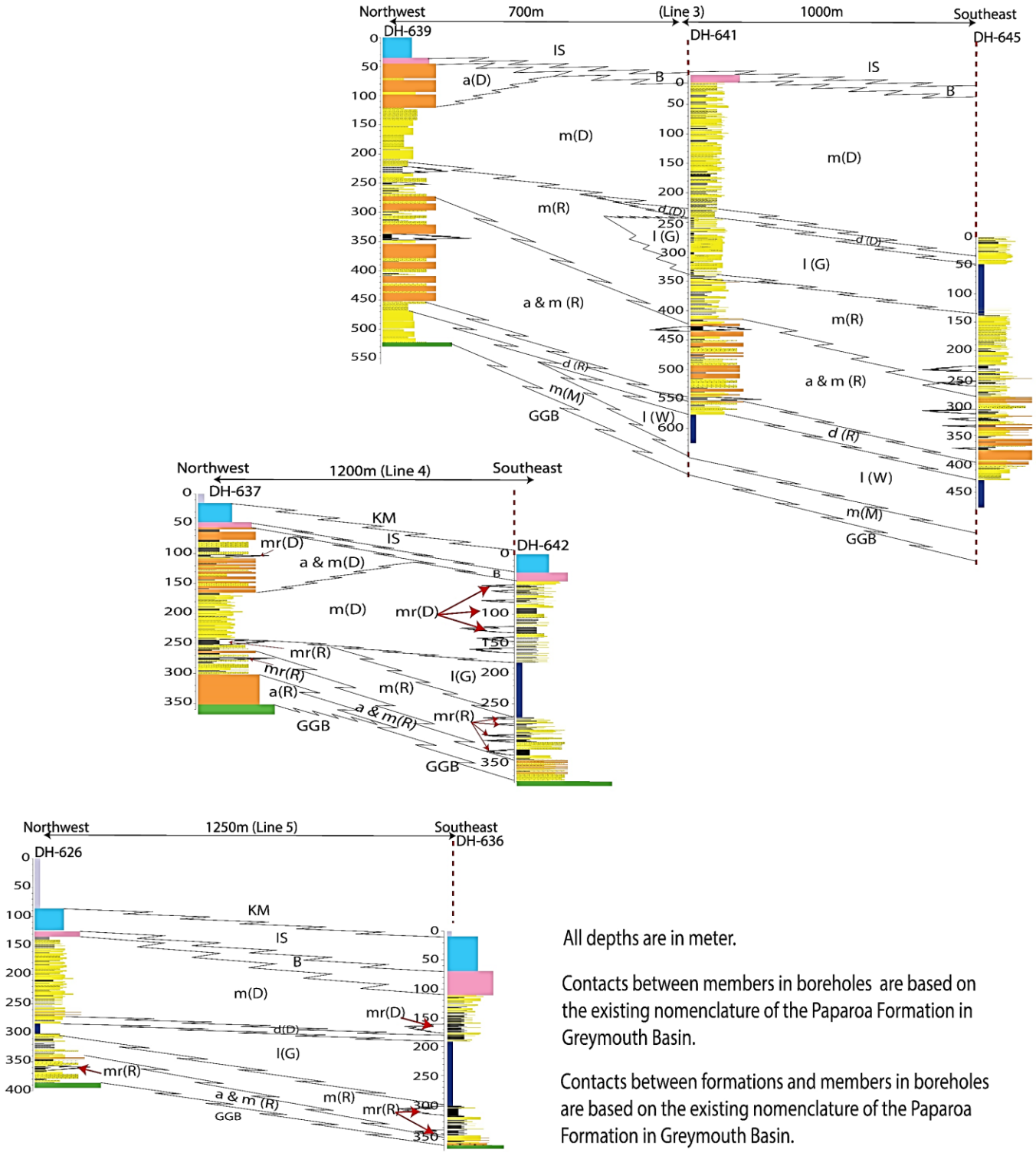


Figure 2. 17: Borehole correlation for line 1-line 5 on the northwestern corner of the basin showing lateral distribution (fence diagram) of conglomerate and associated fine grained sediments among Twelve Mile Beach stratigraphy and eleven drill holes. Line 1-Line 5 are perpendicular to the basin bounding fault.

The alluvial fan/fan delta plain facies association of the Dunollie Member are mostly found in the drill holes located in the northwest (Figure 2.17, Line 1-5). This facies association includes gravelly braided river facies as indicated by the clast-supported, pebble to cobble conglomerates, interbedded with overbank floodplain facies as indicated by the carbonaceous sandstone and siltstones with coaly laminae, and debris flow facies as indicated by matrix supported, poorly sorted pebble to cobble conglomerates.

Unlike at Twelve Mile Beach, the Palaeocene Dunollie Member of the Paparoa Formation in most of the drill holes is gradationally overlain by the Palaeocene to Eocene Brunner Formation and therefore can be difficult to recognize (Figure 2.17, Line 1-5). The contact become easier to identify to the southeast where the correlative Dunollie Member is finer grained than the overlying very coarse grained to granular sandstones of the Brunner Formation. The Brunner Formation is overlain by the glauconitic, fossiliferous, calcareous Island Sandstone of Eocene in age. The contact between Brunner Formation and the Island Sandstone is unconformable and represents the onset of the marine transgression during the Eocene.

In all drill holes, the coarsest conglomerates are located to the northwest, gradually fining and becoming interbedded with finer grained sediments to the southeast (Figure 2.17, Line 1-5). Correlative facies in the basin's centre alternate between thick lacustrine mudstones of the Waiomo and Goldlight members and meandering river channels, oxbow lakes, floodplain and thick mire coals of the Morgan, Rewanui and Dunollie members. The meandering alluvial facies is interpreted to be axial meandering river and floodplain deposits in the basin centre replacing the lacustrine mudstones and commonly interfingering with the alluvial fans and fan deltas to the northwest.

## 2.7 Interpretation and Discussion of Alluvial Fan vs Fan Delta Settings

Alluvial fan conglomerates are difficult to distinguish from fan delta plain conglomerates and the proximal facies would have been the same. All are dominated by clast-supported braided river facies conglomerates with minor debris flow facies present indicating the alluvial fans would have been steamflow dominated fans. The presence of rare angular to subangular clasts in the debris flow facies in the Morgan Member indicates that they travelled a relatively shorter distance. The higher percentage of rounded to subrounded clasts in the debris flow facies in the younger Rewanui and Dunollie members indicates longer transport distances. This suggests that the drainage area became larger through time from the Morgan to Rewanui-Dunollie members so that there was more constant water flow through the canyons that fed the alluvial fans. This might suggest that the hinterland stepped further away or that the rivers feeding the fans cut back into the hinterland and/or captured additional drainages. Downstream on the fans, the gravelly braided river facies became more prevalent indicating high energy stream flows ran consistently over the fan surface. Even further downslope, increasingly abundant overbank floodplain facies record low energy processes between channels approaching the fan delta front.

The criteria that are used to distinguish a fan delta from an alluvial fan setting primarily based on lateral correlation to either lacustrine mudstones or meandering river sandstones and coals in the axis of the basin. However, detailed sedimentary facies analysis of the conglomerates shows previously unidentified shoreline and subaqueous environments recorded by the fan delta front and prodelta facies associations. The fan delta front facies association is characterized by the gravelly mouthbar and the interdistributary bay facies. Subaqueous deposition on the fan delta slope was identified by the presence of abundant load casts and large-scale soft sediment deformation structures indicating slope failure. These were driven by continuous deposition of high bedload, gravel rich sediments at the top of the slope in the mouthbar. Therefore, mouthbar and fan delta slope facies are intrinsically associated and are commonly repeatedly

interbedded. Occasional hyperpycnal flows are interpreted from the presence of clast-supported, reversely graded conglomerate deposits in the gravelly delta slope facies. These grade into the more distal gravelly turbidites facies on the lower delta slope or bottomset fan delta environments. The gravelly turbidites facies is the product of high-density turbidity currents as indicated by the presence of normally graded conglomerate and sandstone beds interbedded with lacustrine mudstones. These grade laterally into lacustrine massive mudstone and lacustrine mudstones with minor thin sandstone facies toward the southeastern low of the centre of the basin.

The type of fan delta is interpreted to be a Hjulstr*ö*m-type fan delta formed on a low angle slope. The internal structure does not show clear distinction between topsets, foresets and bottomsets, and the delta slope facies does not contain steeply dipping foresets such as found in a Gilbert-style fan delta (e.g. Galloway and Hobday 1996; Gobo et al. 2014). The exposure at the Twelve Mile Beach is large and fresh enough to identify a number of soft sediment deformation and delta slope foresets. The presence of abundant convolute bedding and soft sediment deformation at Twelve Mile Beach does indicate a steeper slope but delta slope foresets are not large enough as would be observed in an actual Gilbert-style fan delta. Therefore, we interpret that the overall depositional of conglomerates and associated fine grained sediments took place in a Hjulstr*ö*m-type fan delta environment.

The presence of the fan delta front and prodelta facies associations in both the Waiomo and Goldlight members indicates the existence of two lakes at different times with fan deltas entering each. The thickness of the fan delta front and prodelta facies associations correlative with the Goldlight Member in the Twelve Mile Beach section is about 12 times greater than those correlative with the Waiomo Member (Figure 2.10-Figure 2.14). This suggests that the fan delta developed in the Goldlight Lake probably existed for a significantly longer period of time. This also indicates that the subsidence rate of the basin during the deposition of the Goldlight Member was higher compared to the deposition during the Waiomo Member.

## 2.8 Interpretation and Discussion of the Tectonic Setting of the Greymouth Basin

The distribution of the conglomeratic facies indicates that the northwestern side of the basin was dominated by alluvial fans alternating with fan deltas (Figure 2.17, Line 1-5). To the southeast toward the basin's centre, these facies interfinger with both deeper water lacustrine facies and with meandering channel and mire facies (Newman and Newman 1992; Sherwood et al., 1992; Boyd and Lewis 1995; Ward 1997; Maitra and Bassett 2017). The more proximal debris flow facies are also more common toward the northwest indicating the direction of higher ground. Finally, palaeoflow direction measurements from clast imbrication and cross-bedding also indicate flow from the northwest. This suggests that the highlands were to the northwest and the basin centre was to the southeast. Given the longevity of the alluvial fan/fan delta environments, the highlands were most likely formed by a fault forming a long-lived fault scarp at the apex of the alluvial fans and fan deltas. We interpret this as the primary bounding fault in the Greymouth Rift Basin given the lack of equivalent alluvial fan and fan delta deposits on the eastern side of the basin.

The most probable location of the basin bounding fault would be somewhere offshore of Twelve Mile Beach. One of the petroleum wells (Haku-1), located northwest of the Greymouth Basin, shows that the Eocene Brunner Formation lies directly on Greenland Group basement rocks (Hematite Petroleum 1970). The unconformity between Palaeozoic Greenland Group and Eocene Brunner Formation indicates the main basin boundary fault for the Greymouth Basin must have been located somewhere between the Haku-1 well and Twelve Mile Beach. The most likely candidate is the Cape Foulwind Fault which is recently mapped

in that location as a marine active fault. The fault is interpreted as a normal fault which was reactivated as a reverse fault in the modern compressional tectonic setting as indicated by a number of potential earthquake sources (Barnes and Ghisetti 2013; Figure 1.3; Figure 1.4; Figure 2.1A). It is likely that the Cape Foulwind Fault was active as a normal fault at the time of the deposition of the Paparoa Formation of the Greymouth Basin and controlled the overall subsidence in the basin.

Two tectonic models (Figure 2.18) are presented for the Greymouth Basin that have the master fault of the rift basin located to the northwest as indicated by our detailed facies analysis. Model A represents a continental, half graben, rift basin with interior drainage and filled with a lake in the basin's centre whereas Model B illustrates a continental, rift basin, half-graben with an axial meandering river system in the basin's centre (e.g. Leeder and Gawthorpe 1987; Figure 2.18). Periodic motion on the basin bounding fault maintained the actively rising highlands to the northwest responsible for the thick alluvial fan and fan delta deposits. A half-graben model is chosen, as oppose to a full graben model, based on detailed facies analysis of the finer grained sedimentary rocks present in the basin centre and eastern side (Maitra and Bassett 2017).

Model A illustrates a half graben where the faulted foot-wall margin was steep and produced high energy flows carrying large volumes of coarse-grained sediments (Figure 2.18A). The lower gradient, hanging-wall, hinge side produced lower energy flows carrying a reduced supply of finer grained sediments. Lakes would have formed in the centre, interfingering with alluvial fans on the faulted side resulting in fan deltas and with sandy meandering rivers on the low gradient hinge side resulting in sandy to muddy deltas. The two mudstone members (Waiomo and Goldlight) recorded the lacustrine setting in the basin centre during phases of greater accommodation creation due to rapid subsidence as compared to sediment supply (e.g. Martins-Neto and Catuneanu 2010; Holz et. al. 2015, 2017). The greater thickness of shoreline and subaqueous facies in the Goldlight Member, compared to the Waiomo Member, probably indicates that the shoreline stayed in one location for quite a long time suggesting there was enough subsidence to create accommodation to hold it all. Laterally correlative with the lacustrine mudstones are the alluvial members (Morgan, Rewanui, and Dunollie) which are conglomeratic to the northwest indicating the presence of steeper, fault-controlled palaeotopography. The same alluvial members became sandier to the southeast indicating the location of the half-graben hinge (Maitra and Bassett 2017). The interfingering of alluvial fan facies with both meandering river and lacustrine facies in the southwestern corner suggests that even during lacustrine phases, axial meandering rivers may have flowed into the palaeolakes forming sandy deltas.

Model B is more appropriate for when there were no lakes present in the basin and the depocentre was the site of an axial meandering river system (Figure 2.18B). Differential subsidence would have caused channel migration through time keeping the main channel of the axial meandering river systems adjacent to the alluvial fans (e.g. Leeder and Gawthorpe 1987). When applying this model to the Greymouth Basin, the three alluvial members (Morgan, Rewanui and Dunollie) were deposited across the entire basin but with lateral variations in grain size and sedimentary environments. The conglomeratic alluvial fans were deposited along the steeper, fault-controlled northwestern margin whereas sandy meandering rivers and coaly low-lying mires were deposited in the basin centre and southeastern hinge.

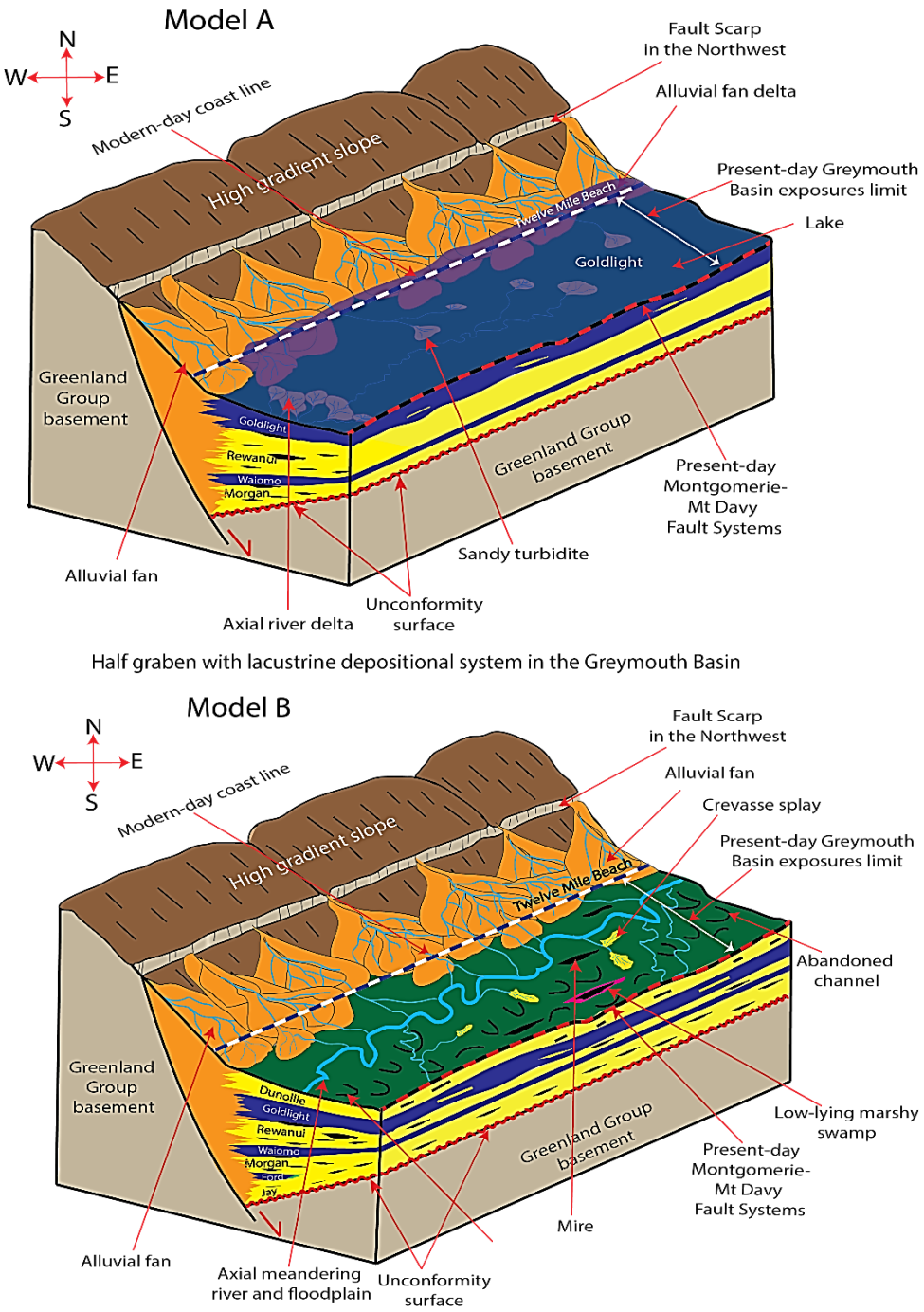


Figure 2. 18: Tectonic models of the Greymouth Basin. Model A illustrates alluvial fans and fan deltas depositional systems when lakes were present in the basin's centre and Model B represents meandering river and floodplain depositional systems when there was no lake in the basin. The back and forth of these two models demonstrate the variation in basin subsidence rate, resulting the change in the ratio of accommodation conditions to sediment supply (A:S) of the basin through time. The change in accommodation space and sediment supply is therefore responsible for the deposition of alternating fluvio-lacustrine members of the Paparoa Formation.

Whether lacustrine or meandering alluvial facies were deposited in the depocentre depends on the balance between the creation of accommodation by subsidence and the amount of sediment supplied to fill it (Leeder and Gawthrope 1987; Martins-Neto and Catuneanu 2010; Holz et. al. 2015, 2017). In the Greymouth Basin, the depocentre alternates between lacustrine and alluvial phases. A lacustrine phase indicates accommodation is greater than sediment supply and may be due to periods of more rapid fault motion leading to more rapid subsidence. This might also result in renewal of uplift and increased alluvial fan/fan delta development. Alluvial phases in the basin's centre may be the result of less activity on faults resulting in less subsidence when compared to sediment supply. The same amount of sediments would gradually fill the accommodation causing the lacustrine mudstone in the basin axis to be replaced with axial meandering rivers. Alternatively, there could be a change in sediment supply, perhaps due to changes in rainfall. However, recent analysis of palaeoclimate indicates there were no cyclical climatic changes happening in the Late Cretaceous to Palaeocene (Ward 1997; Kennedy 2003; Raine et al. 2017).

The present tectonic model differs from previously published models of the Greymouth Basin by locating the major basin bounding fault on the northwestern side of the basin. Most of the previous models depict the eastern margin Montgomerie - Mt Davy Fault System as the basin bounding fault responsible for the overall subsidence (Bowman 1984; Newman 1985; Ward 1997; Kamp et al., 1999). This was recently refuted by Suggate (2014) who concluded that the Montgomerie - Mt Davy faults were not active until very late in the basin's history and thus could not have been the primary basin bounding fault for the majority of the basin's subsidence history. The detailed facies analysis of the conglomerates and associated fine-grained sediments places the primary basin bounding fault to the northwest. The hinge to the southeast was later cross-cut by the younger Montgomerie-Mt Davy Fault System.

## 2.9 Conclusions

The main purpose of this chapter is to conduct a detailed sedimentary facies analysis of the conglomerate deposits in order to understand the palaeogeography and tectonic setting of the northwestern side of the Greymouth Rift Basin.

The lacustrine facies association indicates that lakes existed in the centre of the basin. Three conglomeratic facies associations have been identified along the northwestern margin of the basin. The prodelta facies association is interpreted as being deposited in a delta slope region where high density turbidity currents, subaqueous debris flows, and hyperpycnal flow from the river channels were common. The associated fan delta front facies association is interpreted to have been in high bed load distributary channels at the river mouth and subaqueous, low energy interdistributary bays adjacent to the active channels where channel avulsion is a dominating process of deposition. The jigsaw-like fitted clast textures found in the gravelly mouthbar channels were most likely the product of microvibrations and winnowing by currents due to the interaction between higher energy river mouth channels and the low energy lake. The alluvial fan/fan delta plain facies association is interpreted as being deposited in subaerial environments where the sedimentation processes are dominated by high energy stream flows, low energy overbank floodplain processes, and rare subaerial debris flows.

The deposition of the conglomerates and associated fine grained sediments took place in both alluvial fan and fan delta settings which was controlled by the variable subsidence rate of the Greymouth Basin. The type of alluvial fan is interpreted to be streamflow dominated based on the prevalence of clast-supported braided river facies conglomerates and the relative scarcity of matrix supported debris flow facies conglomerates. The type of fan delta is interpreted to be a Hjulstr*ö*m-type fan delta formed on a lower

angle slope. The greater thickness conglomerate in the northwest indicates an area of high relief. Gradual decrease in conglomerate thickness from the northwest to the southeast of the basin suggests that the primary basin bounding fault was located immediately offshore to the northwest.

# Chapter 3: Lacustrine source rocks of the Greymouth Basin: Sedimentary facies analysis, distribution and palaeogeography, and source rock geochemistry.


## Abstract

The detailed facies analysis of the fine-grained sedimentary rocks of the Paparoa Formation of the Greymouth Basin has been conducted in order to gain a better understanding of lacustrine source rocks in New Zealand. The main focus of this study is twofold; 1) to understand the lateral and vertical distribution of the sedimentary facies in order to interpret the palaeogeography of the Greymouth Basin during Late Cretaceous to Early Palaeocene time, and 2) to delineate the volume of the palaeolacustrine deposits and their source rock potential. The sedimentary facies are broadly classified into four facies associations which include i) lacustrine, ii) delta front, iii) meandering alluvial/delta plain, and iv) mire. The detailed sedimentary facies analysis suggests a half graben with fan deltas on the steep, fault-controlled side to the northwest, a lake in the basin axis, and low gradient, sandy, deltas fed by meandering rivers on the hinge side of the basin to the southeast. A number of organic rich facies have been identified from each facies association. However, the lacustrine facies association has higher petroleum potential based on their dark colour, lateral and vertical distribution along with already proven coaly source rocks.

The lacustrine facies association of Ford, Waiomo and Goldlight members shows promising petroleum potentiality based on their dark colour and higher TOC, S2 and HI content. The Ford Member has TOC content of up to 4.6 wt%, HI of up to 554 mg HC/g TOC, and mostly mixed oil and gas prone source with good to excellent total petroleum potential. The Waiomo Member shows fair to very good petroleum potential with TOC contents of up to 3.08 wt%, HI of up to 554 mg HC/g TOC, and mostly mixed oil and gas prone source rocks. The Goldlight Member has poor potential with TOC contents of up to 2.95 wt%, HI up to 282mg HC/g TOC, and mostly gas prone source rocks with poor to good quantity petroleum potential. Comparing the source rock geochemistry of the three lacustrine members, the Late Cretaceous Ford and the Waiomo mudstones are shown to have higher petroleum potential than the Palaeocene Goldlight mudstones.


## 3.1 Introduction

Increased interest in the hydrocarbon potential of the lacustrine mudstones of the Late Cretaceous to Early Palaeocene Paparoa Formation in the Greymouth Basin has led to this study of the lacustrine members in order to identify and characterize potential lacustrine hydrocarbon source rocks. The Greymouth Basin, the study area, is part of the Late Cretaceous West Coast-Taranaki Rift System in New Zealand of which one part, the Taranaki Basin is currently producing petroleum (Figure 3.1). Cretaceous-Cenozoic waxy coals and coaly/carbonaceous mudstones have already proven to be source rocks for the Taranaki Basin and are interpreted to have sourced large volumes of petroleum deriving from terrestrial woody gymnosperm and/or angiosperm dominated organic matter (Noble et al. 1991; Moore et al. 1992; Curry et al. 1994; Sykes et.al. 2013). Late Cretaceous lacustrine mudstones are also suggested to be potential source rocks in the Taranaki Basin and other offshore basins New Zealand; however, there has been no direct evidence to date (Killops 1994, 2010; Figure 3.1).

Most parts of the West Coast-Taranaki Rift System, including the producing Taranaki Basin, are deeply buried and can only be studied through drillholes and seismic imaging. The Greymouth Basin, however, is

highly accessible. It is known for its high quality, low ash coal deposits and has been extensively drilled for mining exploration. It is filled with the Late Cretaceous to Early Palaeocene non-marine Paparoa Formation which contains organic-rich lacustrine mudstones, mire coals, and meandering alluvial sandstones and mudstones (Morgan 1911; Gage 1952; Nathan et al. 1986; Newman 1985; Sherwood et al. 1992; Boyd and Lewis 1995; Ward 1997). The Paparoa Formation shows promising petroleum potential as suggested by the existence of oil and gas seeps in the area (Morgan 1911; Nathan et al. 1986, 2002). The Cretaceous coals and carbonaceous mudstones in the Greymouth Basin have long been identified as the primary source rocks for existing oil and gas seeps (Hirner and Lyon 1989; Frankenberger et al. 1994). However, more recently, the lacustrine mudstones have also been suggested to be potential source rocks (Cody 2015; Mohnhoff et al. 2017).

Numerous studies on modern and ancient lake deposits around the world suggest that locating and assessing hydrocarbon potential in lacustrine basins is more challenging compared to marine systems because of the complex lithologic and stratigraphic behaviour of lacustrine deposits (Curiale and Stout 1993; Bohacs 1998; Carroll and Bohacs 2001). In addition, available nomenclature is inadequate to understand the complex lateral and vertical facies relationships between coaly, alluvial and lacustrine units. For the Greymouth Basin, the lacustrine mudstone members of the Paparoa Formation are easy to identify and tend to be used as marker beds by the coal companies to separate the coal-bearing members from the non-coal bearing members. The lacustrine units have been previously mapped based on the massive mudstone deep water facies, ignoring the sandier shallow water and shoreline facies which were instead included in the alluvial units and/or interpreted as transitional lithosomes (Gage 1952; Boyd and Lewis 1995; Newman 1985; Ward 1997).

The main purpose of this paper is to understand the petroleum potentiality of the lacustrine mudstones of the Paparoa Formation. A detailed sedimentary facies analysis has been done with a focus on lateral facies transitions so that shallow water and shoreline facies can be identified and distinguished from meandering alluvial facies. The inclusion of the shallow water lacustrine facies with the deep-water facies will increase the volume of identified potential lacustrine source rock in the Paparoa Formation as well as contributing to a better palaeogeographic reconstruction. We have conducted a geochemical study of these lacustrine units in order to analyse their hydrocarbon source rock potential. The proposed sedimentary facies and petrochemical analysis in this chapter can be used as an excellent analogue for the deeply buried Taranaki Basin and other Late Cretaceous frontier basins in New Zealand.

## 3.2 Geological background of Greymouth Basin

The Greymouth Basin is located in the West Coast region of the South Island and is part of the West Coast–Taranaki Rift System (Nathan et. al. 1986, 2002; Laird and Bradshaw 2004; Strogen et.al. 2017). It is bounded by the Cape Foulwind Fault System in the northwest and the Montgomerie-Mount Davy Fault System in the southeast (Suggate 2014; Figure 3.2A). The basin was infilled with Late Cretaceous to Early Palaeocene terrestrial sediments of the Paparoa Formation (commonly known as the Paparoa Coal Measures (Figure 3.2B) (Laird and Bradshaw 2004). The formation is entirely non-marine in origin and is divided into four alluvial members (Jay, Morgan, Rewanui and Dunollie) which are separated by three lacustrine members (Ford, Waiomo and Goldlight) (Gage 1952; Nathan 1986). On the eastern margin and in the centre of the Greymouth Basin, carbonaceous siltstones and mudstones with thinly bedded, normally graded sandstones (Ford, Waiomo and Goldlight Members) are interpreted as lacustrine deposits (Ward 1997; Cody 2015). These are replaced by coal deposits associated with sandstone channels with interbeds of carbonaceous mudstone (Jay, Morgan, Rewanui and Dunollie Members); these are interpreted as raised

mire coals and meandering river sandstones and overbank deposits (Newman 1985; Boyd and Lewis 1995; Ward 1997; Sherwood et al. 1992; Newman and Newman 1992). Correlative conglomerates on the western side of the basin are interpreted as alternating alluvial fan and fan delta deposits (Maitra Chapter 2; Gage 1952; Ward 1997). The Paparoa Formation overlies Greenland Group basement of Early Ordovician age and underlies the transgressive sequence of Eocene Brunner Formation to calcareous Island Sandstone, Kaiata Mudstone and Oligocene Cobden Limestone (Nathan et al. 1986, 2002; Figure 3.2B).

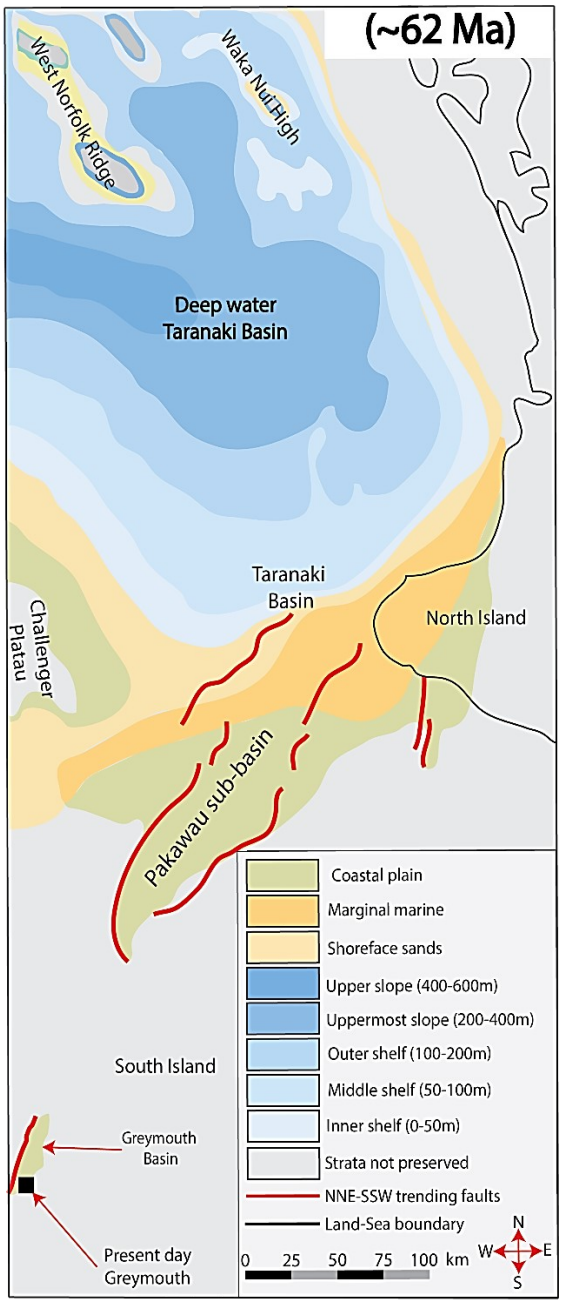


Figure 3. 1: Figure showing the relative position of the Greymouth and the Taranaki Basin at about 62 Myrs ago when marine transgression and post-rift thermal subsidence already started across the Taranaki Basin region. The red lines show parallel to sub-parallel NNE-SSW oriented basin-bounding faults (modified from Strogen et. al. 2017).

The Greymouth Basin is extensively drilled for coal exploration. Coals are found in all alluvial coal-bearing members of the Paparoa Formation (Jay, Morgan, Rewanui and Dunollie) but the economic and mineable coals are restricted to the Morgan and the Rewanui Members (Bowman 1984; Newman 1985; Ward 1997). The Rewanui Member is the thickest coal bearing unit within the Greymouth Basin (Boyd and Lewis 1995; Ward 1997). The coals are waxy in nature, higher bituminous to sub-bituminous in rank, and have low ash and sulphur content (Newman and Newman 1992; Sherwood et al. 1992; Boyd and Lewis 1995; Nathan et al. 2002).

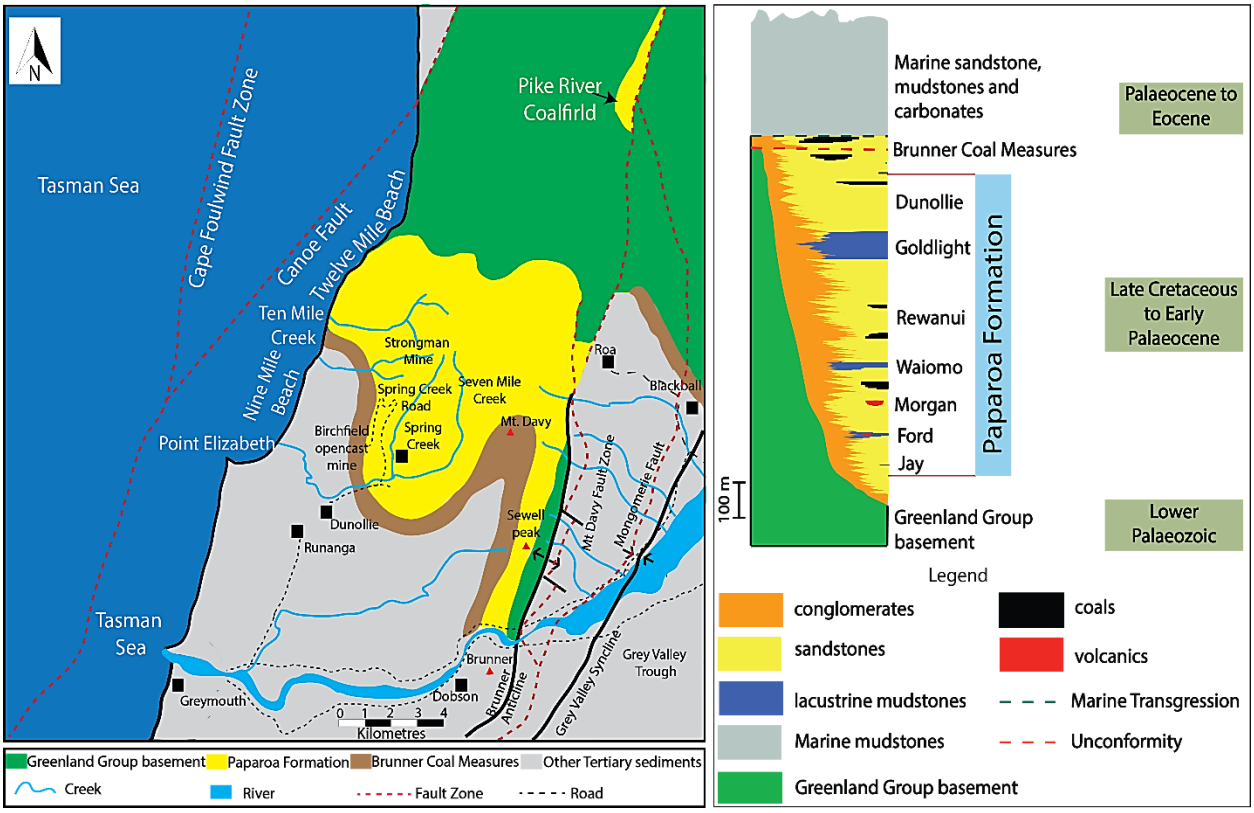


Figure 3. 2: A) Geological and structural map of the study area (modified from Gage 1952, Newman 1985, Suggate 2014, Nathan 1986, Nathan et al. 2002; Rattenbury and Isaac 2012), and B) Generalized stratigraphy of Paparoa Formation, modified from Newman 1985, Nathan 1986, Boyd and Lewis 1995 and Ward 1997.

The presence of petroleum in the Greymouth area has been acknowledged since the early 1900s from several oil and gas seeps and shallow wells drilled in the Katuku anticline in the Arnold Valley, a significant gas blowout in well SFL-1 drilled to the west of Kumara, and high-gravity oil from Niagra-1 drilled to the west of Moana (Morgan 1911; Nathan et al. 2002). However, drilling attempts have not been commercially successful (Beggs et al. 2008). The Taranaki Basin is the only place where petroleum is being produced on a commercial level with the majority of New Zealand hydrocarbon source rocks being coals, carbonaceous rocks, mudstones and shales of Cretaceous to Eocene age of both terrestrial and marine origin (Killops et al. 1994; Herzer et al. 1999; Sykes et al. 2013). Biomarker signatures indicate the oil in the Greymouth Basin has a terrestrial, gymnosperm-dominated source which is interpreted to have migrated from non-marine Late Cretaceous to Early Palaeocene coals (Hirner and Lyon 1989; Frankenberger et al. 1994; Zink and Sykes 2010).

A recent geochemical study of the three lacustrine mudstone units indicates that the lacustrine mudstones also have the potential to generate petroleum (Cody 2015). The massive mudstones and mudstones with thin interbedded normally graded sandstones have TOC values ranging from 1.0 to 4.5 wt. %, HI values ranging from 68 to 552 mHC/gTOC, and thermal maturation ranging from immature to late mature. The "transitional lithosomes" defined by Ward (1997) also contain a significant amount of organic matter including plant stems, plant roots and leaves (Newman 1985; Ward 1997; Cody 2015).

## 3.3 Methods

### 3.3.1 Sedimentary facies analysis

Sedimentary facies analysis has been done by studying outcrop and available drill core in the Greymouth Coal Field (Table 3.1). Outcrops have been chosen based on accessibility and quality, the best of which is the Spring Creek Haul Road section. Stratigraphic sections were measured to the decimetre scale using standard field techniques. Lithological descriptions include bedding thickness and geometry, nature of lower and upper bedding contacts, grain size, sorting, sedimentary structures, and fossils, photographs, and interpreting depositional environments. Stratigraphic columns have been constructed and depositional environments have been interpreted.

Drill holes and cores are more extensive than outcrops, cover a wider area, and, where the outcrops are inaccessible due to dangerous terrain and dense vegetation, are more accessible since the cores are currently located at the Featherston Core Storage near Wellington (Figure 3.3). The selection of drill cores was based on the location, availability and quality of the cores. Core descriptions were taken from the original logs downloaded from NZPM (New Zealand Petroleum and Minerals) website and modified after inspection. Measurements and descriptions were taken in the same manner as investigating the outcrops in the field. Forty drill holes have been inspected of which twenty have been used to develop the sedimentary facies documented with annotated and interpreted stratigraphic columns (Appendix 2). Six drill cores from different parts of the basin have been logged in detail in order to define sedimentary facies.

The drill holes also have geophysical logs available in coal reports downloaded from the NZPM website. The gamma ray and density logs are used here to identify changes in lithology and the presence of coals, respectively. Higher gamma log response is typical of mudstones whereas lower gamma log response is more typical for sandstones. Geophysical logs are presented next to their core log in Appendix 3.

A fence diagram has been developed correlating sedimentary facies among the drill holes and outcrops. The fence diagram displays the lateral and vertical distribution of different sedimentary facies of the Paparoa Formation. Lacustrine mudstones in the centre of the basin are the easiest to identify and form the basis for correlation across the basin following long tradition in the Greymouth Coalfield. Alluvial facies in the basin centre separate each lacustrine interval. The marine Island Sandstone overlying the Paparoa Formation has been added on top of the fence diagram to strengthen correlations for the younger, non-lacustrine members.

In order to understand the distribution of lacustrine mudstones across the basin, isolith maps of each lacustrine unit have been developed. Isolith maps are created by calculating the gross thickness of all lacustrine lithofacies from the stratigraphic columns and drill cores, including the previously unassigned 'transitional lithosomes' of Ward (1997). This focus on lithofacies contrasts with previously published isopach maps which instead focussed on member thickness and may or may not have included the 'transitional' lithosomes (Gage 1952; Newman 1985; Ward 1997).

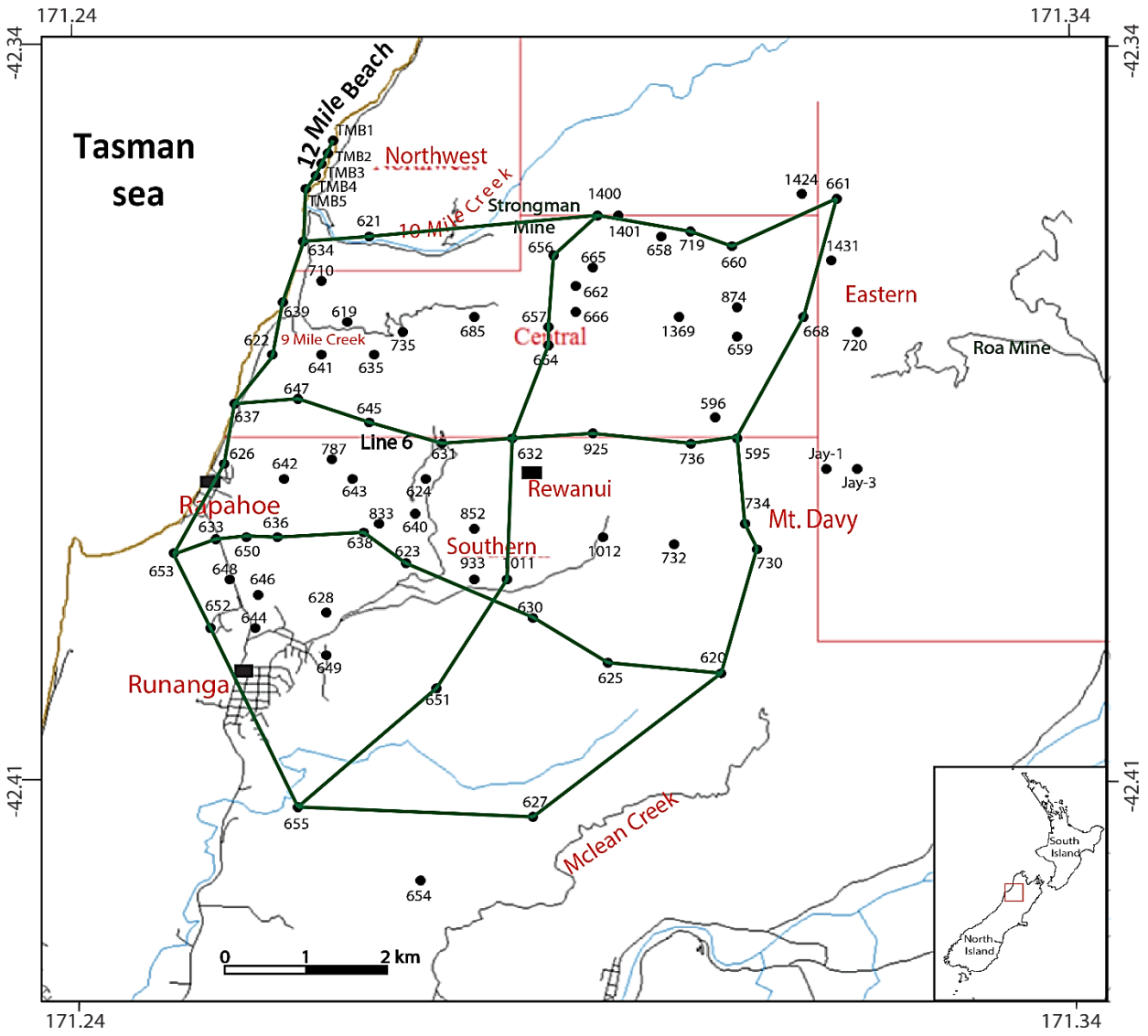


Figure 3. 3: Map of the Greymouth Basin showing the drill holes that have been used to study detailed sedimentary facies of the Paparoa Formation. Inset shows location in New Zealand. The green lines show the lines used to create cross-sections in order to develop a fence diagram.

### 3.3.2 Geochemistry of potential petroleum source rocks

The hydrocarbon potential of the fine grained lithofacies was analysed following the well-established Rock-Eval pyrolysis method (Bissada 1982; Katz 1983; Tissot and Welte 1984; Peter 1986; Demaison and Huizinga 1991; Leythaeuser et al. 1991 and Katz and Liro 1993; Peters and Cassa 1994). The key parameters for source rock analysis that we discuss in this paper are the source rock generative potential, the type and source of the organic matter, and the degree of maturity of the organic matter (Table 3.2; Table 3.3).

Samples were collected from drill cores and outcrops throughout the Greymouth Basin from the lacustrine lithofacies. A total of 183 samples have been collected from the three lacustrine members including 56 samples from the Ford Member, 71 samples from the Waiomo Member, and 56 samples from the Goldlight

Member (Appendix 4). More than one sample was taken from each mudstone lithofacies in each lacustrine member based on the thickness the member. Sample collection depended on the availability of the mudstone members in the drill cores and the outcrops. Most samples were collected from the mudstones with only a few collected from thin sandstone beds with conspicuous plant material (Appendix 4). Ford Member is not penetrated by most of the drill holes and is not common in outcrop; thus, there are fewer samples from the Ford Member. The Goldlight Member is eroded from most of the eastern and central parts of the Greymouth Basin, also resulting in fewer samples. In contrast, the Waiomo Member is available in most of the drill cores as well as accessible outcrops.

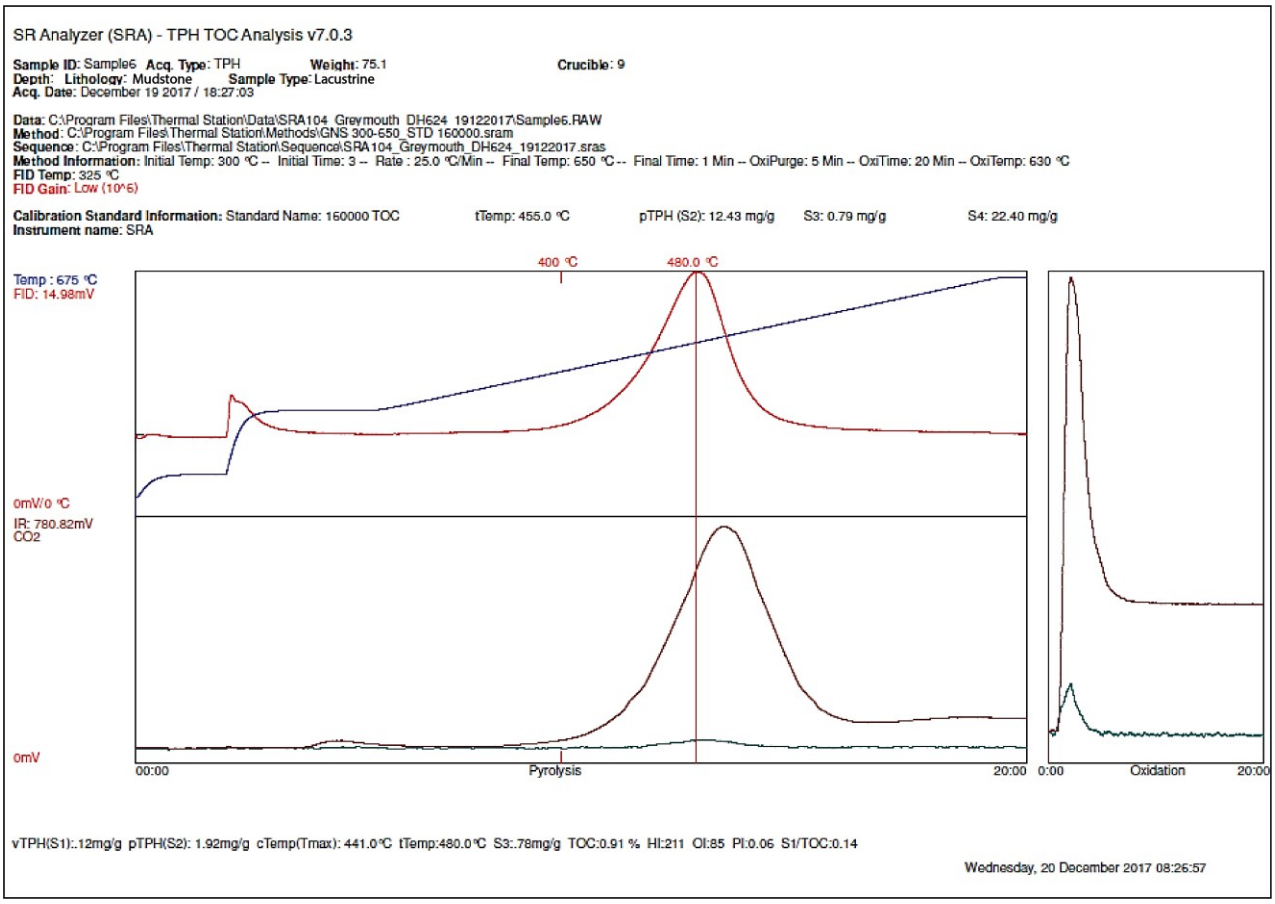


Figure 3. 4: Example graph of preliminary Source Rock Analysis (SRA) at the depth 288.6 m-288.65 m from DH-624 of the Greymouth Basin.

The samples were prepared for geochemical analysis by removing weathered parts in order to get a fresh piece. This was carefully washed and dried in an oven at $40^0$C temperature then crushed to fine powder by mortar and pestle. For dark carbonaceous mudstones with a high volume of organic matter (OM) present, the standard sample weight used was 80 mg or higher to ensure reliable testing. For samples with lower organic matter concentration (light colour), the standard sample weight was increased to 100 mg to ensure testing reliability.

Geochemical analysis was conducted on a Weatherford Laboratories TOC/TPH source rock analyser (SRA) at GNS Science to determine OM richness, kerogen type, and maturity. The SRA uses programmed

pyrolysis to determine source rock characteristics of the powdered samples (Horsfield et al. 1983; Figure 3.4).

The methodology used in this study was based on that described by Espitalié et al. (1977), Peter (1986) and Peters and Cassa (1994). The technique of this method is based on pyrolysis and oxidation of the rock samples. The pyrolysis and oxidation were performed by heating the rock samples in a steady state in order to release i) the hydrocarbons which had previously been generated in the sample during burial and stored in the pore spaces (S1), ii) newly generated hydrocarbon formed by the thermal breakdown of insoluble organic matter present in the rock samples (S2), iii) the oxygen containing compound CO2 (S3). The temperature at which the maximum amount of S2 hydrocarbon is generated is called the temperature of maximum pyrolysis yield ($T_{max}$). As the temperature rises, total organic carbon (TOC) content of the sample from the residual organic matter was determined by oxidation. In order to complete pyrolysis and oxidation, samples were run in the source rock analyser (SRA) over a period of 3 days with each sample taking approximately 45 minutes. The rock samples pyrolised at 300 °C for 3-4 minutes, followed by the temperature rise from 300 °C to 650 °C at the rate of 25 °C/minute during oxidation. The whole heating process took about 25 minutes, followed by cooling the oven at 650 °C for 20 minutes. The other key parametres used for evaluating source rock potential were calculated from the values obtained from pyrolysis and oxidation processes. These parametres are hydrogen index (HI), oxygen index (OI) and production index (PI).

## 3.4 Results of sedimentary facies analysis

Sedimentary facies have been grouped into four facies associations i) lacustrine, ii) delta front, iii) meandering alluvial/delta plain, and iv) mire (Table 3.1) with the fifth conglomeratic alluvial fan-fan delta facies association already covered in Chapter 2. There were two purposes for conducting a detailed analysis of sedimentary facies. One was to develop better palaeogeographic reconstructions, with an emphasis on carbonaceous lacustrine facies, and how those changed through time. A secondary purpose was to adequately assign 'transitional lithosomes' to lacustrine or meandering alluvial environments in order to better understand the distribution of possible lacustrine source rocks in the Greymouth Basin.

### 3.4.1 Lacustrine facies association

The lacustrine facies association is made up of all subaqueous facies. Three subaqueous facies are identified: the lacustrine massive mudstone facies, the lacustrine mudstones with minor sandstone facies, and the sandy turbidites facies.

#### *3.4.1.1 Massive mudstone facies*

*Description:* The massive mudstone facies is generally massive and structureless (Figure 3.5 A). It consists primarily of highly carbonaceous, grey to black mudstone/silty mudstone with occasional purple or brown colouring. Pyrites and tuff bands are rarely present in this facies. Small leaves and freshwater fossils may be locally abundant (Figure 3.5 B and 3.5 C) but no roots are found. Freshwater molluscs from *Hyridella* species and pollen from Nothofagus (southern beech) species were identified by Gage (1952) and Ward (1997). This facies shows uniform high gamma-ray response. It is widely distributed throughout the Greymouth Basin and is easily identified both in outcrop and drill core (Figure 3.6). The facies is commonly associated with the mudstone with minor thin sandstones facies and sandy turbidites facies.

*Interpretations:* The massive mudstone facies is interpreted to have been deposited in the deep water of a freshwater lake characterized by fine-grained, relatively slow sedimentation from suspension beyond the

direct influence of shoreline or deltaic processes (e.g. Anadon et al. 1991; Renaut and Gierlowski-Kordesch 2010). More recent research indicates that thick mudstones may form from muddy hyperpycnal flows loaded by turbulent suspension of silt and clay resulting in with erosional bases (Plint 2014, Zavala 2018), suggesting that the lake shore may have been closer than originally interpreted. The tuff bands found in this facies most likely fell directly on the water surface and settled to the bottom. The presence of pyrite indicates an anoxic environment and may have been formed by early diagenetic alteration within pore fluids at a shallow burial depth (Wells 1995). The *Hyridella* species molluscan fossils found in this facies indicate deposition occurred in a freshwater setting (Marshall et al. 2014). The presence of leaf fossils of genus *Banksiaeformis* and pollen such as *Nothofagus* suggests that the Late Cretaceous had an environment quite similar to that of New Zealand today (Hill and Christophel 1988; Ward 1997; Kennedy 2003; Raine et.al. 2017). The absence of roots indicates that deposition took place in deep water.

Table 3. 1: List of different facies association and their associated lithofacies of the Paparoa Formation

| **Facies association** | **Lithofacies** |
|---|---|
| Lacustrine | Massive mudstone facies |
| | Mudstone with minor sandstone facies |
| | Sandy turbidite facies |
| Delta front | Sandy mouthbar facies |
| | Interdistributary bay facies |
| Meandering alluvial/delta plain | Meandering channel facies |
| | Abandoned channel facies |
| | Crevasse splay facies |
| Mires | Mire coal facies |
| | Low lying marshy swamp facies |

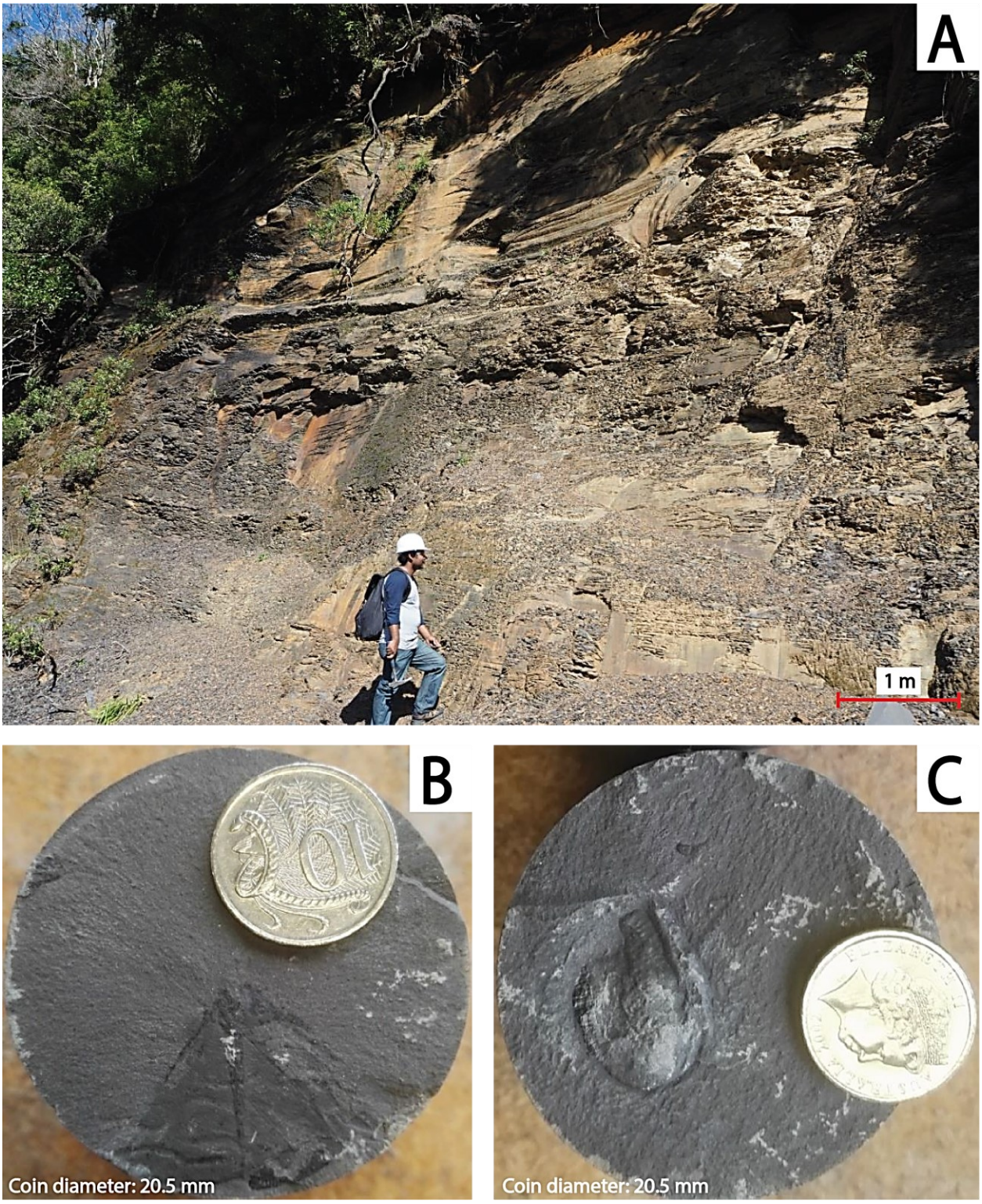


Figure 3. 5: A) Massive mudstone facies of the Goldlight Member at Spring Creek Mine (Seven Mile Stream), and B) leaf fossils at 289.65m and C) fresh water molluscs fossils at 293.98m in DH-624.

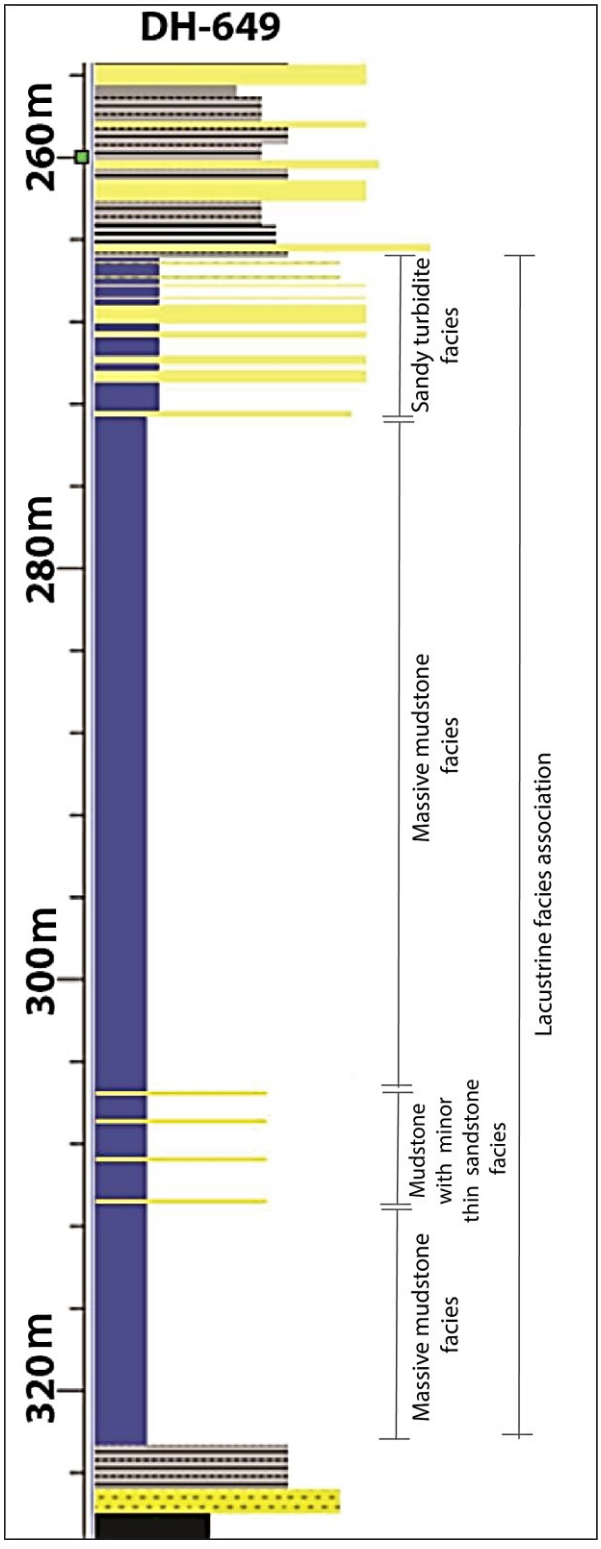


Figure 3. 6: DH-649 showing lacustrine facies association with massive mudstone facies, mudstone with minor thin sandstone facies and sandy turbidites facies.

#### *3.4.1.2 Mudstones with minor thin sandstone facies*

*Description:* The mudstone with minor thin sandstone facies is characterized by carbonaceous mudstones interbedded with thin, brownish grey, fine sandstone and siltstone beds (10% sandstone/siltstone, 90% mudstone) (Figure 3.6 and Figure 3.7). Mudstones are light grey, purple or brown in colour and mostly 6-8 m thick. Interbedded siltstone beds are grey to dark grey and are less than 1 cm thick. Interbedded fine sandstone beds are normally graded with hints of ripple cross-laminations and are less than 3 cm thick. Coarse sandstones are occasionally found. Basal contacts of the thin sandstone or siltstone beds are commonly erosional or sometimes wavy and sharp. The upper contacts are slightly gradational with overlying mudstones. Conspicuous plant debris (~10%) is common in fine-grained sandstone beds. Freshwater molluscs from *Hyridella* species (Gage 1952) and leaves of genus *Banksiaeformis* (Hill and Christophel 1988) are occasionally present. The facies exhibits sudden low gamma-ray spikes in the overall high gamma-ray response recording the presence of the sandstone beds in the mudstones. This facies varies in thickness and can be found in both outcrops and drill cores. This facies is found in the centre of the basin and commonly associated with lacustrine massive mudstone facies.

*Interpretations:* The mudstone with minor thin sandstone facies is interpreted to have been deposited in a lake within the influence of irregular and rare turbidity currents. The fresh water fossils indicate a lacustrine rather than marine setting. The presence of normally graded beds with erosive or sharp bases, conspicuous plant debris, and faint ripples indicates deposition by turbidity currents (e.g. Basilici 1997; Boggs 2006; Sturm and Matter 2009). The turbidite beds likely resulted from exceptional river discharges which could deliver coarser sediments and reworked plant debris and displaced snails and other micro-fossils into deeper water where the resultant deposits became intercalated with the predominant lacustrine muds from suspension settling and/or hyperpycnal underflows (e.g. Span et.al. 1992; Basilici 1997; Renaut and Gierlowski-Kordesch 2010, Plint 2014 and Zavala 2018).

#### *3.4.1.3 Sandy turbidites facies*

*Description:* The sandy turbidites facies comprises mudstones (60%) regularly interbedded with sandstones (30%) and siltstones (10%) (Figure 3.7 and Figure 3.8 A). Mudstones are dark grey to brown, sandy to silty with occasional leaf fossils and minor bioturbation. Mudstone beds range in thickness between 60 cm and 8 m. Mudstones look similar to those of the lacustrine massive mudstone facies and lacustrine mudstone with minor thin sandstone facies except the presence of bioturbation and sandy to silty nature distinguish it from other lacustrine mudstones. Sandstone beds are grey, fine to medium grained, normally graded, and range in thickness from thick (~20 cm - 2 m) to thin (5 – 10 cm). Conspicuous fine plant debris (~10%) is common in fine-grained sandstone beds although coarse plant fragments are rare and roots are absent. Siltstone beds are grey to dark grey and range in thickness between 20 cm and 50 cm. Soft sediment deformation structures such as load casts are common in the siltstone and sandstone beds (Figure 3.8 B and 3.8 C). The presence of soft sediment deformation structures and relatively thicker sandstone beds distinguishes this facies from the lacustrine mudstones with minor thin sandstones facies. This facies shows a serrated pattern in the gamma-ray log. It is only found in drill cores and is primarily located in the eastern and northwestern parts of the basin. This facies is commonly associated with lacustrine massive mudstone facies.

*Interpretations:* The facies is interpreted to have been deposited in a lacustrine environment that was more proximal to the shoreline, probably in the prodelta region, where sedimentation rate was high and turbidity currents were common. These turbidite beds mostly belong to divisions C and D of the Bouma sequence

model. Mudstones and siltstones indicate sedimentation mainly from suspension and/or hyperpycnal underflows between turbidity current events (e.g. Renaut and Gierlowski-Kordesch 2010, Plint 2014 and Zavala 2018). Conspicuous plant debris was transported by the turbidity currents (e.g. Kelts 1988). The soft sediment deformation structures were likely caused by density differences or fluid escape in water-saturated unconsolidated sediments at the top of a slope such as in the prodelta environment (Bhattacharya 2010; Topal and Ozkul 2014).

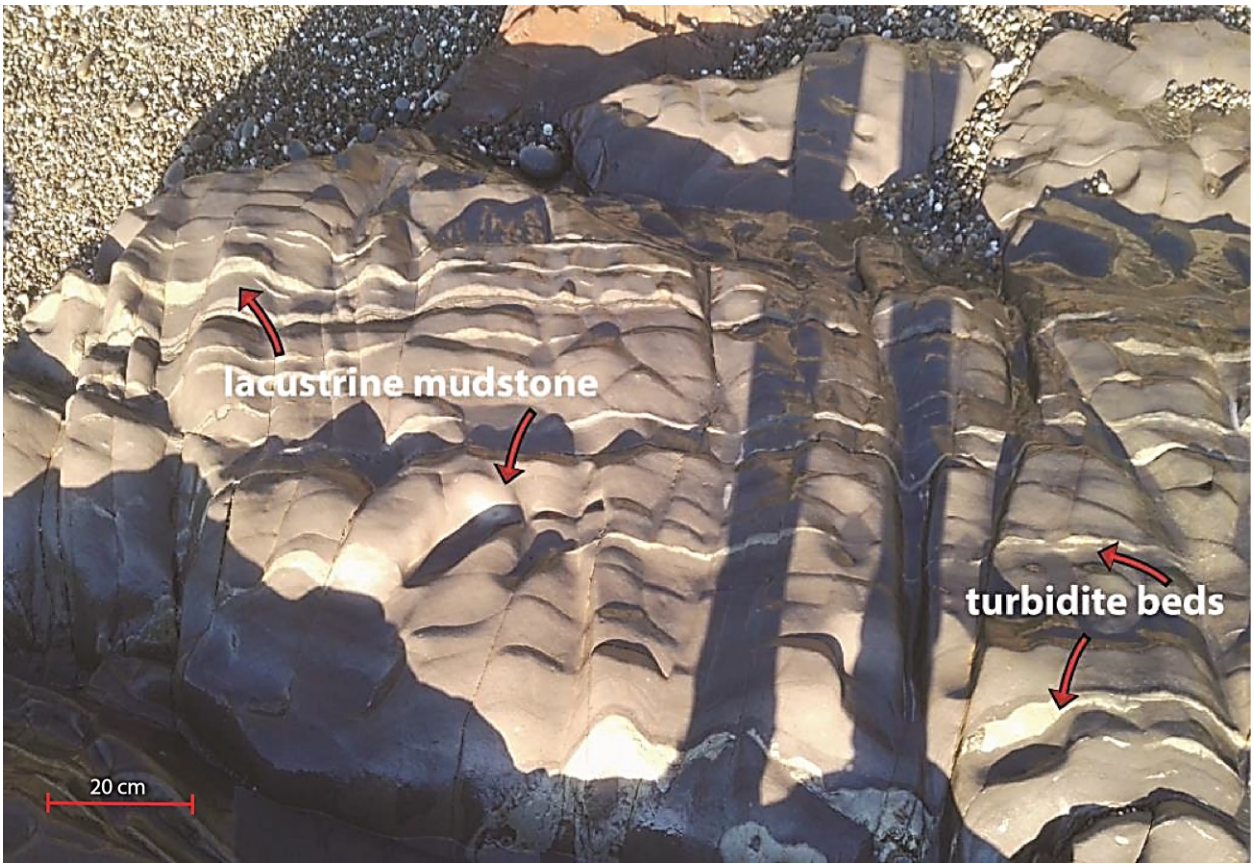


Figure 3. 7: Mudstone with minor thin sandstone facies of the Waiomo Member at Twelve Mile Beach.

### 3.4.2 Delta front facies association

Two facies are identified in the delta front facies association, the sandy mouthbar facies and the interdistributary bay facies.

#### *3.4.2.1 Sandy mouthbar facies*

*Description:* The sandy mouthbar facies is characterized by thick, grey, coarsening and thickening upwards, fine to medium grained, sandstone beds (Figure 3.9A and Figure 3.9B). The sandstone beds are reversely graded with cross-laminations preserved in some locations. Coarse woody material (~10%) can be found in some places which has been altered to coaly fragments. There is no bioturbation and no roots present. Beds range from 30 cm to 10 m thick and show distinct channel shapes. The coarsening upward sequences are easily identifiable in gamma ray logs. The facies is mostly distributed in the eastern, central and some places of the northwestern parts of the basin. It is commonly overlain by meandering alluvial facies

association on delta plain environments and commonly underlain by sandy turbidites facies and rarely by the lacustrine massive mudstone facies. This facies can be identified in both outcrops and drill core.

*Interpretations:* This facies is interpreted to have been deposited in a delta front at the mouth of a river channel where it enters the low energy lake. Sandy mouthbar facies predominantly reflect deposition from rapidly decelerating unidirectional flows in distributary mouthbar environments (e.g. Reading 2009; Collinson and Lewin 2009). Reverse grading within sandstone beds combined with thickening of these beds up sequence is indicative of a prograding mouth bar environment in an alluvially dominated delta where channel enters a lake and dumps the bed load at the mouth of the channel (e.g. Makaske et al. 2002; Jones and Hajek 2007; Bhattacharya 2010).

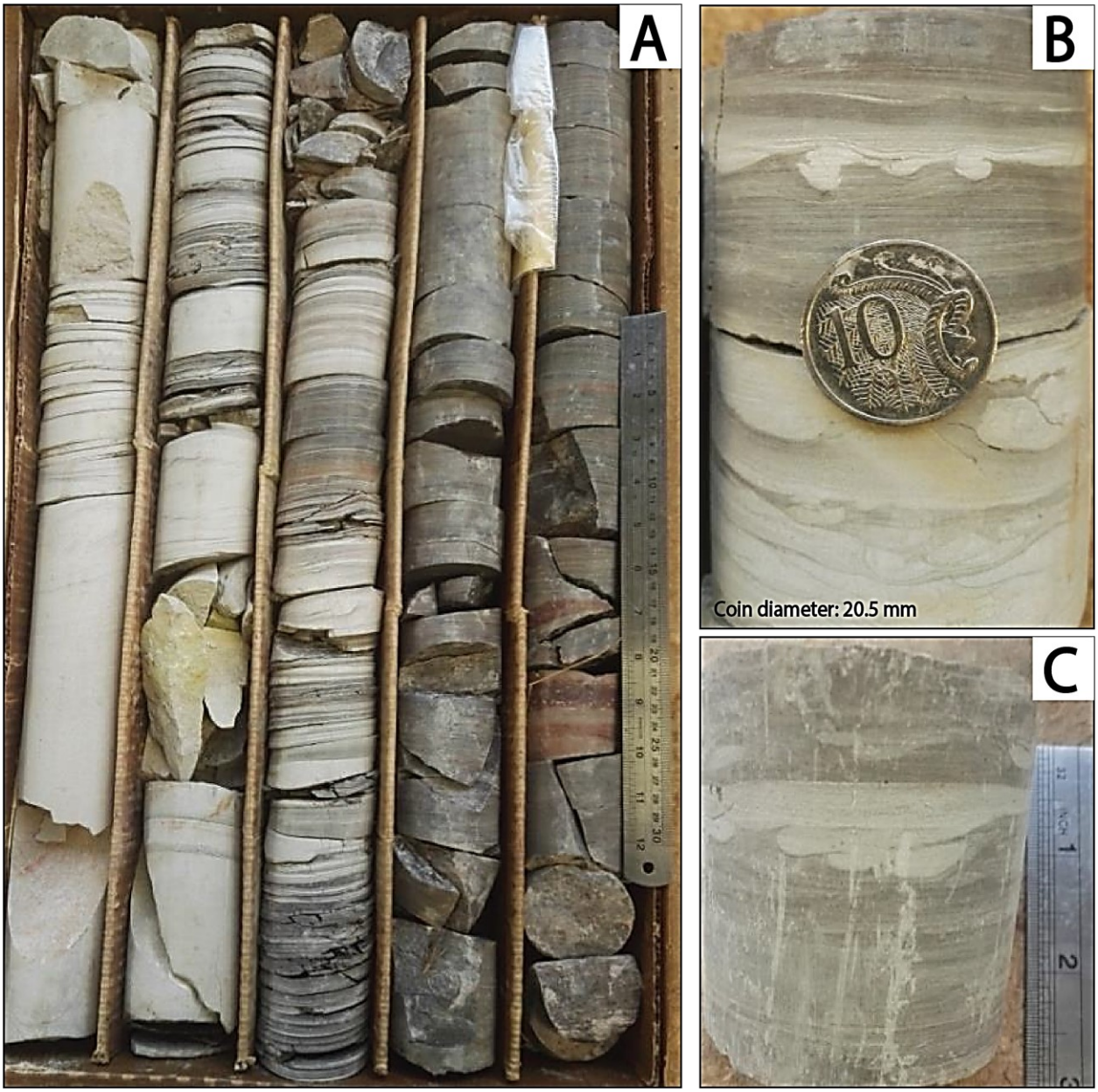


Figure 3. 8: A) Sandy turbidites facies from 275m to 278m in DH-624; Soft sediment structures found in DH-624, B) ripple marks and load casts at 261.80m; C) load casts at 261.98m.

#### *3.4.2.2 Interdistributary bay facies*

*Description:* The interdistributary bay facies is characterized by mudstones and siltstones (80%) with occasional beds of sandstones (20%) (Figure 3.10). Mudstones and siltstones are moderately to weakly carbonaceous, lack leaf fossils, and are moderately to highly bioturbated. Sandstones are grey, very fine to fine grained, and carbonaceous in some places. Sandstone beds lack erosional bases, lack normal grading, and occasionally contain faint current ripple cross-lamination. Carbonaceous sandstones are found in some places. Rootlets are absent but coaly stringers are present (Figure 3.10). Isolated granule and pebble clasts are found in some places. The thickness of this facies ranges from ~70 cm to 4.5 m. In the vertical succession, the facies is commonly associated with the sandy mouthbar facies in the east and the southeast or with the gravelly mouthbar facies in the northwest (Chapter 2). An overall decrease upward in several gamma ray logs is interpreted as coarsening upward cycles, consistent with an association with mouthbar facies.

*Interpretations:* This facies is interpreted to have been deposited in interdistributary bays between channels in the delta frontregionof sandy/muddy low gradient deltas. Sedimentation occurred from settling of suspended fine-grained sediments and organic matter as indicated by the well laminated carbonaceous mudstones and siltstones (e.g. Tye and Kosters 1986). The lack of normal grading in the sandstone beds indicates that sedimentation either didn't take place from turbidity currents or the grain sizes were thoroughly mixed by the more pervasive bioturbation. The association with mouthbar facies indicates close proximity to an active river mouth where channel avulsion was common in a deltaic environment, low-gradient to the southeast and high gradient to the northwest (e.g. Makaske et al. 2002). The overall coarsening upward sequence indicates that deposition took place in the delta front region.

### 3.4.3 Meandering alluvial/delta plain facies association

The meandering alluvial/delta plain facies association includes meandering channel facies, abandoned channel facies and crevasse splay facies.

#### *3.4.3.1 Meandering channel facies*

*Description:* The meandering channel facies is composed of grey to light grey, moderately to well sorted, fine to medium grained sandstones. Occasional granule to pebble conglomerates and coarse to very coarse sandstones are present in some places. The sandstone units range from thick (~1-7.5 m) to thin (~10 cm -1 m) and show distinct channel shapes. Basal scours are found in most of the channels. Coarse coaly fragments and other plant material (~5-10%) are also present. Crossbedding structures are very common in this facies and are well preserved in outcrops and drill cores (Figure 3.11A, 3.11B and 3.11C). In some places, lateral accretion structures can be seen. In gamma ray log, this facies shows multiple fining upward trends as this facies is commonly associated with overlying abandoned channel facies and crevasse splay facies (Figure 3.12 and Figure 3.13). The meandering channel facies is mainly found in the central, eastern and southwestern parts of the Greymouth Basin.

*Interpretations:* This facies is interpreted to have been deposited in channels in an alluvial environment where unidirectional current flow was the dominant depositional process as indicated by cross-bedding. The thick sandstone units are interpreted to have been deposited from continuous but variable flow in a river channel. The distinct channel shapes with basal scours and lag deposits, the presence of crossbeds and lateral accretion beds, and overall fining upward sequences indicate meandering channel deposits (Reading 2009; Miall 2010). The meandering channel facies was deposited in both delta plain settings

when lakes were present in the basin and on alluvial plains when there were no lakes or the lakeshore was more distal.

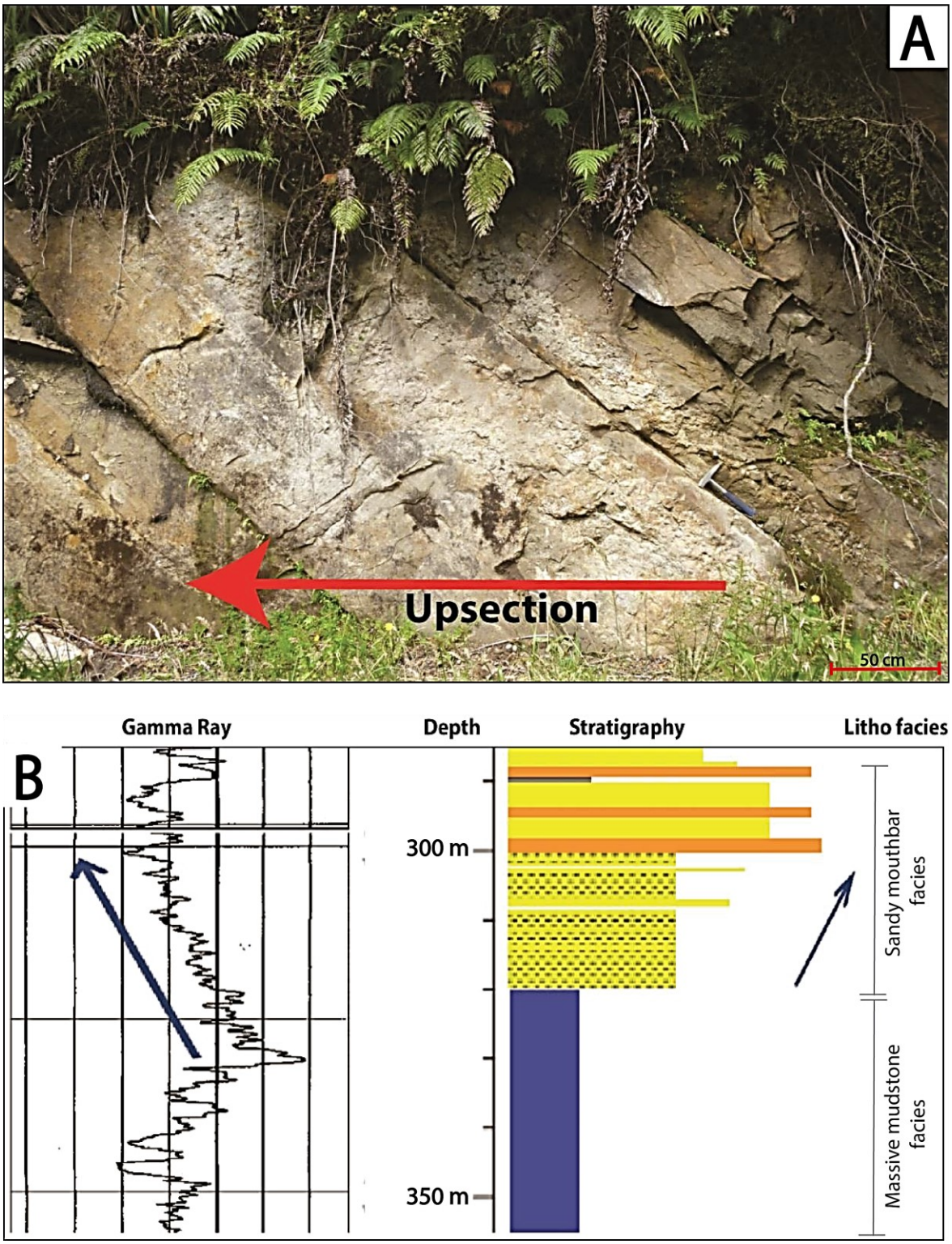


Figure 3. 9: Sandy mouthbar facies A) reverse graded sandstone beds within the Goldlight Member at Ten Mile Creek; B) coarsening upwards sandstone beds in DH-656.


Figure 3. 10: Interdistributary bay facies at Twelve Mile Beach showing bioturbation from burrows in sandstone and siltstones.


Figure 3. 11: A) alternating meandering channel with hints of cross-beds and abandoned channel facies of the Rewanui Member are found inside the tunnel section at Seven Mile Creek Road (modified from Davies 2019), B) cross bedding structure in meandering channel from the lower part of the tunnel section at Seven Mile Creek Road, C) core from DH-637 showing cross lamination in a meandering channel fill are found at 271.3 m in DH-637.

#### *3.4.3.2 Abandoned channel facies*

*Description:* The abandoned channel facies consists of muddy sandstones (20%) with silty carbonaceous mudstone to highly carbonaceous mudstone (50%) fining up to muddy coals at the top (30%) (Figure 3.12 and Figure 3.13). This facies occurs in channel shape lenses. Sandstones are very fine grained and the bed thickness ranges between 20 cm and 3 m. The carbonaceous mudstone beds range from a minimum 20 cm to maximum 2 m. Coals are high in ash content and coal beds range from minimum 40 cm to maximum 1 m. Occasional thin beds of fine sandstones may be present in the mudstones. Rootlets are common in this facies. This facies shows a fining upward nature in the gamma ray log. The coal beds show a positive spike in the density log. The facies commonly overlies the sandy meandering channel facies. The abandoned channel facies is mainly found in the central, eastern and southwestern parts of the Greymouth Basin.

*Interpretations:* This facies is interpreted to have been deposited in abandoned channels which were once the main channel in a meandering river. After abandonment the channel remained as an oxbow lake or a wetland for a substantial length of time as indicated by the presence of muddy sandstones at the bottom and carbonaceous mudstones or muddy coals at the top. Channel abandonment is a common process in meandering alluvial systems and results from channel shifting processes such as meander cut-off and channel-belt avulsion (Slingerland and Smith 2003; Miall 2010; Toonen et. al., 2012). The presence of laminated carbonaceous mudstone suggests slow sedimentation where the organic material is mixed with mud and deposited. Occasional thin beds of sandstone indicate periodic flood events (Bridge 1984; O'Brien and Wells 1986). High ash content indicates episodic input of clastic sediments into the swamps or oxbow lakes from river flooding. The presence of coals indicates the balance among sediment supply, basin subsidence rate and rate of decomposition of the organic matter. Slow decomposition rate of the organic matter retains most of its carbon, suggesting its potentiality as petroleum source rocks. This facies is common in the interpreted delta plain when lakes were present in the basin as well as in non-deltaic alluvial environments when there were no lakes in the basin.

#### *3.4.3.3 Crevasse splay facies*

*Description:* The crevasse splay facies comprises inversely to normally graded, medium to fine sandstone beds (~40-50%) interbedded with laminated silty mudstone to carbonaceous mudstones (~30-40%) with abundant plant material and rootlets (~10-20%) (Figure 3.14A). Sandstones are grey to light grey in colour and contain occasional small cross-beds and ripple marks. Basal scours with underlying beds are not very common but are found in some localities. The individual beds range in thickness from 1 cm to 10 cm thick. However, gross thicknesses of crevasse splay facies ranges from minimum 10 m to maximum 35 m when associated with other floodplain facies. The facies shows coarsening to fining upwards trends in gamma ray logs (Figure 3.12, Figure 3.13 and Figure 3.14B). The facies is commonly overlain and underlain by meandering channel facies and abandoned channel facies, and is mostly found in the central and the eastern sides of the basin.

*Interpretations:* The facies is interpreted to have been deposited on a floodplain in close proximity to an active channel where excess discharge during flooding incises the adjacent levee and deposits as a splay (e.g. Allen 1965; Elliott 1974; Guion 1985). The sandstone beds are interpreted as channelized crevasse splays whereas laminated mudstone and siltstones are interpreted as flood plain deposits (e.g. Bridge 1984). Basal scours indicate the sandstones were deposited from flood events (e.g. O'Brien and Wells 1986). Mudstones and siltstones were deposited from sediment settling when the flooding ceased and water remained stagnant in small depressions for a long time. Coarsening upwards sequences are the product of

levee or splay prograding into the flood basin areas whereas fining upward sequences are produced by abandonment of individual crevasse channel (e.g. Bridge 1984). The association of sandy meandering channel facies over- and under-lying this facies may indicate that the avulsion of a meandering channel was a common process in the Greymouth Basin (e.g. Slingerland and Smith 2003). This facies was deposited in both deltaic and non-deltaic settings when there were lakes in the basin and there were no lakes in the basin, respectively.

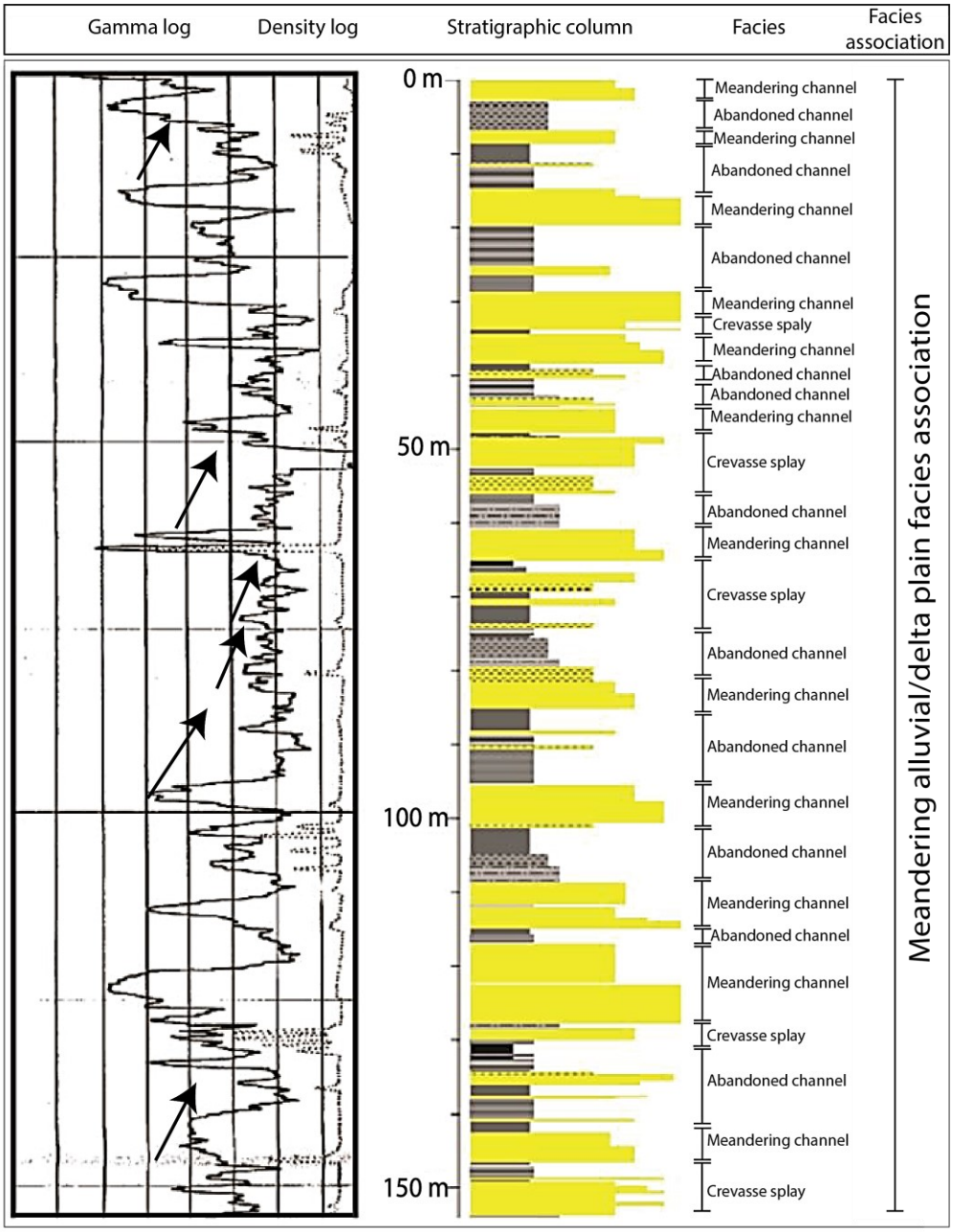


Figure 3. 12: Thick deposits of alternating meandering channel, abandoned channel and crevasse splay facies of meandering alluvial/delta plain facies association of the Rewanui Member are found in DH-658. Meandering channel and abandoned channel facies are showing fining upward trends in gamma ray log whereas coarsening to fining upwards trends are representing crevasse splay facies.

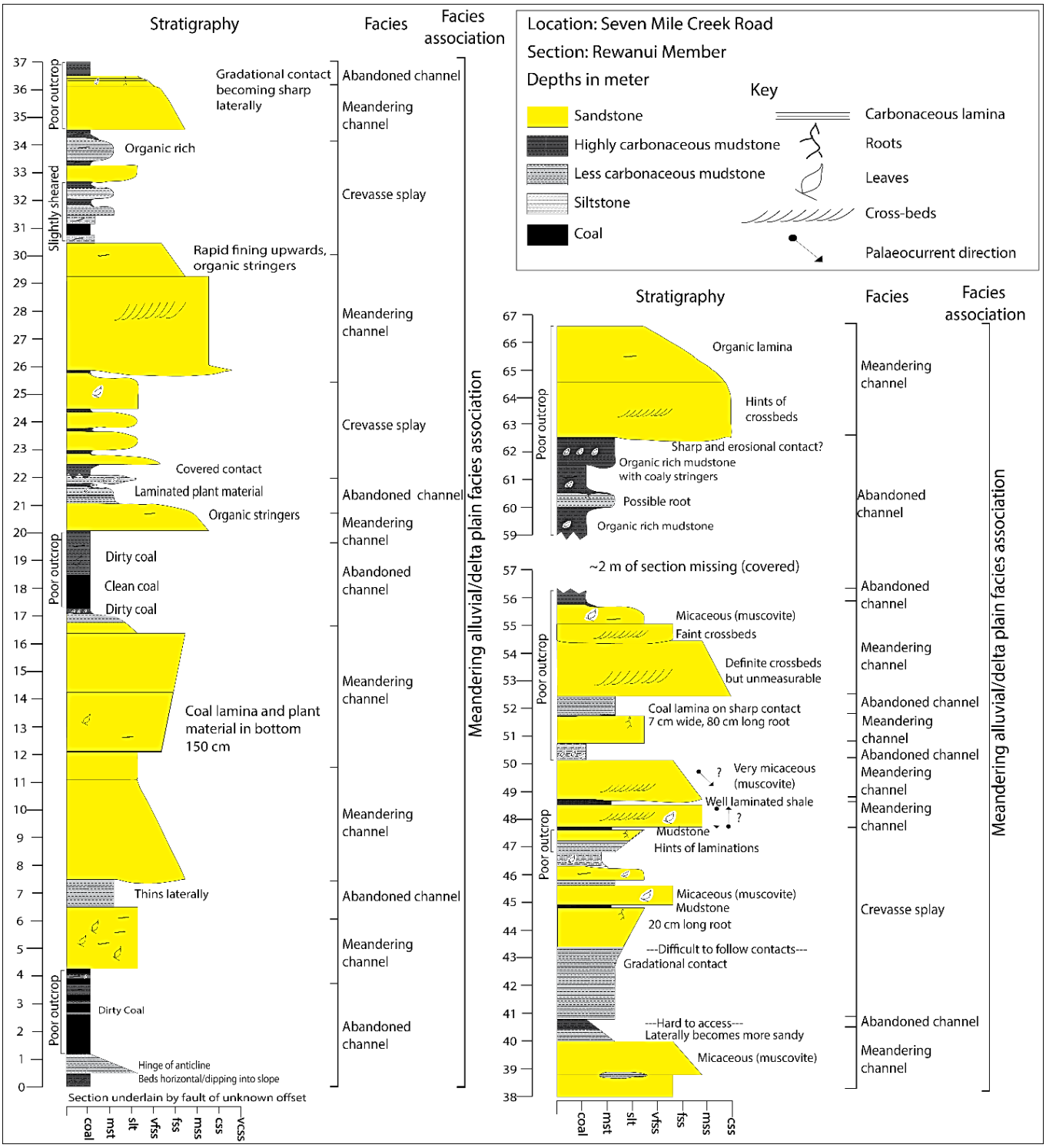


Figure 3. 13: An axial meandering and floodplain system of the Rewanui Member shows alternating meandering channel, abandoned channel and crevasse splay facies of meandering alluvial/delta plain facies association at the Seven Mile Creek road cut section (modified from Davies 2019). Channel sandstones exhibit hints of cross-beds with mostly southerly palaeoflow directions.

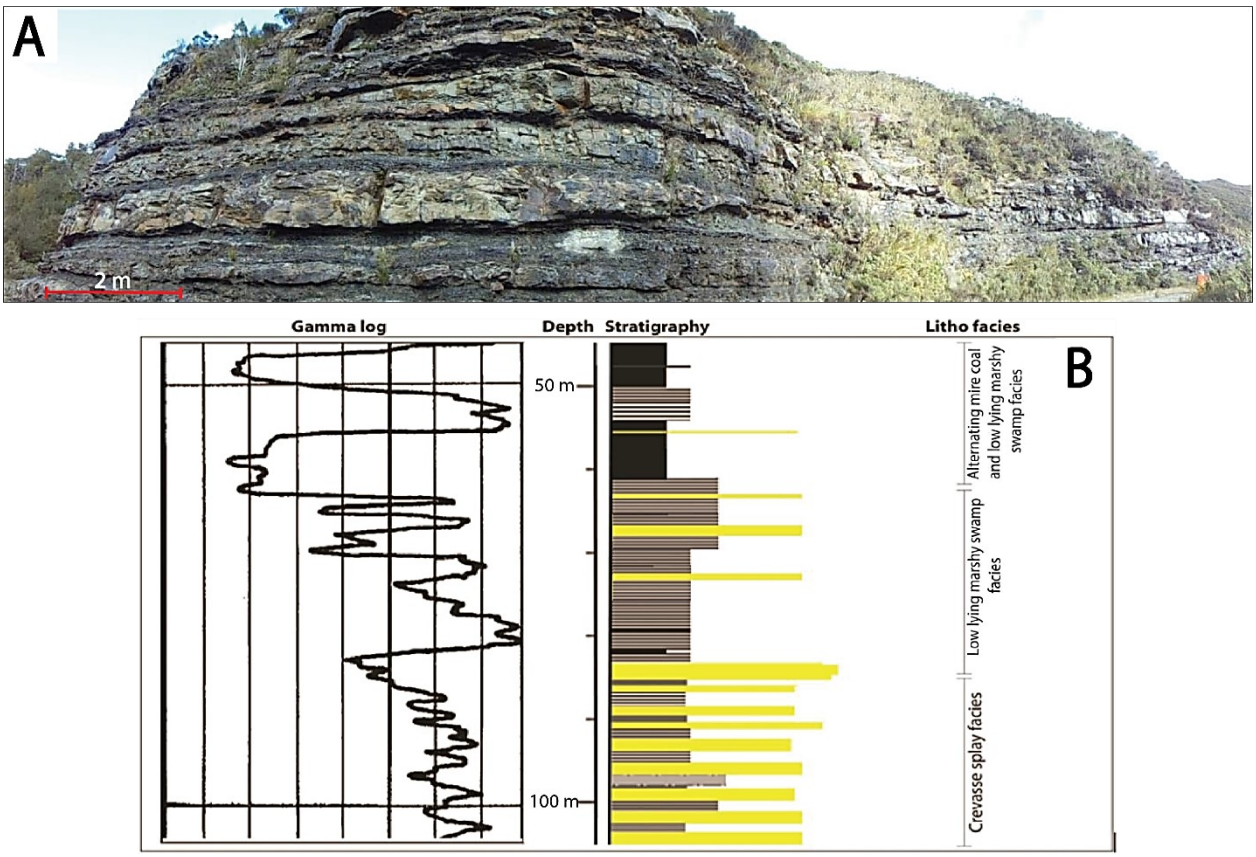


Figure 3. 14: A) Crevasse splay facies at Spring Creek Haul Road, and B) Gamma log showing crevasse splay facies with coarsening and finning upward sequences in DH-656.

### 3.4.4 Mire facies association

The mire facies association includes the mire coal facies and the low-lying marshy swamp facies. In the basin axis, this facies association is found in the upper part of each alluvial member (Jay, Morgan, Rewanui and Dunollie).

#### *3.4.4.1 Mire coal facies*

*Description:* The mire coal facies comprises two subfacies; the first is characterized by black, hard, thick, and clean coals (Figure 3.15A) whereas the second is characterised by alternating bands of clean coals and muddy/dirty coals. The thick clean coals are low in ash and sulphur content. The thick coal seams are typically up to 11 m thick (range 3m-11m) and are lenticular in shape, most having a maximum lateral extent of about 1.5 km (Edbrooke 2000). The clean coal exhibits a uniform nature both in gamma and bulk density logs (Figure 3.15B). The alternating bands of clean and muddy coals show high ash content and low to moderate sulphur values. Pebble layers and isolated pebbles are common. The thicknesses of the alternating clean/muddy coals range from a minimum of 20 cm to a maximum of 3 m. They exhibit a discrete nature in the gamma ray log and a positive spike in the density log (Figure 3.15B). Both subfacies are commonly associated with low lying marshy swamp facies and meandering floodplain facies. The facies is mostly distributed in the basin centre.

*Interpretations:* The facies is interpreted to have been deposited in mire environments where the drainage systems are poorly developed, inhibited by vegetation, and so the clastic input is very low (e.g. Diessel

1992). The very low sediment supply and low bacterial decomposition helps to preserve the organic material in the mire which, upon burial, becomes thick clean coals. The low ash and low sulphur contents of the thick coals indicate they were probably deposited in raised mire conditions where rainfall exceeded evaporation and organic growth was rapid (McCabe 1984; Moore 1987). In addition, rain water is poor in sulphate, is naturally oxygenated, and has low pH (< 7) which reduces sulphate bacteria and thus inhibits bacterial activity resulting in the low sulphur content of this facies (e.g. Casagrande 1987; Gruber and Sachsenhofer 2001). The lack of a detrital influx during flood events, as indicated by the low ash content, probably requires a mire to be raised topographically above the floodplain (e.g. Gruber and Sachsenhofer 2001). The abundance of high ash in the alternating clean and muddy coals indicates that deposition took place in a topographically lower floodplain environment, probably in a low-lying mire setting where minor, low energy, distributary channels brought in sediment during flood events. The presence of pebble layers and isolated pebbles are an indication of larger flood events. The low to moderate sulphur content in the alternating clean/muddy coals suggests a fresh water environment (e.g. Sachsenhofer and Gruber 2001). The raised mire coal facies commonly grades laterally as well as vertically into low lying mire coal facies (McCabe 1984; Moore 1987; Diessel 1992).

#### *3.4.4.2 Low-lying marshy swamp facies*

*Description:* The low-lying marshy swamp facies usually comprises low to high carbonaceous mudstones (~40%), interlaminated with variably carbonaceous siltstones and mudstones (~40%) with abundant roots, twigs and other plant remains (~20%) (Figure 3.13B, Figure 3.16A and Figure 3.16B). Thin beds of carbonaceous, muddy, very fine-grained sandstone are occasionally present. Bioturbation from burrows is common. Laminations are distorted mostly by plant roots and bioturbation (Figure 3.16B). The thickness of this facies ranges from a minimum of 5m to a maximum of 30 m. In general, it shows relatively higher values in the gamma ray log than clean coals because of the presence of fine-grained mudstones and siltstones. This facies also shows serrated nature in gamma ray log because of its association with alternating bands of thin coal beds. In most drill holes, this facies is interbedded with the mire coal facies and may be underlain by the mire coal facies and overlain by the lacustrine massive mudstone facies. The facies is distributed in the centre and the northeastern side of the basin but is more common in the basin centre.

*Interpretations:* This facies is interpreted to have been deposited in wet and low energy areas, probably in a low-lying mire setting in a lower delta plain or along a lake shore. This facies also deposited in low lying areas in a non-deltaic setting. Water depth in these low-lying areas was extremely shallow and marshy (e.g. Coleman et al. 1964). The laminations of carbonaceous mudstones and siltstones indicate a low energy environment where deposition mainly occurred from the settlement of suspended fine-grained clastic material and plant remains. The extremely shallow, marshy environment was favourable for growing vegetation as indicated by the presence of abundant roots. The presence of bioturbation suggests that oxygen levels were high enough to favour the development of burrows (e.g. Bann et al. 2008). The rarity of sandy clastic sediments indicates that the facies was deposited away from an active river system.

## 3.5 Distribution of sedimentary facies

The fence diagram (Figure 3.17) illustrates the distribution of sedimentary facies across the Greymouth Basin. In the basin's centre, sedimentary facies alternate between lacustrine / shoreline facies associations, corresponding to the lacustrine members (Ford, Waiomo, and Goldlight), and meandering alluvial / mire facies associations, corresponding to the coal-bearing members (Jay, Morgan, Rewanui, and Dunollie). The

margins of the basin contain only meandering alluvial and fan delta/alluvial fan facies associations (Chapter 2) of the coal-bearing members (Jay, Morgan, Rewanui, and Dunollie).

During deposition of the lacustrine members, thick deposits of the lacustrine facies association were formed in the centre of the basin comprising the lacustrine massive mudstone facies and the lacustrine mudstones with minor thin sandstones facies grading laterally to the shallower water sandy turbidites facies. Shorelines are indicated by the presence of deltaic sandy mouthbar facies and interdistributary bay facies as well as low lying marshy swamp facies. The northwestern side of the basin was dominated by fan delta facies (Chapter 2) whereas the southern and eastern sides of the basin were dominated by meandering alluvial delta plain facies association comprising meandering channel, abandoned channel, and crevasse splay facies.

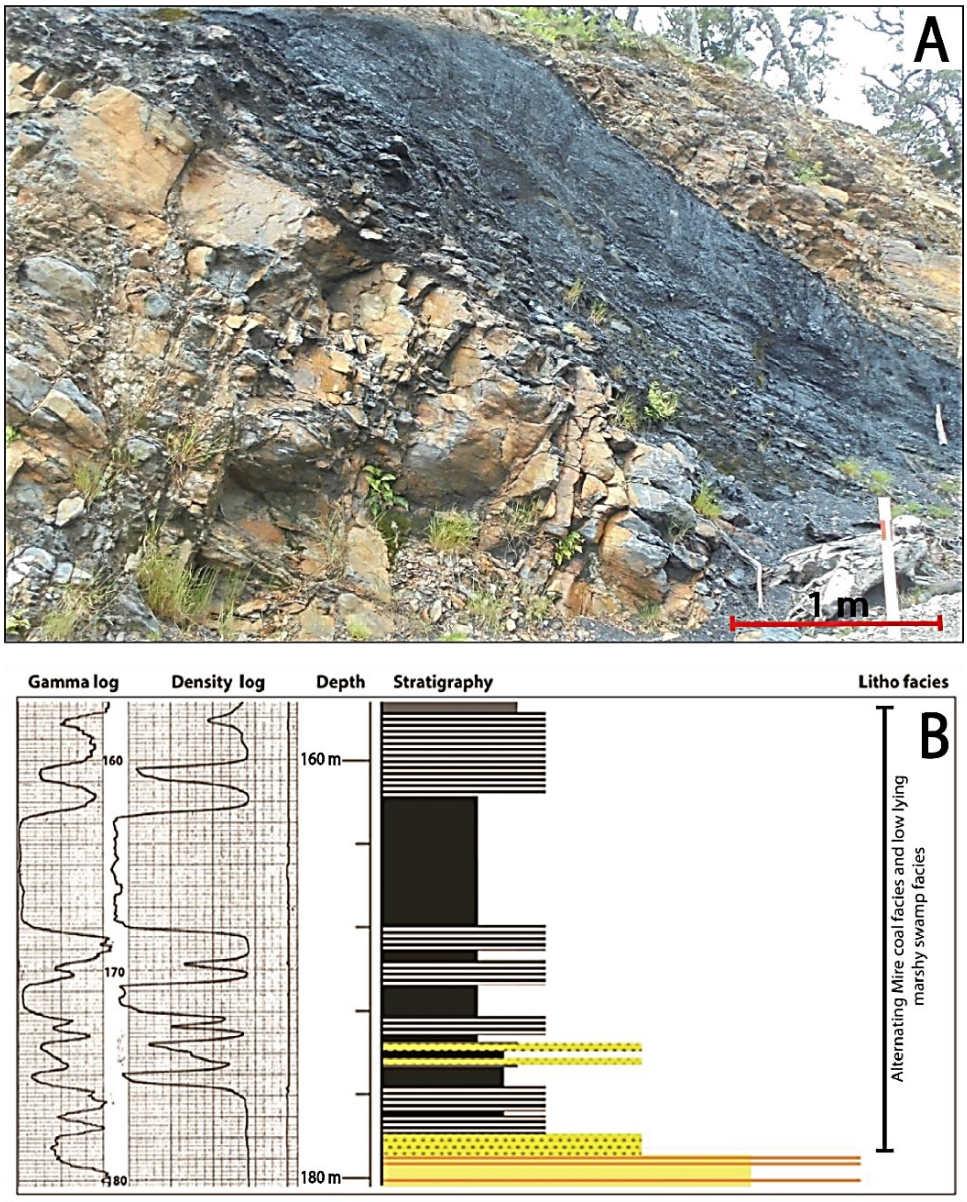


Figure 3. 15: A) Mire coal facies in the Rewanui Member at Roa Mine, B) mire coal facies and associated low lying marshy swamp facies in DH-624.

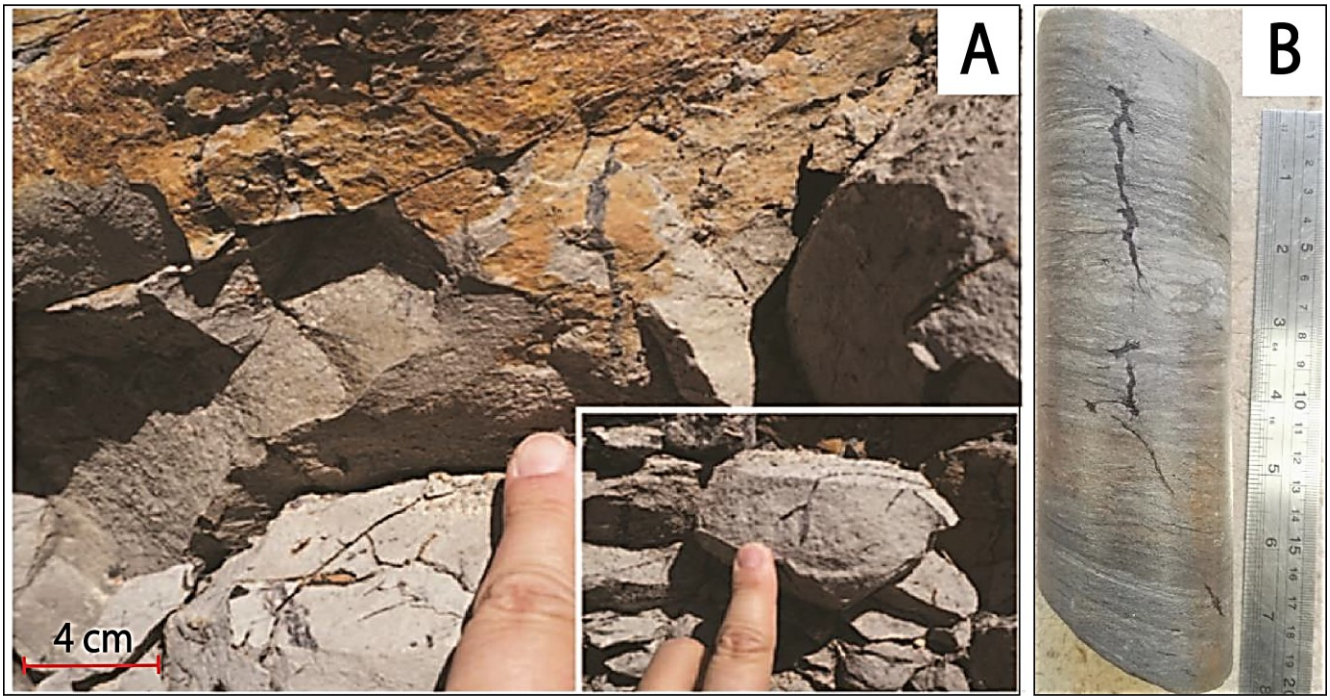


Figure 3. 16: A) Presence of roots and bioturbation in fine grained muddy sandstone in low lying marshy swamp facies at Spring Creek Haul Road, B) Presence of rootlets in laminated carbonaceous mudstone and siltstone in low lying marshy swamp facies at 54.16 m in DH-624.

During deposition of the coal-bearing alluvial members, the centre and southern side of the basin were dominated by the meandering alluvial facies association comprising meandering channel facies, abandoned channel facies and crevasse splay facies (Figure 3.12 and Figure 3.13). Palaeocurrent measurements on cross-beds from the meandering channel facies show palaeoflow was to the south-southwest (Figure 3.13; Davies 2019). The eastern side of the basin was also dominated by the meandering alluvial facies association. The northwestern side of the basin was dominated by the alluvial fan facies association indicating steep topography from the uplifted fault scarp (Chapter 2).

During the transitions from lacustrine to alluvial members, mire coal facies and low-lying marshy swamp facies commonly replaced the lacustrine massive mudstone facies in the centre of the basin. In most places, low-lying marshy swamp facies overlies thick lacustrine facies association. The opposite happened during transitions from alluvial to lacustrine members; the mire facies association is overlain by the lacustrine massive mudstone facies in the centre of the basin.

## 3.6 Interpretation of palaeogeography

The deposition of the thickest alluvial fan and fan delta conglomerate facies on the northwest side of the basin indicates a steep topography in the northwest, most likely fault-controlled (Chapter 2). The lacustrine massive mudstone facies in the basin centre indicates the presence of lakes. The meandering alluvial/delta plain facies association dominates the southeastern margin of the basin indicating a landscape of sandy to muddy meandering river deltas formed on a low gradient topographic slope. Meandering alluvial deltas also would have entered the lakes from the southwest and northeast delineating the overall size of the lakes. The lacustrine mudstones were thickest in the basin centre and onlap fan delta conglomerates and

meandering alluvial delta sandstones as lakes gradually expanded during maximum flooding during deposition of the lacustrine members.

The meandering alluvial facies association periodically replaced the lacustrine facies association in the basin's centre with palaeo-flow parallel to the fault controlled steep topography indicating an axial meandering river and floodplain. Meandering alluvial facies association dominates the southeastern margin of the basin suggesting meandering river tributary systems that flowed from the southeast into an axial meandering river. Alluvial fan facies association dominates the northwestern margin of the basin indicating steep topography existed in that area. The presence of the mire facies association in the basin centre over- and under lying lacustrine mudstone facies association indicates the transition into or out of alluvial phases in the basin.

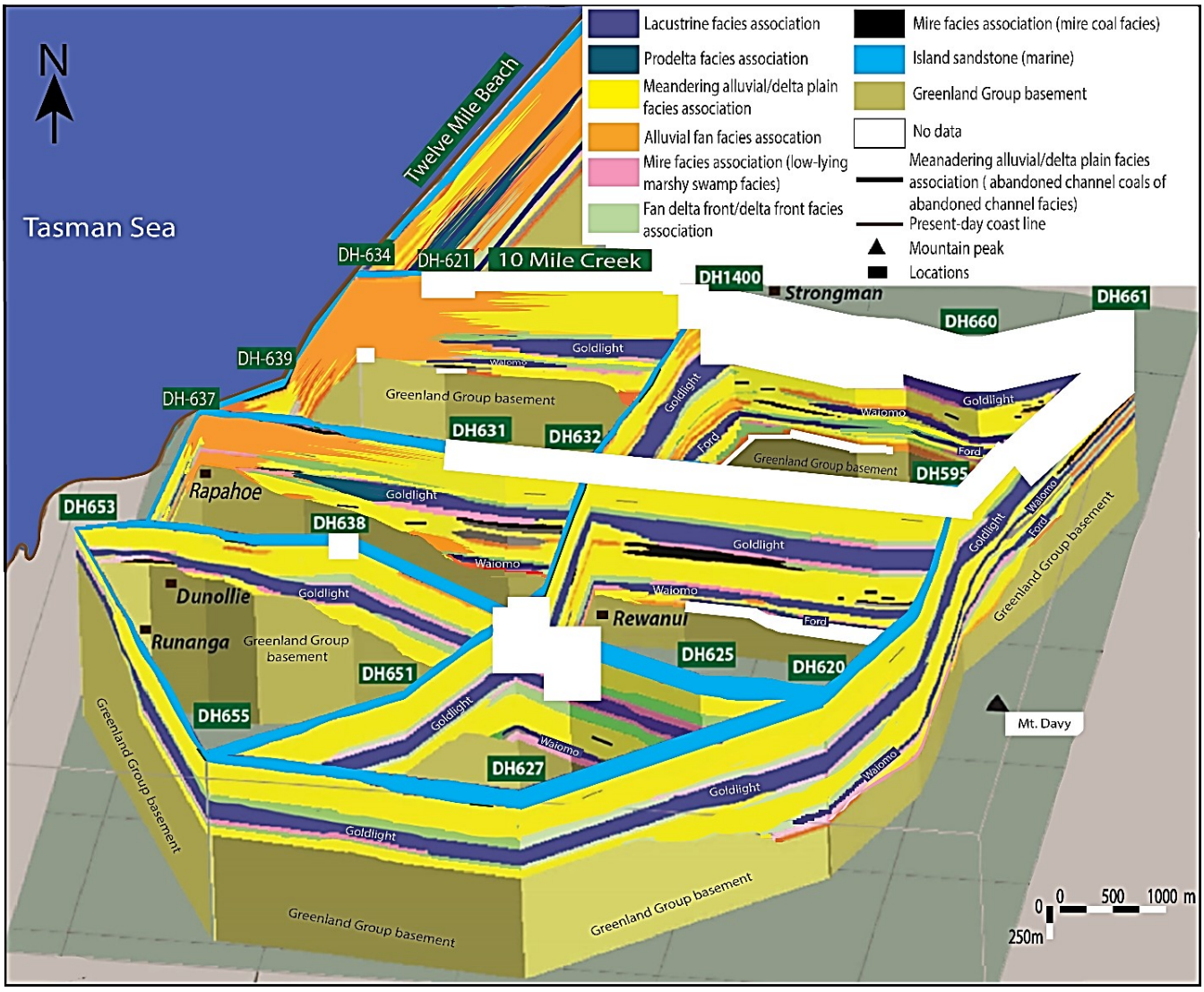


Figure 3. 17: Fence diagram illustrates the distribution of different sedimentary facies of three lacustrine mudstone and four coal-bearing members of the Paparoa Formation of the Greymouth Basin.

The sedimentary facies analysis indicates that shoreline and shallow water facies are more difficult to identify and categorize compared to the deep lacustrine organic facies as they show lateral complexities

when associated with other similar-looking subaerial facies. One of the important tasks in this chapter was to re-examine the "transitional lithosomes" defined by Ward (1997) in order to recognize and differentiate shoreline and subaqueous lacustrine facies. The transitional lithesomes were defined as "interbedded mudstones, siltstones and coarsening upward, fine to medium sandstones with soft sediment deformation structures, fresh water bivalve impressions, leaf fossils, fine detritus and rare thin carbonaceous mudstone beds" and interpreted as subaqueous lacustrine delta by Ward (1997). Detailed sedimentary facies analysis indicates that the "transitional lithosomes" as defined by Simon Ward (1997) are mostly of the sandy turbidites facies, sandy mouthbar facies, and interdistributary bay facies deposited in low gradient meandering river deltas, and low-lying marshy swamp facies deposited away from the deltas. The inclusion of the sandy turbidites facies as lacustrine facies will enlarge the volume of lacustrine facies association in the Greymouth Basin.

The palaeogeography of the Greymouth Basin can be compared with the landscape proposed in half-graben basin models (Model A and Model B) by Leeder and Gawthorpe (1987) (Figure 3.18). Model A represents a continental rift basin with fan deltas on the steep, fault-controlled side, lake in the basin axis, and low gradient, sandy, deltas fed by meandering rivers on the hinge side of the basin. When compared to the Greymouth Basin, the three lacustrine members (Ford, Waiomo, and Goldlight) were most likely deposited in this setting where the lacustrine facies association can be found in the basin axis indicating an asymmetric depo-centre, the correlative alluvial fan/fan-delta facies association during lacustrine deposition can be found to the northwest indicating the presence of steeper, fault-controlled topography, and the correlative sandy/muddy meandering alluvial/delta plain facies association at the time of lacustrine deposition can be found on the southeastern side of the basin indicating the location of the half-graben hinge. Model B illustrates a continental basin with axial meandering river and floodplain during the time when no lake was present in the basin. When applied to the Greymouth Basin, the four alluvial members (Jay, Morgan, Rewanui, and Dunollie) were likely deposited in a half-graben setting similar to Model B. The alluvial fan facies association was deposited along the steeper, fault-controlled northwestern margin whereas axial meandering rivers with mire coals and low-lying marshy swamp facies gradually replacing the lacustrine facies association in the basin centre. Sandy meandering rivers and floodplains continued to occupy the southeastern margin of the basin.

The alternating meandering alluvial and lacustrine facies in the centre of the Greymouth Basin are likely to have been the product of changes in subsidence rate (Figure 3.18). The presence or absence of a lake in the centre of the basin records variation in accommodation conditions (A) in the basin and the balance between sediment supply (S) and subsidence through time (Leeder and Gawthrope 1987; Plint 2001; Martins-Neto and Catuneanu 2010; Holz et. al. 2015, 2017). The creation of a lake in the basin centre records conditions when the sedimentation rate was too low to fill the accommodation space (A>S) created from periods of more rapid subsidence. This interpretation assumes the sediment supply was relatively constant through time as indicated by the lack of climate change during deposition in the Greymouth Basin (Hill and Christophel 1988; Ward 1997; Kennedy 2003; Raine et.al. 2017). These periods of rapid subsidence were followed by periods of slow subsidence when sediment supply was greater than the creation of accommodation space (A<S) and the palaeolakes gradually filled with sediments. The resulting landscape was dominated by an axial meandering river and floodplain system with alluvial fan and meandering rivers entering from the sides of the basin. The back and forth of the variable subsidence rates of the basin give rise the alternating deposition of alluvial and lacustrine sediments through time with the economically productive mires deposited during the transitions.

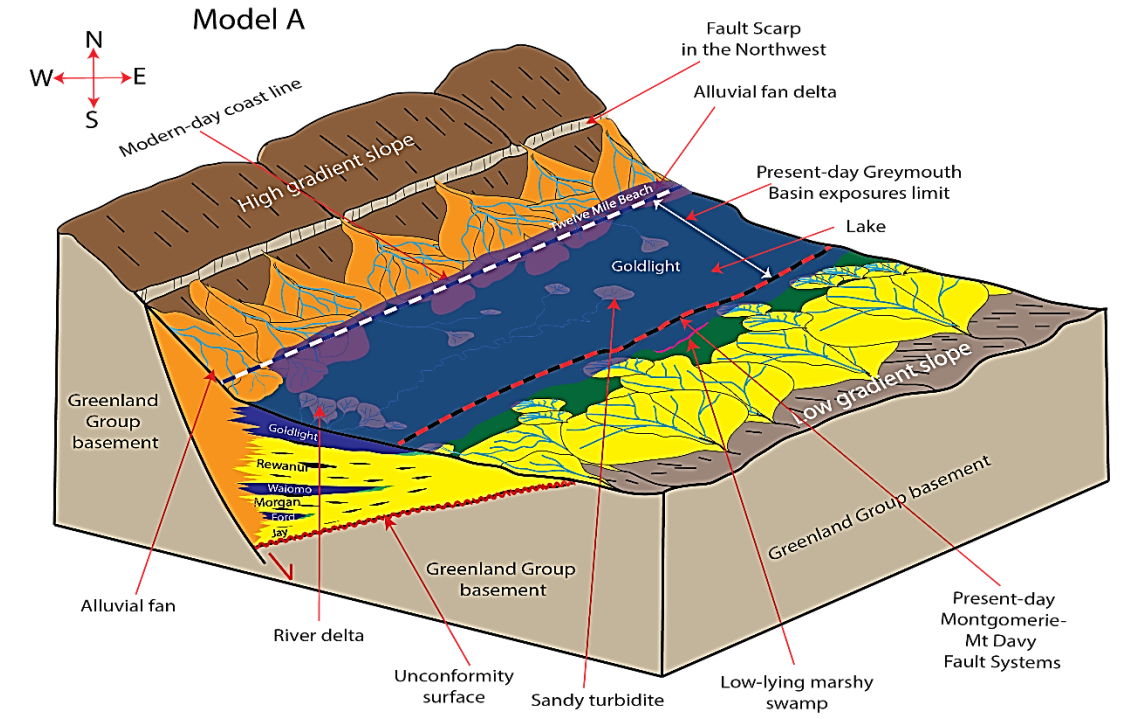


Half graben with lacustrine depositional system in the Greymouth Basin

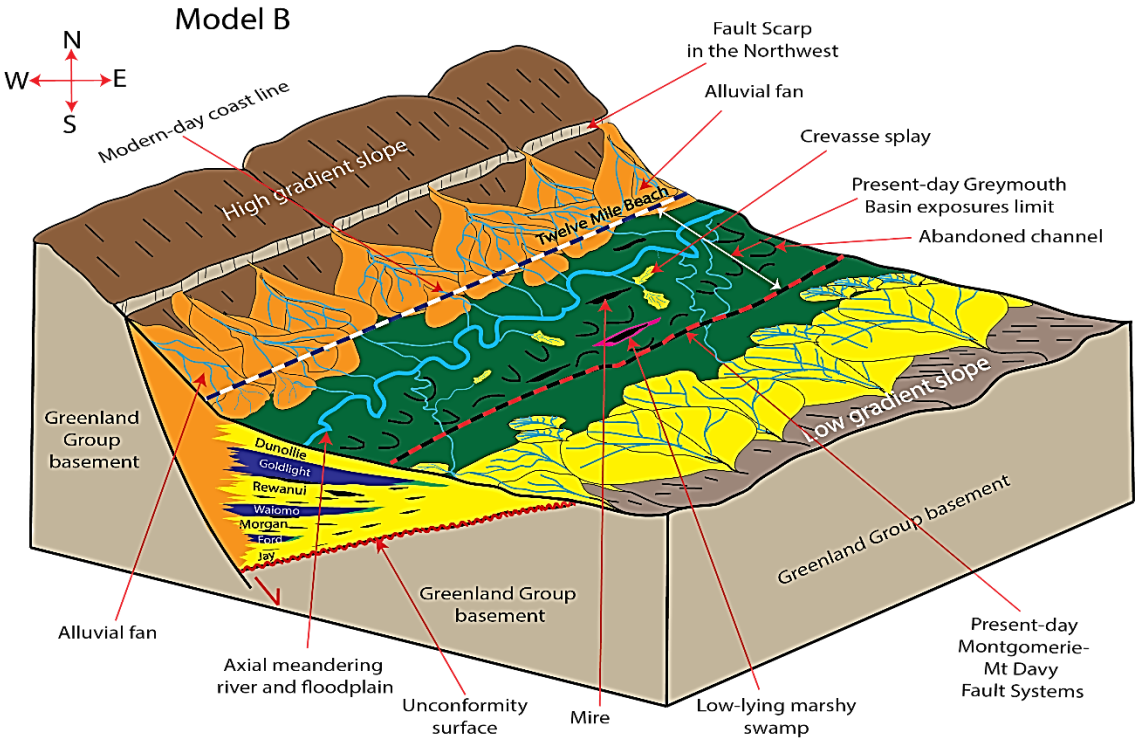


Half graben with axial meandering river and floodplain depositional system in the Greymouth Basin

Figure 3. 18: Palaeogeography of the Greymouth Basin, Model A represents the landscape when there was a lake in the basin centre whereas Model B illustrates the landscape when axial meandering river and floodplain systems dominated the basin centre.

## 3.7 Identification of organic rich facies

Multiple organic rich facies have been identified from the sedimentary facies analysis of the Paparoa Formation as evident from visual percentages of organic content present in each facies. Among these, mire coal and low lying marshy swamp facies from the mire facies association, abandoned channel and crevasse splay facies from the meandering alluvial/delta plain facies association, interdistributary bay facies from the delta front facies association, and lacustrine massive mudstone, lacustrine mudstones with minor sandstones and sandy turbidites facies from the lacustrine facies association are important.

Sedimentary facies analysis indicates that the mire coal facies contains the thickest coals in the Paparoa Formation. Coals are also common in the abandoned channel facies but are commonly thinner than in the mire coals. The large quantity and type of organic material, including stems, roots, spores, pollens and leaves, indicate their potentiality as petroleum source rocks. Biomarker signatures of the Kotuku and Petroleum Creek-3 oils from the Grey Valley to the southeast of the Greymouth Coal Field indicate the oil has a terrestrial, gymnosperm-dominated source and are interpreted to have migrated from the non-marine Late Cretaceous to Early Palaeocene coals and coaly sediments of Paparoa Formation (Frankenberger et al. 1994; Sykes et al. 2014). Geochemistry and maturation properties of the Late Cretaceous coals in the Greymouth Basin have already been studied in detail with a focus to understand the coal rank and their petroleum potential (Newman 1985; Nathan et al. 1986). The results suggest that the coals are source rocks for hydrocarbon generation (Nathan et al. 1986). Since the coals are already proven source rocks in the Greymouth Basin, we will target the less studied facies, in particular the carbonaceous mudstones that are so abundant in the basin.

The meandering alluvial/delta plain facies association contains two facies that are organic rich with the potential of contributing to petroleum generation in the Greymouth Basin. The abandoned channel facies contains silty carbonaceous mudstone to highly carbonaceous mudstone and thin beds of coal. However, the presence of sandstone beds from episodic river flooding may hinder the preservation potential of organic matter in these coals. The crevasse splay facies is also organic rich with laminated silty mudstone to carbonaceous mudstones and contains abundant plant material reaching of about 50-60% volume. Although this facies is scattered all over the basin and throughout the stratigraphy, we believe the facies has minimal source rock potential because it is usually thin and discontinuous, and the detrital carbon could have easily could have become oxidized in the highly bioturbated subaerial environment (Diessel 1992; Miall 1996; Lambiase and Morley 1999). The regular episodic input of clastic materials during flood events may also have hindered the preservation potential of organic matter in this facies. Therefore, the organic material in the meandering alluvial/floodplain facies association may contribute to the other hydrocarbon potentiality of the Greymouth Basin but probably not as much as other source rocks.

The interdistributary bay facies of delta front facies association and the low-lying marshy swamp facies of the mire facies association both could have petroleum potential as evident from the abundance of carbonaceous mudstones with coaly stringers (~80% volume of both facies). These facies may have covered laterally extensive areas between the major distributaries where thin, discontinuous coals may have formed during active deltaic progradation (e.g. Hamilton 1985). Coals are found as thin and discontinuous layers in the interdistributary bay facies which can serve as an important petroleum source rock. However, the associated mudstones are mostly weakly carbonaceous and experienced regular clastic input due to their close proximity to active river mouths which likely reduced their preservation potential as hydrocarbon source rocks. In addition, as the presence coals indicates a subaerial depositional origin, the associated fine-grained deposits were likely to have been oxygenated decreasing their potential as petroleum source rocks.

The presence of high bioturbation is an indication of that. Low-lying marshy swamp facies on palaeolake shores away from active river deltas are more promising as potential source rocks as indicated by highly carbonaceous, laminated mudstones and siltstones with abundant rootlets. However, common bioturbation disrupted the laminations, indicating this facies was also likely to have been oxygenated during its deposition reducing its petroleum potential.

The lacustrine facies association has greater potential for hydrocarbon generation. The lacustrine massive mudstone and lacustrine mudstones with minor sandstone facies are easily recognized by the presence of thick mudstones interpreted as deep-water deposition. The mudstones are carbonaceous as indicated by their dark colour and presence of leaf and fresh water fossils. Interbedded sandstones are very fine grained and have abundant conspicuous plant materials. The sandy turbidites facies also contains dark carbonaceous mudstones with leaf and fresh water fossils, conspicuous plant debris and exhibit rare bioturbation. There is little to no bioturbation evident in the whole lacustrine facies association suggesting an anoxic environment where organic matter was more likely to be preserved. Anoxic conditions exist in deep modern lakes where thermal stratification affects oxygen levels causing them to be too low to support the bacteria necessary for decomposition processes (Lewis 1983; Wilhelm and Adrian 2008). Abundant organic material may be supplied by algal blooms that sink to the bottom of modern lakes when they die becoming preserved in the anoxic deep water environment (Metzger et al. 1985; Volkman 1988). Turbidity currents also supply organic material as they often carry land-derived plant debris and dead aquatic life into the deep water (Kelt 1988) where they can become preserved in the absence of decomposition by bacteria. In the Greymouth Basin, three lacustrine facies associations (Ford, Waiomo and Goldlight) can be identified in three stratigraphic positions and are mappable across the basin in fence diagram (Figure 3.17). Thick, dark colour appearance and presence of leaf and fresh water fossils in all three lacustrine mudstone members of the Greymouth Basin suggest that the deposition likely took place in deep lakes where the organic matter probably supplied by died algal blooms and turbidity currents, and preserved in the absence of decomposed bacteria in anoxic environment.

The coals (the only proven source rock) have been extensively studied and so won't be further investigated here. The meandering fluvial flood plain facies (abandoned channel and crevasse splay facies) are too discontinuous and oxygenated to preserve organic material and so show little promise of petroleum potential. The lacustrine lithofacies are promising but little studied. Therefore, one of the purposes of this chapter is to understand the petroleum potential of the lacustrine facies association.

## 3.8 Distribution of the potential lacustrine source rock facies

In the Greymouth Basin, only the lacustrine facies association are likely to have high petroleum potential along with the proven coaly source rocks. The coal facies distribution across the basin has been previously studied in detail (Gage 1952; Newman 1985; Ward 1997). Therefore, understanding the coaly facies distribution is not a target of this chapter, instead the chapter examines the distribution of potential lacustrine facies across the Greymouth Basin.

Isolith maps have been developed based on lithofacies rather than members in order to understand the distribution of potential lacustrine source rocks in the Greymouth Basin. All fine-grained, carbonaceous, lacustrine lithofacies have been combined to make the isolith maps including the massive mudstone, mudstone with minor thin sandstone, and sandy turbidites facies. These are reported on the isolith maps as pairs of numbers representing the mudstone-rich and sandstone-rich thicknesses respectively. Maximum thicknesses have been determined when lithofacies were completely penetrated in a drill hole. Where a

lithofacies was only partially penetrated in a drill hole, a minimum thickness has been calculated and identified as a partial thickness on the isolith map. Where too little information is present to allow for estimation, the drillhole was not used to create the isolith map. Thicknesses of the lithofacies have been corrected for dip.

### 3.8.1 Ford Member (and Jay Member)

A total of 66 drill holes have been used to prepare the lacustrine isolith maps of the Ford Member, including subaqueous facies from the coeval Jay Member. Only 10 of the drill holes fully intersected lacustrine facies, 17 drill holes record minimum thicknesses and the rest of them intersect Greenland Group basement without intersecting the lacustrine facies association of the Ford Member (Appendix 3; Figures 3.19).

The isolith map (Figure 3.19) shows a maximum thickness of >82m in the northern central part of the basin (DH-657,). Two other locations of increased thickness include 67 m in the northeastern corner (DH-1424) and 41 m to the southeast (DH-1012). The greater thicknesses in two locations (DH-657 and DH-1424) are due to both more complete penetration of total lacustrine facies and by an increased contribution by sandy turbidites facies, the thickest being ~32 m in the north-central part of the basin (DH-657). To the east, the lacustrine facies of >20 m thickness is abruptly terminated by the cross-cutting Montgomerie-Mount Davy Fault System. Thicknesses decrease to the southeast where there are numerous drill holes that intersect Greenland Group basement without intersecting lacustrine facies of the Ford Member. The lacustrine facies of the Ford Member is absent in the northwestern and southwestern parts of the basin.

The thickness variation is probably due to the presence of isolated depo-centres bounded by syn-depositional faults which were formed in the early stages of basin development. The presence of sandy turbidites facies in the depo-centres indicates increased sediment input from deltas at those locations. However, this interpretation may be affected by the thickest lithofacies corresponding to the drill holes with full penetration.

### 3.8.2 Waiomo Member (and Morgan Member)

A total of 65 drill holes have been used to prepare the isolith map of the lacustrine facies of the Waiomo Member, as well as coeval subaqueous facies from the Morgan Member. Most of the drill holes intersect the lacustrine facies of the Waiomo Member completely except two drill holes in the west (DH-641 and DH-645), one drill hole in the northeast (DH-661) and one drill hole in the southeast (DH-600) (Appendix 3; Figure 3.20).

The isolith map shows a maximum thickness of only 87 m (DH-635) in the western part of the study area forming the main depo-centre (Figure 3.20). Three other areas of increased thickness are present in the northeastern corner (36 m in DH-668), the southeastern corner (32 m in DH-620), and the eastern centre of the basin (37 m in DH-261). In the north-central region the lacustrine facies reduce to zero thickness. The lacustrine facies maintain relatively constant thickness across the eastern side of the basin until truncated against the Montgomerie-Mount Davy Fault System in the east. The lacustrine facies of the Waiomo Member is absent in the southwest part of the area where numerous drill holes intersect Greenland Group basement rocks, without intersection of any lacustrine facies association.

The thickest part was probably due to the presence of a single larger depo-centre probably bounded by faults coeval withother smaller fault-bounded depo-centres which were formed during the continuing development of the Greymouth Basin. The faults were presumably syn-depositional in origin. The existence of the smaller depo-centres supports the interpretation that pre-existing isolated depo-centres

existed during the early stage of basin development (Ford time). The abrupt termination of thicker lacustrine facies against the cross-cutting Montgomerie-Mt Davy Fault System suggests the basin was originally wider and that the cross-cutting faults are younger.

The isolith map of the Goldlight Member and coeval members shows a maximum thickness of >186 m (DH-657) in the northern centre of the study area with the northeastern corner removed by erosion (Figure 3.21). The overall thickness decreases to the northwest and south. To the east, the thickness is truncated by the Montgomerie-Mount Davy Fault System. The sandy turbidites facies is thickest in the northwestern and southwestern sides of the basin. The thickest lacustrine facies occur in a NNE-oriented band across the centre of the basin.

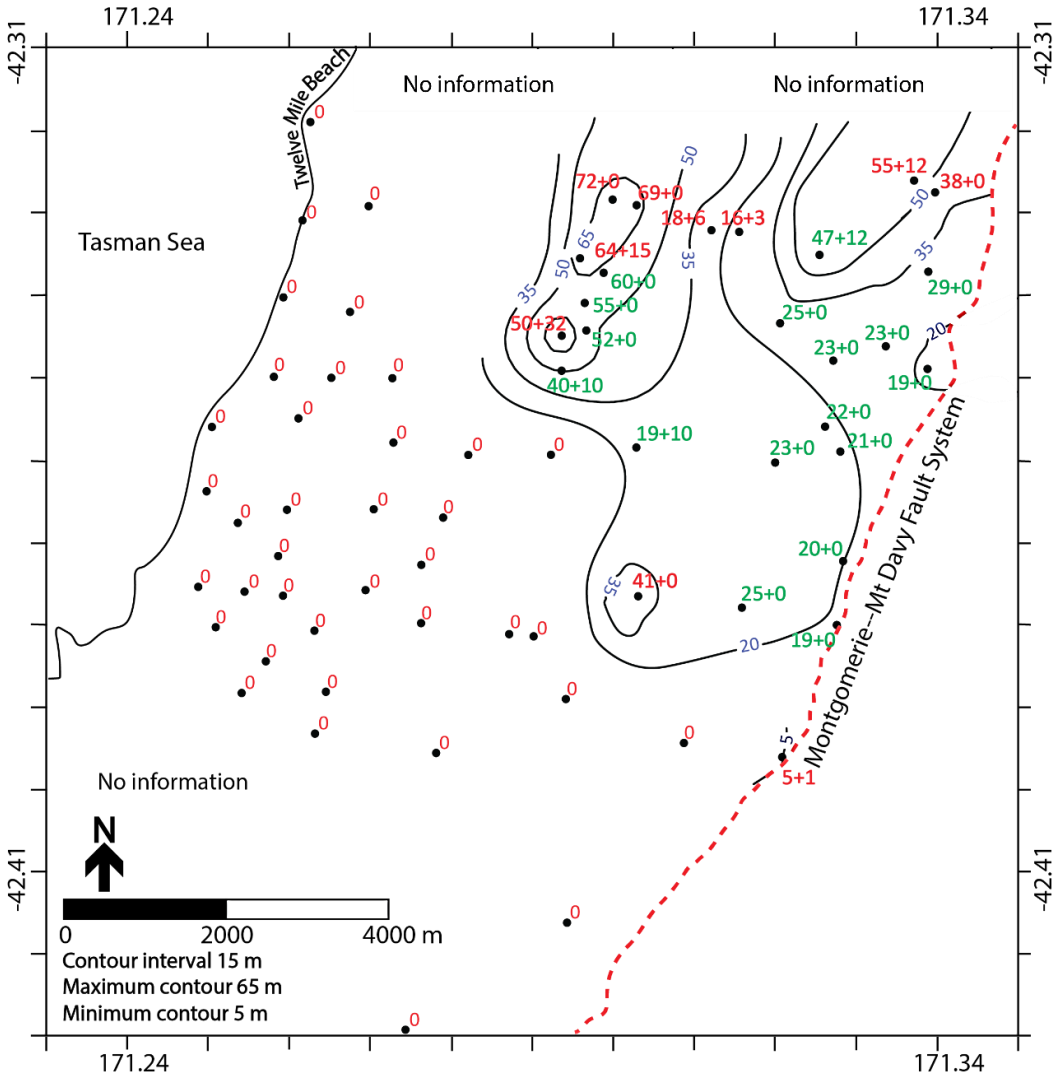


Figure 3. 19: Ford lacustrine facies isolith map showing NNE-SSW orientation of lacustrine deposits and interpreted faults. The calculated thicknesses shown are the sum of muddy lacustrine facies (massive mudstone facies and mudstone with minor sandstone facies) and sandier lacustrine facies (sandy turbidite facies) that may not have been included in the lacustrine Ford Member. Red values represent maximum thickness whereas the green values represent estimated minimum thickness. Zeroes indicate the absence of Ford lacustrine facies in an otherwise stratigraphically complete drill hole.

The northern centre and the northeastern part of the study area contains the greatest thickness of the lacustrine facies, thickening to the NNE (before removal by erosion), indicating that the basin axis was orientated NNE-SSW. The sandy turbidites in the southwestern side of the basin were probably fed from an axial meandering river delta as indicated by the prevalence of the meandering alluvial facies association in the fence diagram (Figure 3.17). The sandy turbidites along the northwestern side of the basin were probably deposited from footwall sourced fan deltas as indicated by the thick subaqueous conglomerate facies of the alluvial fan/fan delta facies association dominating that region in the fence diagram (Chapter 2). The truncation of thick (>140 m), deep water lacustrine massive mudstone facies by the Montgomerie-Mt Davy Fault System in the east indicates the Greymouth Basin was significantly wider at the time of the Goldlight Member.

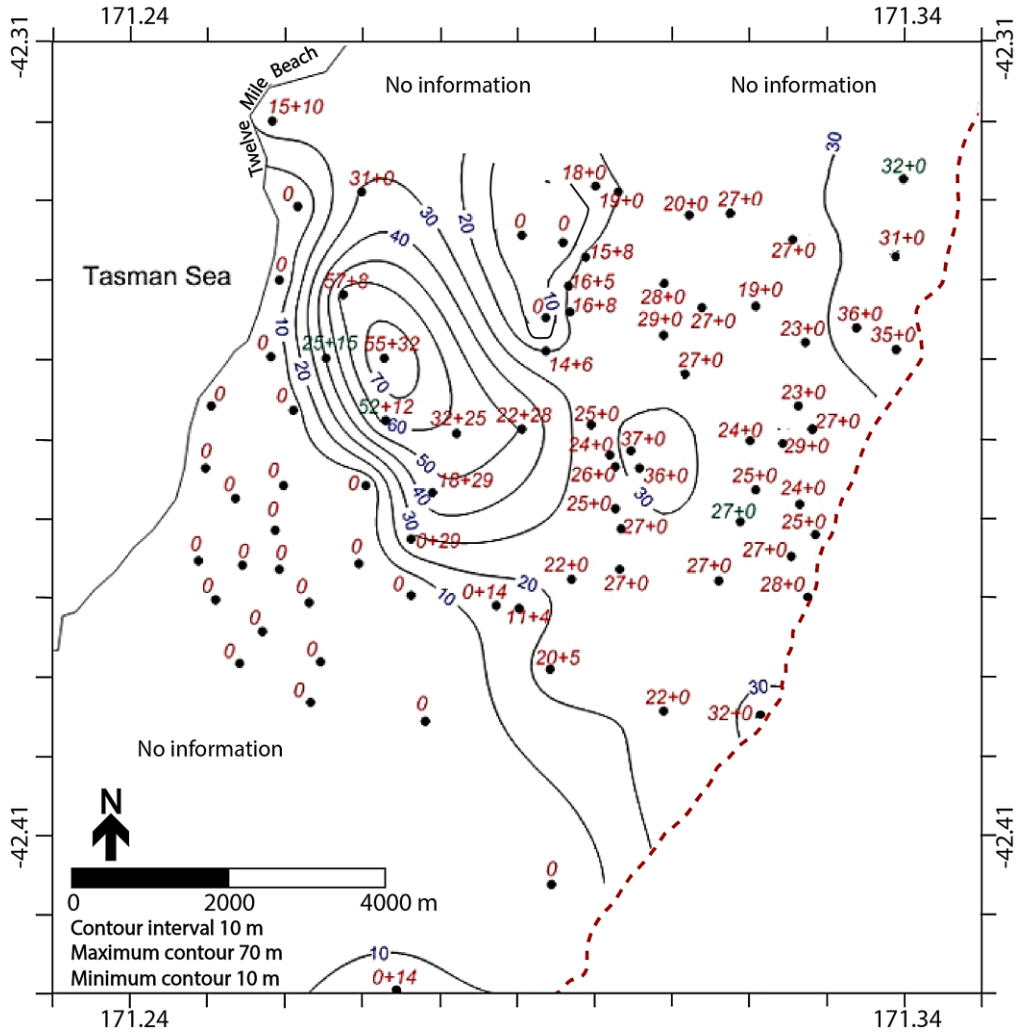


Figure 3. 20: Waiomo lacustrine facies isolith map showing NNE-SSW orientation of lacustrine deposits and interpreted inland and offshore faults. The calculated thicknesses shown are the sum of muddy lacustrine facies (massive mudstone facies and mudstone with minor sandstone facies) and sandier lacustrine facies (sandy turbidite facies) that may not have been included in the lacustrine Waiomo Member. Red values represent maximum thickness whereas the green values represent estimated minimum thickness. Zeroes indicate the absence of Waiomo lacustrine facies in an otherwise stratigraphically complete drill hole.

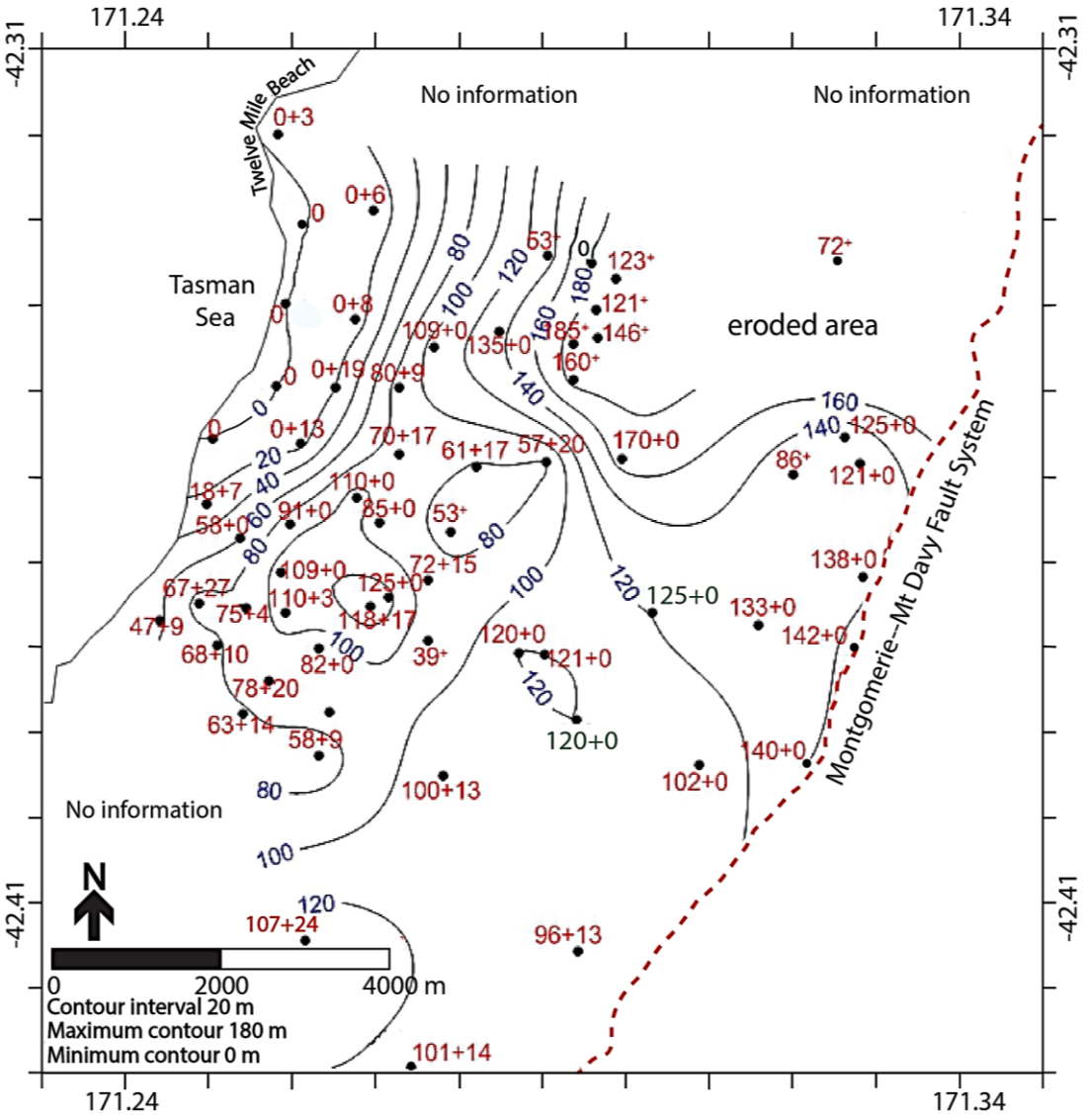


Figure 3. 21: Goldlight lacustrine facies isolith map showing NNE-SSW orientation of lacustrine deposits and interpreted offshore fault. The calculated thicknesses shown are the sum of muddy lacustrine facies (massive mudstone facies and mudstone with minor sandstone facies) and sandier lacustrine facies (sandy turbidite facies) that may not have been included in the lacustrine Goldlight Member. Red values represent maximum thickness whereas the green values represent estimated minimum thickness. When the lacustrine facies association is partially eroded (upper part) in a drill hole, the value is represented with a plus sign the right corner of the value. Zeroes indicate the absence of Goldlight lacustrine facies in an otherwise stratigraphically complete drill hole.

## 3.9 Results and interpretation of the lacustrine source rock geochemistry

Geochemical analysis was done on samples from the lacustrine facies association from each lacustrine member of the Paparoa Formation in order to understand their petroleum potentiality. Among the 56 samples of the Ford Member, 26 samples were collected from the lacustrine massive mudstone facies, 24 of them from the lacustrine mudstones with minor thin sandstone facies and the remaining 6 from the sandy turbidites facies (Appendix 4). Out of the 71 samples collected from the Waiomo Member, 47 were

collected from the lacustrine massive mudstone facies, 16 from the lacustrine mudstones with minor thin sandstone facies, and the remaining 8 from the sandy turbidites facies (Appendix 4). Of the 56 samples from the Goldlight Member, 52 samples were collected from the lacustrine massive mudstone facies and the remaining 4 were collected from the lacustrine mudstones with minor thin sandstone facies (Appendix 4). No samples were collected from the sandy turbidites facies of the Goldlight Member.

The key geochemical parameters that were measured are total volatiles (S1), pyrolysable hydrocarbons (S2), carbon dioxide generation (S3), total organic carbon (TOC), temperature of maximum pyrolysis yield ($T_{max}$), hydrogen index (HI), oxygen index (OI) and production index (PI). Key attributes were then analysed to understand the petroleum potential of the lacustrine mudstones including i) source rock petroleum generative potential parameters, ii) type of kerogen and iii) thermal maturation parameters. Typical values and their application to interpreting the petroleum potential are summarized in Table 3.2, adapted from Peters and Cassa (1994).

Table 3. 2: Summary of key parameters and their values of geochemical analysis adapted from Peters and Cassa (1994).

| Summary table of key parameters (adapted from Peters & Cassa 1994) | | | |
|---|---|---|---|
| Petroleum potential parameters | | | |
| | S1 | S2 | TOC |
| Poor | 0 - 0.5 | 0 - 2.5 | 0 - 0.5 |
| Fair | 0.5 - 1 | 2.5 - 5 | 0.5 - 1 |
| Good | 1 - 2 | 5 - 10 | 1 - 2 |
| Very Good | 2 - 4 | 10 - 20 | 2 - 4 |
| Excellent | >4 | >20 | >4 |
| | | | |
| Kerogen Type and character of expelled products | | | |
| | HI | S2/S3 | Expelled product |
| I | >600 | >15 | Oil |
| II | 300 - 600 | 10 - 15 | Oil |
| II/IIIb | 200 - 300 | 5 - 10 | Mixed |
| III | 50 - 200 | 1 - 5 | Gas |
| IV | <50 | <1 | None |
| | | | |
| Thermal maturation parameters | | | |
| | Ro% | Tmax | PI |
| Immature | 0.2 - 0.6 | <435 | <0.10 |
| Mature - Early | 0.6 - 0.65 | 435 - 445 | 0.10 - 0.25 |
| Mature - Peak | 0.65 - 0.9 | 445 - 450 | 0.25 - 0.40 |
| Mature - Late | 0.9 - 1.35 | 450 - 470 | >0.40 |
| Postmature | >1.35 | >470 | - |

### 3.9.1 Source rock generative potential

Source rock generative potential measures the quantity of kerogen (Tissot and Welte 1984; Peter 1986; Peters and Cassa 1994; Muljana et al., 2012; Table 2). TOC (total organic carbon) and S2 (pyrolysable hydrocarbons) are the two most commonly used parameters to determine the amount of available kerogen

in source rocks. S1 (volatile hydrocarbon) is not useful for determining the total hydrocarbon potential of source rocks as it measures only free hydrocarbons.

#### *3.9.1.1 TOC (Total Organic Carbon)*

The quantity of organic matter within a sample is described as Total Organic Carbon (TOC) and includes both kerogen and bitumen (Peters and Cassa 1994); TOC is what is visibly present as a darker colour when examining a facies in the field or in core. TOC is measured as a percentage during pyrolysis. The higher the value of TOC, the higher the potential for the generation of petroleum (Table 3.2). The minimum acceptable value for TOC is 0.5 wt%. Any values less than that are considered to have too little carbon to be a hydrocarbon source rock (Tissot and Welte 1984; Muljana et al. 2012). A TOC value above 4 wt% indicates excellent source potential. However, TOC alone may not suffice to evaluate source rock potential since it includes inertinite, i.e. oxidized or biodegraded organic matter that is not capable of generating hydrocarbons, even if present in high concentrations (Espitalie et al. 1985; Al-Areeq et al. 2018).

The results show that TOC values of the majority of samples from the lacustrine massive mudstone facies from all members are of good (1-2 wt%) to very good (2-4 wt%) potential (Appendix 4). The Ford Member has 46% of samples between 1-2 wt% and the remaining 54% of samples between 2-4 wt%. 96% of samples from the Waiomo Member show good to very good potential (1-4 wt%) with only 4% showing only fair potential (0.5-1 wt%). Samples from the Goldlight Member show more variation with 2% of poor potential (0-0.5 wt%), 13% of fair potential (0.5-1 wt%), 36% of good potential (1-2 wt%), and 48% of very good potential (2-4 wt%).

TOC values of samples from the lacustrine mudstone with minor thin sandstones facies show good to very good potential (Appendix 4). The Ford Member TOC values indicate 92% of samples have good (50%) to very good petroleum potential (42%); 4% of samples show excellent potential and the remaining 4% show poor potential. One sample from DH656/461.8m has a TOC value above 4 wt% (4.64) indicating excellent petroleum potential. Results from the Waiomo Member indicate that 6% have very good potential, 69% have good, and 25% have fair petroleum potential. TOC values of samples from the Goldlight Member indicate 75% have good and 25% have very good petroleum potential.

Fewer samples were collected from the sandy turbidites facies and, unsurprisingly, they generally show lower TOC values (Appendix 4). The Ford Member samples show 67% of TOC values are 1-2 wt% (good potential) and 33% are 2-4 wt% (very good potential). Waiomo Member samples TOC values are of fair potential (~62%), 25% are of good potential, and 13% are of very good potential.

#### *3.9.1.2 S2 (pyrolysable hydrocarbons)*

S2 measures total hydrocarbon yield from cracking kerogen during pyrolysis. This is sometimes a more realistic measure of source rock potential than TOC because TOC includes "dead carbon" incapable of generating petroleum (Peters and Cassa 1994). Higher measured values for $S_2$ indicate larger amounts of hydrocarbon formation indicating higher petroleum potentiality (Table 3.2). If the $S_2$ value is low, there is not enough organic matter for hydrocarbon formation (Muljana et al., 2012). The minimum acceptable value for $S_2$ is 2.5; any values less than that are considered to be not significant for hydrocarbon source rock potential. Values between 5-10 and 10-20 are considered as good and very good, respectively with values above 20 considered to indicate excellent source potential. We present the analyses by facies, as well as by member.

Results of $S_2$ measurements of hydrocarbon yield from lacustrine massive mudstone facies samples are highly variable across the three lacustrine members (Appendix 4). Those from the Ford Member show 23% below 2.5 indicating poor potential, 69% between 2.5 and 10 indicating fair to good potential, and 8% between 10 and >20 indicating very good to excellent potential. Samples from the Waiomo Member show 19% fall below 2.5 (poor potential), 78% samples fall between 2.5 and 10 (fair to good potential), with only 3% between 10 and 20 (very good potential). Samples from the Goldlight Member show generally lower potential with 42% less than 2.5 (poor potential) and 58% between 2.5 and 10 indicating fair to good potential. The Ford Member is the only member to contain samples of excellent potential.

$S_2$ results of samples from the lacustrine mudstone with minor thin sandstones facies are generally higher (Appendix 4). Samples from the Ford Member have $S_2$ measurements ranging among fair (37%), good (37%), and very good to excellent (18%) potentials with only 8% of the samples having poor potential. One sample (DH656/461.70m), which was collected from thin sandstone beds, shows the highest $S_2$ value (25.08) among all mudstone samples of the Paparoa Formation, indicating that the conspicuous thin sandstone beds have excellent $S_2$ values. $S_2$ analysis of samples from the Waiomo Member are poorer with 25% of poor potential (<2.5), 56% of fair potential (2.5-5), and 19% of good potential (5-10). $S_2$ analysis of samples from the Goldlight Member shows 50% have poor $S_2$ values (<2.5), 25% have fair values (2.5-5), and 25% have good values (5-10). None of the samples from the Waiomo or Goldlight members show excellent values.

Fewer samples were collected from the sandy turbidites facies and all show generally poorer potential (Appendix 4). $S_2$ results of samples from the Ford Member range from 16% with poor potential (<2.5), 67% with fair potential (2.5-5), and 17% with good potential (5-10). Most of the samples from the Waiomo Member show poor potential (~62%) with the remaining 38% having good potential.

#### *3.9.1.3 TOC vs $S_2$*

Comparing TOC and $S_2$ indicates that all three lacustrine members show source rock potential (Figure 3.22). However, some samples from each lithofacies show acceptable TOC values but poor $S_2$ values and thus have poor source rock potential. A threshold value line of 2.5 was used for $S_2$ and of 0.5 for TOC indicate poor potential. Any samples falling below the threshold lines have not been used in further analysis of kerogen type and source maturation. 16% of samples (9/56) from the Ford Member, 24% of samples (17/71) from the Waiomo Member, and 43% of samples (24/56) from the Goldlight Member have poor source rock potential (Appendix 4). From Ford Member, 36% (20/56) shows good potential, 43% (24/56) shows very good potential and 5% (3/56) shows excellent potential. For Waiomo Member, 52% (37/71) shows good potential and 24% shows very good potential. For Goldlight Member, 12% (7/56) shows good potential and 45% (25/56) shows very good potential. Only the Ford Member has some samples which show excellent petroleum potential.

### 3.9.2 Kerogen type and source

The type of organic matter is an important factor for evaluating the petroleum potential of source rocks and has significant influence on the type of hydrocarbon products (Hunt 1979; Tissot and Welte 1984; Al-Areeq et al. 2018). There are two parameters that have been used to determine the type of kerogen and its source, hydrogen index (HI) and oxygen index (OI). HI values indicate the kerogen type and predict their corresponding expelled products of oil or gas. OI values are used to identify the kerogen source as terrestrial (cellulose, spores and pollens) or lacustrine/marine (algae, plankton, other aquatic life) or both. Higher OI values directly impact the HI values of source rocks.

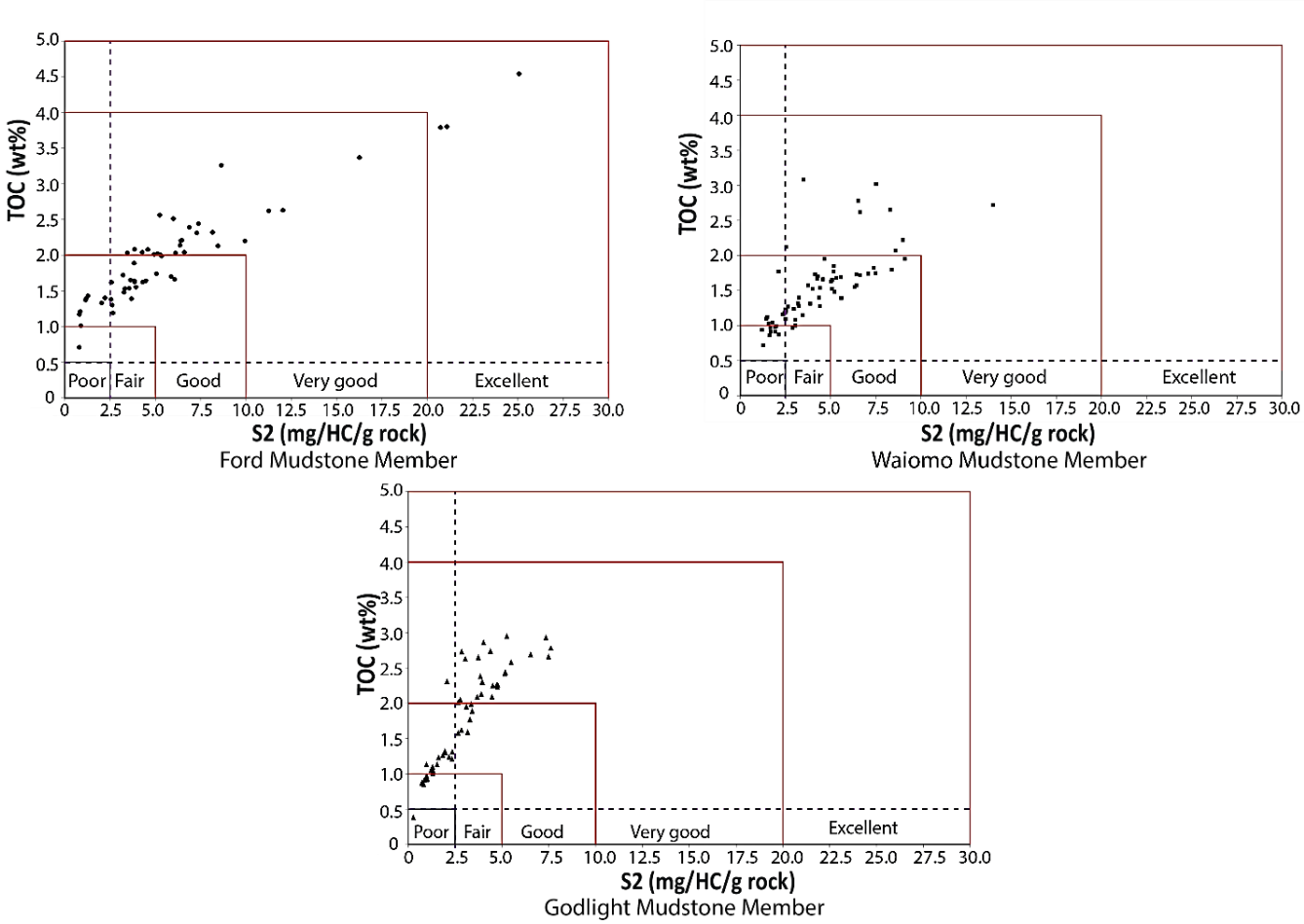


Figure 3. 22: The comparison of TOC vs S2 plot for the Ford, Waiomo and the Goldlight lacustrine members. The Ford mudstone samples are shown in black bullet points whereas the Waiomo and the Goldlight mudstone samples are shown in black squares and black triangles.

### *3.9.2.1 Hydrogen index (HI)*

Hydrogen index (HI) values allow identification of the type of kerogen and its corresponding expelled products, oil or gas. It is calculated as ***HI = (S2/TOC) x 100*** and measured as ***mg HC/g TOC.*** For mature source rocks, HI values for gas-prone kerogens are between 50 and 200, mixed gas-oil prone kerogens are between 200 and 300, and oil-prone kerogens are more than 300 HI (Peters and Cassa 1994; Table 3.2).

HI results from 47 samples from the Ford Member (and coeval Jay Member) vary between 160 and 554. 32% of samples show HI values of 300-600, indicating Type II kerogen with the potential to generate oil (Appendix 4). Approximately 11% of samples show HI values of 50-200, indicating Type III kerogen with the potential to generate gas. The remaining 57% of samples show HI values between 200-300, indicating a mix of Type II and Type III kerogens with the potential to generate both gas and oil.

HI results from 54 samples from the Waiomo Member (and coeval Morgan Member) range from 114 to 514 (Appendix 4). About 47% of the samples show HI values between 300 and 600, suggesting Type II kerogen with the potential to generate oil (Appendix 4). Only 4% of the samples show HI values between 50 and 200, indicating Type III kerogen with the potential to generate gas. About 49% of the samples show

HI values between 200-300, indicating a mix of Type II and Type III kerogens with the potential to generate both gas and oil.

HI results from 32 samples from the Goldlight Member (and coeval Rewanui and Dunollie members) range from 70 to 282 (Appendix 4). 79% of the samples show HI values between 50 and 200, indicating Type III kerogen with the potential to generate gas. The remaining 21% of the samples show HI values between 200 and 300, indicating a mix of Type II and Type III kerogens with the potential to generate both gas and oil. No samples had HI values between 300 and 600.

#### *3.9.2.2 Oxygen index (OI)*

The oxygen index (OI) is related to the amount of oxygen in the kerogen and is measured by $CO_2$ output during S3 phase of pyrolysis (Nunez-Betelu and Baceta 1994; Peters and Cassa 1994). It is calculated as ***OI = (S3/TOC) x 100*** and measured as *mg $C0_2$ /g TOC*. High OI values (>100) are usually found in gas-prone Type III kerogens which indicates terrestrial organic matter (Peters and Cassa 1994). However, weathering may also give anomalously high OI values by elevating S3 during pyrolysis (Peters and Cassa 1994). Organic matter derived from terrestrial (subaerial) origin (cellulose, spore, pollen etc.) have higher weathering/oxidation tendency than those derived from lacustrine or marine (subaqueous) origin (algae, plankton etc.). Oxidation decreases the preservation potential of organic matter and thus OI values over 100 may indicate poor preservation potential rather than just Type III kerogens. Lower OI values (< 100) indicate a lower weathering tendency and thus have higher preservation potential.

OI results from the Ford Member vary from 5 to 237 (n=47). The average is 60 and the median is 34 with a significant number of samples showing values under 20 (Appendix 4). Among these samples, about 78% have OI values less than 100 which indicates less oxidation and therefore higher preservation potential of organic material. The remaining 22% samples show OI values over 100, indicating the organic matter was predominantly derived from terrestrial material which has less preservation potential due to possible oxidation and is therefore unlikely to be productive for gas.

OI results from the Waiomo Member (and coeval Morgan members) vary from 8 to 213 (n=32). The average is 58 and the median is 40 (Appendix 4). 83% have OI values less than 100 with a significant part showing values less than 20 indicating low oxidation and high preservation potential. 17% of samples have OI values over 100, indicating the terrestrial organic matter with low preservation potential.

OI results from the Goldlight Member vary from 13 to 336 (n=54). The average is 74 and the median is 51 (Appendix 4). About 78% of samples have OI values less than 100 with a few samples showing values less than 20 (Appendix 4). The remaining 17% samples show OI values over 100, indicating the organic matter has less preservation potential due to a terrestrial origin with possible high oxidation and therefore unlikely to be productive for gas.

#### *3.9.2.3 Hydrogen index (HI) vs Oxygen index (OI)*

The pyrolysis results can be used to differentiate the type of organic matter by plotting hydrogen index vs oxygen index on a modified Van Krevelen diagram which shows that kerogen Type I is mainly oil-prone with minor gas, Type II is mixed oil and gas prone, Type III is mainly gas prone, and Type IV is incapable of generating hydrocarbons (Espitalie et al. 1985; Peters and Cassa 1994; Muljana et al., 2012; Al-Areeq et al. 2018). It is well established that kerogen type is derived from four classes of organic matter. Type I kerogens, known as liptinite or algenite, are derived from algae, phytoplankton, and micro-organisms; Type II kerogens, known as exinite, are derived from spores, pollens, and cuticles; Type III kerogens, known as

vitrinite, are derived from humic tissues, wood, and cellulose; and Type IV kerogens, inertinite, are derived from charcoal and oxidized tissues (Tissot et. al., 1974; Peters and Cassa 1994).

In this study, the results are plotted on a modified Van Krevelen diagram showing HI vs OI (Figure 3.23). Most of the samples from the Ford and Waiomo members plot between the lines of Type II and Type III kerogens indicating a mixed source derived from both exinite (spore and pollen) and vitrinite (woody/cellulose). The diagram indicates that these members are therefore capable of generating both oil and gas. Approximately 30% of the samples have higher HI values (300-600) suggesting Type II kerogen dominates over Type III. A few samples, three from the Ford Member and one from the Waiomo Member, marginally plot along the Type I kerogen curve line which indicates some of the organic matter probably derived from an alginite source that is capable of generating oil. Samples from the Goldlight Member plot also indicate a mixed kerogen source from vitrinite to exinite. However, most of the samples have HI values in between 50-200 which indicate Type III kerogen dominates over Type II and thus the Goldlight Member is capable to generate only gas.

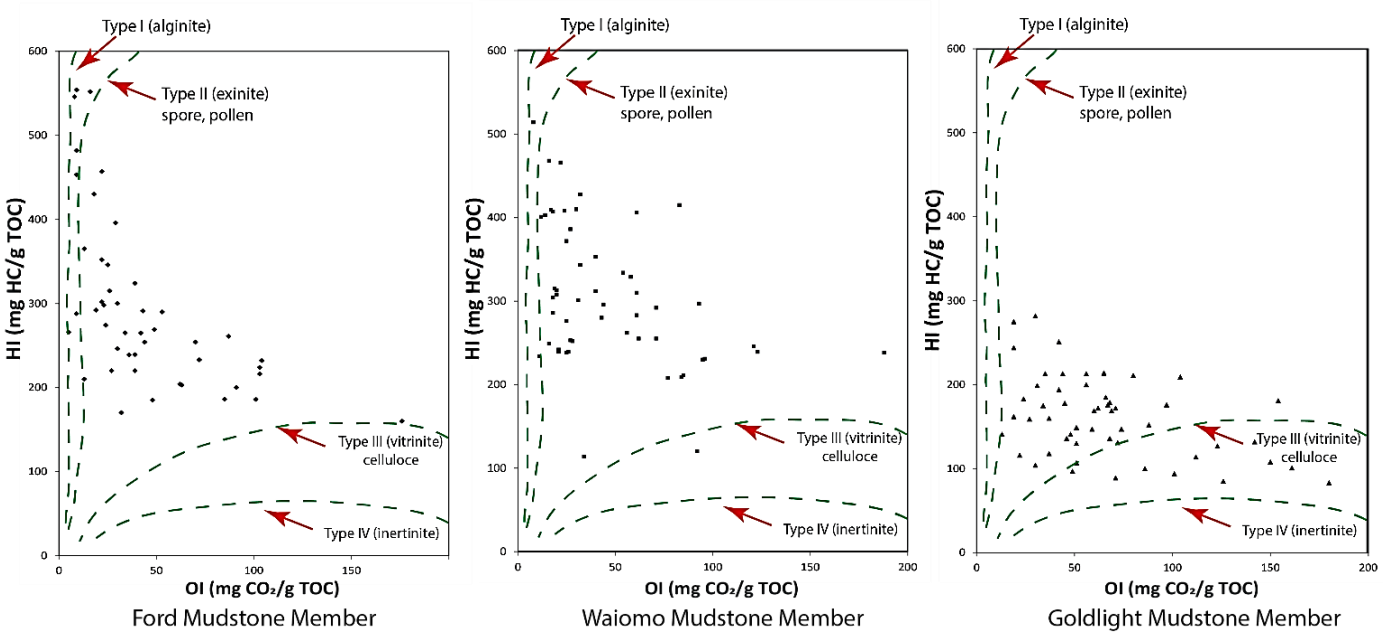


Figure 3. 23: The comparison of HI vs OI plot for the Ford, Waiomo and the Goldlight lacustrine members. The Ford mudstone samples are shown in black bullet points whereas the Waiomo and the Goldlight mudstone samples are shown in black squares and black triangles.

### 3.9.3 Level of thermal maturation

An analysis of thermal maturation level of the organic matter indicates the degree of hydrocarbon generation and expulsion from lacustrine source rocks (Peters and Cassa 1994). Three parameters (Table 3.3), maximum temperature (Tmax), vitrinite reflectance (Ro%), and production index (PI), have been used to determine the level of thermal maturation of oil for each possible lacustrine source rock of the Paparoa Formation.

#### *3.9.3.1 Maximum temperature (Tmax)*

The maximum temperature, Tmax ($^0$C), obtained from interpreting Rock-Eval pyrolysis data, has become a widely used maturation index (Tissot and Welte 1984; Tissot et al. 1987). The value of Tmax increases

in response to increasing maturation of the organic matter (Tissot et al. 1987). Espitalie et al (1986) showed that the range of Tmax variation is narrower for Type I kerogen (435-450°C) than for Type II (420-460°C) and Type III kerogens (400-600°C) due to increasing structural complexities in aliphatic chains. Therefore, Tmax is not considered to be a good maturation index for kerogen Type I, but is recommended for Types II and III (Espitalie et al 1986; Tissot et al. 1987; Muljana et al. 2012). For Type II and Type III kerogen, the Tmax value for the oil threshold is lower and narrower than the Tmax value for the gas threshold. For example, the Tmax value ranges from 430 to 435°C for oil threshold for Type II and Type III kerogen whereas for gas threshold, Tmax is approximately 430 to 455°C for Type II kerogen and 465 to 470°C for Type III kerogen (Espitalie et al. 1986; Tissot et al. 1987; Muljana et al. 2012).

In the present study, Tmax results from the Ford Member vary from 426.3°C to 450.5°C (Appendix 4), indicating that both oil and gas generation have occurred. The oil probably generated from both Type II and Type III kerogens, but the gas was likely only generated from Type II kerogen. The results show that the Ford Member source rock samples are mostly early-mature to peak-mature (~83%) (Figure 3.24).

Tmax results from the Waiomo Member vary from 424.7 to 467°C (Appendix 4), indicating that both oil and gas generation have occurred, probably from both Type II and Type III kerogens. The Tmax vs HI graph of thermal maturation shows that the Waiomo Member source rock samples are mostly early-mature (~64%) (Figure 3.24).

Tmax results from the Goldlight Member vary from 422.2 to 451.3°C (Appendix 4), suggesting the oil probably generated from both Type II and Type III kerogen, but the gas only generated from Type II kerogen. The results show that the Goldlight Member source rock samples are mostly immature (~88%) (Figure 3.24).

Table 3. 3: Summary of key parameters and their values of thermal maturation for oil showing the relation among PI, Tmax and Ro% (adapted from Peters 1986 and Tissot et al. 1987).

| | **Maturation** | **PI** | **Tmax** | **Ro (%)** |
|---|---|---|---|---|
| **Level of thermal maturation** | Top of oil window | 0.1 | 435-445 | 0.6 |
| | Bottom of oil window | 0.4 | 450-470 | 1.35 |

### *3.9.3.2 Maximum temperature (Tmax) vs HI*

A plot of Tmax vs HI is useful to understand how the increase in temperature (Tmax) affects the oil generative potential (HI) of a source rock (Figure 3.24). HI values are expected to be the highest in the immature source rocks and gradually decrease with the onset of hydrocarbon generation (Sykes and Snowdon 2002). However, the plot indicates a trend of increasing HI with increasing Tmax which is unusual. Sykes and Snowdon (2002) studied New Zealand coals and showed that the increase in HI with increase in Tmax is also seen in coals. The authors suggested that this increase was likely due to rearrangement of the coal molecules during diagenesis and catagenesis. The rearrangement probably formed new higher energy bonds which result in an increase in hydrogen generative potential. Similar trend in the lacustrine mudstones of the Paparoa Formation suggests similar rearrangement in hydrocarbon molecules present in lacustrine mudstones occurred during their diagenesis and catagenesis. Based on this information it can be concluded that the lower HI values in some immature samples will increase once they

reach the oil window and the samples which are currently showing higher HI values may have had lower HI when they were immature. This also indicates that the lacustrine mudstones of the Paparoa Formation have actually higher HI values than what has been indicated in the Tmax vs HI plot.

#### *3.9.3.3 Vitrinite reflectance (Ro%)*

Vitrinite reflectance (Ro%) is another popular maturation index. Vitrinite, Type III kerogen, is a common component of coals and is derived from the cellulose cell walls of the higher plants (Teichmuller 1989). The technique measures the ability of tiny vitrinite particles to reflect incident light; as the maturation level increases, the reflectance of vitrinite particles increases, (Al-Areeq et al. 2018). A vitrinite reflection value of 0.6% marks the early stage of oil expulsion whereas the peak and late stage of oil generation are at ~0.8% and ~1.35%, respectively (Waples 1988). Tissot and Weltre (1984) evaluated the Ro% value of the early, peak, and late stage of oil generation for different types of kerogen (Table 3.3).

Vitrinite reflectance was conducted on four samples from the Ford Member; results ranged from 0.63 Ro% to 0.7 Ro%, indicating the source rocks are mostly in the early to peak maturation stage. Vitrinite reflectance on nine samples from the Waiomo Member gave values ranging from 0.43 Ro% to 0.65 Ro%, indicating the host rocks are in the immature to early maturation stage. Vitrinite reflectance was not conducted on samples from the Goldlight Member since it is younger and contains less potential for hydrocarbon generation.

#### *3.9.3.4 Production index (PI)*

The production index is another parameter to determine the level of thermal maturation of hydrocarbon. PI is transformation ratio which measures how much kerogen is converted to free hydrocarbon. PI is calculated as PI= S1/(S1+S2). As the thermal maturity of the source rocks increases PI increases until the expulsion occurs. The threshold value of PI marking the top of the oil window is ~0.1 and continues to 0.4 marking the bottom of oil window (Table 3.3; Al-Areeq et al. 2018).

In this study, the production index of the samples from the Ford Member (n=47) vary from a minimum of 0.03 to a maximum of 0.4, suggesting the Ford Member covers the full window of oil production from early to mature maturation stages (Appendix 4). The production index of samples from the Waiomo Member (n=54) vary from 0.01 to 0.29 suggesting this younger member is near the top of the oil window in early to peak maturation stages. The production index of samples from the overlying Goldlight Member (n=32) varies from 0.01 to 0.15 with 95% of the samples between 0.01 and 0.08, suggesting the youngest lacustrine member has not yet entered the oil window and therefore is still immature (Appendix 4). Only 5% of the Goldlight Member samples fall in the early maturation stage.

## 3.10 Interpretations and Discussion

Worldwide, about 30% of all rift half-grabens contain thick lacustrine mudstones from large, deep lakes (Lambiase and Morley 1999) which have good preservation potential of organic carbon because of their great thickness and long history of deposition (Kelts 1988; Biddle and Christie-Blick 1985). Organic matter found in such lacustrine mudstones commonly comes from the decomposition of algal materials (Bottyococcus algae), microfossils (e.g., plankton), dinoflagellates, fresh water gastropods and bivalves (Kelts 1988; Katz 1995). In addition, the relationship between subsidence, sediment supply, and accommodation in a rift basin can form thick sequences of alluvial sandstones with coals and highly carbonaceous mudstones alternating with the thick sequences of lacustrine sediments. These fine-grained sediments as a whole can be potential source rocks (Kelts 1988; Allen and Allen 1990; Katz 1995; Lambiase

and Morley 1999; Gawthorpe and Leeder 2000). Although the Greymouth Rift Basin has a very limited geochemical database to analyse hydrocarbon source rock potential, the basin is extensively drilled for coal mining and has several accessible outcrops for sedimentary facies analysis. The detailed sedimentary facies analysis of the Greymouth Basin indicates that the lacustrine facies association has the higher petroleum potentiality along with already proven coaly source rocks. The study of drill cores and outcrops can resolve the complexity of potential lacustrine source rock mapping in this basin.

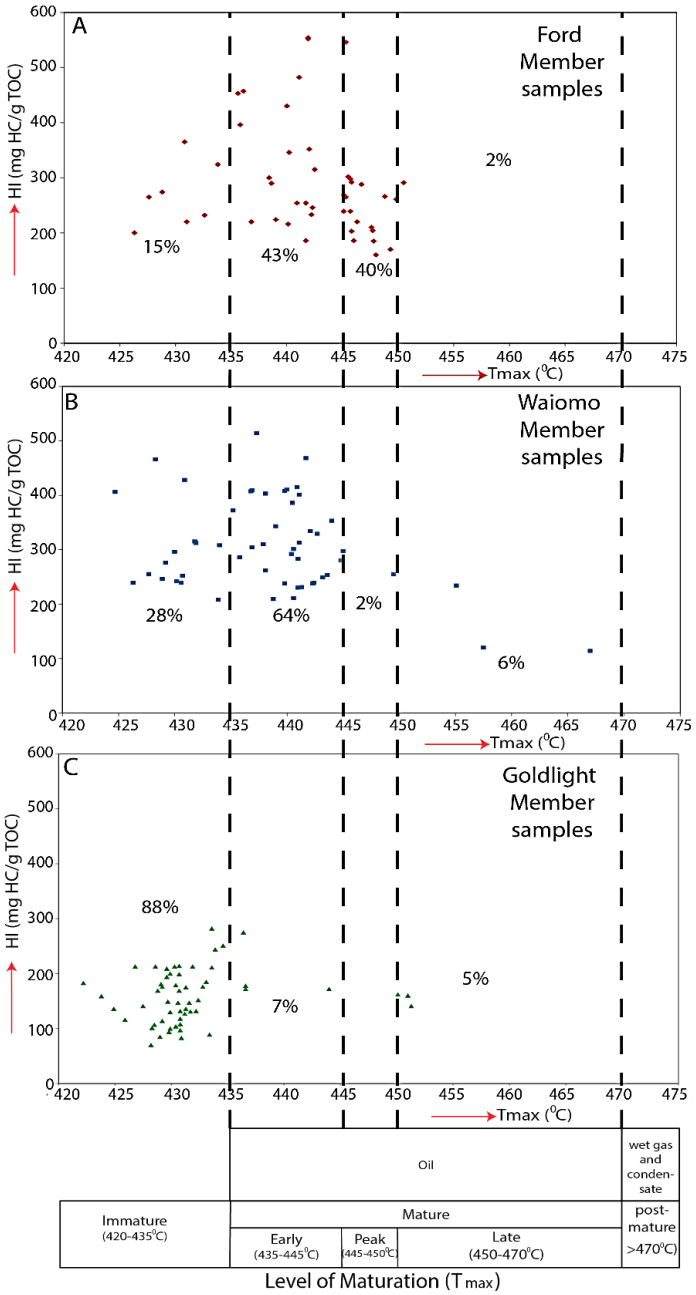


Figure 3. 24: The comparison of Tmax vs HI plot for the Ford, Waiomo and the Goldlight lacustrine members. The Ford mudstone samples are shown in red bullet points whereas the Waiomo and the Goldlight mudstone samples are shown in blue squares and green triangles. The broken black line represents the division in level of thermal maturation.

### 3.10.1 Petroleum potential of the lacustrine facies association

The lacustrine facies association of Ford, Waiomo and Goldlight members show promising petroleum potentiality based on their dark colour and higher TOC and $S_2$ content. TOC and $S_2$ values indicate that all three lithofacies have good to excellent source rock generative potential (Figure 3.25). We found that the Late Cretaceous Ford Member has TOC content of up to 4.6 wt%, HI of up to 554 mg HC/g TOC, and mostly mixed oil and gas to oil prone source with good to excellent total petroleum potential. The Late Cretaceous Waiomo Member has good potential with TOC contents of up to 3.08 wt%, HI of up to 554 mg HC/g TOC, and mostly mixed oil and gas prone source rocks with fair to very good total petroleum potential. The Palaeocene Goldlight Member has poor potential with TOC contents of up to 2.95 wt%, HI up to 282mg HC/g TOC, and mostly mixed oil and gas prone source rocks with poor to good quantity petroleum potential. The best sample (DH656/461.70m) was collected from lacustrine mudstone with minor sandstone facies in the Ford Member and shows the highest $S_2$ value (25.08) and TOC value (above 4 wt%) of all samples from the Paparoa Formation. This sample comes from lacustrine mudstones with minor thin sandstone facies of deep-water origin where turbidite sandstones are very fine sand grading to siltstone in grain size. Although conspicuous plant material is also present in proximal sandy turbidites facies, higher values of $S_2$ and TOC are absent in the turbidite beds of this facies. The grain size of the turbidite sandstone is fine sand grading to medium sand. This suggests that the preservation potential of the conspicuous plant materials present in the turbidite beds is higher and may have excellent source rock potential when they are finger grained and were deposited in deep water as compared to those turbidite deposits where the grain size is mostly fine to medium sand and deposited in more proximal and perhaps more oxygenated lacustrine settings.

### 3.10.2 Kerogen types and sources

The source rock geochemistry indicates that the organic matter in the lacustrine facies association was mostly derived from Type II and Type III kerogens which are dominated by terrestrial-derived exinite (spores and pollens) and vitrinite (cellulose) resulting in mixed gas and oil generation. The occurrence of vitrinite and inertinite in the deep-water environment is interpreted as a resedimentation process (Muljana et al. 2012). In the Greymouth Basin, these spores and pollens were likely transported by meandering rivers, through the delta front mouthbar, and then into deeper water carried by turbidity currents to accumulate within the lacustrine mudstones. Only a few samples from the Ford and Waiomo members exhibit higher HI indicating Type I, algenite kerogen which could result in oil generation.

Mohnhoff et al. (2017) conducted microscopic analysis of the lacustrine mudstones in the Paparoa Formation and identified a mixture of vitrinite and inertinite in all samples (Figure 3.26A). Samples from the Ford and Waiomo members also contain *Botryococcus* algae (Figure 3.26B). A plot of fourteen samples show that those with higher HI values and paraffinic oil potential tended to be richer in liptinitic macerals comprising telalginite (*Botryococcus*) and lamalginite (*Pediastrum*), whereas poorer quality samples were richer in higher plant matter-derived vitrinite and inertinite macerals (Figure 3.27). *Botryococcus* is thought to derive from the hydrogenation of C34 alkenes, termed botryococcenes, which occur in very high concentration in a species of fresh water, green algae *Botryococcusbraunii* (Metzger et al. 1985; Volkman 1988). Colonies of green *Botryococcusbraunii* can be found in temperate or tropical, deep, freshwater lakes around the world, where they often float in large masses and bloom in the presence of elevated levels of dissolved inorganic phosphorus (Wolf et al. 1985; Metzger and Largeau (2005). Holocene sedimentary records in the basinal area of Lake Victoria in Africa show sediments closer to a Type I precursor which is believed to be derived from *Botryococcus* floating algal mats (Kelts 1988).

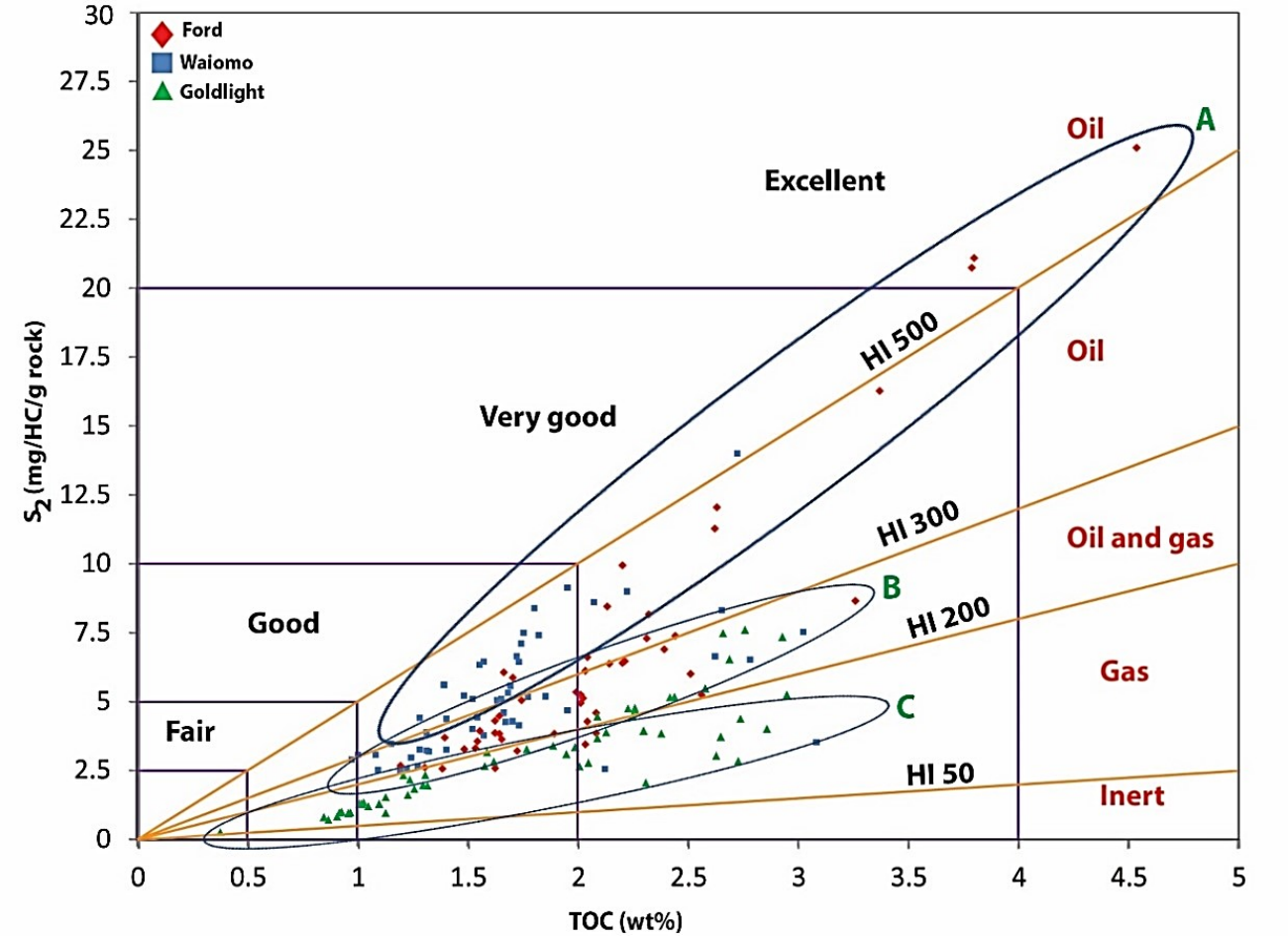


Figure 3. 25: The comparison of among TOC vs S2 vs HI plot for all lacustrine mudstone samples (modified from Mohnhoff et al. 2017).

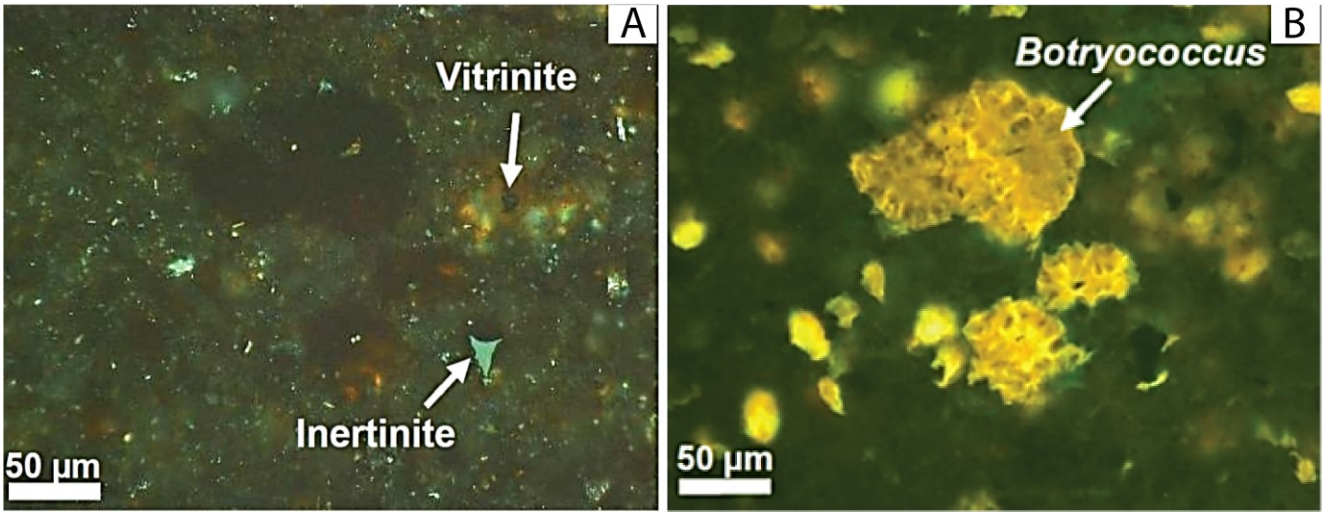


Figure 3. 26: A) Microscopic analysis of the lacustrine mudstone showing the presence of vitrinite and inertinite macerals (photo taken from Mohnhoff et al. 2017), and B) Microscopic analysis of the lacustrine mudstone showing the presence of Botryococcus algae (photos are taken from Mohnhoff et al. 2017).

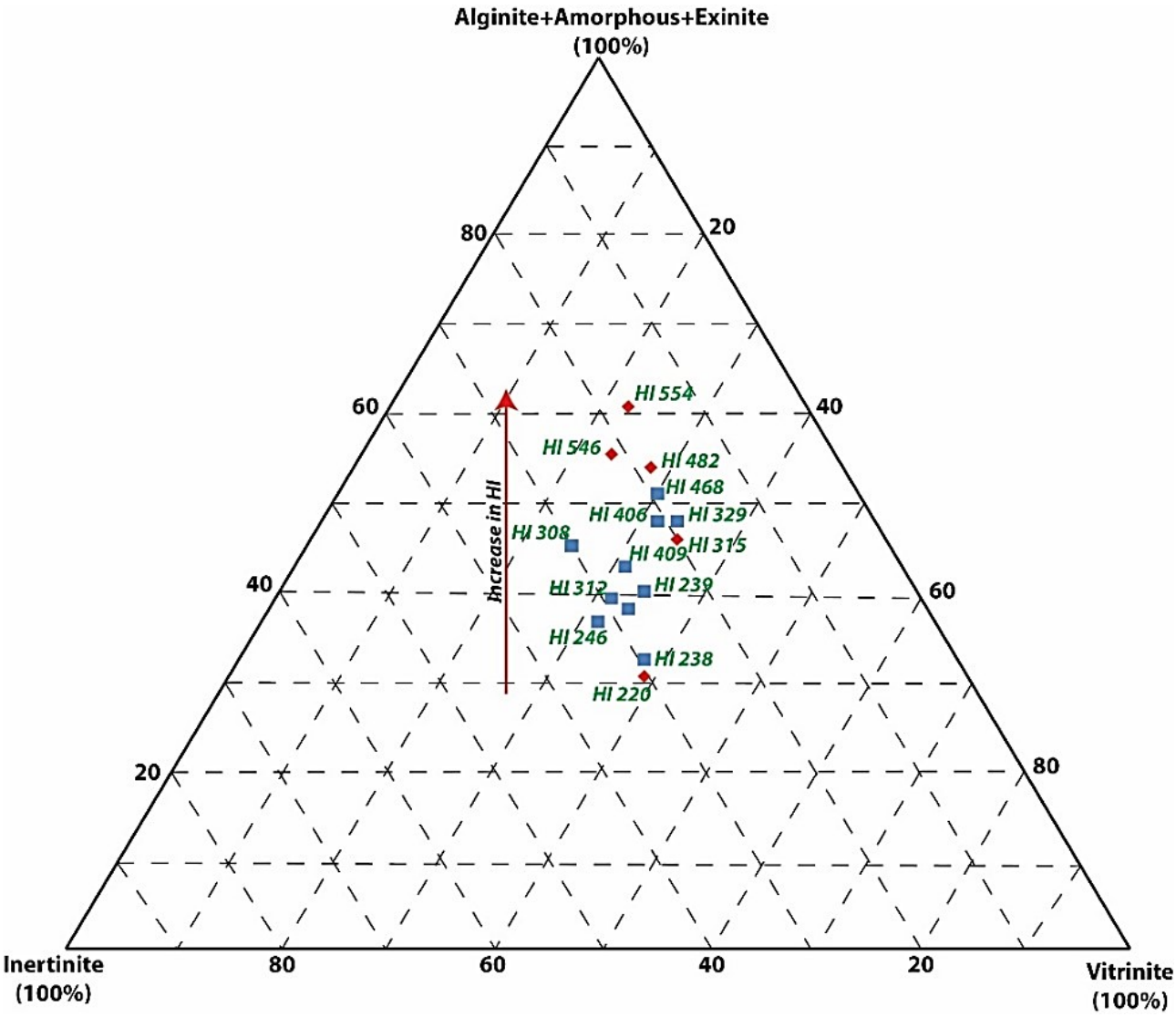


Figure 3. 27: Samples distribution showing higher HI values and paraffinic oil potential tend to be richer in liptinite macerals telalginite (comprising Botryococcus) (slightly modified from Mohnhoff et al. 2017).

### 3.10.3 Preservation potential of the organic matter

The source rock analysis of the three lacustrine members indicates that the Late Cretaceous Ford and Waiomo lacustrine mudstones have higher petroleum potential than the Palaeocene Goldlight lacustrine mudstone despite isolith maps and distribution of sedimentary facies indicating that the Goldlight Lake was larger, deeper and more extensive than the Ford or Waiomo lakes. The thickness distribution of the lacustrine facies association of each member indicates that the Ford Member was restricted to the centre and northeastern side of the basin and was most likely deposited in multiple sub-basins, the thickest at 83 m. The Waiomo Member was widely distributed across the basin with a new depocentre in the northwest of about 72 m thick. The Goldlight Member was the thickest and most extensively distributed across the basin with a maximum thickness of 200m in the centre. This suggests that some change in the lacustrine setting affected the preservation potential of the organic matter.

Higher preservation potential of source rocks often depends on thermal stratification of lake water and has been intensively studied (Lewis 1983; Wilhelm and Adrian 2008; Kirillin and Shatwell 2016; Woolway and Merchant 2019). Thermal stratification is a phenomenon where lake waters separate into three distinct layers. The shallow water surface layer (epilimnion) is warm, heated by direct sunlight. The deep bottom water layer (hypolimnion) is cool and dense with little to no sunlight available to support aquatic life. The middle thermocline layer (metalimnion) separates the epilimnion from the hypolymnion and acts as a barrier that prevents mixing and heat exchange between the top and the bottom layer. Oxygen input in lake water comes from different sources with the majority from atmospheric diffusion at the surface, some from photosynthesis by aquatic plants, and minor amounts from river inflow. The hypolimnion, being deeper, receives very little dissolved oxygen from atmospheric diffusion and river input and is too dark to favour oxygen producing aquatic life. Once the dissolved oxygen level in the hypolimnion of deep lakes reaches 0 mg/l, the water layer becomes anoxic. This leads to oxygen-deficient, reducing conditions in deep lakes which thus become ideal for preservation of organic material.

Thermal stratification in temperate lakes is seasonal. During the warm summer months, there is strong thermal stratification leading to higher preservation of organic matter in anoxic bottom waters of a deep lake. During the autumn and winter months, thermal stratification becomes weaker as the sunlight is not strong enough to effectively warm the epilimnion. This may cause the epilimnion to sink into the hypolimnion causing mixing of the layers (Lewis 1983). Wind can also mix the layers if the density differences between epilimnion and hypolimnion become weaker during autumn and winter. The addition of oxygenated surface waters into deeper waters reduces the preservation potential of organic matter in deep lakes with mixed waters. Warmer climates tend to have more consistent thermal stratification in lakes, thus increasing the preservation potential of organic matter.

In order to have high preservation potential of organic matter in lacustrine sediments, the ideal conditions would be for the palaeolake to be large, deep, in a warmer climate, and have a reducing environment with limited circulation during seasonal stratification. Lake Lugano in Switzerland is an example of a complex, deep (270m), freshwater, temperate lake with sluggish lake circulation throughout the Holocene in an overall reducing environment (Kelts 1988). The geochemical analysis of the lake sediments indicates that they contain an average of 2-6% TOC comprising a combination of dissolved carbon, and detrital input of particulate organic carbon carried by common turbidites (Kelts 1988).

The higher TOC and S2 values of the Ford and Waiomo members indicate higher preservation of the organic matter, suggesting there was strong thermal stratification of the Ford and Waiomo lakes that was probably consistent throughout their life span. This suggests the lakes were deep but with limited circulation which increased the preservation of organic matter. In addition, rapid warming at the end of Early Cretaceous is evident from the change of forest vegetation and appearance of flowering plants, indicates an average temperature of about 12-14 $^{0}$ C (Raine et al. 2017). This would also be likely to improve preservation of organic material due to increased stratification of the lake waters.

In contrast, the Goldlight Lake had poor preservation of organic matter even though it was large and deep. It may be that the large size of the lake meant it was more consistently agitated by winds preventing seasonal stratification. Alternatively, the cooling of the climate during at the end of the Cretaceous (Raine et al. 2017) may have meant the lake water experienced more seasonal temperature changes that drove water circulation and mixing of thermal layers. This would have produced more oxic conditions in the bottom waters of the lake and hindered the preservation of the organic matter in the lake sediments. The K-T boundary, which is also a boundary of climate change, is located at the contact between the Rewanui and

Goldlight members as indicated by the sudden extinction of *Tricolpiteslilliei* and other rare large and/or ornamented angiosperm pollen taxa (PM2), and the rise in abundance of *Triorites minor* (PM3) (Ward 1997).

### 3.10.4 Petroleum potential of the Greymouth Basin

The study of the detail sedimentary facies and geochemical analysis of the Paparoa Formation in the Greymouth Basin shows that the lacustrine mudstone facies have potential for generating both oil and gas as indicated by laminated carbonaceous mudstones and siltstones with leaf and fresh water fossils. Organic matter found in such lacustrine mudstones commonly comes from the decomposition of algal materials (*Bottyococcus* algae), microfossils (e.g., plankton), dinoflagellates, fresh water gastropods and bivalves etc (Kelts 1988; Katz 1995). In general, the lacustrine mudstones facies are the thickest individual facies and can be identified in three stratigraphic positions (Ford, Waiomo and Goldlight) of the Paparoa Formation and are mappable across the basin in a fence diagram. The visual carbon percentages of abandoned channel, crevasse splay, interdistributary bay and low-lying marshy swamp facies indicate that they also have the potential of being hydrocarbon source rocks. However, the presence of moderate to high bioturbation and episodic clastic sediment input from river flood make their preservation potential low and are thought to be less potential as petroleum source rocks. The mire coal facies are already proven source rocks for the Greymouth Basin as indicated by thick, black coals and interlaminated very high carbonaceous mudstones.

### 3.10.5 Comparison with Taranaki Basin and other Late Cretaceous basins in New Zealand

The Greymouth Basin is a small part of the Late Cretaceous West Coast-Taranaki Rift System in New Zealand, of which only one part of it, the Taranaki Basin, is producing petroleum. However, unlike most parts of the Taranaki Basin which are deeply buried and only available via seismic analysis, the sedimentary rocks of the Greymouth Basin are accessible in outcrops and through extensive drill cores. Although the main source rock within the highly prospective Taranaki Basin is Eocene in age (Sykes et al. 2014), Late Cretaceous waxy coals and coaly mudstones are also proven as source rocks along with the Eocene source rocks. Considering the similarities in basin evolution and hydrocarbon source rock characteristics, the onshore Greymouth Basin can provide the best available geological analogue for lacustrine source rocks that are inferred to be present in the Taranaki Basin.

Based on the study of seismic data in offshore New Zealand, it is suggested that there is a strong possibility of finding Late Cretaceous alluvial and lacustrine sediments in three other basins; the Great South Basin of the southeast coast of the South Island, the Bellona Basin to the west of Taranaki and Challenger Plateau, and the Deepwater Solander Basin south of Fiordland. Several wells and seismic data have highlighted a thick sequence of terrestrial and transgressive Cretaceous syn-rift sandstones, mudstones and coals present in the Great South Basin (Uruski 2010; Killops et al. 1997; Barrier 2017). The studies on the Solander Basin reveal that this basin is characterized by Cretaceous lacustrine mudstones, alluvial sandstones and coals, and thus fulfills all necessary conditions for trapping potential hydrocarbon source rocks (Uruski 2010). The Bellona Basin is the least studied basin among the three basins. However, current knowledge from the plate reconstructions study suggested that the Bellona Basin may have formed adjacent to the Gippsland Basin in Australia (Uruski 2010). The Gippsland Basin has organic rich, non-marine lacustrine mudstones and coals along with marginal marine shales (Bhattacharjee 2005). Given the similarities in basin formation, it is likely that the Bellona Basin contains a similar sequence of hydrocarbon potential source rocks. If lacustrine mudstones are present in the Great South, Bellona and Deepwater Solander Basins, sedimentary facies and geochemical analysis of the Paparoa Formation of the Greymouth Basin can also be an analogue

for them. This suggests high TOC and a range of HI values, and therefore a capability of generating both oil and gas.

## 3.11 Conclusions

Late Cretaceous to Early Palaeocene non-coal bearing lacustrine sedimentary rocks in the Greymouth Basin are suggested to be potential source rocks from several oil seeps discoveries. The main purpose of this study is to conduct detailed facies analysis of the fine-grained sedimentary rocks of the Paparoa Formation in order to understand the distribution of different lacustrine facies, their relationships to other fine-grained and coal-bearing facies, and examine the source rock potential of the lacustrine facies. The results have been used as an analogue for the Taranaki and other Late Cretaceous basins in New Zealand.

Sedimentary facies of potential hydrocarbon source rocks have been grouped into four facies associations i) lacustrine, ii) delta front, iii) meandering alluvial/delta plain and iv) mires. The reconstruction of palaeogeography of the Greymouth Basin has been developed by constructing a fence diagram. The palaeogeography of the Greymouth Basin indicates that the Paparoa Formation was depositied in a half graben with alternating alluvial fan and fan deltas on the steep, fault-controlled side, lake in the basin axis, and low gradient, sandy, deltas fed by meandering rivers on the hinge side of the basin. A number of hydrocarbon source rocks have been identified based on their visual carbon percentages. The lithofacies of the lacustrine facies association are considered to have highest petroleum potential based on their dark colour, highest thickness and deep water origin. The thickness distribution of the lacustrine facies association of each member indicates that the Ford Member is about 82 m thick and is restricted to the centre and northeastern side of the basin. The Waiomo Member is widely distributed across the basin with a new depocentre in the northwest of about 87 m thick. The Goldlight Member is the thickest and most extensively distributed across the basin with a maximum thickness of 200m in the centre.

About 40% of Ford and Waiomo lacustrine massive mudstone samples fall in the excellent to very good range with S2 values ranging between 10 and 25, and TOC values ranging from 2% to 4.6% and HI values in between 300-600, indicating they are capable for generating both oil and gas. Most of the Goldlight lacustrine massive mudstone samples plotted as having good petroleum potential with S2 values between 2 and 10 and TOC values between 0.5 and 4. However, 80% of the Goldlight samples have lower HI values (<200), indicating they are only capable of generating gas.

The sedimentary facies analysis of the Paparoa Formation can be used as an analogue for the Taranaki Basin as the latter is deeply buried and only available via seismic. Based on the seismic data, it is suggested that the lacustrine mudstones are also present in other Late Cretaceous, deeply buried basins in New Zealand. Given the similarities in basin formation, it is likely that the lacustrine mudstones present in these Late Cretaceous basins could also have hydrocarbon potential.

# Chapter 4: Tectonic evolution of the Greymouth Basin, West Coast, New Zealand


## Abstract

The Greymouth Basin, in which the thick sequence of Paparoa Formation was deposited, is part of the same Late Cretaceous to Early Palaeocene rift tectonics along the West Coast that produced the Taranaki Basin. The purpose of this chapter is to understand the basin evolution through time by investigating the distribution of sedimentary facies through isolith maps, a basal unit map and a fence diagram of detailed facies correlations.

The cross-sections and fence diagram demonstrate the half-graben geometry of the Greymouth Basin. Alluvial fan facies dominate to the NW, meandering channel facies dominate to the SE, and the basin axis contains facies that alternate between alluvial and lacustrine depositional phases from Late Cretaceous to Early Palaeocene. The lacustrine mudstone facies onlaps alternating alluvial fan and gravelly braided river facies to the NW near the basin-bounding fault, and both thickens and widens upsection. Isolith maps of the conglomerate and lacustrine facies show an overall NNE-SSW trend for the basin axis and reveal that older units comprise several isolated smaller lakes that later connect and become wider through time, expanding toward the northwest. The basal unit map shows that the conglomerates step westward through time with increasingly younger Paparoa Formation members directly overlying the basement.

The meandering channel facies with scattered abandoned channel facies in the basin centre indicate phases of slow to moderate subsidence rates in the basin. These alternate with mire and lacustrine facies in the basin centre suggesting phases of increased subsidence rate. Conglomerate facies mark normal fault scarps that became progressively more connected until they formed a major border fault to the northwest. This fault was responsible for the lateral and vertical facies changes across the basin during its greatest expansion. The results suggest that the Greymouth Rift Basin evolved from small sub-basins that widened, deepened and amalgamated through time.

The sedimentation pattern and the evolution of faulting suggest the basin likely formed in a pure extensional setting where no, or minimal, strike-slip movement occurred. All of the revised isolith maps show the same NNE-SSW orientation which suggests the Greymouth Basin did not change orientation during its subsidence history. Therefore, we suggest the change from WNW-ESE to NNE-SSW may have occurred during the ~15 Ma gap between deposition of the underlying mid-Cretaceous Pororari Group and the overlying Late Cretaceous to Early Palaeocene Paparoa Formation. These results can be compared with the West Coast-Taranaki rift phase where a number of Late Cretaceous sub-basins have NNE-SSW orientation approximately perpendicular to many of the earlier mid-Cretaceous rift basins.


## 4.1 Introduction

Rift systems are complex features commonly developed as collections of stepping, intersecting, and/or parallel normal faults with associated rift basins (Nelson et al. 1992; Busby and Ingersoll 1995; Withjack et al. 2002). They are commonly associated with the initial stage of continental break-up where the extension may lead to lithospheric rupture and the formation of a new ocean basin (Klepeis and Vine 2013). Rift basins are elongate crustal depressions bounded on one or both sides by basement-involved normal faults (Withjack et al. 2002). Two normal faults facing each other with the down-dropped block forming the basin in the centre are referred to as a full graben structure (Nelson et al. 1992; Withjack et al. 1998,

2002). Half-graben structures or tilt blocks are formed when the basins are bounded by single, steep normal faults on one side and low angle hinge zones on the other side (Leeder and Gawthorpe 1987; Roberts and Yielding 1994; Leeder 1995; Roberts and Bally 2002; Withjack et al. 2002). The asymmetric nature of the half-graben has a major impact on deposition and the distribution of sedimentary facies across a basin (Leeder and Gawthorpe 1987; Gawthorpe and Leeder 2000). Thick, coarse-grained, alluvial fan conglomerates may be deposited along the steep fault-controlled margin where both the gradient of the slope and subsidence are greatest. Lower energy fluvial fan environments depositing fine-grained sandstones and mudstones are associated with the shallowly dipping hanging wall on the hinge side of the basin. The slightly off-set central part of the basin commonly forms lacustrine environments when subsidence rate is high but sediment supply is low; this may be replaced with meandering alluvial environments where either subsidence rate is lower or sediment supply is greater (Leeder 1995, 1999; Einsele 2013). Alternating alluvial and lacustrine sequences in a half-graben basin result from variable subsidence rates in the basin and the tilting nature of the fault blocks (Leeder and Gawthorpe 1987; Gawthorpe and Leeder 2013; Holz et al. 2013, 2015).

The Cretaceous break-up of Gondwana resulted in a series of extensional basins in New Zealand and has been previously documented by many authors (Laird 1981, 1992, 1993; Bishop 1992; Nathan et al. 1986; Turnbull et al. 1993; King and Thrasher 1996; Gaina et al. 1998; Cook et al. 1999; Laird and Bradshaw 2004; King et al. 2011; Strogen et.al. 2017; Mortimer et al. 2017). The Greymouth Basin is part of the West Coast–Taranaki Rift System (80– 55 Ma) mainly observed in the West Coast (Greymouth Basin), southern Taranaki (Taranaki Basin), and Western Southland (Waiau Basin) regions (Strogen et al. 2017). A better understanding of the tectonic evolution of the Greymouth Basin will contribute more information to the context of the formation of the other contemporary basins of West Coast–Taranaki Rift System.

The Greymouth Basin, filled with the Late Cretaceous to Early Palaeocene sediments of the Paparoa Formation, has been variably modelled as a complex full-graben rift basin (Bowman 1984), a half-graben rift basin with the bounding fault on the eastern side (Ward 1997; Newman and Newman 1992; Kamp et al. 1999), a transtensional rift basin (Laird 1993, 1994; Bassett et al. 2006), and a sag basin (Gage 1952; Suggate 2014). In most cases where a fault was postulated it was located on the eastern side of the basin primarily based on the presence of the Montgomerie - Mt Davy Fault System marking the eastern boundary of the Paparoa Formation (Gage 1952; Newman 1985; Bishop 1992; Ward 1997; Kamp et al 1999). However, more recent work has suggested that the Montgomerie - Mt Davy faults were not active until very late in the basin's history and thus could not have been the primary basin bounding fault for the majority of the basin's subsidence history (Suggate 2014). Other authors suggest that thick conglomerate deposits indicate high relief and therefore the basin bounding fault lay to the northwest (Bassett et al. 2014; Chapter 2).

Isopach maps of different members of the Paparoa Formation have been interpreted as indicating a change in basin orientation from WNW-ESE to NNE-SSW approximately mid-way through the basin's depositional history (Gage 1952; Newman 1985; Ward 1997). However, more recent work suggests no dramatic change in basin orientation occurred, based on isopach maps created from new drill hole data illustrating thickness changes in lacustrine members (Cody 2015).

This study presents a tectono-stratigraphic model for the Greymouth Basin based on new detailed sedimentary facies analysis, isolith maps of lithofacies rather than members, a basal unit map, and a fence diagram connecting cross-sections developed from facies correlations. The questions framing this research are the following:

1) What is the tectonic setting of the Greymouth Basin? Is it purely extensional, transtensional, or a sag basin?
2) Did the basin change its orientation from WNW-ESE to NNE-SSW and if it did, why?
3) How did the Greymouth Basin evolve?
4) What does this indicate about the West Coast-Taranaki Rift System?

## 4.2 Formation and lithostratigraphy of the Greymouth Basin

The formation of the Greymouth Basin is directly associated with the mid to Late Cretaceous breakup of Gondwana and the opening of the Tasman Sea separating New Zealand from Australia (Laird 1994; Laird and Bradshaw 2004). Two temporally distinct phases of rifting have been recognized in New Zealand during this time (Strogen et al. 2017). The first phase, the Zealandia Rift phase, was during the mid-Cretaceous (c. 105 – 83 Ma) and produced half-grabens and metamorphic core complexes striking NW to WNW; it coincided with the opening of the Southern Ocean and rifting from Antarctica (Strogen et al. 2017). The second phase, the West Coast–Taranaki Rift System phase, was active during the latest Cretaceous-Palaeocene (c. 80– 55 Ma) and produced NNE-striking extensional half-grabens; it coincided with active sea floor spreading in the Tasman Sea (Strogen et al. 2017). These two phases were separated by a short period (c. 83 – 80 Ma) of uplift and erosion representing a break-up unconformity (Strogen et al. 2017). The Greymouth Basin, the subject of this study, is the product of the second rifting phase and contains more than 800 metres of Late Cretaceous to Early Palaeocene sedimentary rocks in seven members (Gage 1952; Nathan 1978; Nathan et. al. 1986, 2002; Strogen et.al. 2017).

The Greymouth Basin is located in the West Coast region of the South Island and is bounded by the modern shoreline at Twelve Mile Beach in the west and the Montgomerie - Mt Davy Fault System in the east (Suggate 2014; Figure 4.1A). The Late Cretaceous to Early Palaeocene Paparoa Formation is characterized by non-marine deposits composed of conglomerates, coals, coaly mudstones, sandstones and lacustrine mudstones (Figure 4.1B; Gage 1952; Nathan et al. 1986; Newman and Newman 1992, Boyd and Lewis, 1995; Ward 1997; Chapter 2; Chapter 3). The non-marine deposits are interpreted as a typical terrestrial rift succession comprising fault proximal alluvial fans/braided alluvial facies and hinge side sandy/muddy river delta/meandering alluvial and floodplain systems grading laterally to basin axis lacustrine mudstone facies alternating with meandering alluvial systems with adjacent raised mires (Ward 1997; Cody 2015; Chapter 2; Maitra and Bassett 2016, 2017, 2018). The Paparoa Formation is divided into seven members encompassing alternating coal bearing alluvial and lacustrine facies. The coal-bearing alluvial phases are represented by the Jay, Morgan, Rewanui and Dunollie members from the oldest to the youngest. These four members are separated by three lacustrine phases; the Ford, Waiomo and Goldlight members from the oldest to the youngest (Figure 4.1B; Gage 1952; Nathan 1978; Nathan et. al. 1986, 2002; Boyd and Lewis 1995; Ward 1997). The Paparoa Formation overlies Greenland Group basement rocks of Early Ordovician age and underlies the transgressive sequence of Palaeocene Brunner Formation to calcareous Island Sandstone, Eocene Kaiata Mudstone and Oligocene Cobden Limestone (Gage 1952; Nathan 1978; Nathan et. al. 1986, 2002).

## 4.3 Previous Greymouth Basin models

The Greymouth Basin has been variably modelled by different authors. However, it has been interpreted as a rift basin by most authors. Bowman (1984) modelled the Greymouth Basin as a complex full graben basin with two major persistent parallel depo-centre zones separated by a more stable palaeo-high of a small horst

in the middle (Chapter 1; Figure 1.7). The grabens were slightly asymmetric. Bowman's (1984) model shows subsidence and sediment thicknesses being largely controlled by NNE-SSW deep seated syn-depositional faults. The western margin active fault scarp was a major NNE trending fault, likely the Cape Foulwind Fault offshore to the west. The eastern margin of the basin was controlled by major basement faulting, originally identified by Bowman as the Montgomerie-Mt Davy Fault System, and was active from the Late Cretaceous to the Palaeocene.

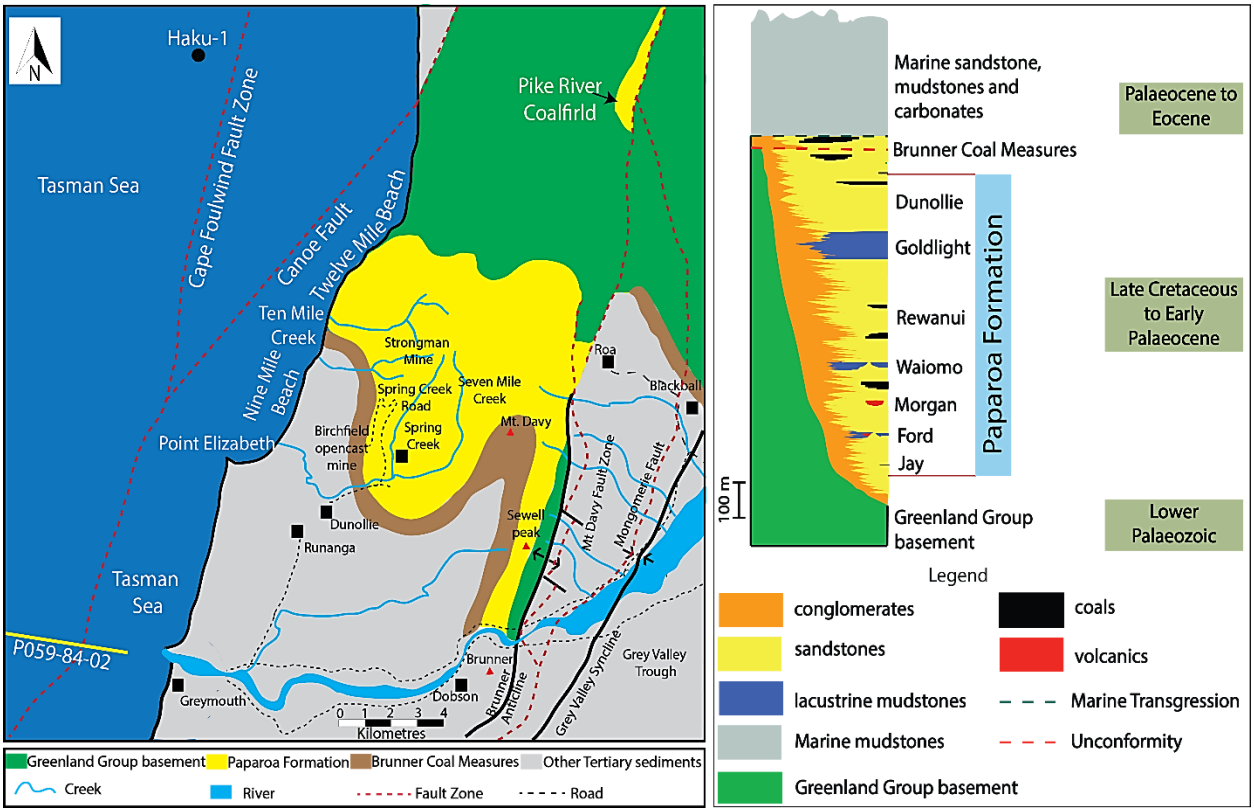


Figure 4. 1: A) Geological and structural map of the study area (modified from Gage 1952, Newman 1985, Suggate 2014, Nathan 1986; Nathan et al. 2002; Rattenbury and Isaac 2012) of the Greymouth Basin. The Haku-1 well in the northwest offshore is used to define the extreme northwest limit of the Greymouth Basin whereas the yellow line in the southwest is an offshore seismic, representing Takutai half graben and refers the figure 2.21. B) Generalized stratigraphy of Paparoa Formation, modified from Newman 1985, Nathan 1986, Boyd and Lewis 1995 and Ward 1997 and Chapter 3.

The rift basin model proposed by Newman (1981, 1985) stated that the Greymouth Basin has two major structural trends, WNW-ESE for the older members and NNE-SSW for the younger members with the transition within the Morgan to Waiomo members (Chapter 1; Figure 1.8). Newman identified the eastern margin as the location of the majority of the basin subsidence. Later, Ward (1997), Newman's student, interpreted the Greymouth Basin as a half-graben where the eastern margin fault (Montgomerie - Mt Davy Fault System) was responsible for the overall subsidence and sediment distribution (Chapter 1; Figure 1.9).

An alternative theory suggested that extension of the Greymouth Basin could have been accommodated as oblique movement on NNE – SSW faults, likely reactivated transform faults from spreading in the Tasman Sea (Laird 1994; Bishop 2010). These palaeo-reconstruction models and the interpretations about the changes in the primary extension directions of the basin led to ideas about the Greymouth Basin as a

transtensional basin. Strike-slip fault movement was also suggested based on provenance analysis of the Paparoa Formation that concluded that the Greymouth Basin formed in a transtensional setting (Bassett et al. 2006). The provenance study was done by cathodoluminescence analysis of detrital quartz grains indicating a predominantly metamorphic source. From this data, Bassett et al. (2006) concluded that the Greymouth Basin must have moved past the Paparoa Metamorphic Core Complex with sinistral transcurrent movement during the Late Cretaceous. However, the regional basement geology does not support any large scale (tens of km) sinistral offset of the Greymouth Basin suggesting no significant strike slip motion has occurred in the vicinity of the Paparoa Core Complex since its formation (Nathan et. al. 2002; Monteith 2015).

More recently, Suggate (2014) interpreted the Greymouth Basin as a downwarping sag basin similar to the Mawhera basin in the West Coast (Suggate and Waight 1999; Suggate 2013). The sag basin concept of the Greymouth Basin was proposed by Suggate (2014) based on one of the oldest sedimentary cross-sections produced by Gage (1952) who interpreted no faulting in the eastern part of the Greymouth Basin during the whole of the Late Cretaceous and Early Palaeocene depositional phase. Suggate (2014) presented evidence that the Montgomerie - Mt Davy Fault System post-dates Greymouth Basin deposition, truncating outcrops rather than being a basin bounding fault. This interpretation was based on revision of the cross-section through the Brunner Anticline suggesting the onset of uplift was a result of the future Montgomerie - Mt Davy Fault System prior to deposition of the Brunner Formation during Palaeocene to Eocene time (Suggate 2014). Therefore, the Montgomerie - Mt Davy Fault Zone was re-interpreted as post-dating the Paparoa Formation.

Previous studies of the Greymouth Basin have highlighted two primary extension directions of the basin based on isopach maps of different members of the Paparoa Formation, indicating a syn-depositional change in basin orientation (Gage 1952; Newman 1985; Ward 1997). The previously interpreted WNW-ESE orientation of the Jay and Ford members was distinctly different from the interpreted NNE-SSW orientation of the youngest Rewanui, Goldlight and Dunollie members with the transition taking place during the Morgan and Waiomo members. A dramatic 90º change to the primary extension direction from N-S to E–W during deposition of the Paparoa Formation was also proposed by Bishop (2010). The interpretation was that the older Jay and Ford members were deposited in a WNW-ESE trending basin (Bishop 1992) which followed the same orientation as the Paparoa Metamorphic Core Complex and the underlying Hawks Crag Breccia of the Pororari Group (Herd 2007; Sagar and Palin 2011; Schulte et al. 2014). The NNE-SSW orientation of the younger members was interpreted to be the result of the basin bounding NNE-striking Cape Foulwind Fault Zone of the Takutai half-graben located offshore (Bishop 1992; Ward 1997). The resulting palaeo-reconstruction model featured a narrow transtensional corridor along the west coast of New Zealand that aligns parallel with the primary extension directions during this time (Laird 1994; Bishop 2010). Cody (2015) recently argued that there was no dramatic change in basin orientation based on another set of revised isopach maps. Strogen et al. (2017) also concluded that the West Coast–Taranaki Rift System was produced from NNE-SSW striking extensional half-grabens based on geometries in the Taranaki Basin to the north.

## 4.4 Methods

Outcrops, as well as extensive drill cores and geophysical logs, are available throughout the Greymouth Basin due to its history as an economic source of coal. Measured sections, core logs and borehole descriptions have been used to conduct a detailed sedimentary facies analysis of the Paparoa Formation

(Chapters 2 and 3). The detailed sedimentary facies analysis presented earlier provides the basis for the following methods that have been used to determine the tectonic evolution of the Greymouth Basin.

### 4.4.1 Basal unit map

A basal unit map was created to show which member sits directly on the basement Greenland Group. It can be used to identify which side of the basin has the oldest member directly overlying the basement and which side of the basin has younger members deposited directly on top of the basement. The detailed sedimentary facies analysis and correlations resulted in redefining some member designations within cores at some locations. This map will help us to understand the younging direction of basin development.

### 4.4.2 Fence diagram

A fence diagram has been developed based on the correlation of detailed sedimentary facies among the bore holes and the outcrops. The easiest sedimentary facies to correlate is the lacustrine massive mudstone facies in each lacustrine interval. Therefore, the lacustrine massive mudstone facies are first identified in each core or outcrop. The other subaqueous facies (gravelly and sandy turbidites, gravelly delta slope facies etc.) and shoreline facies (gravelly and sandy mouthbar facies, interdistributary bay facies, low lying marshy swamp facies etc.) deposited in each lacustrine interval are then correlated with the lacustrine massive mudstone facies as lateral facies representing the lacustrine interval. This first correlation is made in order to understand the size and extent of lakes in each interval. The subaerial components (debris flow facies, gravelly braided river facies, meandering channel facies, overbank floodplain facies etc.) during the lacustrine phases are interpreted as delta plain environments correlated with the shoreline and subaqueous components of the delta. Alluvial components then replace the lacustrine interval in the basin centre. The subaerial mire coal facies are used as tools to understand the onset of each lacustrine phase, whereas the subaerial axial meandering river and associated floodplain facies are used as tools to understand the beginning of each alluvial phase. The Paparoa Formation in the fence diagram starts with the oldest Jay alluvial phase at the base and ends with the youngest Dunollie alluvial phase at the top. The addition of the Brunner Formation on top of the Paparoa Formation is to understand the continuous development of the basin through time into the post-rift phase. The Island Sandstone is added to infer the time when the overall terrestrial depositional systems of the basin change to a shallow marine depositional setting during New Zealand's transgressive phase.

### 4.4.3 Conglomerate isolith maps

Conglomerate isolith maps are developed in order to understand the relative abundance of conglomerates as well as their distribution in each alluvial or lacustrine phase. These isolith maps represent the distribution of steep fans adjacent to local highs. Conglomerate deposits from alluvial fans and fan deltas, including both subaerial and subaqueous facies, have been used to prepare these isolith maps (Chapter 2;). As conglomerates are found in both alluvial and lacustrine phases, conglomerate isolith maps are presented in four maps. These are named, from the oldest to the youngest, the Jay-Ford, Morgan-Waiomo, Rewanui-Goldlight, and the Dunollie conglomerate isolith maps. There is no lacustrine phase found after the deposition of the Dunollie Member of the Paparoa Formation when deposition changes in the basin to widespread marine transgression recorded by the Island Sandstone.

### 4.4.4 Lacustrine isolith maps

Lacustrine isolith maps are developed in order to understand the thickness and distribution of the sediments deposited subaqueously. All subaqueous components are included in these, including conglomeratic ones,

making them different from previous isopach maps based on the lacustrine members. Subaerial facies, deposited during lacustrine and alluvial phases, are excluded from these isolith maps and are used to separate different lakes from the oldest to the youngest. Subaerial facies such as mire coals, low-lying marshy swamps and mouthbar facies are excluded whereas subaqueous facies such as interdistributary bays and delta slopes are included in the isolith maps. Therefore, lacustrine isolith maps are interpreted as being subaqueous and show the gross thickness of all subaqueous facies. These maps include three subdivisions which are named, from the oldest to the youngest, the Ford, the Waiomo, and the Goldlight lacustrine isolith maps.

Several revisions in the identification of different members in older borehole logs and outcrops were taken into consideration when creating the lacustrine isolith maps. The correlation of detailed sedimentary facies was most important in this process, with information from previous publications also being relevant. The redefinition of lacustrine mudstones by Ward (1997) for certain bore holes located in the central part of the basin has been used to create the Ford lacustrine isolith map. The sedimentary facies of the Waiomo Member at Twelve Mile Beach defined by Cody (2015) have been modified to include interdistributary bay facies, gravelly mouthbar facies, gravelly delta slope facies, gravelly turbidites facies, lacustrine mudstones with minor sandstone facies and lacustrine massive mudstone facies (Chapters 2 and 3). The thick conglomerate deposits of the Rewanui Member that contain load casts and soft sediment deformation are identified as coeval lateral facies to the lacustrine Goldlight Member since the facies indicate subaqueous deposition (Chapter 2). The bore holes in the northwestern part of the basin are correlated with the detailed stratigraphy developed for Twelve Mile Beach outcrop (Chapter 2). The inclusion of the thick section of subaqueous conglomerates creates overlap between the Goldlight lacustrine isolith map and the Rewanui-Goldlight conglomerate isolith map.

## 4.5 Results

### 4.5.1 Basal unit map

The basal unit map shows the bore holes that penetrate to the basement (Figure 4.2). The Jay Member, the basal member, sits directly on the basement in the central and northeastern parts of the basin. The Morgan Member sits directly on the basement in the southeast and covers a wide region to the northwest. The southwestern side of the basin has the Rewanui Member directly overlying the Greenland Group basement stretching across to the southeastern side. In almost all cases, the basal unit is an alluvial member, the Jay, Morgan or Rewanui members. There are only two bore holes which have an exception, showing lacustrine members sitting directly on the basement; the Waiomo Member in the northwest (DH-624) and the Ford Member in the centre (DH-1012). However, faulting in these locations has disrupted the stratigraphy, making it questionable whether Waiomo and Ford members can be identified as originally resting on basement or not.

### 4.5.2 Sedimentary facies distribution

The distribution of sedimentary facies indicates that the northwestern side of the basin is dominated by fan deltas alternating with alluvial fans whereas the southern and eastern sides of the basin are dominated by sandy meandering rivers and floodplains to sandy/muddy deltas (Figure 4.3). Thick, organic-rich, deep-water lacustrine facies are at the centre of the basin with marshy or delta front facies marking the shorelines. Thick, low ash coal facies are interpreted as mire complexes which commonly replace the lacustrine mudstones in the centre of the basin adjacent to axial meandering rivers. In general, fan-delta conglomerates

shift westward and get thicker mirrored by the lacustrine mudstones which also get thicker and shift westward onlapping fan delta conglomerates.

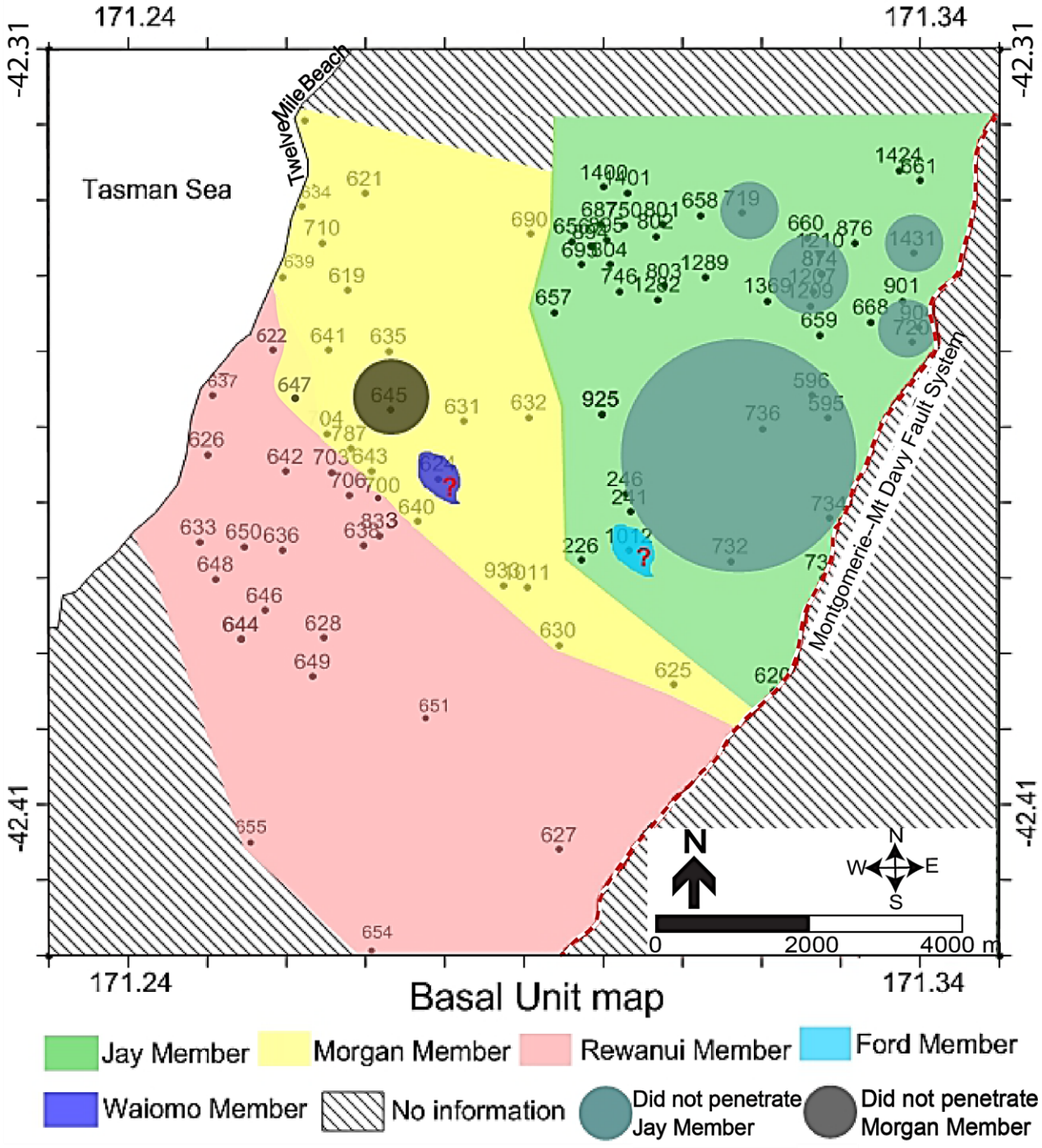


Figure 4. 2: Basal unit map showing westward and southwestward propagation of the younger alluvial members of the Paparoa Formation. In the central and the northeastern side of the basin, the Jay Member is underlain by the Greenland Group basement whereas the Morgan Member directly sits on the basement in the southeast and the northwest. The Rewanui Member covers the southwest and the northwest side of the basin, sitting on top of the Greenland Group basement.

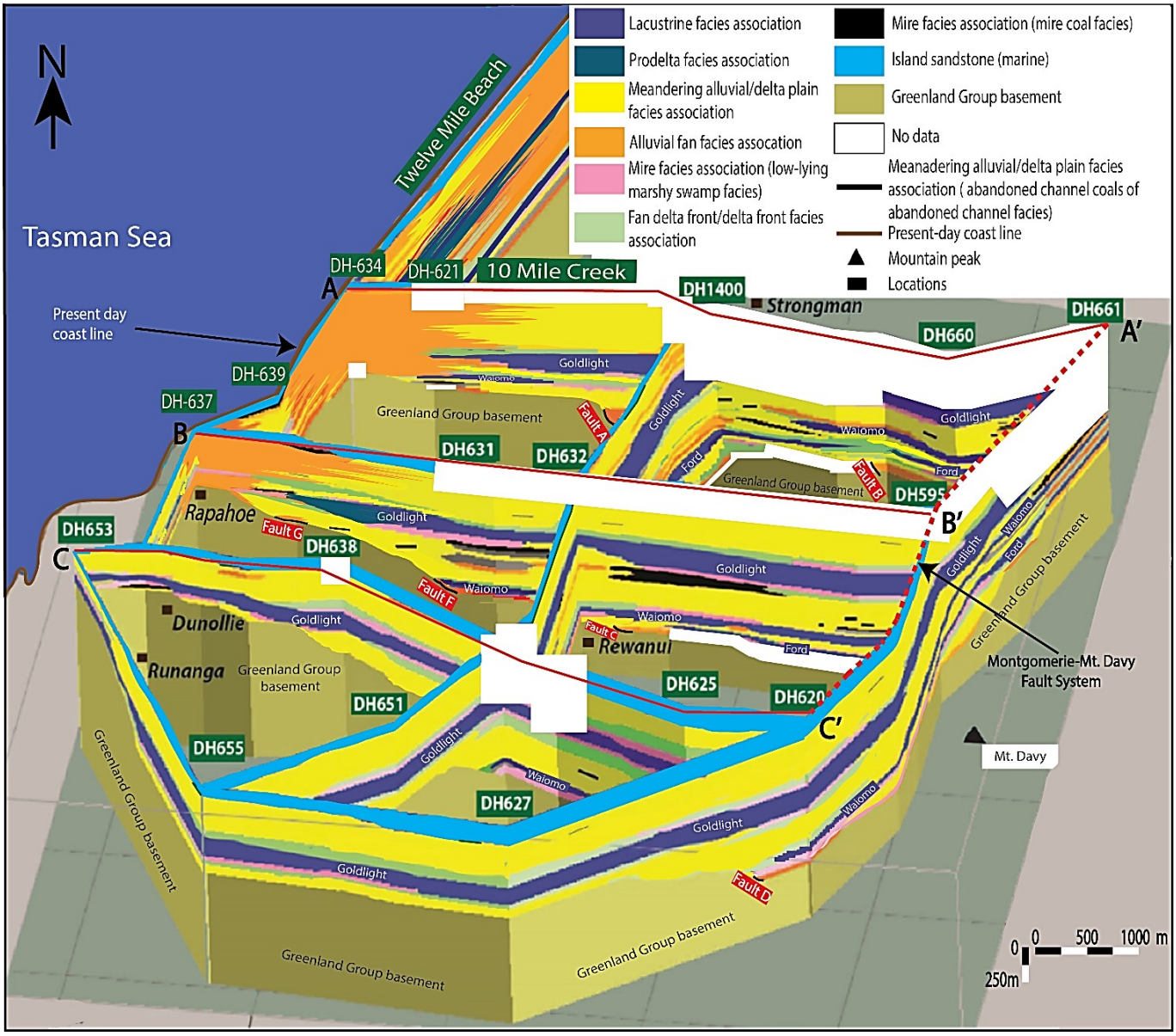


Figure 4. 3: Fence diagram illustrating the distribution of sedimentary facies in the Greymouth Basin. Cross-sections AA', BB' and CC' are shown in more detail in Figures 4.11A, 4.11B and 4.11C. Syn-despositional faults are drawn in the fence diagram based on the presence of thick conglomerates. The red dashed line shows the cross-cutting Montgomerie-Mt Davy Fault System.

Alluvial fan and fan delta conglomerate facies deposited in the Jay and Ford members are restricted to the central and northeastern parts of the overall basin. Conglomerate facies deposited in the Morgan and Waiomo members are found in the northwestern part of the basin and are thinner than in the conglomerates of the Jay Member. Conglomerate facies are the thickest in the Rewanui and Goldlight members and are restricted to the northwestern side of the basin. Conglomerate facies in the Dunollie Member are thinner and also are restricted to the northwestern side of the basin. Conglomerate facies thickness gradually decreases from the northwest to the southeast and south in the basin where sandstone facies dominate

instead. Meandering channels, sandy meandering delta and associated floodplain facies dominate in the centre, the east, the southeast and the southwest regions of the basin.

The lacustrine mudstone facies of the Ford Member are only found in the central and northeastern parts of the basin whereas the lacustrine mudstone facies of the Waiomo Member are found in isolated depo-centres in the northwest and the northeast that merge to the south. The lacustrine mudstone facies of the youngest Goldlight Member is widely distributed across the basin except in the northwestern corner of the basin where it is replaced by subaqueous fan delta slope facies instead.

The conglomerate facies of the Dunollie Member is overlain by conglomerates of the Palaeocene Brunner Member of the Brunner Formation in the west whereas the sandstone facies of the Dunollie Member in the east is overlain by the Eocene Brunner Coal Measures of the Brunner Formation. The Brunner Formation is found across the entire basin except in the coastal Twelve Mile Beach outcrop. The Island Sandstone overlies the Brunner Formation across the entire basin but sits directly on the gravelly braided river facies of the Dunollie Member at Twelve Mile Beach.

### 4.5.3 Conglomerate isolith maps

The gravel-rich facies, such as debris flow facies, gravelly braided river facies, gravelly mouthbar facies, gravelly turbidites facies and gravelly delta slope facies are used to prepare the conglomerate isolith maps. In general, the conglomerate isoliths get thicker with time and step westward.

#### *4.5.3.1 Jay-Ford conglomerate isolith map*

In order to understand the gross thickness of conglomerates deposited in the Jay alluvial phase, existing data from Gage (1952) and Ward (1997) are combined with this study's detailed sedimentary facies analysis of conglomerates (Chapter 2). According to Gage (1952), three subdivisions of Jay conglomerates have been described: Jay (i) (breccia, breccia-conglomerates), Jay (ii) (conglomerates, minor sandstones) and Jay (iii) (Sandstone, shales, coal seams, minor conglomerates). Gage (1952) concluded the total thicknesses of the Jay Member ranges from 0 to 1500 feet (~457 metres). Ward (1997) re-assigned the Jay (i) subdivision of the Jay Member to Pororari Group based on the angularity of the clasts. However, angular clasts also occur in the debris flow facies and alluvial fan facies of the Paparoa Formation and there is no other evidence such as changes in clast composition to support a Pororari Group assignment (Steadman 2017). Therefore, the Jay (i) subdivision is not correlated with Pororari Group in this study and is instead interpreted as the lowermost part of the Jay Member following Gage (1952).

Jay conglomerates rest on the Greenland Group basement in the centre and northeastern region of the basin and are interpreted as alluvial fan and braided river facies. Conglomerate thicknesses from the gravelly delta slope facies, gravelly mouthbar facies and the interdistributary bay facies of the correlatives of the Ford Member are added to the thickness of the Jay conglomerates. The correlation of the detailed sedimentary facies indicates Jay and Ford members were not present in the northwestern or southwestern parts of the Greymouth Basin indicated by 0 thickness on the isolith map. Most of the bore holes that encounter Jay conglomerates do not penetrate to Greenland Group basement (Appendix 3). Therefore, estimating the thickness of the conglomerate for this isolith map remains uncertain and is only a minimum in many locations.

The Jay-Ford conglomerate isolith map shows multiple, small, isolated traces of conglomerates which are in depocentres elongated to the NNE-SSW (Figure 4.4). Unfortunately, due to the limited number of bore holes drilled to basement, it is difficult to interpret overall thicknesses or whether the conglomerates were

deposited in multiple depocentres or fewer larger ones. Multiple depo-centres have been interpreted based on the variation in conglomerate thicknesses. Five faults are identified (Fault A, Fault B, Fault B', Fault C, and Fault D) based on the multiple depo-centres. The maximum thickness of greater than 110 metres can be found in the central part of the basin. The minimum complete thickness is 1.4 metres found in the southeastern region. Conglomerates are found in both the Jay and Ford members in the central part of the basin.

#### *4.5.3.2 Morgan-Waiomo conglomerate isolith map*

Conglomerate deposits resting on the Greenland Group basement at Twelve Mile Beach belong to the Morgan Member as shown on the last published geological map of the Greymouth area (Nathan 1978) and the bore holes close to the Twelve Mile Beach are correlated accordingly (Chapter 2). In order to calculate the gross thicknesses of the Morgan-Waiomo conglomerate isolith, all conglomerate facies from subaerial, subaqueous and shoreline components are combined (Appendix 3).

The Morgan-Waiomo conglomerate isolith map shows conglomerates in four isolated depo-centres located in the northwestern and central region of the basin (Figure 4.5). Therefore, three new faults (Fault E, Fault F and Fault G) and a pre-existing fault (Fault A) are drawn based on four depo-centres. The maximum thickness is 28 metres whereas the minimum thickness is estimated as 17.7 metres. The thickness gradually decreases from northwest to the southeast in each depocentre and elongates in a NNE-SSW orientation. The presence of multiple depocentres suggests the conglomerates were deposited in multiple sub-basins.

#### *4.5.3.3 Rewanui-Goldlight conglomerate isolith map*

It is difficult to correlate the individual conglomerate deposits of the Rewanui and Goldlight members from the stratigraphic column at Twelve Mile Beach. The thick conglomerate section with imbricated clasts, large cross-bedded structures, load casts and soft sediment deformation above the gravelly turbidites facies of the lacustrine Waiomo Member is included in the Rewanui-Goldlight conglomerate isolith map except for the 21 metres of the vertical column that has been interpreted as Dunollie Member conglomerates (Chapter 2). The sedimentary facies of drillholes close to Twelve Mile Beach are also interpreted and are used to calculate the gross thickness of conglomerate deposits for developing the Rewanui-Goldlight conglomerate isolith map (Appendix 3).

Rewanui-Goldlight conglomerate isolith map shows the same NNE-SSW trend as the other isolith maps. The conglomerates are restricted to the northwestern side of the basin in a single depo-centre and are much thicker (Figure 4.6). Fault E is drawn in the northwest which probably get larger as indicated by much thicker conglomerate deposition compared to the conglomerates deposited during Morgan-Waiomo time. The maximum thickness is 200 metres at Twelve Mile Beach whereas the minimum thickness is estimated at approximately 1 metre at the southwest. The isolith map covers a large area compared to the previous maps. The conglomerate thicknesses gradually decrease from the northwest to the southeast which suggests the conglomerates were most likely deposited in a single large basin that extended further to the northwest.

#### *4.5.3.4 Dunollie conglomerate isolith map*

The Dunollie conglomerate isolith map is the only alluvial phase without a paired lacustrine phase and represents the end of active subsidence in the Greymouth Basin. Therefore, the only relevant conglomerate facies are the subaerial braided river facies. There are multiple problems that must be taken into account when developing the Dunollie conglomerate isolith map. The contact between the Rewanui Member conglomerates and those of the Dunollie Member at Twelve Mile Beach is difficult to identify as the

conglomerates look nearly identical and correlation into the basin doesn't provide the answer. The top 24 m conglomerate section of the Twelve Mile Beach is interpreted as the Dunollie Member due to the absence of large cross-bedded and soft sediment deformation structures indicating subaqueous deposition (Chapter 2). As the Dunollie Member is not economic for coal deposits, another problem is that the drill holes that encounter the Dunollie Member tend to be inadequately described in existing lithological logs or even uncored (Appendix 3). And finally, the Dunollie Member is often eroded from the tops of the mountains and thus any thickness is a minimum.

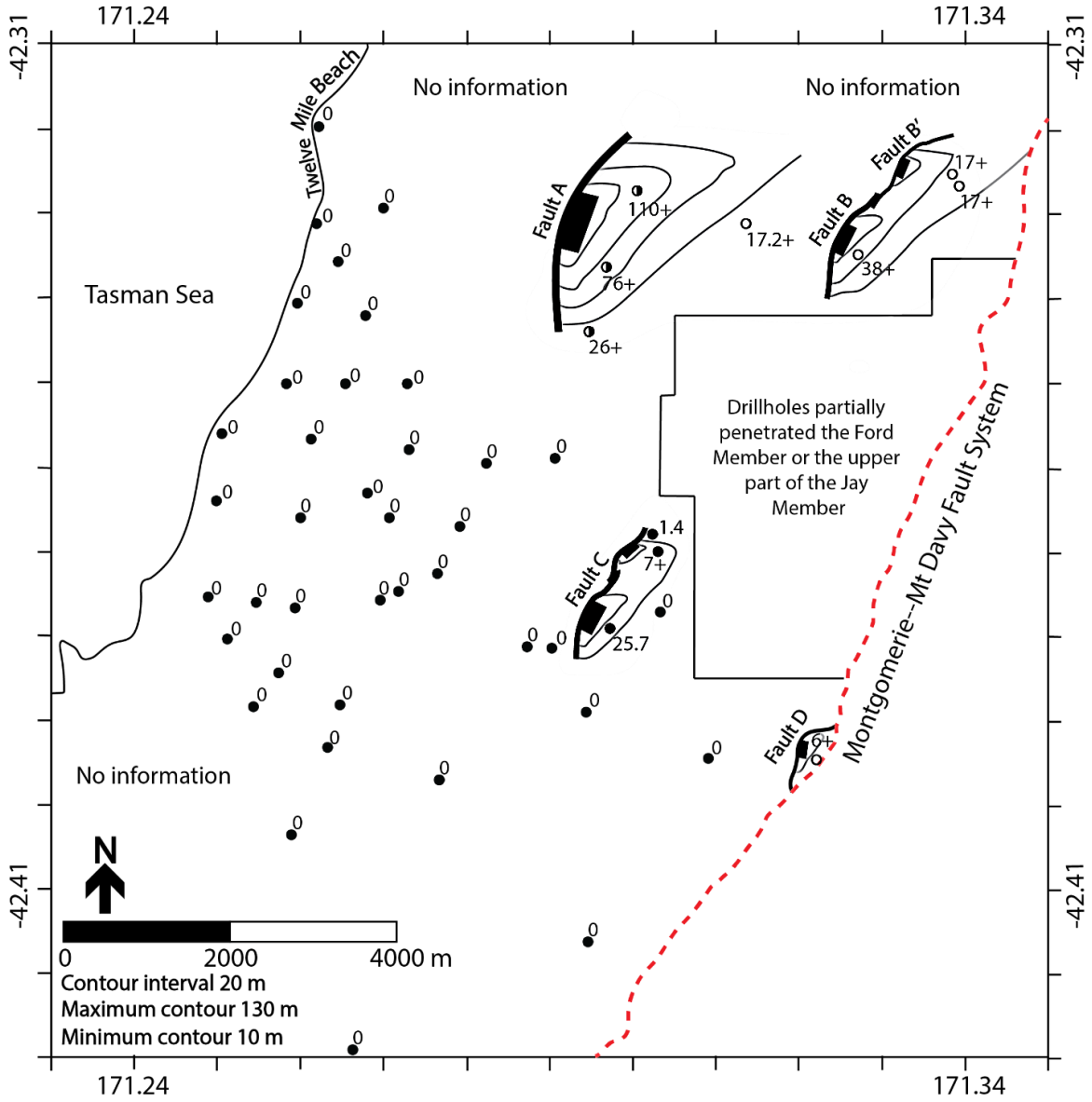


Figure 4. 4: Jay-Ford conglomerate isolith map showing NNE-SSW orientation of conglomerate deposits and interpreted faults. Black circles represent the drillholes. Half black and half white circles represent the drillholes that have both alluvial fan and fandelta conglomerates. Zero value represents either the drillholes have no Jay conglomerates or the drillholes have no Jay Member. The thickness values followed by a plus sign represent the drillholes that partially penetrate the Jay conglomerates. Four faults (Fault A, Fault B, Fault B', Fault C and Fault D) are drawn based on the distribution of conglomerates.

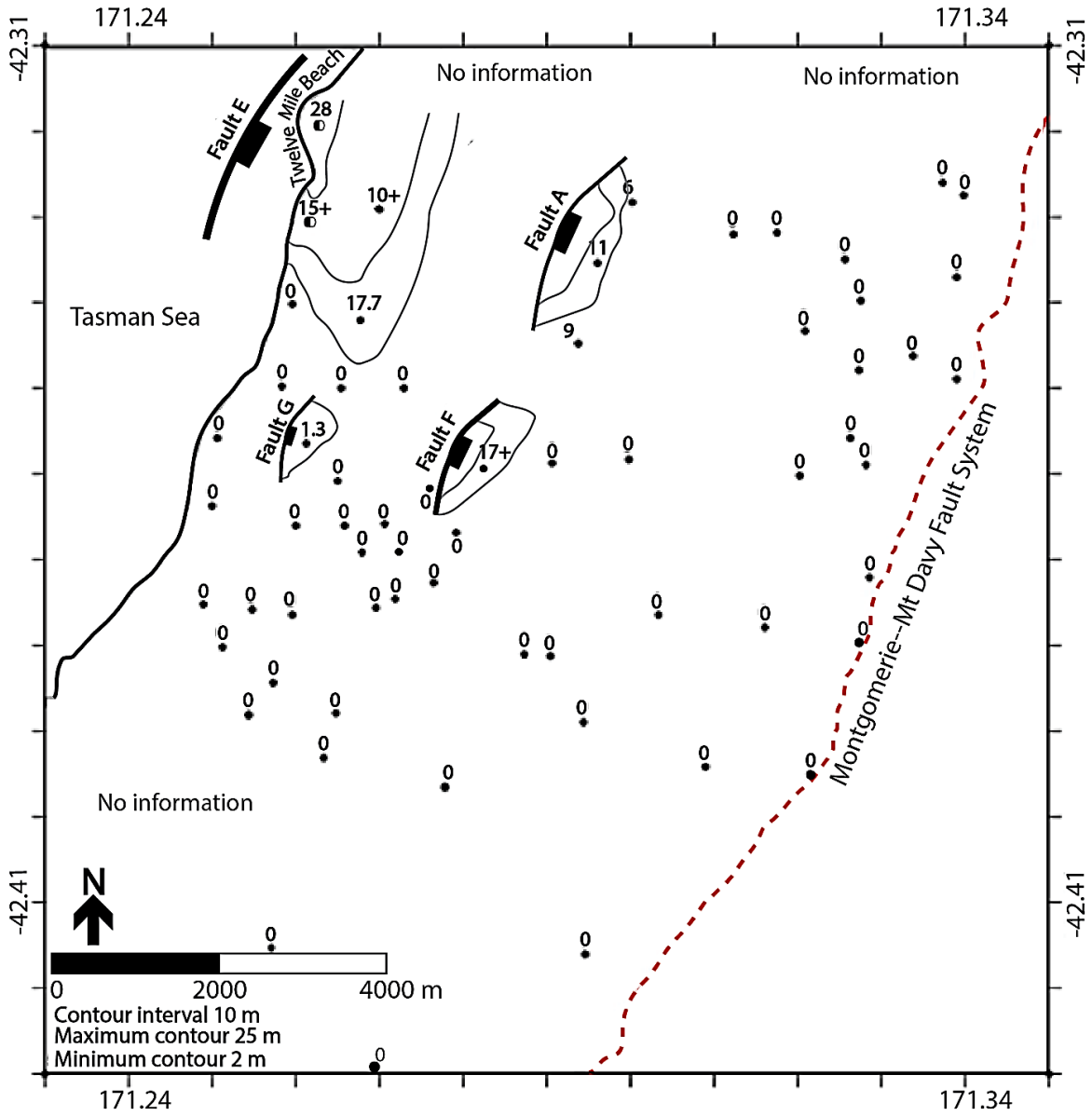


Figure 4. 5: Morgan-Waiomo conglomerate isolith map showing NNE-SSW orientation of conglomerate deposits and interpreted faults. Black circles represent the drillholes. Half black and half white circles represent the drillholes that have both alluvial fan and fandelta conglomerates. Zero value represents either the drillholes have no Morgan conglomerates or the drill holes have no Member Member. The thickness values followed by a plus sign represent the drillholes that partially penetrate the Morgan conglomerates. Four faults (Fault A, Fault E, Fault F and Fault G) are drawn based on the distribution of conglomerates.

Dunollie conglomerates cover less area compared to the Rewanui-Goldlight conglomerates, but still occur in the same NNE-SSW orientation (Figure 4.7). Fault E was probably responsible for the deposition of the Dunollie conglomerates. The maximum thickness is 119 metres(?) whereas the minimum is estimated at 4 metres. The thickness decreases from northwest to southeast. The Dunollie conglomerate isolith map suggests the conglomerates were deposited in a large single depo-centre with some of the basin located further west into the modern offshore region.

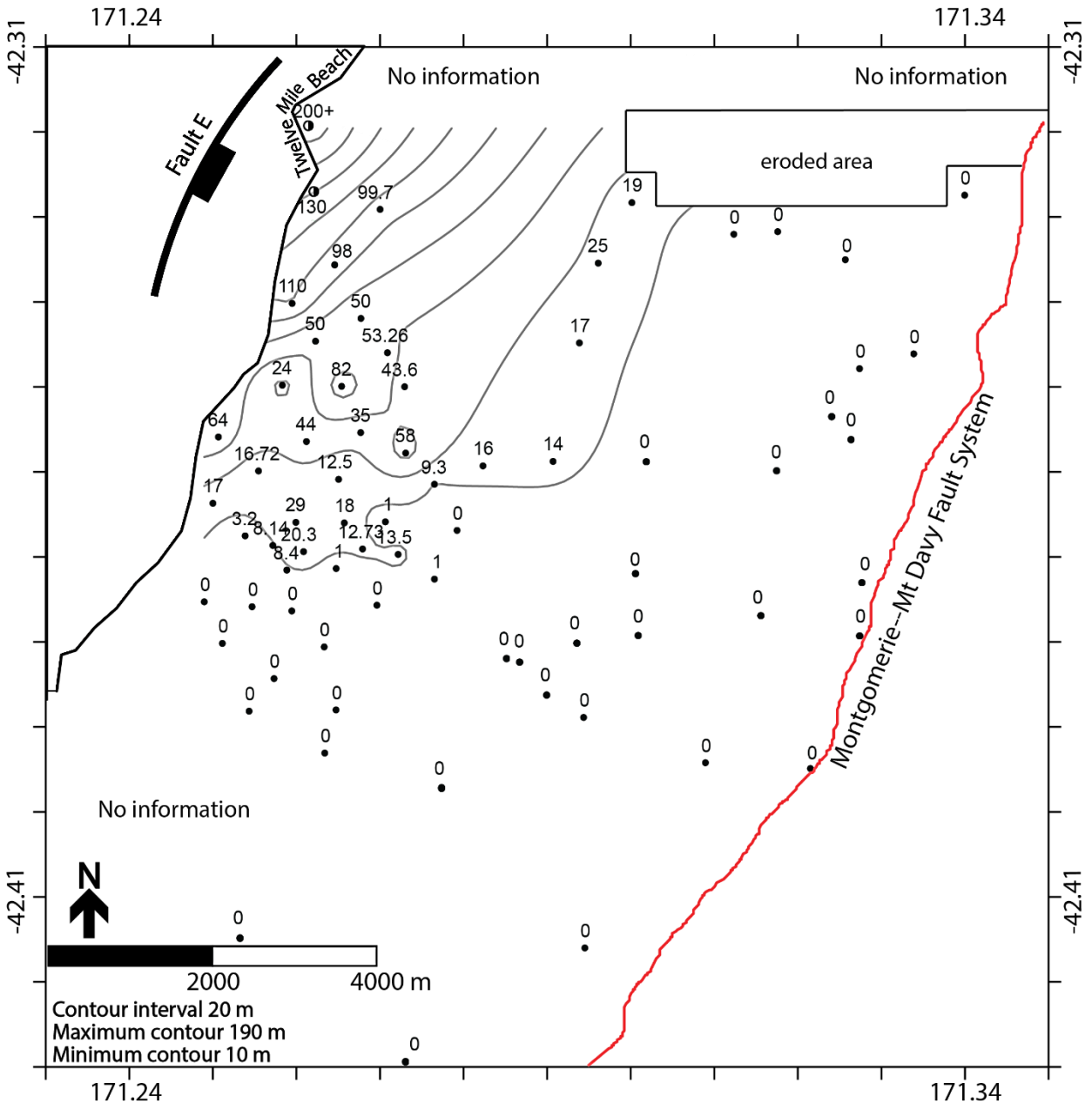


Figure 4. 6: Rewanui-Goldlight conglomerate isolith map showing NNE-SSW orientation of deposits and interpreted offshore fault. Black circles represent the drillholes. Half black and half white circles represent the drillholes that have both alluvial fan and fandelta conglomerates. Zero value represents either the drillholes have no Rewanui-Goldlight conglomerates or the drill holes have no Rewanui Member. Fault E is drawn based on the distribution of conglomerates.

### 4.5.4 Lacustrine facies isolith maps

The subaqueous gravel-rich and sand-rich facies, such as the lacustrine mudstone facies, the sandy turbidites facies, the gravelly turbidites facies and the gravelly delta slope facies, are used to prepare the lacustrine facies isolith maps. The overall finding of the lacustrine facies isolith maps indicates the basin started with small isolated depocentres that became larger through time and migrated westward.

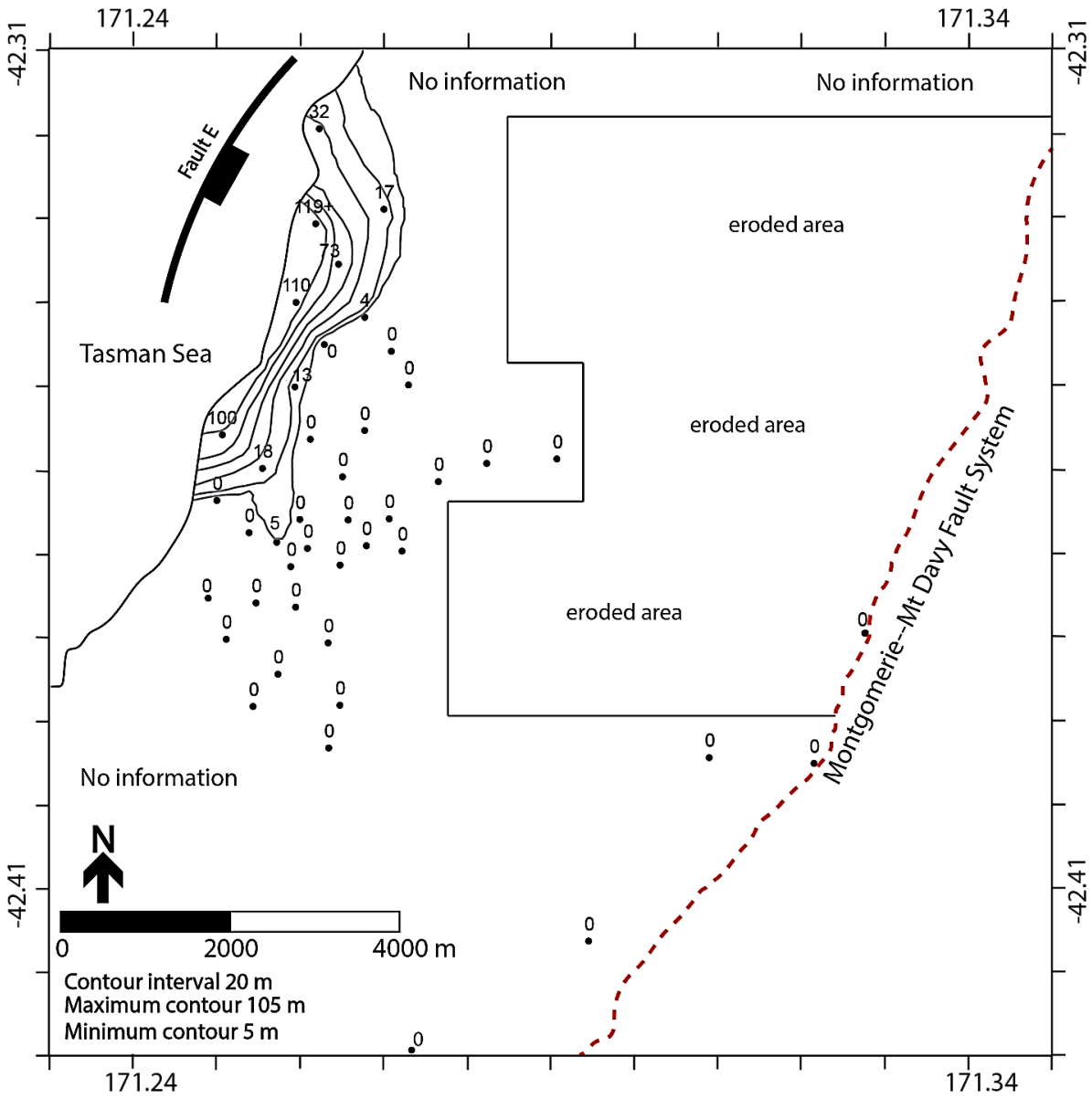


Figure 4. 7: Dunollie conglomerate isolith map showing NNE-SSW orientation of conglomerate deposits and interpreted offshore fault. Black circles represent the drillholes. Zero value represents the drillholes which have no Dunollie conglomerates. The thickness values followed by a plus sign represent the drillholes that partially penetrate the Dunollie conglomerates. Fault H is drawn based on the distribution of conglomerates.

#### *4.5.4.1 Ford lacustrine facies isolith map*

The Ford lacustrine facies isolith map follows a more or less NNE-SSW orientation (Figure 4.8). Four faults (Fault A, Fault B, Fault C and Fault D) are identified based on the thickest lacustrine mudstones supported by the presence of conglomerates from the Jay-Ford conglomerate isolith map. The maximum thickness is 82 metres whereas the minimum thickness is estimated at approximately 4 metres. There are three depocentres identified from the isolith map which are located in the central, the northeastern, and the southeastern parts of the wider basin. The largest depocentre was in the central area where the maximum

thickness was encountered. The northeastern depocentre contains ~67 metres maximum thickness whereas the maximum thickness in the southeastern depocentre is 41 metres. The northeastern and the southeastern depocentres are truncated by the younger Montgomerie-Mt Davy Fault System in the east. The multiple depocentres are interpreted from the thickness variations in dillholes, however, it is unclear whether these are strictly separated or whether they connect slightly.

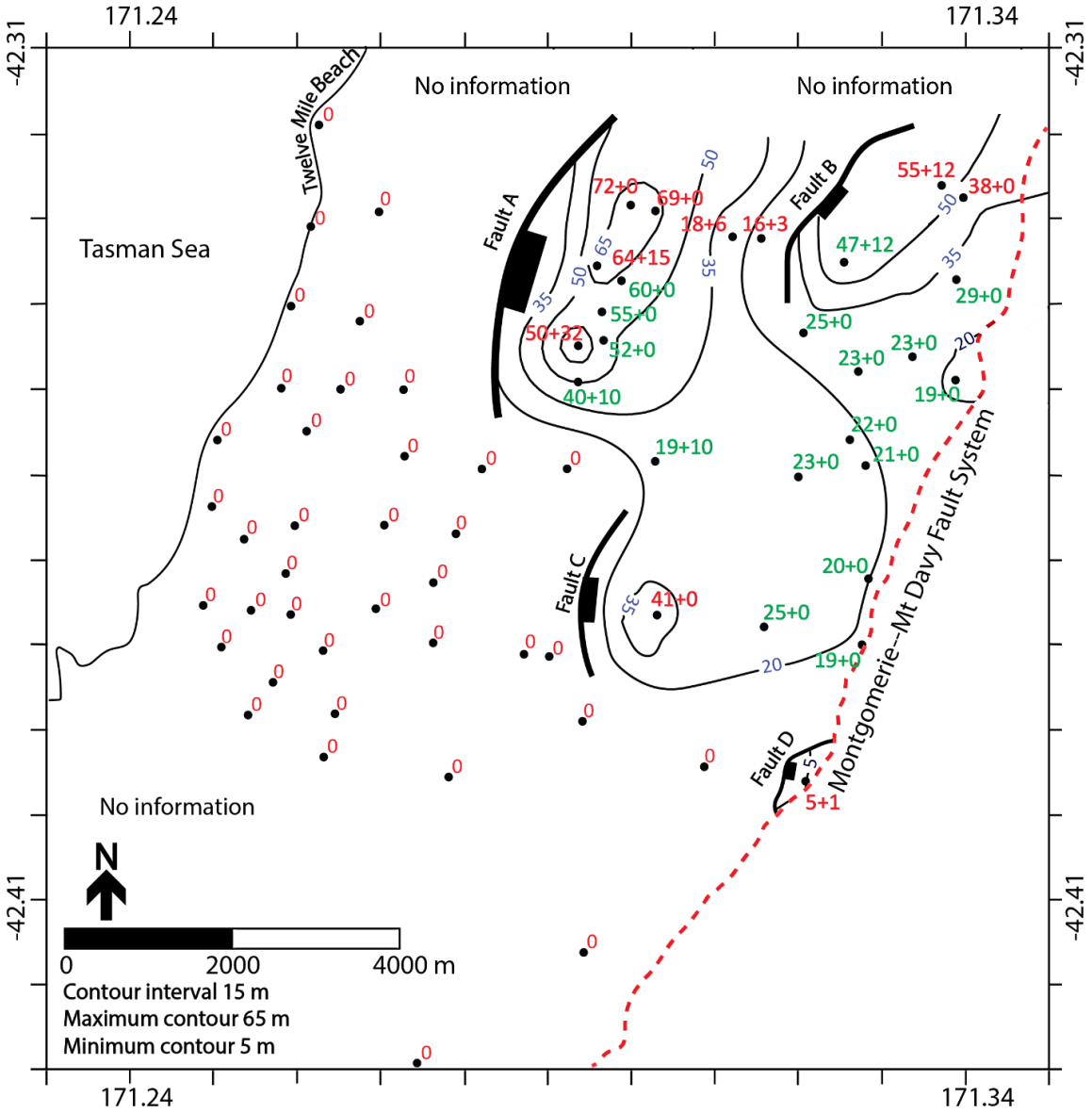


Figure 4. 8: Ford lacustrine facies isolith map showing NNE-SSW orientation of lacustrine deposits and interpreted faults. The calculated thicknesses shown are the sum of muddy lacustrine facies (massive mudstone facies and mudstone with minor sandstone facies) and sandier lacustrine facies (sandy turbidite facies) that may not have been included in the lacustrine Ford Member. Red values represent maximum thickness whereas the green values represent estimated minimum thickness. Zeroes indicate the absence of Ford lacustrine facies in an otherwise stratigraphically complete drill hole. Four faults and their orientations are interpreted based on the thickest lacustrine mudstones supported by the presence of conglomerates from the Jay-Ford conglomerate isolith map in Figure 4.4.

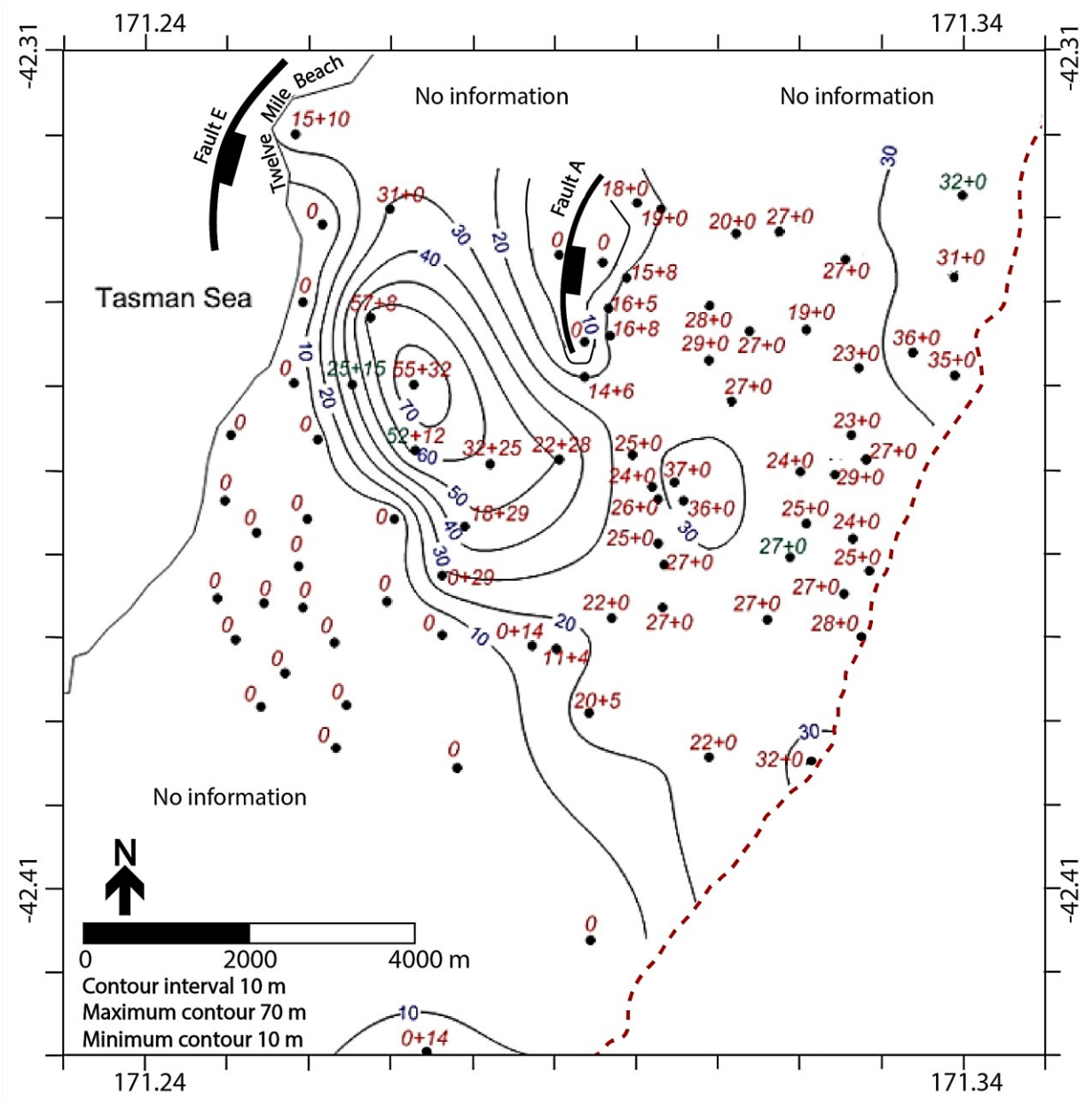


Figure 4. 9: Waiomo lacustrine facies isolith map showing NNE-SSW orientation of lacustrine deposits and interpreted inland and offshore faults. The calculated thicknesses shown are the sum of muddy lacustrine facies (massive mudstone facies and mudstone with minor sandstone facies) and sandier lacustrine facies (sandy turbidite facies) that may not have been included in the lacustrine Waiomo Member. Red values represent maximum thickness whereas the green values represent estimated minimum thickness. Zeroes indicate the absence of Waiomo lacustrine facies in an otherwise stratigraphically complete drill hole. Two faults and their orientations are interpreted based on the thickest lacustrine mudstones supported by the presence of conglomerates from the Morgan-Waiomo conglomerate isolith map in Figure 4.5.

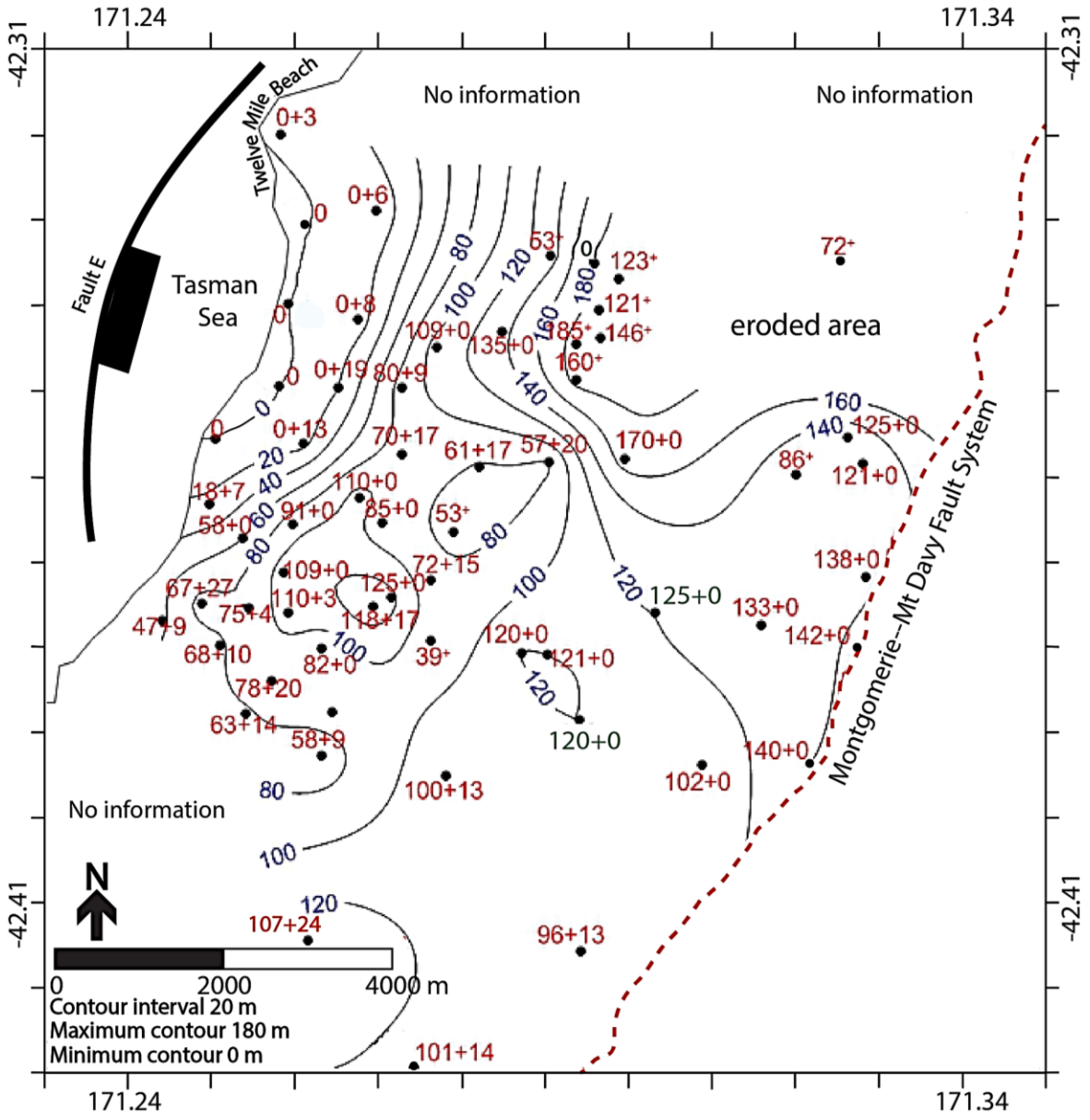


Figure 4. 10: Goldlight lacustrine facies isolith map showing NNE-SSW orientation of lacustrine deposits and interpreted offshore fault. The calculated thicknesses shown are the sum of muddy lacustrine facies (massive mudstone facies and mudstone with minor sandstone facies) and sandier lacustrine facies (sandy turbidite facies) that may not have been included in the lacustrine Goldlight Member. Red values represent maximum thickness whereas the green values represent estimated minimum thickness. When the lacustrine facies association is partially eroded (upper part) in a drill hole, the value is represented with a plus sign the right corner of the value. Zeroes indicate the absence of Goldlight lacustrine facies in an otherwise stratigraphically complete drill hole. Fault E and its orientation is interpreted based on the distribution of conglomerates from the Rewanui-Goldlight conglomerate isolith map in Figure 4.6.

### *4.5.4.2 Waiomo lacustrine facies isolith map*

Waiomo lacustrine facies isolith map shows multiple depo-centres which are oriented mostly in the NNE-SSW direction (Figure 4.9). One depocentre is identified on the northwest side and two relatively smaller

depocentres are found in the centre and the northeast. Another depocentre, identified in the southeastern corner of the basin, contains the maximum thickness of 37 metres. The northeastern and the southeastern depocentres are truncated by the younger Montgomerie-Mt Davy Fault System in the east. The maximum thicknesses of the other depocentres are as follows: the northwestern one is 87 metres and the northeastern two are 36 metres and 37 metres thick, respectively. Fault E and its orientations are drawn based on the presence of conglomerates and highest lacustrine mudstone deposits. Pre-existing Fault A from Figure 4.8 separates the Waiomo Lake in the northcentral part of the basin. Pre-existing Fault F and Fault G from Figure 4.5 are probably inundated by the Waiomo Lake in the central part of the basin whereas pre-existing Fault B, Fault C and Fault D from Figure 4.4 and Figure 4.8 are probably inundated by the Waiomo Lake in the northeast and the southeast part of the basin.

#### *4.5.4.3 Goldlight lacustrine facies isolith map*

Goldlight lacustrine facies isolith map shows a uniform thickness distribution indicating the lake was extensive and deposited in a single depocentre (Figure 4.10). Multiple depocentres are found but they were connected together into a single lake. The closely spaced contour lines suggest the shoreline had a high gradient, and sedimentary facies indicate it was deposited on a delta slope. The minimum thickness of the Goldlight lacustrine facies is ~17 metres thick in the northwest adjacent to the fan delta slope. Most of the drillholes located in this area contain shoreline facies indicating this area was likely a lake shore during the deposition of the Goldlight Member. The other depocentres are found to the centre and to the southeast at ~186 metres and ~140 metres thick, respectively. Fault E was probably the most prominent fault during the presence of Goldlight Lake. All other pre-existing faults were inundated as the basin subsided through time. The Goldlight isolith map is truncated by the younger Montgomerie-Mount Davy Fault System in the east.

## 4.6 Interpretation of Results

This section will provide an interpretation of the basin and fault geometry, and a reconstruction of the faults at each fluvio-lacustrine interval of the Greymouth Basin. The fault reconstructions are the basis of the development of the tectonic model to explain the evolution of the Greymouth Basin from Late Cretaceous to the Early Palaeocene.

### 4.6.1 Basin geometry

The overall basin shows a half-graben geometry with footwall sourced fan deltas alternating with alluvial fans and braided river facies in the northwest. The basin centre is characterized by mire coals during alluvial phases alternating with lacustrine mudstones during lacustrine phases.

The NNE-SSW orientations of the conglomerate and lacustrine facies isolith maps indicate that the axes of the overall basin and its sub-basins are orientated in that direction. The faults controlling their geometry have been interpreted as following the same trends.

Northwestward and southwestward expansion of the younger alluvial members (Morgan, Rewanui and Dunollie members) of the Paparoa Formation over the Greenland Group basement rocks indicate the widening of the Greymouth Basin through time. The younger members sitting unconformably on the basement towards the west also indicate the unconformity surfaces become younger from east to west from the Late Cretaceous to the Early Palaeocene (Figure 4.3). The thicknesses of the conglomerates follow the same pattern with early conglomerates restricted to the east (Jay Member) stepping northwestward through time (Morgan, Rewanui and Dunollie members).

The conglomerate isolith maps cannot independently identify whether there were multiple isolated basins or a single basin that widened westward. In order to resolve this, we integrate the information from the lacustrine isolith maps to interpret multiple depocentres that most likely represent deposition in multiple isolated basins. When combined with the sedimentary facies, all lines of evidence indicate that the palaeo-sub-basins started out as isolated from each other (Jay-Ford), became more connected through time (Morgan-Waiomo), until they formed a large single basin (Rewanui-Goldlight-Dunollie).

### 4.6.2 Fault geometry

We interpret the location of faults based on the presence of the thickest alluvial fan/fan delta conglomerate and lacustrine mudstone facies in each fluvio-lacustrine paired interval. The distribution of the sedimentary facies across the basin then adds detail to interpreting changing palaeogeography and the locations of valleys and hills through time.

Choosing the strike of the fault lines was difficult, particularly if based only on the presence of conglomerates. However, when we consider the conglomerates as being an indication of a steep slope and the steep slope as being the indication of a fault scarp, in many locations the strike of the fault was clear. When combined with the thicknesses of the lacustrine facies, some of the ambiguous faults became clearer. Therefore, we have drawn the orientation of the faults in an NNE-SSW strike direction on both sets of isolith maps.

We use the direction of thinning of the conglomerates to indicate the direction of dip for the interpreted faults. Conglomerates will be thickest immediately adjacent to a fault and will thin away from it. This is particularly clear for the younger Rewanui-Goldlight and Dunollie conglomerate isolith maps that thin from the northwest to the southeast indicating a southeastward dipping fault. The smaller faults are identified by the thinner conglomerate deposits but these also thin to the southeast in most cases indicating fault dip to the southeast. As the thickest conglomerates are found at the western edges of each depocentre, we have drawn the faults as dipping to the southeast.

### 4.6.3 Timing of Faults in the Greymouth Basin

The interpreted faults are shown in several cross-sections and in the fence diagram (Figure 4.3, Figure 4.11). Cross-sections are chosen from the northern, central and southern parts of the Greymouth Basin and are oriented NW-SE to be perpendicular to the faults in order to cover both the basin margins and the basin axis. The location of the faults step westward through time. The cross-section line A-A$^{/}$ illustrates the cross-section across the northern part of the Greymouth Basin and covers approximately 10.9 km in length (Figure 4.11A). Cross-section B-B$^{/}$ represents the middle part of the Greymouth Basin and covers approximately 8.9 km in distance (Figure 4.11B). Cross-section C-C$^{/}$ represents the southern part of the Greymouth Basin and covers approximately 9.2 km in distance (Figure 4.11C).

#### *4.6.3.1 Jay-Ford interval*

The conglomerate and lacustrine isolith maps (Figure 4.4, Figure 4.8) are used to interpret the location, strike, and dip direction of four faults (Fault A, Fault B, Fault B', Fault C and Fault D) during the Jay-Ford time which are then illustrated on the cross-sections (Figure 11). Fault A and Fault C are present in both the conglomerate and lacustrine facies isolith maps where two different depo-centres are apparent in the same locations. Fault B and Fault B', present in Figure 4.3, were probably connected in Figure 4.8. However, the interpretation of Fault D is more tentative because it is identified based on only the conglomerate thickness due to the lack of a lacustrine depo-centre in that location.

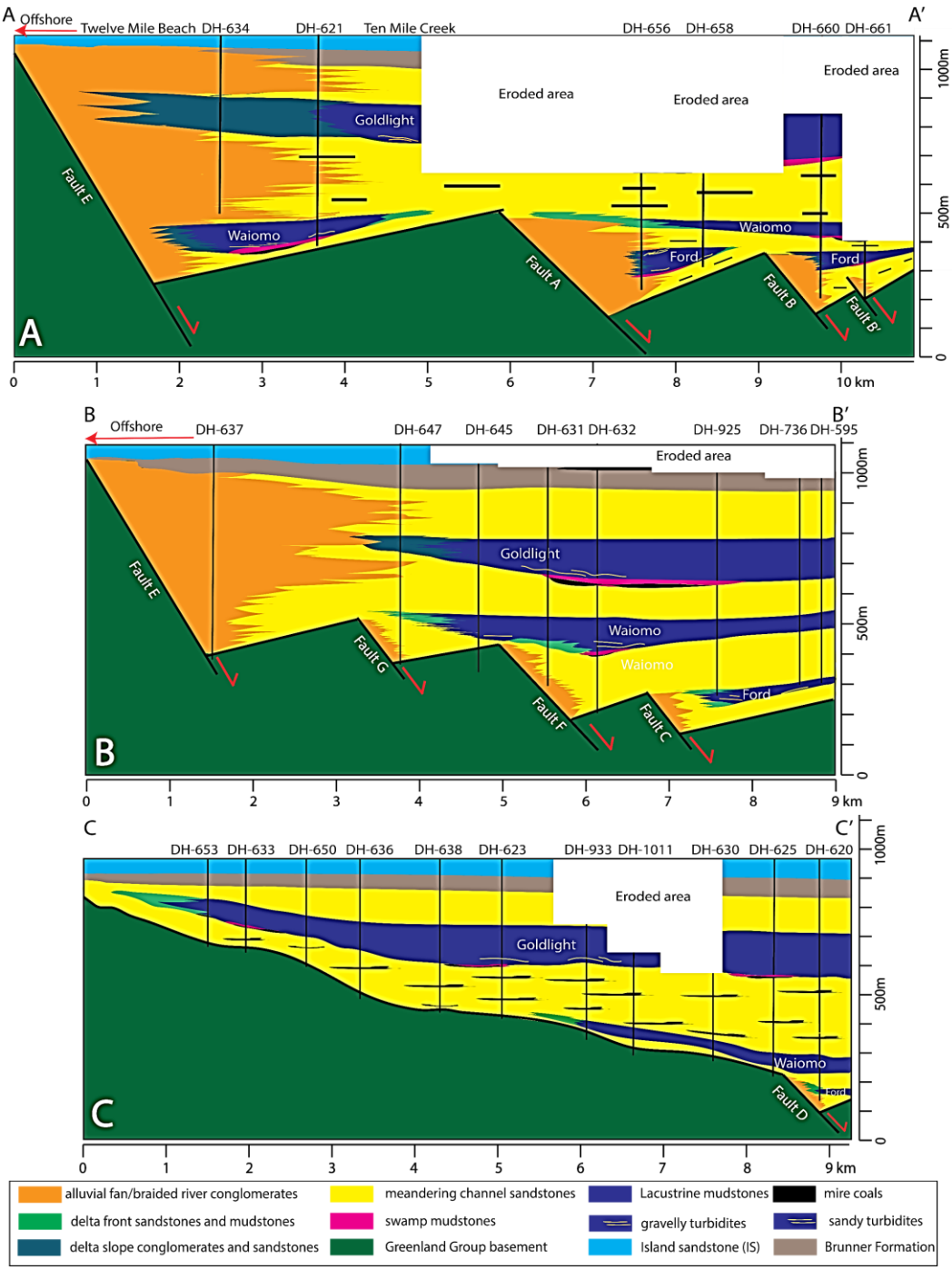


Figure 4. 11: Cross-section with interpreted faults showing the northern (A), central (B) and southern (C) part of the Greymouth Basin. Cross-section A-A' shows two Ford lacustrine sub-basins bounded by Fault A and Fault B, two Waiomo lacustrine sub-basins bounded by Fault A and Fault E and single Goldlight lacustrine basin bounded by Fault E. Cross-section B-B' illustrates single Ford lacustrine basins bounded by Fault C, single Waiomo lacustrine sub-basins bounded by Fault G and single Goldlight lacustrine basin bounded by Fault E. Cross-section C-C' shows single Ford lacustrine basins bounded by Fault D, the Waiomo and the Goldlight lacustrine basins are onlapping against the pre-existing fluvial deposits of Morgan Member and the Rewanui Member, respectively.

The basal stratigraphy of Jay and Ford members in the northeastern part of the basin in cross-section A-A' is characterized by two isolated sub-basins which are bounded by Fault A and Fault B (Figure 4.11A). Thick conglomerates were deposited adjacent to the faults during Jay and Ford time and two lakes filled these basins during the Ford lacustrine phase. Cross-section B-B' represents the central part of the basin where the basal stratigraphy of Jay and Ford members is characterized by one single basin which is bounded by Fault C (Figure 4.11B). The southern part of the basin is illustrated in cross-section C-C' where the basal stratigraphy of Jay and Ford members is restricted in single small basin which is bounded by Fault D (Figure 4.11C).

#### *4.6.3.2 Morgan-Waiomo interval*

During the Morgan-Waiomo time, conglomerate and lacustrine deposition step westward. The new conglomerate thicknesses in the northwestern part of the basin suggest the presence of three new faults (Fault E , Fault F and Fault G) (Figure 4.3, Figure 4.5, Figure 4.9). Fault E is likely located further offshore to the west given the facies at Twelve Mile Beach indicate a long-lived fan delta shoreline (Figure 4.11B andC). Fault F and Fault G is likely located further southwest from Fault A and connected where significant thicknesses of Morgan-Waiomo conglomerates have been identified in three bore holes (Figure 4.11B). Fault A in the central part of basin is still active as indicated by the presence of conglomerate in Figure 4.5. Fault C and Fault D on the eastern and central side of the basin is apparent as a lacustrine depo-centre in the Waiomo lacustrine facies isolith map lending credence to the earlier interpretation during Jay-Ford time (Figure 4.11C). The Waiomo lacustrine facies isolith map suggests the presence of another depo-centre further east from Fault A, where the location of Fault B is drawn in Figure 4.4 and Figure 4.8.

Cross-section line A-A$^{/}$ across the northern part of the Greymouth Basin (Figure 4.11A) show the deposition of the Morgan Member on basement as the basin steps to the northwest. Conglomerates indicate that a new fault Fault E became active in the northwestern part of the basin. In the Waiomo Member, two isolated lacustrine depo-centres are identified; one associated with the older Fault A and the other associated with the newly developed Fault E. In cross-section B-B', two new faults, Fault F and Fault G, along with Fault E steps to the northwest (Figure 4.11B). The Faults F and G are associated with the Waiomo Member in the western part of the basin whereas the eastern side of the basin continued to subside over the inactive Fault C. Fault F was probably inundated during the expansion of the Waiomo Lake. Cross-section C-C' does not show any faults during Morgan-Waiomo time and likely represents the basin away from the faults in the basin axis.

#### *4.6.3.3 Rewanui-Goldlight interval*

Conglomerates increase in thickness on the northwestern side of the basin in the Rewanui-Goldlight members (Figure 4.3, Figure 4.6, Figure 4.10). This may be the result of two possibilities; either smaller and isolated basin bounding faults linked together, making the Fault E larger. Fault E is considered the more likely option due to the southwestward expansion of the basin during Rewanui time as seen in the basal unit map (Figure 4.2). Thicker and wider conglomerate distribution in the northwestern side of the basin, found on the Rewanui-Goldlight conglomerate isolith map (Figure 4.6), strongly support that Fault E was significantly larger during the Rewanui-Goldlight time compared to the length of Fault E which was activated during the Morgan-Waiomo time.

In cross-section line A-A$^{/}$ (Figure 4.11A), the deposition of the Rewanui conglomerates are likely associated with of Fault E in the west which continued to be active for the later extensive Goldlight lacustrine phase and the Dunollie alluvial phase which cover the whole basin. Cross-section B-B$^{/}$ (Figure

4.11B) shows the same thing as Faults F and G likely became inactive once Fault E in the west offshore became more active and got larger. Cross-section C-C/ (Figure 4.11C) does not show any faults. This part represents the basin away from the faults, and is likely the southernmost extent of the basin axis as it expanded.

#### *4.6.3.4 Dunollie interval*

The presence of thick conglomerates on the Dunollie conglomerate isolith map indicates the faults were still active during that time (Figure 4.3, Figure 4.7). Fault E, shown on cross-section line A-A/, was responsible for the development of Dunollie alluvial phase that covers the whole basin. Deposition of the Brunner Formation infills the basin but also sits directly on basement in the offshore Haku-1 well indicating that Fault E had become inactive by that time (Palaeocene to Eocene).

#### *4.6.3.5 Fault timing in summary*

Stratigraphically, Faults A, B, B' C and D are older than Faults E, F and G (Figure 4.3). Fault E is probably the youngest as this fault was active till the deposition of the Dunollie Member. The stratigraphic younging was accompanied by westward stepping with the formation of new faults and the increasing width of the basin. The new faults coincided with the cyclic alternation of alluvial and lacustrine facies. Each fluvio-lacustrine cycle started with widening of the basin and the development of a new fault along the northwestern margins at each step followed by increased accommodation and deposition of lacustrine facies.

Alternating alluvial and lacustrine sediments of a half-graben basin are the product of fluctuation in subsidence rate (Leeder and Gawthorpe 1987). Rapid subsidence rate of the basin created accommodation for the deposition of lacustrine mudstones in the basin centre indicating that accommodation was greater than sediment supply (Einsele 1992; Leeder 1995, 1999; Holz et. al. 2013, 2015; Martins-Neto and Catuneanu 2010). A decrease in basin subsidence rate caused the lacustrine mudstone in the basin centre to be replaced with axial meandering rivers (e.g. Leeder and Gawthorpe 1987; Martins-Neto and Catuneanu 2010; Holz et. al. 2015). Widening of the basin due to the stepping of the faults to the west coincided with variable subsidence rates in the basin and was responsible for producing the cycle of alternating alluvial and lacustrine sediments.

## 4.7 Tectonic-sedimentary models of the Greymouth Basin

### 4.7.1 Greymouth Basin evolution

Five stages of basin development of the Greymouth Basin from Late Cretaceous to Early Palaeocene time are interpreted based on analysis of the sedimentary facies distribution and the fault reconstructions. The stages of basin development include the Jay-Ford stage, the Morgan-Waiomo stage, the Rewanui-Goldlight stage, the Dunollie-Palaeocene Brunner stage and the Eocene Brunner-Island Sandstone stage

During the Jay-Ford stage, several isolated, low accommodation and fault controlled small basins formed in the central and the northeastern parts of the Greymouth Basin (Figure 4.12 and Figure 4.13, interpreted from the multiple depocentres identified in the lacustrine isolith maps. The central sub-basin was larger than the sub-basin located in the northeast as indicated by the presence of relatively thicker lacustrine mudstone facies and thick conglomerate facies deposited on the basin margin to the west, indicating a steep margin of the faults. This fault is interpreted as a basin bounding fault during the deposition of the Jay-Ford stage. The axial river systems were not well developed at this stage, indicating rapid subsidence rates and

accommodation creation was greater than sediment supply. The steeper side of the basin is interpreted based on the deposition of fan-delta facies along the faults during the Ford lacustrine interval and is marked as a basin bounding fault during that time. This stage illustrates that the main lake was surrounded by a few smaller, isolated lakes across the area as indicated by the Jay-Ford conglomerate and Ford lacustrine isolith maps.

During the Morgan-Waiomo stage, the existing central basin bounding faults was probably less active and a new fault system developed in the northwest as indicated by the northwestward propagation of conglomerate facies with less conglomerate facies deposition along the older bounding fault (Fault A) during the Jay-Ford stage in the centre (Figure 4.14and Figure 4.15). The Morgan conglomerates deposited along these faults were restricted to the northwestern part of the basin as indicated by the Morgan-Waiomo conglomerate isolith map and the Waiomo lacustrine isolith map (Figure 4.5 and Figure 4.9). The presence of two isolated lakes in the northwest and in the eastern side of the basin indicates two main depo-centres with the old depo-centre in the northeast joined by the new depo-centre in the northwest. The economic mire coal facies of the Morgan Member are primarily distributed in the eastern depo-centre, indicating the basin was wide enough to develop axial river systems with slow subsidence which allowed deposition of coals and carbonaceous mudstones. The westward propagation of conglomerate facies indicates widening of the basin. Widening of the basin to the west is also indicated by the basal unit map where the Morgan Member directly sits on the Greenland Group basement. The overall thickness of the Morgan-Waiomo stage is less compared to the overall thickness of the earlier Jay-Ford stage as the basin was widening during that time.

During the Rewanui-Goldlight stage, the northwest fault system likely developed a larger fault due to the linkage of the smaller, isolated basin bounding faults as indicated by the thickest fan-delta conglomerate deposition at Twelve Mile Beach (Figure 4.16 and Figure 4.17. This also suggests that the northwestern margin fault likely controlled the overall subsidence of the basin and therefore can be identified as the main basin bounding fault of the Greymouth Basin. The widening of the basin is indicated by the presence of alluvial facies during Rewanui time. The presence of economic mire coals in this stage indicates that the basin was large and wide enough to develop axial meandering river system in the basin axis. The great thickness of the widely distributed overlying Goldlight mudstone indicates a long-lived increase in subsidence rate in the basin that created more accommodation and allowed thick lacustrine mudstone to be deposited.

During the Dunollie-Palaeocene Brunner stage, the basin bounding fault was most likely responsible for depositing conglomerates on the western margin as indicated by the presence of thick conglomerate facies to the northwest. A likely decrease in basin subsidence rate with continuing high sediment supply started filling up available accommodation space as indicated by the widespread deposition of the Palaeocene Brunner Formation above the Dunollie Member of the Paparoa Formation. The deposition stepped out over the rift shoulders and became widespread across NZ, indicating that active faulting ceased and was replaced by thermal cooling and subsidence. This also suggests the basin was wide enough to open to the sea during this stage.

The overall lacustrine setting changes to a marine setting during the Eocene Brunner-Island Sandstone stage as indicated by the deposition of marginal marine Eocene Brunner and transgressive Island Sandstone on top of the Palaeocene Brunner Formation. This marks the end of the fluvial-lacustrine deposition of the Greymouth Basin. It is the beginning of the New Zealand wide transgression and thermal subsidence, evidenced by the deposition of the upper part of the Haerenga Supergroup. This includes Brunner Formation

and Island Sandstone, which is interpreted as a package of laterally equivalent terrestrial (Brunner Formation), marginal marine (Island Sandstone) and marine facies (Kaiata Formation) that record overall marine transgression as a result of palaeobathymetric deepening from the Late Cretaceous to the Late Eocene (Mortimer et al. 2014).

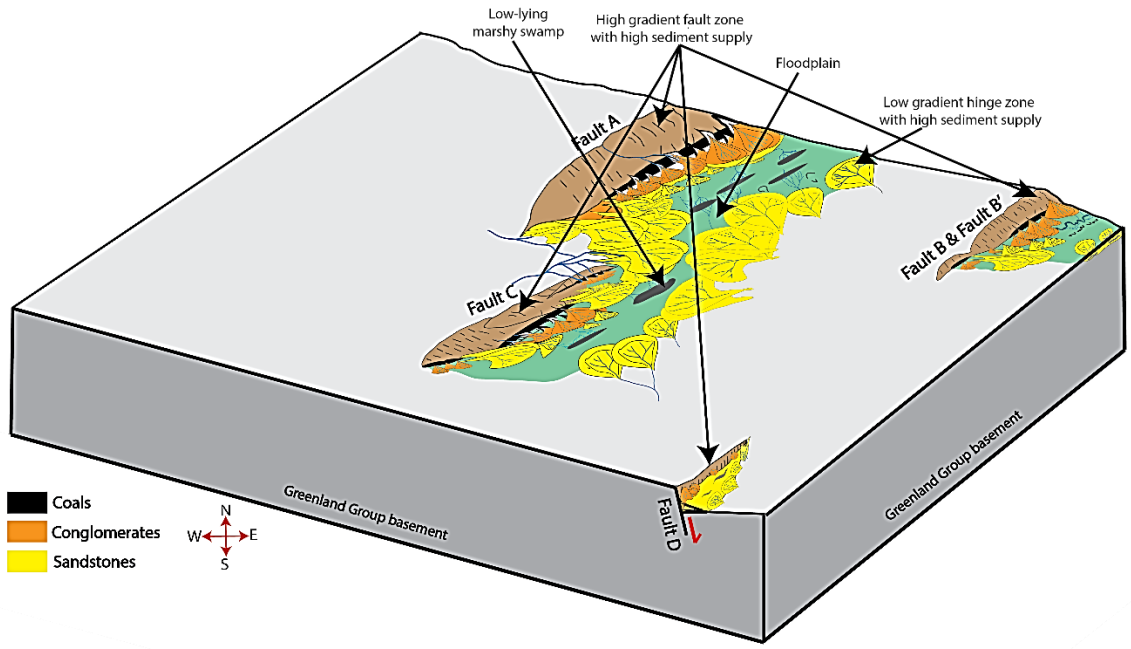


Figure 4. 12: The development of the Jay alluvial phase in the Greymouth Basin illustrating the deposition of scattered conglomerates along the interpreted faults.

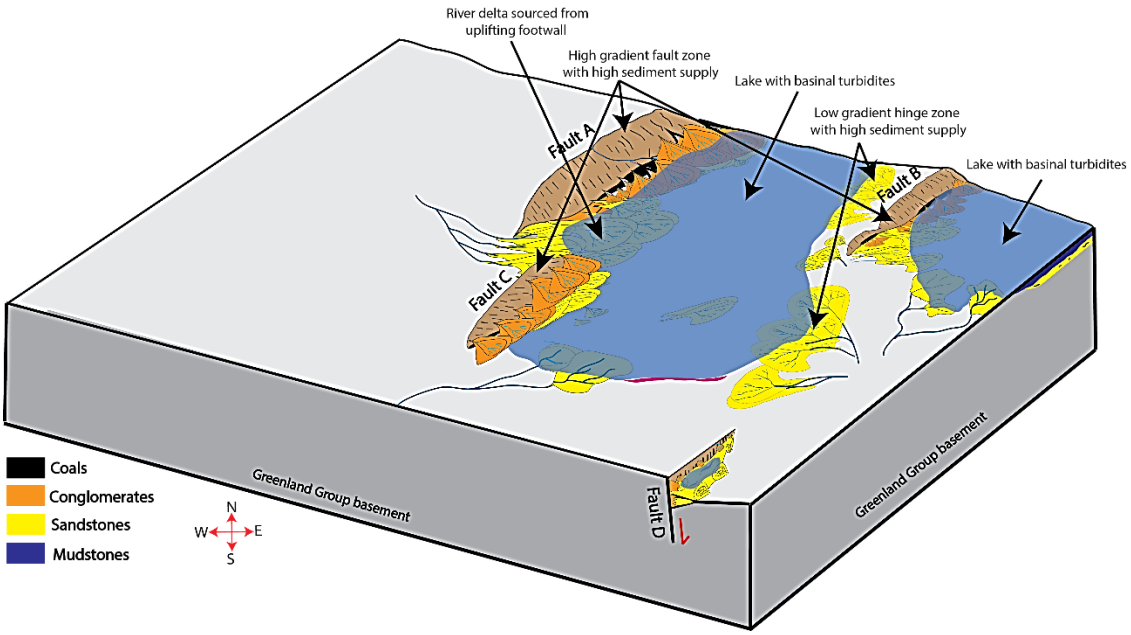


Figure 4. 13: The development of the Ford lacustrine phase in the Greymouth Basin illustrating the linkage of the faults in the centre and the deposition of Ford mudstones in isolated basins.

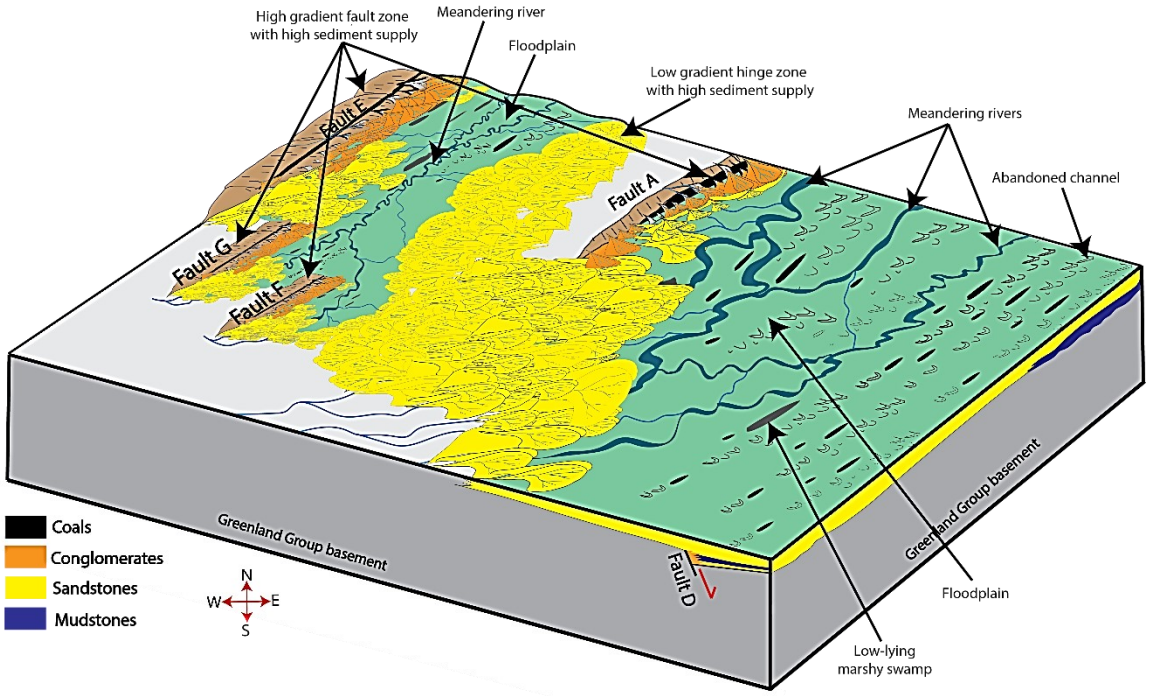


Figure 4. 14: The development of the Morgan alluvial phase in the Greymouth Basin illustrating the activation of a new fault in the northwest. Axial meandering river and floodplain systems are well developed in the northeast. In the northwest, axial meandering river systems are not well developed.

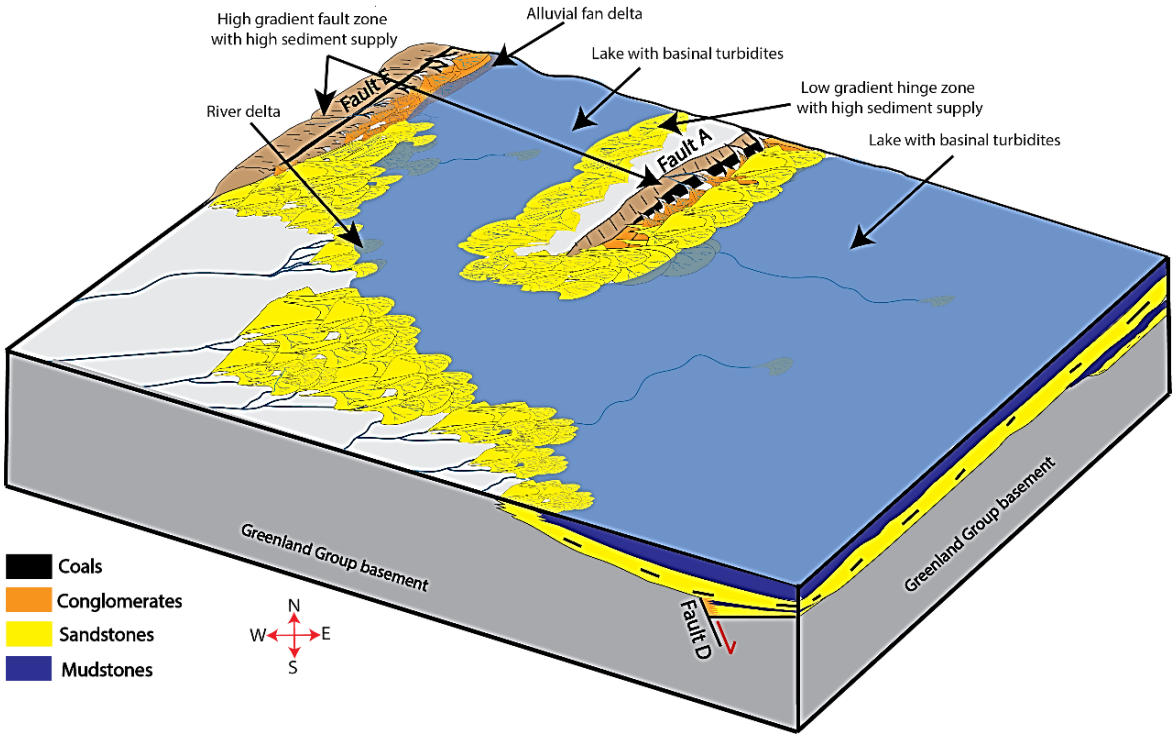


Figure 4. 15: The development of the Waiomo lacustrine phase in the Greymouth Basin illustrating two distinct depo-centres in the northwest and the northeast to the southeast.

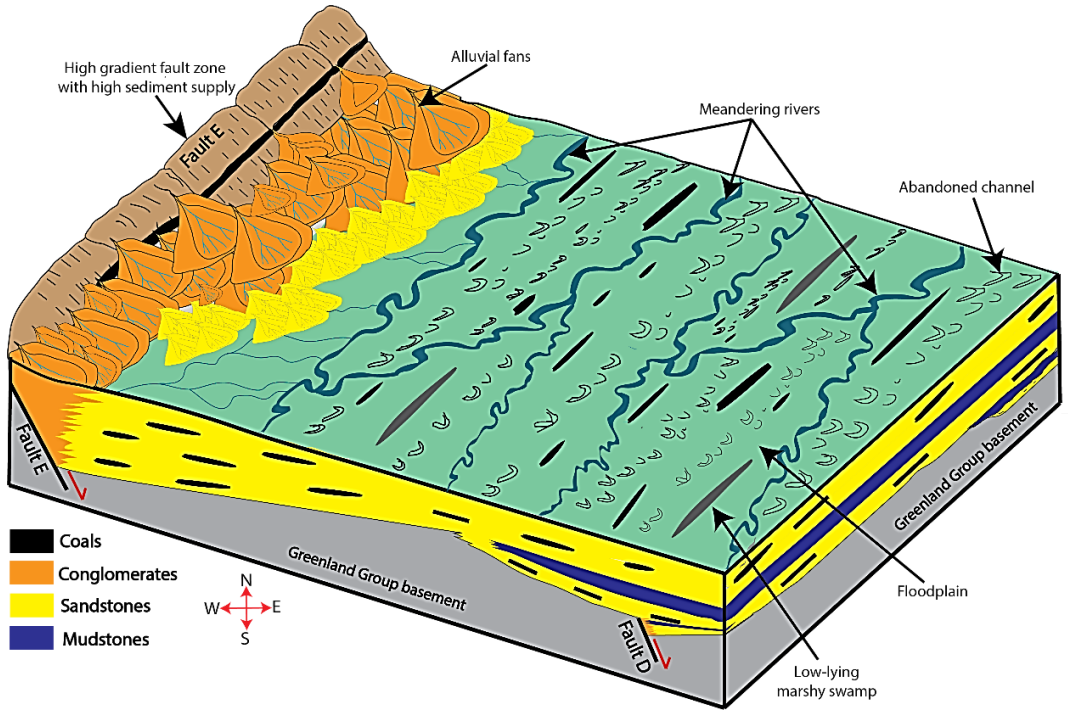


Figure 4. 16: The development of the Rewanui alluvial phase in the Greymouth Basin illustrating the activation of a new fault and/or the existing fault in the northwest. Two axial meandering river and floodplain systems are well developed in the northwest and the northeast side of the basin. The primary basin fault is showing in the offshore west.

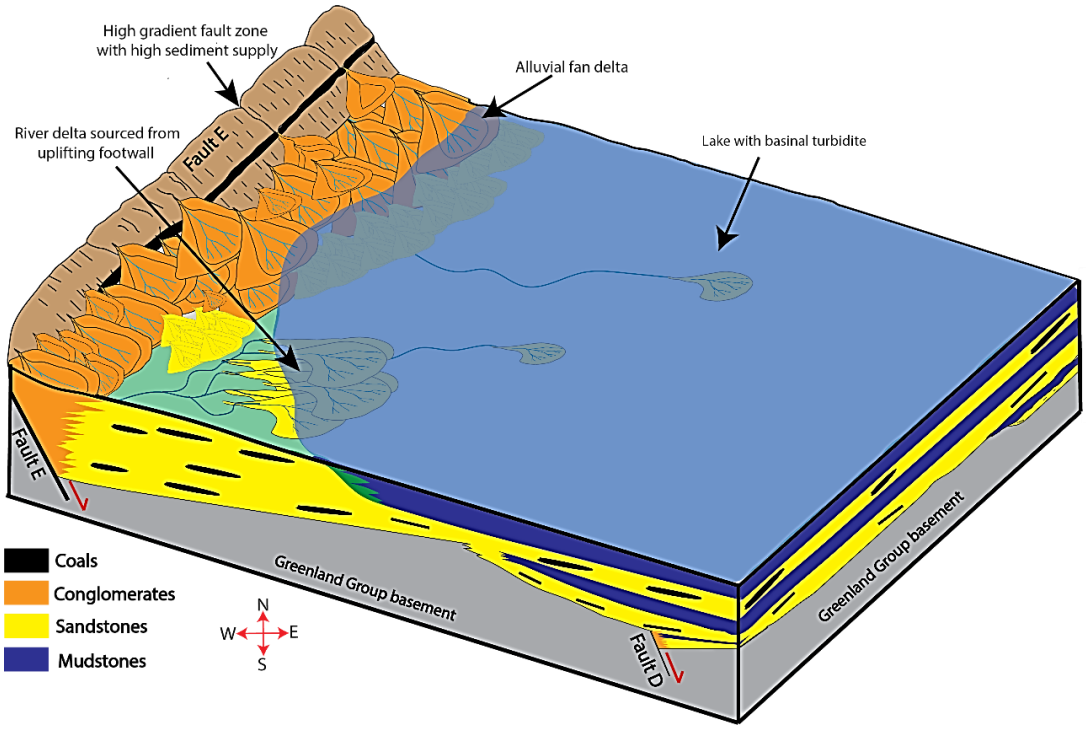


Figure 4. 17: The development of the Goldlight lacustrine phase in the Greymouth Basin illustrating a single lake basin controlled by the primary basin bounding fault.

It is apparent based on the above discussion that the Greymouth Basin evolved from small, isolated sub-basins in the Late Cretaceous to a wide, continuous basin in the Early Palaeocene by the mechanism of linking small, normal faults. The oldest alluvial-lacustrine phase (Jay-Ford phase) records small isolated sub-basins separated by alluvial fan conglomerate facies adjacent to axial lakes marking the locations of small, discontinuous normal faults. Conglomerate deposits step northwestward and thicken up-section as the small faults became amalgamated to form a single border fault during the youngest lacustrine phase (Goldlight lacustrine phase).

The evolution of the Greymouth Basin can be compared with the rift basin evolution model proposed by Gawthorpe and Leeder (2000) (Figure 4.18A and Figure 4.18B). The model illustrates that the initiation phase of fault growth within a developing rift basin can be characterized by low surface topography developed from the isolated displacement of normal faults. The isolated topography eventually becomes larger structures by connecting the small faults throughout the basin evolution. Major displacements of normal faults occur along the basin margins which are continuous and through-going whereas minor faults within the basin become inactive through time. The depo-centres of the half-grabens are associated with these different stages of fault development which become the predominant catchment zones for sediments.

### 4.7.2 Comparison with the offshore Takutai Half-graben

The half-graben geometry of the Greymouth Basin is interpreted as being similar to the structure of the Takutai half-graben, identified from a seismic line offshore to the west of the Greymouth Basin (Bishop 2010; Figure 4.1A, Figure 4.19A and 4.19B). The half-graben geometry of the Takutai Basin is indicated by fault proximal alluvial fans/fan deltas (dipping westward) and hinge side sandy/muddy river delta/meandering alluvial and floodplain systems (dipping eastward) grading laterally to basin axis lacustrine mudstone facies alternating with meandering alluvial systems and adjacent raised mires. The transparent reflectors in the seismic profile indicate probable lacustrine facies, whereas the strong reflectors suggest the presence of coals and alluvial sediments (e.g. Barrier et. al 2017). Sub-basins are identified from the eastward propagation of the new fault systems and the likely inactivation of the pre-existing fault systems as the basin widened through time. From the seismic line, two probable lacustrine intervals are identified where the older lacustrine mudstones were deposited in two isolated sub-basins (Figure 4.21B). The isolated lacustrine mudstones were separated by an intra-basin high visible on the seismic line. The youngest lacustrine basin in the seismic profile is widely distributed and covers the two older sub-basins identified in the profile. The interpretation of two isolated basins in the older Takutai half-graben is very similar to what we interpreted for the older Jay-Ford and Morgan-Waiomo lacustrine phases in the Greymouth Basin. The lakes were separated by an intra-basin high similar to what we see in the Greymouth Basin. In the later stage, a single lake basin covers the underlying inactive faults and formed as the basin widened, similar to what was interpreted for the Goldlight mudstone in the Greymouth Basin.

The eastern end of the Takutai half-graben is deformed and truncated by the NNE-striking Cape Foulwind Fault Zone, interpreted as the major basin bounding fault for the Takutai Basin. The Cape Foulwind Fault was also the likely primary basin bounding fault for the Greymouth Basin and may have been linked with the basin bounding fault of the Takutai half-graben along a transfer zone (e.g. Gawthorpe and Hurst 1993). Such inter-basin transfer zones link individual half-grabens where major border faults are located on the opposite sides of the rift with fault dips in opposite directions, whereas an intra-basin transfer zone links individual fault segments within a half-graben or within inter-basin transfer zones (Figure 4.20; Rosendahl et al. 1987; Leeder and Gawthorpe 1987; Gawthorpe and Hurst 1993). These features are commonly found in large scale half-grabens in elongate rift zones where transverse or oblique structural elements are

important along with extensional segments (Gibbs 1984; Rosendahl et al. 1987; Leeder and Gawthorpe 1987; Larsen 1988; Peacock and Sanderson 1991). Examples of these features are found in Lake Tanganyika and Lake Malawi in the East African Rift, Red Sea of the Gulf of Suez Rift, and the Gulf of Evvia in central Greece (Rosendahl et al. 1987; Ebinger et al. 1987; Gawthorpe et al. 1990; Roberts and Jackson 1991).

### 4.7.3 Comparison to other rift systems

The new tectonic model for the evolution of the Greymouth Rift Basin can be comparable with many rift systems around the world. For example, the Plio-Pleistocene Corinth Rift in Greece (Gawthorpe et al. 2018), the Hammam Faraun fault system in the Suez Rift in Egypt (Gawthorpe et al. 2003), Late Jurassic rifting in the northern North Sea (Cowie et al. 2005), the modern rift of Lake Baikal (Agar and Klitgord, 1995) etc. A similar pattern of fault development was identified in the rift basins mentioned above which began with the initiation and growth of a distributed conjugate fault network and the early development of depo-centres with segment growth and linkage of the faults. These eventually merged into a large fault system dipping inward towards the rift axis as extension progressed through time. The cessation of a number of pre-existing small fault segments during rift development leading to the overtopping of many of the intra-basin highs by younger sedimentary fill. When comparing with Greymouth Basin, we found that the fault sizes and the associated isolated basin sizes were small during the Jay-Ford stage. As the basin widened through time during the Morgan-Waiomo stage and the Rewanui-Goldlight stage as indicated by the development of a new fault system in the northwest, some of the palaeo-basin bounding faults in the centre and the northeast during the initiation of the basin became inactive and got overtopped by younger sediments. The new fault system in the west became larger through time and acted as the main basin bounding fault of the Greymouth Basin. The overall deposition of the basin was eventually controlled by the main basin bounding fault.

## 4.8 Discussion

The discussion will refer back to the questions framing this research. This section places our tectonic evolution models of the Greymouth Basin into the wider context of the West-Coast Taranaki Rift System.

### 4.8.1 Question 1: What is the tectonic setting for the Greymouth Basin? Rift or other?

A significant factor in the formation of interior sag basins is the lack of major normal faulting during the subsidence (Middleton 1989). However, the Taranaki Basin and other concurrent parallel basins in the West Coast-Taranaki Rift System are interpreted as rift basins bounded by normal faults (Strogen et.al. 2017). Fault construction and half-graben geometry of the Greymouth Basin also supports the idea that the basin was not formed as a sag basin. Instead, the evidence justifies that the Greymouth Basin is formed in a fault-controlled rift basin where small, isolated normal faults were developed during the initiation of the basin. These faults linked together and progressively stepped northwestward as the basin became larger and deeper through time, remaining as the master basin bounding fault and controlling the subsidence of the basin.

The sedimentary facies analysis of the Greymouth Basin suggests asymmetrical half-graben geometries along NNE-SSW striking and southeastward dipping normal faults. Fault reconstructions also suggest the widening of the basin through time. The asymmetrical half-graben geometry with a basin bounding fault to the northwest refutes the idea of a complex full graben geometry as proposed by Bowman (1984). The widening of the Greymouth Basin suggests the activation of faults in different time intervals contradicting Bowman's (1984) idea of two persistent parallel depo-centres. However, a palaeo-high did exist during the

older depositional phases, but with a half-graben rather than the full graben geometry as proposed by Bowman (1984).

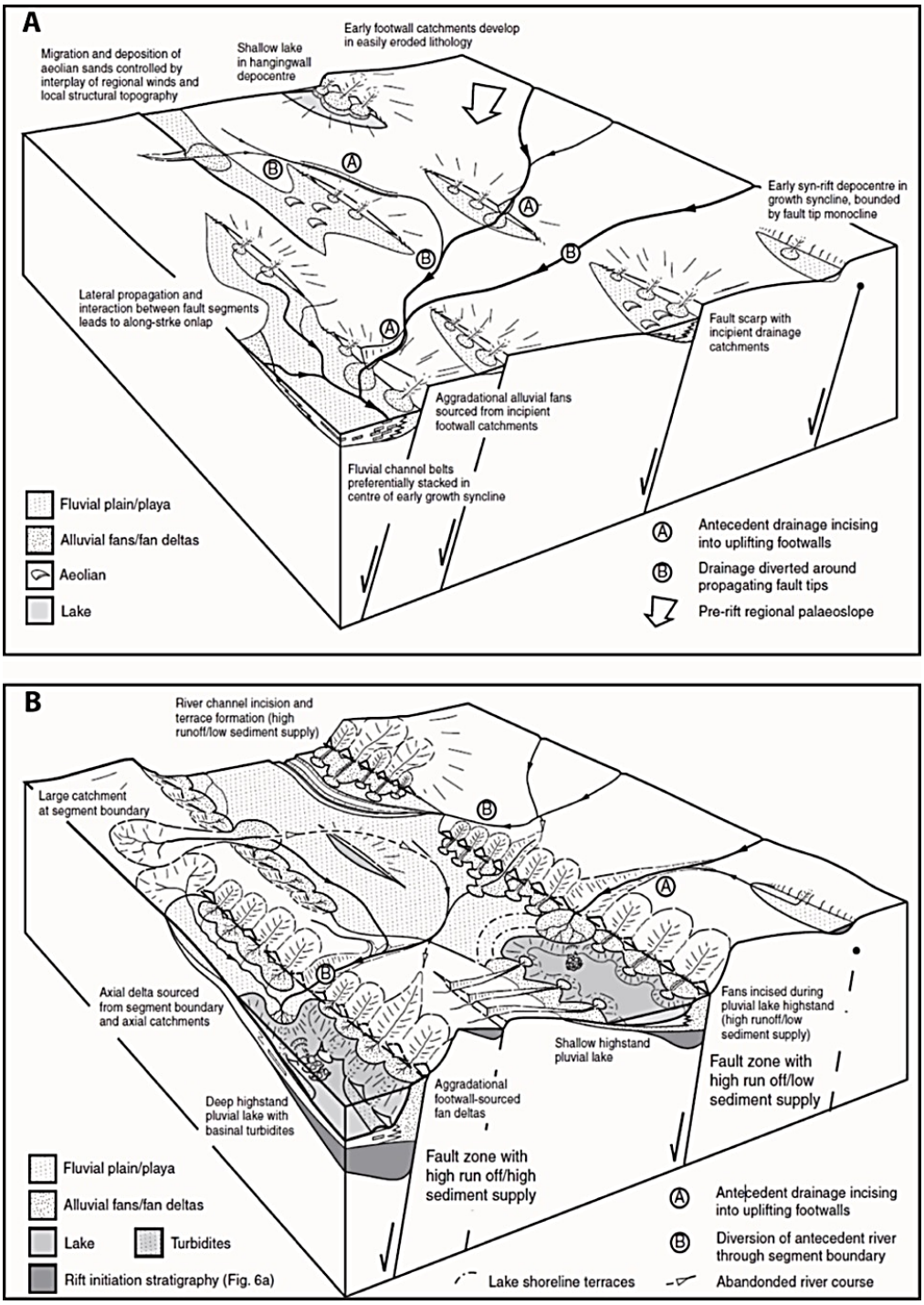


Figure 4. 18: Tectono-sedimentary evolution of a continental rift basin (Gawthorpe and Leeder 2000). A) Deposition during the initiation of a rift phase which shows scattered isolated basins with alluvial fan deposition along the faults. B) The interaction of faults leads to enlargement of basin and subsequent depositional settings including lakes. High energy sediments are sourced from the footwall while the low angle hanging wall sources finer, low energy sediments.

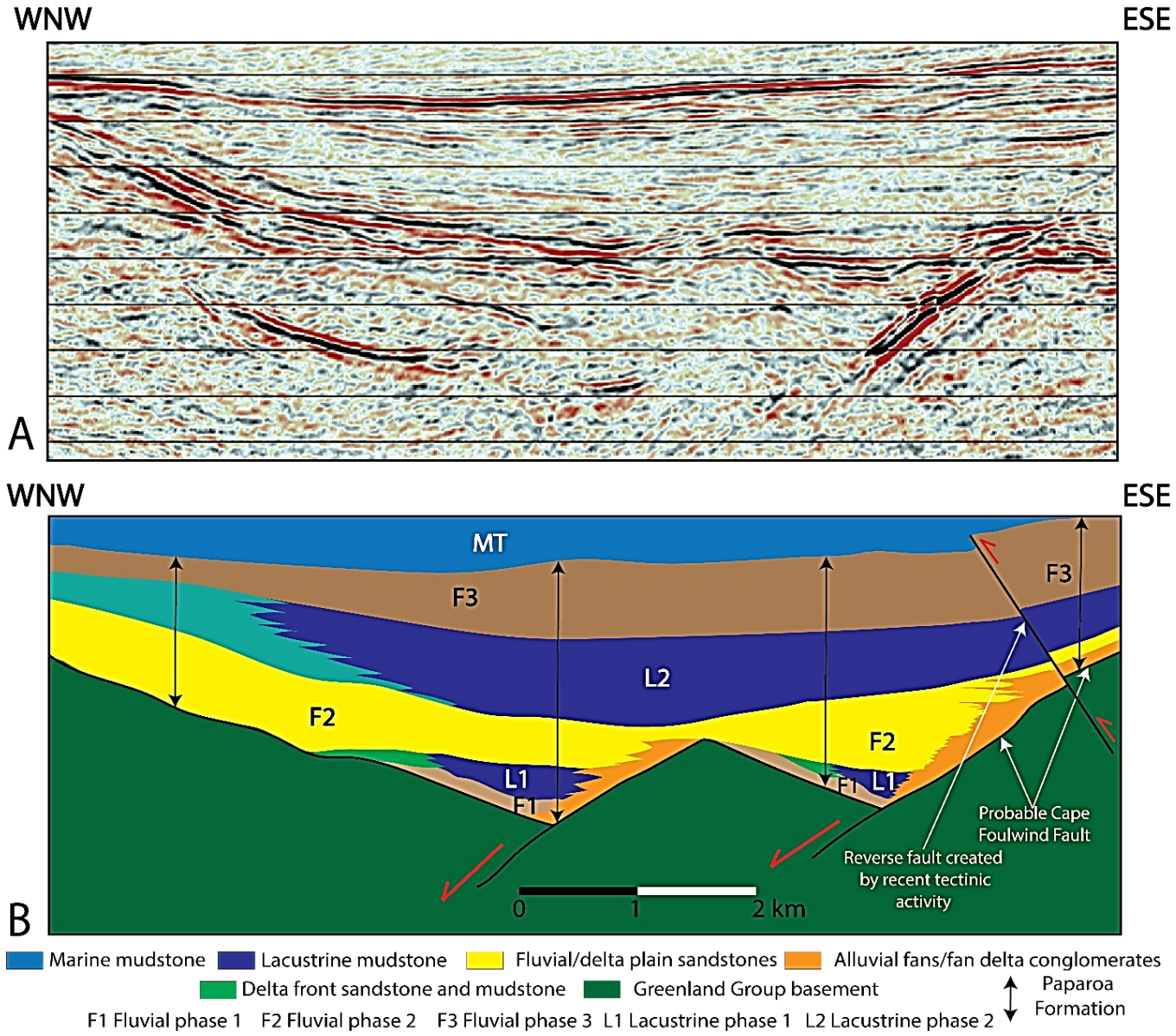


Figure 4. 19: A) Seismic image from offshore west of the Greymouth Basin (P059-84-02). The location is shown in Figure 4.1A. The half-graben is interpreted as Takutai half-graben (Bishop 1992; Suggate 2013). B) Interpreted faults and the potential presence of lacustrine phase 1 (older) and lacustrine phase 2 (younger) which are separated by three alluvial phases.

Newman (1981, 1985) and Ward (1997) identified the Montgomerie - Mt Davy Fault System on the eastern margin as responsible for the majority of the basin subsidence and interpreted it as the main basin bounding fault of the Greymouth Basin. However, Suggate (2014) showed that the Montgomerie - Mt Davy Fault System resulted from Neogene inversion of the Late Cretaceous to Early Palaeocene Paparoa Formation. This indicates the eastern margin Montgomerie - Mt Davy Fault System was not active until late in the basin's history and could not be responsible for the overall subsidence of the Greymouth Basin. Another piece of evidence against the location of the basin bounding fault to the east is the abrupt truncation of the thick lacustrine facies by the Montgomerie-Mt Davy Fault System. This indicates they were likely offset

due to the activation of this younger fault system. In addition, the presence of the thickest conglomerate section during the Rewanui-Goldlight stage in the northwest indicates the presence of a major basin bounding fault to the west which refutes the eastern margin fault as being the major basin bounding fault for the Greymouth Basin. Overall, the evidence indicates that the primary fault for the basin was to the northwest in a half-graben geometry, contradicting what Newman (1985, 1987) and Ward (1997) interpreted.

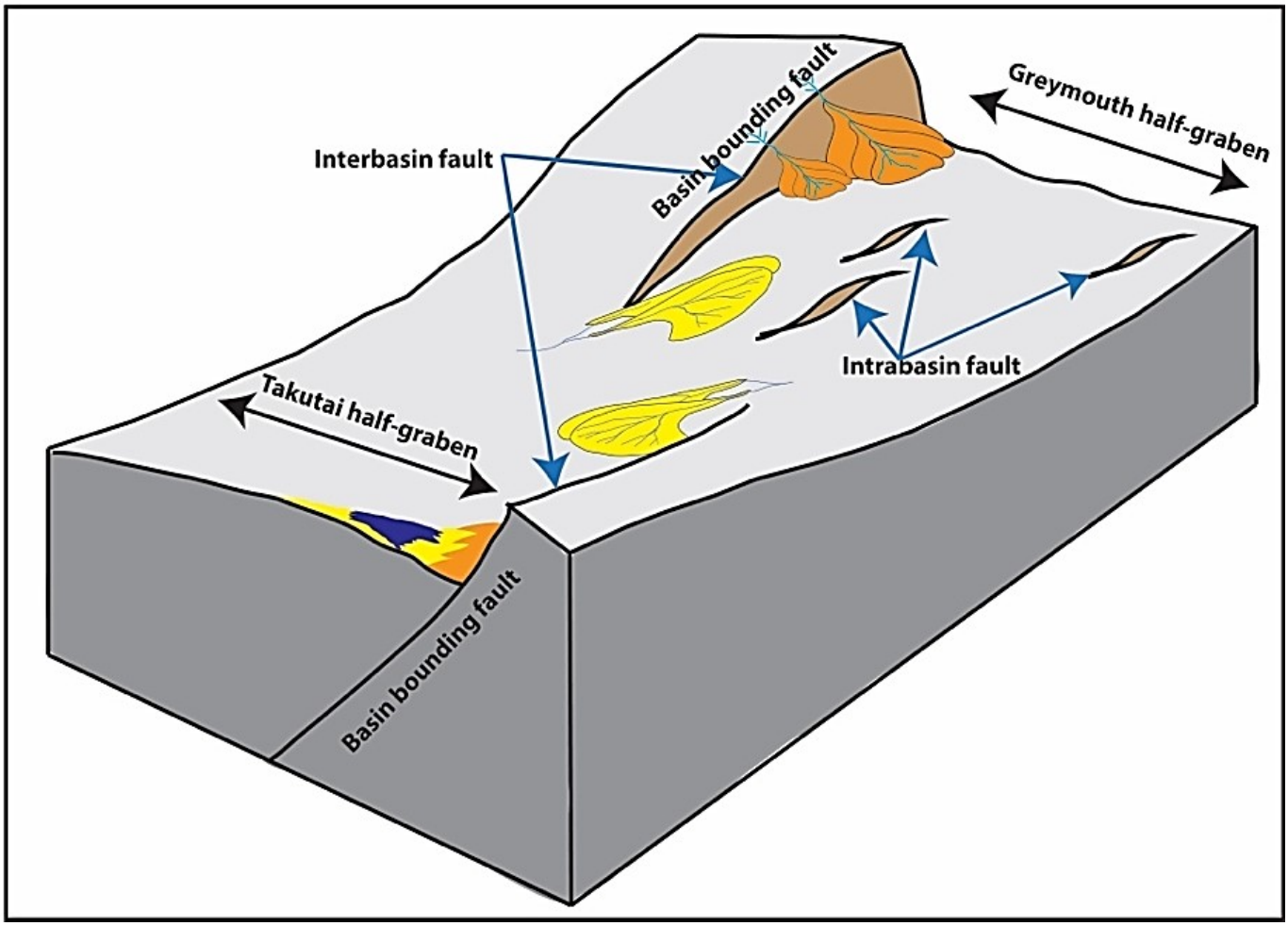


Figure 4. 20: Diagram illustrating the interaction of the interbasin faults and intra basin faults in a rift basin (modified from Gawthorpe and Hurst 1993). Two interbasin border faults show the possibility of the formation of the Greymouth half-graben in the northwest and the Takutai half-graben in the southwest. The interaction and linkage of the intrabasin faults in the Greymouth Basin may be responsible for the large border fault in the northwest.

Studies from the transtensional/strike-slip and extensional basins around the world show that the asymmetrical half-graben geometry and the alternating fluvio-lacustrine sediments are commonly associated with both types of basins (Nilsen and Sylvester 1995; Leeder 1999; Gawthorpe and Leeder 2000; Wu et al. 2009). However, revisiting reworked volcanic sediments and their origin may add more information to interpret the basin geometry and tectonic setting. Reworked volcanic conglomerate facies and the presence of interbedded tuffs and lavas in the Paparoa Formation indicate active volcanism during the deposition of Paparoa Formation (Gage 1952; Bishop 1992). Intrusive dykes and volcaniclastics are

rare in the Paparoa Formation, have limited aerial extent, and have been interpreted as being the result of localised eruptions (Gage 1952; Laird 1968; Nathan 1978; Newman 1985; Bishop 1992). Recent geochemical analysis of a basalt clast conglomerate found in the Morgan Member in the centre of the basin suggests that they were derived from tholeiitic magma (Steadman 2018). Volcanic activity is common in both pure rifting and transtensional basins. However, purely extensional half-graben, asymmetrical rift basins often have eruptions of tholeiitic magma with a greater amount of volcanism (Tatar et al., 2007; Mathieu et al., 2011), than transtensional basins where volcanism is less common and usually more alkaline in composition (Einsele 1992; Leeder 1995; Leeder 1999; Tatar et al. 2007). As the volcaniclastics are rare yet tholeiitic in the Paparoa Formation, the Greymouth Basin is interpreted as being probably formed due to pure but passive extension associated with Tasman Sea spreading (e.g. Gaina et al. 1998; Bradshaw and Laird 2004).

From the interpretation of fault geometry and facies distribution, we negate the idea of the Greymouth Basin being formed as a sag basin. Attempts to distinguish a transtensional from an extensional basin have not yielded any clear outcome although the evidence is more inclined towards the Greymouth Rift Basin having most likely formed in a purely extensional regime. Therefore, the asymmetrical half-graben geometry and alternating fluvio-lacustrine sediments of the Greymouth Basin are most likely the product of an extensional rift tectonic setting where the basin bounding fault was located on the northwest.

### 4.8.2 Question 2: Did the Basin change orientation?

The previous lacustrine isopach maps have been revised as isolith maps in this paper with the inclusion of some new drill hole data, the revised sedimentary facies analysis, and better mapping of the shoreline facies association. The lacustrine units had been previously mapped based on the mudstone-rich deep-water facies only, ignoring the sandier low gradient deltaic facies and gravelly subaqueous facies that were instead included in the alluvial units (Gage 1952; Ward 1997). Including all subaqueous facies changes the thicknesses of lacustrine units and the distribution of the lacustrine facies association of the basin. Combining information from the lacustrine facies isolith maps with the conglomerate isolith maps and the distribution of sedimentary facies has led to a more complete tectonic model to understand the change in basin orientation and the regional tectonics. All of the revised isolith maps in this paper show the same NNE-SSW orientation which suggests the Greymouth Basin did not change orientation during its subsidence history.

The stability of the extension direction affects the interpretation of the regional tectonics of the Greymouth Basin from the Late Cretaceous to the Early Palaeocene. Its NNE-SSW orientation was different from the WNW-ESE orientation of the faults in the underlying Metamorphic Core Complex (Herd 2007; Sagar and Palin 2011; Schulte et al. 2014). For the older members of the Paparoa Formation to have been deposited in a WNW-ESE orientated basin, the primary extension of the Greymouth Basin would be required to change. We suggest the change instead occurred during the ~15 Ma gap between deposition of the underlying of the Pororari Group and the overlying Paparoa Formation (Gage 1952; Nathan 1978). This corresponds with interpretations made in the Taranaki Basin where detailed seismic mapping and stratigraphic analysis of the West Coast-Taranaki rift phase indicate that the Pakawau, Kiwa and Maui sub-basins have a NE orientation approximately perpendicular to many of the earlier mid-Cretaceous rift basins (Strogen et.al. 2017).

The question still remains of how the dramatic 90º change of the primary extension directions between the metamorphic core complexes and the West Coast-Taranaki Rift System occurred in the ~15 Ma time gap.

We try to resolve this complexity using studies of present spreading centres such as the Afar triple junction. The Afar triple junction is located where the modern the Red Sea, Gulf of Aden and the East African Rift Zones meet. It involves three major plates (the Arabian, Nubian and Somalian plates) which are rifting apart to form three complex zones with each rift at approximately 120º angles to each other (Wolfenden 2004). It may be possible that there was a similar geometry during the West Coast-Taranaki Rift System with a third failed rift arm needed to form a complete triple junction. Major spreading centres with a third failed rift arm would form a number of microplates, and these microplates would accrete to an adjacent larger plate (Bird 1999). No such association of microplates have yet been found.

### 4.8.3 Question 3: What does the evolution of the Greymouth Basin indicate about the West Coast-Taranaki Rift System?

The depositional history of New Zealand indicates that the continent experienced a long period of subduction in a position along the eastern boundary of Gondwana (Laird 1981, Bradshaw 1989; Laird and Bradshaw 2003) followed by rifting that produced metamorphic core complexes which resulted in hot and thinned crust (Tulloch and Kimbrough 1989; Laird and Bradshaw 2004; Herd 2007; Schulte et al. 2014). Rifting during the West Coast-Taranaki Rift System thinned the crust further due to a slightly different rifting orientation (Mortimer 2004; Strogen et.al. 2017). Therefore, the condition of the lithosphere was hot, thin, and weak. Shorter rift segments in the Afar Rift in the East African Rift System have been attributed to rifting of hot thin crust (Ebinger 1999). Ebinger (1999) discussed the relationship between the elastic lithospheric condition and the formation of different fault segments in the extensional basin geometry of the active East African Rift system and compared the results with the faults found in the Baikal and Aegean Rifts. The comparison suggests that the Baikal Rift, which is greater than 80 km in length, was developed in the cold thick lithosphere. The Aegean Rift in the Mediterranean and Afar Rift in East Africa both show short border faults (less than 30 km in length) bounding narrow basins. The shorter border fault of the Aegean Rift develops within weak lithosphere whereas the shorter border faults of the Afar Rift develop as a new segmentation within highly stretched and intruded lithosphere. This suggests that the reason for the formation of shorter fault bounded rift basins in the West Coast-Taranaki Rift System was due to them being formed in crust that had already been highly stretched and intruded during the development of the metamorphic core complexes in the mid-Cretaceous.

The West Coast-Taranaki Rift phase produced a number of NNE-SSW oriented parallel to sub-parallel half-graben basins at the same time as the productive Taranaki Basin to the north (Strogen et.al. 2017; Figure 4.21; Figure 4.22). Most of the previous interpretations regarding the Taranaki Basin and associated sub-basins have been made using seismic data combined with limited outcrops and well data. In comparison, the Greymouth Basin is extensively drilled for coal exploration and has greater outcrop availability. Understanding the distribution of different sedimentary facies in the Greymouth Basin, it is highly possible that the Taranaki and other sub-basins in the West Coast Taranaki Rift phase have the same asymmetric facies distribution. Applying the information about the evolution of the Greymouth Basin, it can be concluded that the West Coast-Taranaki Rift basins experienced similar basin development histories. The basins likely initiated from small sub-basins that progressively widened and deepened from the amalgamation of active normal fault segments through time.

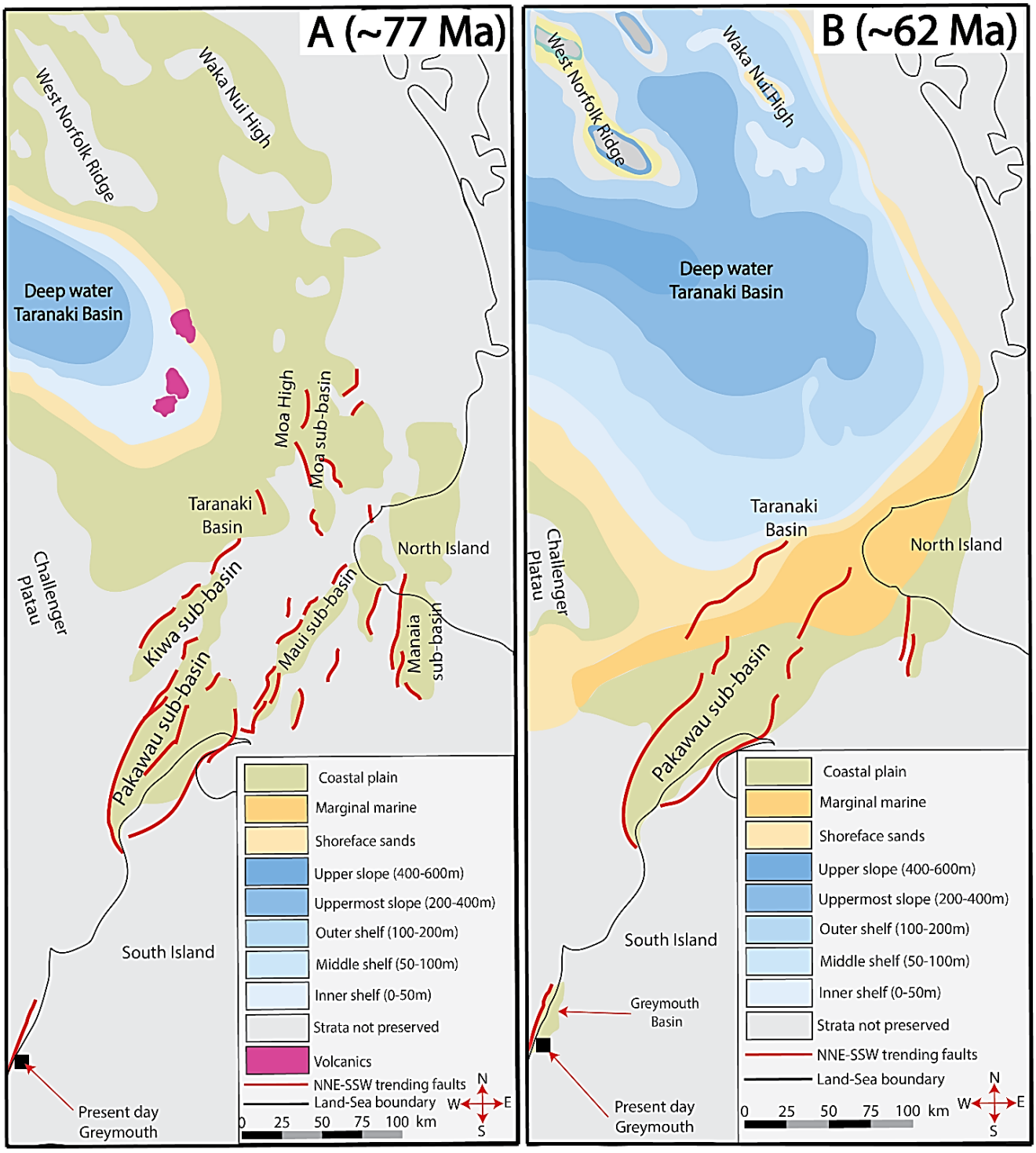


Figure 4. 21: A) Onset of the West Coast Taranaki rift phase in the Taranaki Basin region. Several subparallel to parallel NNE-SSW trending basins was initiated during this time. Greymouth basin was not formed during the onset of the West Coast Taranaki rift phase, B) Formation of the Greymouth Basin during the late West Coast Taranaki rift phase showing the same NNE-SSW orientation like other sub-basins. Marine transgression and post-rift thermal subsidence already started across the Taranaki Basin region (modified from Strogen et. al. 2017).

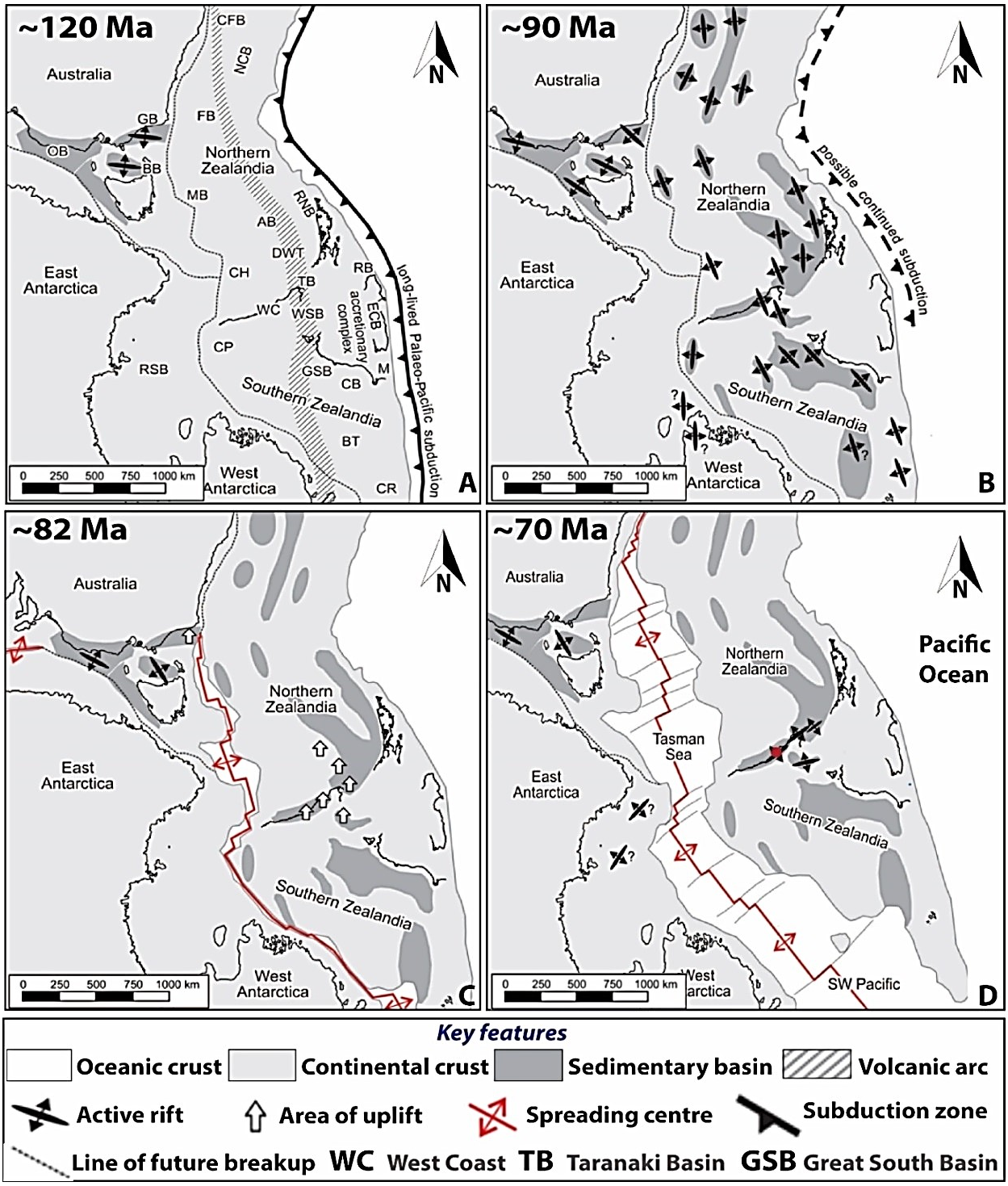


Figure 4. 22: Tectonic reconstruction for the Zealandia–Australia–Antarctica region from 120 Ma to 70 Ma (Strogen et. al. 2017), (A) the active convergent plate boundary system at the eastern margin of Gondwana; (B) first phase of rifting (Zealandia rift phase) with NW to WNW trending half grabens; (C) Initiation of separation of New Zealand from Australia by sea floor spreading in the west and a short period of uplifting and erosion phase to the east from the spreading centre, and (D) second phase of rifting (West Coast–Taranaki rift phase) with N to NE trending half grabens; the red dot is the location of Greymouth Basin.

## 4.9 Conclusions

An analysis of the distribution of the sedimentary facies of the Late Cretaceous-Early Palaeocene Paparoa Formation of the Greymouth Basin indicates half-graben rift basin geometry with the main border fault located to the northwest. The basin axis was filled with alternating alluvial and lacustrine sediments that were associated with episodes of widening of the basin with continued extension.

Sedimentary facies distribution across the basin shows alluvial fan and fan deltas alternated with braided river conglomerates in the centre to northeastern side of the basin during the Jay-Ford stage. During the Morgan-Waiomo and the Rewanui-Goldlight, these conglomerate facies shift to the northwestern side of the basin. Sandy meandering channels and floodplain facies dominated the eastern and southern parts whether a lake was present in the basin's centre or not. The sedimentary facies distribution suggests an asymmetrical half-graben rift basin. A gradual decrease in conglomerate thickness from northwest to southeastward suggests that the primary basin bounding fault was located towards the northwest. Conglomerate and lacustrine facies isolith maps indicate the deposition of the Paparoa Formation occurred in a NNE-SSW oriented basin. The basal bounding surface youngs to the northwest and southwest with increasingly younger sediments sitting directly on the basement. This all suggests a widening and deepening of the basin resulting from the main basin bounding fault stepping westward.

The Greymouth Basin evolved from small sub-basins that widened and deepened through time via small-displacement normal fault segments. Normal fault segments became more connected as the sub-basins amalgamated until they formed a major border fault. The major border fault controlled the subsidence of the late syn-rift phase of the basin. The basin did not change its orientation part way through its subsidence history as had been suggested by previous researchers; rather the faults progressively shifted westward and got larger and more connected as the basin subsided and enlarged similar to what has been found in other rift basins around the world.

# Chapter 5: Sequence stratigraphy in the Late Cretaceous to Early Palaeocene Greymouth Rift Basin


## Abstract

Lacustrine sequence stratigraphy provides a useful framework to understand the primary controlling factors of sedimentation in terrestrial rift basins. Sequence stratigraphic analysis on sedimentary facies of the Late Cretaceous to Early Palaeocene Paparoa Formation in the Greymouth Rift Basin, New Zealand, improves the understanding of the factors that were involved in the cyclic alluvial and lacustrine sedimentation. The basin formed a NNE-SSW striking half-graben with the steep gradient, fault-bounded margin to the northwest and the low gradient, hinge side to the southeast. Alluvial fans and fan deltas originated along the steep faults to the northwest, lakes alternating with meandering rivers and raised mires developed along the axis, and low gradient meandering river fans and deltas were to the southeast hinge and in the axis to the northeast and southwest.

A detailed sedimentary facies and sequence stratigraphic analysis revealed five sequences with consequent depositional phases and system tracts. The oldest depositional sequence (SQ1) overlies the basal unconformity with Greenland Group and comprises an alluvial depositional phase with progradational facies. SQ1 represents deposition in the rift initiation stage. The rift development stage records the highest thickness of sediments and combines three depositional sequences (SQ2, SQ3 and SQ4), each starting with marshy swamp phase at the base, overlying lacustrine phase which grades into deltaic infill phase and alluvial phase at the top. SQ2, SQ3 and SQ4 represent three complete depositional sequences, each of which consisting a transgressive system tract of retrogradational depositional pattern, a highstand system tract of clear progradational depositional pattern and a lowstand system tract with an overall progradational depositional pattern. Each complete depositional sequence is bounded by upper and lower sequence boundaries except SQ4 where the upper sequence boundary is replaced by an unconformity and correlative conformable surface. The rift termination stage records the youngest depositional sequence (SQ5) and consists of an alluvial phase of overall progradational depositional pattern. This is an incomplete depositional sequence which is underlain by an unconformity and correlative conformable surface at the base, and overlain by a marine transgressive surface, marking the end the lacustrine setting of the Greymouth rift basin and the onset of the marine transgression.

SQ1 is distributed in locally restricted and fault-controlled small basins, indicating the accommodation was too low relative to sediment supply due to slow subsidence of the basin to record any lacustrine phase. SQ2, SQ3 and SQ4 are distributed in large and deep fault bounded basins which became connected as the small basins amalgamated until they formed a major border fault. This suggests that each complete depositional sequence represents an episodic basin subsidence of rapid creation of accommodation due to basin extension and new fault activation to the west. This is commonly followed by a longer period of tectonic quiescence when decrease in basin subsidence rate allowed deltaic systems to prograde to infill the lakes until the basin was dominated by axial alluvial systems. SQ5 distributed all over the basin except at Twelve Mile Beach and deposited on large, low gradient surface as the basin widened and open to the sea, suggesting the sediment supply exceeded the accommodation condition as rifting of the Greymouth Basin probably came to an end and extensional basin subsidence stopped. Most of the sedimentation of the Greymouth Basin, particularly the Paparoa Formation, was occurred during the rift initiation and the rift

development phases. Therefore, sequence stratigraphic analysis of the Greymouth Basin suggests that the primary factor that controls the cyclic alluvial-lacustrine variation in Paparoa Formation is tectonic.

## 5.1 Introduction

Conventional sequence stratigraphic concepts, developed in relatively stable tectonic regions such as passive margins with a marine shoreline, are generally viewed as not applicable to lacustrine settings (Withjack et. al., 2002; Martins-Neto and Catuneanu 2010; Selim 2017; Holz et. al. 2013). Because lakes are small and isolated, unlike oceans, they are more affected by a local variation such as changes in basin subsidence rates, climate and inflow vs outflow. However, lacustrine sequence stratigraphy focusing on maximum flooding and expansion of lakes can be used for correlation and to better constrain those local variations, particularly in active tectonic settings. Lacustrine sequence stratigraphy has been widely applied to rift basins, most of which exhibit alternating alluvial and lacustrine sedimentary facies as a result of variations in tectonic activity, climate, and sediment supply (Currie 1997; Melchor 2007; Wei et. al., 2017). Cyclicity of sedimentary facies in rift basins is primarily generated from episodic pulses of extension and creation of accommodation (Blair and Bilodeau 1988; Folkestad and Satur 2008). In addition, the climate can have a profound influence because it affects hydrologic systems (Gore 1989). Many lakes located in rift basins are sensitive to climate variations, such as rainfall and evaporation rates, which change the hydrological conditions and can increase or decrease lake levels (Butzer and Isaac 1972; Street and Grove 1976; Williams et. al., 1977). Such hydrological variations can be superimposed on lacustrine sequences formed by changes in basin subsidence or can act alone where the tectonic setting promotes stable and continuous subsidence such as in distal foreland basins or central cratons.

The Late Cretaceous to Early Palaeocene Paparoa Formation of the Greymouth Basin is interpreted as a rift basin (Ward 1997) controlled by normal faults located toward the northwest with the half-graben hinge to the southeast (Chapter 2; Chapter 4). The formation is accessible in outcrop and has been extensively drilled for coal exploration (Figure 5.1). Sedimentary lithofacies comprise braided river alluvial fan and fan delta conglomerates to the northwest, and meandering alluvial and deltaic sandstones in the hinge to the southeast (Gage 1952; Nathan et al. 1986; Newman and Newman 1992; Boyd and Lewis 1995; Chapter 2; Chapter 3; Figure 5.2). The basin axis is characterized by alternating deposition of meandering alluvial and lacustrine sedimentary facies (Bowman et al 1984; Ward 1997; Cody 2015; Chapter 2; Chapter 3; Chapter 4) comprising four different alluvial phases separated by three different lacustrine phases. Raised and low-lying mire coals are also common in the basin axis (Gage 1952; Nathan et al. 1986; Newman and Newman 1992; Boyd and Lewis 1995). Such cyclicity in sedimentary facies suggests that sequence stratigraphy would be a useful tool to interpret the relative importance of tectonic versus climatic controlling factors in the Greymouth Basin. Thus, the main purpose of this study is to conduct a lacustrine sequence stratigraphic analysis in order to better tectonic versus climatic controls for each alluvial-lacustrine sequence.

## 5.2 Cyclic sedimentation and sequence stratigraphy

### 5.2.1 Marine vs non-marine sequence stratigraphy

The fundamental idea of sequence stratigraphy was developed from the centuries-old controversy over the origin of cyclic sedimentation and the relative importance of eustatic and tectonic factors on sea level change (Emery 1996). The word "sequence" refers to cyclic sedimentary deposits whereas the word “stratigraphy” deals with the processes of forming of different sedimentary deposits and their lateral as well as vertical changes through time and space on the Earth's surface (Emery 1996; Emery and Myers 1996; Catuneanu 2006). Sequence stratigraphy deals with genetically related sedimentary strata bounded by

unconformities and their correlative conformities (Posamentier and Vail 1988; Posamentier and Allen 1999; Catuneanu 2006).

The fundamental idea of non-marine sequence stratigraphy is that the development of an individual sequence is due to variation in the ratio of accommodation creation (A – tectonically driven subsidence with sediment load) to sediment supply rate (S - controlled largely by topography, climate and source area lithology) (Plint et al. 2001; Catuneanu 2006). Therefore, the classical marine sequence stratigraphy, in which specific sequences develop following a predictable order during a complete cycle of eustatic sea-level change, is not applicable (Holz et al. 2013; 2015). Eustatic sea-level, in non-marine sequence stratigraphy, is not a factor and can be ignored.

Nonmarine sequence stratigraphy has evolved through time and different concepts have been applied to understand the internal stacking patterns of genetically related deposits (system tracts) in different geological settings (Shanley and McCabe 1994; Oslen et.al. 1995; Currie 1997; Bohacs et al., 2000; Keighley et al. 2003; Martins-Neto and Catuneanu 2010; Holz et. al., 2013 Wei et. al., 2017; Selim 2017). Typical marine sequence stratigraphy defines a sequence with four major systems tracts; lowstand systems tracts (LST), transgressive systems tracts (TST), highstand systems tracts (HST) and falling stage systems tracts (FSST)/forced regressive system tracts (FRST) (Shanley and McCabe 1994; Van Wagoner 1995; Batezelli 2017; Wei et al. 2017). These are problematic to apply to systems with no shoreline or obvious base level (i.e. lake level). Therefore, several authors have argued that using the systems tracts that typically refer to sea-level change creates problems for the analysis of non-marine sequence stratigraphy (Oslen et. al. 1995; Currie 1997; Scherer et al. 2015).

### 5.2.2 Rift basin tectonic sequence stratigraphy

The variation in accommodation in a rift basin results from episodic pulses of extension (rapid subsidence) followed by long tectonic quiescence (slow subsidence) (Martins-Neto and Catuneanu 2010; Hou et al. 2020). Due to the asymmetry of the half-grabens and their subsidence controlled by a single major boundary fault, the creation of accommodation within a rift basin is asymmetric, and zones of high accommodation rate develop close to zones with no accommodation or even erosion (Holz et al. 2013).

The concepts, terminologies and models of tectonic sequence stratigraphy are broadly discussed in Martins-Neto and Catuneanu (2010). Martins-Neto and Catuneanu (2010) demonstrates that a full sequence stratigraphic cycle observed in the rift basins includes two major depositional trends, a short retrogradational trend and a dominating progradational trend. The cycle starts with a retrogradation trend of fining upward succession, corresponding to the episodic basin subsidence with short stages of rapid creation of accommodation. The cycle ends with a progradational trend of coarsening upward successions, corresponding to the longer periods of time of tectonic quiescence. Therefore, only two major system tracts can be identified in a non-marine sequence developed in rift basins; the transgressive system tracts (TST) and the highstand system tracts (HST). The TSTs correspond to the retrogradation depositional trend. Lacustrine transgressions are simply the time when accommodation rate (A) exceeds the rate of sediment supply (S). This condition tends to prevail when subsidence rate speeds up for a while. The HSTs correspond to the progradational depositional trend. Lacustrine highstand are simply the time when rate of sediment supply (S) exceeds the rate the accommodation creation (A), and gradually fills the available accommodation by the progradation of alluvial, fluvial and deltaic depositional systems. This condition tends to prevail when longer stages of tectonic quiescence establish after each stage of extensional subsidence. The maximum flooding surfaces/flooding surfaces are the part of the highstand system tracts

and are the only approximately time-significant surfaces in a full stratigraphic cycle. The maximum flooding surfaces record times when subsidence rate was at its highest, relative to sedimentation rate. The initial flooding surfaces/first flooding surfaces/basal flooding surfaces represent the onset of transgression whereas the presence of first turbidite facies in lacustrine package represents the onset of progradation. The position of the maximum flooding surfaces is likely to be nearer the basal flooding surfaces. Lowstand system tracts (LST) and falling stage system tracts (FSST)/forced regressive system tracts in the non-marine rift basins tend to be poorly developed or absent as the subsidence is continuous and there is no loss of accommodation. In reality, all that is observed in a rift basin is that deltaic and alluvial systems gradually prograde into the unfilled accommodation (i.e. the lake), resulting in coarsening upward sequences and an upward decrease in water depth. This should not be confused with an upward decrease in accommodation, or with a 'lowstand' or 'forced regression'. Therefore, a typical non-marine rift sequence tends to start with a basal flooding surface culminating in lacustrine deposits at the base, overlain by a maximum flooding surface and then by prograding delta and alluvial deposits. The sequence boundary in non-marine rift basins is related to rapid tectonic subsidence and the consequent generation of accommodation. The basal flooding surface, in this case, represents the onset of rapid tectonic subsidence and is identified as the rift sequence boundary. A complete stratigraphic cycle or a sequence in a rift basin is bounded by upper and lower sequence boundaries.

However, applying Martins-Neto and Catuneanu (2010) model in many rift basins is somewhat problematic, particularly when a rift sequence doesn't start with a deep-water lacustrine deposit. Prosser (1993) mentioned that a basal alluvial dominated interval could be found below the basal flooding surface in many rift basins, representing the early stage of rift initiation. Martins-Neto and Catuneanu (2010) model doesn't clearly demonstrate how rift initiation alluvial deposits can be correlated in a rift sequence stratigraphic analysis. In order to solve this problem, Holz et al. (2013, 2015) proposed a conceptual sequence stratigraphic model for the Reconcavo Rift Basin in Brazil where a three-fold scheme of tectonic system tracts are linked with alternation of accommodation generation and sediment supply. According to the model, a phase of initial slow subsidence in the basin (rift initiation system tract) is followed by increasing subsidence rates (rift development system tract) and ends with slow subsidence rates (rift termination system tract) where the subsidence is primarily controlled by one major basin bounding fault. This model can be tied to Gawthorpe and Leeder's (2000) rift tectonic model which illustrates that the initiation phase of fault growth within a rift basin is characterized by low surface topography developed from displacement on discontinuous small normal faults which eventually become larger structures by connecting resulting in the amalgamation of multiple sub-basins. Major displacements of large continuous normal faults occur along the basin margins which are continuous and through-going whereas minor faults within the basin become inactive through time. The depocentres of the half-grabens are associated with these different stages of fault development which become the predominant catchment zones for sediments.

Other names for defining different system tracts have also been suggested. For example, 'Aggradational' and 'Degradational' system tracts were proposed by Currie (1997) according to changes in stacking patterns of alluvial architectural elements due to changes in base level and available accommodation. 'Low-Accommodation' and 'High-Accommodation' system tracts were introduced by Martinsen et al. (1999) where the generation and destruction of the accommodation space with respect to sediment supply were the main focus of study.

### 5.2.3 Lacustrine cyclic sedimentation: tectonic versus climatic factors

Cyclic sediments are repetitive patterns of different sedimentary facies forming a sequence (Oslen et.al. 1995; Emery and Myers 1996; Hinnov and Bazykin 2001; Goldhammer 2013). Actively subsiding, complex, non-marine tectonic settings such as rift and foreland basins often contain cyclic sedimentation that could be due to a variety of factors including fluctuation in subsidence rate, climate and changes in outflow in the basin (Schuster and Costa 1986; Scholz et al., 1998; Scholz 2001; Martins-Neto and Catuneanu 2010; Holz et al. 2013, 2015). Each factor may influence the sedimentation independently or in conjunction with other factors.

Changes in tectonic subsidence rate is the primary factor for developing cyclic variation in sediments in rift basins. The cyclicity in sedimentary facies results from changes in the ratio of the creation of accommodation (A) and sediment supply (S) (Plint et al. 2001; Martins-Neto and Catuneanu 2010). The alternation of alluvial and lacustrine facies in the Brazilian Reconcavo Rift Basin suggests that the incipient rift basins, created from isolated and restricted faults, had low accommodation due to a low rate of subsidence and were easily infilled with alluvial facies such that S>A. Lacustrine facies were deposited when the initial faults linked and created greater accommodation forming a larger and deeper basin with a higher rate of subsidence such that A>S (Holz et al. 2013). The cyclic variation in sediments of the Minas Basin indicates that the thicker cycles were deposited due to rapid subsidence towards the fault-bounded side of the basin whereas decreasing cycle thicknesses up-section reflects a decreasing rate of tectonic subsidence within the basin (Martel and Gibling 1991).

Cyclic deposits in many rift basins alternatively may be dramatic indicators of climate change (Smoot and Oslen 1988, 1994). Classic ideas of cyclic lake level changes have been ascribed to Pleistocene climate changes of alternating glaciations and interglaciations controlling the hydrologic condition by fluctuations in rainfall and evaporation (Hammen 1974; Seltzer 1994; Schutt et al. 2008; Fan and Guangliang 2012; Phan 2014; Walther et al. 2017). For example, Lake Estanya in Spain experienced significant hydrological changes over the last 21,000 years indicated by moderate to shallow lake levels in the generally arid and cold climate of the Late Glacial Period during the Late Quaternary and higher lake levels in the relatively warm Interglacial Period during the Holocene (Morellón et al. 2009). Studies have examined the relative importance of rainfall versus evaporation in controlling cyclic lacustrine sequence stratigraphy. Scholz et al. (1998) compared lakes from low latitude (Lake Malawi and Lake Tanganyika) versus high latitude (Lake Baikal) rift basins and found that lake levels are extremely dynamic in low-latitude systems due to the predominance of evaporation in the hydrologic cycle whereas precipitation dominates over evaporation in the higher latitude lakes. Climatic variations controlled the Quaternary lake levels and the sedimentation in ~ 58 lakes in Africa where lake level rises were caused by regional increases in rainfall and runoff, broadly correlating with periods of decreased global temperatures which developed cloud covers and constant seasonal precipitation (Street and Grove 1976). In Lake Malawi in the southern part of the East African Rift, the total loss of annual lake water is primarily through evaporation (90%) with very little lost through the lake's outlets (10%) (Scholz 2001). This produces seasonal fluctuations of 1–2 m in this enormous lake, and long-term changes in water level are measured in the hundreds of meters over time frames of hundreds to thousands of years (Owen et al., 1990; Scholz 2001). The Main Ethiopian Rift, Aden Rift and Afar Depression in East Africa are regions in rainfall deficit and the existence of many lake basins developed in these regions are directly dependant on inflows from permanent rivers or numerous springs from the surrounding highlands (Gasse and Street 1978). Studies on Late Quaternary lake levels in southern Afar and the adjacent Ethiopian Rift showed that the change in lake levels was primarily controlled by moister

conditions during phases of high lake level even in the volcanically and tectonically active regions (Williams et al. 1977).

The other factor that can control the cyclic variation in sediments is changes in the outflow of the lakes and inflow from upstream rivers. Unlike closed lake systems where rising and falling of the lake level and alternating shallowing (coarsening) upward and deepening (fining) upward cycles depends on the climatic variation, an outflow of an open lake system can independently control fluctuations in lake levels (Gore 1989; Martel and Gibling 1991). Many large-scale landslides around the world cause river damming in the upstream inflow which eventually creates a new lake system or blocks water inflows from being transported to the original lakes (Schuster and Costa 1986; Ermini et al. 2006; Coico et al. 2013; Storm 2013). These dams leave the lake sediment starved, leading to cyclic variations in lithology. The most common initiation mechanisms for dam-forming landslides are excessive rainfall and snowmelt (climatic factors), earthquakes (tectonic factor affecting subsidence rate) and volcanic eruptions (Schuster and Costa 1986; Costa and Schuster 1988; Fan et al. 2012).

In many basins, both tectonic and climatic changes affect cyclic sedimentation. For example, lacustrine sequence stratigraphic analysis of the Miocene Rubielos de Mora Basin in Spain indicates that basin subsidence was responsible for the generation of first and second-order sequences, whereas third and fourth-order sequences were the result of climatically forced processes (Anadón et al. 1991). Analysis on modern shoreline deposits of the Dead Sea in Israel suggests that the major fluctuations in lake level are controlled by climate (e.g. rainfall), whereas minor fluctuations are the result of basin subsidence (Machlus et al. 2000; Bartov et al. 2002; Bartov et al. 2006). Sedimentary facies analysis of the Lunpola Rift Basin in Tibet indicate that climate variation interacted with the basin tectonics at the later stage of rifting to control the deposition of a widespread evaporite layer distributed across the basin under relatively warm and arid climatic conditions (Wei et al. 2017).

### 5.3 Greymouth Rift Basin

The Late Cretaceous to Palaeocene Greymouth Rift Basin is located in the West Coast region of the South Island of New Zealand and is part of the West Coast-Taranaki Rift System (Strogen et.al. 2017). It is bounded on the west by the Cape-Foulwind Fault Zone and on the east by the cross-cutting Montgomerie-Mt Davy Fault Zone (Suggate 2014; Chapter 4; Figure 5.1). The basin was infilled with Late Cretaceous to Early Palaeocene non-marine sediments of the Paparoa Formation (Laird 1993, 1994; Laird and Bradshaw 2004) which unconformably overlie Ordovician Greenland Group basement rocks and conformably underlie Palaeocene Brunner Formation in places (Gage 1952; Nathan et al. 1986; Boyd and Lewis 1995; Mortimer et al. 2014; Figure 5.2).

The Paparoa Formation exhibits cyclic deposition of alluvial-lacustrine rocks where three lacustrine members are separated by four alluvial members (Gage 1952; Newman 1985; Boyd and Lewis 1995; Ward 1997; Cody 2015; Figure 5.2). Three lacustrine members are named the Ford, Waiomo and Goldlight mudstone members from the oldest to the youngest (Nathan 1978; Figure 5.2). The oldest Ford Member lacustrine mudstones are distributed in several isolated sub-basins in the central and the northeastern parts of the main rift basin (Chapter 4; Figure 5.2). The younger Waiomo Member lacustrine mudstones are found in mainly two sub-basins in the northwestern and the northeastern parts of the main basin (Cody 2015; Chapter 4; Figure 5.2). The youngest Goldlight Member lacustrine mudstones are the thickest and are distributed across the entire Greymouth Basin (Gage 1952; Newman 1985; Ward 1997; Cody 2015; Chapter 4). Associated with each lacustrine member are alluvial fan-deltas and meandering river deltas

from the rift faults and hinge zones, respectively (Chapters 2, 3 and 4). The lacustrine facies association includes organic-rich lacustrine massive mudstone facies that have been interpreted as potential source rocks capable of generating both oil and gas (Cody 2015; Mohnhoff et al. 2017).

The three lacustrine members are separated by four coal-bearing alluvial members named, from oldest to youngest, the Jay, Morgan, Rewanui, and Dunollie. The overall depositional environments associated with each alluvial member are an alluvial fan, braided rivers, and meandering rivers with floodplain deposits. Alluvial fan and braided river conglomerates of the Jay Member alluvial phase are restricted to the central and the northeastern side of the basin along interpreted faults (Chapter 2 and Chapter 4). Alluvial fan and braided river conglomerates of the younger alluvial phases (Morgan, Rewanui and Dunollie) are restricted to the northwest side of the basin deposited along the interpreted basin-bounding master fault of the rift (Chapter 4). Meandering river and associated floodplain systems were developed mostly in the basin axis and the southeastern hinge side of the basin (Chapter 2; Chapter 3; Chapter 4; Figure 5.2).

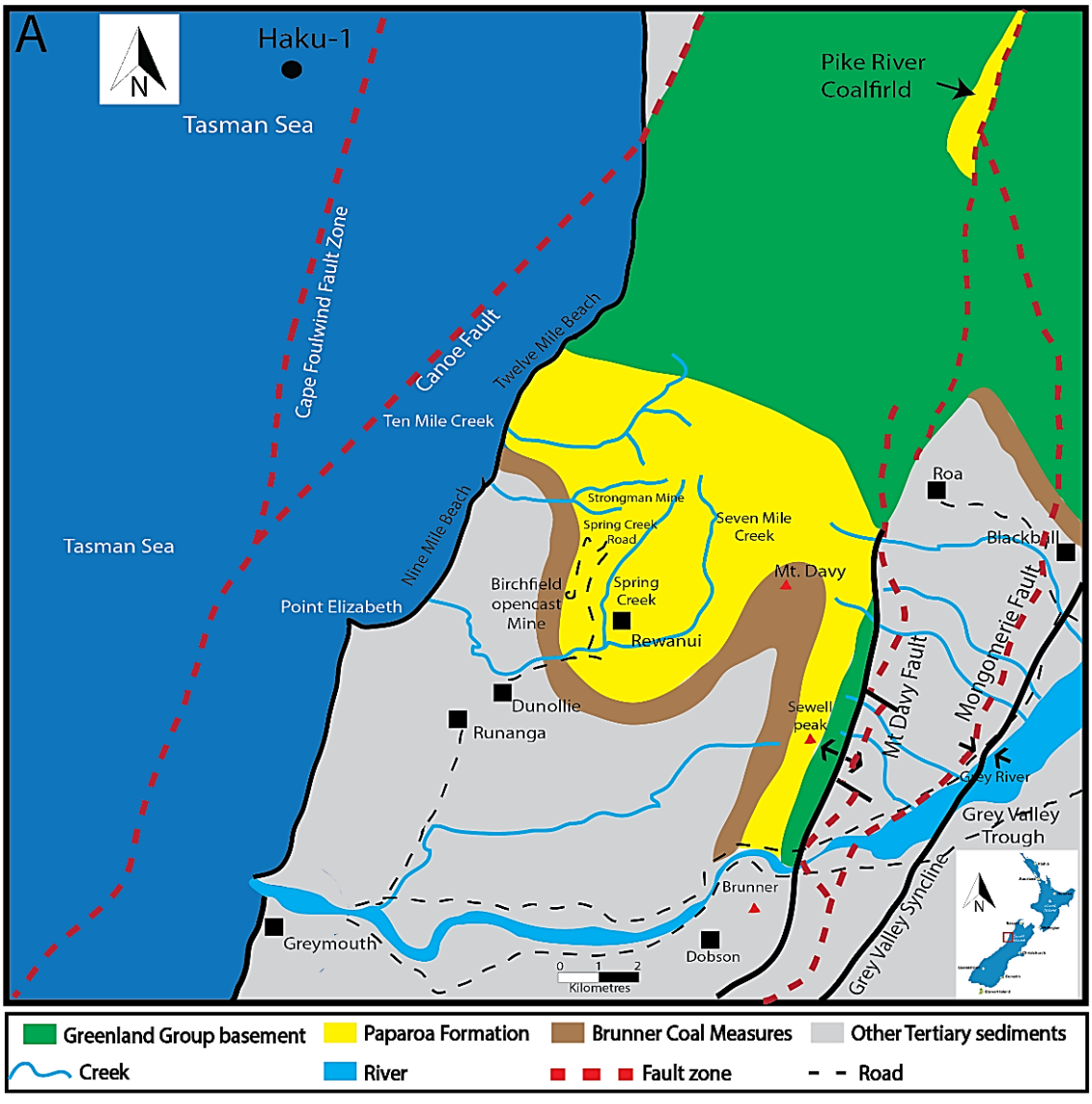


Figure 5. 1: A) Geological and structural map of the study area (modified from Gage 1952, Newman 1985, Suggate 2014, Nathan 1986; Nathan et al. 2002; Rattenbury and Isaac 2012) of the Greymouth Basin.

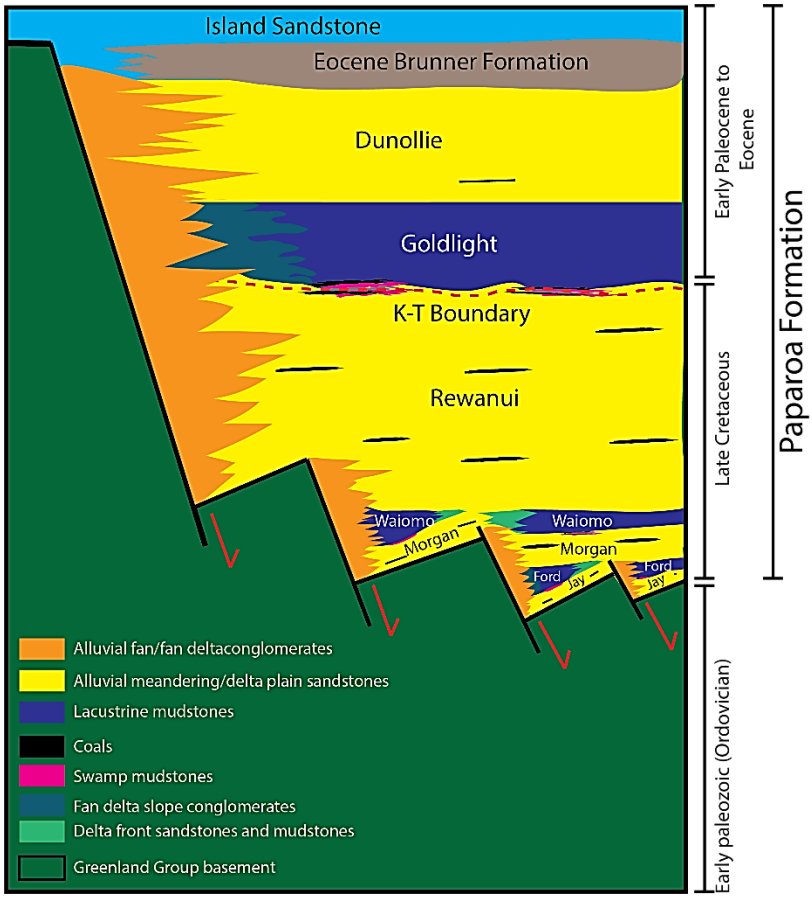


Figure 5. 2: Generalized stratigraphy of Paparoa Formation based on Gage 1952, Newman 1985, Boyd and Lewis 1995 and Chapter 4.

## 5.4 Methods

Sedimentary facies and lacustrine sequence stratigraphy have been analyzed in multiple drill cores combined with detailed measured sections from the outcrop (Chapter 2). Typical data from drill holes include core logs and geophysical logs. These are constructed into a fence diagram based on sedimentary facies to identify lateral variability across the Greymouth Rift Basin. Sequence stratigraphy improved the correlation between drill holes.

### 5.4.1 Sedimentary facies analysis

Detailed sedimentary facies analysis is used to map out lateral and temporal variation within the basin with a particular focus on how facies are identified (Figure 5.3). For the purpose of sequence stratigraphic analysis, sedimentary facies are grouped into the subaqueous, shoreline and subaerial facies. Subaqueous facies include all lacustrine, prodelta, and fan delta slope facies. Shoreline facies include facies that were deposited in the river mouths, and delta and fan delta fronts, as well as away from them. Subaerial facies include all alluvial, floodplain, and mire facies.

Using the detailed facies analysis, we construct a lake-level curve for each borehole, identifying shoreline, subaerial and subaqueous facies as a simple method to understand i) the identification of phases where either lacustrine or alluvial environments dominated in the basin centre, ii) the size of the lakes, and iii) the interpreted balance between subsidence rate and sediment supply. In the lake level curve, shorelines mark

the centre of the horizontal scales of lake level curve, the subaerial facies are drawn to the left and the subaqueous facies are drawn to the right side of the curve. In this simple visual, facies migration and changes in the size of the palaeo-lakes become immediately obvious when the water level curve changes its position from the left side to right, or vice-versa.

A fence diagram and detailed cross-sections are created with a particular focus on how the shoreline, subaerial and subaqueous facies are distributed laterally as well as vertically across the basin. The lake level curve and the maximum flooding surfaces are used for correlation. We use cross-sections and the fence diagram in order to correlate the complete depositional sequences into the alluvially dominated basin margins as well as in the basin axis where the lakes form.

### 5.4.2 Sequence Stratigraphy Analysis

We offer an an integrative approach to analize the sequence startigraphy of the Greymouth Basin, based on the Martins-Neto and Catuneanu (2010) model and Holz et al. (2013, 2015) model. The reason behind the approach is that the Paparoa Formation in the Greymouth Basin starts with an alluvial phase (the oldest Jay Member), sitting directly on the Greenland Group basement. Applying only the Martins-Neto and Catuneanu (2010) model in the Greymouth Basin cannot define the oldest alluvial phase clearly as a complete depositional sequence/stratigraphic cycle. Therefore, we introduce the Holz et al. (2013, 2015) model to define the oldest alluvial phase and to demonstrate a complete sequence stratigraphic analysis for all members of the Paparoa Formation and the lower part of the transgressive Haerenga Supergroup identifying rift initiation, rift development and rift termination stages. In our sequence stratigraphic analysis, we use the word ‘stage’ instead of defining them as system tracts as described in the Holz et al. (2013, 2015) model. For example, rift initiation stage, rift development stage and rift termination stage instead of rift initiation system tract, rift development system tract and rift termination system tract.

The centre of the Greymouth Basin is the easiest area to identify the cyclicity of the sediments. We use detailed sedimentary facies analysis and lake level curves from the centre of the basin to define different depositional phases; marshy swamp, lacustrine, deltaic infill, and alluvial phases. These are then extrapolated to the basin margins where the depositional environments do not record the cyclicity seen in the basin’s axis.

The depositional phases occur in specific depositional sequences, defining sequence stratigraphic systems tracts. Identifying depositional sequences help to identify the multiple alluvial-lacustrine cycles of the Paparoa Formation and correlate disparate facies from across the basin. A complete depositional sequence/stratigraphic cycle consists of all four depositional phases or at least three depositional phases; lack two or more depositional phases make a depositional sequence incomplete unless they are extrapolated in the basin margins as part of a complete depositional sequence (Figure 5.3). System tracts represent base-level changes during the presence and the absence of a lake in the basin. The presence and the absence of a lake in the basin is simply because the subsidence provides accommodation, and rate changes cause the deepening and the shallowing events as the ratio between accommodation and sediment supply shifts back and forth.

A sequence boundary is usually defined as a widespread subaerial/erosional unconformity in the basin (Figure 5.3). In rift basins, subsidence and consequent sedimentation is continuous, hence there is no subaerial/erosional unconformity. Therefore, a sequence boundary in a rift basin is used to mark changes in subsidence rate and the creation of large accommodation. Where a depositional sequence is complete and starts with either a marshy swamp phase or a lacustrine phase, a sequence boundary (SB) is identified

and marked by a basal flooding surface (Figure 5.3). A tectonic sequence boundary is replaced by an unconformity (U) in two situations; i) where a depositional sequence is incomplete and starts with an alluvial phase directly sitting on the Greenland Group basement, and ii) where a complete depositional sequence in the basin centre correlates to the basin margins during widening and starts with an alluvial phase directly sitting on the Greenland Group basement (Figure 5.3).

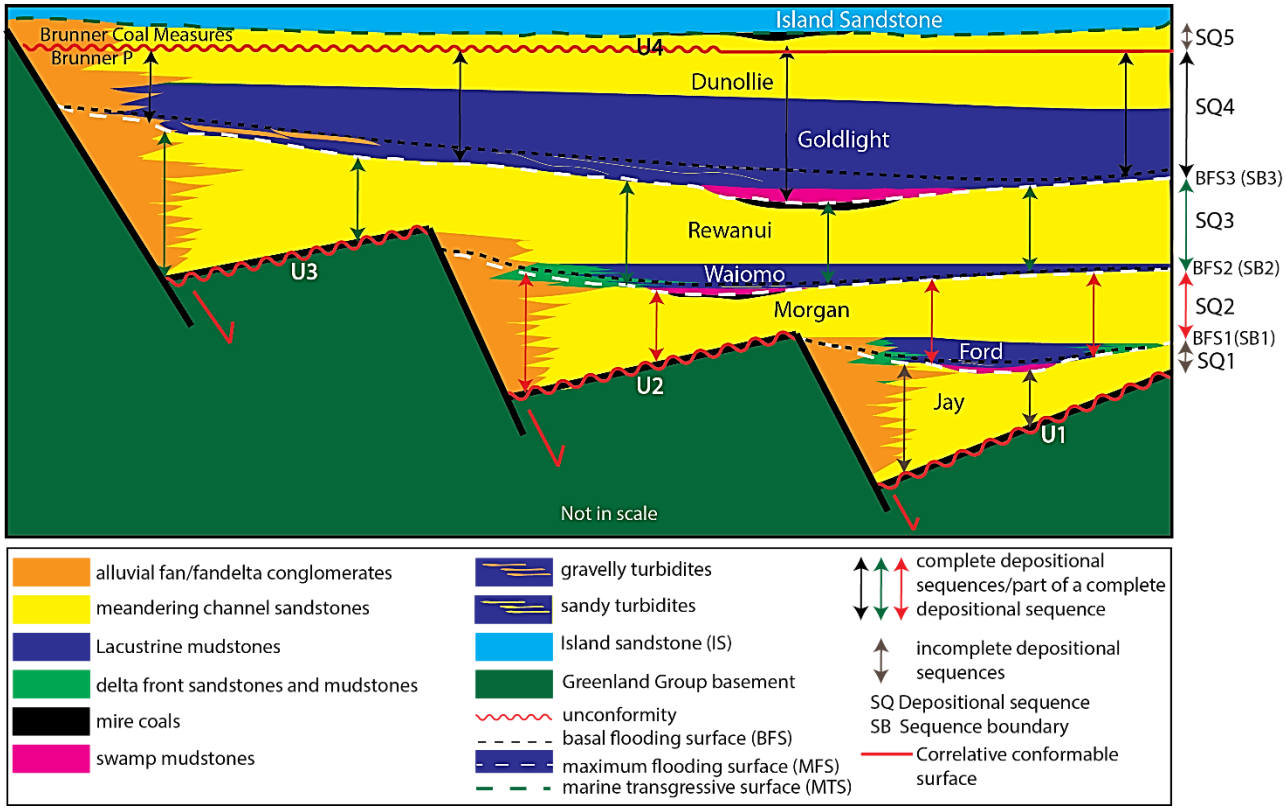


Figure 5. 3: A schematic diagram shows a sequence stratigraphic framework for the Greymouth Basin.

## 5.5 Results: Sedimentary facies analysis

### 5.5.1 Sedimentary facies groups

Detailed sedimentary facies analysis of the Paparoa Formation was presented in Chapters 2 and 3. In order to draw lake level curves and conduct a sequence stratigraphic analysis, these were grouped into three facies groups; subaqueous, shoreline and subaerial. Each facies group includes a number of individual facies.

The subaqueous facies group includes lacustrine and prodelta facies association. The lacustrine facies association includes massive mudstone facies, mudstones with minor sandstone facies and sandy turbidites facies. The massive mudstone facies consists of grey to black mudstone/silty mudstone with rare small leaves and fresh water fossils and is interpreted as deposited in the centres of lakes away from shoreline influences. The facies shows thick, uniform nature of high gamma response due to the presence of homogeneous mudstone. The mudstones with minor sandstone facies consists of normally graded, thin, brownish grey, fine sandstone and siltstone beds with conspicuous plant debris interpreted as turbidites derived from a distal shoreline. Turbidite beds are thicker, contain convolute bedding and common load casts, and are more proximal to shorelines in the sandy turbidites facies. This facies is interpreted as deposited in underwater delta slope of river delta setting that is lower in gradient and sourced from the basin

axis and hinge side of the basin. The gravelly turbidites facies comprises normally graded sandstone beds with lenses of conglomerates and isolated dropstones. Moderate to well-sorted, clast or matrix-supported, rounded to subrounded, pebble to cobble sized, highly deformed conglomerates and sandstones form the gravelly delta slope facies. These two facies are also more proximal to the shorelines but are interpreted to have been deposited in underwater slopes of high gradient alluvial fan-deltas, sourced from the fault-bounded side of the basin (Chapter 2; Chapter 3).

The shoreline facies group includes a number of facies. The gravelly mouth bar facies mainly consists of thick and coarsening upward conglomerate beds interpreted as deposited in the shoreline delta front of alluvial fan-deltas. The sandy mouthbar facies is characterized by thick, coarsening upwards sandstone beds interpreted as deposited at the river mouth of river delta, commonly on the hinge side of the basin or in the basin's axis from the northeast or southwest. The interdistributary bay facies has highly bioturbated carbonaceous mudstones and sandstones interbedded with the occasional conglomerate bed or coaly stringer, deposited in shallow water along fan-delta shorelines and associated with the gravelly mouthbar facies in the northwest, and sandy mouthbar facies in the northeast and the southeast. The low-lying marshy swamp facies comprises thinly interbedded siltstones, sandstones, carbonaceous mudstones and silty coals with abundant leaf matter, spore, pollens, and vertical rootlets and is interpreted as deposited along low energy shorelines away from an active river delta (Chapter 2; Chapter 3).

The subaerial facies group includes gravelly, sandy and coaly facies. The debris flow facies is poorly sorted conglomerate and breccia, interpreted as deposited from subaerial debris flows. The gravelly braided river facies comprises clast-supported, cobble to boulder-sized, rounded to subangular, moderate to poorly sorted, imbricated conglomerates with thin sandstone lenses interpreted as deposited on the delta plain of alluvial fan-deltas or in the lower part of an alluvial fan when there were no lakes in the basin. Due to the presence of overall coarse-grained sedimentation in the basin margin, the overall gamma-ray value is low for the gravelly braided river facies. The meandering channel facies primarily consists of cross-bedded, medium to coarse-grained sandstones interpreted as deposited on the delta plain of meandering river deltas or as part of a meandering river system during the absence of lakes in the basin. The abandoned channel facies consists of carbonaceous silty mudstone/highly carbonaceous mudstone fining up to muddy coals interpreted as oxbow lakes to marshes. The crevasse splay facies comprise thin coarsening to fining upward sandstone and interlaminated siltstone and carbonaceous mudstone beds with plant material interpreted as flood deposits. These facies are located proximal to the active meandering river channel and are interpreted as having been deposited as floodplain facies of the meandering river systems. Gamma-ray value is comparatively higher due to the presence of mostly fine-grained sandstones and mudstones.

The mire coal facies has two sub-facies. The thick, dark black, waxy and clean coals with fragmented leaf fossils. This facies is interpreted as likely deposited in raised mires isolated from local drainage systems as indicated by its thick, clean, low ash coals and wide lens-shaped geometry. The alternating clean and muddy coals with high sulphur and high ash content are likely deposited as low-lying mire facies and is commonly associated with the raised mire coal facies or lateral to low lying marshy swamp facies. Coals and carbonaceous mudstone deposits are identified from the spike of the density log (Figure 5.4).

### 5.5.2 Distribution of sedimentary facies in the Greymouth Basin

The fence diagram (Figure 5.4; Chapter 2 and Chapter 3) shows the results of the detailed sedimentary facies analysis, correlation, and distribution of different sedimentary facies across the Greymouth Basin.

Lateral changes in facies are most obvious in the cross-sections perpendicular to the interpreted basin-bounding faults in the northwest, across the basin axis, and to the hinge side in the southeast.

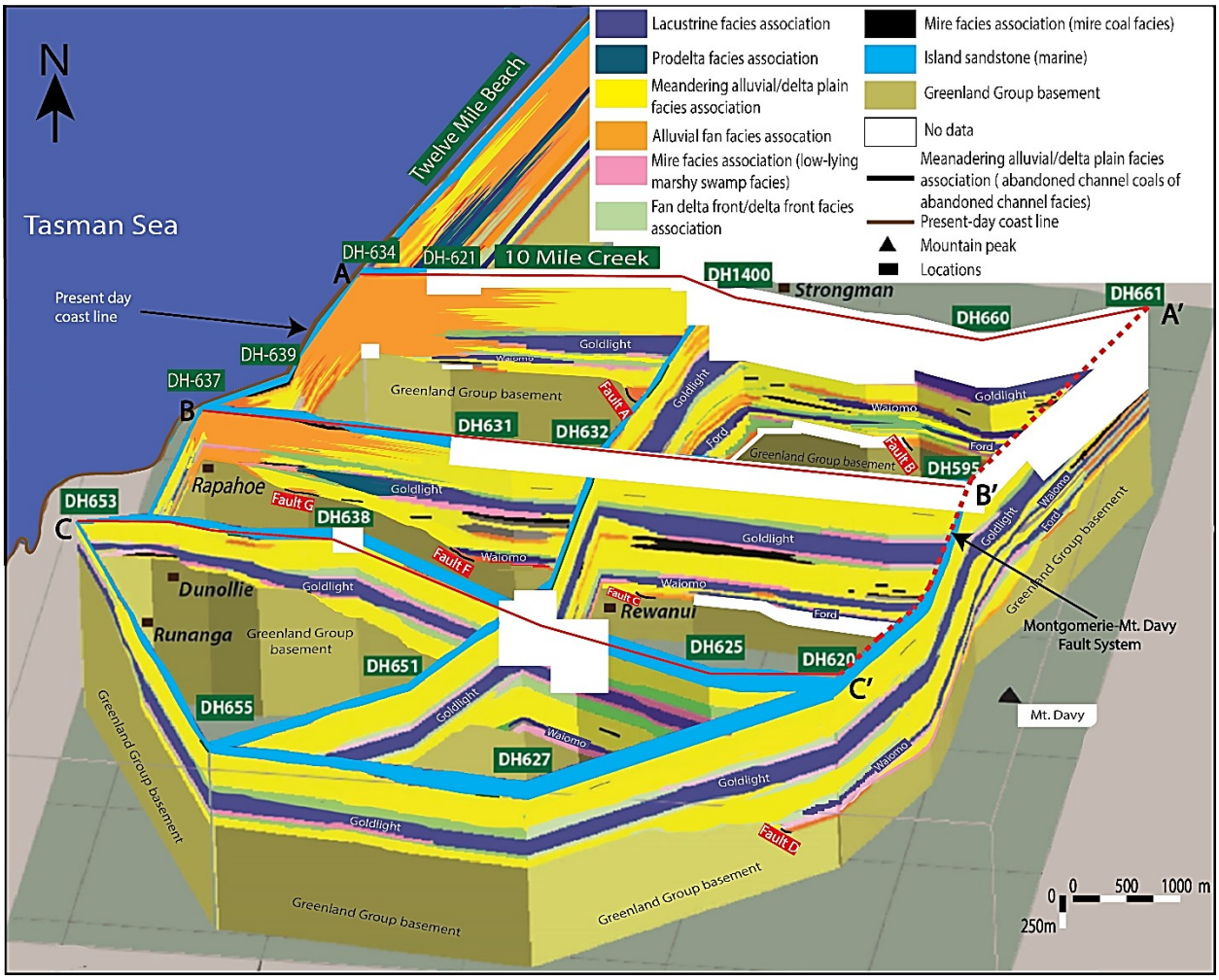


Figure 5. 4: Fence diagram illustrating the distribution of alternating fluvio-lacustrine deposits of the Paparoa Formation in the Greymouth Basin, which highlights the basin development through time. The detail of the cross-sections (AA', BB' and CC') are demonstrated in Figure 4.11. Syn-depositional faults (Fault A, Fault B, Fault C, Fault D and Fault F) are drawn in the fence diagram on the basis of the presence of conglomerates. Red broken line represents the eastern margin Montgomerie-Mt Davy Fault System that postdates the deposition of the Paparoa Formation.

The centre of the basin contains lacustrine massive mudstone facies, and lacustrine mudstone with minor sandstones facies (Chapter 3). Sandy turbidites facies deposited proximal to lake from active river delta whereas low lying marshy swamp facies deposited along the lake edges away from active river delta. The lacustrine facies alternate with meandering alluvial facies in the basin axis. These are characterized by meandering channel facies and associated abandoned channel and crevasse splay facies. Mire coal facies can be found when there is no lake infilling the basin.

Sandy to muddy meandering river deltas entered the palaeolakes from the southeastern hinge side or along the basin axis from the northeast or southwest (Chapter 3). The deltas contain a subaerial delta plain system, a shoreline delta front, and subaqueous delta slope system. The subaerial delta plain is characterized by

meandering channel facies, abandoned channel facies and crevasse splay facies. Sandy mouthbar facies and interdistributary bay facies are found in shoreline delta fronts whereas sandy turbidites facies are common in subaqueous delta slope systems. During alluvial phases, the meandering alluvial systems were present but joined the axial meandering alluvial system as tributaries.

Gravelly fan deltas entered the palaeolakes from steeper fault-controlled topography (Chapter 2). The subaerial fan delta plains comprise debris flow and gravelly braided river facies. Gravelly mouth bar facies and interdistributary bay facies make up the shoreline delta front whereas gravelly delta slope and gravelly turbidites facies are common in the subaqueous delta slope systems. Debris flow and gravelly braided river facies are also present during alluvial phases of each depositional sequence in the basin margin interfingering with meandering channel facies, abandoned channel facies and crevasse channel facies in the basin axis. Alluvial fan and fan delta facies record steep fault-controlled sides of the basin with the thickest and largest to the northwest in the upper units.

## 5.6 Results: Sequence stratigraphy analysis

### 5.6.1 Depositional phases and lacustrine systems tracts

Four depositional phases (Figure 5.5) can be identified based on the facies in the basin centre. The phases are marshy swamp, lacustrine, deltaic infill, and alluvial. The basin margins remain alluvial but change between gravelly alluvial fans or fan deltas, and meandering rivers or meandering river deltas. A complete depositional sequence is made up of four depositional phases, starting with a marshy swamp phase is overlain by the lacustrine phase, which grades to the deltaic infill phase and finally to the alluvial phase at the top (Figure). As subsidence was continuous and sediment supply was almost constant during the time of the deposition of the Paparoa Formation (Chapter 2; Chapter 3; Chapter 4), a lowstand system tract was not developed in the Greymouth Basin. As there was no negative accommodation in the Greymouth Basin due to continuous subsidence throughout the deposition, forced regressive system tracts (FRST) were also absent. However, when the lake is infilled and completely disappeared, the depositional regimes change to alluvial setting and spread across the basin. The decrease in subsidence rate in the basin during that time allow the alluvial sediments to fill up the low accommodation space. Therefore, a low accommodation system tract with an overall progradation pattern is developed over the highstand system tract. A complete depositional sequence is, therefore contains a transgressive system tract at the base, a highstand system tract in the middle, and a low accommodation system tract at the top. The gamma-ray references have only been used from the basin centre in order to understand the depositional trend for each systems tract.

A marshy swamp phase is defined by the existence of thinly bedded carbonaceous mudstones, sandstone and silty coals, underlying thick mire coals in the basin centre. This phase comprises low-lying marshy swamp facies of the shoreline facies group. The marshy swamp phase is identified as a transgressive systems tract (TST). The TST is easy to identify in the basin axis where the depositional trend grades upward from mire to low lying marshy swamp. In the basin margin, mostly the low-lying marshy swamp facies of the shoreline facies group has been identified as the TST. TST start with a basal flooding surface. In the gamma-ray log, TST is characterized by a short fining upward sequence and identified as retrogradation depositional patterns.

A lacustrine phase is defined by the existence of thick lacustrine mudstones in the basin's centre. This phase consists of various lacustrine facies of the subaqueous facies group with the associated lateral shoreline and subaerial facies. The lacustrine phases represent the lower part of highstand systems tracts ($HST^{l}$) which starts with a maximum flooding surface at the base. In the basin axis, the depositional trend is uniform due

to the presence of a deep lake. The presence of thin sandstone beds (mudstone with minor thin sandstone facies) indicate the onset of progradation. In the fault-controlled basin margin, the depositional trend changes upward from proximal lacustrine to fan delta, indicating the onset of progradation. In the hinge side of the basin, depositional trend grades upward from proximal lacustrine to meandering delta, indicating the onset of progradation. In the gamma-ray log, $HST^{l}$ is usually characterized by a slightly coarsening upward depositional pattern.

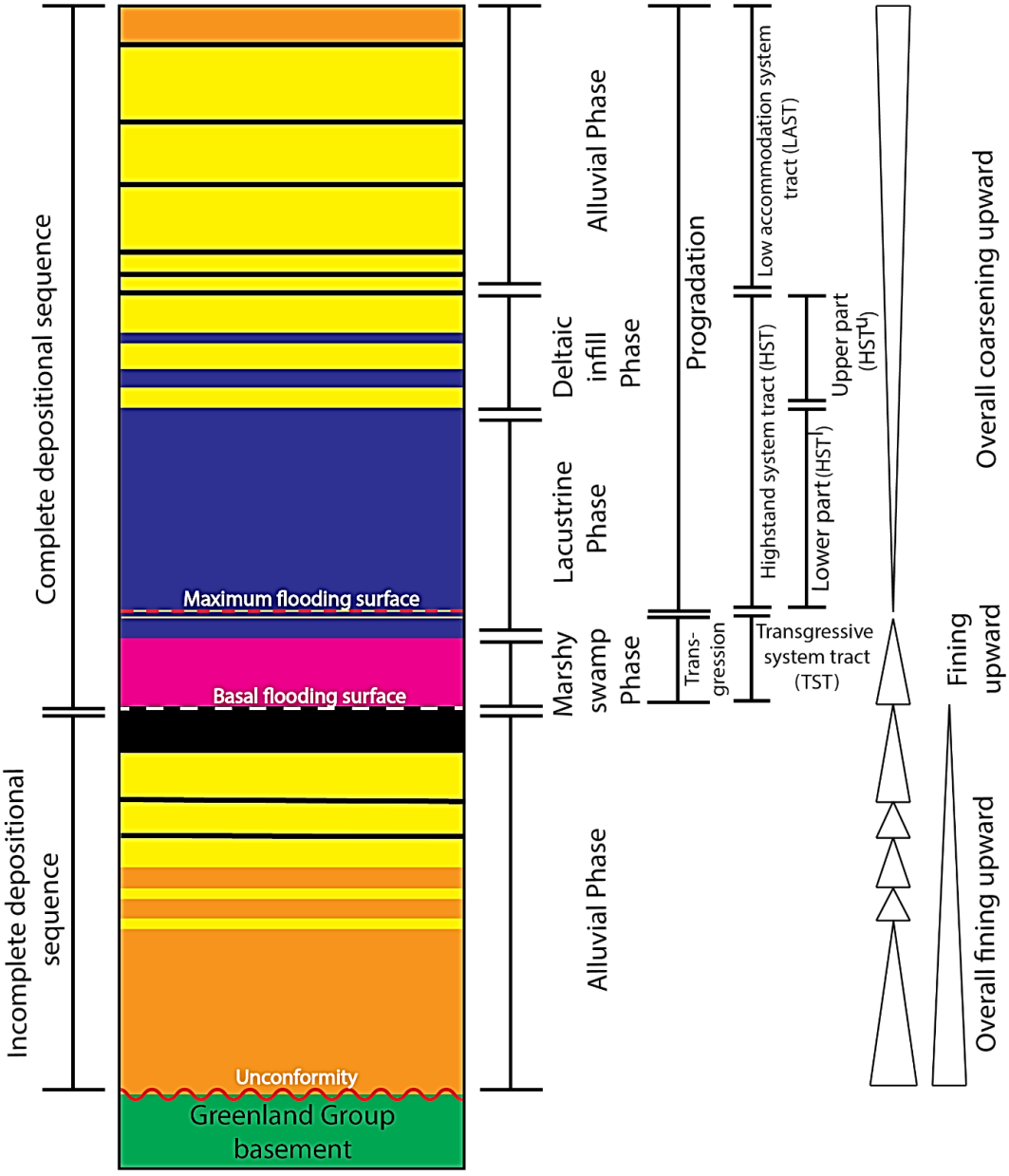


Figure 5. 5: Different depositional phases and corresponding system tracts of each fluvio-lacustrine interval of the Paparoa Formation, Greymouth Basin.

A deltaic infill phase overlies each lacustrine phase and is defined by the progradation of delta facies. This phase consists of various shoreline facies, replacing the lacustrine facies in the centre of the basin. The two basin margins continue to deposit the various deltaic or alluvial facies of the subaerial facies group as lateral

correlatives. The deltaic infill phase represents the upper part of the highstand system tract ($HST^u$). The depositional trend changes upward from fan delta to alluvial fan in the fault-controlled basin margin. In the hinge side of the basin, their lateral correlatives are low gradient sandy meandering deltas which change upward to subaerial meandering channels and floodplain. In the basin axis, a coarsening upward mouthbar from axial meandering delta represent the depositional trend. In the gamma-ray log, $HST^u$ is characterized by a sharp coarsening upward trend and is identified by overall progradational depositional patterns.

An alluvial phase is defined by the presence of thick subaerial facies in the basin axis during the times when there was no palaeolake. This phase overlies the lacustrine phase and comprises all facies of the subaerial facies group excluding the mire coal facies. The alluvial phase defines the low accommodation systems tracts (LAST). Near the faulted basin margin, the depositional trend shows alternating alluvial fans and braided rivers. In the basin axis, the depositional trend includes axial meandering channel grading upward to channel abandonment. The depositional trend changes somewhere in the transition from basin margin to basin axis, showing interfingering alluvial fan and axial meandering channel facies. In the gamma-ray log, LAST shows an overall coarsening upward trend with multiple small-scale fining upward trends and identified as a progradational depositional pattern.

The next step was to identify the sequence boundary unconformities. In order to define a sequence boundary (SB), widespread subaerial/erosional unconformable surfaces need to be formed in a rift basin (Figure 5.3; Figure 5.6). However, as the subsidence was continuous in the Greymouth Basin, and thus there was no negative accommodation during the rifting process, a genuine widespread subaerial/erosional unconformity (sequence boundary) was not formed. The only subaerial unconformity found in the Greymouth Basin is the basal contact between the Palaeozoic Greenland Group and the Paparoa Formation. In the basin axis, the basal flooding surfaces are defined as sequence boundaries in order to identify the base of a complete stratigraphic cycle and to understand the timing of the onset of more rapid subsidence. Correlating these sequence boundaries (basal flooding surfaces) in the basin margins is difficult since i) the cyclic sedimentation is not found in the basin margin (Chapter 3; Chapter 4), and ii) an alluvial phase directly sits on the Greenland Group basement as the basin widened through time (Chapter 4). The maximum flooding surface represents the greatest lateral extent of lacustrine and shoreline facies which is placed at the first appearance of thin sandstone packages (mudstone with thin sandstone facies) in the basin centre and in the first appearance of sandy turbidite facies in the shoreline (Figure 5.6).

### 5.6.2 Sequences in the Greymouth Basin

Five depositional sequences are identified in the Greymouth Basin (Figure 5.7); these are, from oldest to youngest, depositional sequence 1 (SQ1), depositional sequence 2 (SQ2), depositional sequence 3 (SQ3), depositional sequence 4 (SQ4) and depositional sequence 5 (SQ5). SQ1 is included in the rift initiation stage. SQ2, SQ3 and SQ4 make the rift development stage and record the highest thickness of sediments in the Greymouth Basin. SQ5 is included in the rift termination stage. SQ5 is not a part of this study but it is included for completeness of the sequence stratigraphic analysis of the Greymouth Basin. SQ5 represents wide spread alluvial deposition prior to marine transgression in Eocene time of the Waka Supergroup rocks of the Zealandia megasequence (Mortimer et al. 2014), and marks the end of the lacustrine setting of the Greymouth Basin.

The easiest depositional phases to identify and correlate among the bore holes are the lacustrine phases. Three lacustrine phases (from the oldest to the youngest Ford, Waiomo, and Goldlight) are found in the Paparoa Formation where the older Ford and Waiomo lacustrine phases were developed in isolated basins

while the Goldlight lacustrine phase was developed in a single basin (Chapter 3). Among the three lacustrine phases, the Goldlight lacustrine phase mudstone is the thickest and most extensive across the basin. The maximum flooding of the Goldlight Lake has therefore been used as the zero level for correlation across the basin and for sequence stratigraphic analysis (Figure 5.7). Basal flooding surfaces, maximum flooding surfaces and sequence boundaries are identified and drawn on the detailed cross-sections and summary fence diagram. Cross-section A-A$^{/}$ (Figure 5.8A) covers ~ 10.9 km across the northern part of the Greymouth Basin. The northeastern side of the cross-section is interpreted to contain three older normal faults which young northwestward to one additional fault, the youngest of which is interpreted as the northeast-striking, basin-bounding, normal fault based on the distribution of conglomerate facies (Chapter 4). Cross-section B-B$^{/}$ (Figure 5.8B) covers ~ 8.9 km across the central part of the Greymouth Basin with four normal faults interpreted as younging to the northwest (Chapter 4). Cross-section C-C$^{/}$ (Figure 5.8C) covers ~ 9.2 km across the southern part of the Greymouth Basin with only a single, very small normal fault interpreted at the base of the section. The details of the sequences are described below.

#### *5.6.2.1 Depositional sequence 1 (SQ1)*

SQ1 consists of the Jay Member of the Paparoa Formation and is the oldest depositional sequence of the Greymouth Basin which unconformably overlies Greenland Group basement. The Jay Member consists of only alluvial sediments. SQ1 is an incomplete depositional sequence as it sits directly on basement and is not a part of a full depositional sequence. Therefore, there is no lower sequence boundary, instead it is replaced by a subaerial unconformity (U1) (Figures 5.8A, B, C).

SQ1 is interpreted to have been deposited in an alluvial dominated environment. The alternating debris flow facies and gravelly braided river facies were located adjacent to interpreted normal faults (Figure 5.7; Chapter 4). These facies thinned towards the east and south. Sandy meandering channel and floodplain facies (crevasse splay and abandoned channel facies) were found in the basin axes and on the hinge sides of the small isolated sub-basins.

The distribution of SQ1 in locally restricted fault bounded shallow, disconnected basins indicates low accommodation space relative to sediment supply (S>A) due to low subsidence rate of the basin which allowed the alluvial sediments to fill the available accommodation easily and did not record any deep-water lacustrine sediments.

#### *5.6.2.2 Depositional sequence 2 (SQ2)*

SQ2 consists of the Ford and the Morgan members of the Paparoa Formation (Figure 5.8). This sequence started with a basal flooding surface (BFS1 at the base (SB1)), indicating the onset of more rapid subsidence of the basin at the beginning of the Ford Member, resulting in high accommodation space relative to sediment supply (A>S).

During the TST, low lying marshy swamp facies in the basin axis represented the marshy swamp phase. Basal flooding surface (BFS1) is placed at the base of the marshy swamp phase.

During the HST$^{l}$, the lacustrine phase shows a slightly progradational depositional pattern and records massive mudstone facies and mudstone with minor sandstone facies. These facies were deposited in the axes of isolated sub-basins in the northeast amalgamating into a single lake to the south. This indicates that the disconnected fault bounded small basins during the rift initiation stage started to connect and formed a basin of sufficient size and depth to create a larger lake during the Ford lacustrine phase. The appearance of mudstone with minor sandstone facies in the basin centre represents the maximum flooding (MF1) of

the Ford lacustrine phase. To the west, MF1 is correlated with locally derived fault proximal fan-delta facies on the faulted basin margin. To the east and the south, MF1 is correlated with low lying marshy swamp facies and locally derived delta with meandering river and floodplain facies.

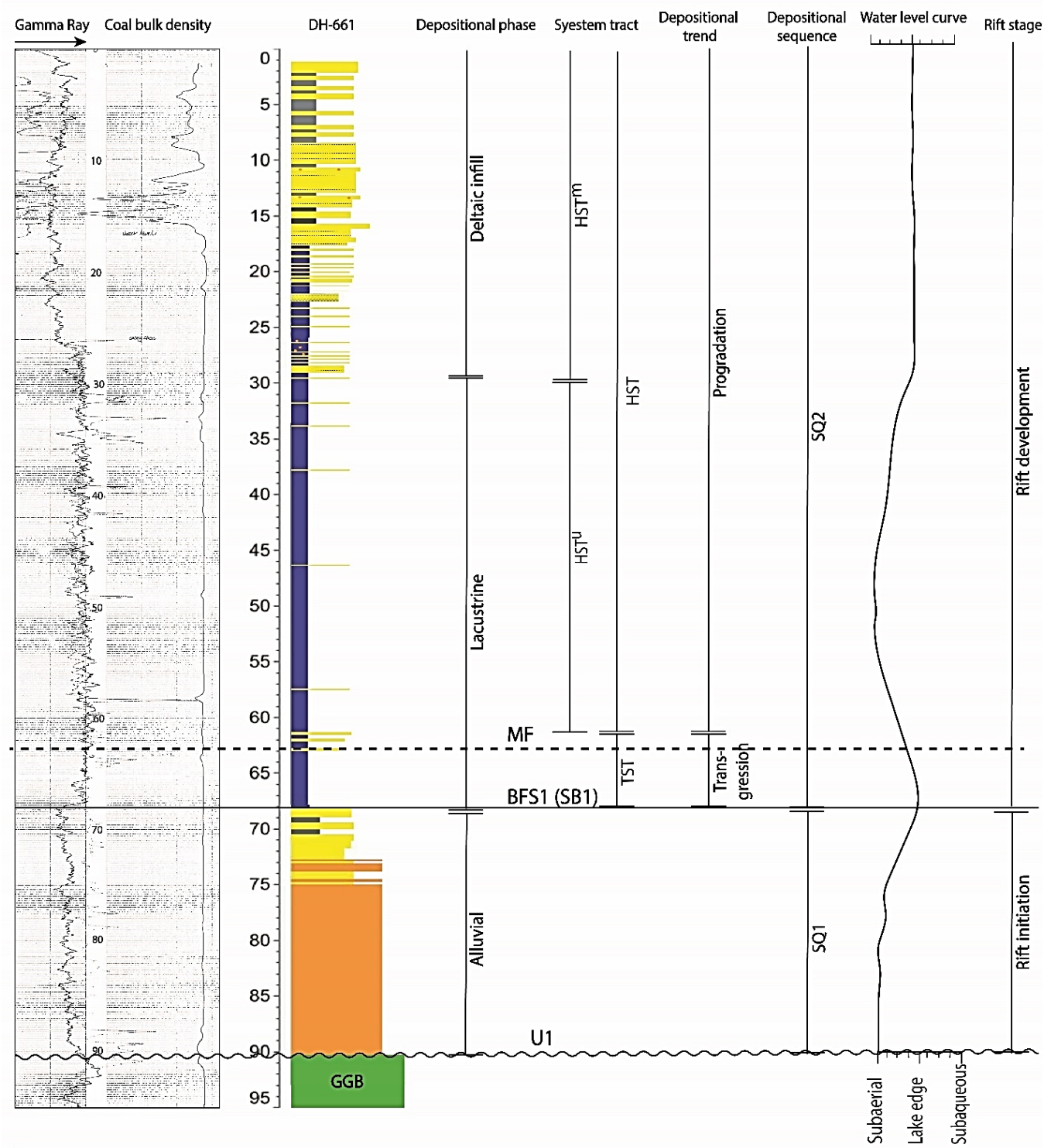


Figure 5. 6: Application of sequence stratigraphy in drill hole DH-661.

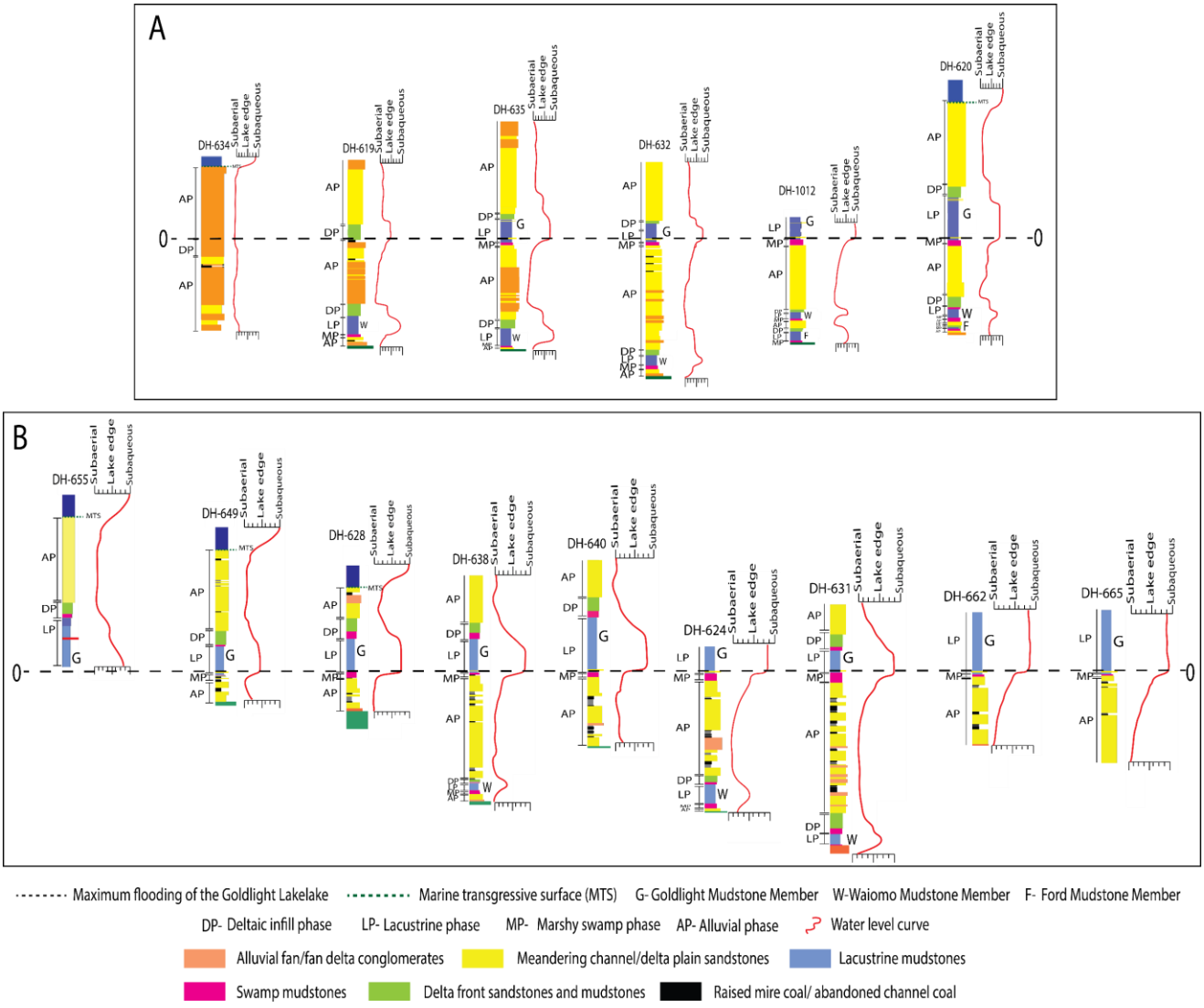


Figure 5. 7: Borehole to borehole correlation with maximum flooding of the Goldlight Lake from A) southwest to northeast, and B) from west to east of the Greymouth Basin.

During the HST$^{u}$, the deltaic infill phase was recorded by progradation of deltas and fan deltas until the lakes of the Ford lacustrine phase become entirely infilled. HST$^{u}$ corresponds to the gravelly mouthbar facies and the interdistributary bay facies on the shoreline fan delta front with the correlative debris flow and gravelly braided river facies on the fan delta plain in the western margin. HST$^{u}$ corresponds to the sandy mouthbar and interdistributary bay facies on the shoreline delta front with the correlative meandering channel facies on the delta plain in the eastern margin. From the south to the basin axis, HST$^{u}$ correlates to the meandering channel facies, abandoned channel facies and crevasse channel facies on the delta plain of the axial meandering river delta with their correlative sandy mouthbar and interdistributary bay facies on the shoreline delta front.

During the LAST, gravelly braided river facies and overbank floodplain facies of the Morgan Member are found proximal to the fault in the northwestern side of the basin thinning and fining to the southeast (Figures 5.7 and Figure 5.8). Along the smaller fault in the centre of the basin debris facies are found instead, which also fine and thin towards the east. Meandering channel facies can be found to the east and southeast

marking both basin axes and the hinge zones. The rate sediment supply increases during the LAST relative to the rate of basin subsidence, leading to the decrease in available accommodation condition.

SQ2 is a complete depositional sequence starting with marshy swamp phase at the base, grading up to the lacustrine phase then the deltaic infill phase and finally to the alluvial phase at the top. SQ2 in the basin axis when correlates to the basin margin to the west, only the alluvial phase of the Morgan Member is identified. The alluvial phase of the Morgan Member is considered as part of the complete SQ2 sequence as the phase records the evidences when the basin starts to widen due to the development of a new fault system to the northwest. This alluvial phase sits unconformably on the Greenland Group basement and marks the subaerial unconformity (U2) (Figure 5.9D).

#### *5.6.2.3 Depositional sequence 3 (SQ3)*

SQ3 consists of the Waiomo and Rewanui members of the Paparoa Formation. SQ3 starts with a basal flooding surface (BFS2) forming the sequence boundary (SB2), indicating the onset of more rapid subsidence of the basin at the beginning of SQ3, resulting in high accommodation relative to sediment supply (A>S).

Low lying marshy swamp facies found in the northwest and the centre of the basin mark the beginning of the TST (Figures 5.8). Basal flooding surface (BFS2) is placed at the base of the marshy swamp phase.

The $HST^{l}$ connects transgression to maximum flooding of the Waiomo Lake. During the $HST^{l}$ of the Waiomo Lake, there were two sub-basins with two lakes, one in the west and the other in the centre. The centre of both sub-basins filled with lacustrine massive mudstone facies with correlative gravelly turbidites facies and gravelly delta slope facies in the western margin of the lake in the west. Sandy turbidites facies are found in the hinge zone to the east and to the south and in the axial meandering river delta. The thickness of lacustrine mudstones gradually decreased towards the hinge side of the sub-basin, located on the west. To the east and to the south, lacustrine mudstones are truncated by the Montgomerie-Mt Davy Fault System. The maximum flooding surface (MF2) is associated with massive mudstone with minor sandstone facies which are found in two sub-basins in the northwest and the northeast which amalgamate into a single lake to the south (Figures 5.7 and Figure 5.8). On the basin margin of the sub-basin to the west, MF2 is correlated with coeval locally-derived fault-proximal fan-deltas with gravelly mouthbar facies and interdistributary bay facies. On the basin margin of the sub-basin in the east, MF2 goes through the contemporary low-lying marshy swamp facies correlating with sandy meandering delta on the hinge zone to the east and to the south.

During the $HST^{u}$, both Waiomo lakes filled with prograding fan delta gravelly mouthbar and interdistributary bay facies with correlative delta plain debris flow facies, gravelly braided river and overbank floodplain facies from their fault proximal western margins (Figures 5.8). In both sub-basin axes as well as their hinge zones, prograding delta sandy mouthbar facies infilled the lakes grading upward into the meandering river and floodplain facies of the delta plain.

During the LAST, debris flow facies, gravelly braided river facies and overbank floodplain facies of the Rewanui Member get thicker along the large fault and spread away from the fault of the northwestern side to the east and to the southwest. In the basin axis and on the hinge side to the east and southeast, sandy meandering river and floodplain facies (meandering channel facies, abandoned channel facies and crevasse splay facies) are common and widely distributed across the basin. Coals from abandoned channel facies are common throughout the Rewanui Member. The contact between Waiomo and Rewanui members is slightly erosional at Twelve Mile Beach on the northwestern part of the basin where it is marked by a layer of rip-

up clasts of lacustrine mudstones of the Waiomo Member at the base of a large alluvial channel at the base of the Rewanui Member (Figure 5.9B). This contact exists further inland where a thick conglomerate channel is found on top of gently dipping mudstones of the Waiomo Member (Figure 5.9C). This contact is probably a localised channel base-scour, indicating the onset of an alluvial phase.

SQ3 is a complete depositional sequence starting with marshy swamp phase at the base, overlain by lacustrine phase, then deltaic infill phase and alluvial phase at the top. When correlating SQ3 from the basin axis to the faulted basin margin to the west, the depositional sequence comprises only the alluvial phase of the Rewanui Member making it an incomplete sequence. However, this alluvial phase of the Rewanui Member is considered as part of a complete depositional sequence SQ3 as this phase records continuous widening of the basin during the rift development stage. This alluvial phase sits unconformably on the Greenland Group basement and marks the subaerial unconformity (U3) (Figure 5.8).

#### *5.6.2.4 Depositional sequence 4 (SQ4)*

SQ4 consists of the Goldlight and the Dunollie members of the Paparoa Formation as well as the Palaeocene Brunner Formation. This sequence starts with a basal flooding surface (BFS3) forming the sequence boundary (SB3), indicating the onset of rapid subsidence of the basin resulting in high accommodation relative to sediment supply (A>S).

During the TST, low-lying marshy swamp facies replaced the thick mire coal facies in the basin axis and the northeastern side of the basin as the base level rose. The northeastern side of the basin was later removed by uplift and erosion along the Montgomerie-Mt Davy fault zone.

During the HST$^{l}$, thick gravelly delta slope facies were deposited from locally derived fan-deltas on the fault proximal northwestern side of the basin coeval with the lacustrine massive mudstone facies of the very large Goldlight Lake in the greatly enlarged basin centre. Along the basin axis in the southwestern side, the Goldlight Lake was fed by locally derived sandy deltas where thick sandy turbidites facies were commonly found with contemporaneous lacustrine massive mudstone facies in the basin centre. During maximum flooding (MF3), the Goldlight Member lacustrine massive mudstone facies and lacustrine mudstones with minor sandstone facies were widely spread across the basin with correlative gravelly delta slope facies in the northwest and sandy turbidites facies in the southwest. Lacustrine massive mudstone facies to the northeast were eroded whereas to the southeast they were truncated by the Montgomerie-Mt Davy Fault System.

During the HST$^{u}$, progradation of wide spread gravelly fan-deltas and sandy meandering deltas filled the Goldlight Lake. Thick gravelly mouthbar facies and interdistributary bay facies were found on the fan delta front on the northwestern side with contemporaneous debris flow, gravelly braided river, and overbank floodplain facies on the fan delta plain. To the southwest, sandy mouthbar facies were common on the delta front with correlative meandering channel facies, abandoned channel facies and crevasse splay facies on the delta plain. On the hinge to the southeast, prograding sandy delta mouthbar facies infill the lake grading upward into the meandering river and floodplain facies of the delta plain. The facies to the east and northeast were removed by erosion or truncated by later faults.

During the LAST, the northwestern side of the basin was characterized by debris flow and gravelly braided river facies of the Dunollie Member. In the basin axis as well as in the east and south, the basin was filled with widely distributed meandering channel facies, abandoned channel facies and crevasse splay facies. Coals from abandoned channel facies were common in this alluvial phase.

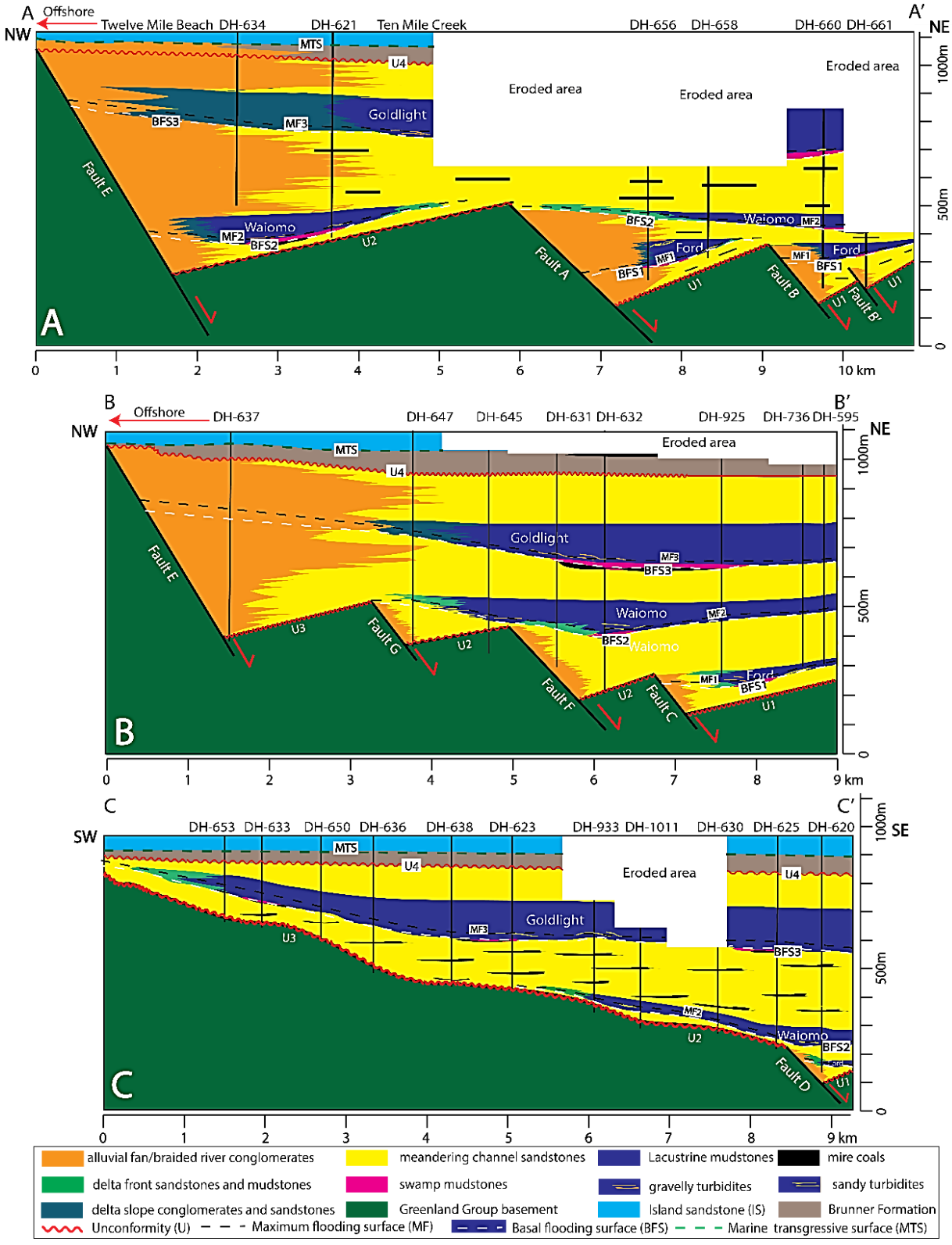


Figure 5. 8: A) Cross-section of the sedimentary facies and key sequence stratigraphic analysis from the northwest to the northeast of the Greymouth Basin; B) northwest to the northeast in the central part of the Greymouth Basin, and C) Southwest to southeast part of the Greymouth Basin. Cross-section A-A' shows

two Ford lacustrine sub-basins bounded by Fault A and Fault B, two Waiomo lacustrine sub-basins bounded by Fault A and Fault E and single Goldlight lacustrine basin bounded by Fault E. Cross-section B-B' illustrates single Ford lacustrine basins bounded by Fault C, single Waiomo lacustrine sub-basins bounded by Fault G and single Goldlight lacustrine basin bounded by Fault E. Cross-section C-C' shows single Ford lacustrine basins bounded by Fault D, the Waiomo and the Goldlight lacustrine basins are onlapping against the pre-existing fluvial deposits of Morgan Member and the Rewanui Member, respectively.

Although the main purpose of this research is to look at the Late Cretaceous to Early Palaeocene Paparoa Formation, we include the Palaeocene Brunner Formation in this sequence in order to understand the eventual termination of the lacustrine setting by marine transgression in the Greymouth Basin. The sedimentary facies analysis has not been done for the Palaeocene Brunner Formation. Instead, the stratigraphic relationship of this formation with overlying and underlying deposits across the basin has been taken from the literature.

Nunweek (2001) divided the Palaeocene Brunner Formation into the Brunner Conglomerate Member and the Brunner P Member and further proposed to include these two members into the Paparoa Formation because of their limited distribution in the Greymouth Basin and not being associated with the Eocene marine transgression. Monteith (2015) revised the formation and member names, proposing the Ikes Peak Formation instead of the Palaeocene Brunner Formation where Hall Ridge Conglomerate Member replaces the Brunner Conglomerate Member, and the Birchfield Sandstone Member replaces the Brunner P Member. Newman (1985) mentioned that sedimentation in the Greymouth Basin ceased almost immediately with the end of major spreading at c. 60 Ma and an unconformity began to develop on the basin surfaces (Newman 1985). Palynological data suggested that there was a depositional break of ~ 10 myrs in the centre of the basin within the Brunner sequence suggesting the presence of an unconformity between the Palaeocene Brunner Formation and the Eocene Brunner Formation (Figure 5.8; Raine 1984; Newman 1985). This unconformity likely correlates with the contact between highly bleached gravelly braided river facies of the Dunollie Member and the overlying Island Sandstone at Twelve Mile Beach (Gage 1952; Nathan 1978; Monteith 2015). This unconformable surface at the basin margin probably becomes conformable at the basin centre through to the east side of the basin. This unconformable and correlative conformable surface (U4) marks the termination of fault-controlled subsidence in the Greymouth Basin.

#### *5.6.2.5 Depositional sequence 5 (SQ5)*

SQ5 consists of the Eocene Brunner Formation, commonly known as Brunner Coal Measures (BCM). This sequence is introduced here to understand the rift termination stage of the Greymouth Basin followed by the marine transgression. The majority of the BCM were deposited by meandering rivers on large, low gradient surfaces, with the coals and fine-grained sediments accumulating on the floodplains (Flores and Sykes 1996; Monteith 2015). The presence of incised stream conglomerates and prograding deltaic deposits in the BCM indicates erosion in low gradient surfaces (Titheridge 1993; Monteith 2015). A distinctively high percentage of quartz in the BCM indicates increased chemical weathering, suggesting the landscape at the time had been extensively subaerially weathered for some time prior to deposition during a period of peneplanation and production of a weathered quartzose residuum (Suggate 1950). All these above criteria suggest a longer period of tectonic quiescence in the Greymouth Basin, allowing alluvial and deltaic sediments to fill the available accommodation in low gradient surfaces (S>A) followed by a time of sediment starvation which allowed chemical weathering of the existing sediments and produced quartzose residuum. The rifting was terminated during this time. Relict topography of the earlier basins has influenced deposition of the BCM in the Greymouth Basin (Nathan 1978; Newman 1985; Monteith 2015).

The upper part of BCM is considered as the lowest member of a regional transgressive sequence all over New Zealand from the Eocene to Oligocene (Lever 1999; Nunweek 2001; Monteith 2015). The TST starts with the deposition of mire coals and continues beyond the end of the deposition of the basin-wide Island Sandstone (Figures 5.8; Figure 5.9A). The Island Sandstone represents the end of non-marine deposition and the initiation of the first marine formation. The upper part of the Haerenga Supergroup is commonly marked by greensands, unconformities and other indicators of enhanced marine transgression and reduction in clastic sediment supply around the Eocene–Oligocene boundary (Mortimer et al. 2014). The New Zealand wide transgressive sequence is not part of this research but is included for completeness.

## 5.7 Discussion of the causative factors controlling the lacustrine sequence stratigraphy

One of the main purposes of the sequence stratigraphic analysis of the Greymouth Basin is to understand the primary factors that control lake level changes and the overall cyclicity of sedimentary facies. These could be due to several factors, such as climatic variation, sea-level change, changes in outflow conditions and changes in tectonic activity and subsidence rates. We will discuss here the possible evidence and relative importance for various factors that control lake levels and resultant cyclicity of the basin.

### 5.7.1 Cyclical Variations in water inflow from local climate changes

Local climate changes due to heavy rainfall, glaciation, and/or evaporation can cause fluctuation in lake level which eventually contribute to the cyclic variation in sedimentation (Scholz et al. 1998; Morellón et al. 2009). During the formation of the Late Cretaceous Greymouth Basin, the geographic position of New Zealand (between $78^0$ S and $68^0$ S) (Raven and Axelrod 1972) indicates a higher latitude system. The position also suggests relatively low temperatures and long winter nights with high rainfall and cloud cover (Grindley 1978). However, this was contradicted by more recent leaf fossil studies from New Zealand Cretaceous coals in South Island, suggesting that New Zealand landmasses during that time were covered by broadleaf-podocarp forests with varying proportions of angiosperms (Ward 1997; Kennedy 2003; Raine et.al., 2017). This indicates a temperate climate during the Late Cretaceous with the annual temperature ranging between $12^0$ C and $15^0$ C, a similar temperature to that of present-day New Zealand that does not coincide with a climate of prolonged heavy rainfall. In addition, the KTB (Cretaceous-Tertiary boundary) is identified at the beginning of the deposition of the Goldlight lacustrine phase with no significant change in climate (Ward 1997 and Kennedy 2003). Therefore, cyclical changes in rainfall are unlikely to have been the factor controlling lake level changes.

### 5.7.2 Cyclical variations in water outflow from landslide damming

Landslide damming, in many parts of the world, is often responsible for changing sedimentation in lakes (Schuster and Costa 1986; Ermini et al. 2006; Coico et al. 2013; Storm 2013). However, the tectonic evolution indicates that the smaller fault systems in the Greymouth Basin linked together through time and became a larger basin bounding fault located to the northwest. This fault was responsible for the majority of basin subsidence during Rewanui alluvial and Goldlight lacustrine phases. In order to develop a large and deep lake similar to the Goldlight Lake, the landslide dam would have had to have been huge and therefore would likely not exist for long enough. Therefore, landslide dams cannot be the factor for controlling cyclic sedimentation in Greymouth Basin.

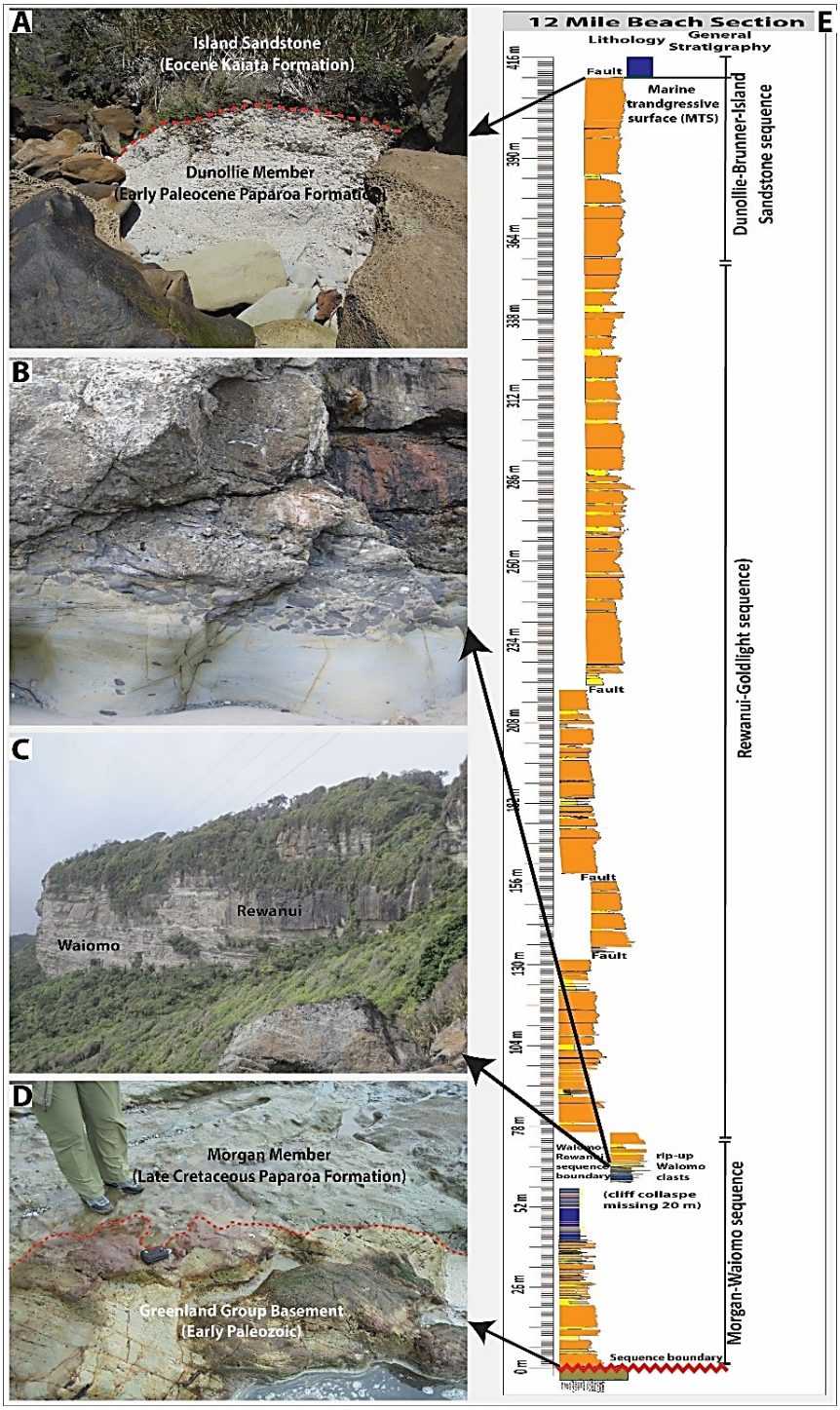


Figure 5. 9: Twelve Mile Beach stratigraphy showing (E). A) First marine transgressive surface (MTS) above SQ5, B) Rip-up clasts in the lower Rewanui section represent slight erosional surface between the Waiomo and Rewanui members in SQ3. C) A probable localised channel base-scour between the Waiomo and Rewanui members in SQ3 showing a gravelly braided river facies which have an erosional contact with the underlying Waiomo lacustrine mudstone facies, indicating the onset of an alluvial phase, and D) Unconformable sequence boundary (U2) between Greenland Group basement and SQ2 depositional sequence.

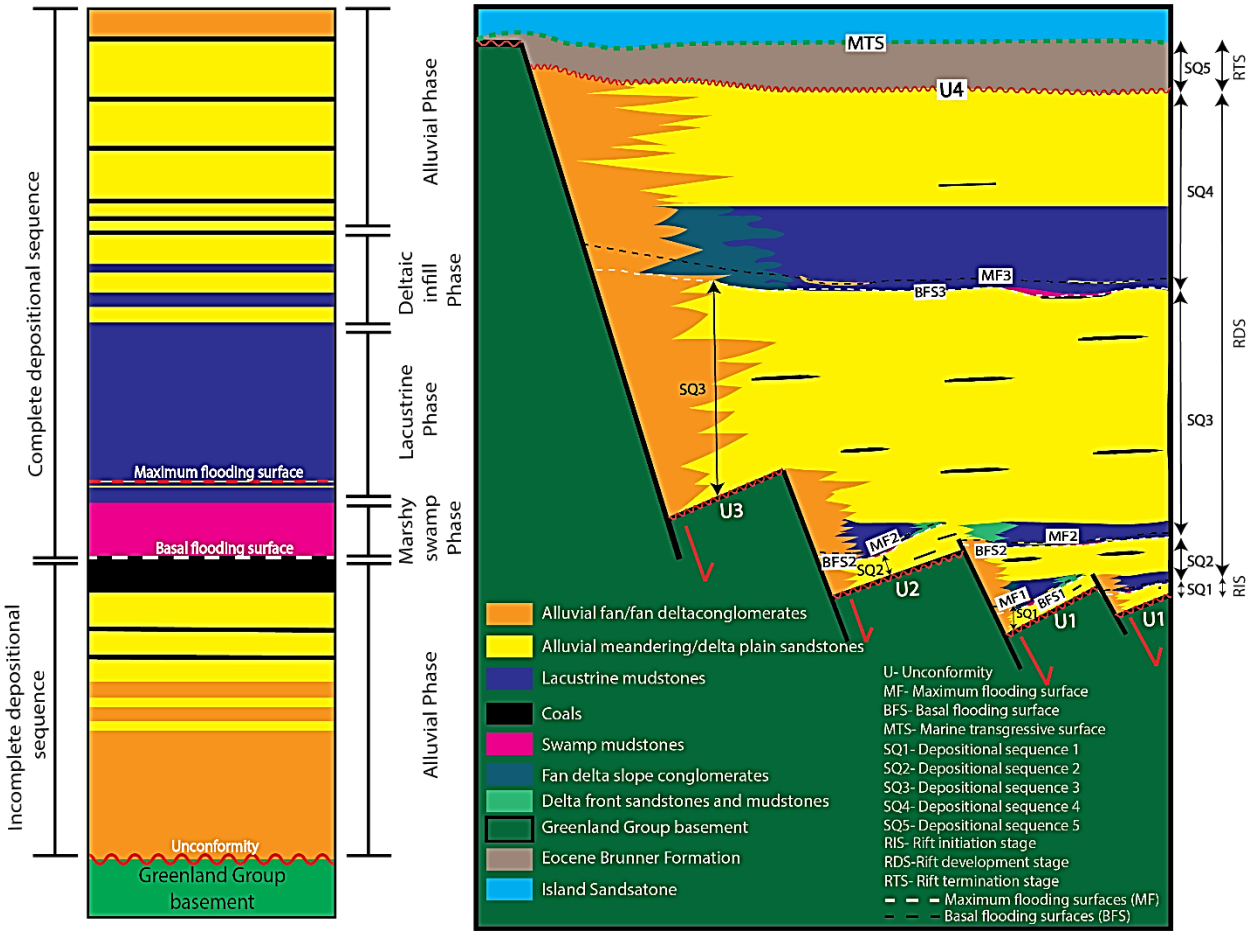


Figure 5. 10: A detailed sequence stratigraphic approach for the Greymouth Basin showing different depositional phases, depositional sequences and important key surfaces.

### 5.7.3 Cyclical variations in base level from basin subsidence

Having ruled out other options, variation in subsidence rates through time is the most likely cause of the cyclic sedimentation in the Greymouth Basin. The facies change from basin margin to basin centre to hinge as indicated by the deposition of fan delta conglomerate facies on the fault-controlled margin to the west, lacustrine mudstones in the centre and sandy meandering delta in the axis and in the hinge zone to the east. This indicates a typical half-graben, rift basin geometry. The vertical facies distribution in the Greymouth Basin indicates three alluvial-lacustrine sequences (Figure 5.3; Figure 5.7; Chapters 2, 3). Each lacustrine phase therefore represents a time of increased subsidence without a larger influx of sediments to infill the newly widened basins, indicated by the presence of thick lacustrine mudstone facies across ever wider areas. In addition, continuing extension led to thinning of the crust under the basin resulting in increased subsidence over time. This was followed by longer periods of tectonic quiescence, allowing deltaic and alluvial facies to gradually prograde into the unfilled accommodation. The oldest sequences recorded small sub-basins infilled by isolated lakes separated by alluvial fan conglomerate facies marking the locations of small, discontinuous normal faults. Conglomerate deposits stepped northwestward and thickened up-section as the small faults became inactive or amalgamated to form a single border fault during the youngest sequence. In this way, the Greymouth Basin records a developing rift basin where smaller normal faults amalgamated as the basin widened over time (e.g. Gawthorpe and Leeder 2000; Chapter 4). The cyclic

sequences record stepped, rather than incremental, widening of the rift basin. Rift basins around the world exhibit variations in subsidence rates during the evolution of the basin from initiation to fault amalgamation and widening, through the final transition to thermal subsidence as extension ceases (Leeder 1995; Martins-Neto and Catuneanu 2010; Holz et al. 2013, 2015).

A detailed sequence stratigraphic analysis of the Greymouth Basin reveals the shifting balance between subsidence rate and the rate of sediment supply through time. During the rift initiation stage, accommodation was very low due to low subsidence rates in multiple small sub-basins. Sediment supply exceeded the available accommodation conditions as indicated by the presence of small, restricted fault bounded half grabens which were easily filled up with alluvial sediments and did not record any lacustrine facies. During the rift development stage, the sequence boundaries (SB1, SB2 and SB3) represent the onset of increased subsidence rates in the basin, indicated by the presence of either marshy swamp or lacustrine facies in the basin axis. Progressive creation of new faults to the northwest widened the basin forming correlative unconformities (U1 and U2). During the rift termination stage, a change in basin tectonics allowed conglomerates to spread more fully into the centre of the basin suggesting a decrease in subsidence rate. This was followed by more passive infilling with even less fault activity and marked the beginning of the New Zealand-wide transgression of passive margin development where subsidence was controlled by thermal cooling and sediment loading. The Greymouth Basin opened to the sea with the deposition of the calcareous Island Sandstone followed by deposition of deeper marine Kaiata Mudstone and Oligocene limestones (Figure 5.10).

Based on the above observations, the alternation of alluvial and lacustrine phases in the members of the Paparoa Formation better fits an interpretation of subsidence variation from rift basin tectonics rather than cyclicity from climate variation and/or outflow of streams. Therefore, we conclude that the primary factor for the Greymouth Basin, like most rift basins around the world, that controls the cyclic sedimentation is tectonic subsidence as the basin widens and faults link up.

## 5.8 Discussion of lacustrine sequence stratigraphy terminology

The lacustrine sequence stratigraphy of the Greymouth Basin is illustrated in Figure 5.12. In this section we will compare and correlate our sequence stratigraphic framework with the terminologies and models proposed by different authors in other rift basins around the world.

Martinsen et al. (1999) and Scherer et al. (2015) felt new terminology was needed because lacustrine non-marine deposition records a delicate balance between the creation of accommodation space and sediment supply (A/S). They defined two new systems tracts; 1) A Low-Accommodation Systems Tract (LAST) comprising amalgamated alluvial channel deposits, and 2) A High-Accommodation Systems Tract (HAST) comprising either alluvial channels encased in overbank deposits or a lacustrine dominated succession. The HAST takes place where the A/S ratio is close to or above 1, meaning sediment supply cannot fill the available accommodation and flooding occurs. The LAST occurs where A/S ratio is between 0 and 1 but close to 0, meaning sediment supply fills the accommodation and some bypass may occur. When the A/S ratio is negative, a sequence boundary occurs, meaning no accommodation exists which results in sediment bypass and erosion.

Applying Low and High Accommodation Systems Tracts to our sequence stratigraphic analysis of the Greymouth Basin results in the combined marshy swamp, lacustrine and deltaic infill phases corresponding to HAST. We also introduced the alluvial phase as LAST. The HAST phases were deposited when higher accommodation outpaced sediment supply in the basin. The basal flooding surfaces and maximum flooding

of the lake can be correlated with HAST. The alluvial phases corresponding to LAST were deposited during low subsidence rates in the basin when sediment supply outpaced the available accommodation. The sequence boundaries are the basal flooding surfaces at the beginning of the increase in subsidence rates. The sequence boundaries were replaced by laterally correlative subaerial unconformities when the A/S ratio was negative during widening of the basin and the inception of new faults to the northwest. This way of analyzing the lacustrine sequences allows us to focus on changes in subsidence rate assuming that sediment supply was relatively constant.

We compare the rift tectonic systems tracts developed by Holz et al. (2013, 2015) for the Reconcavo Rift Basin in Brazil to the sequences of the Greymouth Basin. The rift initiation systems tract is represented by the oldest depositional sequence (SQ1) where sedimentation was restricted to isolated multiple sub-basins, mostly in the northeastern part of the basin. During the deposition of SQ2, SQ3 and SQ4, the basin progressively widened to the northwest. Several isolated lacustrine basins in multiple sub-basins amalgamated to a single lacustrine basin during the deposition of SQ3. A thick sequence of subaqueous fan-deltas deposits in the northwest indicates the basin was large and deep with more accommodation due to the activation of large basin-bounding faults. Therefore, SQ2, SQ3 and SQ4 can be compared with rift development system tracts. The youngest depositional sequence (SQ5) is interpreted to have been deposited when the basin was mostly overfilled with sediments and widened enough to open to the sea.

Holz et al.'s (2013, 2015) tectonic sequence stratigraphic framework combined with the Gawthorpe and Leeder (2000) rift tectonic model has been used for the Triassic half-graben Ischigualasto-Villa Union lake Basin in Argentina in order to understand the vertical and lateral facies variability and to examine the significance of tectonic and other controls on syn-rift deposition (Melchor 2007). Melchor (2007) concluded that variations in the character of successive sequences were primarily controlled by tectonic evolution of the half-graben including changes in subsidence rate and the growth and evolution of the border fault zone. Changes in water balance and lake level, as well as autocyclic processes like delta lobe switching, also played an important role. In comparison to the Greymouth Basin, we conclude that the successive sequences of the Greymouth Basin show an evolution from Late Cretaceous small, isolated lake basins (Ford and Waiomo Lakes) to an Early Palaeocene large lake basin (Goldlight Lake) through the linkage of northwestward propagating normal faults.

The conceptual rift basin sequence stratigraphic model of Martins-Neto and Catuneanu (2010) demonstrates different phases in the development of a rift basin. The underfilled phase is defined as the maximum accommodation developed due to rapid subsidence in a basin. A lacustrine system would be developed in this phase. The filled phase is defined as the stage when accommodation is generated from small tectonic pulses of fault reactivation. A fan-delta system would be developed in this phase. The alluvial phase is defined as the minimum accommodation retained after completely filling up the lake. Meandering rivers and floodplain systems commonly replace the lake in the basin axis during this phase. The overfilled phase is defined as the stage when mechanical subsidence of the basin shifts to thermal subsidence. Therefore, no new accommodation is generated. An alluvial system would be developed in this phase and the sediment supply would gradually fill all available accommodation.

The presence of three cyclic alluvial-lacustrine phases in the Paparoa Formation indicates that the Greymouth Basin mostly experienced alternating underfilled and filled phases through time. As the subsidence was continuous in the Greymouth Basin, the underfilled and filled phases of the Greymouth Basin coincided with the rift development stage when three complete depositional sequences (SQ2, SQ3, SQ4) were deposited. The overfilled phase of the Greymouth Basin corresponds with the rift termination

stage when the youngest depositional sequence (SQ5) was deposited. During this stage, the overall mechanism of subsidence of the basin started shifting to thermal subsidence with less accommodation available.

Therefore, the sequence stratigraphic terminologies that we have used in the Greymouth Basin can be compared and correlated with various other terminologies proposed by other authors. However, as the primary factor of the cyclic deposition of the Greymouth Basin is tectonic subsidence, the use of transgressive system tract (TST) and the highstand system tract (HST) are a better fit (Figure 5.10).

## 5.9 Conclusions

Sequence stratigraphic analysis combines three separate lacustrine phases with alternating axial meandering alluvial phases infilling the Greymouth Basin. Five depositional sequences are defined; among them the oldest depositional sequence (SQ1) representing the initiation stage of rifting whereas the three successive deposition sequences (SQ2, SQ3 and SQ4) address the development stage of Greymouth Basin rifting. The youngest depositional sequence (SQ5) represents the rift termination stage. The sequences developed during rift initiation and rift termination phases (SQ1 and SQ5) are incomplete comprising only alluvial basin fill. Whereas each of the sequences deposited during the rift development stage corresponded to a full sequence of lacustrine to alluvial basin fill. A full sequence (SQ2/SQ3/SQ4) represents transgressive, highstand and low accommodation systems tracts that are the products of the balance between the changes in basin subsidence and sediment supply. Transgressive systems tracts (TST) contain low lying marshy swamp laminated mudstones and siltstones and correlate with the basal flooding surfaces and the maximum flooding of the lakes. Highstand systems tracts help correlate depositional facies across the basin; i) massive mudstones in the basin centre correlated with locally derived alluvial fan and fan-deltas in the basin margin during the lacustrine phase, and ii) fan delta facies along the steep northern margin of the basin correlated with the sandy fan delta facies spread widely along the hinge side southern and eastern margin during the deltaic infill phase. Low accommodation systems tracts are gravelly braided alluvial fans correlated with sandy meandering alluvial systems across the basin with scattered dirty coals and organic-rich mudstones from abandoned channels in the basin axis during the alluvial phase.

The sequence boundaries related to SQ2, SQ3 and SQ4 (SB1, SB2, SB3) likely recorded episodes of increased subsidence rates that increased the accommodation. This was followed by a time of decreased subsidence rates permitting deltaic systems to prograde into the lake basin eventually completely infilling it and changing to alluvial systems across the basin. The sequence boundaries are laterally correlative with subaerial unconformities (U1 and U2) as the basin widened due to progressive creation of new faults to the northwest. The sequence stratigraphic analysis concludes that the cyclic variation of the alluvial-lacustrine deposits of the Paparoa Formation was primarily controlled by episodic tectonic activity in the basin associated with the expansion and maturing of the Greymouth Rift Basin.

# Chapter 6: Summaries, discussions and future works

This thesis presents the detailed sedimentary facies analysis, hydrocarbon source rock potential, sequence stratigraphy, and tectonic evolution of the Greymouth Basin from the Late Cretaceous to the Early Palaeocene based on extensive drill cores, geophysical logs, and outcrop descriptions. The primary method included in this research was detailed sedimentary facies analysis of conglomerates and fine-grained rocks. We prepared fence diagram, isopach maps of conglomerates and lacustrine facies in order to understand the distribution of different facies and the palaeogeography of the Greymouth Basin. Finally, we developed tectonic models to illustrate the tectonic evolution of the Greymouth Basin from Late Cretaceous to Early Palaeocene, and a framework for understanding the lacustrine sequence stratigraphy of the Greymouth Basin. The results obtained from the above analysis can be used as an analogue for other Late Cretaceous basins in New Zealand which are deeply buried and only available via seismic. The following section provides an overall summary of the major finding of this research and highlights their significance in the context of the formation of the Greymouth Basin.

## 6.1 Sedimentary facies analysis of conglomerates

The detailed sedimentary facies analysis of coarse grained lithologies presented in Chapter 2 has highlighted the importance of the thick conglomerate deposits in the northwestern part of the Greymouth Basin during deposition of the latest Cretaceous-Palaeocene Paparoa Formation. Most of the sedimentary facies are defined at Twelve Mile Beach and Ten Mile Creek outcrops were then applied to nearby conglomerate-bearing drill holes where they were more difficult to correlate due to the small diameter.

The sedimentary facies analysis of the conglomerate and associated finer grained deposits has resulted in an interpretation of alluvial fans shed off highlands in the northwest that entered palaeolakes to the southeast as fan deltas. Sometimes no palaeolakes existed in the basin and the alluvial fans interfingered with axial meandering river deposits (Chapter 3). The palaeolakes were identified by the existence of thick lacustrine facies association deposits to the southeast. The massive mudstone facies is interpreted to have been deposited from suspension settling in deep freshwater lakes, whereas the mudstones with minor thin sandstones facies is interpreted to have been deposited by suspension settling alternating with infrequent, small scale, turbidity currents. The conglomerate sedimentary facies have been grouped into alluvial fan/fan delta plain, fan delta front, and fan delta slope facies associations.

The alluvial fan/fan delta plain facies association contains debris flow, gravelly braided river, and overbank floodplain facies. The debris flow facies is rare but more common toward the northwest and is composed of poorly sorted, matrix supported, angular to subangular to sometimes subrounded conglomerates. It is interpreted to have been deposited by debris flow processes in proximal alluvial fan environments or at the top of fan delta slopes (e.g., Nemec and Steel 1984; Blair 1999). The gravelly braided river facies makes up the majority of deposits and comprises clast-supported, cobble to boulder-sized, rounded to subangular, moderate to poorly sorted conglomerate with thin sandstone lenses. It is interpreted to be the product of high energy stream flow in an alluvial fan and travelled relatively short distance before deposition (e.g. Kazanci 1988; Turkmen et al. 2007; Miall 2010). Carbonaceous sandstone and mudstones with abundant rootlets are interpreted as overbank floodplain facies. These are also rare but are more common in association with fan delta front facies indicating a more distal or lower gradient setting proximal to an active channel with episodic floods alternating with low energy environments (Reading 1996). These facies are interpreted to have been deposited as either alluvial fans during alluvial phases when axial meandering

rivers occupied the centre of the basin or as fan delta plain during lacustrine phases when palaeolakes occupied the centre; the subaerial portion of the fan being the same in both cases.

The delta front facies association marks the shoreline and the transition to subaqueous fan delta environments. The interdistributary bay facies contains slightly carbonaceous, bioturbated, wavy bedded, rarely rippled, fine grained sandstones with rare coaly stringers deposited in a low energy, subaqueous setting (e.g. Jones et al. 2008). The gravelly mouthbar facies is composed of thick, Clast-supported, cobble conglomerate beds with pockets of fitted clast textures. These were deposited in active channel mouths where strong currents winnowed out the fines to create the fitted clast textures. One of the most striking features, the fitted clast textures occur in lenses, have no matrix, and show jigsaw-like fitted edges with sharp contacts and angular indentations on clast interfaces. They are interpreted to have been deposited in the river mouth channels where the fitted textures formed from abrasion and microvibrations from jostling of clasts, clast collisions, and winnowing of fines by continual current flow (Schumm and Stevens 1973; Nelson and Hood 2016). The long term microvibration and in situ abrasion of the clasts continued until they formed the intricate indented nature of the clast contacts. The interbedded nature of the gravelly mouthbar facies and the interdistributary bay facies, as well as the coarsening up sequences, indicate channel avulsion was dominant because of high sediment loads.

The fan delta slope facies association is divided into gravelly delta slope facies and gravelly turbidites facies. The gravelly delta slope facies consists of interbedded conglomerates and sandstones with the presence of numerous load casts and associated soft sediment deformation features. The abundance of large load cast features and deformed bedding in the thick conglomerate deposits indicates deposition was subaqueous in origin. This suggests both a steep delta slope and high sedimentation rates where bedload flows were deposited at the top of the slope or flowed down the slope as hyperpycnal flows during large flood events and storms (e.g. Zavala and Pan 2018). This facies is interpreted to have been deposited in a relatively steep, subaqueous, fan delta slope environment. The gravelly turbidites facies is composed of mostly grey to yellowish brown sandstones with common siltstone beds, occasional conglomerate lenses and dropstones. This facies was interpreted to have been deposited from high energy turbidity currents proximal to the channel mouth but further downslope than the gravelly delta slope facies (e.g. Boggs 2006; Renaut and Gierlowski-Kordesch 2010). The presence of dropstones is an interesting feature. Dropstones are often used to indicate nearby glaciers with melting icebergs carrying coarser material out into deep water. However, recent leaf fossil and pollen studies indicate a temperate climate during the Late Cretaceous when deposition took place to what we see today in New Zealand making nearby glaciers unlikely (Ward 1997; Kennedy 2003; Raine et.al. 2017). The dropstones indent the beds under them so they dropped from a height, likely from the floating logs or grass mats on the surface of the palaeolake (Emery 1955, 1965; Postma et. al. 1988; Bennett et al. 1996).

Once the sedimentary facies were defined, they were then correlated according to their individual depositional environments in order to understand their distribution. The fence diagram illustrates the distribution of conglomerate facies; they are restricted to the northwestern corner of the basin with their abundance and thickness decreasing to the southeast. Proximal facies such as the debris flow facies are also more common to the northwest. Taken together, this suggests a highland area existed to the northwest with a steep gradient down to the nearby palaeolake forming a fan delta setting. The creation of such a steep gradient and the long-lived supply of gravels indicate the highlands were probably the result of prolonged uplift on a fault. We interpreted this fault as a possible basin bounding fault of the Greymouth Basin. This contradicts with most of the previous studies where the proposed basin bounding fault of the Greymouth

Basin was located on the eastern margin (the Montgomerie-Mount Davy Fault System) which was responsible for the majority of the basin's subsidence (Newman 1981, 1985; Ward 1997; Kamp et al 1999). However, the most recent study indicates the eastern margin fault was not active until the late in the basin history and could not have been the primary basin bounding fault (Suggate 2014). The detailed study of conglomerates and associated fine grained sediments on the northwestern side of the basin highlighted the presence of a new basin bounding fault nearby offshore to the west which leads to rethinking the tectonic setting of the Greymouth Basin. The abundance of conglomerates in the northwest, their decrease to the southeast, and the presence of palaeolakes alternating with axial meandering rivers in the basin centre indicate a half graben geometry for the rift basin with the primary basin-bounding fault to the northwest. The most probable basin bounding fault would be the Cape Foulwind Fault which is located offshore of Twelve Mile Beach but inshore of the Haku-1 well where younger sediments lie directly on basement.

## 6.2 Sedimentary facies analysis of finer sediments and hydrocarbon potential source rocks

Sedimentary facies analysis of the lacustrine facies and other potential hydrocarbon source rock facies in Chapter 3 examines the hydrocarbon producing potential of the Greymouth Basin. The basin has been extensively mined for coal but several gas seeps and surface oil discoveries suggest it may also be a petroleum prospect. It is part of the Late Cretaceous West Coast-Taranaki Rift System where waxy coaly facies of Late Cretaceous age are already proven source rocks in the Taranaki Basin and Late Cretaceous lacustrine mudstones have been suggested to have potential. A recent geochemical study by Cody (2015) showed that the three lacustrine mudstone units of the Paparoa Formation in the Greymouth Basin have both Type II and Type III kerogen and, therefore, they have the potential of being oil generating source rocks and a shale gas resource. The main purpose of this research is to define and identify potential hydrocarbon source rock facies of the Greymouth Basin. The results can be an accessible analogue for Taranaki and other Late Cretaceous frontier basins in New Zealand which are deeply buried and only available via seismic analysis, whereas the Greymouth Basin is accessible in outcrops and through extensive drill cores.

The sedimentary facies analysis has resulted in four broad classifications of source rock types based on facies associations. The lacustrine facies association includes lacustrine massive mudstone facies, lacustrine mudstone with minor thin sandstones, and sandy turbidites facies. The lacustrine massive mudstone facies consists of massive, laminated grey to dark grey mudstones and siltstones. Several snails and molluscs fossils from *Hyridella* species found in this facies indicate a freshwater setting (Fossil Record Database; Gage 1952; Ward 1997). The lacustrine mudstones with minor thin sandstone facies are thin, discontinuous fine-grained sandstone beds interbedded with lacustrine mudstones. This facies is interpreted to have been deposited in a subaqueous lacustrine environment within the influence of turbidity currents (e.g. Span et.al. 1992; Basilici 1997; Renaut and Gierlowski-Kordesch 2010). The sandy turbidites facies is also interbedded with the lacustrine massive mudstone facies and composed of normally graded sandstone beds with abundant soft sediment deformation features such as convolute bedding, fluid escape structures and load casts. The facies was deposited in low gradient delta slope to prodelta environments where the sands were transported out into deeper water as the deltas prograded into the palaeolakes (e.g. Renaut and Gierlowski-Kordesch 2010). The presence of soft sediment deformation suggests high sedimentation rates in a low gradient delta slope.

The delta front facies association comprises the sandy mouthbar facies and the interdistributary bay facies. The sandy mouthbar facies is composed of thick, grey, fine to medium grained, and coarsening and thickening upwards, sandstone beds whereas the interdistributary bay facies is characterized by moderately

to highly carbonaceous, interlaminated siltstones and mudstones with plant remains. This facies association is interpreted to have been deposited at the mouth of a meandering river channel in a low gradient delta where it enters the lake (e.g. Makaske et al. 2002; Jones and Hajek 2007; Bhattacharya 2010). Coarsening and thickening upwards beds indicates prograding mouthbar environments where channel avulsions dominate.

The alluvial meandering facies association is divided into the meandering channel facies, abandoned channel facies and crevasse splay facies. The meandering channel facies is characterized by rare pebble conglomerate lag at the base and very coarse grained sandstones fining to medium sandstones at the top. Basal scouring and crossbedding are common in this facies. This facies is interpreted to have been deposited in a subaerial delta plain environment at the times when lakes existed in the basin centre and deposited in a meandering river floodplain at the times when there was no lake in the basin centre. Channel meandering, meander cut-off, cut-bank erosion, and channel shifting are the dominating processes (e.g. Slingerland and Smith 2003; Reading 2009). The abandoned channel facies consists of muddy sandstones with silty carbonaceous mudstone to highly carbonaceous mudstones grading up to coals with common rootlets. The facies was deposited in an environment which was once the part of the main channel, and after the abandonment it remained as a wetland for a substantial length of time (Slingerland and Smith 2003; Miall 2010; Toonen et. al. 2012). The crevasse splay facies comprises inversely to normally graded, fine to medium sandstones at the base which fine up to laminated silty mudstone and carbonaceous mudstones at the top. This facies was mainly deposited in close proximity to an active channel where episodic flooding events with excess discharge incise the levee and deposit as splays (e.g. Allen 1965; Elliott 1974; Guion 1985; Slingerland and Smith 2003).

The mire facies association includes mire coal facies and low-lying marshy swamp facies. The mire coal facies is divided in to two sub-facies. The thick coals are clean, black, hard, fragmented, and low ash, and likely deposited in raised mire conditions which was topographically high above floodplains where drainage systems were poorly developed (McCabe 1984; Moore 1987; Gruber and Sachsenhofer 2001). The alternating clean and muddy coals with high ash were likely deposited in low-lying mire setting in lower floodplain where drainage systems occasionally affected the mires and brought detrital influx during flood events (e.g. Sachsenhofer and Gruber 2001). The facies is overlain by the low-lying marshy swamp facies as indicated by moderately to highly carbonaceous, interlaminated siltstones and mudstones with abundant roots, twigs, other plant remains and common bioturbation. The presence of plant roots indicates the facies was deposited in subaerial, low energy and marshy environments in a low-lying mire setting in a lower floodplain delta or along lake edge during the presence of lakes (Coleman et al. 1964; Hamilton 1985; Bann et al. 2008).

The sedimentary facies distribution on the southern and eastern sides of the Greymouth Basin are dominated by meandering channel facies, abandoned channel facies and crevasse splay facies from floodplains to muddy low gradient axial meandering river deltas during the presence of the lake. The lacustrine massive mudstone facies are at the centre of the basin with low-lying marshy swamp facies at the edge. Thick, low ash coal is interpreted as mire coal facies and commonly replaces the lacustrine mudstone facies in the centre of the basin. When lakes are absent in the basin, the meandering channel facies, the abandoned channel facies and the crevasse splay facies are deposited from the axial meandering river and cover the southern and eastern sides. The overall facies distribution indicates a half-graben geometry of the Greymouth Basin with a basin bounding fault in the northwest (e.g. Leeder and Gawthorpe 1987). The eastern side of the basin is truncated against the Montgomerie - Mt Davy Fault System, suggesting part of

the basin is missing which makes difficult to conclude whether the Greymouth Rift Basin was formed as a graben or half-graben. However, sedimentary facies analysis of older alluvial and lacustrine members indicates that the eastern side was lower gradient than the western side, which, therefore, suggests half graben geometry.

The sedimentary facies analyses indicate a number of rocks that may have the potential to be petroleum source rocks according to their visible carbon percentage. In the meandering alluvial/delta plain facies association, the abandoned channel facies with ~60% carbonaceous material and the crevasse splay facies with ~30-40% carbonaceous material are thought to have hydrocarbon potential but due to their subaerial depositional origin they are more prone to oxygenated and bioturbated which made their preservation potential low. In addition, these facies are discontinuous and thin, and therefore not mappable in the fence diagram. The interdistributary bay facies of the delta front facies association contains about 80% carbonaceous mudstones and siltstones with a number of coaly stringers and occasional thin beds of coals which also make this facies potential as hydrocarbon source rocks. However, this facies is highly bioturbated and affected by regular deposition of sands from flood events which may reduce their preservation as potential source rocks. Interlaminated, carbonaceous siltstone and mudstone with abundant rootlets of the low-lying marshy swamp facies of the mire facies association can also be a potential source rock facies for the Greymouth Basin. However, the laminations are heavily disrupted by bioturbation and plant roots, meaning the facies was oxygenated during their deposition which likely decomposed the organic matter present in this facies and reduced the petroleum potential. The mire coal facies of the mire facies association are already proven hydrocarbon (both generation and expulsion) source rocks (Frankenberger et al. 1994; Zink and Sykes 2010).

The lacustrine massive mudstone and the lacustrine mudstones with minor sandstone facies of the lacustrine facies association are considered to have higher petroleum potential as indicated by their dark colour, presence of massive mudstone abundant leaf and fresh water fossils (Gage 1952; Ward 1997). The lack of bioturbation indicates that the deposition likely took place in anoxic, deep lake environments where the preservation of organic matter was high. About 60% lacustrine mudstones with leaf and fresh water fossils, 20% sandstones with conspicuous carbonaceous materials and rare bioturbation makes the sandy turbidites facies of the lacustrine facies association also potential as hydrocarbon source rocks. In addition, this facies are widely distributed both in basin margin as well as in the basin axis and can be mapped along with the lacustrine mudstone facies in a fence diagram. In general, the lacustrine mudstones facies is the thickest as an individual facies among all of the facies and was identified in three stratigraphic positions (Ford, Waiomo and Goldlight) of the Paparoa Formation. The isolith map of the lacustrine facies association of each member indicates that the Ford Member was deposited in multiple smaller basins to the centre and the northeastern side of the basin and the thickest at 82 m. The Waiomo Member was widely distributed across the basin with a new depocentre in the northwest of about 87 m thick. The Goldlight Member was the thickest and most extensively distributed across the basin with a maximum thickness of 200m in the centre.

Sedimentary facies analysis indicates that the “transitional lithosomes”, defined by Simon Ward (1997), are mostly sandy turbidites facies, sandy mouthbar facies, interdistributary bay facies and low-lying marshy swamp facies of low gradient meandering river delta. The inclusion of the potential sandy turbidites facies enlarged the interpreted size of the lakes and increases the volume of potential lacustrine source rocks.

The geochemical analysis of the potential lacustrine facies association indicates that all three litho-facies have good to excellent source rock potential (Figure 3.23). The result suggests that the Late Cretaceous Ford Member has TOC content of up to 4.6 wt%, HI of up to 554 mg HC/g TOC, and mostly mixed oil and

gas to oil prone source (Type II and Type III) with good to excellent total petroleum potential. The Late Cretaceous Waiomo Member has good potential with TOC contents of up to 3.08 wt%, HI of up to 554 mg HC/g TOC, and mostly mixed oil and gas prone source rocks (Type II and Type III) with fair to very good total petroleum potential. The very high HI values in Ford and Waiomo members (554 mg HC/g TOC) indicate that they may have Type I (alginate) oil prone kerogen as indicated by the presence of liptinitic macerals comprising telalginite (*Botryococcus*) and lamalginite (*Pediastrum*) (Mohnhoff et al. 2017). The Palaeocene Goldlight Member has poor potential with TOC contents of up to 2.95 wt%, HI up to 282mg HC/g TOC, and mostly gas prone source rocks with poor to good quantity petroleum potential. The maturation properties suggest that the Ford Member is mostly in the early to peak maturation stage whereas the Waiomo Member is mostly in the immature to early maturation stage. The Goldlight Member is mostly in immature stage.

The geochemical analysis indicates the Ford and the Waiomo have higher petroleum potential than the Goldlight although the Goldlight Member exhibits the highest thickness. The higher preservation potential of the organic matter present in the Ford and the Waiomo members was likely because of the strong thermal stratification of the Ford and Waiomo lakes that was probably consistent throughout their life span. The cooling of the climate at the end of Late Cretaceous likely changed the thermal stratification of the large, extensive Goldlight Lake by driving water circulation in the lake and mixing the thermal layers which hindered the preservation potential of the organic matter present at the lake bottom (e.g Lewis 1983). Therefore, Late Cretaceous-Palaeocene Paparoa Formation of the Greymouth Basin provides the best available geological analogue for fluvio-lacustrine source rocks that are inferred to be present in some New Zealand offshore sedimentary basins including the Taranaki Basin.

### 6.3 Tectonic evolution of the Greymouth Rift Basin

The tectonic evolution of the Greymouth Basin in Chapter 4 presents a tectono-stratigraphic model to understand how the Greymouth Basin evolved from Late Cretaceous to Early Palaeocene and its implications in the context of the formation of the West Coast-Taranaki Rift System. Here I developed conglomerate and the lacustrine facies isolith maps as well as a basal unit map to interpret the probable location of the main basin bounding fault and various smaller intra-basin faults. The aim is to understand how the faults interconnect and propagate through time as the basin widens and deepens with continued extension.

The basal unit map shows how the basin widened through time with the Jay Member sitting directly on Greenland Group basement in the central, northeastern and southeastern parts of the basin. In the northwestern part of the basin, the Morgan Member sits directly on the Greenland Group basement. In the southwestern side of the basin, the Rewanui Member sits on basement. The north- to southwestward propagation of which members lie directly on basement indicates that the basal bounding surface youngs to the northwest. This suggests a widening of the basin to the north- and southwest through time.

The Jay-Ford conglomerate isolith map shows a NNE-SSW orientation of the conglomerate deposits. Conglomerates are deposited in isolated basins which were mainly restricted to the central and eastern part of the basin. The Ford lacustrine facies isopach map shows several NNE-SSW oriented isolated sub-basins. The Morgan-Waiomo conglomerate isolith map follows the same orientation but the conglomerates were shifted westward and mainly restricted to the northwestern part of the basin. The Waiomo lacustrine facies isolith map shows two main depocentres, one located in the northwest and the other in the northeast. The depocentres are aligned approximately NNE-SSW. The depocentres are either coeval or slightly migrate

toward each other to the south. The Rewanui-Goldlight conglomerates were thicker and restricted to the northwestern corner of the basin. The thickness of the conglomerate isolith map also exhibits NNE-SSW orientation with the conglomerates thinning to the southeast. The Goldlight lacustrine facies isolith map is widely spread across the basin. The orientation is approximately NNE-SSW in direction. The Dunollie conglomerate isolith map also shows a NNE-SSW orientation of the deposits where the conglomerate thickness also decreases from the northwest to the east. The approximately NNE-SSW orientation of all isolith maps indicates that the Greymouth Basin has not changed its orientation during deposition as suggested by previous authors (Gage 1952; Newman 1981, 1985; Ward 1997).

Faults have been interpreted for each interval by combining information from both the conglomerate and lacustrine isolith maps. Faults have been inferred based on the presence of thick conglomerates indicating higher relief topography with lacustrine facies indicating adjacent depocentre lows. Larger faults have been drawn where thick conglomerate deposits exist and deep lacustrine depocentres are identified. Thinner conglomerates and smaller lacustrine depocentres, however, indicate smaller faults. There are five faults (Fault A, Fault B, Fault C, Fault D and Fault G) interpreted in the central, northeastern and the southeastern parts of the basin. Fault E, Fault F and Fault H are located in the northwestern side of the basin (Figure 4.11).

The tectonic model for the Greymouth Basin interprets the Jay conglomerates as initially depositing along small, disconnected faults forming small, isolated depocentres. Lacustrine mudstones of the Ford Member were deposited in these depocentres (Figure 4.12; 4.13). Over time with continuing extension, new fault systems developed in the northwest during the deposition of the Morgan and the Waiomo members. Morgan Member conglomerates record a widening of the basin as they were deposited along faults developed to the northwest. The activation of new faults in the northwestern side of the basin created two depo-centres across the basin during the deposition of the Waiomo Member (Figure 4.14; 4.15). Thick conglomerates deposited during the deposition of the Rewanui Member indicate that the basin became more active on the northwestern side as the existing fault to the northwest became larger. This larger fault is interpreted as the main basin bounding fault of the Greymouth Basin which is eventually controlled the majority of the basin subsidence. The basin got wider and larger during the deposition of Rewanui to Goldlight members (Figure 4.16; 4.17). In short, the Greymouth Basin evolved from Late Cretaceous small, isolated Ford lake basins to gradually enlarged Waiomo lakes and eventually to an Early Palaeocene large Goldlight lake basin through the linkage of northwestward propagating normal faults (e.g Leeder and Gawthorpe 1987; Gawthorpe and Leeder 2013; Holz et al. 2013, 2015). The half-graben geometry and alternating fluvio-lacustrine sediments of the Greymouth Basin is most likely the product pure extensional rift tectonics where the basin bounding fault is located on the northwest (e.g Leeder and Gawthorpe 1987). Applying the information about the evolution of the Greymouth Basin, it can be concluded that Late Cretaceous basins of the West Coast-Taranaki Rift System experienced a similar basin development history initiating from small sub-basins that widened and deepened through time from the amalgamation of active normal fault segments.

## 6.4 Sequence stratigraphy of the Greymouth Basin

The lacustrine sequence stratigraphy of the Greymouth Basin in chapter 5 examines the primary factors that control the alternating cycle of axial meandering alluvial and lacustrine fill of the Paparoa Formation. To start, we categorize all sedimentary lithofacies as subaerial, shoreline and subaqueous facies. The subaqueous lithofacies group includes lacustrine massive mudstones and lacustrine mudstones with minor thin sandstone facies, gravelly turbidites facies, sandy turbidites facies and gravelly delta slope facies. The

subaerial lithofacies group combines debris flow facies, gravelly braided river facies and overbank floodplain facies in the northwest, and meandering channel facies, abandoned channel facies and crevasse splay facies in the east and the south. The shoreline lithofacies are interpreted as transitional facies between subaerial and subaqueous facies which includes mire coal facies and low-lying marshy swamp facies mostly in the basin centre, alternating gravelly mouthbar and interdistributary bay facies in the northwest, and alternating sandy mouthbar and interdistributary bay facies in the east and the southeast.

Four depositional phases and their corresponding system tracts have been defined using the facies present in the basin's centre. The marshy swamp phase or transgressive systems tract (TST) includes the low-lying marshy swamp facies from the shoreline lithofacies group. It shows a short fining upward trends in gamma-ray logs. It starts with a basal flooding surface at the base. Marshy swamp phase is overlain by lacustrine phases. The lacustrine phase corresponds with highstand systems tract ($HST^{l}$) and consists of lacustrine massive mudstone and lacustrine mudstones with minor thin sandstone facies of the subaqueous lithofacies group in the basin centre. This includes the maximum flooding surface of the lakes at the base as indicated by the thin turbidite package in massive mudstones and is characterized by a thick uniform nature of the high gamma-ray response of slightly coarsening upward trends. The lacustrine phase is overlain by the deltaic infill phase. It corresponds with highstand systems tract ($HST^{u}$) which comprises deltaic gravelly mouthbar, sandy mouthbar, and interdistributary bay facies from the shoreline lithofacies group; and gravelly turbidite, sandy turbidite, and gravelly delta slope facies from the subaqueous lithofacies group. It shows coarsening upward trends in gamma-ray logs. The alluvial phase or low accommodation systems tracts (LAST) comprises all facies of the subaerial lithofacies group excluding the mire facies association and overlies the deltaic infill phase. It shows low gamma-ray values in basin margin localities due to the overall coarse-grained nature of the sedimentary facies, and comperatively high gamma-ray values in basin axis localities due to the presence of finergrained sandstones and mudstones in the meandering alluvial facies association. However, the overall trend shows a coarsening upward pattern.

Five depositional sequences are identified and tied to different rifting phases of the Greymouth Basin. A complete depositional sequence consists of four devotional phases, starting with a marshy swamp or lacustrine phases at the base and grading upward to deltaic infill phase and alluvial phase at the top. Transgressive, highstand and low accommodation systems tracts are identified in a complete depositional sequence. The basal flooding surfaces are interpreted as sequence boundaries. An incomplete depositional sequence consists of only the alluvial phase. A sequence boundary is replaced by an unconformity when an incomplete depositional sequence sits directly on the basement. The oldest depositional sequence consists of an alluvial phase and therefore is interpreted as an incomplete depositional sequence (SQ1). SQ1 unconformably overlies Greenland Group basement in the northeast side of the basin (Figure 5.6). Three successive complete depositional sequences SQ2, SQ3 and SQ4 are interpreted as complete depositional sequences as indicated by the presence of four or at least three depositional phases in the basin axis. Each sequence in the basin axis starts with a marshy swamp phase which is overlain by a lacustrine phase and grades towards a deltaic infill phase and alluvial phase at the top. Each complete depositional sequence in the basin axis correlates with an alluvial phase unconformably sitting on the basement to the basin margin in the northwest. Each complete depositional sequence is divided into the transgressive, highstand and low accommodation system tract. The transgressive system tracts start with a basal flooding surface and shows a short trend of retrogradational depositional pattern up to the maximum expansion of the lake (maximum flooding surface). The highstand system tracts start with a maximum flooding surface at the base, and include lacustrine and deltaic infill phase. The highstand system tracts show a sharp progradational

depositional pattern. The low accommodation system tracts include alluvial phases show an overall progradational depositional pattern. The youngest depositional sequence (SQ5) unconformably overlies SQ4. It is comprised of mostly alluvial phase and is, therefore, interpreted as an incomplete depositional sequence. The Island Sandstone deposited on top of the SQ5 represents the end of non-marine deposition and the initiation of the first marine transgression.

SQ1 is distributed in small, restricted fault-controlled basins with alluvial and braided river facies along the faults, thinning towards east and becoming sandier away from the fault. Locally restricted fault bounded shallow, disconnected basins indicates low accommodation space relative to sediment supply (S>A) due to low subsidence rate of the basin. This sequence corresponds to the rift initiation stage. The complete depositional sequences (SQ2/SQ3/SQ4) are distributed throughout the basin as indicated by the westward stepping of the fault through time and younger unconformable surface to the northwest and southwest with ever younger sediments sitting directly on the basement. This also indicate the widening and deepening of the basin. Each of this depositional sequence indicates the onset of the rapid subsidence of the basin with high accommodation conditions, followed by a longer period of tectonic quiescence with low subsidence rate and gradual decrease in accommodation space relative to sediment supply. These sequences were formed during the rift development stage. SQ5 is distributed in large, low gradient surfaces and dominated by meandering rivers with coals and fine-grained sediments accumulating on the floodplains, followed by an increased chemical weathering, suggesting a longer period of tectonic quiescence with extensive subaerial exposer of the sediments. The low accommodation space and the constant sediment supplies (S>A) during this time allowed the alluvial sediments to fill the available accommodation prior to the extensive subaerial weathering and marine transgression. SQ5 was deposited during the termination stage of Greymouth rifting. Widening and thickening of the Greymouth Basin associated with the rift basin development where the primary driving force is episodic tectonic activity. Therefore, we conclude that, like most of the rift basins across the world, the primary factor that controls the cycle of alluvial and lacustrine sedimentation of the Greymouth Basin is tectonic.

## 6.5 The Greymouth Basin and the West Coast-Taranaki Rift Systems

The depositional history of the Greymouth Basin suggests that the stability of the extension direction affects the interpretation of the regional tectonics of the Greymouth Basin from the Late Cretaceous to the Early Palaeocene as indicated by the presence of NNE-SSW and WNW-ESE oriented faults in the underlying Metamorphic Core Complex (Herd 2007; Sagar and Palin 2011; Schulte et al. 2014). The conglomerate and lacustrine facies isolith maps indicate that the basin orientation did not change during the deposition of the Paparoa Formation in the Greymouth Basin which contradicts previous models (Gage 1952; Newman 1985; Ward 1997). We suggest the change may have occurred during the ~15 Ma gap between deposition of the underlying of the Pororari Group and the overlying Paparoa Formation (Gage 1952; Nathan 1978). This coincides with interpretations made in the Taranaki Basin where detailed seismic mapping and stratigraphic analysis of the West Coast-Taranaki rift phase indicates that the Pakawau, Kiwa and Maui sub-basins have a NE orientation approximately perpendicular to many of the earlier mid-Cretaceous rift basins (Strogen et.al. 2017).

The depositional history of New Zealand indicates that a long period of subduction along the eastern boundary of Gondwana (Laird 1981, Bradshaw 1989; Laird and Bradshaw 2003) was followed by rifting that produced metamorphic core complexes in hot and thinned crust (Tulloch and Kimbrough 1989; Laird and Bradshaw 2004; Herd 2007; Schulte et al. 2014). Rifting during the West Coast-Taranaki Rift System continued to thin the crust as a result of rifting in a slightly different orientation (Mortimer 2004; Strogen

et.al. 2017). Therefore, the lithosphere was hot, thin, and weak which suggests the reason for the formation of shorter fault bounded rift basins in the West Coast-Taranaki Rift System was due to them being formed in crust that had already been highly stretched and intruded during the development of the metamorphic core complexes in the mid-Cretaceous similar to what postulated for the Afar Rift in the East African Rift System (Ebinger 1999).

The West Coast-Taranaki Rift phase produced a number of NNE-SSW oriented parallel to sub-parallel half-graben basins at the same time as the productive Taranaki Basin to the north (Strogen et.al. 2017; Figure 4.24 and Figure 4.25). Most of the previous interpretations regarding the Taranaki Basin and associated sub-basins have been made using seismic data combined with limited outcrops and well data. In comparison, the Greymouth Basin is extensively drilled for coal exploration and has greater outcrop availability.Understanding the distribution of different sedimentary facies in the Greymouth Basin, it is highly possible that the Taranaki and other sub-basins in the West Coast Taranaki Rift phase have the same asymmetric facies distribution. Applying the information about the evolution of the Greymouth Basin, it can be concluded that the West Coast-Taranaki Rift basins experienced same basin development history initiating from small sub-basins that widened and deepened through time from the amalgamation of active normal fault segments through time.

## 6.6 Suggestions for future works

The following additional investigations can be done to further understand the source rock potentials, depositional history and evolution of the Greymouth Basin and the West Coast Taranaki Rift Systems.

- The Greymouth Basin has proven coaly source rocks and potential lacustrine mudstone source rocks. The other source rocks from shoreline, subaerial and subaqueous environments are also available in the Greymouth Basin. Future work can be done to the understand the total volume of the source rock potential of the Greymouth Basin by adding other potential source rocks that obviously increase the total volume of potential lacustrine source rocks in the Greymouth Basin.
- The present work can be extended further by looking at the Pike River Basin and the other basins further north that connect the Greymouth Basin to the Taranaki Basin to add more information regarding the formation of the West Coast Taranaki Rift Systems.
- Additional future work should be done through high resolution seismic acquisition in offshore Greymouth, particularly in the Takutai Basin area. If the Greymouth Basin is economic, the Takutai must have some graben structures with potential alluvial and lacustrine source rock facies that may also have economic potential.

# References


Agar, S. M., and Klitgord, K. D. (1995). Rift flank segmentation, basin initiation and propagation: a neotectonic example from Lake Baikal. *Journal of the Geological Society, 152*(5), 849-860.

Agarwal, R., and Bhoj, R. (1992). Evolution of Kosi river fan, India: structural implications and geomorphic significance. *International Journal of Remote Sensing, 13*(10), 1891-1901.

Al-Areeq, N. M., Al-Badani, M. A., Salman, A. H., and Albaroot, M. A. (2018). Petroleum source rocks characterization and hydrocarbon generation of the Upper Jurassic succession in Jabal Ayban field, Sabatayn Basin, Yemen. *Egyptian journal of petroleum*, *27*(4), 835-851.

Allen, J.R.L. (1977). The possible mechanics of convolute lamination in graded sand beds. *Journal of Geologocal Society, London*, 134, 19-31.

Allen, J.R.L. (1982). Sedimentary structures: their character and physical basis, *New York (Elsevier),* 11,663.

Anadón, P., Cabrera, L., Julia, R., and Marzo, M. (1991). Sequential arrangement and asymmetrical fill in the Miocene Rubielos de Mora Basin (northeast Spain). *Lacustrine facies analysis*, 257-275.

Anderson, H., Webb, T., and Jackson, J. (1993). Focal mechanisms of large earthquakes in the South Island of New Zealand: implications for the accommodation of Pacific-Australia plate motion. *Geophysical Journal International, 115*(3), 1032-1054.

Anderson, H., Beanland, S., Buck, G., Darby, D., Downes, G., Haines, J., Jackson, J., Robinson, R. and Webb, T. (1994). The 1968 May 23 Inangahua, New Zealand, earthquake: an integrated geological, geodetic, and seismological source model. *New Zealand Journal of Geology and Geophysics, 37*(1), 59-86.

Bann, K. L., Jones, B. G., Tye, S. C., Maceachern, J. A.and Fielding, C. R. (2008). Ichnological and sedimentologic signatures of mixed wave-and storm-dominated deltaic deposits: Examples from the Early Permian Sydney Basin, Australia. In Hampson, G., Steel, R., Burgess, P., and Dalrymple, R., eds., *Recent advances in model of siliciclastic shallow marine stratigraphy: SEPM Special Pulication,* 90, 293-332.

Barnes, P., and Ghisetti, F. (2013). Offshore faulting and earthquake sources, West Coast, South Island: Stage 2. *MBIE Envirolink West Coast Regional Council Advice*.

Basilici, G. (1997). Sedimentary facies in an extensional and deep-lacustrine depositional system: the Pliocene Tiberino Basin, Central Italy. *Sedimentary Geology, 109*(1-2), 73-94.

Bartov, Y., Stein, M., Enzel, Y., Agnon, A., and Reches, Z. e. (2002). Lake levels and sequence stratigraphy of Lake Lisan, the late Pleistocene precursor of the Dead Sea. *Quaternary Research, 57*, 17-31.

Bartov, Y., Agnon, A., Enzel, Y., and Stein, M. (2006). Late Quaternary faulting and subsidence in the central Dead Sea basin. *Israel Journal of Earth Sciences, 55*(1).

Bassett, K. N., and Orlowski, R. (2004). Pahau Terrane type locality: Fan delta in an accretionary prism trench-slope basin. *New Zealand Journal of Geology and Geophysics, 47*(4), 603-623.

Bassett, K., Ettmuller, F., and Bernet, M. (2006). Provenance analysis of the Paparoa and Brunner Coal Measures using integrated SEM-cathodoluminescence and optical microscopy. *New Zealand Journal of Geology and Geophysics, 49*(2), 241-254.

Bassett, K., Cody, E., Monteith, F., and Maitra, M. (2014). Greymouth coal field: a fault-bounded basin, but which side. *Geoscience Society of New Zealand Annual Conference*. New Plymouth, New Zealand, 24-27 November 2014.

Bates, C. (1953). Rational theory of delta formation. *AAPG Bulletin*, 37, 2119-2162.

Bechtel, A., Jia, J., Strobl, S. A., Sachsenhofer, R. F., Liu, Z., Gratzer, R., and Püttmann, W. (2012). Palaeoenvironmental conditions during deposition of the Upper Cretaceous oil shale sequences in the Songliao Basin (NE China): Implications from geochemical analysis. *Organic geochemistry, 46*, 76-95.

Beggs, J., Ghisetti, F., and Tulloch, A. (2008). Basin and petroleum systems analysis of the West Coast region, South Island, New Zealand, *PESA Eastern Australasian Basins Symposium III,* 1-7.

Bennett, M. R., Doyle, P., and Mather, A. E. (1996). Dropstones: their origin and significance. *Palaeogeography, Palaeoclimatology, Palaeoecology, 121*(3-4), 331-339.

Berryman, K. (1980). Late Quaternary movement on White Creek Fault, South Island, New Zealand. *New Zealand Journal of Geology and Geophysics, 23*(1), 93-101.

Bhattacharjee SK 2005. Unlocking the Gippsland Basin. Offshore 65: 112 – 117.

Bhattacharya, J. P. (2010). Deltas. In James, N. P. and Dalrymple, R. W., eds., Facies Models 4, *Geological Association of Canada*, 6, 233-264.

Biddle, K. T. & N. Christie-Blick, 1985, Glossary – strike-slip deformation, basin formation and sedimentation. In: K. T. Biddle & N. Christie-Blick, (eds.,) Strike-Slip Deformation, Basin Formation and Sedimentation. *SEPM Special Publications, 37,* 375–384.

Bird, R. T., Naar, D. F., Tebbens, S. F., and Kleinrock, M. C. (1999). Episodic triple-junction migration by rift propagation and microplates. *Geology, 27*(10), 911-914. https://doi.org/10.1130/0091-7613(1999)027<0911:Etjmbr>2.3.Co;2

Bishop, D. J. (1992). Extensional tectonism and magmatism during the middle Cretaceous to Paleocene, North Westland, New Zealand. *New Zealand Journal of Geology and Geophysics, 35*(1), 81-91. https://doi.org/10.1080/00288306.1992.9514502

Bishop, D. J., and Buchanan, P. G. (1995). Development of structurally inverted basins: a case study from the West Coast, South Island, New Zealand. In Buchanan, J. G. and Buchanan, P. G. eds., Basin Inversion, *Geological Society Special Publication, 88*, 549-585.

Bissada, K. (1982). Geochemical constraints on petroleum generation and migration—a review. *Proceedings at the ASEAN Council on Petroleum*, 69-87.

Blair, T. C., and Bilodeau, W. L. (1988). Development of tectonic cyclothems in rift, pull-apart, and foreland basins: Sedimentary response to episodic tectonism. *Geology, 16*(6), 517-520.

Blair, T. C., and McPherson, J. G. (1994). Alluvial fans and their natural distinction from rivers based on morphology, hydraulic processes, sedimentary processes, and facies assemblages. *Journal of Sedimentary Research, 64*(3a), 450-489.

Blair, T. C. (1999). Sedimentology of the debris-flow-dominated Warm Spring Canyon alluvial fan, Death Valley, California. *Sedimentology, 46*(5), 941-965.

Blair, T. (2002). Alluvial-fan sedimentation from a glacial-outburst flood, Lone Pine, California, and contrasts with meteorological flood deposits. Flood and Megaflood Processes and Deposits: Recent and Ancient Examples. *International Association of Sedimentologists Special Publication*, 32, 111-140.

Blair, T. C., and McPherson, J. G. (2009). Processes and forms of alluvial fans. *Geomorphology of desert environments, Springer*, 413-467.

Boggs, S. Jr., (2006). Continental (terrestrial) environments. In: Boggs S., Fifth Edition. *Principles of Sedimentology and Stratigraphy,* 213– 247.

Bohacs, K. M. (1998). Contrasting expressions of depositional sequences in mudrocks from marine to nonmarine environments. In Schieber J., Zimmerle W., and Sethi P., eds., Shales and mudstones I. *Basin studies, sedimentology, and paleontology*, 33–78.

Bohacs, K. M., Carroll, A. R., Neal, J. E., and Mankiewicz, P. J. (2000). Lake-basin type, source potential, and hydrocarbon character: an integrated sequence-stratigraphic-geochemical framework. In GierlowskiKordesch E. H. and Kelts K. R., eds., Lake basins through space and time*: AAPG Studies in Geology, 46*, 3-34.

Boyd, R.J., Lewis, D.W. (1995): Sandstone diagenesis relating to varying burial depth and temperature in Greymouth Coalfiled, South Island, New Zealand. *New Zealand Journal of Geology and Geophysics*, *38(3)*, 333-348.

Bowman, R. G. (1984). Greymouth coalfield report-Part 1 (Geology and coal resources), New Zealand Coal Resources Survey Report. *Ministry of Energy, Wellington, New Zealand*, 84.

Bowman, R. G., Caffyn, P., Duff, S. W. (1984). Greymouth Coalfield. New Zealand Coal Resources Survey Report. *Ministry of Energy, Wellington, New Zealand*, *1*, 211.

Bowman, V. C., Francis, J. E., Riding, J. B., Hunter, S. J., and Haywood, A. M. (2012). A latest Cretaceous to earliest Paleogene dinoflagellate cyst zonation from Antarctica, and implications for phytoprovincialism in the high southern latitudes. *Review of Palaeobotany and Palynology, 171*, 40-56.

Bradshaw, J. (1993). A review of the Median Tectonic Zone: terrane boundaries and terrane amalgamation near the Median Tectonic Line. *New Zealand Journal of Geology and Geophysics, 36*(1), 117-125.

Brewer, P. A., Leeks J.L. and Lewin J., (1992). Direct measurement of in-channel abrasion processes, Erosion and Sediment Transport Monitoring Programmes in River Basins, *Proceedings of the Oslo 1 Symposium IV*, 21-29.

Bridge, J. S., (1984). Large-scale facies sequences in alluvial overbank environments: Journal of Sedimentary Petrology, 54, 583-588.

Busby, C. J. and Ingersoll, R. V., (1995). Tectonics of sedimentary basins, *Blackwell Science Oxford*, 478pp.

Butzer, K. W., Isaac, G. L., Richardson, J. L., and Washbourn-Kamau, C. (1972).Radiocarbon dating of East African lake levels. *Science, 175*(4026), 1069-1076.

Carroll, A. R., and Bohacs, K. M. (2001). Lake-type controls on petroleum source rock potential in nonmarine basins. *AAPG Bulletin, 85*(6), 1033-1053.

Casagrande, D. (1987). Sulphur in peat and coal. In Scott, A. C. eds., Coal and Coal-bearing strata: Recent Advances. *Geological Society Special Publication, London, 32(1)*, 87-105.

Catuneanu, O., Khalifa, M. A., and Wanas, H. (2006). Sequence stratigraphy of the lower cenomanianbahariya formation, Bahariya Oasis, Western Desert, Egypt. *Sedimentary Geology, 190*(1-4), 121-137.

Catuneanu, O. (2006). *Principles of sequence stratigraphy*: *Elsevier*, 375pp.

Chang, T. S., and Chun, S. S. (2012). Micro-characteristics of sustained, fine-grained lacustrine turbidites in the Cretaceous Hwangsan Tuff, SW Korea. *Geosciences Journal, 16*(4), 409-420.

Coleman, J. M., Gagliano, S. M., and Webb, J. E. (1964). Minor sedimentary structures in a prograding distributary. *Marine Geology, 1*(3), 240-258.

Cook, R.A.; Sutherland, R.; Zhu, H. (et al.) (1999). Cretaceous - Cenozoic geology and petroleum systems of the Great South Basin, New Zealand. Lower Hutt: *Institute of Geological and Nuclear Sciences monograph. 20,* 190.

Cody, E.N. (2015). Sedimentology and Hydrocarbon Potential of the Paparoa Coal Measures Lacustrine Mudstones. (Unpublished master's thesis). *University of Canterbury, Christchurch, New Zealand*.

Colella, A. (1988). Fault-controlled marine Gilbert-type fan deltas. *Geology, 16*(11), 1031-1034.

Collinson, J.D., (1996). Alluvial sediments, In: Reading, H.G. (Ed.), S*edimentary Environments and Facies. 3rd edn. Blackwell Science, Oxford*, 37–82.

Collinson, J. D., and Lewin, J. (2009). Modern and ancient alluvial systems: *John Wiley and Sons*, 574 pp.

Colombo, F. (1994). Normal and reverse unroofing sequences in syntectonic conglomerates as evidence of progressive basinward deformation. *Geology, 22*(3), 235-238.

Costa, J. E., and Schuster, R. L. (1988). The formation and failure of natural dams. *Geological Society of America Bulletin, 100*(7), 1054-1068.

Cowie, P. A., Underhill, J. R., Behn, M. D., Lin, J., and Gill, C. E. (2005). Spatio-temporal evolution of strain accumulation derived from multi-scale observations of Late Jurassic rifting in the northern North Sea: A critical test of models for lithospheric extension. *Earth and Planetary Science Letters, 234*(3-4), 401-419.

Curiale, J. A., and Stout, S. A. (1993). Monitoring tectonically controlled marine to lacustrine transitions using organic facies—Ridge basin, California, USA. *Chemical Geology, 109*(1-4), 239-268.

Currie, B. S. (1997). Sequence stratigraphy of nonmarine Jurassic–Cretaceous rocks, central Cordilleran foreland-basin system. *Geological Society of America Bulletin, 109*(9), 1206-1222.

Curry, D.J., Bohacs, K.M., (1994). The influence of sequence stratigraphic position on the oil generation potential of coals. In: Emerging Concepts in Organic Petrology and Geochemistry. *Delegate Manual, Joint Meeting of the Canadian Society for Coal Science and Organic Petrology andThe Society for Organic Petrology (TSOP 19th Annual Meeting)*, Abstract A3.1.1.

Demaison, G., and Huizinga, B. J. (1991). Genetic classification of petroleum systems (1). *AAPG Bulletin, 75*(10), 1626-1643.

Diessel C. F. K. (1992). Coal-bearing depositional systems. *Springer-Verlag, New York; Berlin*, 721 pp.

Dorsey, R. J., Umhoefer, P. J., and Renne, P. R. (1995). Rapid subsidence and stacked Gilbert-type fan deltas, Pliocene Loreto basin, Baja California Sur, Mexico. *Sedimentary Geology, 98*(1-4), 181-204.

Ebinger, C. J., Rosendahl, B., and Reynolds, D. (1987). Tectonic model of the Malaŵi rift, Africa. *Tectonophysics, 141*(1-3), 215-235.

Edbrooke, S., Sykes, R., and Pocknall, D. (1994). *Geology of the Waikato coal measures, Waikato coal region, New Zealand* (Vol. 6): Institute of Geological and Nuclear Sciences Limited.

Einsele, G., (1992). Sedimentary Basins: Evolution, Facies and Sediment Budgets. *Springer, New York,* 628 pp.

Elliott, T. (1974). Interdistributary bay sequences and their genesis. *Sedimentology, 21*(4), 611-622.

Emery, D., and Myers, K. (1996). Sequence stratigraphy: *Oxford, U. K., Blackwell*. 297 pp.

Emery, K.O. (1955). Transportation of rocks by driftwood. *Journal of Sedimentary Petrology*, 25, 51-57.

Emery, K.O. (1965). Organic transportation of marine sediments. In M.N. Hill eds., *The Sea. Wiley, New York*, 776 793.

Ermini, L., Casagli, N., and Farina, P. (2006). Landslide dams: analysis of case histories and new perspectives from the application of remote sensing monitoring techniques to hazard and risk assessment. *Italian Journal of Engineering Geology and Environment,* 1, 45-52.

Espitalie, J., Deroo, G., and Marquis, F. (1985). Rock-Eval pyrolysis and its applications. *Revue De L InstitutFrancais Du Petrole, 40*(5), 563-579.

Falk, P. D., and Dorsey, R. J. (1998). Rapid development of gravelly high-density turbidity currents in marine Gilbert-type fan deltas, Loreto Basin, Baja California Sur, Mexico. *Sedimentology, 45*(2), 331-349.

Fan, X., van Westen, C. J., Xu, Q., Gorum, T., and Dai, F. (2012). Analysis of landslide dams induced by the 2008 Wenchuan earthquake. *Journal of Asian Earth Sciences, 57*, 25-37.

Fernández, L., Agueda, J., Colmenero, J., Salvador, C., and Barba, P. (1988). A coal-bearing fan-delta complex in the Westphalian D of the Central Coal Basin, Cantabrian Mountains, northwestern Spain: implications for the recognition of humid-type fan deltas. In Nemec, W., and Steel, R. J., eds., Fan Deltas: Sedimentology and Tectonic Settings*, London, Blackie and Son,* 286-302.

Figueiredo, F. T., Almeida, R. P., Freitas, B. T., Marconato, A., Carrera, S. C., and Turra, B. B. (2016). Tectonic activation, source area stratigraphy and provenance changes in a rift basin: The Early Cretaceous Tucano Basin (NE-Brazil). *Basin Research, 28*(4), 433-445.

Flint, S., and Turner, P. (1988). Alluvial fan and fan-delta sedimentation in a forearc extensional setting: The Cretaceous Coloso Basin of northern Chile. In Nemec, W., and Steel, R. J., eds., Fan deltas: Sedimentology and tectonic settings. *Blackie, Glasgow, 387*-399.

Folkestad, A., and Satur, N. (2008). Regressive and transgressive cycles in a rift-basin: Depositional model and sedimentary partitioning of the Middle Jurassic Hugin Formation, Southern Viking Graben, North Sea. *Sedimentary Geology, 207*(1-4), 1-21.

Frankenberger, A., Brooks, R., Varela-Alvarez, H., Collen, J., Filby, R., and Fitzgerald, S. (1994). Classification of some New Zealand crude oils and condensates by means of their trace element contents. *Applied Geochemistry, 9*(1), 65-71.

Gaina, C., Müller, R. D., Roest, W. R., and Symonds, P. (1998). The opening of the Tasman Sea: a gravity anomaly animation. *Earth Interactions, 2*(4), 1-23.

Gage, M. 1952: The Greymouth coalfield. *New Zealand Geological Survey Bulletin, 45*, 232p.

Galloway, W. E., & Hobday, D. K. (Eds.). (1996). Alluvial fans. In Terrigenous clastic depositional systems, *Berlin: Springer Science+Business Media*, 29-59.

Gasse, E., and Street, F. (1978). Late Quaternary lake-level fluctuations and environments of the northern Rift Valley and Afar region (Ethiopia and Djibouti). *Palaeogeography, Palaeoclimatology, Palaeoecology, 24*(4), 279-325.

Gawthorpe, R., Hurst, J., and Sladen, C. (1990). Evolution of miocene footwall-derived coarse-grained deltas, Gulf of Suez, Egypt: Implications for exploration (1). *AAPG Bulletin, 74*(7), 1077-1086.

Gawthorpe, R., and Hurst, J. M. (1993). Transfer zones in extensional basins: their structural style and influence on drainage development and stratigraphy. *Journal of the Geological Society, 150*(6), 1137-1152.

Gawthorpe, R., and Leeder, M. (2000). Tectonic-sedimentary evolution of active extensional basins. *Basin Research, 12*(3-4), 195-218.

Gawthorpe, R. L., Jackson, C. A.L., Young, M. J., Sharp, I. R., Moustafa, A. R., and Leppard, C. W. (2003). Normal fault growth, displacement localisation and the evolution of normal fault populations: the Hammam Faraun fault block, Suez Rift, Egypt. *Journal of Structural Geology, 25*(6), 883-895.

Gawthorpe, R. L., Leeder, M. R., Kranis, H., Skourtsos, E., Andrews, J. E., Henstra, G. A., Mack, G., Muravchik, M., Turner, J., and Stamatakis, M. (2018). Tectono-sedimentary evolution of the Plio-Pleistocene Corinth rift, Greece. *Basin Research, 30*(3), 448-479. https://doi.org/10.1111/bre.12260.

Ghisetti, F. C., and Sibson, R. H. (2006). Accommodation of compressional inversion in northwestern South Island (New Zealand): Old faults versus new?. *Journal of Structural Geology*, *28*(11), 1994-2010.

Gibbs, A. (1984). Structural evolution of extensional basin margins. *Journal of the Geological Society, 141*(4), 609-620.

Gilbert, R. (1990). Rafting in glacimarine environments. In: Dowdeswell, J.A., Scourse, J.D. eds., Glacimarine Environment: Processes and Sediments. *Geological Society (London) Special Publications, 53*(1), 105-120.

Gobo, K., Ghinassi, M., and Nemec, W. (2014). Reciprocal changes in foreset to bottomset facies in a Gilbert-type delta: response to short-term changes in base level. *Journal of Sedimentary Research, 84*(11), 1079-1095.

Gore, P. J. (1989). Toward a model for open-and closed-basin deposition in ancient lacustrine sequences: the Newark Supergroup (Triassic-Jurassic), eastern North America. *Palaeogeography, Palaeoclimatology, Palaeoecology, 70*(1-3), 29-51.

Grindley, G. (1978). Palaeomagnetic data from New Zealand. *Exploration Geophysics, 9*(3), 140-143.

Gruber, W., and Sachsenhofer, R. (2001). Coal deposition in the Noric Depression (Eastern Alps): raised and low-lying mires in Miocene pull-apart basins. *International Journal of Coal Geology, 48*(1-2), 89-114.

Guion, P. D. (1985). Crevasse splay deposits and roof-rock quality in the Threequarters Seam (Carboniferous) in the East Midlands Coalfield, UK. In: Rahmani, R.A., Flores, R.M. eds., *Sedimentology of coal and coal-bearing sequences*, *International Association of Sedimentologists Special Publication*, 7, 291-308.

Guy, M. (1992): Facies analysis el the Kopervik sand interval, Kilda Filed, Block 16/26, t-. K. North Sea. - In: Hardman. R.F.P. ted.l: Exploration Britain: Geological Insights for the next decade, *Special Publication of Geological Society, London*, 67, 187-220.

Hamilton, D. S. (1985). Deltaic depositional systems, coal distribution and quality, and petroleum potential, Permian Gunnedah Basin, NSW, Australia. *Sedimentary Geology, 45*(1-2), 35-75.

Hammen van der T. (1974). The Pleistocene changes of vegetation and climate in tropical South America. *Journal of Biogeography*, 3-26.

Harvey, A. (1984). Debris flows and alluvial deposits in Spanish Quaternary alluvial fans: implications for fan morphology. in Koster, F. E. M., and Steel, R. J., eds., Sedimentology of Gravels and Conglomerates*, Canadian Society of Pctroteum Geologists*, 10, 123-132.

Harvey, A. M., Mather, A. E., and Stokes, M. (2005). Alluvial fans: geomorphology, sedimentology, dynamics—introduction. A review of alluvial-fan research. *Geological Society, London, Special Publications, 251*(1), 1-7.

Hein F. J. (1982). Depositional mechanisms of deep sea coarse elastic sediments, Cap Enrage Formation, *Canadian Journal of Earth Sciences*, 19, 276-287.

Hematite Petroleum, (1970). Haku-1 Well Report. Ministry of Economic Development, New Zealand. Unpublished Report.

Herd, M. E. J. (2007). Continental Extensional Tectonics – The Paparoa Metamorphic Core Complex of Westland, New Zealand. *Master of Science, University of Canterbury, New Zealand*.

Herzer, R., Sykes, R., Killops, S., Funnell, R., Burggraf, D., Townend, J., Raine, I., and Wilson, G. (1999). Cretaceous carbonaceous rocks from the Norfolk Ridge system, Southwest Pacific: implications for regional petroleum potential. *New Zealand Journal of Geology and Geophysics, 42*(1), 57-73.

Higgs, R. (1990). Sedimentology and tectonic implications of Cretaceous fan-delta conglomerates, Queen Charlotte Islands, Canada. *Sedimentology, 37*(1), 83-103.

Hill, R. S., and Christophel, D. C. (1988). Tertiary leaves of the tribe Banksieae (Proteaceae) from southeastern Australia. *Botanical Journal of the Linnean Society, 97*(2), 205-227.

Hirner, A. V., and Lyon, G. L. (1989). Stable isotope geochemistry of crude oils and of possible source rocks from New Zealand—1: carbon. *Applied Geochemistry, 4*(2), 109-120.

Holz M., Troccoli E. B., Vieira M. P (2014). Sequence Stratigraphy of Continental Rift Basins I: A Conceptual Discussion of Discrepant Models. In: Rocha R., Pais J., Kullberg J., Finney S. eds., STRATI 2013. *Springer Geology, Springer*. https://doi.org/10.1007/978-3-319-04364-7_2.

Holz, M., Moreira, F., Troccoli E. (2015). A conceptual sequence stratigraphic model for continental rift successions based on the Reconcavo Basin, Cretaceous, Brazil, *2nd International Congress on Stratigraphy*, *Graz, Austria*.

Holz, M., Vilas-Boas, D.B., Troccoli, E.B., Santana, V.C., Vidigal-Souza, P.A. (2017). Conceptual models for sequence stratigraphy of continental rift successions. In: Montenari, M. eds., Stratigraphy & Timescales. *Academic Press*, 119–186.

Horsfield, B., H. D., and Ho, T. T. Y. (1983), Some potential applications of pyrolysis to basin studies: *Journal of the Geological Society, 140(3),* 431–443, doi:10.1144/gsjgs.140.3.0431.

Horton, B., and DeCelles, P. G. (2001). Modern and ancient alluvial megafans in the foreland basin system of the central Andes, southern Bolivia: Implications for drainage network evolution in fold-thrust belts. *Basin Research, 13*(1), 43-63.

Hou, Y., Wang, H., Fan, T., Zhang, H., Yang, R., Li, Y., and Long, S. (2020). Rift-related sedimentary evolution and its response to tectonics and climate changes: A case study of the Guaizihu sag, Yingen-Ejinaqi Basin, China. *Journal of Asian Earth Sciences*, *195*, 104370.

Ilgar, A., and Nemec, W. (2005). Early Miocene lacustrine deposits and sequence stratigraphy of the Ermenek Basin, Central Taurides, Turkey. *Sedimentary Geology, 173*(1-4), 233-275.

Imbrie, J., Hays, J., Martinson, D., McIntyre, A., Mix, A., Morley, J. J., Pisias, N. G., Prell, W., and Shackleton, N. (1984). The orbital theory of Pliestocene climate: support from a revised chronology of the maribe d18O record. In Berger, A., Imbrie, J., Hays, J. D., Kukla, G., and Saltzman, B. *Milankovitch and Climate*, 269-305.

Jones, H., and Hajek, E. (2007). Characterizing avulsion stratigraphy in ancient alluvial deposits. *Sedimentary Geology, 202*(1-2), 124-137.

Kamp P. J. J., Whitehouse I. W. S., Newman J., (1999). Constraints on the thermal and tectonic evolution of Greymouth coalfield, *New Zealand Journal of Geology and Geophysics* 42, 447-467.

Katz, B. J. (1983). Limitations of 'Rock-Eval'pyrolysis for typing organic matter. *Organic Geochemistry, 4*(3-4), 195-199.

Katz, B. (1995). The Green River Shale: an Eocene carbonate lacustrine source rock. In *Petroleum source rocks, Springer*, 309-324.

Katz, B. J., and Liro, L. M. (1993). The Waltman Shale Member, Fort Union Formation, Wind River basin: a Paleocene clastic lacustrine source system. In Keefer, W. R., Metzger, W. J. and Godwin L. H. eds., Oil and Gas and Other Resources of the Wind River Basin, Wyoming. *Wyoming Geological Association, Casper*, 163–174.

Kazanci N., (1988). Repetitive deposits of alluvial fan-deltas and fan-delta wedges at a fault-controlled margin of the Pleistocene-Holocene Burdur Lake graben, southwestern Anatolia, Turkey. In Nemec, W., and Steel, R. J., eds., Fan deltas: Sedimentology and tectonic settings. *Blackie, London,* 186-196.

Kearey, P., Klepeis, K. A., and Vine, F. J. (2013). *Global tectonics*. *Blackwell Scientific Publications*, *New York, 302 pp.*

Keighley, D., Flint, S., Howell, J., and Moscariello, A. (2003). Sequence stratigraphy in lacustrine basins: a model for part of the Green River Formation (Eocene), southwest Uinta Basin, Utah, USA. *Journal of Sedimentary Research, 73*(6), 987-1006.

Kelts, K. (1988). Environments of deposition of lacustrine petroleum source rocks: an introduction. *Geological Society, London, Special Publications, 40*(1), 3-26.

Kennedy E.M. (2003). Late Cretaceous and Paleocene terrestrial climates of New Zealand: Leaf fossil evidence from South Island assemblages. *New Zealand Journal of Geology and Geophysics*, 46, 295-306.

Kereszturi, Á., Hargitai, H., and Postma, G. (2015). Delta. Encyclopedia of Planetary Landforms, *Springer Science + Business Media,* 551-560.

Killick, M. (1988). Sedimentary and tectonic controls of fan-delta facies and development: an example from the Infracambrian of the High Atlas, Morocco. In Nemec, W., and Steel, R. J., eds., Fan Deltas: Sedimentology and Tectonic Settings: *Blackie, London*, 212-225.

Killops, S. D., Woolhouse, A. D., Weston, R. J., and Cook, R. A. (1994). A geochemical appraisal of oil generation in the Taranaki Basin, New Zealand.*AAPG Bulletin, 78*(10), 1560-1585.

Killops, S., Cook, R., Sykes, R., and Boudou, J. (1997). Petroleum potential and oil-source correlation in the Great South and Canterbury Basins. *New Zealand Journal of Geology and Geophysics, 40*(4), 405-423.

Kimbrough, D., Tulloch, A., Geary, E., Coombs, D., and Landis, C. (1993). Isotopic ages from the Nelson region of South Island New Zealand: Crustal structure and definition of the Median Tectonic Zone. *Tectonophysics, 225*(4), 433-448.

King, P. R., and Thrasher, G. P. (1996). Cretaceous Cenozoic geology and petroleum systems of the Taranaki Basin, New Zealand (Volume 2). *Institute of Geological and Nuclear Sciences Monogram,* 13.

King, P.R., Naish, T.R., Browne, G.H., Field, B.D. and Edbrooke, S.W. (compilers) (2011). Cretaceous to Recent sedimentary patterns in New Zealand. *Institute of Geological and Nuclear Sciences Folio Series*, 1a, 35 pp.

Kirillin, G., and Shatwell, T. (2016). Generalized scaling of seasonal thermal stratification in lakes. *Earth-Science Reviews, 161*, 179-190.

Kochel, R. C., and Johnson, R. A. (1984). Geomorphology and sedimentology of humid-temperate alluvial fans, central Virginia. In Koster, E.H., and Steel, R.J., eds., Sedimentology of Gravels and Conglomerates. *Canadian Society of Petrnleum Geologists Memoir*, *10*, 109-122.

Laird, M.G. (1981): The Late Mesozoic fragmentation of the New Zealand segment of Gondwana. In Cresswell, M.M.; Vella, P. (eds.) *Gondwana Five. Proceedings of the 5$^{th}$International Gondwana Symposium, Wellington, 1980.A.A. Balkema*, 311-318.

Laird, M.G. (1993): Cretaceous continental rifts: New Zealand region. In Ballance, P.F. (ed.) *South Pacific Sedimentary Basins. Sedimentary Basins of the World, 2.Elsevier*, 37- 49.

Laird, M.G. (1994): Geological aspects of the opening of the Tasman Sea. In Vander Lingen, G.J., Swanson, K.M., Muir, R.J. (eds.) *Evolution of the Tasman Sea Basin. A.A.Balkema, Rotterdam*, 1-17.

Laird, M.G., and Bradshaw J.D., (2004). The break-up of a long-term relationship: The Cretaceous separation of New Zealand from Gondwana. *Gondwana Research*, 7(1), 273-286.

Lambiase, J. J., and Morley, C. K. (1999). Hydrocarbons in rift basins: the role of stratigraphy. *Philosophical Transactions of the Royal Society of London. Series A: Mathematical, Physical and Engineering Sciences, 357*(1753), 877-900.

Larsen, V., and Steel, R. (1978). The sedimentary history of a debris-flow dominated, Devonian alluvial fan–a study of textural inversion. *Sedimentology, 25*(1), 37-59.

Larsen, P. H., (1988). Relay structures in a Lower Permian basement-involved extension system, East Greenland, *Journal of Structural Geology*, 10, 3– 8.

Leeder, M. R. and Gawthorpe, R. L. (1987). Sedimentary models for extensional tilt-block/half-graben basins. *Geological Society, London, Special Publications, 28*(1), 139-152. https://doi.org/10.1144/gsl.Sp.1987.028.01.11

Leeder, M.R., 1995. Continental Rifts and Proto-Oceanic Rift Troughs. In: Busby, C. J., Ingersoll, R. V., eds., Tectonics of Sedimentary Basins. *Blackwell Science*. 119 – 148.

Leeder, M.R. (1999), Sedimentology in Sedimentary Basins. *In: Leeder MR, Sedimentology and Sedimentary Basins: From Turbulence to Tectonics. Blackwell Science*. 497 – 530.

Leleu, S., and Hartley, A. J. (2018). Constraints on syn-rift intrabasinal horst development from alluvial fan and aeolian deposits, Triassic Fundy Basin, Nova Scotia. In: Ventra, D. and Clarke, L.E. eds., Geology and Geomorphology of Alluvial and Fluvial Fans: Terrestrial and Planetary Perspectives. *Geological Society, London, Special Publications, 440*(1), 79-101. https://doi.org/10.1144/SP440.8

Lever, H. (1999). Paleogeography, sedimentology and basin development of the Eocene Rapahoe Group in the Punakaiki-Westport area. *University of Canterbury* (Unpublished M.Sc thesis), 237 pp.

Lewis Jr, W. M. (1983). A revised classification of lakes based on mixing. *Canadian Journal of Fisheries and Aquatic Sciences, 40*(10), 1779-1787.

Leythaeuser D. and Poelchau H. S. (1991) Expulsion of petroleum from type III kerogen source rocks in gaseous solution: Modelling of solubility fractionation. In England, W. A. and Fleet, A. J., eds., Petroleum Migration. *Geological Society, London, Special Publication, 59*(1), 33-46.

Lourens, L., andHilgen, F. (1997). Long-periodic variations in the Earth's obliquity and their relation to third-order eustatic cycles and late Neogene glaciations. *Quaternary International, 40*, 43-52.

Lowe, D.R. (1975). Water escape structures in coarse-grained sediments, *Sedimentology*, 31,749-745.

McCabe, P. J. (1984). Depositional environments of coal and coal-bearing strata. in Rahmani, R.A., and Flores, R.M., eds., Sedimentology of coal and coal-bearing sequences: *International Association of Sedimentologists, Special Publication,* 7, 13-42.

MacEachern, J.A., Pemberton, S.G., Gingras, M.K., Bann, K.L. (2010). Ichnology and facies models. In: James, N.P., Dalrymple, R.W. eds., Facies Models, edition 4: *Geological Association of Canada, St. Johns, Newfoundland*, 19–58.

Machlus, M., Enzel, Y., Goldstein, S. L., Marco, S., and Stein, M. (2000). Reconstructing low levels of Lake Lisan by correlating fan-delta and lacustrine deposits. *Quaternary International, 73*, 137-144.

Maejima W., (1988). Marine transgression over an active alluvial fan: the early Cretaceous Arida Formation, Yuasa-Aridagawa Basin, southeastern Japan, *Fan Deltas: Sedimentology and Tectonic Setting*, Eds. W. Nemec and R.J. Steel, 1988 Blackie and Son, 303-317.

Maitra, M. K., and Bassett, K. (2017). Detailed facies analysis and sequence stratigraphy of potential lacustrine source rocks, Greymouth Basin, New Zealand. *Calgary Geoconvention, Canada*.

Makaske, B., Smith, D. G., and Berendsen, H. J. (2002). Avulsions, channel evolution and floodplain sedimentation rates of the anastomosing upper Columbia River, British Columbia, Canada. *Sedimentology, 49*(5), 1049-1071.

Maltman, A.J., and Bolton, A., (2003). How sediments become mobilized. In: Van Rensbergen, P., Hillis, R.R., Maltman, A.J., Morley, C.K., eds., Subsurface Sediment Mobilization: *Geological Society London Special Publications*, 216, 9–20.

Marshall, B. A., Fenwick, M. C., and Ritchie, P. A. (2014). New Zealand recent Hyriidae (Mollusca: Bivalvia: Unionida). *Molluscan Research, 34*(3), 181-200.

Martel, A., and Gibling, M. (1991). Wave-dominated lacustrine facies and tectonically controlled cyclicity in the Lower Carboniferous Horton Bluff Formation, Nova Scotia, Canada. In Anadon, P., Cabrera, L., Kelts, K., eds., Lacustrine Facies Analysis. *International Association of Sedimentologists Special Publication*, *13*, 223–243.

Martins-Neto, M., and Catuneanu, O. (2010). Rift sequence stratigraphy. *Marine and Petroleum Geology, 27*(1), 247-253.

Martinsen, O. J., Ryseth, A., Hellland-Hansen, W., Flesche, H., Torkildsen, G., and Idil, S. (1999). Stratigraphic base level and alluvial architecture: Ericson sandstone (Campanian), rock springs uplift, SW Wyoming, USA. *Sedimentology, 46*(2), 235-263.

Mastalerz, K. (1995). Deposits of high-density turbidity currents on fan-delta slopes: an example from the upper Visean Szczawno Formation, Intrasudetic Basin, Poland. *Sedimentary Geology, 98*(1-4), 121-146.

McConnico, T., and Bassett, K. N. (2007). Gravelly Gilbert-type fan delta on the Conway Coast, New Zealand: Foreset depositional processes and clast imbrications. *Sedimentary Geology, 198*(3-4), 147-166.

McPherson, J. G., Shanmugam, G., and Moiola, R. J. (1988). Fan deltas and braid deltas: conceptual problems. In Nemec, W., and Steel, R. J., eds., Fan Deltas: Sedimentology and Tectonic Settings: *Blackie, London*, 14-22.

Melchor, R. N. (2007). Changing lake dynamics and sequence stratigraphy of syn-rift lacustrine strata in a half-graben: an example from the Triassic Ischigualasto–Villa Unión Basin, Argentina. *Sedimentology, 54*(6), 1417-1446.

Metzger, P., Berkaloff, C., Casadevall, E., andCoute, A. (1985). Alkadiene-and botryococcene-producing races of wild strains of Botryococcusbraunii. *Phytochemistry, 24*(10), 2305-2312.

Metzger, P.; Largeau, C. (2005). "*Botryococcusbraunii*: a rich source for hydrocarbons and related ether lipids". *Applied Microbiology and Biotechnology*, **66** (25), 486–96.

Mills, P. C. (1983). Genesis and diagnostic value of soft-sediment deformation structures—a review. *Sedimentary Geology, 35*(2), 83-104.

Miall, A.D. (1996). The Geology of Alluvial Deposits. *Springer-Verlag, New York*, 582.

Miall, A.D. (2010). Alluvial deposits. In: James, N.P., Dalrymple, R.W. (Eds.), Facies Models 4. *Geol. Assoc., Canada, St. John's, Newfoundland*, 105–137.

Middleton, M. (1989). A model for the formation of intracratonic sag basins. *Geophysical Journal International, 99*(3), 665-676.

Mohnhoff D., Crouch E.M., Naeher S., and Sykes R. (2017). Understanding petroleum source rock properties of mid-Cretaceous to Paleocene lacustrine mudstones in New Zealand basins. *New Zealand Petroleum Conference, Wellington, New Zealand.*

Moldowan, J. M., and Seifert, W. K. (1980). First discovery of botryococcane in petroleum. *Journal of the Chemical Society, Chemical Communications* (19), 912-914.

Monteith, F. D. (2015). Late Palaeocene-Eocene tectonic-sedimentary evolution of North Westland, Soult Island: An analysis of the Brunner Coal Measures and their basal contact. *University of Canterbury* (Unpublished master's thesis), Christchurch, New Zealand.

Moore, P. (1987). Ecological and hydrological aspects of peat formation. In Scott, A. C., eds., Coal and Coal-bearing Strata: Recent Advances. *Geological Society, London, Special Publications, 32*, 7-15.

Moore, P., Burns, B., Emmett, J., and Guthrie, D. (1992). Integrated source, maturation and migration analysis, Gippsland Basin, Australia. *Australian Petroleum Exploration Association Journal, 32*(1), 313-324.

Morellón, M., Valero-Garcés, B., Vegas-Vilarrúbia, T., González-Sampériz, P., Romero, Ó., Delgado-Huertas, A., . . . Corella, J. P. (2009). Lateglacial and Holocene palaeohydrology in the western Mediterranean region: the Lake Estanya record (NE Spain). *Quaternary Science Reviews, 28*(25-26), 2582-2599.

Moretti, M., Soria, J. M., Alfaro, P., and Walsh, N. (2001). Asymmetrical soft-sediment deformation structures triggered by rapid sedimentation in turbiditic deposits (Late Miocene, Guadix Basin, southern Spain). *Facies, 44*(1), 283-294.

Morgan, P.G. (1911). The geology of the Greymouth Subdivision, North Westland. *New Zealand Geological Survey Bulletin, 13*.

Mortimer, N., Gans, P., Calvert, A., and Walker, N. (1999). Geology and thermochronometry of the east edge of the Median Batholith (Median Tectonic Zone): a new perspective on Permian to Cretaceous crustal growth of New Zealand. *Island Arc, 8*(3), 404-425.

Mortimer, N. (2004). New Zealand's geological foundations. *Gondwana Research, 7*(1), 261-272.

Mortimer, N., Nathan, S., Jongens, R., Kawachi, Y., Ryland, C., Cooper, A., Stewart, M. and Randall, S. (2013). Regional metamorphism of the Early Palaeozoic Greenland Group, South Westland, New Zealand. *New Zealand Journal of Geology and Geophysics, 56*(1), 1-15.

Mortimer, N., Rattenbury, M. S., King, P. R., Bland, K. J., Barrell, D. J. A., Bache, F., andEdbrooke, S. W. (2014). High-level stratigraphic scheme for New Zealand rocks.*New Zealand Journal of Geology and Geophysics*, *57*(4), 402-419.

Mortimer, N., Campbell, H.J. et al. (2017). Zealandia: Earth's hidden continent. *GSA Today*, 27, 8, https://doi.org/10.1130/GSATG321A.1.

Muir, R., Ireland, T., Weaver, S., Bradshaw, J., Evans, J., Eby, G., and Shelley, D. (1998). Geochronology and geochemistry of a Mesozoic magmatic arc system, Fiordland, New Zealand. *Journal of the Geological Society, 155*(6), 1037-1053.

Muljana, B., Watanabe, K., and Rosana, M. F. (2012). Source-rock Potential of the Middle to Late Miocene Turbidite in Majalengka Sub-basin, West Java Indonesia: Related to Magmatism and Tectonism. *Journal of Novel Carbon Resource Sciences, 6*, 15-23.

Nathan, S. (1978). Sheet S44—Greymouth. Geological map of New Zealand 1:63 360. Lower Hutt, New Zealand, *Department of Scientific and Industrial Research*, *Wellington, New Zealand*.

Nathan, S., Anderson, H. J., Cook, R. A., Herzer, R., Hoskins, R., Raine, J., and Smale, D. (1986). Cretaceous and Cenozoic sedimentary basins of the West Coast region, South Island, New Zealand: *New Zealand Geological Survey basin studies1.* Wellington, Department of Scientific and Industrial Research.

Nathan, S., Rattenbury, M. S. and Suggate, R. P. (compilers) (2002). Geology of the Greymouth area: scale 1:250,000. Lower Hutt: Institute of Geological and Nuclear Sciences. Institute of Geological and Nuclear Sciences 1:250,000 geological map 12. 58 p. + 1 folded map.

Nelson, R., Patton, T., and Morley, C. (1992). Rift-Segment Interaction and Its Relation to Hydrocarbon Exploration in Continental Rift Systems (1). *AAPG Bulletin, 76*(8), 1153-1169.

Nelson C.S. and SD Hood S.D., (2016). The enigma of intricately fitted beach boulders near Raglan, New Zealand, *New Zealand Journal of Geology and Geophysics*, 59 (3), 367-381.

Nemec, W., and Steel, R. J. (1984). Alluvial and coastal conglomerates: Their significant features and comments of gravelly mass-flow deposits. In Koster, E. H., and Steel, R. J., eds., Sedimentology of Gravels and Conglomerates. *Canadian Society of Petroleum Geologists*, Memoir, *10,* 1-31.

Nemec, W. (1990). Deltas—remarks on terminology and classification. In Colella, A., and Prior, D.B., eds., Coarse-grained deltas. *International Association of Sedimentologists Special Publication*, *10*, 3-12.

Newman, J. 1981: Development of the Late Cretaceous-Paleocene Paparoa Coal Measure Basin at Greymouth. The interrelationship of differential subsidence, sedimentary facies, coal seam distribution and coal seam character. *Report to Lime and Marble Ltd. for Mines Division, Ministry of Energy*, New Zealand.

Newman, J., (1985). Paleoenvironments, coal properties, and their inter-relationships in Paparoa and selected Brunner Coal Measures on the West Coast of the South Island. *University of Canterbury* (Unpublished PhD thesis), Christchurch, New Zealand.

Newman, J. and Newman.N.A. (1992). Tectonic and paleoenvironmental controls on the distribution and properties of Upper Cretaceous coals on the West Coast of the South Island, New Zealand. In: McCabe, P. J., Parish, J. T., eds., Controls on the distribution and quality of cretaceous coals. *Geological Society of America Special Paper, 267*, 347-368.

Nilsen T. H. and Sylvetser A.G. (1995). Strike-slip Basins. *In: Busby, C. J., and Ingersoll, R. V., eds.,* Tectonics of Sedimentary Basins. *Blackwell Science.*425 – 458.

Noble, R., Wu, C., and Atkinson, C. (1991). Petroleum generation and migration from TalangAkar coals and shales offshore NW Java, Indonesia. *Organic geochemistry, 17*(3), 363-374.

Nunweek, C. N. (2001). Depositional controls on peat accumulation and coal characteristics, Dunollie and Brunner coal measures, Southern Rapahoe Sector, Greymouth (Unpublished Masters thesis). University of Canterbury, Christchurch, New Zealand.

Nunez-Betelu, L., and Baceta, J. (1994). Basics and application of Rock-Eval/TOC pyrolysis: an example from the uppermost Paleocene/lowermost Eocene in the Basque Basin, Western Pyrenees. *Munibe. Cienciasnaturales, 46*, 43-62.

O'Brien, P., and Wells, A. (1986). A small, alluvial crevasse splay. *Journal of Sedimentary Research, 56*(6), 876-879.

Orton, G. (1988). A spectrum of Middle Ordovician fan deltas and braidplain deltas, North Wales: a consequence of varying alluvial clastic input. In Nemec, W. and Steel, R. J. eds., Fan deltas: sedimentology and tectonic settings. *Glasgow, Blackie*, 23–49.

Owen, R., Crossley, R., Johnson, T., Tweddle, D., Kornfield, I., Davison, S., Eccles, D., and Engstrom, D. (1990). Major low levels of Lake Malawi and their implications for speciation rates in cichlid fishes. *Proceedings of the Royal Society of London. B. Biological Sciences, 240*(1299), 519-553.

Owen, G. (1996). Experimental soft-sediment deformation: structures formed by the liquefaction of unconsolidated sands and some ancient examples. *Sedimentology, 43*(2), 279-29.

Owen, G., and Moretti, M., (2011). Identifying triggers for liquefaction–induced soft–sediment deformation in sands. *Sedimentary Geology*, 235 (3–4), 141–147.

Peacock, D. C. P. and Sanderson D.J., (1991). Displacements, segment linkage and relay ramps in normal fault zones, Journal of Structural Geology, 13, 721–733.

Peters, K. (1986). Guidelines for evaluating petroleum source rock using programmed pyrolysis. *AAPG Bulletin, 70*(3), 318-329.

Peters, K., and Cassa, M. (1994). Applied source rock geochemistry, in Msgoon, L.B., Dow, W. G. eds., the petroleum system from source to trap. *American Association of Petroleum Geologists Memoir*, *60,* 93-120.

Phan, V. H. (2014). Observing changes in lake level and glacial thickness on the Tibetan Plateau with the ICESat laser altimeter. Ph. D. Thesis, *Delft University of Technology, Delft, The Netherlands*.

Plint, A. G., 2014, Mud dispersal across a Cretaceous prodelta: Storm-generated, wave-enhanced sediment gravity flows inferred from mudstone microtexture and microfacies: *Sedimentology, 61 (3)*, 609–647, doi:10.1111/sed.12068.

Postma, G. (1983). Water escape structures in the context of a depositional model of a mass flow dominated conglomeratic fan-delta (Abrioja Formation, Pliocene, Almeria Basin, SE Spain). *Sedimentology, 30*(1), 91-103.

Postma, G. (1984). Mass-flow conglomerates in a submarine canyon: Abrioja fan-delta, Pliocene, southeast Spain. *Sedimentology of Gravels and Conglomerates,* 10, 237−258.

Postma, G. (1990). Depositional architecture and facies of river and fan deltas: a synthesis. In *Coarse-grained deltas* (Vol. 10, pp. 13-27): International Association of Sedimentologists, Special Publication 10.

Postma, G. (1991). Water escape structures in the context of a depositional model of a mass flow dominated conglomeratic fan-delta (Abrioja Formation, Pliocene, Almeria Basin, SE Spain). *Deep-Water Turbidite Systems*, 276-276.

Postma, G. (2003). Fan delta. *Sedimentology*, 444-447.

Postma, G. and Cruickshank, C. (1988) Sedimentology of a late Weichselian to Holocene terraced fan delta, Varangerfjord, northern Norway. *In: Fan Deltas: Sedimentology and Tectonic Settings (Eds W. Nemec and R.J. Steel)*, 144–157, Blackie, London.

Postma, G., and Roep, T. B. (1985). Resedimented conglomerates in the bottomsets of Gilbert-type gravel deltas. *Journal of Sedimentary Research, 55*(6), 874-885.

Postma, G., Nemec, W., and Kleinspehn, K. L. (1988). Large floating clasts in turbidites: a mechanism for their emplacement. *Sedimentary Geology, 58*(1), 47-61.

Postma, G., Babic, L., Zupanic, J., and Roe, S. (1988). Delta front failure and associated bottomset deformation in a marine, gravelly Gilbert-type fan delta. *Fan Deltas: Sedimentology and Tectonic Settings*, 91-102.

Prior, D. B., Bornhold, B. D., and Johns, M. W. (1984) Depositional characteristics of a submarine debris flow. *Journal of Geology,* 91,707-727.

Raine, J.I. (1984). Outline of a Palynological Zonation of Cretaceous to Paleogene Terrestrial Sediments in West Coast Region, South Island, New Zealand. New Zealand Geological Survey Report 109. 82 pp.

Raine, I., Kennedy, L., Ciowes C. (2017). A vegetation and paleoclimate record from New Zealand Cretaceous coal measures. NZ Petroleum Geoscience Workshop. 28-29 September 2017.

Rattenbury, M. S. and Isaac, M. J., (2012). The QMAP 1:250 000 Geological Map of New Zealand project. *New Zealand Journal of Geology and Geophysics*, 55:393–405. doi:10.1080/00288306.2012.725417

Raven, P. H., and Axelrod, D. I. (1972). Plate tectonics and Australasian paleobiogeography. *Science, 176*(4042), 1379-1386.

Ravn, R. and Steel, R. J. (1998). Architecture of Marine Rift-Basin Successions. *AAPG Bulletin, 82 (1998)*.https://doi.org/10.1306/1d9bc3a9-172d-11d7-8645000102c1865d

Reading, H. G. (2009). Sedimentary environments: processes, facies and stratigraphy: *John Wiley and Sons,* 688 pp.

Rees, C., Palmer, J., and Palmer, A. (2018). Gilbert-style Pleistocene fan delta reveals tectonic development of North Island axial ranges, New Zealand. *New Zealand Journal of Geology and Geophysics, 61*(1), 64-78.

Renaut, R.W., Gierlowski-Kordesch E.H., (2010). Lakes. In: James NP, Dalrymple RW Facies Models 4. *Geological Association of Canada*, 541 – 575.

Rhine, J. L., and Smith, D. G. (1988). The late Pleistocene Athabasca braid delta of northeastern Alberta, Canada: a paraglacial drainage system affected by aeolian sand supply. In *Fan Deltas: Sedimentology and Tectonic Settings* (pp. 158-169): Blackie and Son.

Ricci Lucchi, F. (1968): Channelized deposits in the middle Miocene flysch of Romagna (Italy). *Giornale di Geologia*, 36, 203-282.

Roberts, S. and Jackson, J.A. (1991). Active normal faulting in central Greece: an overview. *In* Roberts, A.M., Yielding, G. and Freeman, B., eds., *The Geometry of Normal Faults. Geological Society London Special Publication*, *56*, 125-142.

Roberts, A., and Yielding, G., (1994). Continental extensional tectonics, *in* Hancock, P.L., *eds., Continental Deformation: New York, Pergamon*, 223–250.

Roberts, D.G. and Bally A.W., (2002). From rifts to passive margins: A continuum of extension. In Roberts, D.G. and Bally A.W., eds., Regional Geology and Tectonics: Phanerozoic Rift Systems and Sedimentary Basins. *Elsevier, Amsterdam, 1B*, 19-31.

Rogers, D., Astin, T., Anadon, P., Cabrera, L., and Kelts, K. (1991). Ephemeral lakes, mud pellet dunes and wind-blown sand and silt: reinterpretations of Devonian lacustrine cycles in north Scotland. In:

Anadon, P., Cabrera, L., Kelts, K., eds., Lacustrine Facies Analysis. *International Association Sedimentologists Special Publication*, 13, 199–221.

Rohais, S., Eschard, R., and Guillocheau, F. (2008). Depositional model and stratigraphic architecture of rift climax Gilbert-type fan deltas (Gulf of Corinth, Greece). *Sedimentary Geology, 210*(3-4), 132-145.

Rosendahl, B. R. (1987). Architecture of continental rifts with special reference to East Africa. *Annual Review of Earth and Planetary Sciences, 15*(1), 445-503.

Rosendahl, B. R., D. J. Reynolds, P. M. Lorber, C. F. Burgess, J. McGill, D. Scott, J. J. Lambiase, and S. J. Derksen, (1986), Structural expressions of rifting: lessons from Lake Tanganyika, Africa, *in* L. E. Frostick, R. W. Renaut, I. Reid, and J.-J. Tiercelin, eds., Sedimentation in the east-African rifts: *Geological Society, London, Special Publication,* 25, 29–43.

Ruble, T. E., Lewan, M., and Philp, R. (2001). New insights on the Green River petroleum system in the Uinta basin from hydrous pyrolysis experiments. *AAPG Bulletin, 85*(8), 1333-1371.

Ryan B. and Ledda A.(1998). A review of sulphur in coal: with specific reference to the Telkwa deposits, Northwestern British Columbia. Geological Fieldwork. *British Columbia Geological Survey Branch.*

Sagar, M. W., and Palin, J. M. (2011). Emplacement, metamorphism, deformation and affiliation of mid-Cretaceous orthogneiss from the Paparoa Metamorphic Core Complex lower-plate, Charleston, New Zealand. *New Zealand Journal of Geology and Geophysics, 54*(3), 273-289. https://doi.org/10.1080/00288306.2011.562904

Sanders, J.E. (1956). Oriented phenomena produced by sedimentation from turbidity currents and in subaqueous slope deposits, *Journal of Sedimentary Petrology*, 26, 178-179.

Sanders, J.E. (1965). Primary sedimentary structures formed by turbidity currents and related resedimentation mechanisms. In Middleton, G. V., eds., Primary sedimentary structures and their hydrodynamic interpretation, *Society for Sedimentary Geology*, *12*, 192-219.

Scherer, C. M., Goldberg, K., and Bardola, T. (2015). Facies architecture and sequence stratigraphy of an early post-rift alluvial succession, Aptian Barbalha Formation, Araripe Basin, northeastern Brazil.*Sedimentary Geology, 322*, 43-62.

Scholz, C. A. (2001). Applications of seismic sequence stratigraphy in lacustrine basins. In Last, W.M., Smol, J.P., eds., Tracking Environmental Change Using Lake Sediments. Basin Analysis, Coring and Chronological Techniques. *Springer, Berlin, 1,* 7-22.

Schulte, D. O., Ring, U., Thomson, S. N., Glodny, J., andCarrad, H. (2014). Two-stage development of the Paparoa Metamorphic Core Complex, West Coast, South Island, New Zealand: Hot continental

extension precedes sea-floor spreading by ~25 m.y. *Lithosphere, 6*(3), 177-194. https://doi.org/10.1130/l348.1.

Schumm, S.A., and Stevens, M.A., (1973). Abrasion in place: A mechanism for rounding and size reduction of coarse sediments in rivers*: Geology*, 1, 37-40.

Schuster, R. L., and Costa, J. E. (1986). A perspective of landslide dams. In Schuster, R. L., eds., Landslide dams: Processes, risk, and mitigation: *American Society of Civil Engineers Geotechnical Special Publication*, *3*, 1-20.

Schütt, B., Berking, J., Frechen, M., and Yi, C. (2008). Late Pleistocene lake level fluctuations of the Nam Co, Tibetan Plateau, China. *ZeitschriftfürGeomorphologie, Supplementary Issues, 52*(2), 57-75.

Seifert, W. K., and Moldowan, J. M. (1980). Palaeoreconstruction by biological markers. *Journals Geochimica et Cosmochimica Acta*, 45, 783-794.

Selim, S. (2017). Facies and architecture of a coarse-grained alluvial-dominated incised valley fill: a case study from the Oligocene Gebel Ahmar Formation, Southern Tethyan-shelf (northern Egypt). *Proceedings of the Geologists' Association, 128*(2), 234-255.

Selker, J.S. (1993), Expressions for the formation of load casts in soft sediments, Journal of Sedimentary Petrology, 63, 1149-1151.

Seltzer, G. O. (1994). A lacustrine record of late Pleistocene climatic change in the subtropical Andes. *Boreas, 23*(2), 105-111.

Shanley, K. W., and McCabe, P. J. (1994). Perspectives on the sequence stratigraphy of continental strata. *AAPG Bulletin, 78*(4), 544-568.

Sherwood, A., Lindqvist, J., Newman, J., and Sykes, R. (1992). Depositional controls on Cretaceous coals and coal measures in New Zealand. In McCabe, P. J., Parrish, J. T., eds., Controls on the distribution and quality of Cretaceous coals. *Geological Society of America Special Papers, 267*, 325-346.

Sibson, R. H., and Ghisetti, F. C. (2010). Characterising the seismic potential of compressional inversion structures, NW South Island. *Earthquake Commission, EQC Project*, *8*(547), 38.

Singh, H., Parkash, B., and Gohain, K. (1993). Facies analysis of the Kosimegafan deposits.*Sedimentary Geology, 85*(1-4), 87-113.

Slingerland, R., and Smith, N. D. (2004). River avulsions and their deposits. *Annu. Rev. Earth Planet. Sci., 32*, 257-285.

Smoot, J. P., and Olsen, P. E. (1988). Massive mudstones in basin analysis and paleoclimatic interpretation of the Newark Supergroup. *Developments in Geotectonics, Elsevier,22,* 249-274.

Smoot, J. P., and Olsen, P. E. (1994). Climatic cycles as sedimentary controls of rift-basin lacustrine deposits in the Early Mesozoic Newark Basin based on the continuous core. In Lomando, A.J., Schreiber, B.C., and Harris, P.M., eds., Lacustrine Reservoirs and Depositional Systems. *Society for Sedimentary Geology Core Workshop*, *19*, 201–237.

Sohn, Y.K., (1997). On traction carpet sedimentation. *Journal of Sedimentary Research,* 67, 502–509.

Sohn, Y., Kim, S., Hwang, I., Bahk, J., Choe, M., and Chough, S. (1997). Characteristics and depositional processes of large-scale gravelly Gilbert-type foresets in the Miocene Doumsan fan delta, Pohang Basin, SE Korea. *Journal of Sedimentary Research, 67*(1), 130-141.

Sohn, Y. K., Rhee, C. W., and Kim, B. C. (1999). Debris flow and hyperconcentrated flood-flow deposits in an alluvial fan, northwestern part of the Cretaceous Yongdong Basin, Central Korea. *The Journal of Geology, 107*(1), 111-132.

Song, Z., Qin, Y., George, S. C., Wang, L., Guo, J., and Feng, Z. (2013). A biomarker study of depositional paleoenvironments and source inputs for the massive formation of Upper Cretaceous lacustrine source rocks in the Songliao Basin, China.*Palaeogeography, Palaeoclimatology, Palaeoecology, 385*, 137-151.

Span, D., Dominik, J., Loizeau, J.-L., Belzile, N., andVernet, J.-P. (1992). Phosphorus trapping by turbidites in deep-lake sediments. *Chemical Geology, 102*(1-4), 73-82.

Stahl, T. (2014). Active Tectonics and Geomorphology of the central South Island, New Zealand: Earthquake Hazards of Reverse Faults. University of Canterbury, Christchurch, New Zealand.

Steadman, R. D. (2017). Provenance and porosity analysis of the Greymouth Basin, New Zealand. University of Canterbury (Unpublished master's thesis), Christchurch, New Zealand.

Steel, R., Hogseth, K., Skar, T., and Line Ros, S. (1995). Sequence architecture in a alluvial succession: sequence stratigraphy in the Upper Cretaceous Mesaverde Group, Price Canyon, Utah. *Journal of Sedimentary Research B, 65*, 265-280.

Stirling, M.W., McVerry, G., Gerstenberger, M., Litchfield, N.J., Van Dissen, R.J., Berryman, K.R., Barnes, P.M., Wallace, L., Villamor, P., Langridge, R., Lamarche, G., Nodder, S., Reyners, M., Bradley, B., Rhoades, D., Smith, W., Nicol, A., Pettinga, J., Clark, K., Jacobs, K., (2012). National Seismic Hazard Model for New Zealand. *Bulletin of the Seismological Society of America*, 102, 1514-1542, doi:10.1785/0120110170.

Stow, D. A. V., Reading, H. G., Collinson, J. D., (1996). Deep seas. In Reading, H. G., eds., *Sedimentary Environments: Processes, Facies and Stratigraphy, 3rd Edition, Blackwell Science,* 395 – 453.

Street, F. A., and Grove, A. (1976). Environmental and climatic implications of late Quaternary lake-level fluctuations in Africa. *Nature, 261*(5559), 385.

Strogen, D. P., Seebeck, H., Nicol, A., and King, P. R. (2017). Two-phase Cretaceous–Paleocene rifting in the Taranaki Basin region, New Zealand; implications for Gondwana break-up. *Journal of the Geological Society, 174*(5), 929-946. https://doi.org/10.1144/jgs2016-160

Strom, A. (2013). Geological prerequisites for landslide dams' disaster assessment and mitigation in Central Asia. In *Progress of Geo-Disaster Mitigation Technology in Asia* (pp. 17-53): Springer.

Stromberg, S.G. and Bluck, B. (1998). Turbidite facies, fluid escape structures and mechanisms of emplacement of the Oligo-Miocene Aljibe Flysch, Gibraltar Arc, Betics, southern Spain, *Sedimentary Geology*, 115, 267-288.

Sturm, M., and Matter, A. (2009). Turbidites and varves in Lake Brienz (Switzerland): deposition of elastic detritus by density. *Lake Sediments, 104*, 147.

Suggate, R. P. (2013). Late Cretaceous and Paleogene stratigraphy and structure linking offshore with onshore north Westland, New Zealand. *New Zealand Journal of Geology and Geophysics, 56*(4), 263-275. https://doi.org/10.1080/00288306.2013.844720

Suggate, R. P. (2014). Extensional basin development and subsequent inversion in Greymouth Coalfield. *New Zealand Journal of Geology and Geophysics, 58*(1), 1-12. https://doi.org/10.1080/00288306.2014.978341

Suggate, P., and Waight, T. E. (1998). Geology of the Kumara-Moana area. *Institute of Geological and Nuclear Sciences geological map 24*, 1 map+120 p.

Sultwold, H.H. Jr (1959): Nomenclature of load deformation in turbidites. – *Geological Society of American Bulletin*, 70, 1247-1248.

Sykes, R., and Snowdon, L. (2002). Guidelines for assessing the petroleum potential of coaly source rocks using Rock-Eval pyrolysis. *Organic geochemistry, 33*(12), 1441-1455.

Sykes, R., Volk, H., George, S., Ahmed, M., Higgs, K., Johansen, P., and Snowdon, L. (2014). Marine influence helps preserve the oil potential of coaly source rocks: Eocene Mangahewa Formation, Taranaki Basin, New Zealand. *Organic geochemistry, 66*, 140-163.

Tambach, T. J., Veld, H., and Griffioen, J. (2009). Influence of HCl/HF treatment on organic matter in aquifer sediments: a Rock-Eval pyrolysis study. *Applied Geochemistry, 24*(11), 2144-2151.

Thul D (2012). Niobara source rock maturity in the Denver Basin: A study of differential heating and tectonics on petroleum prospectivity using programmed pyrolysis. Masters thesis Colourado School of Mines, Colourado, USA.

Tissot, B., Durand, B., Espitalie, J., and Combaz, A. (1974). Influence of nature and diagenesis of organic matter in formation of petroleum. *AAPG Bulletin, 58*(3), 499-506.

Tissot, B., and Welte, D. (1984). Petroleum Formation and Occurrence, 2nd edn, *Springer-Verlag, Berlin, Germany,* 699.

Tissot, B. P. and D. H. Welte (1984). Petroleum formation and occurrence: *Berlin, Springer-Verlag*, 699.

Tissot, B., Pelet, R., andUngerer, P. (1987). Thermal history of sedimentary basins, maturation indices, and kinetics of oil and gas generation. *AAPG Bulletin, 71*(12), 1445-1466.

Toonen, W. H., Kleinhans, M. G., and Cohen, K. M. (2012). Sedimentary architecture of abandoned channel fills. *Earth surface processes and landforms, 37*(4), 459-472.

Topal, S., andÖzkul, M. (2014). Soft-sediment deformation structures interpreted as seismites in the Kolankaya formation, Denizli basin (SW Turkey). *The Scientific World Journal, 2014,* 1-13. http://dx.doi.org/10.1155/2014/352654

Turnbull, I.M., Uruski, C.I. et al., (1993). Cretaceous and Cenozoic sedimentary basins of western Southland, South Island, New Zealand. *Institute of Geological and Nuclear Sciences Monograph*, 1, Lower Hutt, New Zealand

Tanaka, J., and Maejima, W. (1995). Fan-delta sedimentation on the basin margin slope of the Cretaceous, strike-slip Izumi Basin, southwestern Japan. *Sedimentary Geology, 98*(1-4), 205-213.

Teichmüller, M. (1989). The genesis of coal from the viewpoint of coal petrology. *International Journal of Coal Geology, 12*(1-4), 1-87.

Tulloch, A.J.; Kimbrough, D.L. (1989). The Paparoa metamorphic core complex, New Zealand: Cretaceous extension associated with the fragmentation of the Pacific margin of Gondwana. *Tectonics, 8*, 1217-1234.

Turkman I, Aksoy E, Taşgin CK, (2007). Alluvial and lacustrine facies in an extensional basin: The Miocene of Malataya basin, Eastern Turkey. *Journal of Asian Earth Science,* 30,181 – 198.

Tye, R., and Kosters, E. (1986). Styles of interdistributary basin sedimentation: south-central Louisiana: *Gulf Coast Assoc. Geol. Socs. Trans, 36*, 575-588.

Uruski, C. I., 2010, New Zealand's deepwater frontier: *Marine and Petroleum Geology, 27(9),* 2005–2026, doi: 10.1016/j.marpetgeo.2010.05.010.

Van Houten, F. B. (1962). Cyclic sedimentation and the origin of analcime-rich Upper Triassic Lockatong Formation, west-central New Jersey and adjacent Pennsylvania. *American Journal of Science, 260*(8), 561-576.

Van Houten, F.B. (1964). Cyclic lacustrine sedimentation, Upper Triassic Lockatong Forma1ion, central New Jersey and adjace111 Pennsylvania. Kans., Slate Geol. Surv., Bull., 169: 497 - 531.

Van Wagoner, J. C. (1995). Sequence stratigraphy and marine to nonmarine facies architecture of foreland basin strata, Book Cliffs, Utah, USA. In Van Wagoner, J.C., and Bertram, G.T., eds., Sequence Stratigraphy of Foreland Basin Deposits. *American Association of Petroleum Geologists, Memoir*, *64*, 137–223.

Van Wagoner, J., Posamentier, H., Mitchum, R., Vail, P., Sarg, J., Loutit, T., and Hardenbol, J. (1988). An overview of the fundamentals of sequence stratigraphy and key definitions.

Van Wagoner, J. C., Posamentier, H. W., Mitchum, R. M. Jr., Vail, P. R., Sarg, J. F., Loutit, T. S., and Hardenbol, J. (1988). An overview of sequence stratigraphy and key definitions. In Wilgus, C. K., Hastings, B. S., Kendall, C. G. St. C., Posamentier, H. W., Ross, C. A., and Van Wagoner, J. C., eds., Sea Level Changes–An Integrated Approach, *Society for Sedimentary Geology Special Publication, 42,* 39–45.

Van Loon, A., and Brodzikowski, K. (1987). Problems and progress in the research on soft-sediment deformations. *Sedimentary Geology, 50*(1-3), 167-193.

Van Loon, A. (1992). The recognition of soft-sediment deformations as early-diagenetic features–a literature review. In *Developments in Sedimentology* (Vol. 47, pp. 135-189): Elsevier.

Ventra, D., and Clarke, L. E. (2018). Geology and geomorphology of alluvial and alluvial fans: current progress and research perspectives. *Geological Society, London, Special Publications, 440*(1), 1-21.

Volkman, J. (1988). Biological marker compounds as indicators of the depositional environments of petroleum source rocks. In Fleet, A. J. et al., eds., Lacustrine petroleum source rocks. *Geological Society, London, Special Publications, 40*(1), 103-122.

Wadsworth, J., Diessel, C., Boyd, R., Ratcliffe, K., and Zaitlin, B. (2010). The sequence stratigraphic significance of paralic coal and its use as an indicator of accommodation space in terrestrial sediments. in: Ratcliffe, K.T., Taitlin, B.A., eds., Application of modern stratigraphic techniques: Theory and case histories. *Society for Sedimentary Geology Special Publication, 94*, 201-221.

Wanas, H., Sallam, E., Zobaa, M., and Li, X. (2015). Mid-Eocene alluvial-lacustrine succession at Gebel El-Goza El-Hamra (Shabrawet area, NE Eastern Desert, Egypt): facies analysis, sequence stratigraphy and paleoclimatic implications. *Sedimentary Geology, 329*, 115-129.

Walther, M., Dashtseren, A., Kamp, U., Temujin, K., Meixner, F., Pan, C. G., and Gansukh, Y. (2017). Glaciers, Permafrost and Lake Levels at the Tsengel Khairkhan Massif, Mongolian Altai, During the Late Pleistocene and Holocene. *Geosciences, 7*(3), 73.

Waples DW. (1994). Maturity modelling: Thermal indicators, hydrocarbon generation, and oilcracking. *American Association of Petroleum Geologists Bulletin,*60, 285-306.

Ward, S. (1995). Controls on sedimentology and coal occurrence in the Rewanui Coal Measure Member, Western Greymouth Coalfield (Rapahoe Sector). *Proceedings, 6th New Zealand Coal Conference, Wellington, October 1995,*151-161.

Ward, S. (1996). Application of lithostratigraphic and chronostratigraphic analysis to seam modelling in the Rapahoe Sector, western Greymouth Coalfield, The changing face of West Coast mining. *The Australasian Institute of Mining and Metallurgy, New Zealand Branch, 29th Annual Conference, Greymouth*.173-199.

Ward S.D., (1997). Lithostratigraphy, palynostratigraphy and basin analysis of the Late Cretaceous to early Tertiary Paparoa Group, Greymouth Coalfield, New Zealand. PhD Thesis, *University of Canterbury*, New Zealand.

Wei, W., Lu, Y., Xing, F., Liu, Z., Pan, L., andAlgeo, T. J. (2017). Sedimentary facies associations and sequence stratigraphy of source and reservoir rocks of the lacustrine Eocene Niubao Formation (Lunpola Basin, central Tibet). *Marine and Petroleum Geology, 86*, 1273-1290.

Weissmann, G., Hartley, A., Nichols, G., Scuderi, L., Olson, M., Buehler, H., and Banteah, R. (2010). Alluvial form in modern continental sedimentary basins: distributive alluvial systems. *Geology, 38*(1), 39-42.

Wellman, H., (1971). Geology of the Kotuku Oilfield, Westland-New Zealand: *New Zealand Geological Survey report*, *48*, 46 p.

Wells, N. A., (1984). Sheet debris flow and sheetflood conglomerates in Cretaceous cool-maritime alluvial fans, South Orkney Island, Antarctica, In: Koster, E.H. and Steel R.J. (Eds.), *Sedimentology of gravels and conglomerates, Canadian Society of Petroleum Geologists*, 10, 133-145.

Wescott, W., (1988). A late Permian fan-delta system in the southern Morondava Basin, Madagascar. In Nemec W, and Steel R. J., eds., *Fan deltas: Sedimentology and tectonic settings. Blackie, Glasgow*, 226-238.

Wescott, W. A., and Ethridge, F. G. (1980). Fan-delta sedimentology and tectonic setting--Yallahs fan delta, southeast Jamaica. *AAPG Bulletin, 64*(3), 374-399.

Wilhelm, S., and Adrian, R. (2008). Impact of summer warming on the thermal characteristics of a polymictic lake and consequences for oxygen, nutrients and phytoplankton. *Freshwater Biology, 53*(2), 226-237.

Williams, M., Bishop, P. M., Dakin, F. M., and Gillespie, R. (1977). Late Quaternary lake levels in southern Afar and the adjacent Ethiopian Rift. *Nature, 267*(5613), 690.

Withjack, M. O., Schlische, R. W., and Olsen, P. E. (1998). Diachronous rifting, drifting, and inversion on the passive margin of central eastern North America: an analog for other passive margins. *AAPG Bulletin, 82*(5), 817-835.

Withjack, M. O., Schlische, R. W., and Olsen, P. E. (2002). Rift-basin structure and its influence on sedimentary systems. In: Renaut, R.W., Ashley, G.M., eds., Sedimentation in Continental Rifts. *Society for Sedimentary Geology Special Publication*, 73, 57-81.

Wolf, Fred R.; Nonomura, Arthur M.; Bassham, James A. (1985). "Growth and Branched Hydrocarbon Production in a Strain of Botryococcusbraunii (Chlorophyta)1". *Journal of Phycology*, 21 (3): 388. doi:10.1111/j.0022-3646.1985.00388.x.

Wolfenden, E., Ebinger, C., Yirgu, G., Deino, A., andAyalew, D. (2004). Evolution of the northern Main Ethiopian rift: birth of a triple junction. *Earth and Planetary Science Letters, 224*(1-2), 213-228.

Woolway, R. I., and Merchant, C. J. (2019). Worldwide alteration of lake mixing regimes in response to climate change. *Nature Geoscience, 12*(4), 271.

Wu, J. E., McClay, K., Whitehouse, P., and Dooley, T. (2009). 4D analogue modelling of transtensional pull-apart basins. *Marine and Petroleum Geology, 26*(8), 1608-1623

Zavala, C., and Pan, S. (2018). Hyperpycnal flows and hyperpycnites: Origin and distinctive characteristics. *Lithologic Reservoirs, 30*(1), 1-27.

Zink, K.-G., Sykes, R. (2010). Geochemical database and interpretation of 10 oils from several New Zealand basins, *GNS Science Report 2009/13*. 59p.

# Appendix 1: Twelve Mile Beach stratigraphy

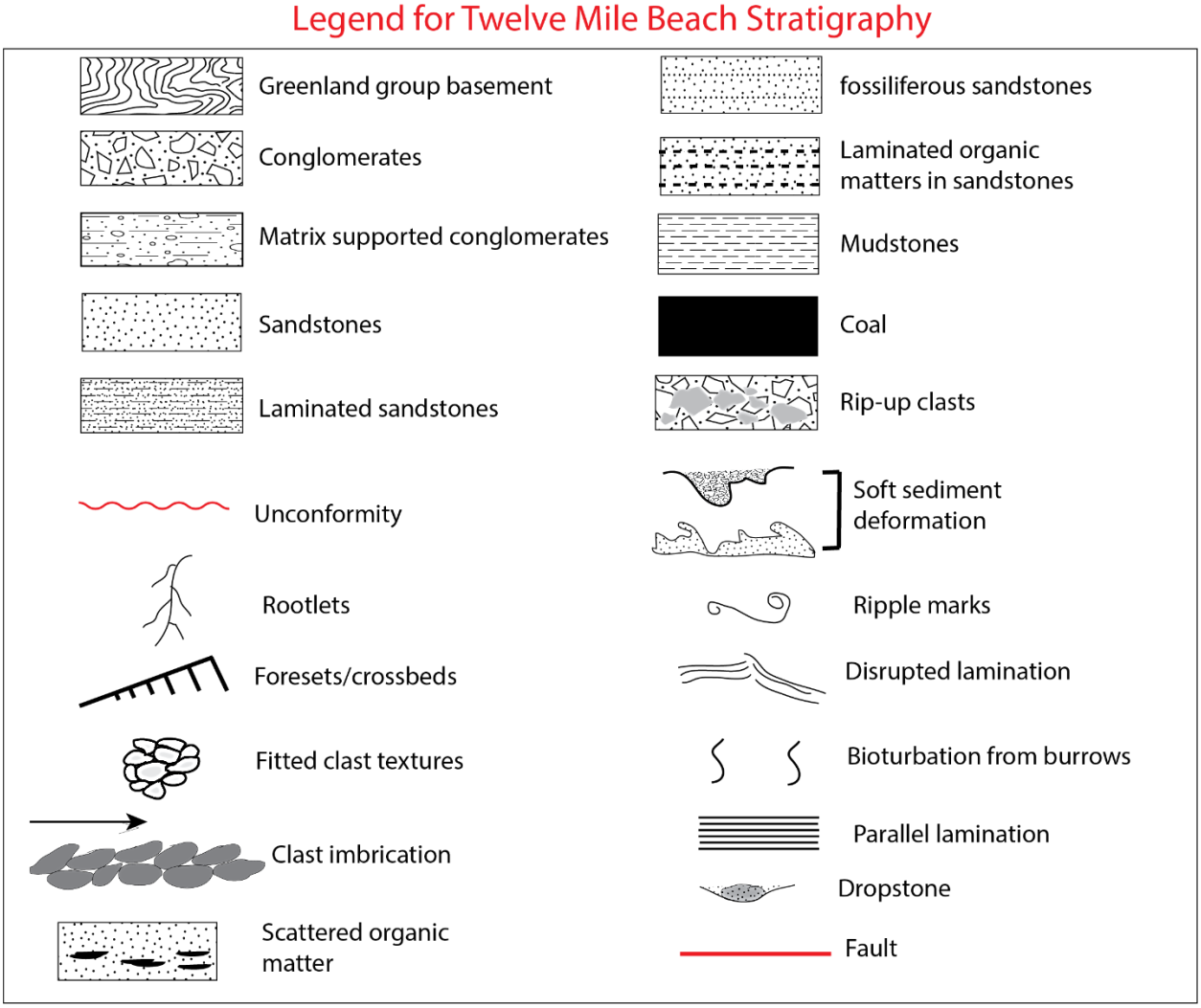

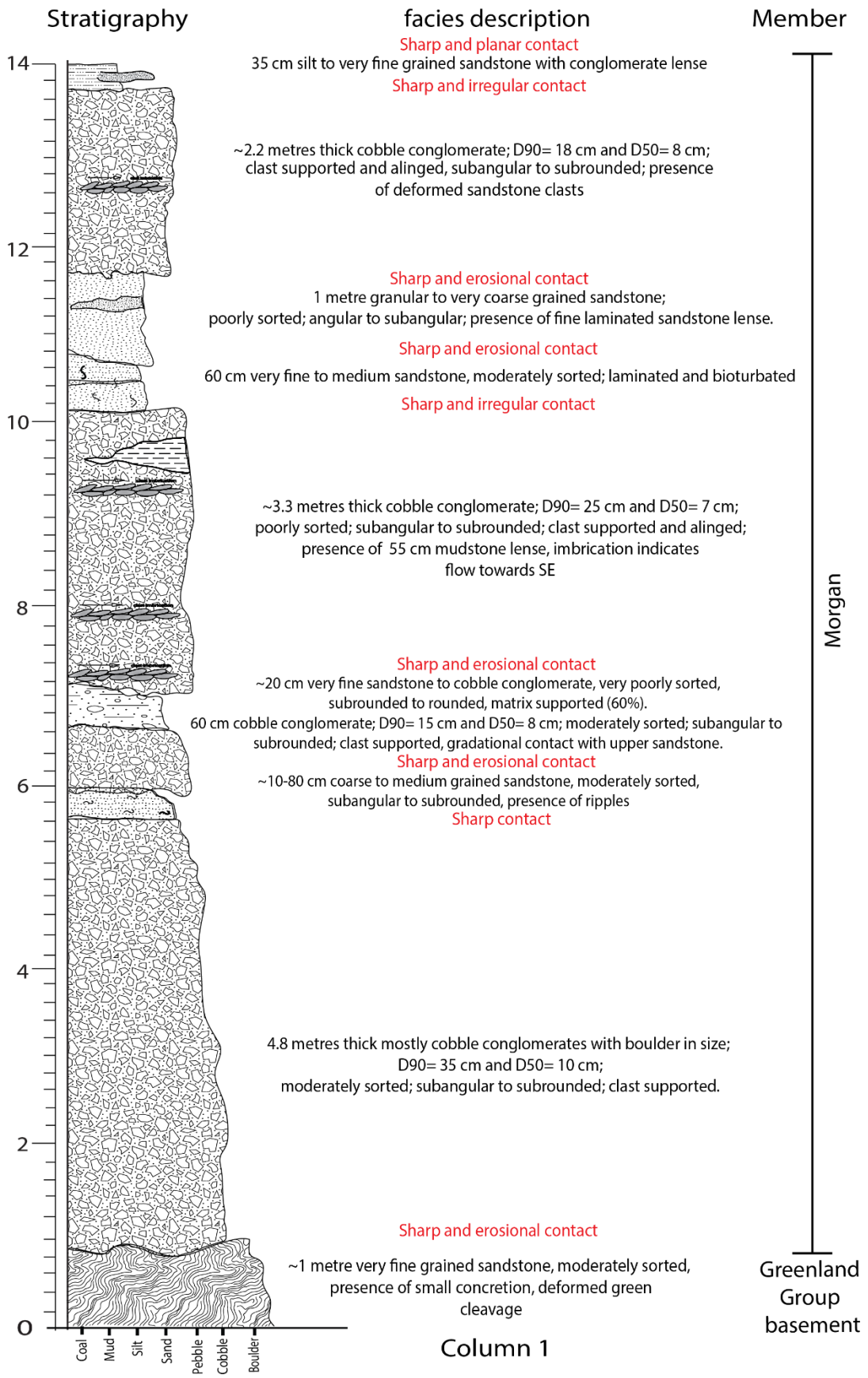
Stratigraphy
facies description
Member
Sharp and planar contact
35 cm silt to very fine grained sandstone with conglomerate lense
Sharp and irregular contact
~2.2 metres thick cobble conglomerate; D90= 18 cm and D50= 8 cm;
clast supported and alinged, subangular to subrounded; presence
of deformed sandstone clasts
Sharp and erosional contact
1 metre granular to very coarse grained sandstone;
poorly sorted; angular to subangular; presence of fine laminated sandstone lense.
Sharp and erosional contact
60 cm very fine to medium sandstone, moderately sorted; laminated and bioturbated
Sharp and irregular contact
~3.3 metres thick cobble conglomerate; D90= 25 cm and D50= 7 cm;
poorly sorted; subangular to subrounded; clast supported and alinged;
presence of 55 cm mudstone lense, imbrication indicates
flow towards SE
Sharp and erosional contact
~20 cm very fine sandstone to cobble conglomerate, very poorly sorted,
subrounded to rounded, matrix supported (60%).
60 cm cobble conglomerate; D90= 15 cm and D50= 8 cm; moderately sorted; subangular to
subrounded; clast supported, gradational contact with upper sandstone.
Sharp and erosional contact
~10-80 cm coarse to medium grained sandstone, moderately sorted,
subangular to subrounded, presence of ripples
Sharp contact
4.8 metres thick mostly cobble conglomerates with boulder in size;
D90= 35 cm and D50= 10 cm;
moderately sorted; subangular to subrounded; clast supported.
Sharp and erosional contact
~1 metre very fine grained sandstone, moderately sorted,
presence of small concretion, deformed green
cleavage
14
12
10
8
6
4
2
0
Coal
Mud
Silt
Sand
Pebble
Cobble
Boulder
Column 1
Morgan
Greenland
Group
basement

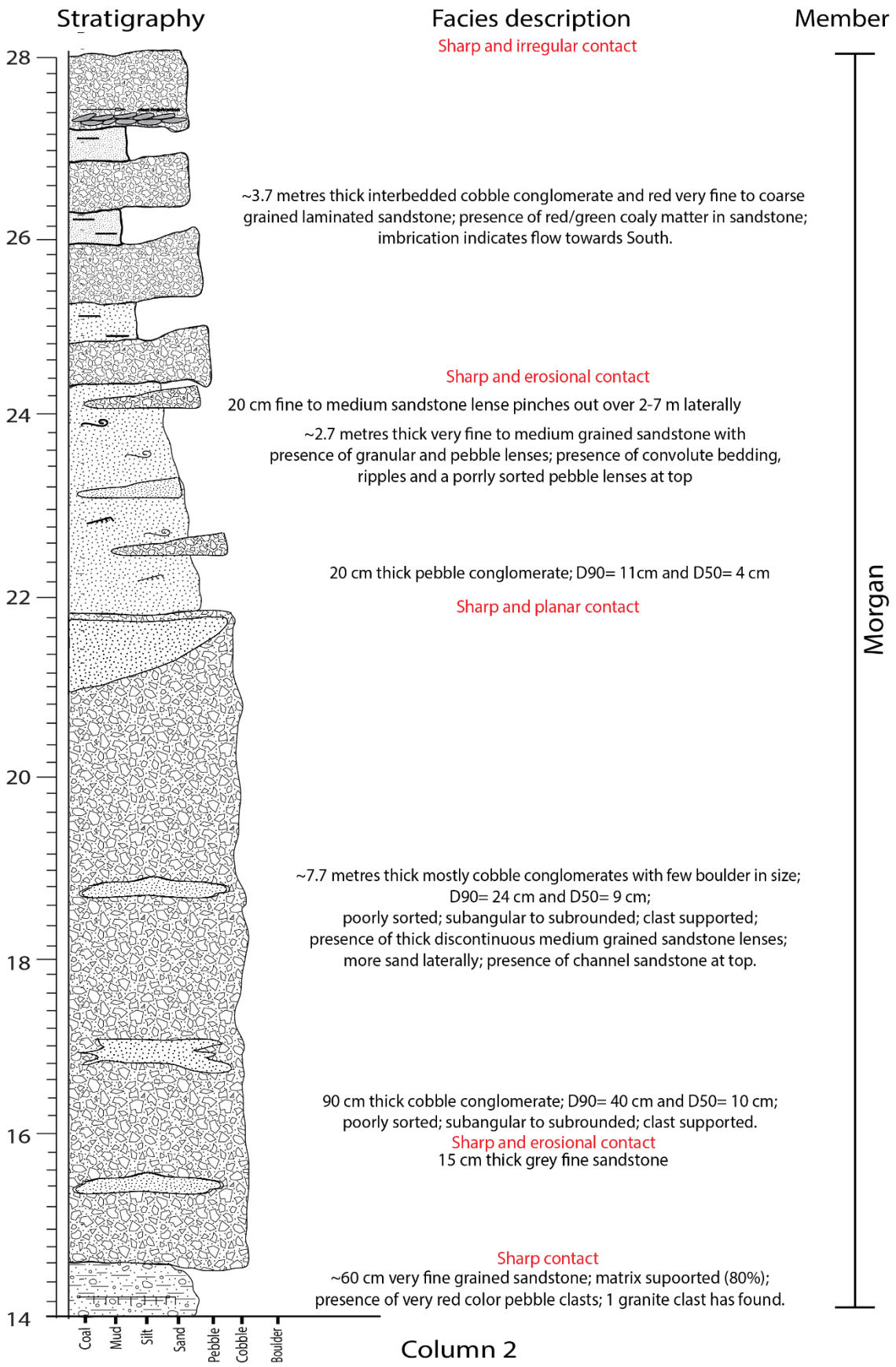
Stratigraphy
Facies description
Member
Sharp and irregular contact
~3.7 metres thick interbedded cobble conglomerate and red very fine to coarse grained laminated sandstone; presence of red/green coaly matter in sandstone; imbrication indicates flow towards South.
Sharp and erosional contact
20 cm fine to medium sandstone lense pinches out over 2-7 m laterally
~2.7 metres thick very fine to medium grained sandstone with presence of granular and pebble lenses; presence of convolute bedding, ripples and a porrly sorted pebble lenses at top
20 cm thick pebble conglomerate; D90= 11cm and D50= 4 cm
Sharp and planar contact
~7.7 metres thick mostly cobble conglomerates with few boulder in size; D90= 24 cm and D50= 9 cm; poorly sorted; subangular to subrounded; clast supported; presence of thick discontinuous medium grained sandstone lenses; more sand laterally; presence of channel sandstone at top.
90 cm thick cobble conglomerate; D90= 40 cm and D50= 10 cm; poorly sorted; subangular to subrounded; clast supported.
Sharp and erosional contact
15 cm thick grey fine sandstone
Sharp contact
~60 cm very fine grained sandstone; matrix supoorted (80%); presence of very red color pebble clasts; 1 granite clast has found.
Morgan
28
26
24
22
20
18
16
14
Coal
Mud
Silt
Sand
Pebble
Cobble
Boulder
Column 2

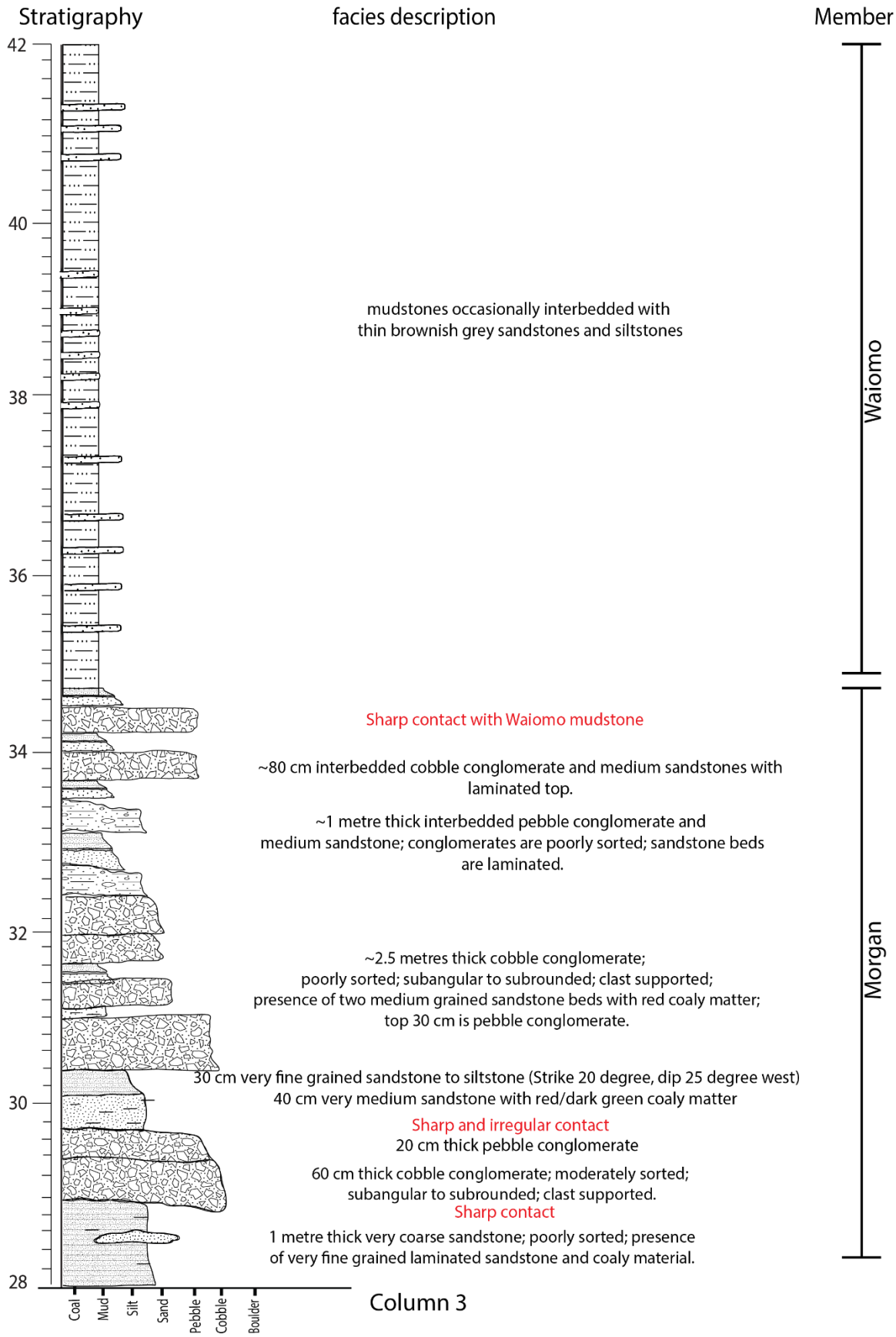
Stratigraphy
facies description
Member
42
40
38
36
34
32
30
28
mudstones occasionally interbedded with
thin brownish grey sandstones and siltstones
Waiomo
Sharp contact with Waiomo mudstone
~80 cm interbedded cobble conglomerate and medium sandstones with
laminated top.
~1 metre thick interbedded pebble conglomerate and
medium sandstone; conglomerates are poorly sorted; sandstone beds
are laminated.
~2.5 metres thick cobble conglomerate;
poorly sorted; subangular to subrounded; clast supported;
presence of two medium grained sandstone beds with red coaly matter;
top 30 cm is pebble conglomerate.
30 cm very fine grained sandstone to siltstone (Strike 20 degree, dip 25 degree west)
40 cm very medium sandstone with red/dark green coaly matter
Sharp and irregular contact
20 cm thick pebble conglomerate
60 cm thick cobble conglomerate; moderately sorted;
subangular to subrounded; clast supported.
Sharp contact
1 metre thick very coarse sandstone; poorly sorted; presence
of very fine grained laminated sandstone and coaly material.
Morgan
Coal
Mud
Silt
Sand
Pebble
Cobble
Boulder
Column 3

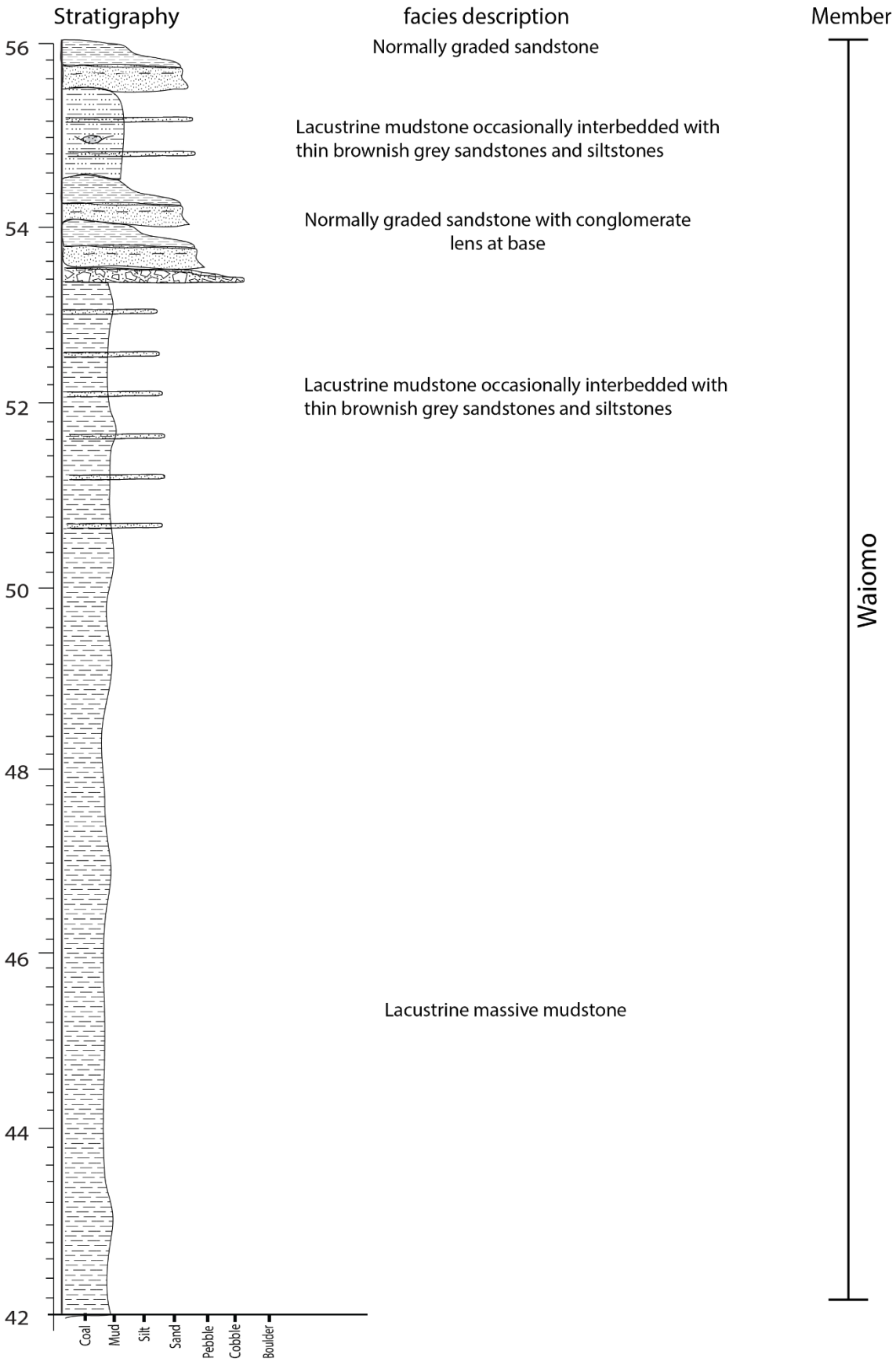
Stratigraphy
facies description
Member
56
54
52
50
48
46
44
42
Normally graded sandstone
Lacustrine mudstone occasionally interbedded with thin brownish grey sandstones and siltstones
Normally graded sandstone with conglomerate lens at base
Lacustrine mudstone occasionally interbedded with thin brownish grey sandstones and siltstones
Lacustrine massive mudstone
Waiomo
Coal
Mud
Silt
Sand
Pebble
Cobble
Boulder

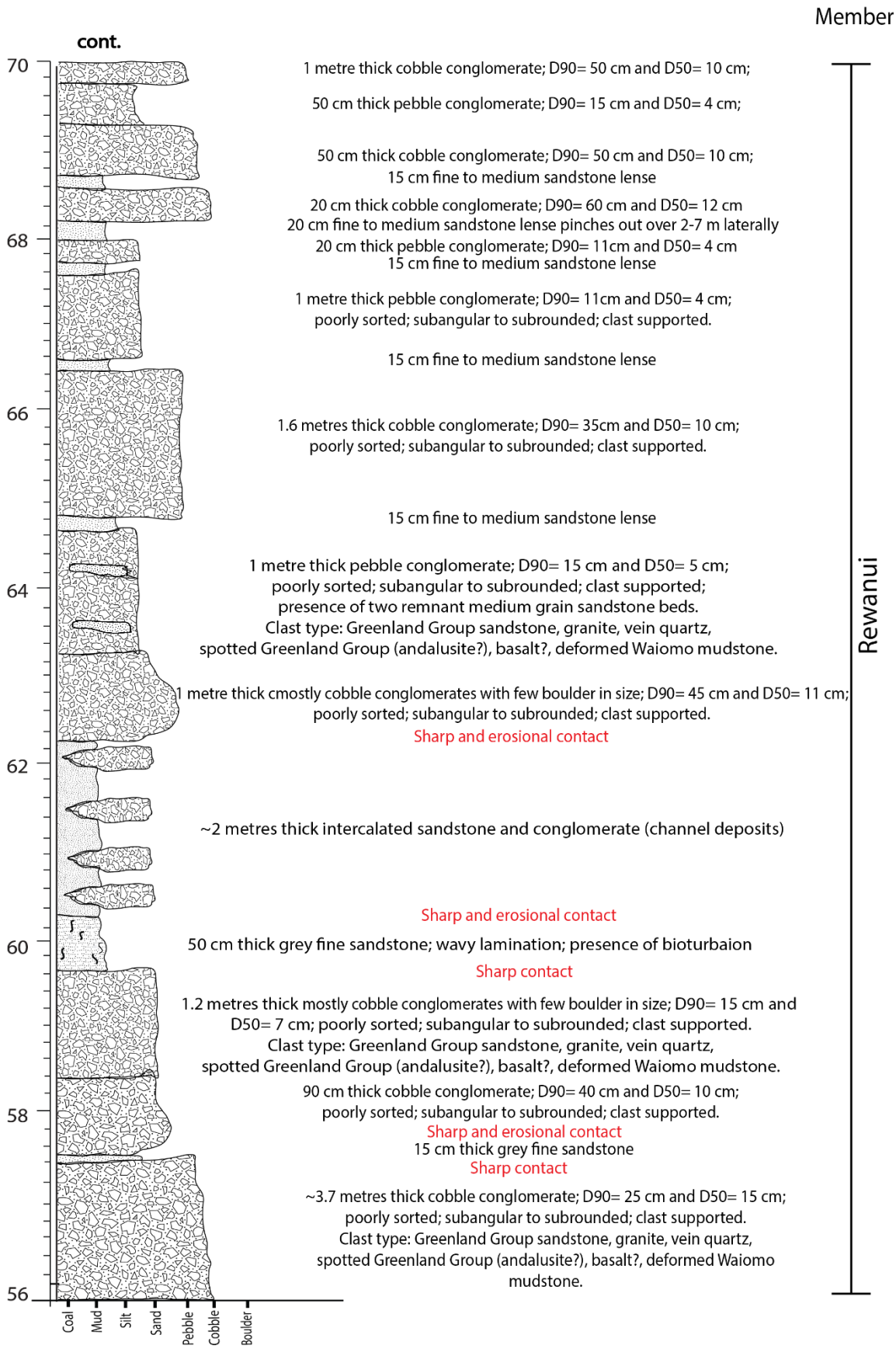
Member
cont.
70
68
66
64
62
60
58
56
1 metre thick cobble conglomerate; D90= 50 cm and D50= 10 cm;
50 cm thick pebble conglomerate; D90= 15 cm and D50= 4 cm;
50 cm thick cobble conglomerate; D90= 50 cm and D50= 10 cm;
15 cm fine to medium sandstone lense
20 cm thick cobble conglomerate; D90= 60 cm and D50= 12 cm
20 cm fine to medium sandstone lense pinches out over 2-7 m laterally
20 cm thick pebble conglomerate; D90= 11cm and D50= 4 cm
15 cm fine to medium sandstone lense
1 metre thick pebble conglomerate; D90= 11cm and D50= 4 cm;
poorly sorted; subangular to subrounded; clast supported.
15 cm fine to medium sandstone lense
1.6 metres thick cobble conglomerate; D90= 35cm and D50= 10 cm;
poorly sorted; subangular to subrounded; clast supported.
15 cm fine to medium sandstone lense
1 metre thick pebble conglomerate; D90= 15 cm and D50= 5 cm;
poorly sorted; subangular to subrounded; clast supported;
presence of two remnant medium grain sandstone beds.
Clast type: Greenland Group sandstone, granite, vein quartz,
spotted Greenland Group (andalusite?), basalt?, deformed Waiomo mudstone.
1 metre thick cmostly cobble conglomerates with few boulder in size; D90= 45 cm and D50= 11 cm;
poorly sorted; subangular to subrounded; clast supported.
Sharp and erosional contact
~2 metres thick intercalated sandstone and conglomerate (channel deposits)
Sharp and erosional contact
50 cm thick grey fine sandstone; wavy lamination; presence of bioturbaion
Sharp contact
1.2 metres thick mostly cobble conglomerates with few boulder in size; D90= 15 cm and
D50= 7 cm; poorly sorted; subangular to subrounded; clast supported.
Clast type: Greenland Group sandstone, granite, vein quartz,
spotted Greenland Group (andalusite?), basalt?, deformed Waiomo mudstone.
90 cm thick cobble conglomerate; D90= 40 cm and D50= 10 cm;
poorly sorted; subangular to subrounded; clast supported.
Sharp and erosional contact
15 cm thick grey fine sandstone
Sharp contact
~3.7 metres thick cobble conglomerate; D90= 25 cm and D50= 15 cm;
poorly sorted; subangular to subrounded; clast supported.
Clast type: Greenland Group sandstone, granite, vein quartz,
spotted Greenland Group (andalusite?), basalt?, deformed Waiomo
mudstone.
Rewanui
Coal
Mud
Silt
Sand
Pebble
Cobble
Boulder

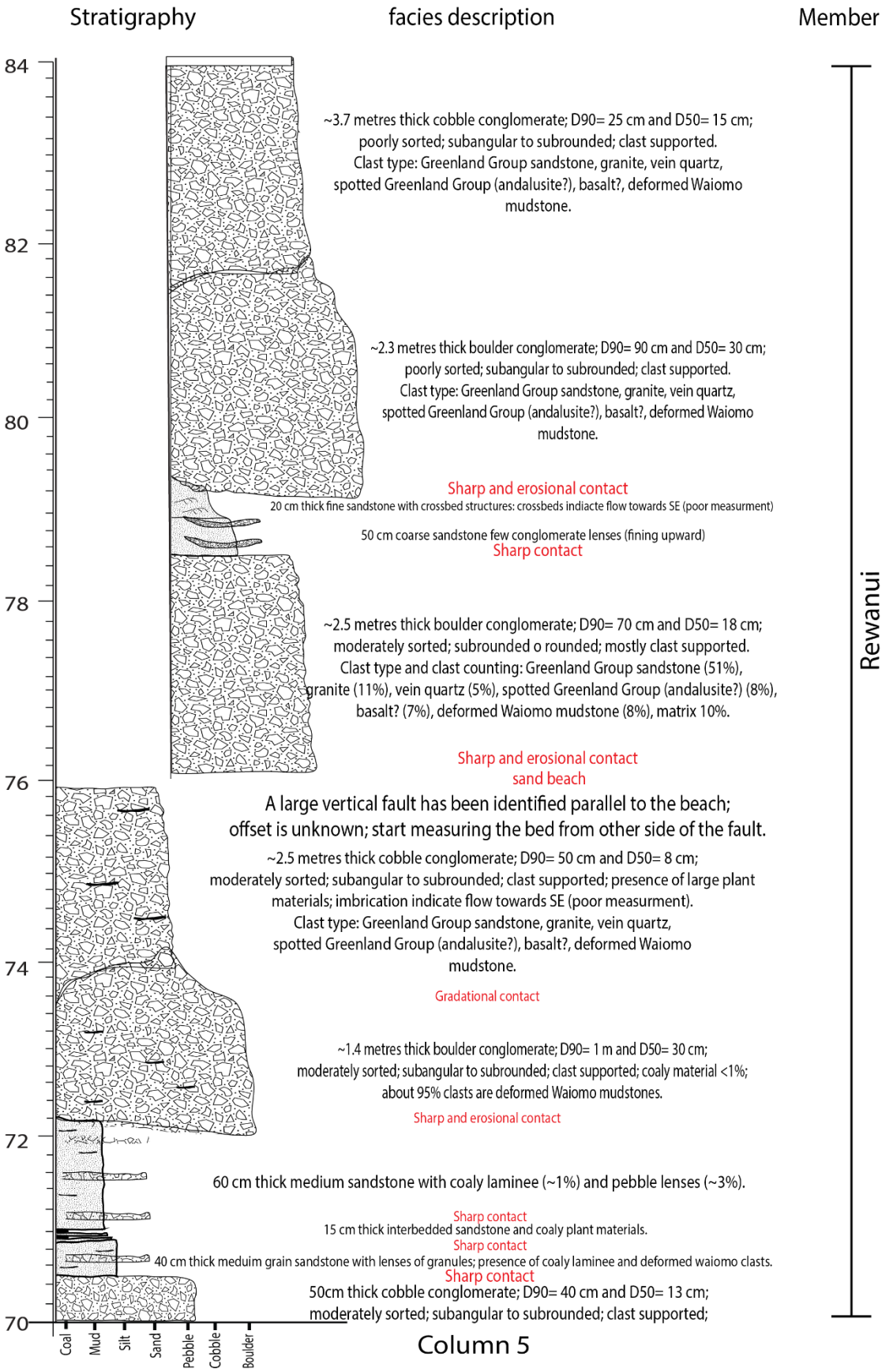
Stratigraphy
facies description
Member
84
82
80
78
76
74
72
70
~3.7 metres thick cobble conglomerate; D90= 25 cm and D50= 15 cm; poorly sorted; subangular to subrounded; clast supported. Clast type: Greenland Group sandstone, granite, vein quartz, spotted Greenland Group (andalusite?), basalt?, deformed Waiomo mudstone.
~2.3 metres thick boulder conglomerate; D90= 90 cm and D50= 30 cm; poorly sorted; subangular to subrounded; clast supported. Clast type: Greenland Group sandstone, granite, vein quartz, spotted Greenland Group (andalusite?), basalt?, deformed Waiomo mudstone.
Sharp and erosional contact
20 cm thick fine sandstone with crossbed structures: crossbeds indiacte flow towards SE (poor measurment)
50 cm coarse sandstone few conglomerate lenses (fining upward)
Sharp contact
~2.5 metres thick boulder conglomerate; D90= 70 cm and D50= 18 cm; moderately sorted; subrounded o rounded; mostly clast supported. Clast type and clast counting: Greenland Group sandstone (51%), granite (11%), vein quartz (5%), spotted Greenland Group (andalusite?) (8%), basalt? (7%), deformed Waiomo mudstone (8%), matrix 10%.
Sharp and erosional contact
sand beach
A large vertical fault has been identified parallel to the beach; offset is unknown; start measuring the bed from other side of the fault.
~2.5 metres thick cobble conglomerate; D90= 50 cm and D50= 8 cm; moderately sorted; subangular to subrounded; clast supported; presence of large plant materials; imbrication indicate flow towards SE (poor measurment). Clast type: Greenland Group sandstone, granite, vein quartz, spotted Greenland Group (andalusite?), basalt?, deformed Waiomo mudstone.
Gradational contact
~1.4 metres thick boulder conglomerate; D90= 1 m and D50= 30 cm; moderately sorted; subangular to subrounded; clast supported; coaly material <1%; about 95% clasts are deformed Waiomo mudstones.
Sharp and erosional contact
60 cm thick medium sandstone with coaly laminee (~1%) and pebble lenses (~3%).
Sharp contact
15 cm thick interbedded sandstone and coaly plant materials.
Sharp contact
40 cm thick meduim grain sandstone with lenses of granules; presence of coaly laminee and deformed waiomo clasts.
Sharp contact
50cm thick cobble conglomerate; D90= 40 cm and D50= 13 cm; moderately sorted; subangular to subrounded; clast supported;
Coal
Mud
Silt
Sand
Pebble
Cobble
Boulder
Rewanui

Column 5

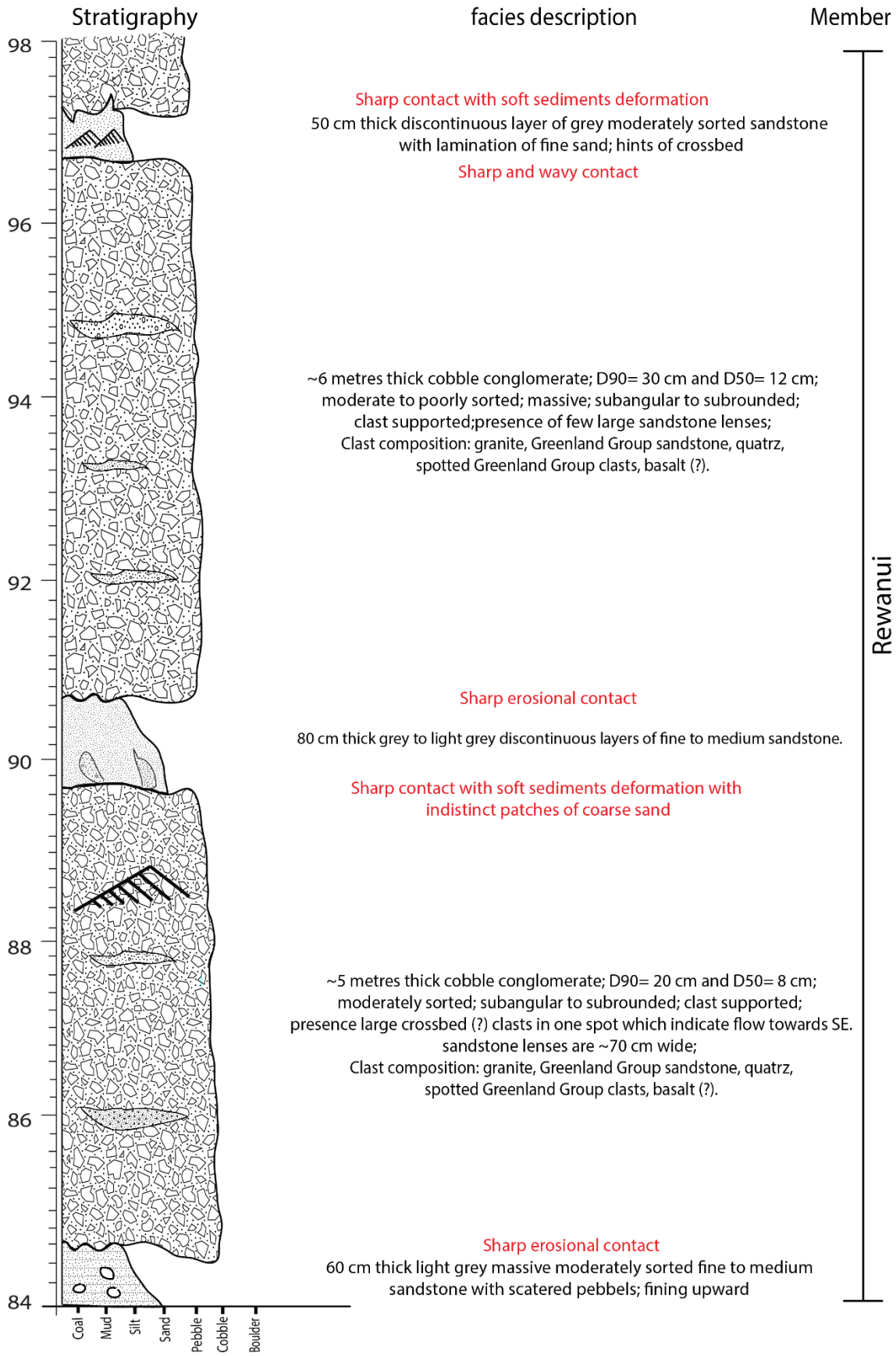
Stratigraphy
facies description
Member
98
96
94
92
90
88
86
84
Coal
Mud
Silt
Sand
Pebble
Cobble
Boulder
Sharp contact with soft sediments deformation
50 cm thick discontinuous layer of grey moderately sorted sandstone with lamination of fine sand; hints of crossbed
Sharp and wavy contact
~6 metres thick cobble conglomerate; D90= 30 cm and D50= 12 cm; moderate to poorly sorted; massive; subangular to subrounded; clast supported;presence of few large sandstone lenses; Clast composition: granite, Greenland Group sandstone, quatrz, spotted Greenland Group clasts, basalt (?).
Sharp erosional contact
80 cm thick grey to light grey discontinuous layers of fine to medium sandstone.
Sharp contact with soft sediments deformation with indistinct patches of coarse sand
~5 metres thick cobble conglomerate; D90= 20 cm and D50= 8 cm; moderately sorted; subangular to subrounded; clast supported; presence large crossbed (?) clasts in one spot which indicate flow towards SE. sandstone lenses are ~70 cm wide; Clast composition: granite, Greenland Group sandstone, quatrz, spotted Greenland Group clasts, basalt (?).
Sharp erosional contact
60 cm thick light grey massive moderately sorted fine to medium sandstone with scatered pebbels; fining upward
Rewanui

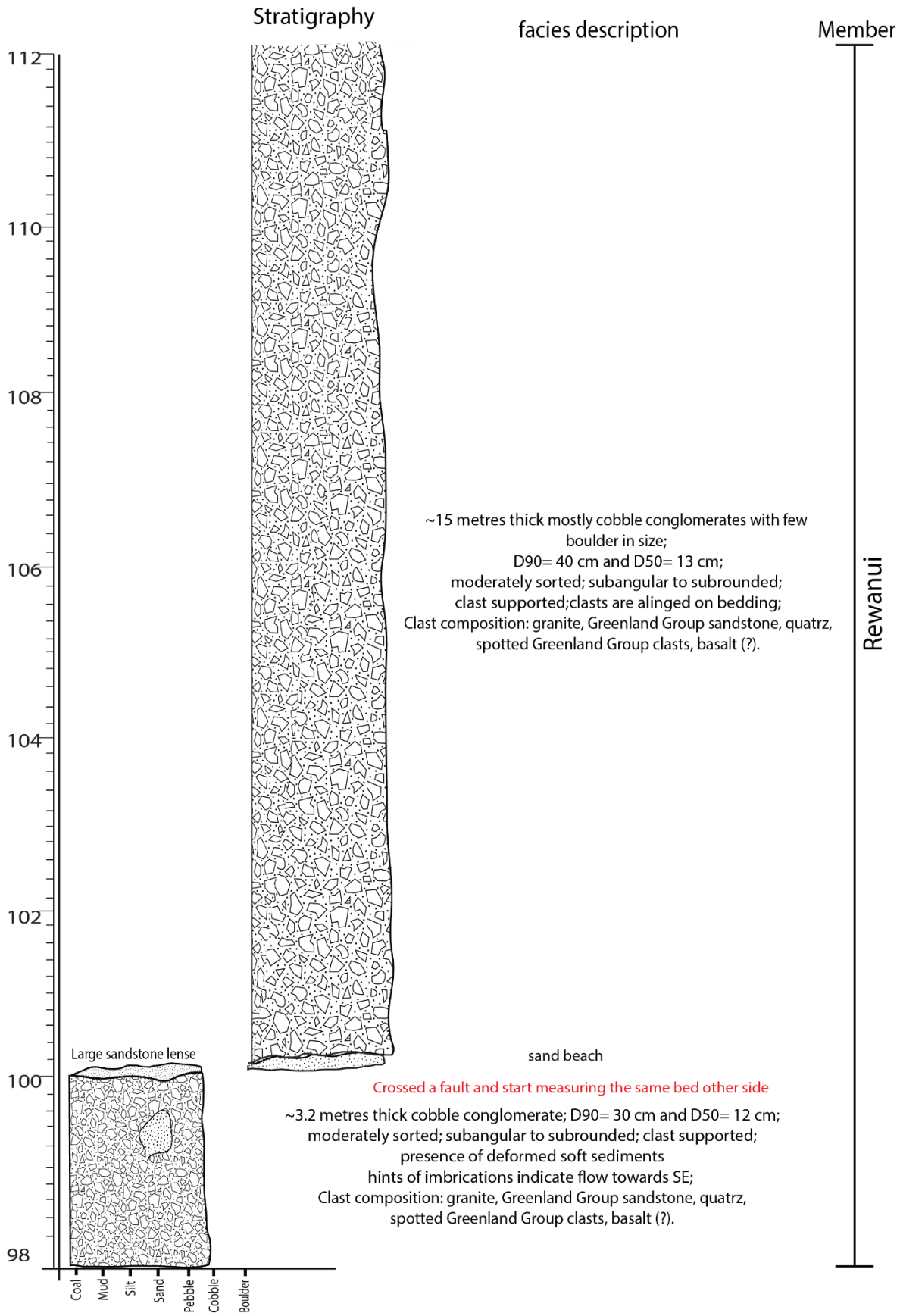
Stratigraphy
facies description
Member
112
110
108
106
104
102
100
98
Large sandstone lense
~15 metres thick mostly cobble conglomerates with few boulder in size;
D90= 40 cm and D50= 13 cm;
moderately sorted; subangular to subrounded;
clast supported;clasts are alinged on bedding;
Clast composition: granite, Greenland Group sandstone, quatrz, spotted Greenland Group clasts, basalt (?).
Rewanui
sand beach
Crossed a fault and start measuring the same bed other side
~3.2 metres thick cobble conglomerate; D90= 30 cm and D50= 12 cm;
moderately sorted; subangular to subrounded; clast supported;
presence of deformed soft sediments
hints of imbrications indicate flow towards SE;
Clast composition: granite, Greenland Group sandstone, quatrz, spotted Greenland Group clasts, basalt (?).
Coal
Mud
Silt
Sand
Pebble
Cobble
Boulder

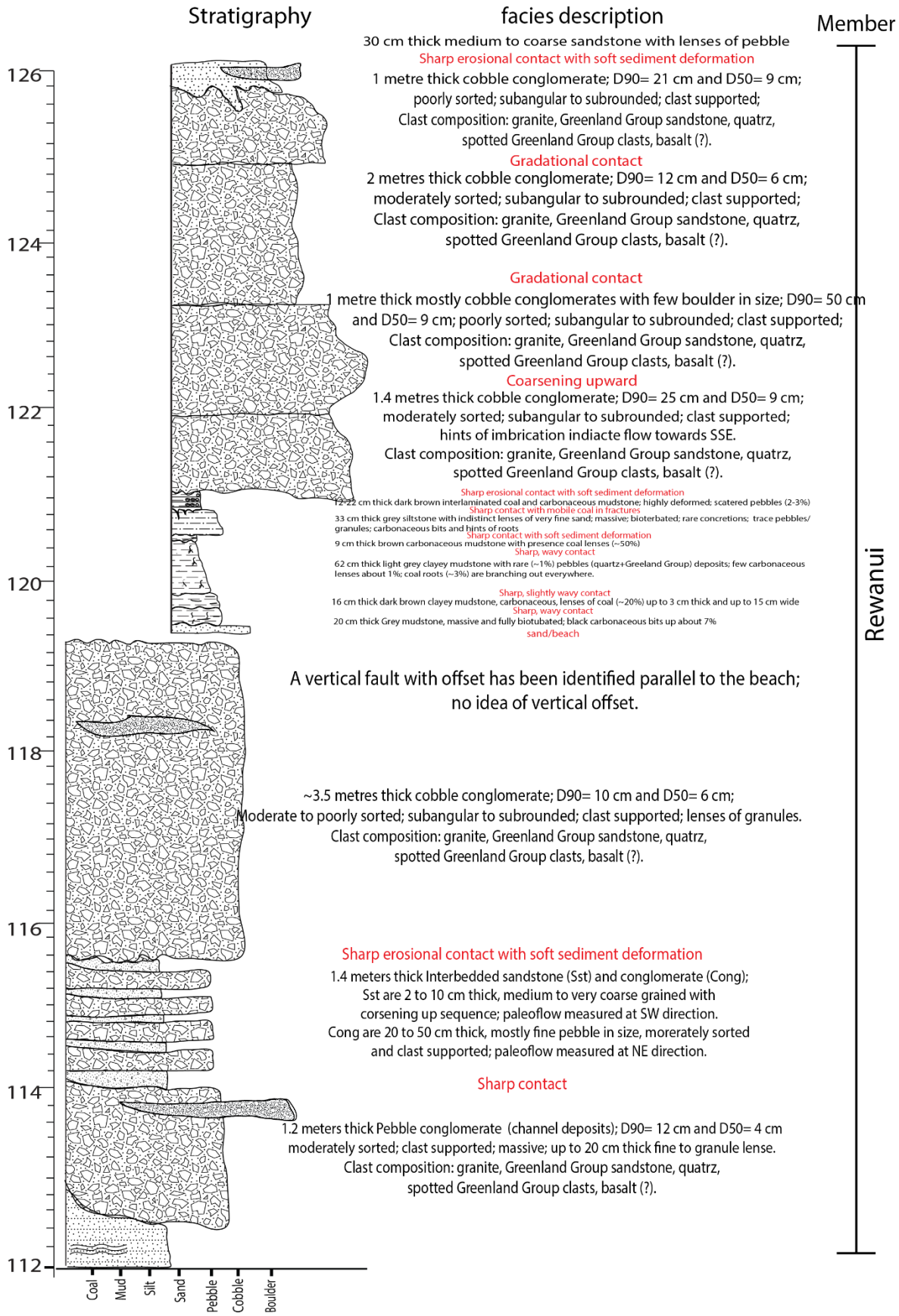
Stratigraphy
facies description
Member
30 cm thick medium to coarse sandstone with lenses of pebble
Sharp erosional contact with soft sediment deformation
1 metre thick cobble conglomerate; D90= 21 cm and D50= 9 cm;
poorly sorted; subangular to subrounded; clast supported;
Clast composition: granite, Greenland Group sandstone, quatrz,
spotted Greenland Group clasts, basalt (?).
Gradational contact
2 metres thick cobble conglomerate; D90= 12 cm and D50= 6 cm;
moderately sorted; subangular to subrounded; clast supported;
Clast composition: granite, Greenland Group sandstone, quatrz,
spotted Greenland Group clasts, basalt (?).
Gradational contact
1 metre thick mostly cobble conglomerates with few boulder in size; D90= 50 cm
and D50= 9 cm; poorly sorted; subangular to subrounded; clast supported;
Clast composition: granite, Greenland Group sandstone, quatrz,
spotted Greenland Group clasts, basalt (?).
Coarsening upward
1.4 metres thick cobble conglomerate; D90= 25 cm and D50= 9 cm;
moderately sorted; subangular to subrounded; clast supported;
hints of imbrication indiacte flow towards SSE.
Clast composition: granite, Greenland Group sandstone, quatrz,
spotted Greenland Group clasts, basalt (?).
Sharp erosional contact with soft sediment deformation
12-22 cm thick dark brown interlaminated coal and carbonaceous mudstone; highly deformed; scatered pebbles (2-3%)
Sharp contact with mobile coal in fractures
33 cm thick grey siltstone with indistinct lenses of very fine sand; massive; bioterbated; rare concretions; trace pebbles/
granules; carbonaceous bits and hints of roots
Sharp contact with soft sediment deformation
9 cm thick brown carbonaceous mudstone with presence coal lenses (~50%)
Sharp, wavy contact
62 cm thick light grey clayey mudstone with rare (~1%) pebbles (quartz+Greeland Group) deposits; few carbonaceous
lenses about 1%; coal roots (~3%) are branching out everywhere.
Sharp, slightly wavy contact
16 cm thick dark brown clayey mudstone, carbonaceous, lenses of coal (~20%) up to 3 cm thick and up to 15 cm wide
Sharp, wavy contact
20 cm thick Grey mudstone, massive and fully biotubated; black carbonaceous bits up about 7%
sand/beach
A vertical fault with offset has been identified parallel to the beach;
no idea of vertical offset.
~3.5 metres thick cobble conglomerate; D90= 10 cm and D50= 6 cm;
Moderate to poorly sorted; subangular to subrounded; clast supported; lenses of granules.
Clast composition: granite, Greenland Group sandstone, quatrz,
spotted Greenland Group clasts, basalt (?).
Sharp erosional contact with soft sediment deformation
1.4 meters thick Interbedded sandstone (Sst) and conglomerate (Cong);
Sst are 2 to 10 cm thick, medium to very coarse grained with
corsening up sequence; paleoflow measured at SW direction.
Cong are 20 to 50 cm thick, mostly fine pebble in size, morerately sorted
and clast supported; paleoflow measured at NE direction.
Sharp contact
1.2 meters thick Pebble conglomerate (channel deposits); D90= 12 cm and D50= 4 cm
moderately sorted; clast supported; massive; up to 20 cm thick fine to granule lense.
Clast composition: granite, Greenland Group sandstone, quatrz,
spotted Greenland Group clasts, basalt (?).
126
124
122
120
118
116
114
112
Coal
Mud
Silt
Sand
Pebble
Cobble
Boulder
Rewanui

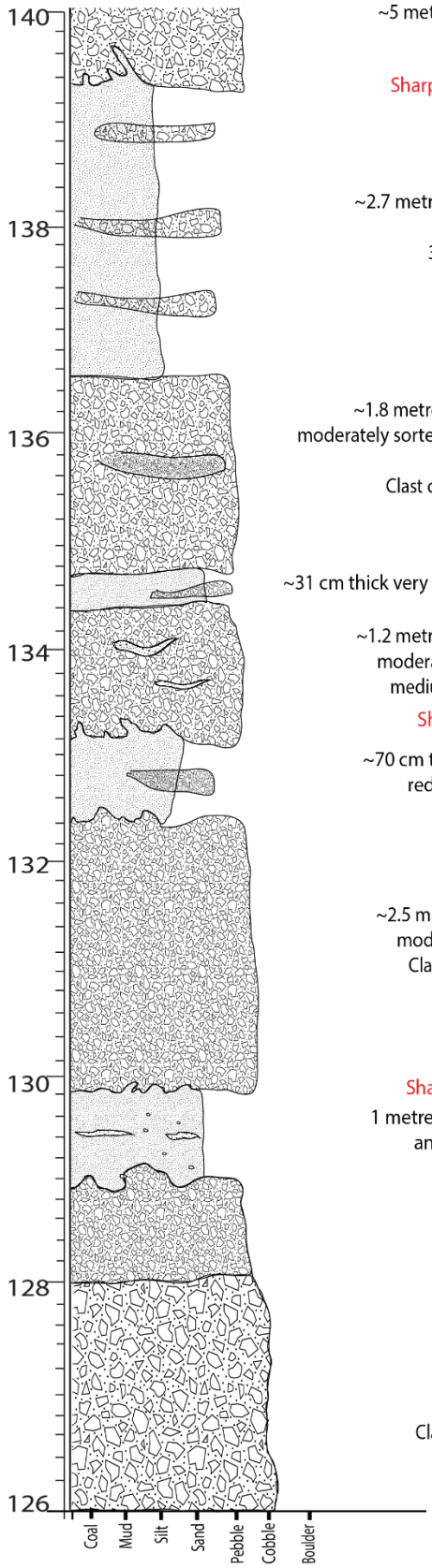


facies description

~5 metres thick cobble conglomerate; D90= 28 cm and D50= 11 cm;
poorly sorted; subangular; clast supported.

Sharp and erosional contact with deformed soft sediments

~2.7 metres thick grey fine grained sandstone; moderate to well sorted;
presence of burrows which are mottled in color;
3 cobble lenses; 12 cm thick red mudstone at the top.
bedding attitude: 110, 10 NE

Sharp contact

~1.8 metres thick cobble conglomerate; D90= 22 cm and D50= 9 cm;
moderately sorted; subangular to subrounded; mostly clast supported (5% matrix);
presence of a 3 metres long granule lense.
Clast composition: granite, Greenland Group sandstone, quatrz,
spotted Greenland Group clasts, basalt (?).

Sharp contact

~31 cm thick very coarse to coarse, moderately sorted sandstone with granule lense.

Sharp contact

~1.2 metres thick cobble conglomerate; D90= 14 cm and D50= 7 cm;
moderately sorted; subangular to subrounded; clast supported;
medium to coarse sand lenses with soft sediment deformation.

Sharp and erosional contact with deformed soft sediments

~70 cm thick fine to medium grain sandstone; mottled/biotubated;
red/greenish grey burrows; discontinuous pebble lense.

Sharp and deformed contact

~2.5 metres thick cobble conglomerate; D90= 17 cm and D50= 8 cm;
moderately sorted; subangular to subrounded; clast supported;
Clast composition: granite, Greenland Group sandstone, quatrz,
spotted Greenland Group clasts, basalt (?).

Sharp and erosional contact with deformed soft sediments

1 metre thick mottled medium grained sandstone with rare pebbles
and discontinuous lenses; sst are moderate to well sorted.

Sharp and deformed contact

cobble conglomerate; D90= 16 cm and D50= 7 cm;
moderately sorted; subangular to subrounded;
clast supported;

~15 metres thick cobble conglomerate;
D90= 40 cm and D50= 13 cm;
moderately sorted; subangular to subrounded;
clast supported;clasts are allinged on bedding;
Clast composition: granite, Greenland Group sandstone, quatrz,
spotted Greenland Group clasts, basalt (?).

Member

Rewanui

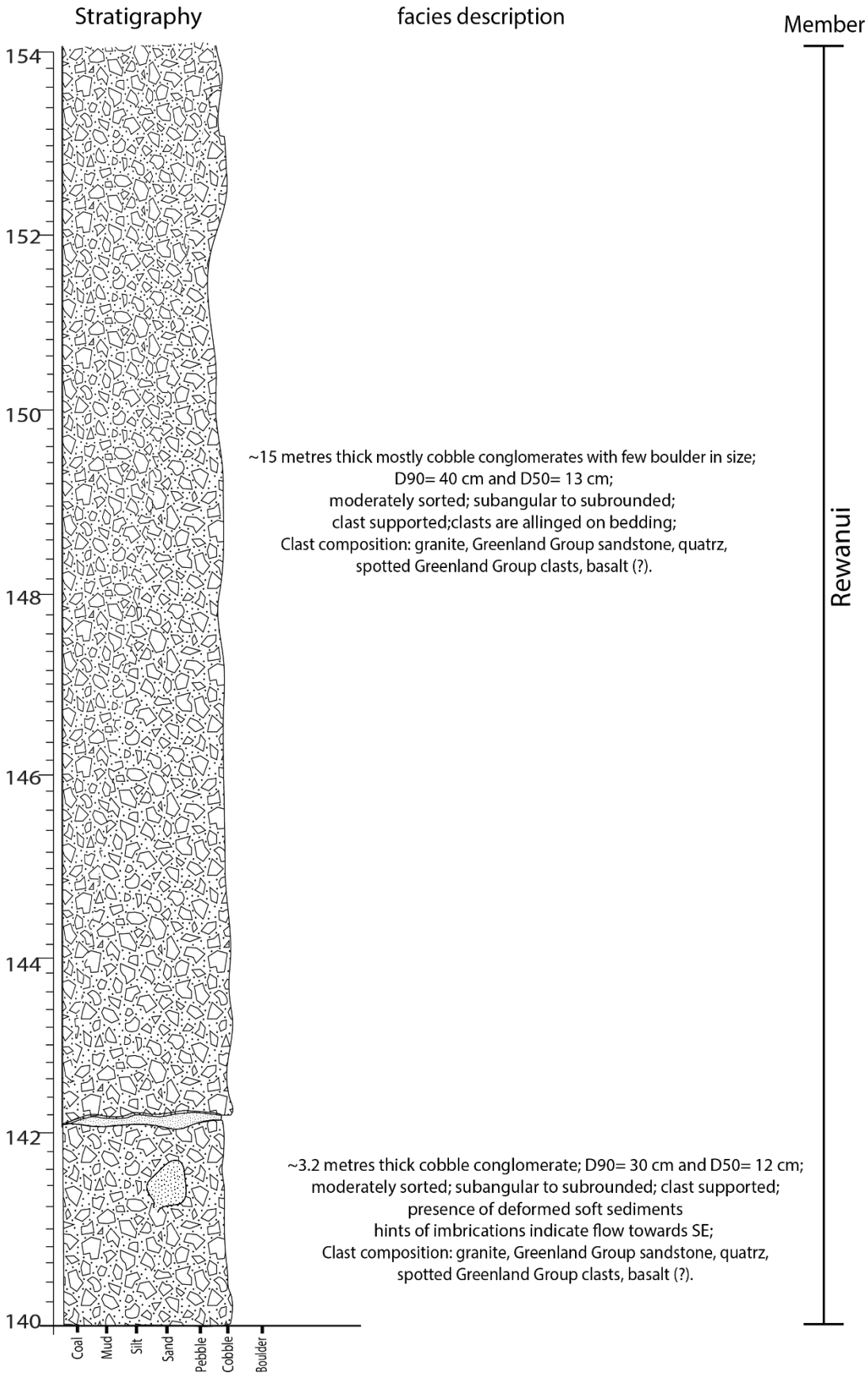
Stratigraphy
facies description
Member
154
152
150
148
146
144
142
140
~15 metres thick mostly cobble conglomerates with few boulder in size;
D90= 40 cm and D50= 13 cm;
moderately sorted; subangular to subrounded;
clast supported;clasts are allinged on bedding;
Clast composition: granite, Greenland Group sandstone, quatrz,
spotted Greenland Group clasts, basalt (?).
~3.2 metres thick cobble conglomerate; D90= 30 cm and D50= 12 cm;
moderately sorted; subangular to subrounded; clast supported;
presence of deformed soft sediments
hints of imbrications indicate flow towards SE;
Clast composition: granite, Greenland Group sandstone, quatrz,
spotted Greenland Group clasts, basalt (?).
Rewanui
Coal
Mud
Silt
Sand
Pebble
Cobble
Boulder

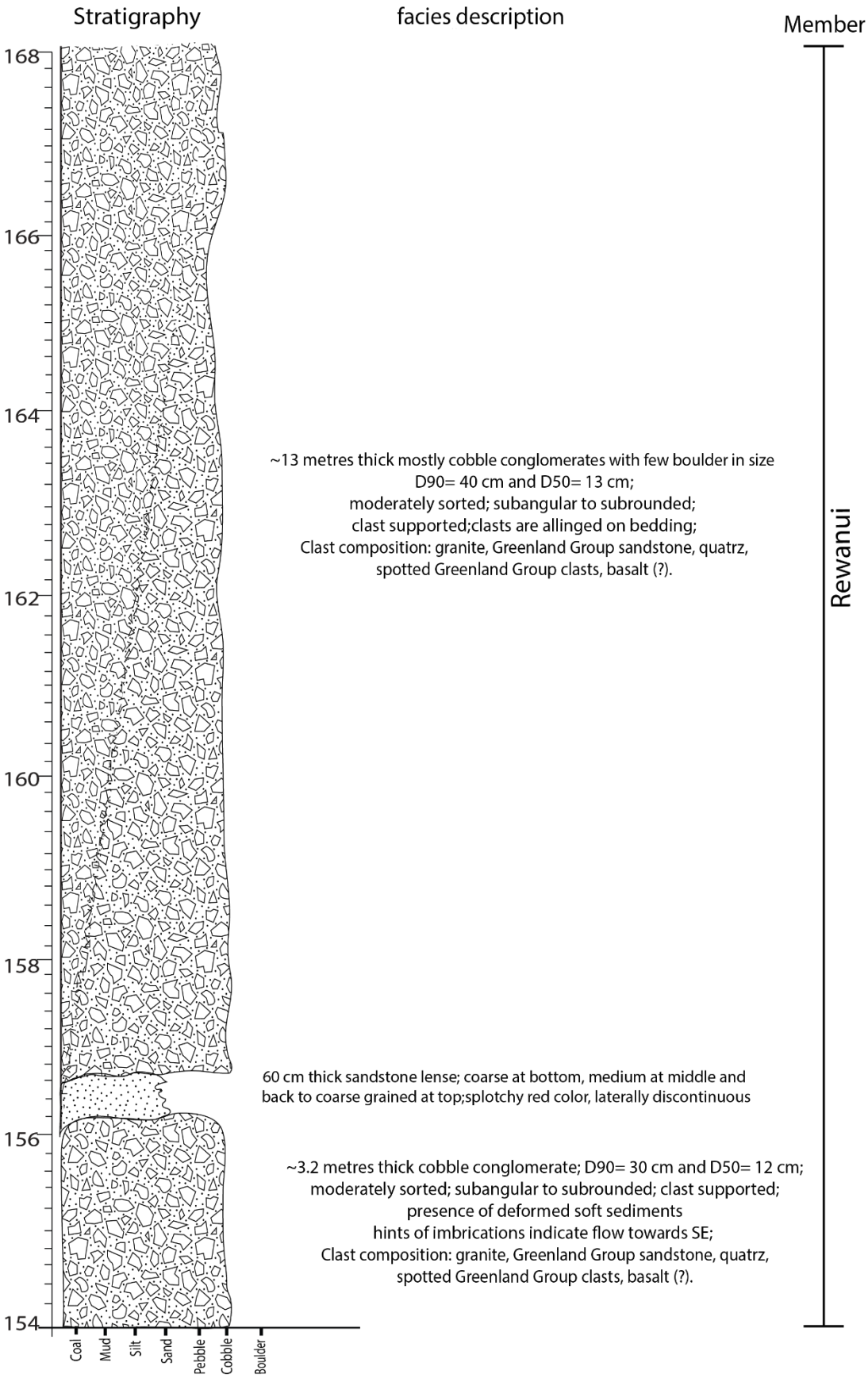
Stratigraphy
facies description
Member
168
166
164
162
160
158
156
154
~13 metres thick mostly cobble conglomerates with few boulder in size
D90= 40 cm and D50= 13 cm;
moderately sorted; subangular to subrounded;
clast supported;clasts are allinged on bedding;
Clast composition: granite, Greenland Group sandstone, quatrz,
spotted Greenland Group clasts, basalt (?).
60 cm thick sandstone lense; coarse at bottom, medium at middle and
back to coarse grained at top;splotchy red color, laterally discontinuous
~3.2 metres thick cobble conglomerate; D90= 30 cm and D50= 12 cm;
moderately sorted; subangular to subrounded; clast supported;
presence of deformed soft sediments
hints of imbrications indicate flow towards SE;
Clast composition: granite, Greenland Group sandstone, quatrz,
spotted Greenland Group clasts, basalt (?).
Rewanui
Coal
Mud
Silt
Sand
Pebble
Cobble
Boulder

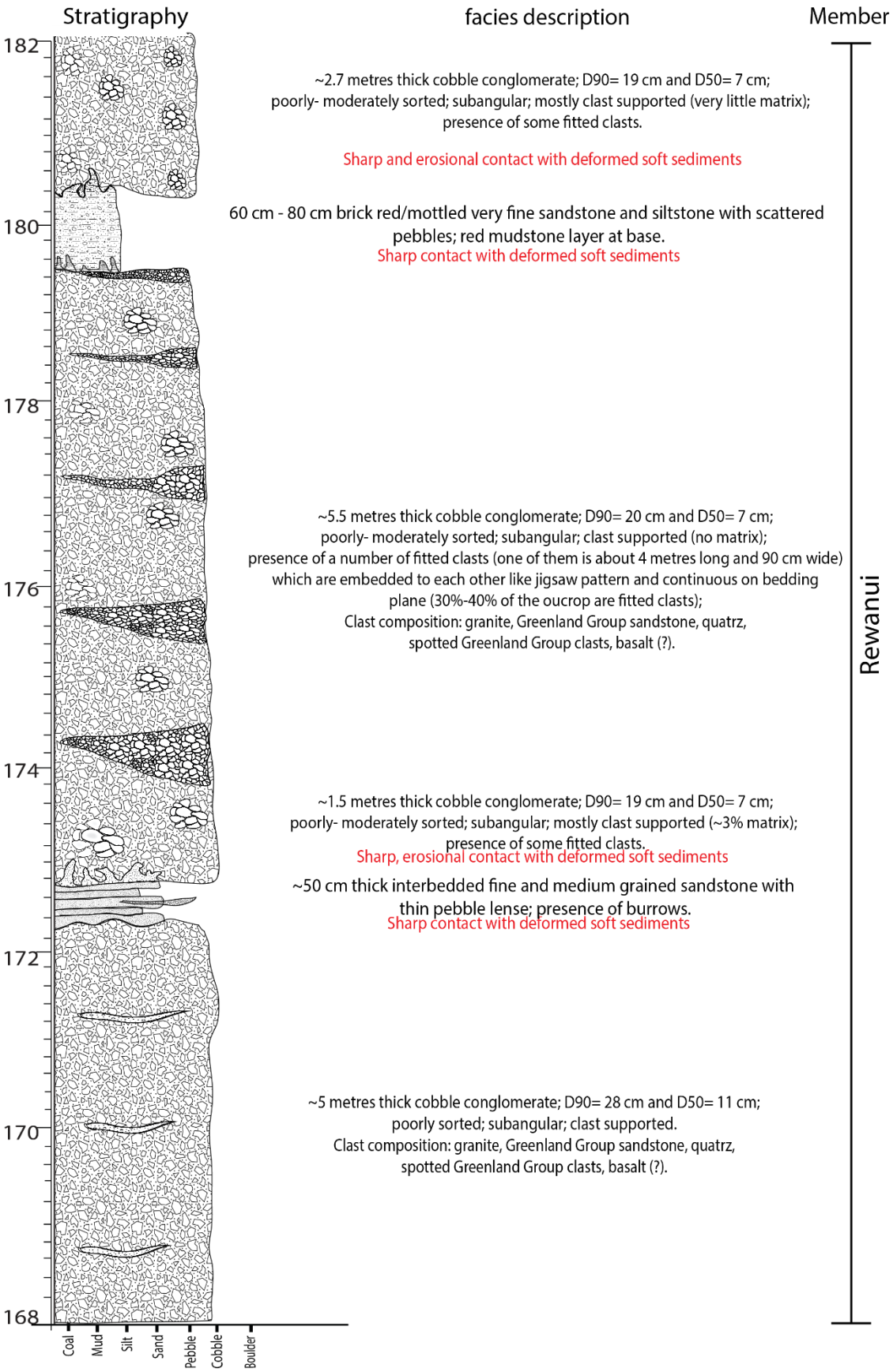
Stratigraphy
facies description
Member
182
180
178
176
174
172
170
168
~2.7 metres thick cobble conglomerate; D90= 19 cm and D50= 7 cm;
poorly- moderately sorted; subangular; mostly clast supported (very little matrix);
presence of some fitted clasts.
Sharp and erosional contact with deformed soft sediments
60 cm - 80 cm brick red/mottled very fine sandstone and siltstone with scattered pebbles; red mudstone layer at base.
Sharp contact with deformed soft sediments
~5.5 metres thick cobble conglomerate; D90= 20 cm and D50= 7 cm;
poorly- moderately sorted; subangular; clast supported (no matrix);
presence of a number of fitted clasts (one of them is about 4 metres long and 90 cm wide) which are embedded to each other like jigsaw pattern and continuous on bedding plane (30%-40% of the oucrop are fitted clasts);
Clast composition: granite, Greenland Group sandstone, quatrz, spotted Greenland Group clasts, basalt (?).
~1.5 metres thick cobble conglomerate; D90= 19 cm and D50= 7 cm;
poorly- moderately sorted; subangular; mostly clast supported (~3% matrix);
presence of some fitted clasts.
Sharp, erosional contact with deformed soft sediments
~50 cm thick interbedded fine and medium grained sandstone with thin pebble lense; presence of burrows.
Sharp contact with deformed soft sediments
~5 metres thick cobble conglomerate; D90= 28 cm and D50= 11 cm;
poorly sorted; subangular; clast supported.
Clast composition: granite, Greenland Group sandstone, quatrz, spotted Greenland Group clasts, basalt (?).
Rewanui
Coal
Mud
Silt
Sand
Pebble
Cobble
Boulder

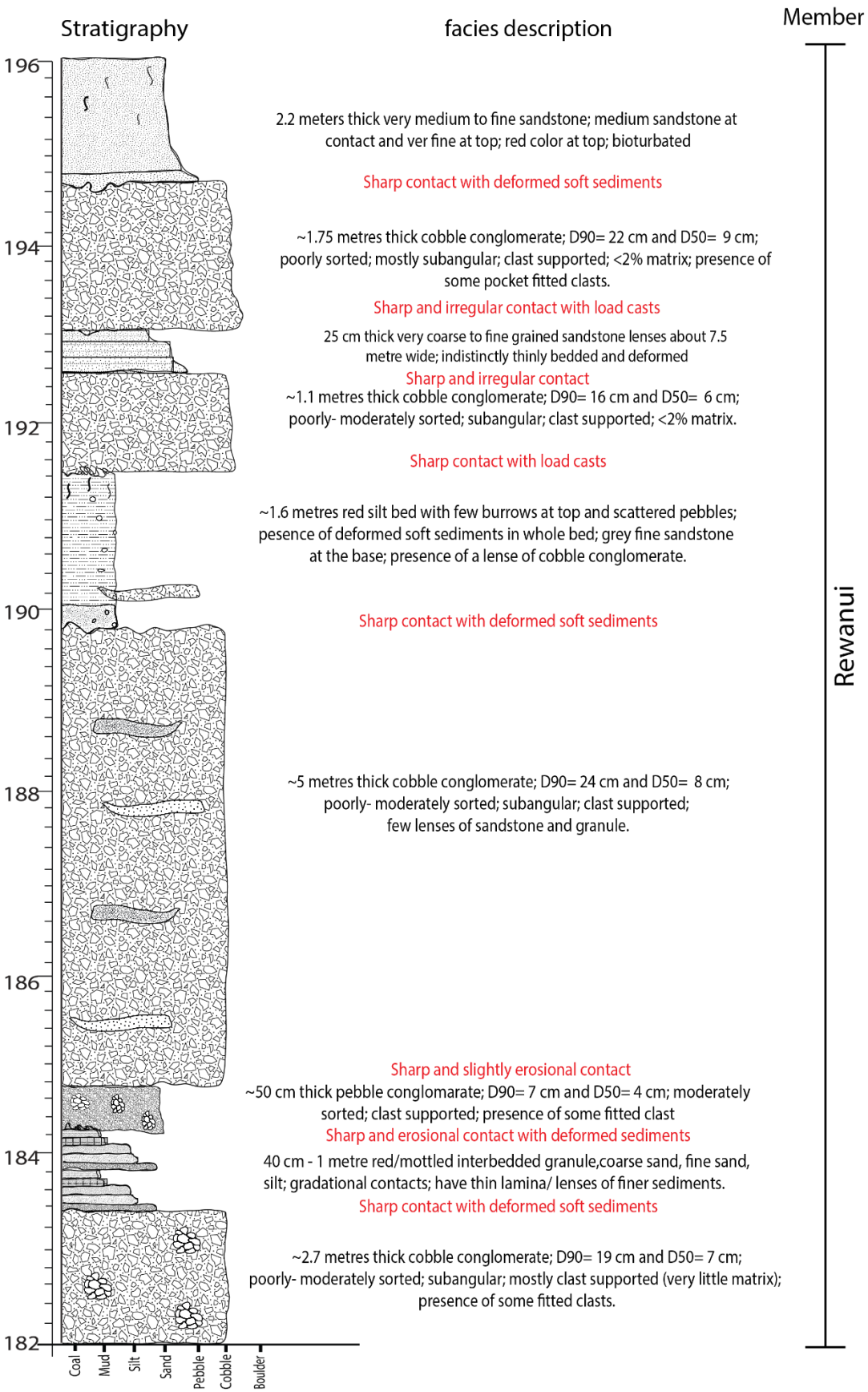
Stratigraphy
facies description
Member
196
194
192
190
188
186
184
182
2.2 meters thick very medium to fine sandstone; medium sandstone at contact and ver fine at top; red color at top; bioturbated
Sharp contact with deformed soft sediments
~1.75 metres thick cobble conglomerate; D90= 22 cm and D50= 9 cm; poorly sorted; mostly subangular; clast supported; <2% matrix; presence of some pocket fitted clasts.
Sharp and irregular contact with load casts
25 cm thick very coarse to fine grained sandstone lenses about 7.5 metre wide; indistinctly thinly bedded and deformed
Sharp and irregular contact
~1.1 metres thick cobble conglomerate; D90= 16 cm and D50= 6 cm; poorly- moderately sorted; subangular; clast supported; <2% matrix.
Sharp contact with load casts
~1.6 metres red silt bed with few burrows at top and scattered pebbles; pesence of deformed soft sediments in whole bed; grey fine sandstone at the base; presence of a lense of cobble conglomerate.
Sharp contact with deformed soft sediments
~5 metres thick cobble conglomerate; D90= 24 cm and D50= 8 cm; poorly- moderately sorted; subangular; clast supported; few lenses of sandstone and granule.
Sharp and slightly erosional contact
~50 cm thick pebble conglomarate; D90= 7 cm and D50= 4 cm; moderately sorted; clast supported; presence of some fitted clast
Sharp and erosional contact with deformed sediments
40 cm - 1 metre red/mottled interbedded granule,coarse sand, fine sand, silt; gradational contacts; have thin lamina/ lenses of finer sediments.
Sharp contact with deformed soft sediments
~2.7 metres thick cobble conglomerate; D90= 19 cm and D50= 7 cm; poorly- moderately sorted; subangular; mostly clast supported (very little matrix); presence of some fitted clasts.
Rewanui
Coal
Mud
Silt
Sand
Pebble
Cobble
Boulder

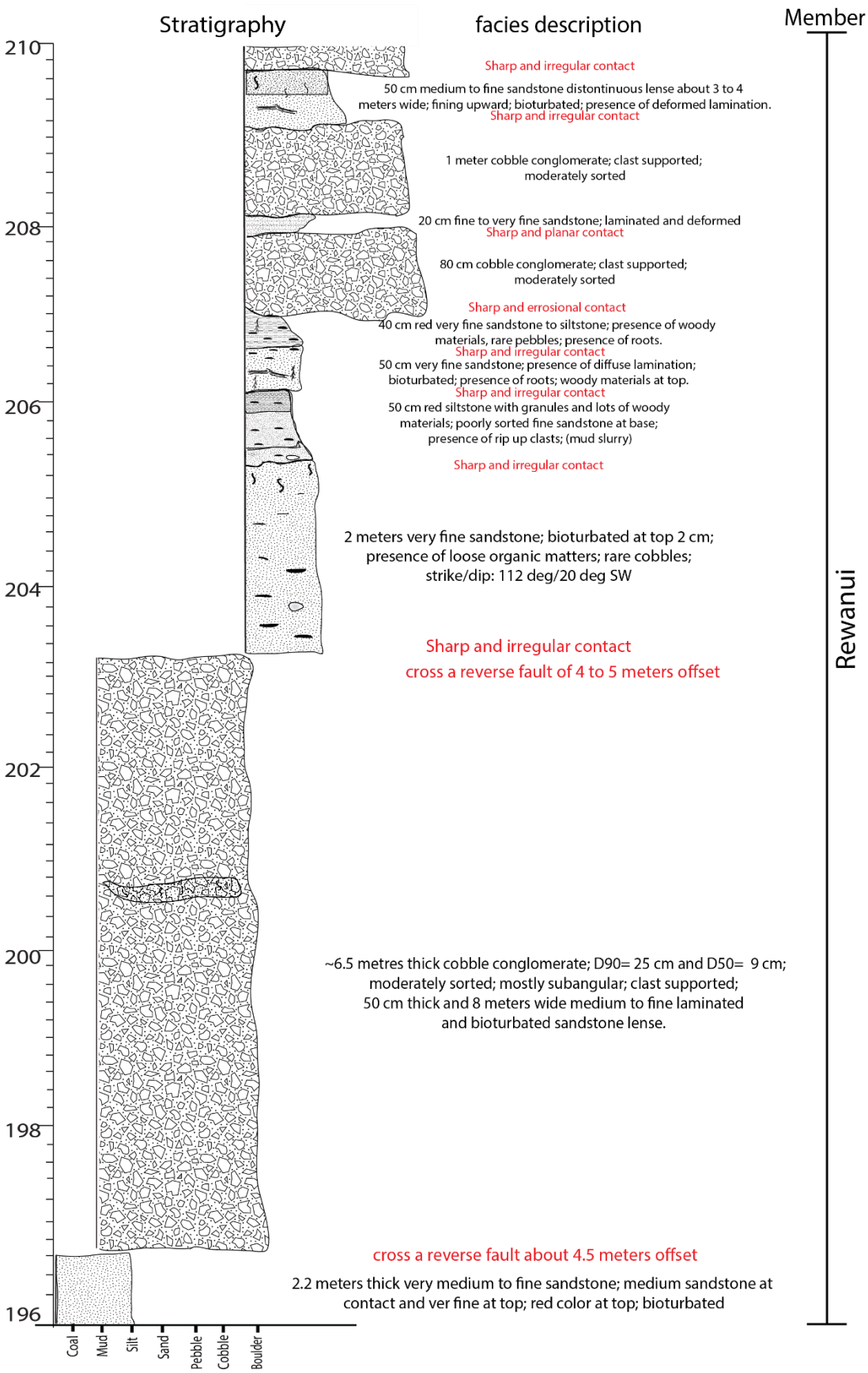
Stratigraphy
facies description
Member
210
208
206
204
202
200
198
196
Sharp and irregular contact
50 cm medium to fine sandstone distontinuous lense about 3 to 4 meters wide; fining upward; bioturbated; presence of deformed lamination.
Sharp and irregular contact
1 meter cobble conglomerate; clast supported; moderately sorted
20 cm fine to very fine sandstone; laminated and deformed
Sharp and planar contact
80 cm cobble conglomerate; clast supported; moderately sorted
Sharp and errosional contact
40 cm red very fine sandstone to siltstone; presence of woody materials, rare pebbles; presence of roots.
Sharp and irregular contact
50 cm very fine sandstone; presence of diffuse lamination; bioturbated; presence of roots; woody materials at top.
Sharp and irregular contact
50 cm red siltstone with granules and lots of woody materials; poorly sorted fine sandstone at base; presence of rip up clasts; (mud slurry)
Sharp and irregular contact
2 meters very fine sandstone; bioturbated at top 2 cm; presence of loose organic matters; rare cobbles; strike/dip: 112 deg/20 deg SW
Sharp and irregular contact
cross a reverse fault of 4 to 5 meters offset
~6.5 metres thick cobble conglomerate; D90= 25 cm and D50= 9 cm; moderately sorted; mostly subangular; clast supported; 50 cm thick and 8 meters wide medium to fine laminated and bioturbated sandstone lense.
cross a reverse fault about 4.5 meters offset
2.2 meters thick very medium to fine sandstone; medium sandstone at contact and ver fine at top; red color at top; bioturbated
Rewanui
Coal
Mud
Silt
Sand
Pebble
Cobble
Boulder

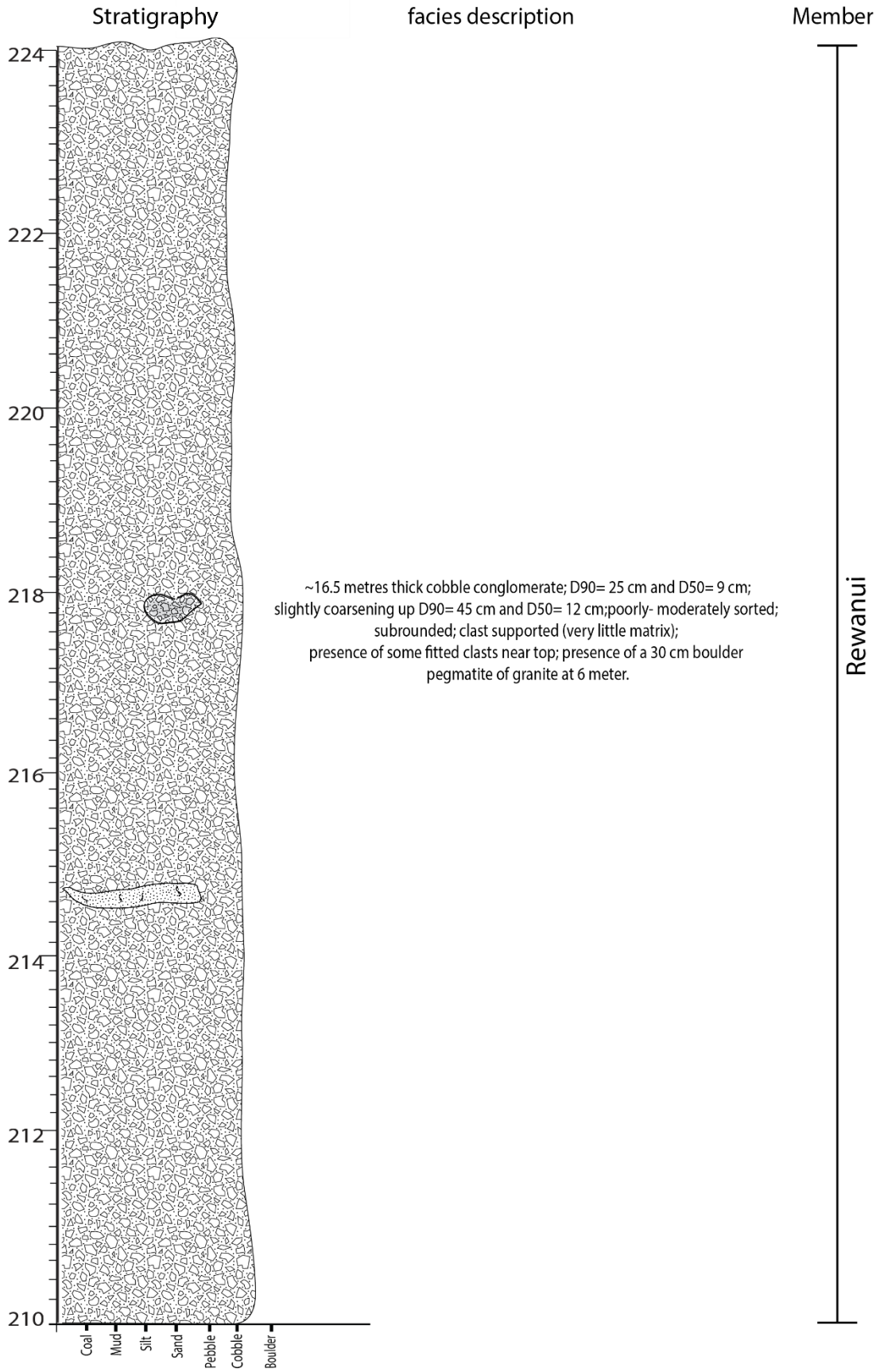
Stratigraphy
facies description
Member
224
222
220
218
216
214
212
210
~16.5 metres thick cobble conglomerate; D90= 25 cm and D50= 9 cm;
slightly coarsening up D90= 45 cm and D50= 12 cm;poorly- moderately sorted;
subrounded; clast supported (very little matrix);
presence of some fitted clasts near top; presence of a 30 cm boulder
pegmatite of granite at 6 meter.
Rewanui
Coal
Mud
Silt
Sand
Pebble
Cobble
Boulder

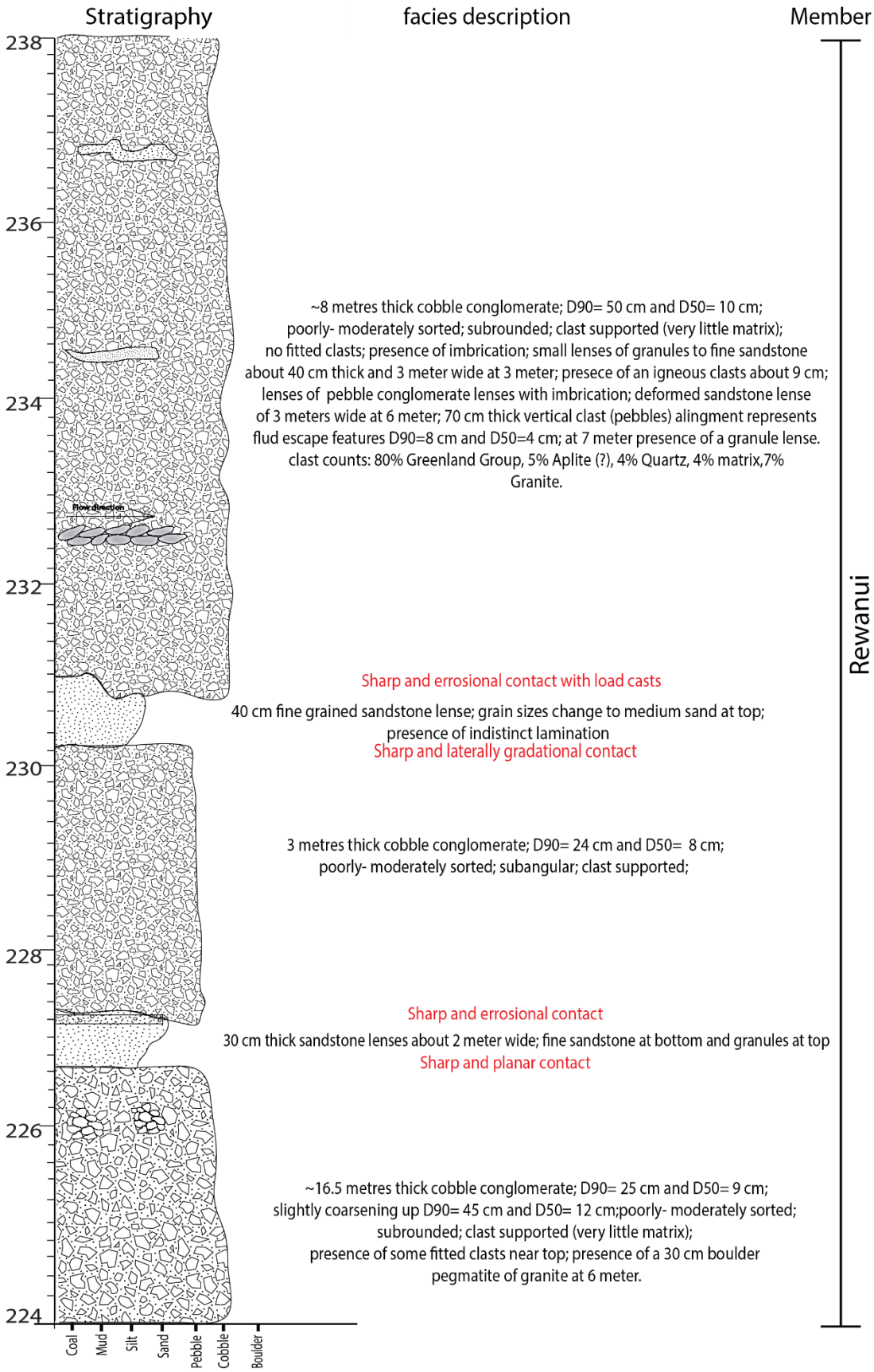
Stratigraphy
facies description
Member
238
236
234
232
230
228
226
224
Flow direction
~8 metres thick cobble conglomerate; D90= 50 cm and D50= 10 cm;
poorly- moderately sorted; subrounded; clast supported (very little matrix);
no fitted clasts; presence of imbrication; small lenses of granules to fine sandstone
about 40 cm thick and 3 meter wide at 3 meter; presece of an igneous clasts about 9 cm;
lenses of pebble conglomerate lenses with imbrication; deformed sandstone lense
of 3 meters wide at 6 meter; 70 cm thick vertical clast (pebbles) alingment represents
flud escape features D90=8 cm and D50=4 cm; at 7 meter presence of a granule lense.
clast counts: 80% Greenland Group, 5% Aplite (?), 4% Quartz, 4% matrix,7%
Granite.
Sharp and errosional contact with load casts
40 cm fine grained sandstone lense; grain sizes change to medium sand at top;
presence of indistinct lamination
Sharp and laterally gradational contact
3 metres thick cobble conglomerate; D90= 24 cm and D50= 8 cm;
poorly- moderately sorted; subangular; clast supported;
Sharp and errosional contact
30 cm thick sandstone lenses about 2 meter wide; fine sandstone at bottom and granules at top
Sharp and planar contact
~16.5 metres thick cobble conglomerate; D90= 25 cm and D50= 9 cm;
slightly coarsening up D90= 45 cm and D50= 12 cm;poorly- moderately sorted;
subrounded; clast supported (very little matrix);
presence of some fitted clasts near top; presence of a 30 cm boulder
pegmatite of granite at 6 meter.
Rewanui
Coal
Mud
Silt
Sand
Pebble
Cobble
Boulder

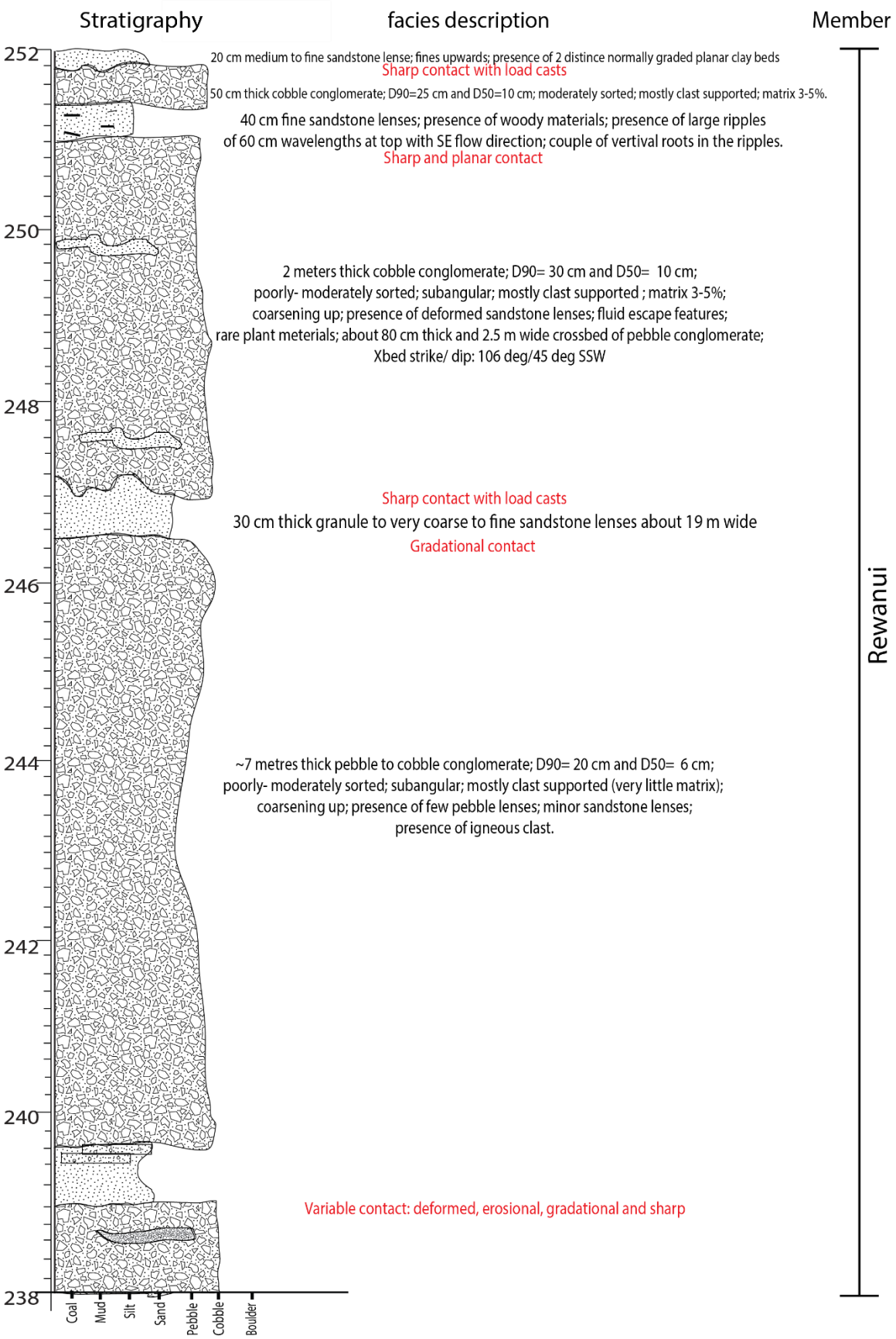
Stratigraphy
facies description
Member
252
250
248
246
244
242
240
238
20 cm medium to fine sandstone lense; fines upwards; presence of 2 distince normally graded planar clay beds
Sharp contact with load casts
50 cm thick cobble conglomerate; D90=25 cm and D50=10 cm; moderately sorted; mostly clast supported; matrix 3-5%.
40 cm fine sandstone lenses; presence of woody materials; presence of large ripples
of 60 cm wavelengths at top with SE flow direction; couple of vertival roots in the ripples.
Sharp and planar contact
2 meters thick cobble conglomerate; D90= 30 cm and D50= 10 cm;
poorly- moderately sorted; subangular; mostly clast supported ; matrix 3-5%;
coarsening up; presence of deformed sandstone lenses; fluid escape features;
rare plant meterials; about 80 cm thick and 2.5 m wide crossbed of pebble conglomerate;
Xbed strike/ dip: 106 deg/45 deg SSW
Sharp contact with load casts
30 cm thick granule to very coarse to fine sandstone lenses about 19 m wide
Gradational contact
~7 metres thick pebble to cobble conglomerate; D90= 20 cm and D50= 6 cm;
poorly- moderately sorted; subangular; mostly clast supported (very little matrix);
coarsening up; presence of few pebble lenses; minor sandstone lenses;
presence of igneous clast.
Variable contact: deformed, erosional, gradational and sharp
Coal
Mud
Silt
Sand
Pebble
Cobble
Boulder
Rewanui

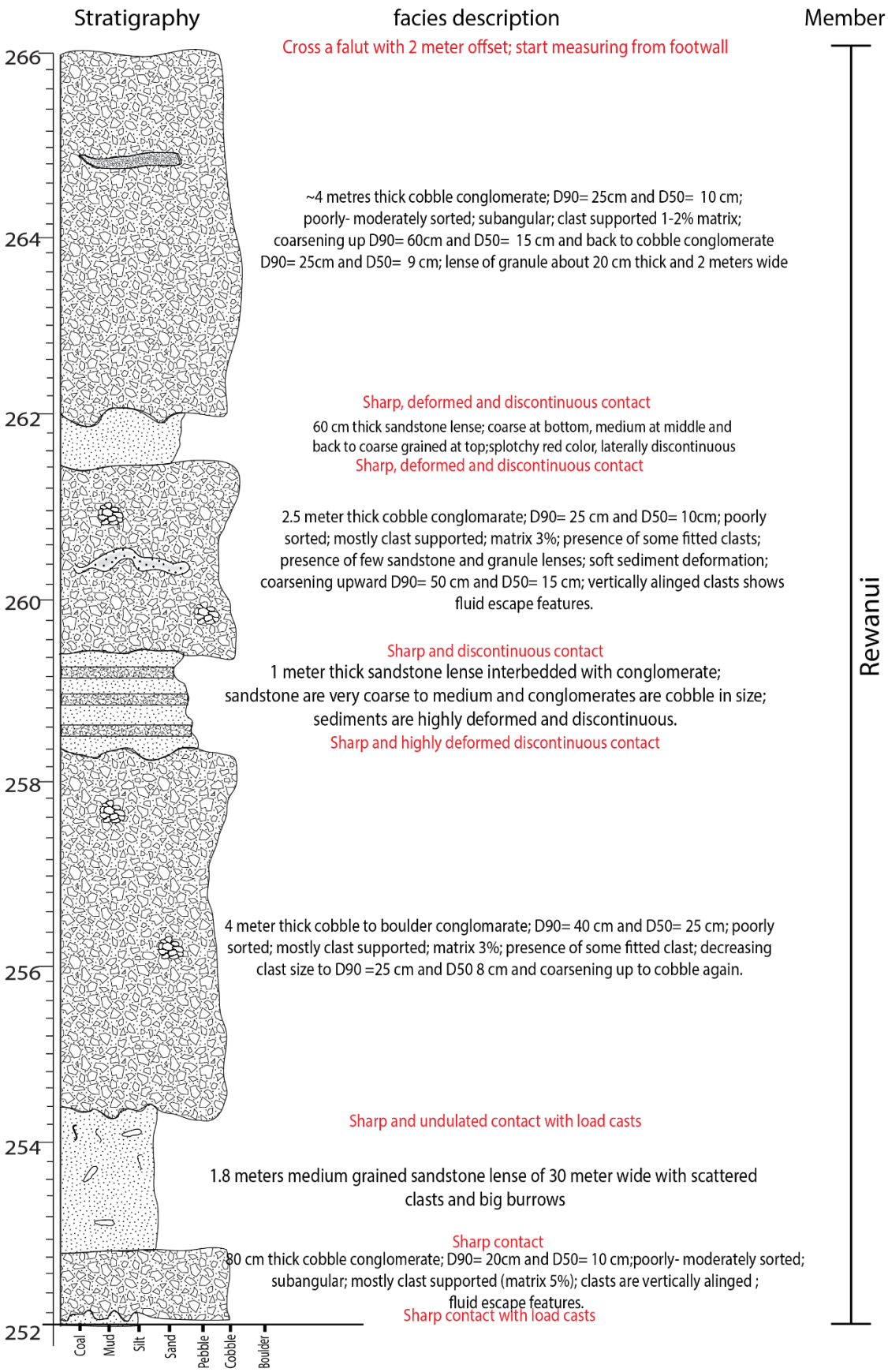
Stratigraphy
facies description
Member
Cross a falut with 2 meter offset; start measuring from footwall
266
264
262
260
258
256
254
252
~4 metres thick cobble conglomerate; D90= 25cm and D50= 10 cm; poorly- moderately sorted; subangular; clast supported 1-2% matrix; coarsening up D90= 60cm and D50= 15 cm and back to cobble conglomerate D90= 25cm and D50= 9 cm; lense of granule about 20 cm thick and 2 meters wide
Sharp, deformed and discontinuous contact
60 cm thick sandstone lense; coarse at bottom, medium at middle and back to coarse grained at top;splotchy red color, laterally discontinuous
Sharp, deformed and discontinuous contact
2.5 meter thick cobble conglomarate; D90= 25 cm and D50= 10cm; poorly sorted; mostly clast supported; matrix 3%; presence of some fitted clasts; presence of few sandstone and granule lenses; soft sediment deformation; coarsening upward D90= 50 cm and D50= 15 cm; vertically alinged clasts shows fluid escape features.
Sharp and discontinuous contact
1 meter thick sandstone lense interbedded with conglomerate; sandstone are very coarse to medium and conglomerates are cobble in size; sediments are highly deformed and discontinuous.
Sharp and highly deformed discontinuous contact
4 meter thick cobble to boulder conglomarate; D90= 40 cm and D50= 25 cm; poorly sorted; mostly clast supported; matrix 3%; presence of some fitted clast; decreasing clast size to D90 =25 cm and D50 8 cm and coarsening up to cobble again.
Sharp and undulated contact with load casts
1.8 meters medium grained sandstone lense of 30 meter wide with scattered clasts and big burrows
Sharp contact
80 cm thick cobble conglomerate; D90= 20cm and D50= 10 cm;poorly- moderately sorted; subangular; mostly clast supported (matrix 5%); clasts are vertically alinged ; fluid escape features.
Sharp contact with load casts
Coal
Mud
Silt
Sand
Pebble
Cobble
Boulder
Rewanui

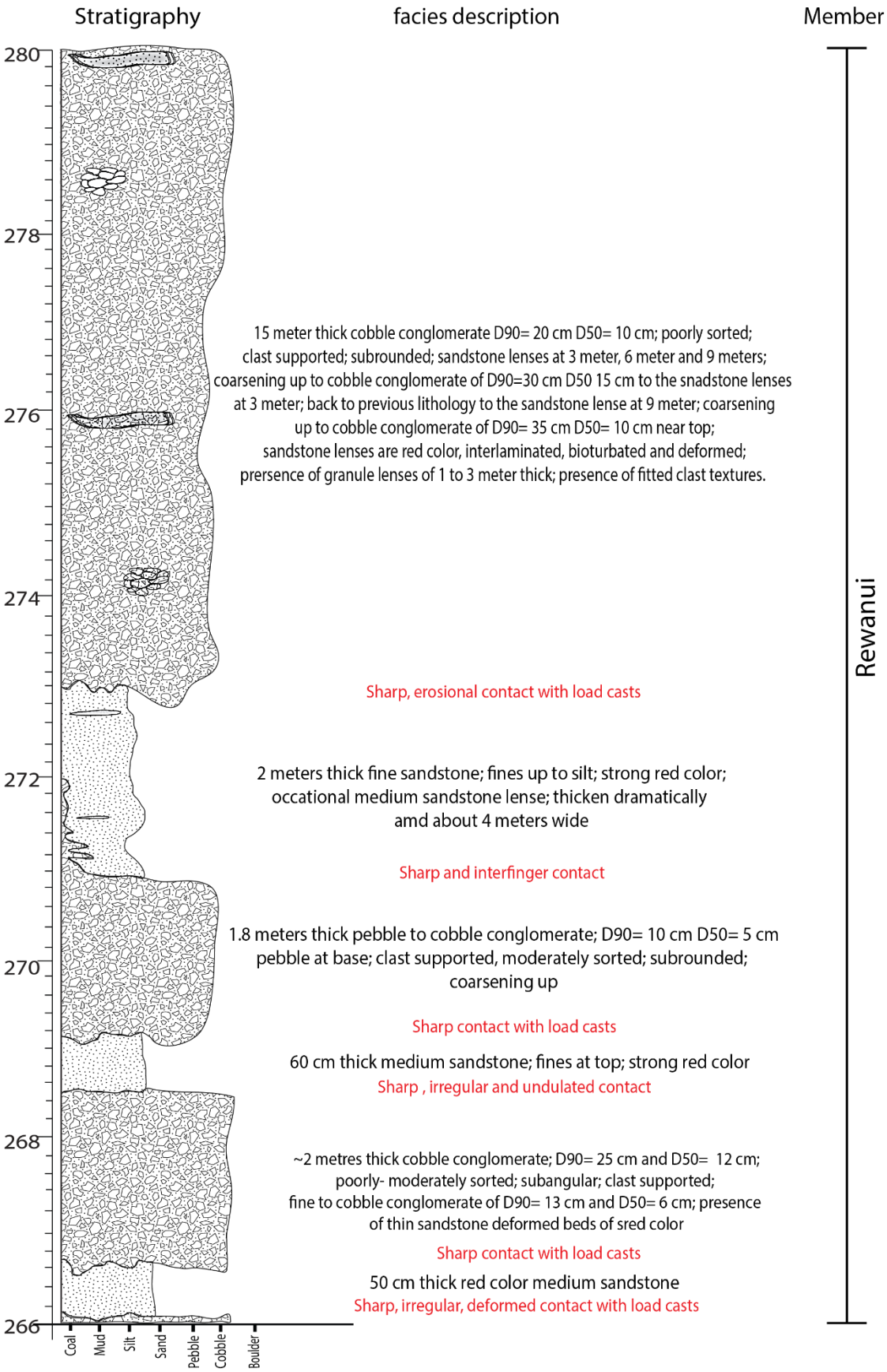
Stratigraphy
facies description
Member
280
278
276
274
272
270
268
266
15 meter thick cobble conglomerate D90= 20 cm D50= 10 cm; poorly sorted;
clast supported; subrounded; sandstone lenses at 3 meter, 6 meter and 9 meters;
coarsening up to cobble conglomerate of D90=30 cm D50 15 cm to the snadstone lenses
at 3 meter; back to previous lithology to the sandstone lense at 9 meter; coarsening
up to cobble conglomerate of D90= 35 cm D50= 10 cm near top;
sandstone lenses are red color, interlaminated, bioturbated and deformed;
prersence of granule lenses of 1 to 3 meter thick; presence of fitted clast textures.
Sharp, erosional contact with load casts
2 meters thick fine sandstone; fines up to silt; strong red color;
occational medium sandstone lense; thicken dramatically
amd about 4 meters wide
Sharp and interfinger contact
1.8 meters thick pebble to cobble conglomerate; D90= 10 cm D50= 5 cm
pebble at base; clast supported, moderately sorted; subrounded;
coarsening up
Sharp contact with load casts
60 cm thick medium sandstone; fines at top; strong red color
Sharp , irregular and undulated contact
~2 metres thick cobble conglomerate; D90= 25 cm and D50= 12 cm;
poorly- moderately sorted; subangular; clast supported;
fine to cobble conglomerate of D90= 13 cm and D50= 6 cm; presence
of thin sandstone deformed beds of sred color
Sharp contact with load casts
50 cm thick red color medium sandstone
Sharp, irregular, deformed contact with load casts
Coal
Mud
Silt
Sand
Pebble
Cobble
Boulder
Rewanui

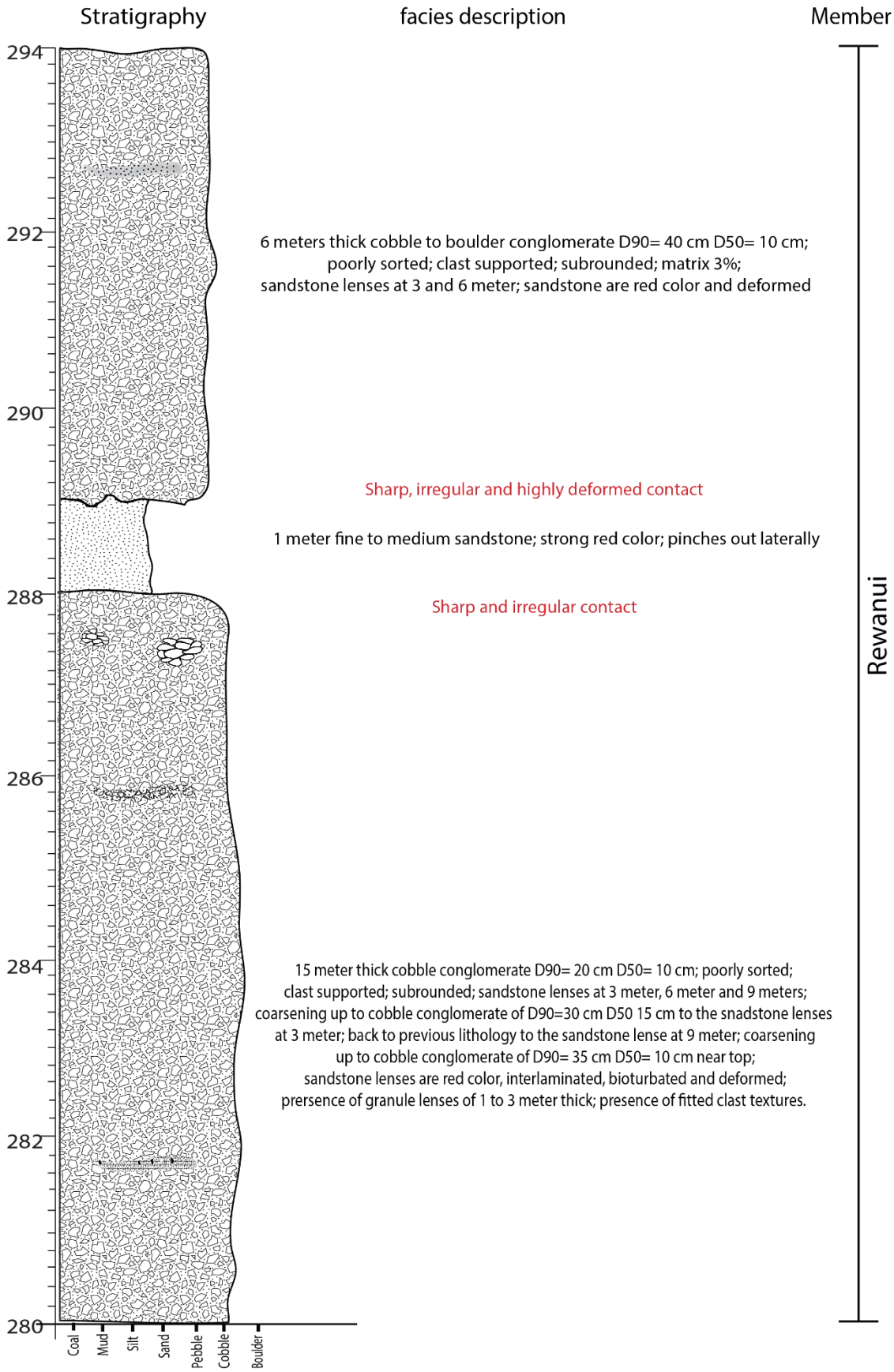
Stratigraphy
facies description
Member
294
292
290
288
286
284
282
280
6 meters thick cobble to boulder conglomerate D90= 40 cm D50= 10 cm;
poorly sorted; clast supported; subrounded; matrix 3%;
sandstone lenses at 3 and 6 meter; sandstone are red color and deformed
Sharp, irregular and highly deformed contact
1 meter fine to medium sandstone; strong red color; pinches out laterally
Sharp and irregular contact
15 meter thick cobble conglomerate D90= 20 cm D50= 10 cm; poorly sorted;
clast supported; subrounded; sandstone lenses at 3 meter, 6 meter and 9 meters;
coarsening up to cobble conglomerate of D90=30 cm D50 15 cm to the snadstone lenses
at 3 meter; back to previous lithology to the sandstone lense at 9 meter; coarsening
up to cobble conglomerate of D90= 35 cm D50= 10 cm near top;
sandstone lenses are red color, interlaminated, bioturbated and deformed;
prersence of granule lenses of 1 to 3 meter thick; presence of fitted clast textures.
Rewanui
Coal
Mud
Silt
Sand
Pebble
Cobble
Boulder

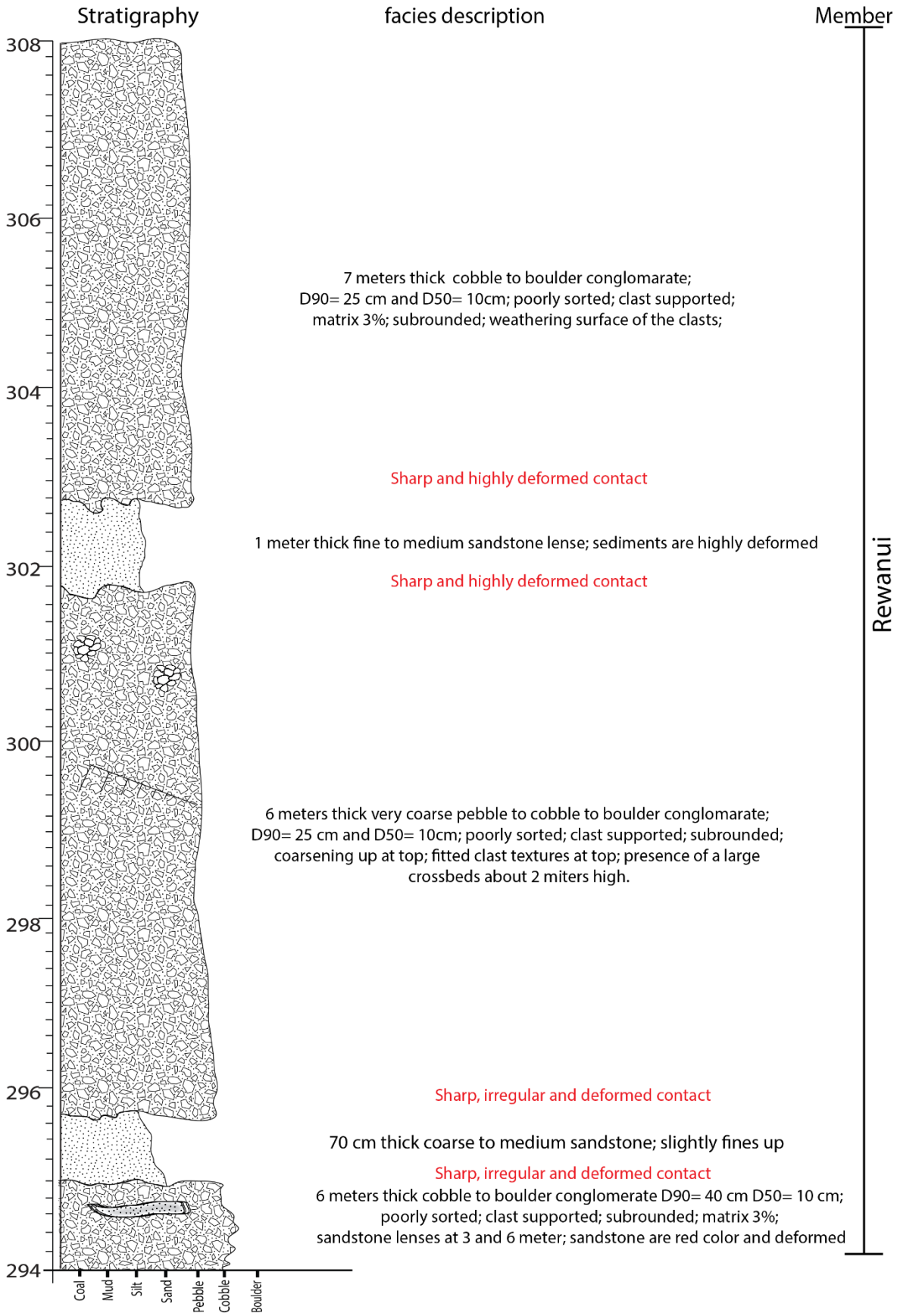
Stratigraphy
facies description
Member
308
306
304
302
300
298
296
294
Coal
Mud
Silt
Sand
Pebble
Cobble
Boulder
7 meters thick cobble to boulder conglomarate;
D90= 25 cm and D50= 10cm; poorly sorted; clast supported;
matrix 3%; subrounded; weathering surface of the clasts;
Sharp and highly deformed contact
1 meter thick fine to medium sandstone lense; sediments are highly deformed
Sharp and highly deformed contact
6 meters thick very coarse pebble to cobble to boulder conglomarate;
D90= 25 cm and D50= 10cm; poorly sorted; clast supported; subrounded;
coarsening up at top; fitted clast textures at top; presence of a large
crossbeds about 2 miters high.
Sharp, irregular and deformed contact
70 cm thick coarse to medium sandstone; slightly fines up
Sharp, irregular and deformed contact
6 meters thick cobble to boulder conglomerate D90= 40 cm D50= 10 cm;
poorly sorted; clast supported; subrounded; matrix 3%;
sandstone lenses at 3 and 6 meter; sandstone are red color and deformed
Rewanui

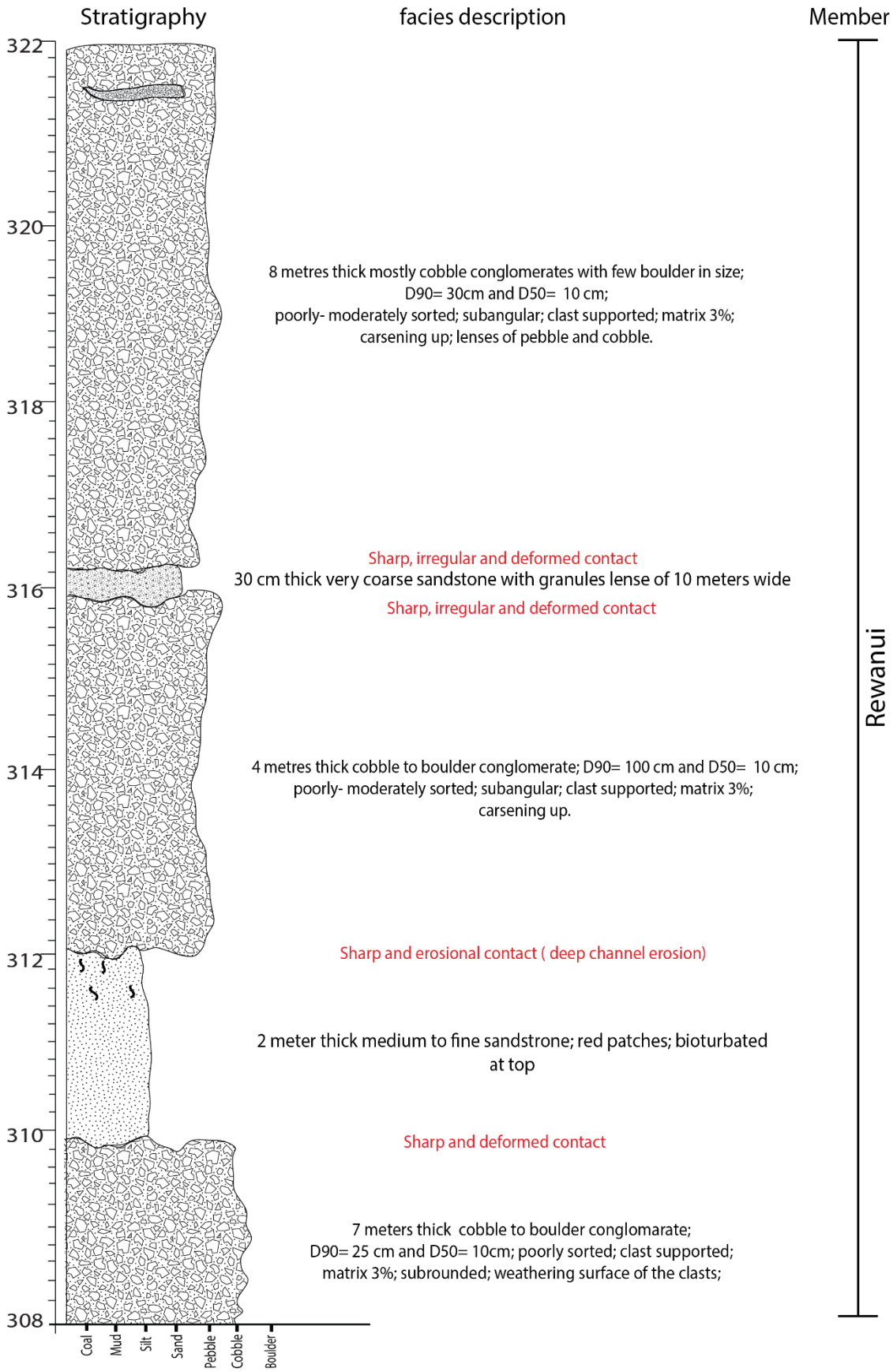
Stratigraphy
facies description
Member
322
320
318
316
314
312
310
308
8 metres thick mostly cobble conglomerates with few boulder in size;
D90= 30cm and D50= 10 cm;
poorly- moderately sorted; subangular; clast supported; matrix 3%;
carsening up; lenses of pebble and cobble.
Sharp, irregular and deformed contact
30 cm thick very coarse sandstone with granules lense of 10 meters wide
Sharp, irregular and deformed contact
4 metres thick cobble to boulder conglomerate; D90= 100 cm and D50= 10 cm;
poorly- moderately sorted; subangular; clast supported; matrix 3%;
carsening up.
Sharp and erosional contact ( deep channel erosion)
2 meter thick medium to fine sandstrone; red patches; bioturbated
at top
Sharp and deformed contact
7 meters thick cobble to boulder conglomarate;
D90= 25 cm and D50= 10cm; poorly sorted; clast supported;
matrix 3%; subrounded; weathering surface of the clasts;
Rewanui
Coal
Mud
Silt
Sand
Pebble
Cobble
Boulder

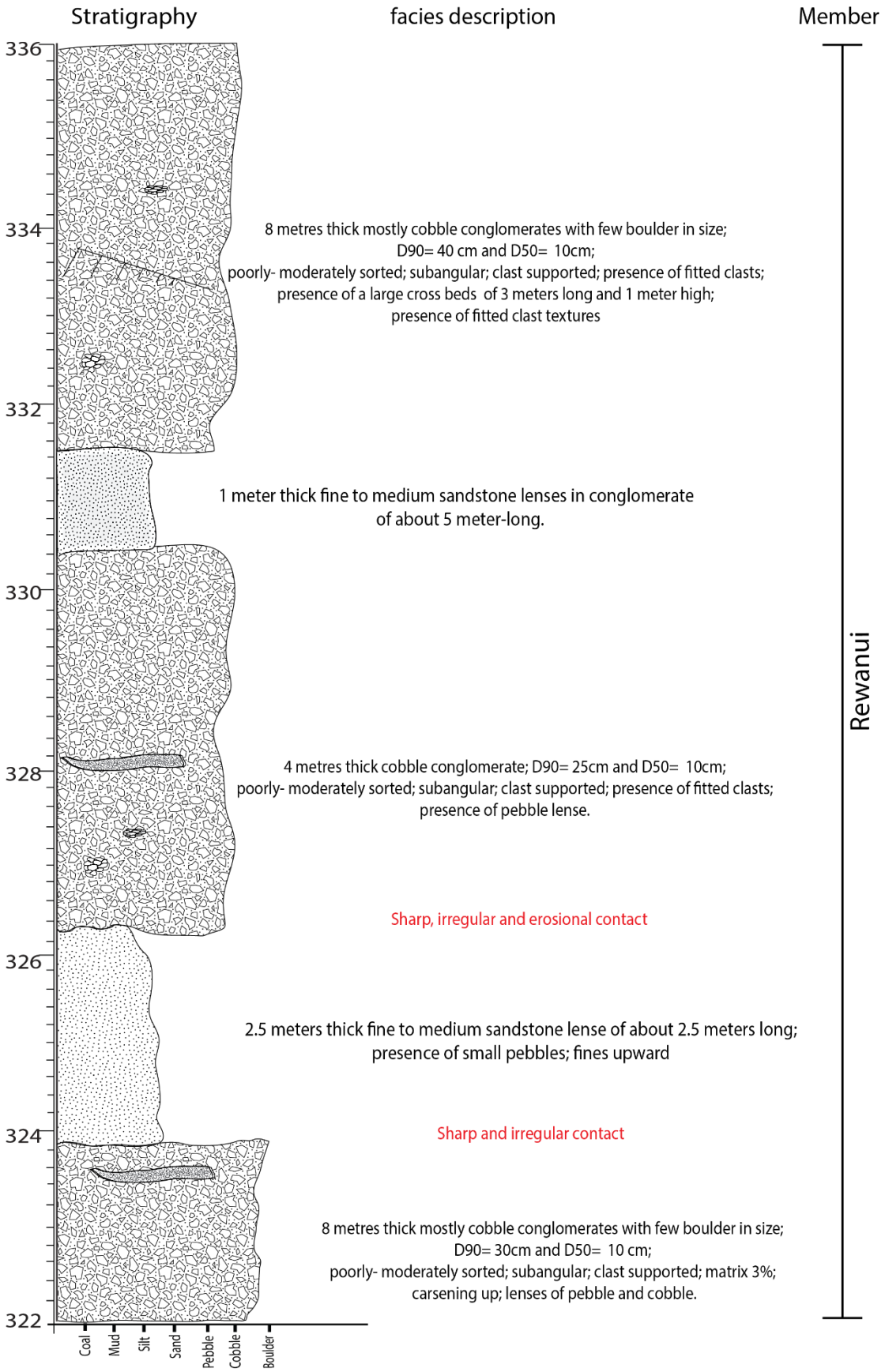
Stratigraphy
facies description
Member
336
334
332
330
328
326
324
322
8 metres thick mostly cobble conglomerates with few boulder in size;
D90= 40 cm and D50= 10cm;
poorly- moderately sorted; subangular; clast supported; presence of fitted clasts;
presence of a large cross beds of 3 meters long and 1 meter high;
presence of fitted clast textures
1 meter thick fine to medium sandstone lenses in conglomerate
of about 5 meter-long.
4 metres thick cobble conglomerate; D90= 25cm and D50= 10cm;
poorly- moderately sorted; subangular; clast supported; presence of fitted clasts;
presence of pebble lense.
Sharp, irregular and erosional contact
2.5 meters thick fine to medium sandstone lense of about 2.5 meters long;
presence of small pebbles; fines upward
Sharp and irregular contact
8 metres thick mostly cobble conglomerates with few boulder in size;
D90= 30cm and D50= 10 cm;
poorly- moderately sorted; subangular; clast supported; matrix 3%;
carsening up; lenses of pebble and cobble.
Rewanui
Coal
Mud
Silt
Sand
Pebble
Cobble
Boulder

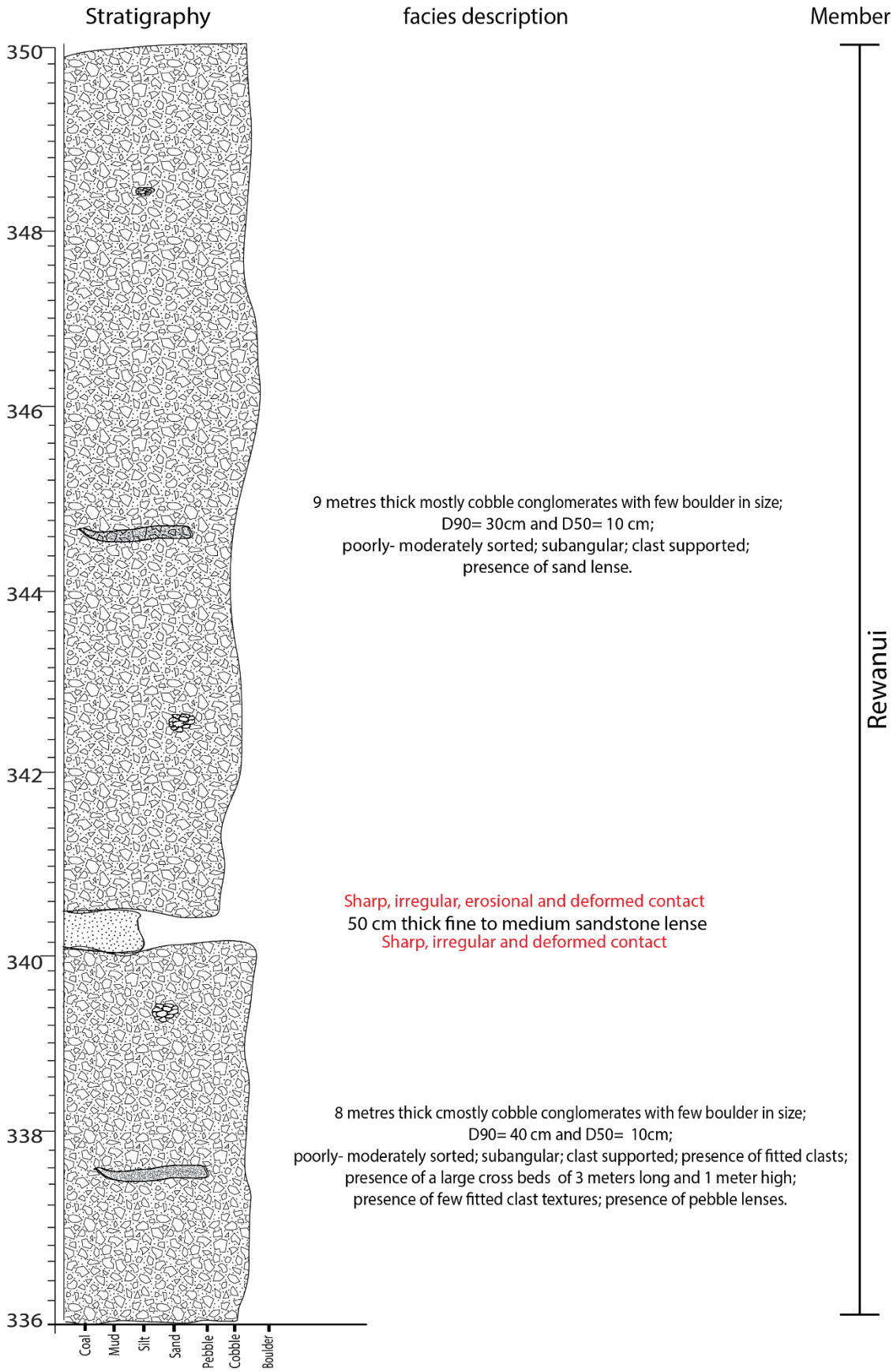
Stratigraphy
facies description
Member
350
348
346
344
342
340
338
336
9 metres thick mostly cobble conglomerates with few boulder in size;
D90= 30cm and D50= 10 cm;
poorly- moderately sorted; subangular; clast supported;
presence of sand lense.
Sharp, irregular, erosional and deformed contact
50 cm thick fine to medium sandstone lense
Sharp, irregular and deformed contact
8 metres thick cmostly cobble conglomerates with few boulder in size;
D90= 40 cm and D50= 10cm;
poorly- moderately sorted; subangular; clast supported; presence of fitted clasts;
presence of a large cross beds of 3 meters long and 1 meter high;
presence of few fitted clast textures; presence of pebble lenses.
Rewanui
Coal
Mud
Silt
Sand
Pebble
Cobble
Boulder

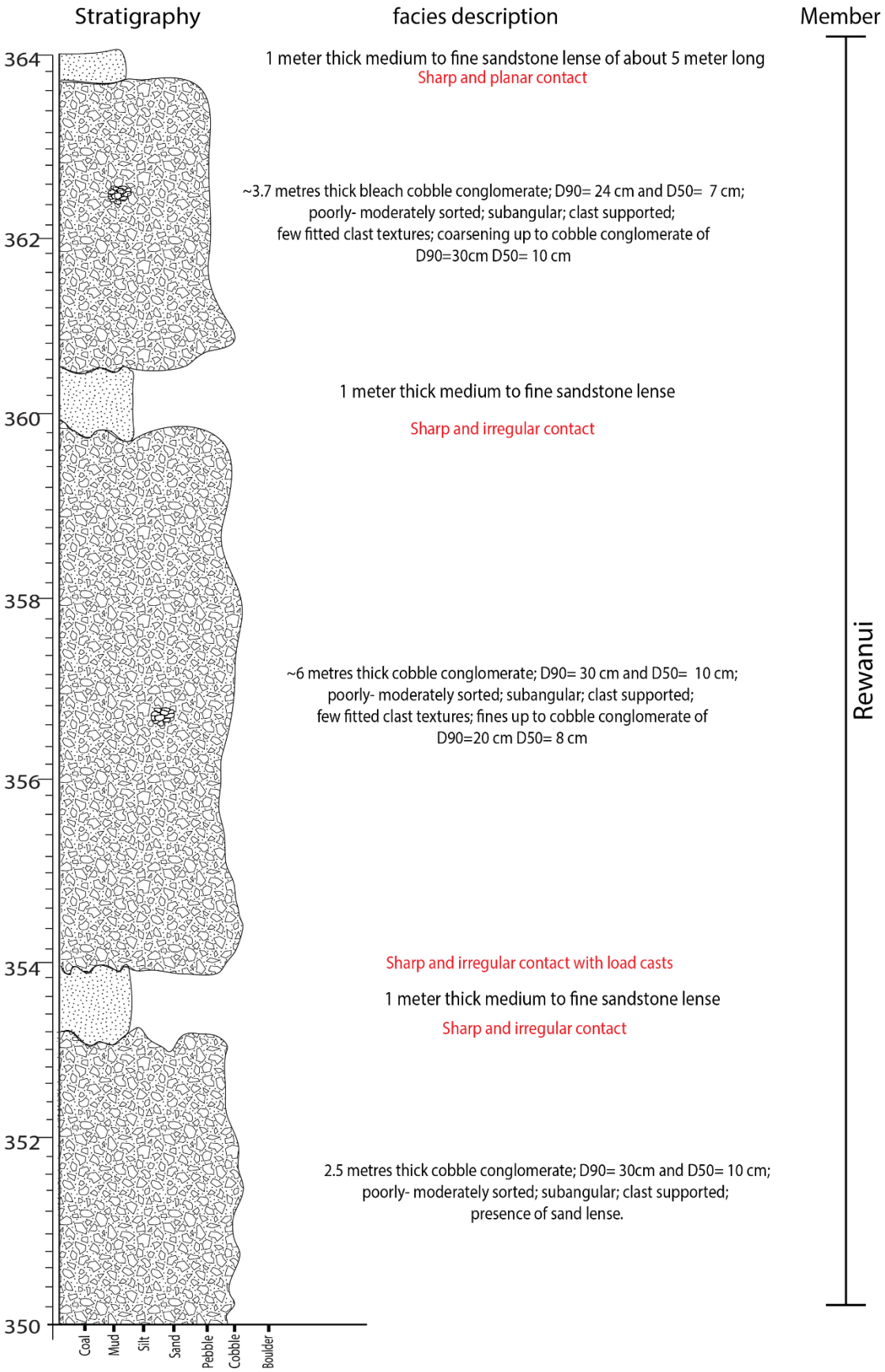
Stratigraphy
facies description
Member
364
362
360
358
356
354
352
350
1 meter thick medium to fine sandstone lense of about 5 meter long
Sharp and planar contact
~3.7 metres thick bleach cobble conglomerate; D90= 24 cm and D50= 7 cm;
poorly- moderately sorted; subangular; clast supported;
few fitted clast textures; coarsening up to cobble conglomerate of
D90=30cm D50= 10 cm
1 meter thick medium to fine sandstone lense
Sharp and irregular contact
~6 metres thick cobble conglomerate; D90= 30 cm and D50= 10 cm;
poorly- moderately sorted; subangular; clast supported;
few fitted clast textures; fines up to cobble conglomerate of
D90=20 cm D50= 8 cm
Sharp and irregular contact with load casts
1 meter thick medium to fine sandstone lense
Sharp and irregular contact
2.5 metres thick cobble conglomerate; D90= 30cm and D50= 10 cm;
poorly- moderately sorted; subangular; clast supported;
presence of sand lense.
Rewanui
Coal
Mud
Silt
Sand
Pebble
Cobble
Boulder

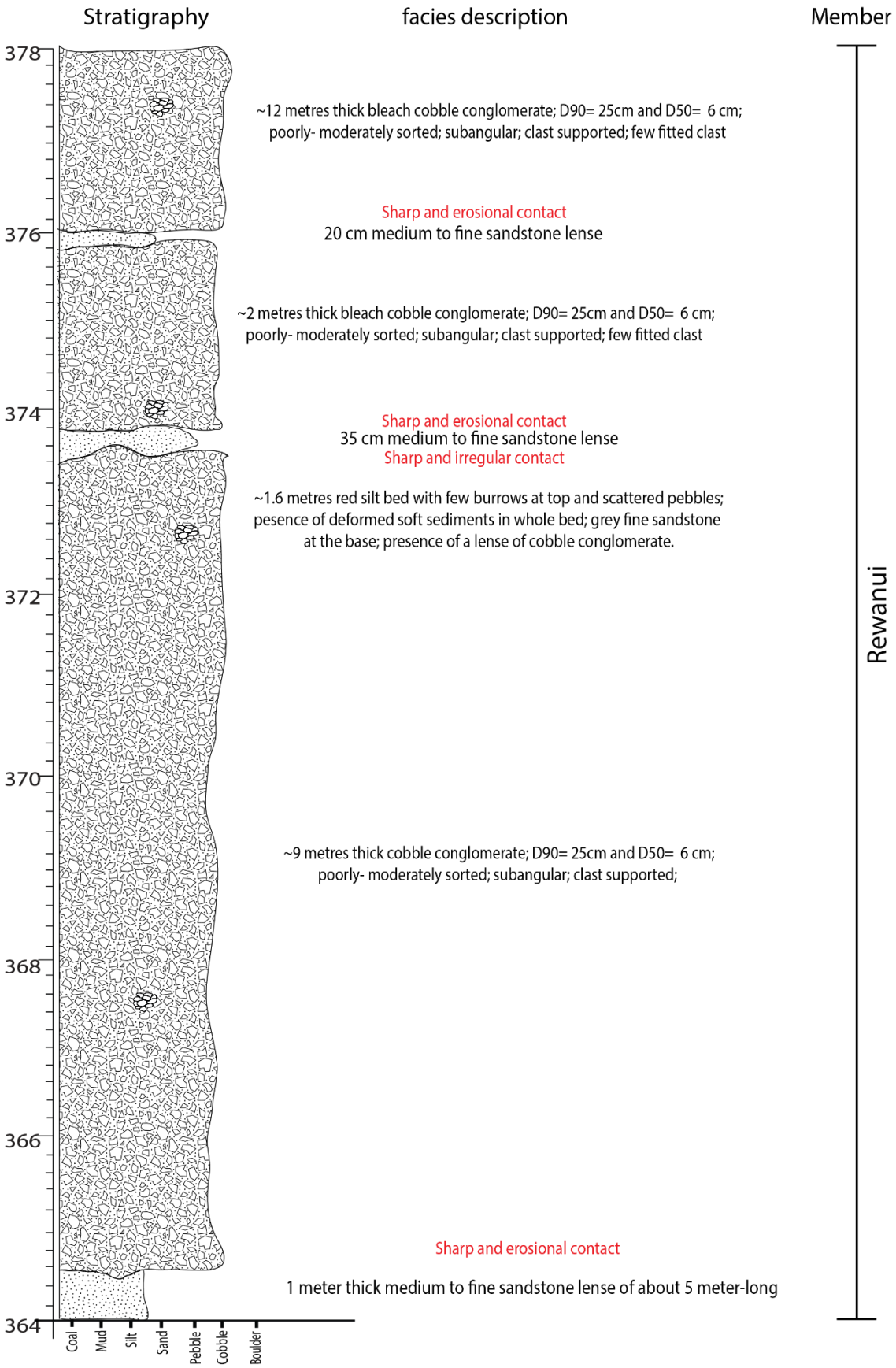
Stratigraphy
facies description
Member
378
376
374
372
370
368
366
364
~12 metres thick bleach cobble conglomerate; D90= 25cm and D50= 6 cm; poorly- moderately sorted; subangular; clast supported; few fitted clast
Sharp and erosional contact
20 cm medium to fine sandstone lense
~2 metres thick bleach cobble conglomerate; D90= 25cm and D50= 6 cm; poorly- moderately sorted; subangular; clast supported; few fitted clast
Sharp and erosional contact
35 cm medium to fine sandstone lense
Sharp and irregular contact
~1.6 metres red silt bed with few burrows at top and scattered pebbles; pesence of deformed soft sediments in whole bed; grey fine sandstone at the base; presence of a lense of cobble conglomerate.
~9 metres thick cobble conglomerate; D90= 25cm and D50= 6 cm; poorly- moderately sorted; subangular; clast supported;
Sharp and erosional contact
1 meter thick medium to fine sandstone lense of about 5 meter-long
Rewanui
Coal
Mud
Silt
Sand
Pebble
Cobble
Boulder

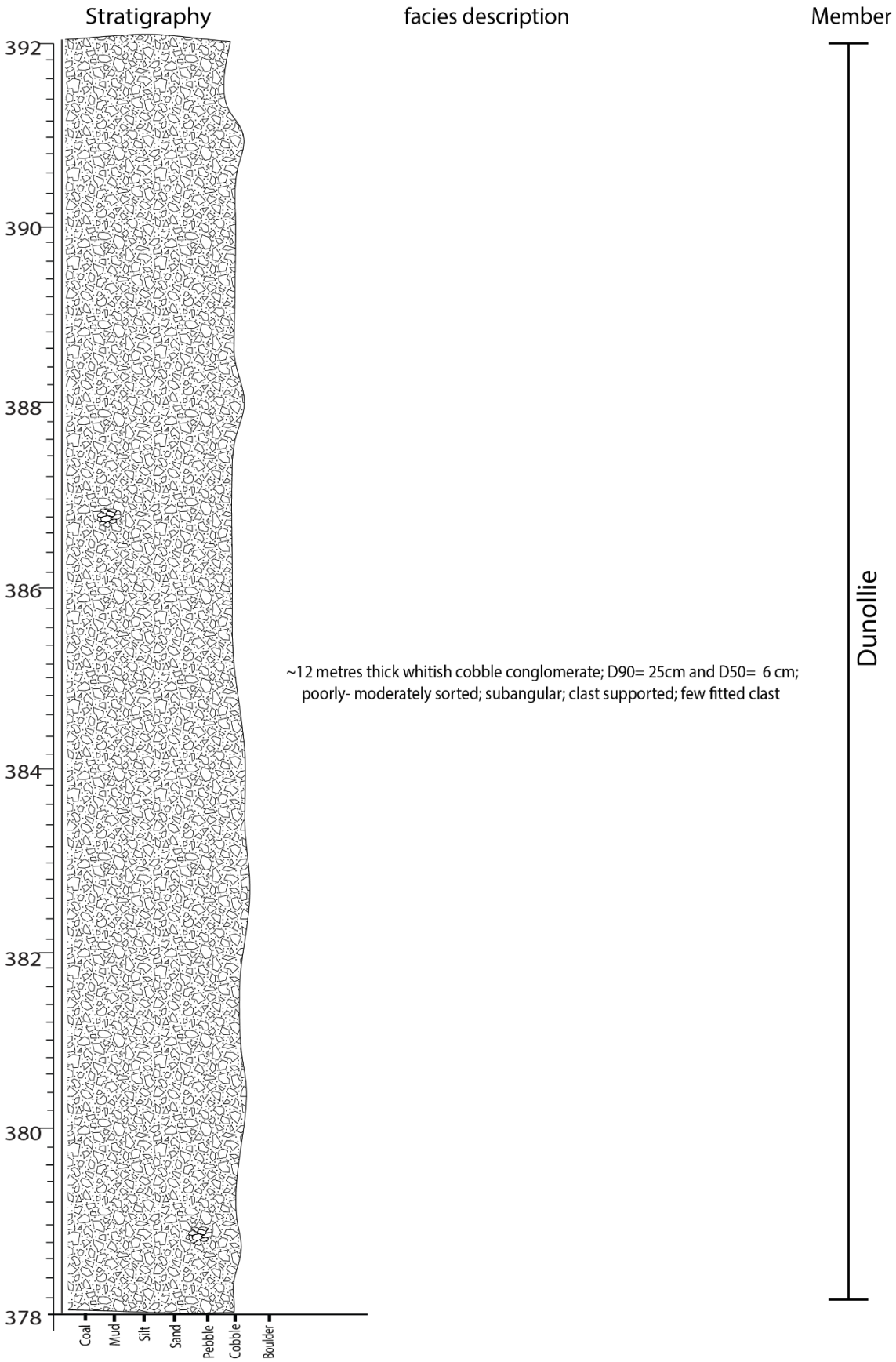
Stratigraphy
facies description
Member
392
390
388
386
384
382
380
378
~12 metres thick whitish cobble conglomerate; D90= 25cm and D50= 6 cm;
poorly- moderately sorted; subangular; clast supported; few fitted clast
Dunollie
Coal
Mud
Silt
Sand
Pebble
Cobble
Boulder

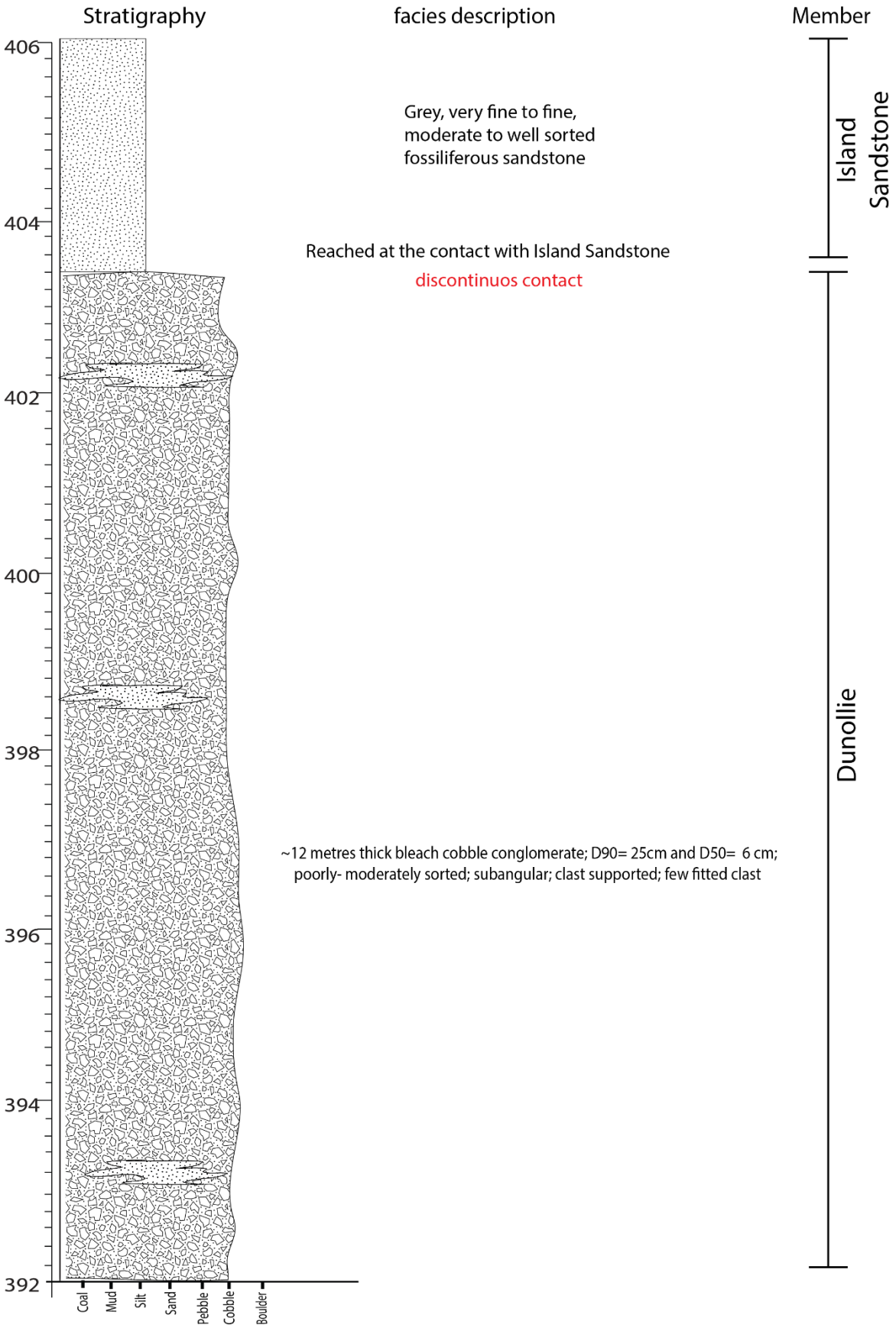
Stratigraphy
facies description
Member
406
404
402
400
398
396
394
392
Grey, very fine to fine,
moderate to well sorted
fossiliferous sandstone
Reached at the contact with Island Sandstone
discontinuos contact
~12 metres thick bleach cobble conglomerate; D90= 25cm and D50= 6 cm;
poorly- moderately sorted; subangular; clast supported; few fitted clast
Island Sandstone
Dunollie
Coal
Mud
Silt
Sand
Pebble
Cobble
Boulder

# Appendix 2: Drill hole data

## Legend for drill hole stratigraphy

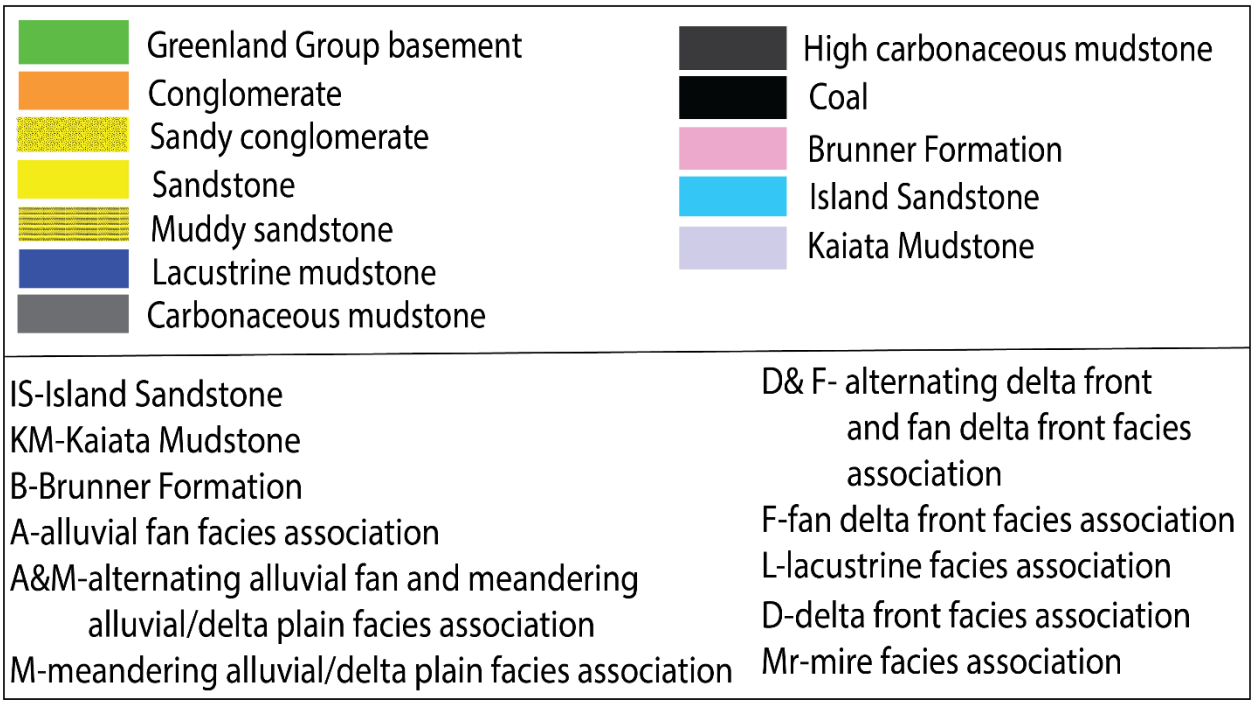


IS-Island Sandstone
KM-Kaiata Mudstone
B-Brunner Formation
A-alluvial fan facies association
A&M-alternating alluvial fan and meandering alluvial/delta plain facies association
M-meandering alluvial/delta plain facies association
D& F- alternating delta front and fan delta front facies association
F-fan delta front facies association
L-lacustrine facies association
D-delta front facies association
Mr-mire facies association

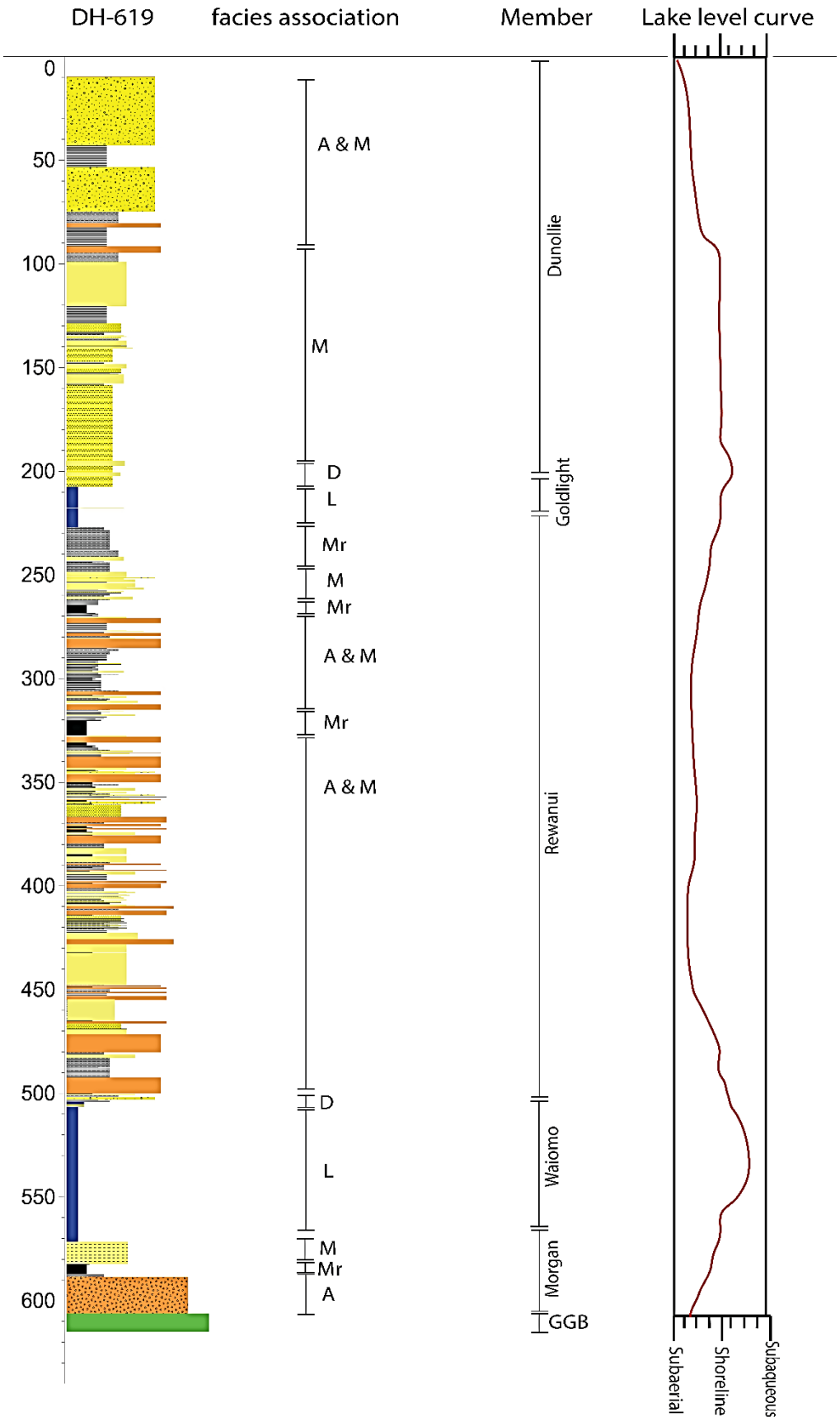
DH-619
facies association
Member
Lake level curve
0
50
100
150
200
250
300
350
400
450
500
550
600
A & M
M
D
L
Mr
M
Mr
A & M
Mr
A & M
D
L
M
Mr
A
Dunollie
Goldlight
Rewanui
Waiomo
Morgan
GGB
Subaerial
Shoreline
Subaqueous

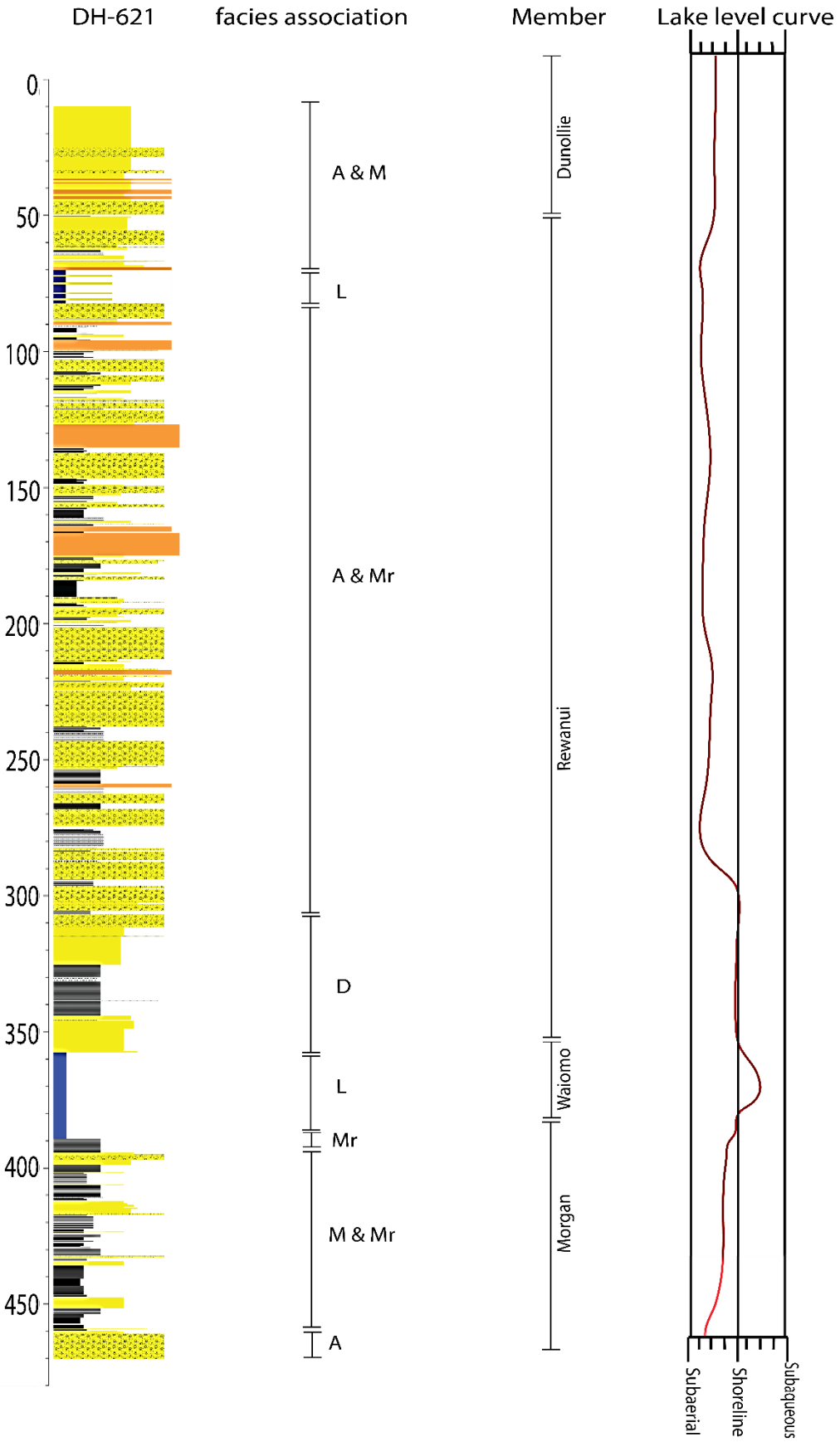
DH-621
facies association
Member
Lake level curve
0
50
100
150
200
250
300
350
400
450
A & M
L
A & Mr
D
L
Mr
M & Mr
A
Dunollie
Rewanui
Waiomo
Morgan
Subaerial
Shoreline
Subaqueous

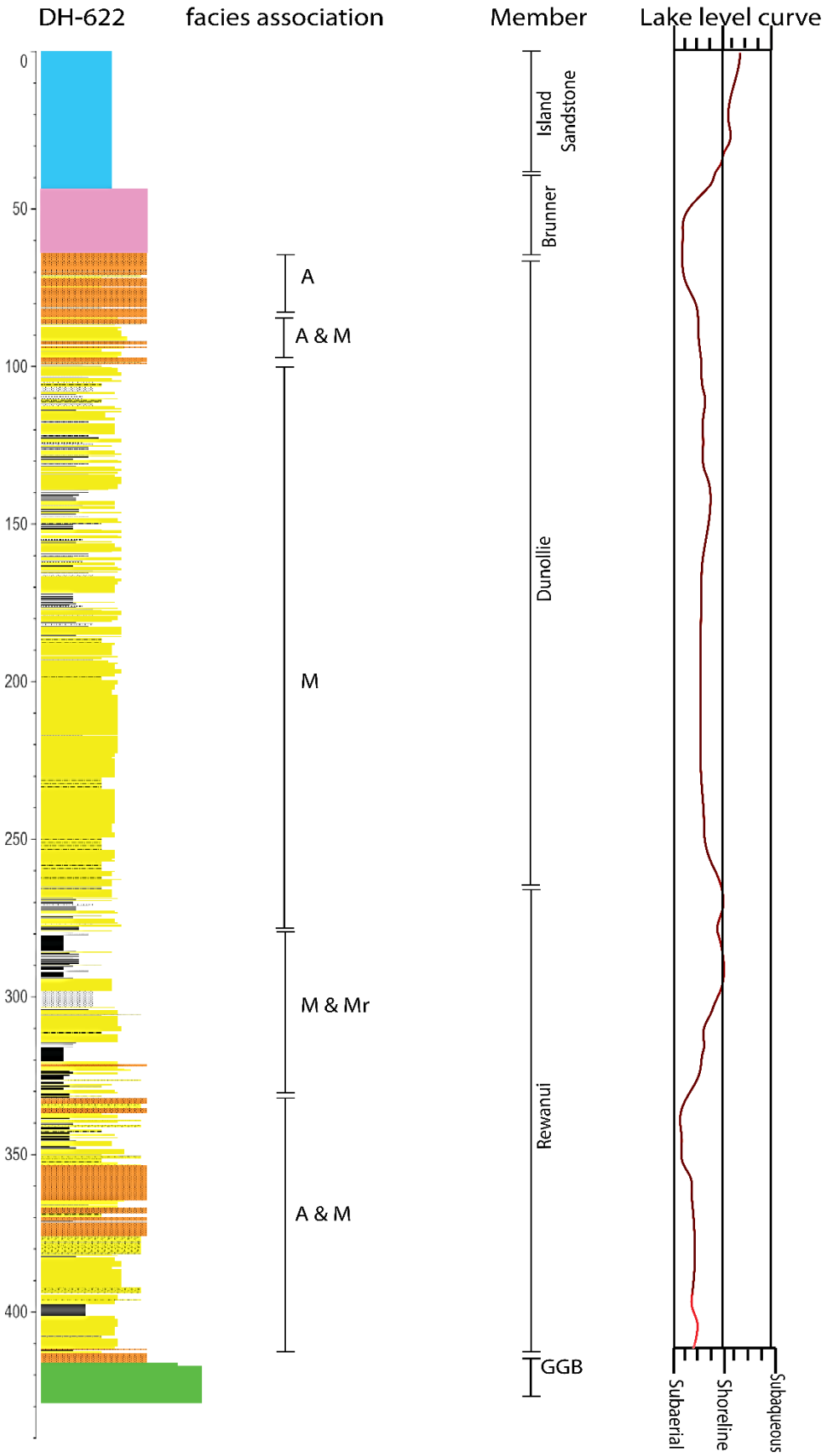
DH-622
facies association
Member
Lake level curve
0
50
100
150
200
250
300
350
400
A
A & M
M
M & Mr
A & M
Island Sandstone
Brunner
Dunollie
Rewanui
GGB
Subaerial
Shoreline
Subaqueous

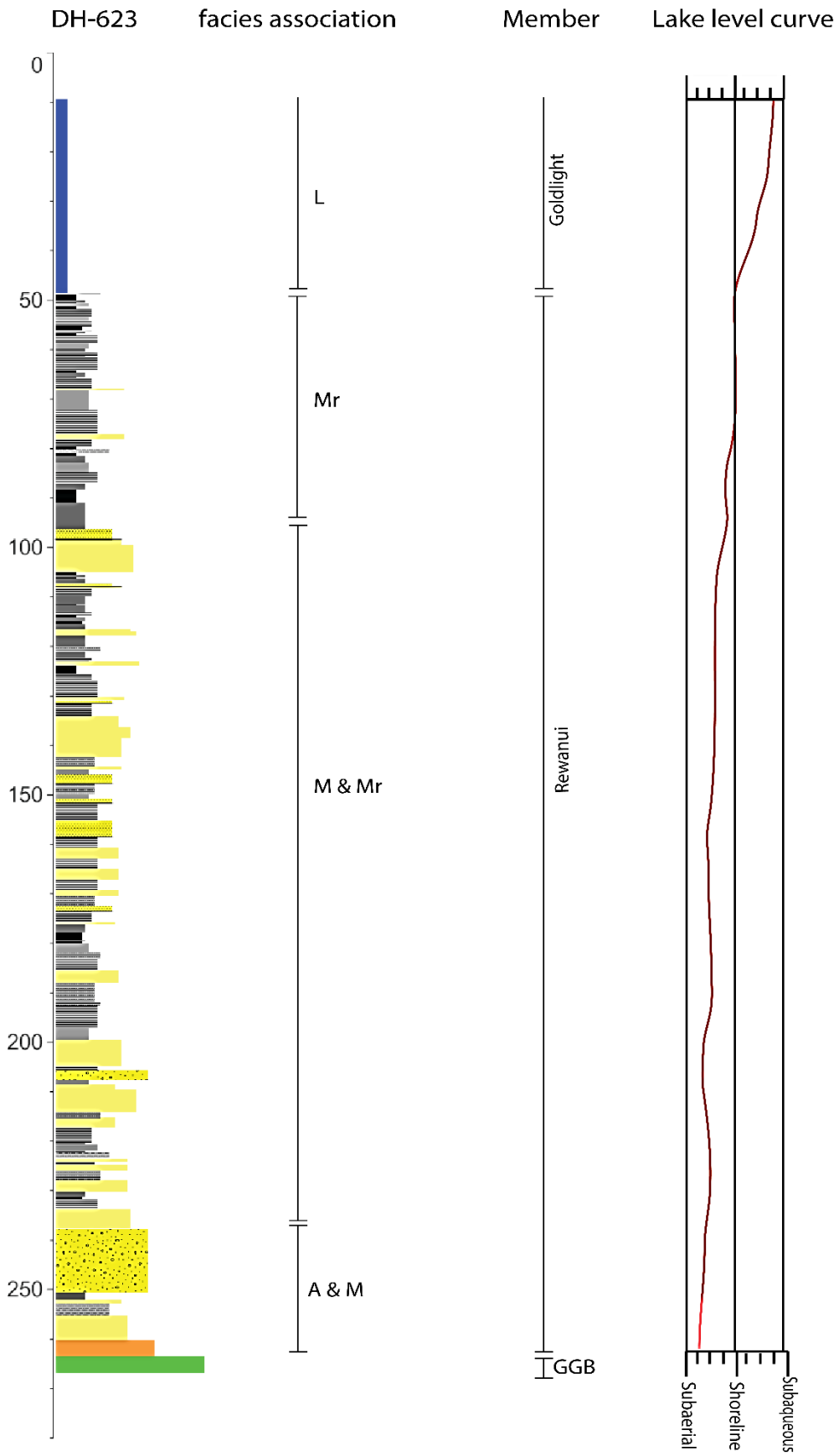
DH-623
facies association
Member
Lake level curve
0
50
100
150
200
250
L
Mr
M & Mr
A & M
Goldlight
Rewanui
GGB
Subaerial
Shoreline
Subaqueous

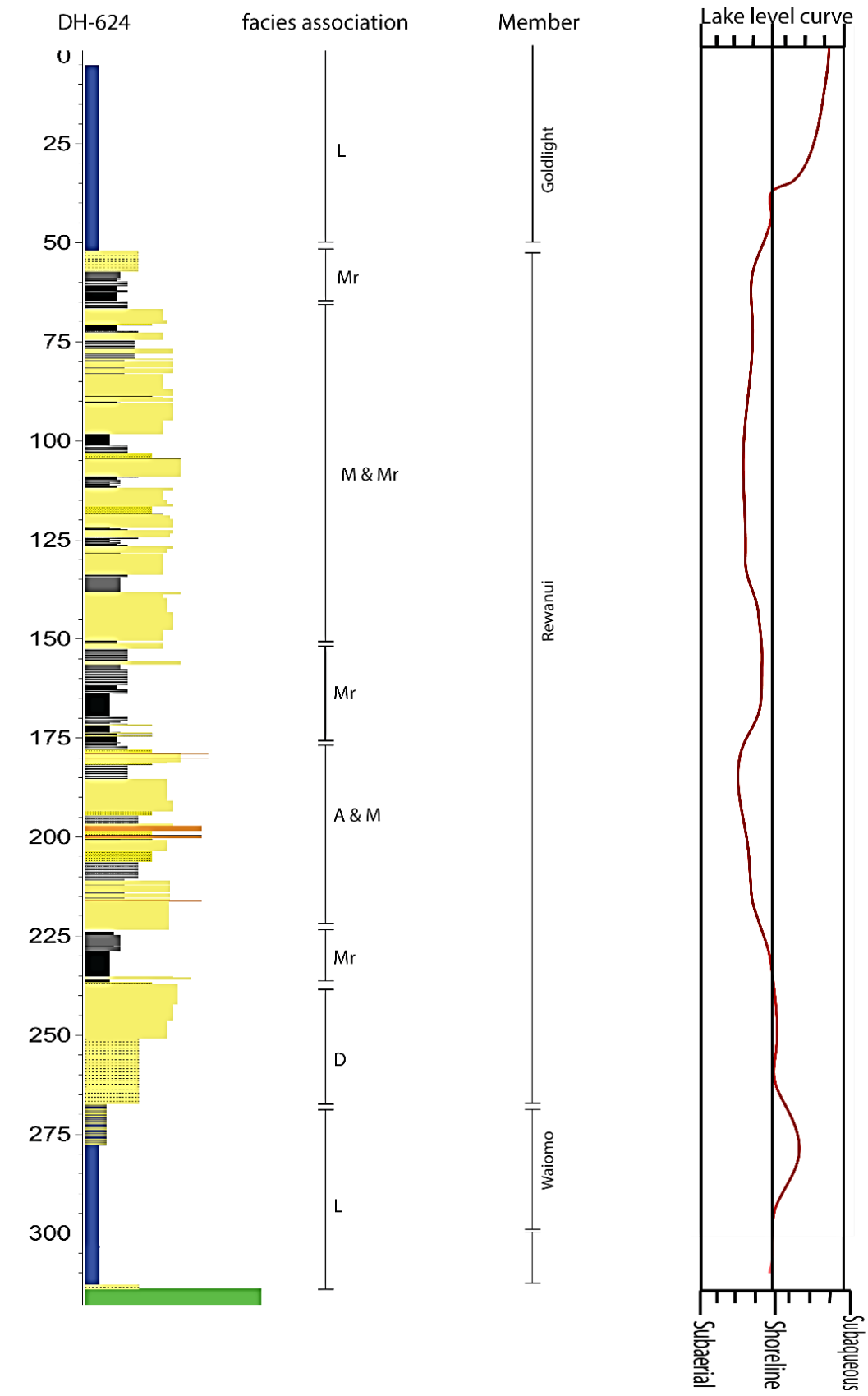
DH-624
facies association
Member
Lake level curve
0
25
50
75
100
125
150
175
200
225
250
275
300
L
Mr
M & Mr
Mr
A & M
Mr
D
L
Goldlight
Rewanui
Waiomo
Subaerial
Shoreline
Subaqueous

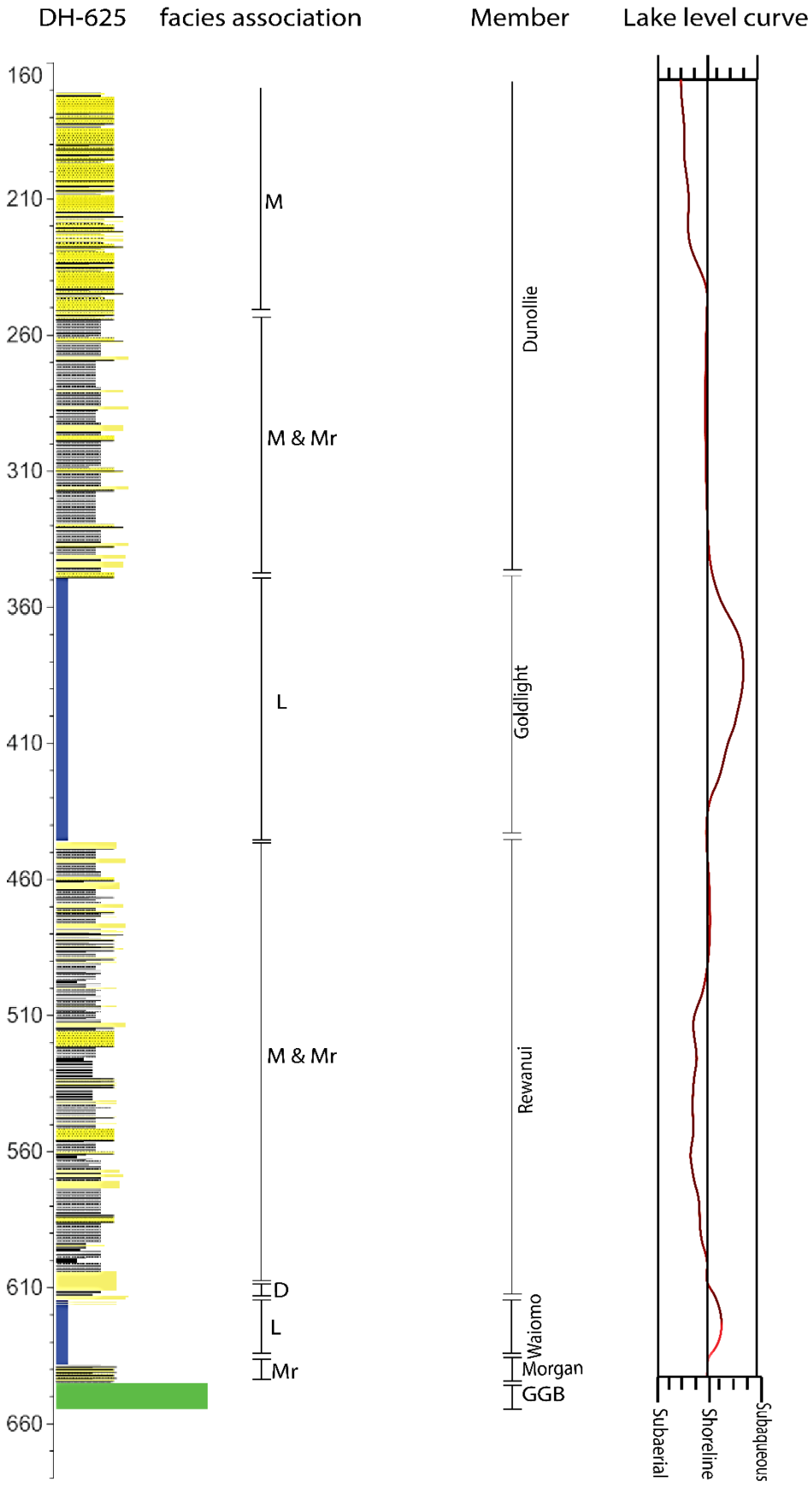
DH-625
facies association
Member
Lake level curve
160
210
260
310
360
410
460
510
560
610
660
M
M & Mr
L
M & Mr
D
L
Mr
Dunollie
Goldlight
Rewanui
Waiomo
Morgan
GGB
Subaerial
Shoreline
Subaqueous

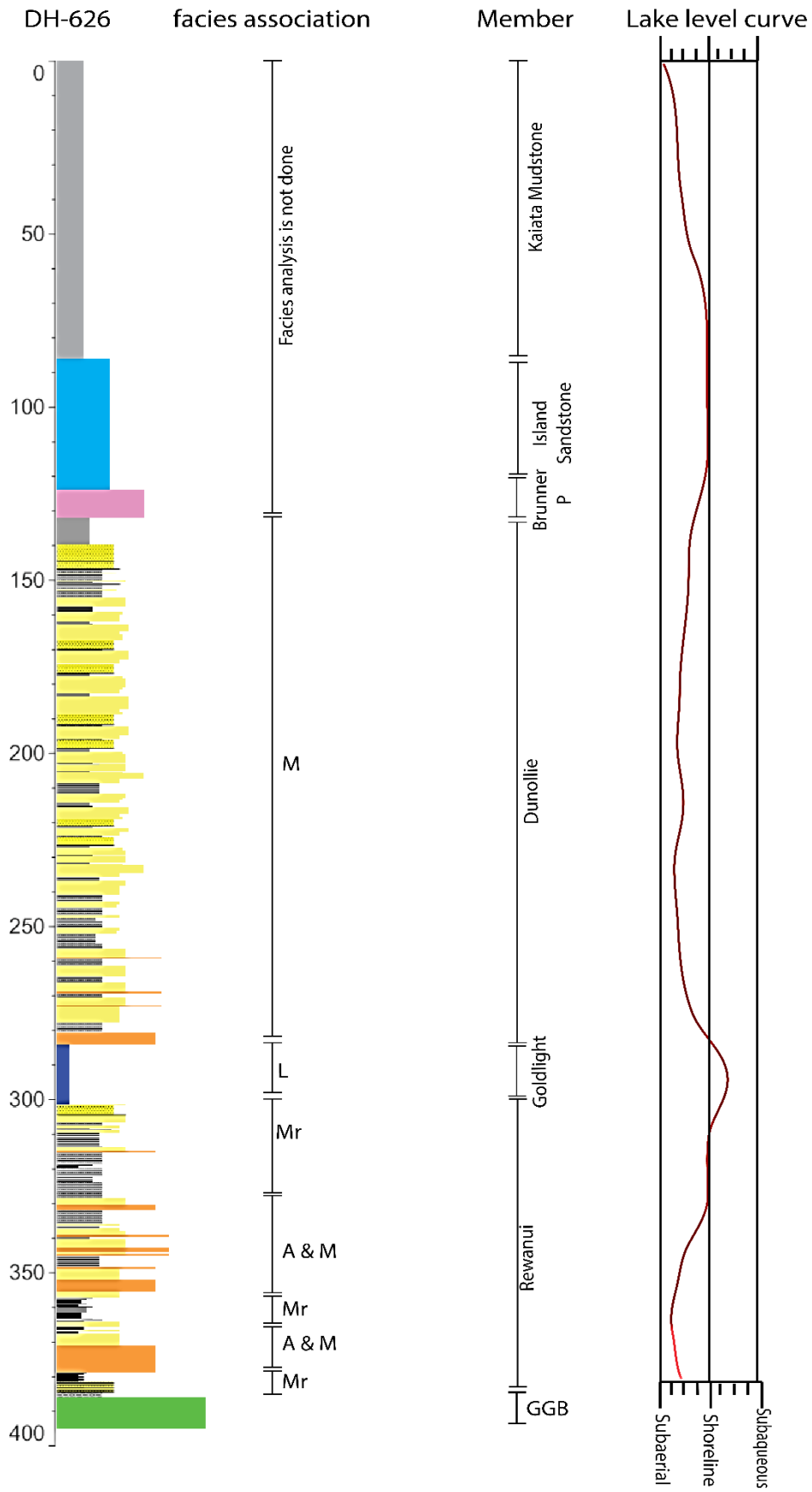
DH-626
facies association
Member
Lake level curve
0
50
100
150
200
250
300
350
400
Facies analysis is not done
M
L
Mr
A & M
Mr
A & M
Mr
Kaiata Mudstone
Brunner Island Sandstone P
Dunollie
Goldlight
Rewanui
GGB
Subaerial
Shoreline
Subaqueous

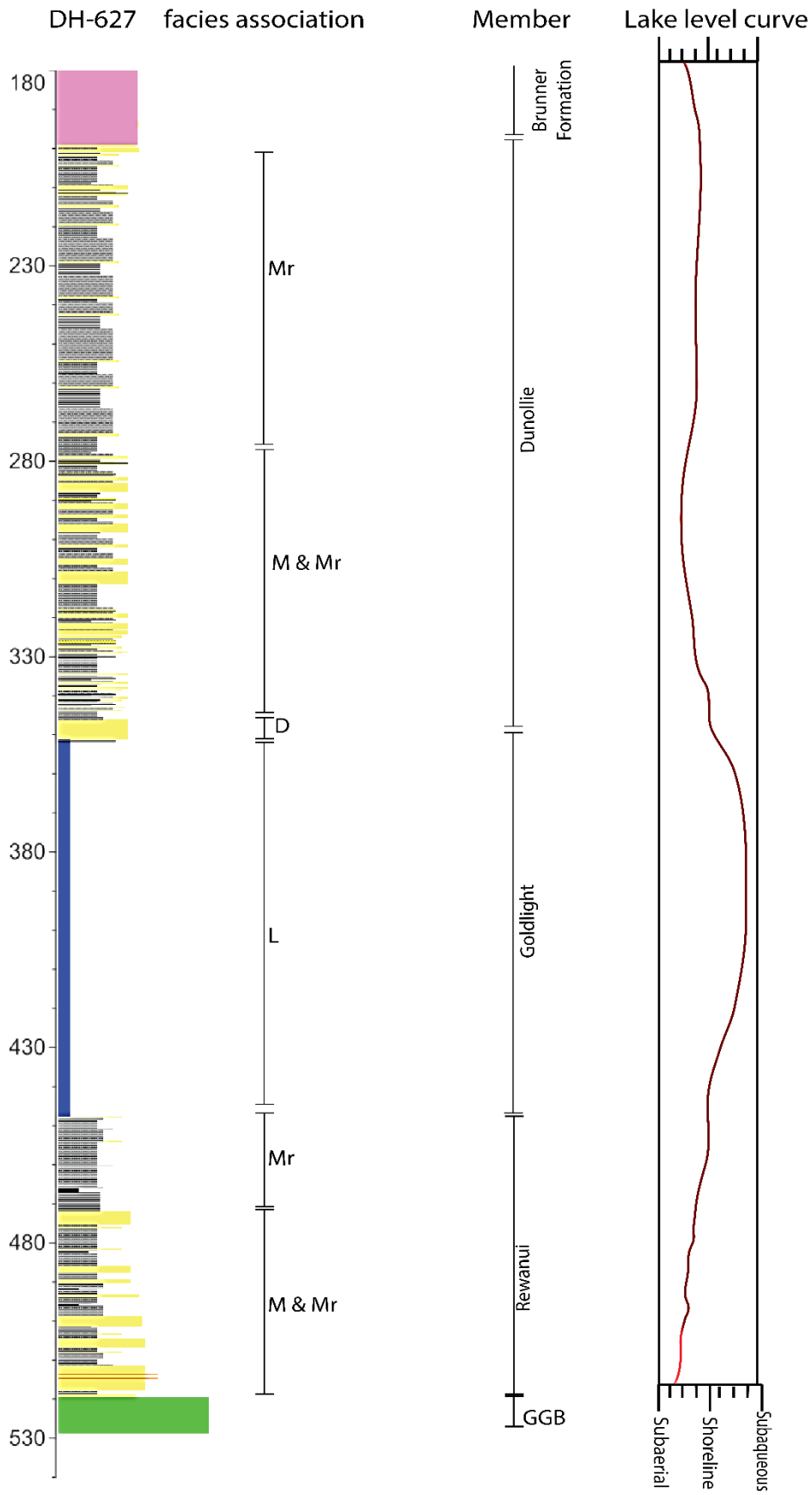
DH-627
facies association
Member
Lake level curve
180
230
280
330
380
430
480
530
Mr
M & Mr
D
L
Mr
M & Mr
Brunner Formation
Dunollie
Goldlight
Rewanui
GGB
Subaerial
Shoreline
Subaqueous

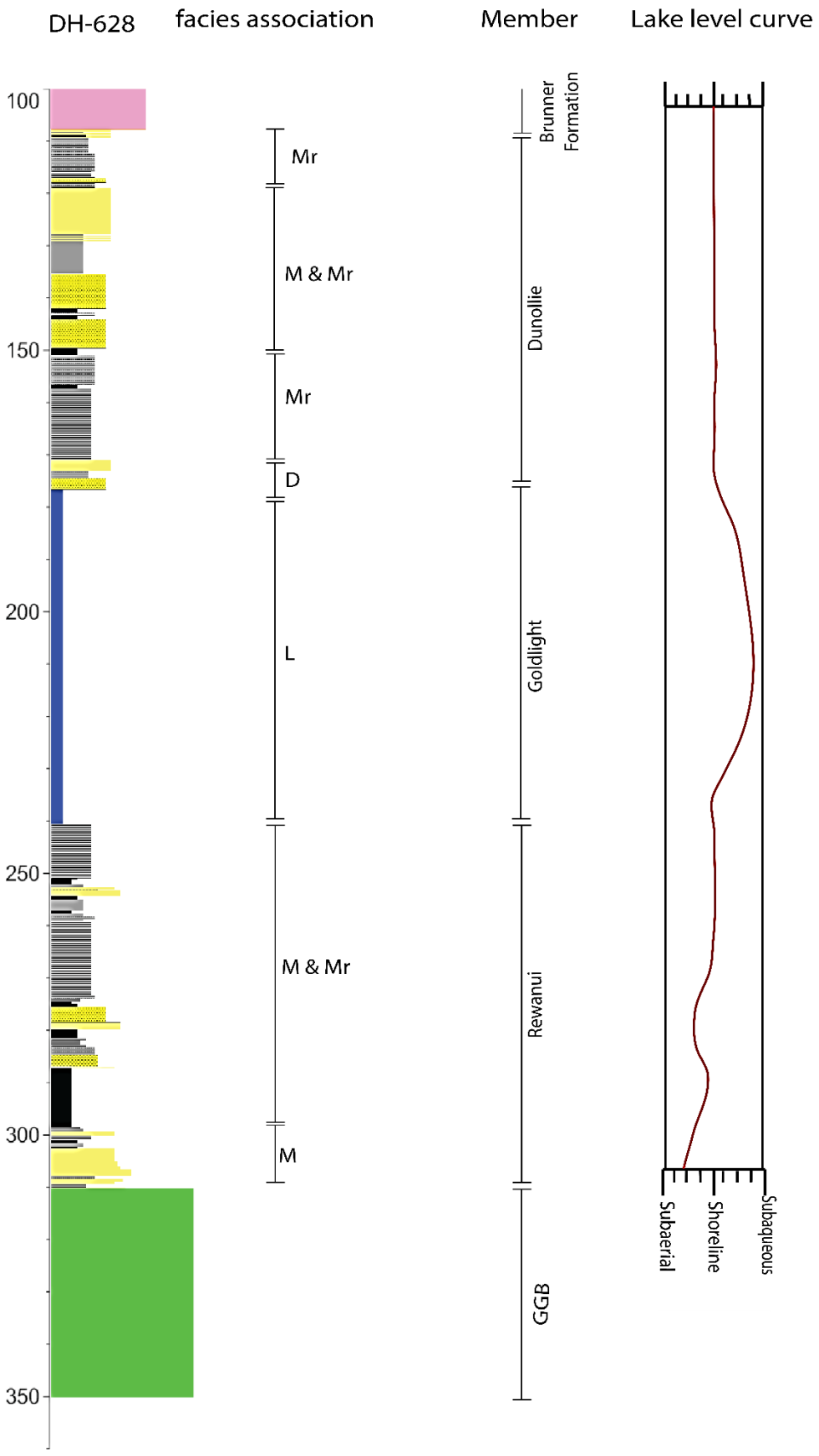
DH-628
facies association
Member
Lake level curve
100
150
200
250
300
350
Mr
M & Mr
Mr
D
L
M & Mr
M
Brunner Formation
Dunollie
Goldlight
Rewanui
GGB
Subaerial
Shoreline
Subaqueous

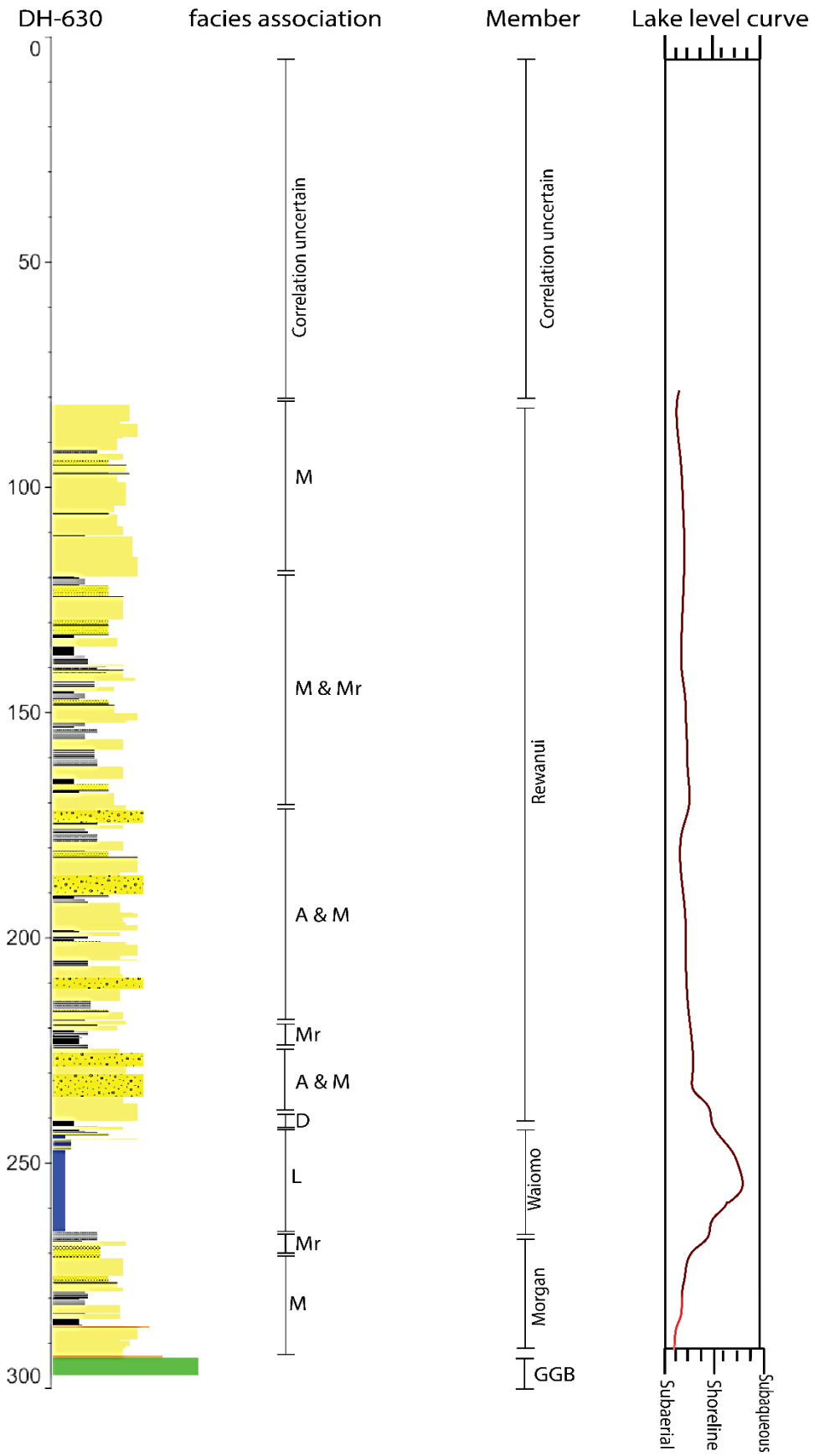
DH-630
facies association
Member
Lake level curve
0
50
100
150
200
250
300
Correlation uncertain
M
M & Mr
A & M
Mr
A & M
D
L
Mr
M
Correlation uncertain
Rewanui
Waiomo
Morgan
GGB
Subaerial
Shoreline
Subaqueous

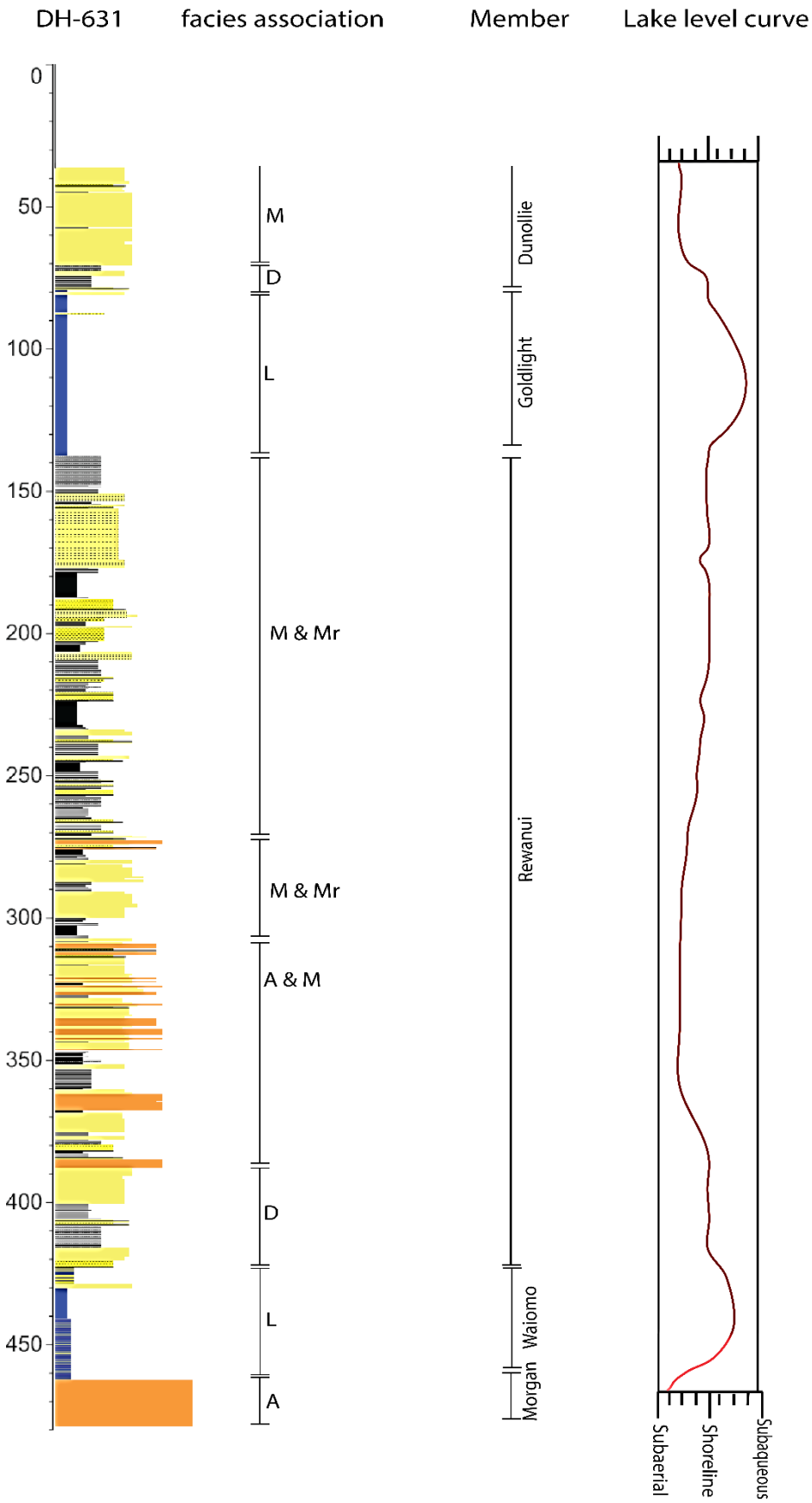
DH-631
facies association
Member
Lake level curve
0
50
100
150
200
250
300
350
400
450
M
D
L
M & Mr
M & Mr
A & M
D
L
A
Dunollie
Goldlight
Rewanui
Waiomo
Morgan
Subaerial
Shoreline
Subaqueous

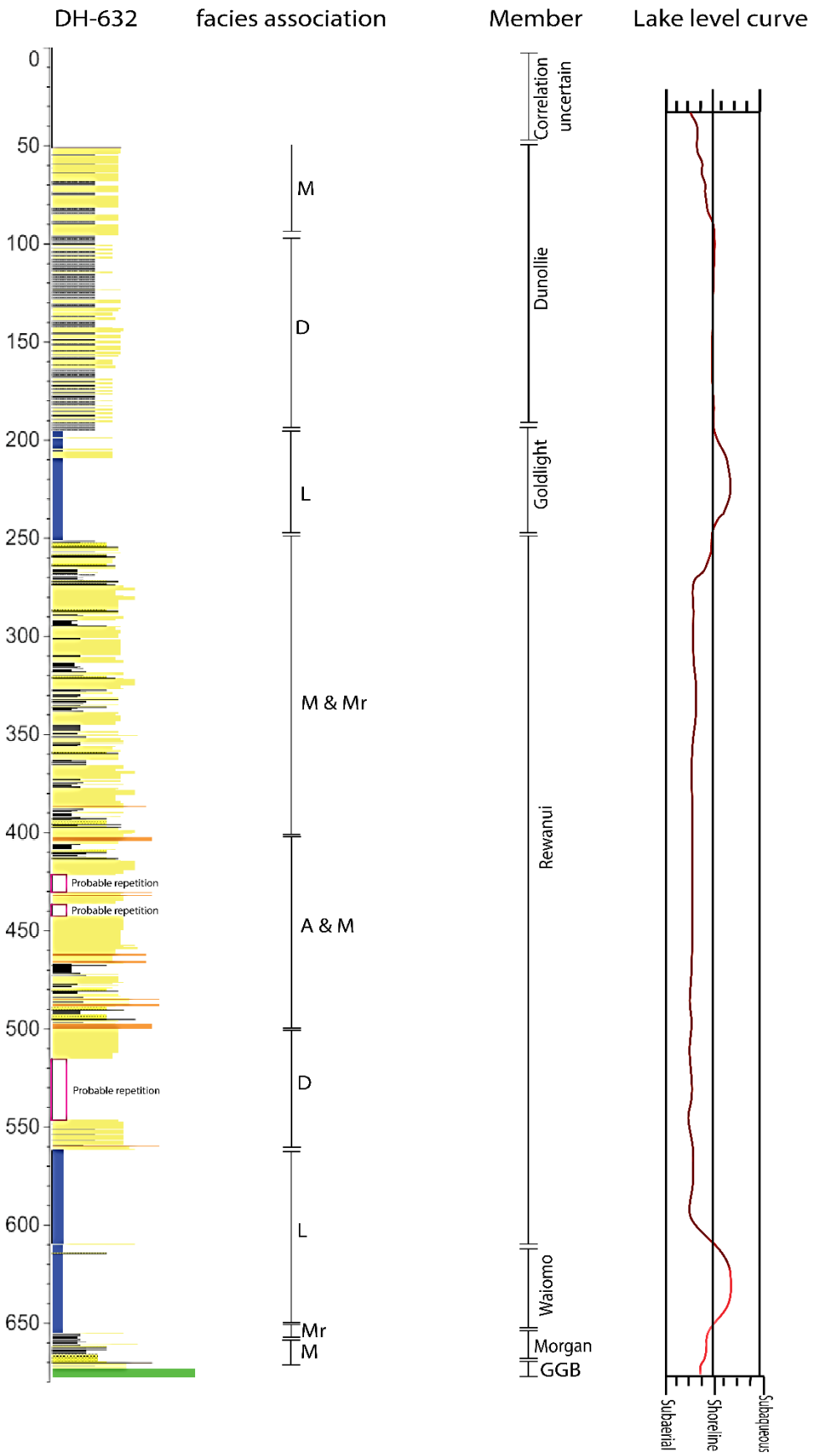
DH-632
facies association
Member
Lake level curve
0
50
100
150
200
250
300
350
400
450
500
550
600
650
Probable repetition
Probable repetition
Probable repetition
M
D
L
M & Mr
A & M
D
L
Mr
M
Correlation uncertain
Dunollie
Goldlight
Rewanui
Waiomo
Morgan
GGB
Subaerial
Shoreline
Subaqueous

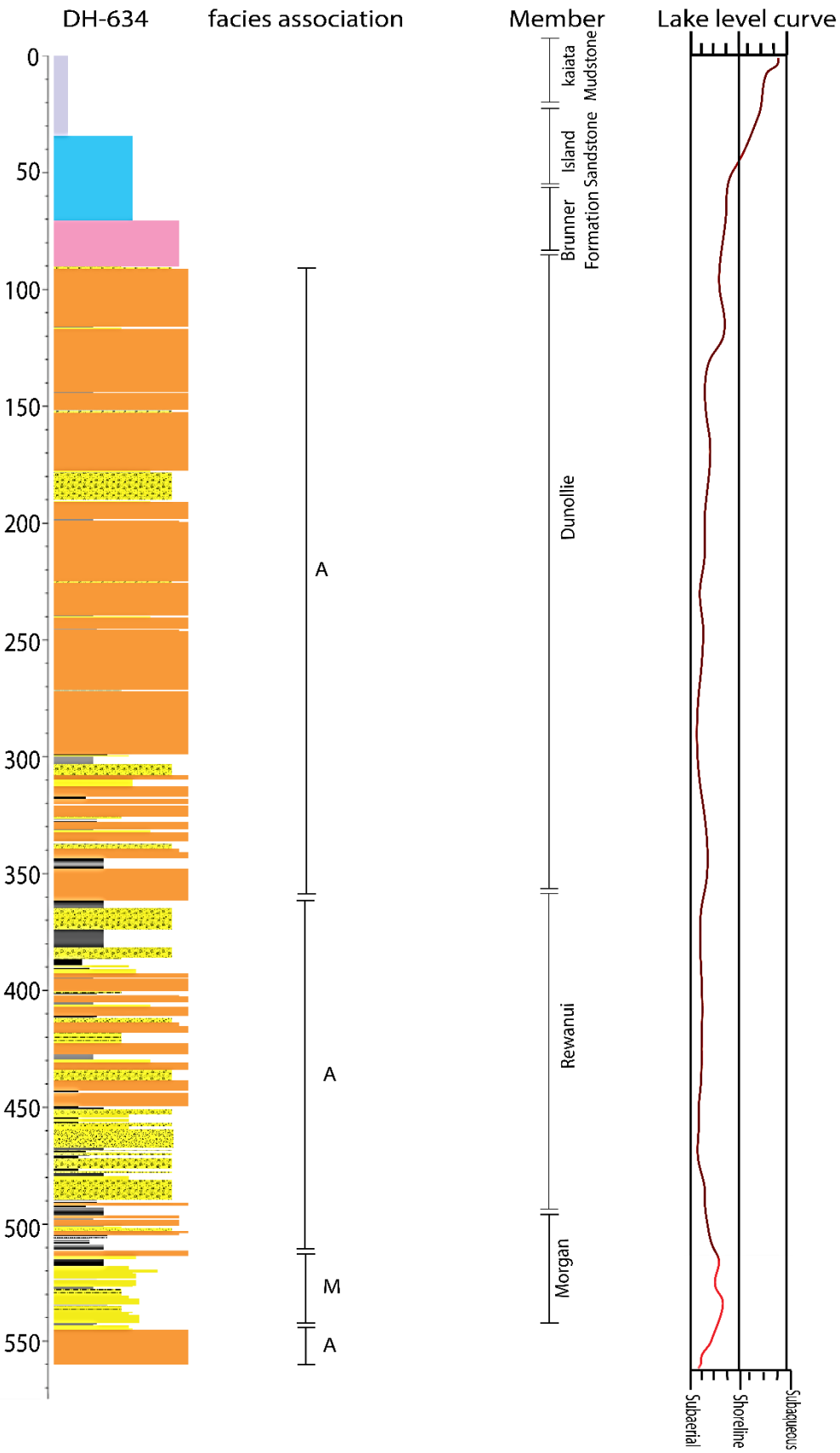
DH-634
facies association
Member
Lake level curve
0
50
100
150
200
250
300
350
400
450
500
550
A
A
M
A
kaiata Mudstone
Island Sandstone
Brunner Formation
Dunollie
Rewanui
Morgan
Subaerial
Shoreline
Subaqueous

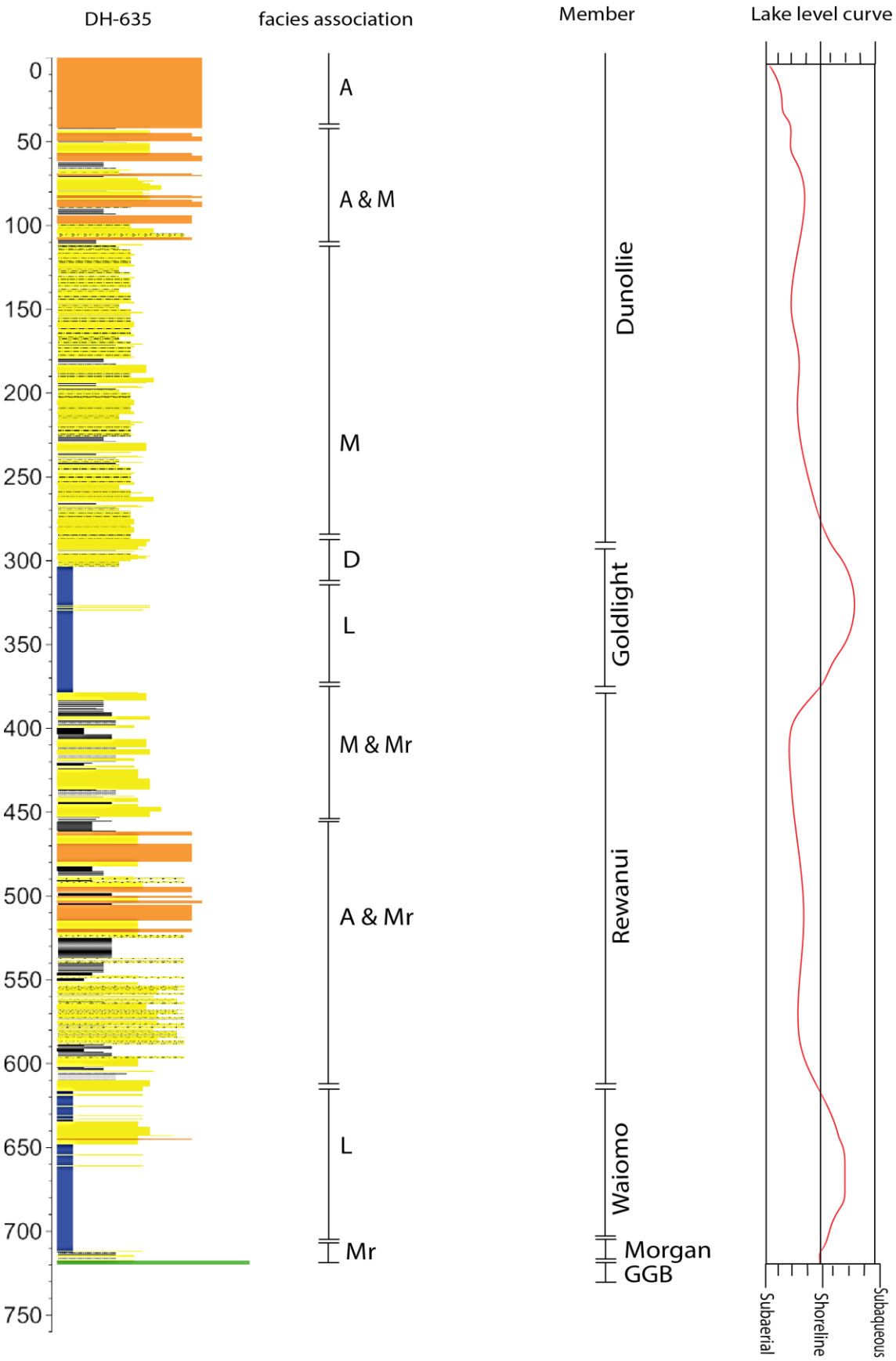
DH-635
facies association
Member
Lake level curve
0
50
100
150
200
250
300
350
400
450
500
550
600
650
700
750
A
A & M
M
D
L
M & Mr
A & Mr
L
Mr
Dunollie
Goldlight
Rewanui
Waiomo
Morgan
GGB
Subaerial
Shoreline
Subaqueous

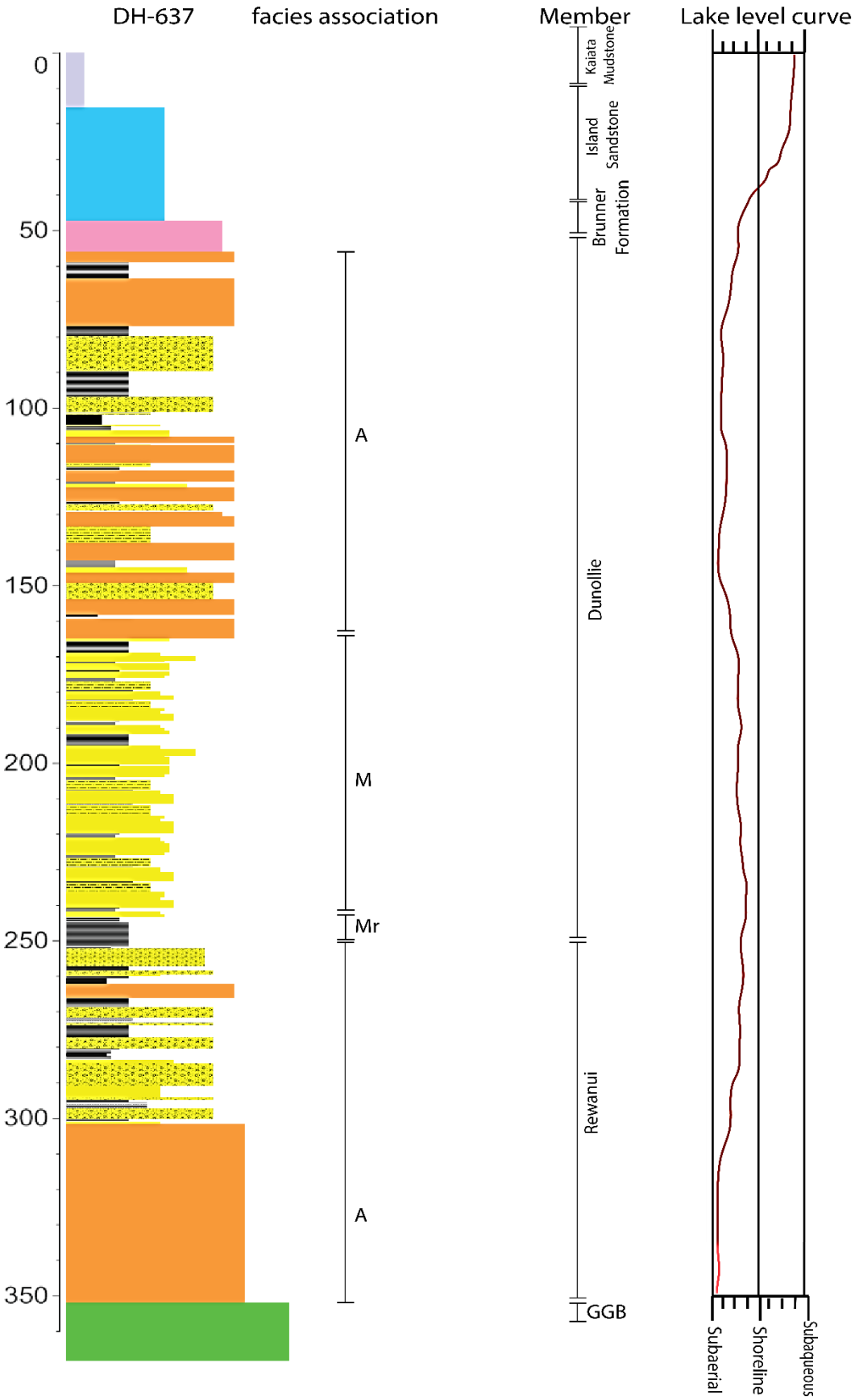
DH-637
facies association
Member
Lake level curve
0
50
100
150
200
250
300
350
A
M
Mr
A
Kaiata Mudstone
Island Sandstone
Brunner Formation
Dunollie
Rewanui
GGB
Subaerial
Shoreline
Subaqueous

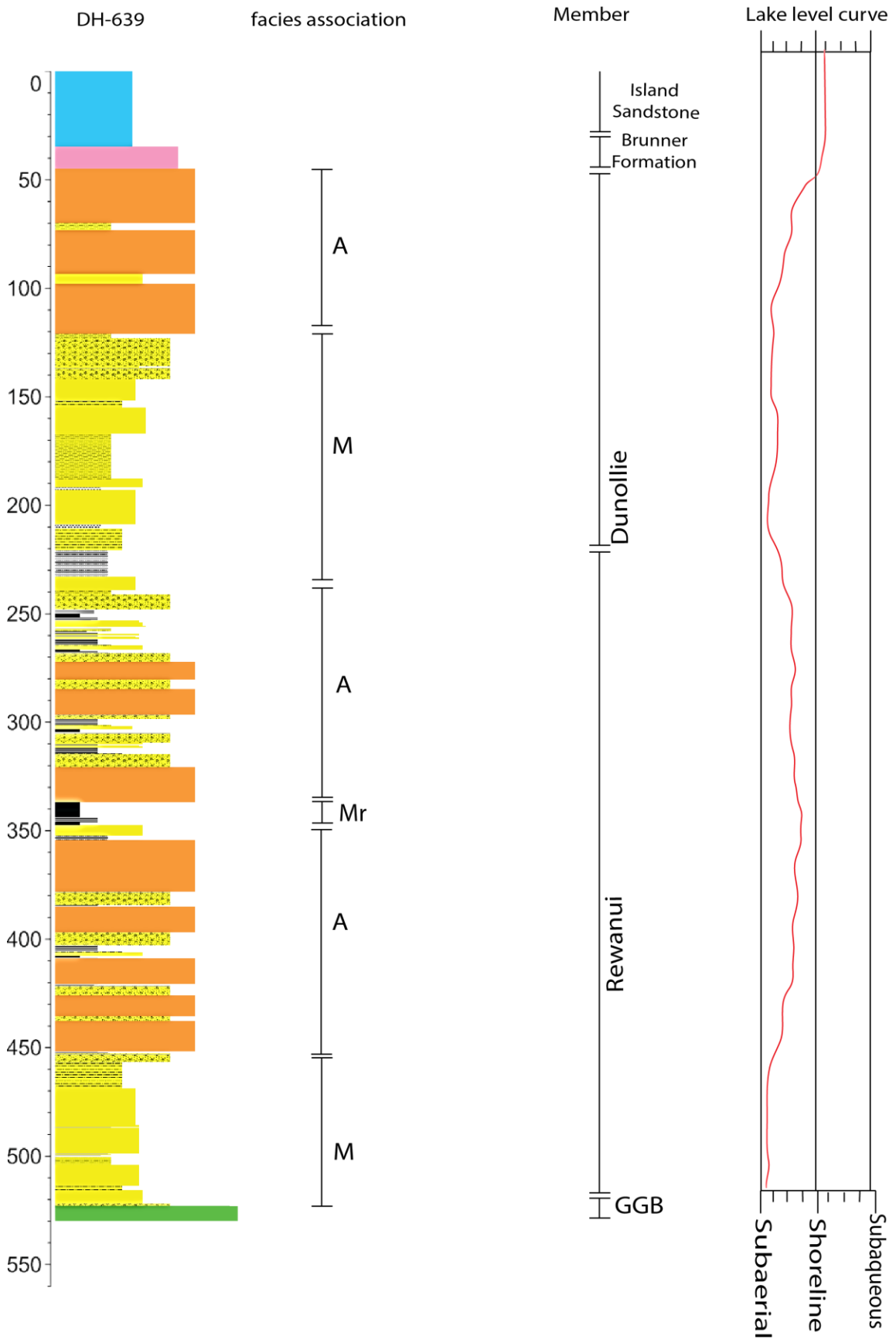
DH-639
facies association
Member
Lake level curve
0
50
100
150
200
250
300
350
400
450
500
550
A
M
A
Mr
A
M
Island Sandstone
Brunner Formation
Dunollie
Rewanui
GGB
Subaerial
Shoreline
Subaqueous

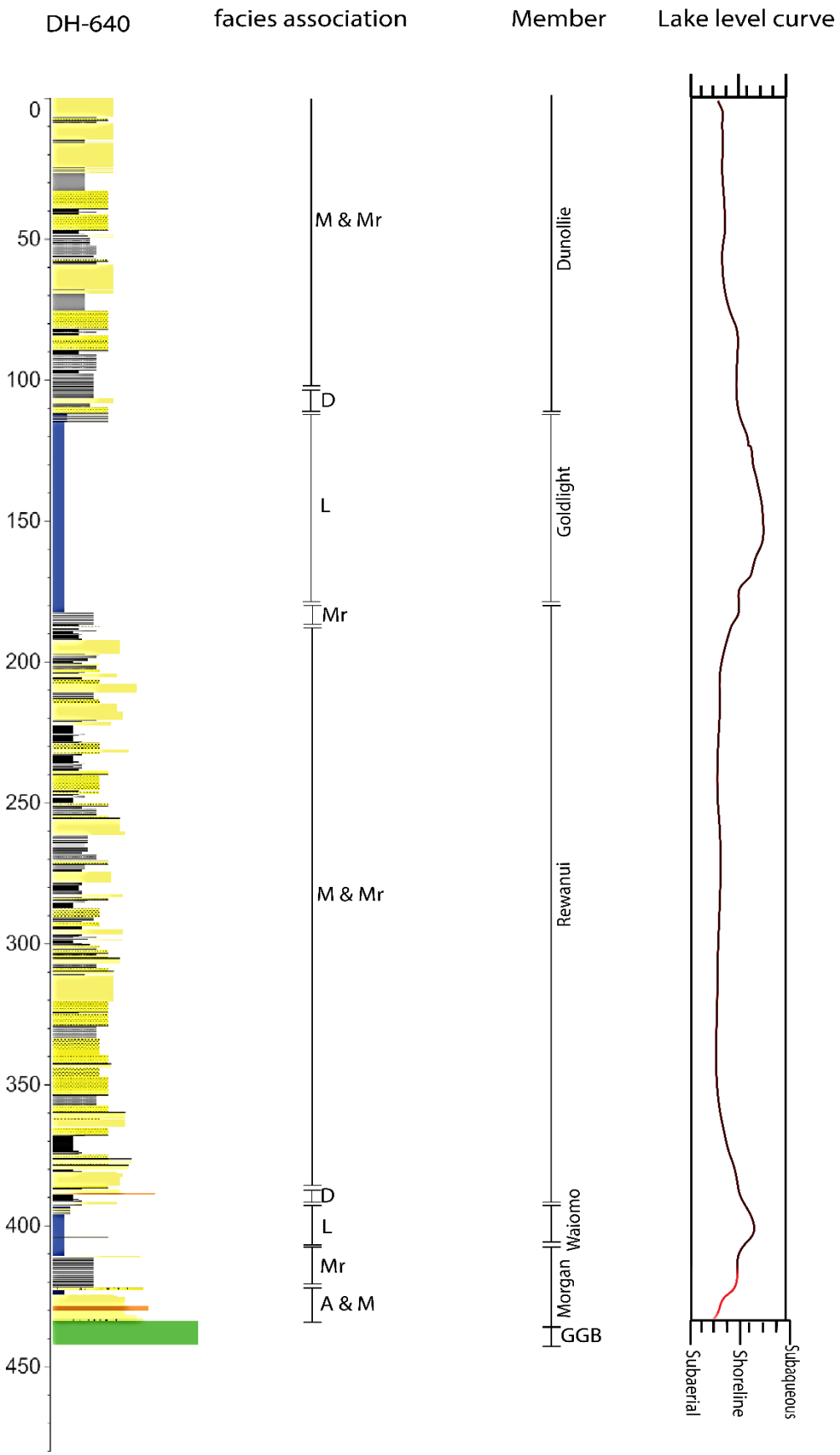
DH-640
facies association
Member
Lake level curve
0
50
100
150
200
250
300
350
400
450
M & Mr
D
L
Mr
M & Mr
D
L
Mr
A & M
Dunollie
Goldlight
Rewanui
Waiomo
Morgan
GGB
Subaerial
Shoreline
Subaqueous

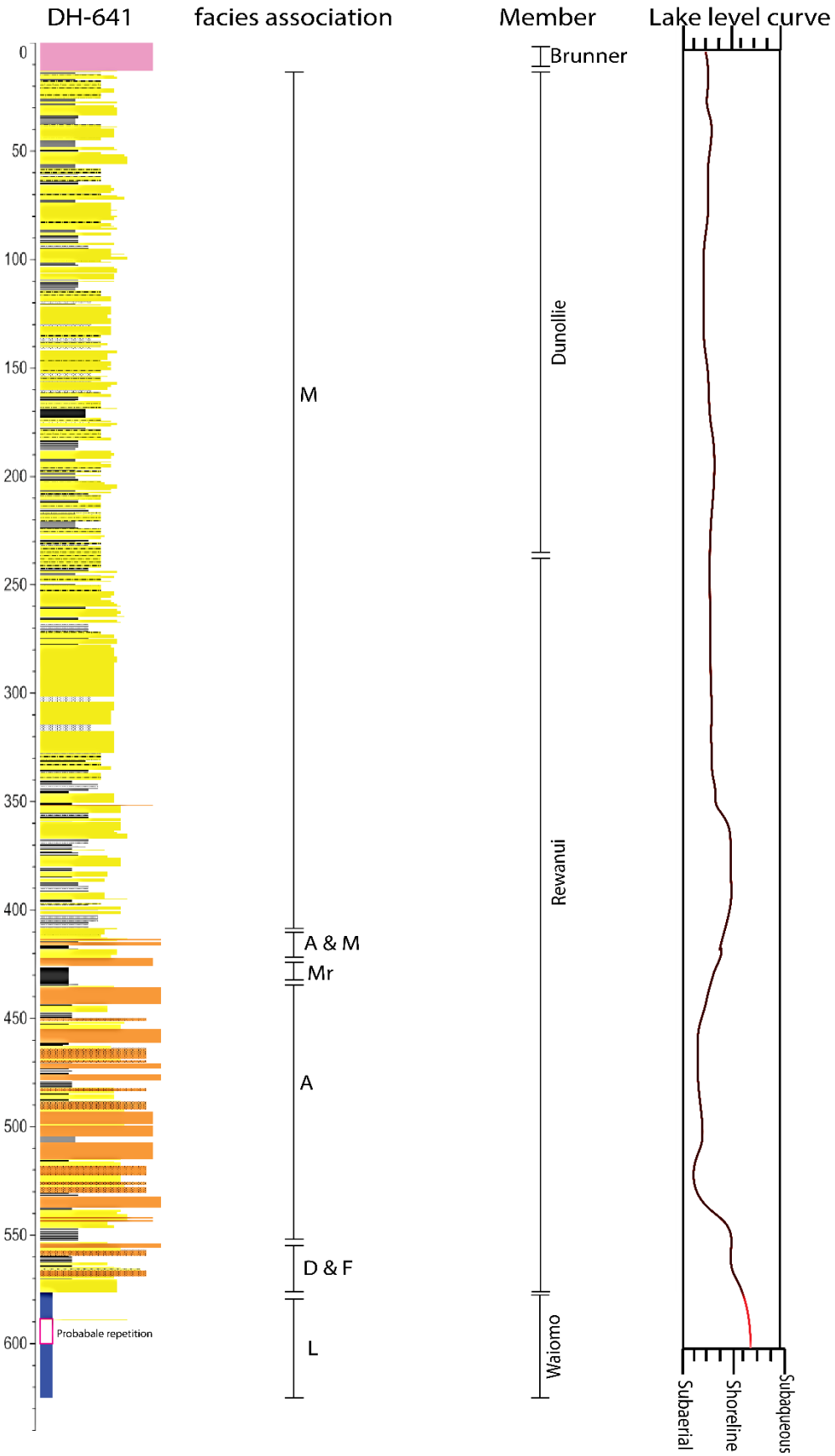
DH-641
facies association
Member
Lake level curve
0
50
100
150
200
250
300
350
400
450
500
550
600
Probabale repetition
M
A & M
Mr
A
D & F
L
Brunner
Dunollie
Rewanui
Waiomo
Subaerial
Shoreline
Subaqueous

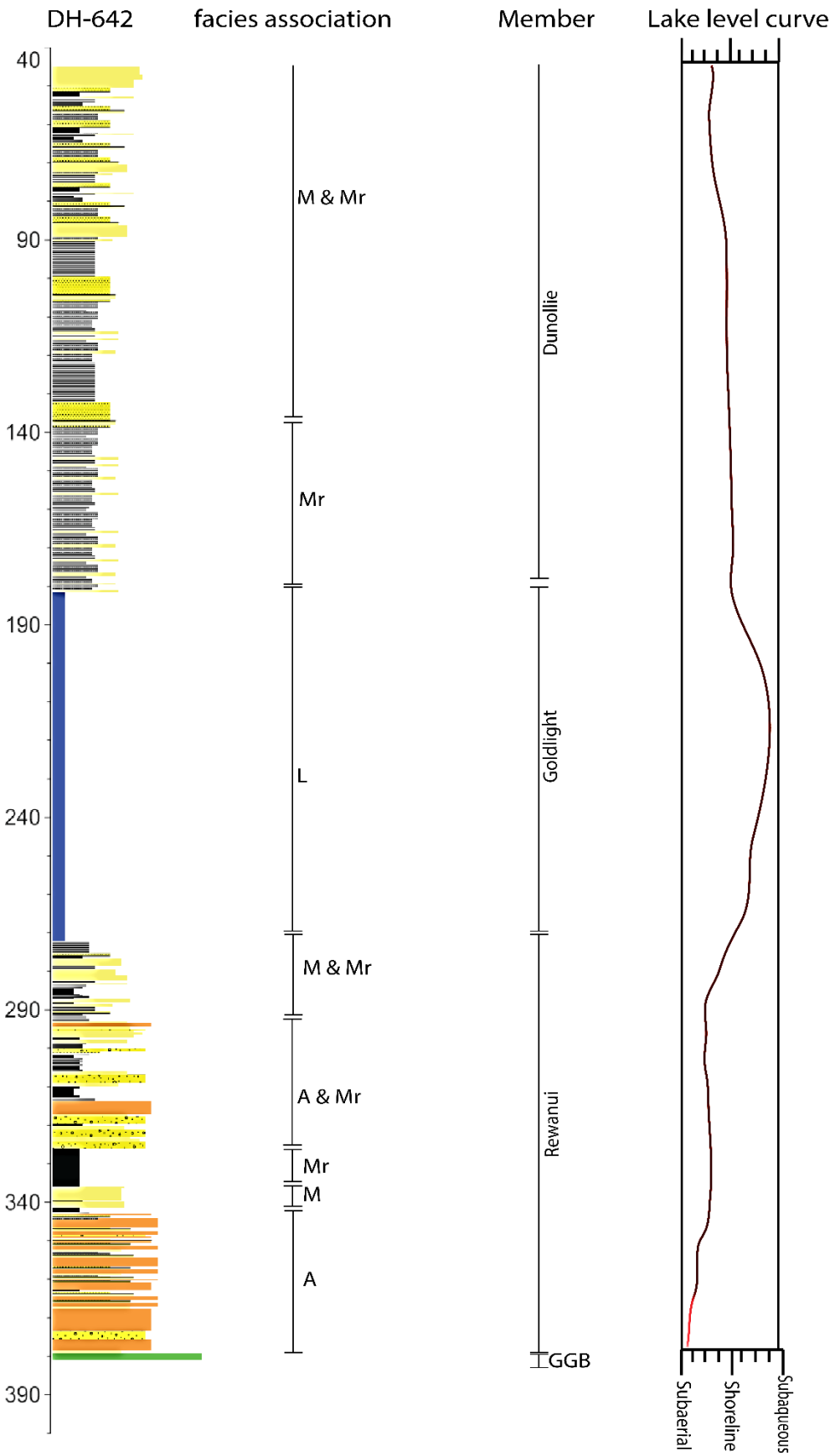
DH-642
facies association
Member
Lake level curve
40
90
140
190
240
290
340
390
M & Mr
Mr
L
M & Mr
A & Mr
Mr
M
A
Dunollie
Goldlight
Rewanui
GGB
Subaerial
Shoreline
Subaqueous

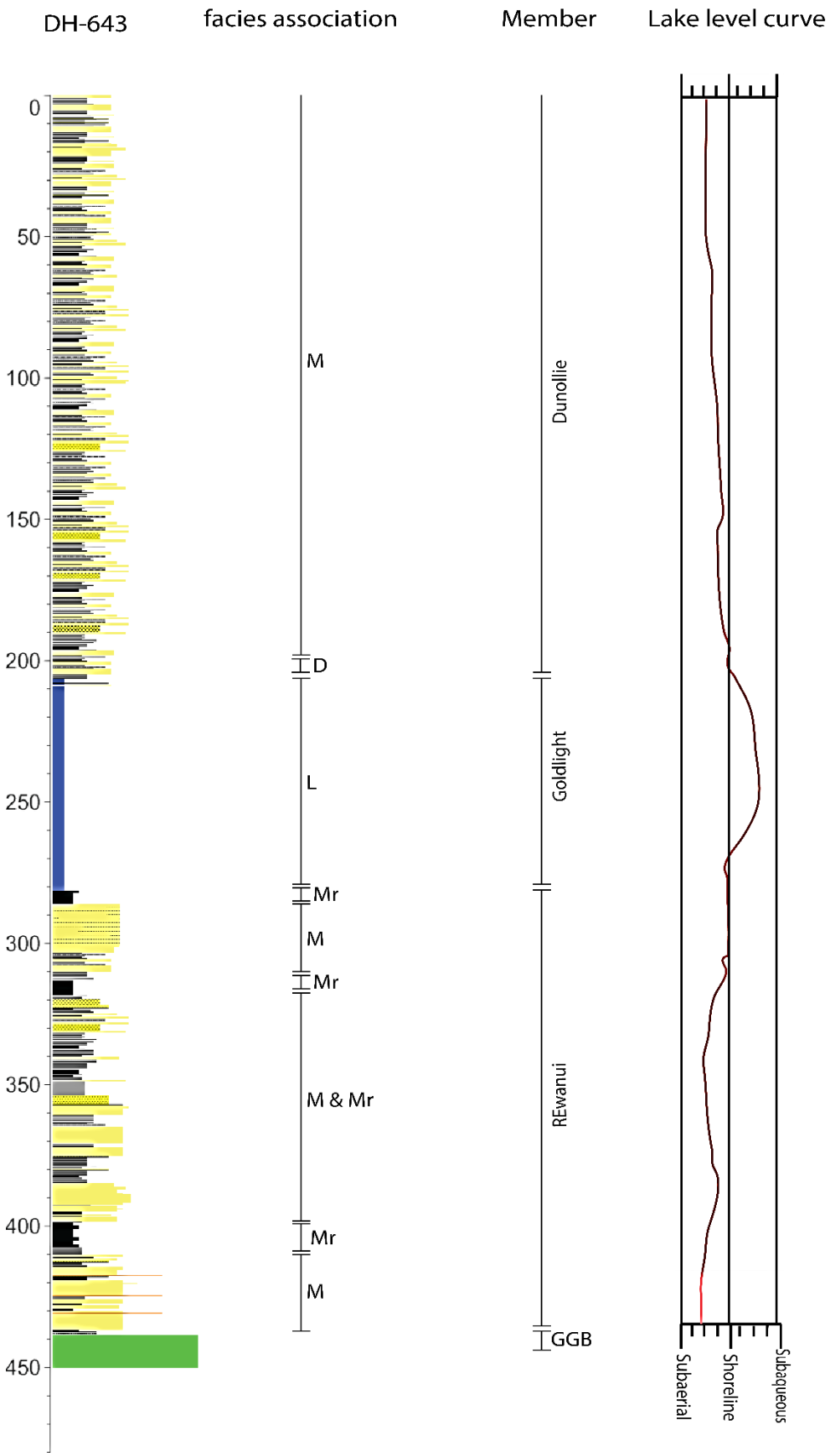
DH-643
facies association
Member
Lake level curve
0
50
100
150
200
250
300
350
400
450
M
D
L
Mr
M
Mr
M & Mr
Mr
M
Dunollie
Goldlight
REwanui
GGB
Subaerial
Shoreline
Subaqueous

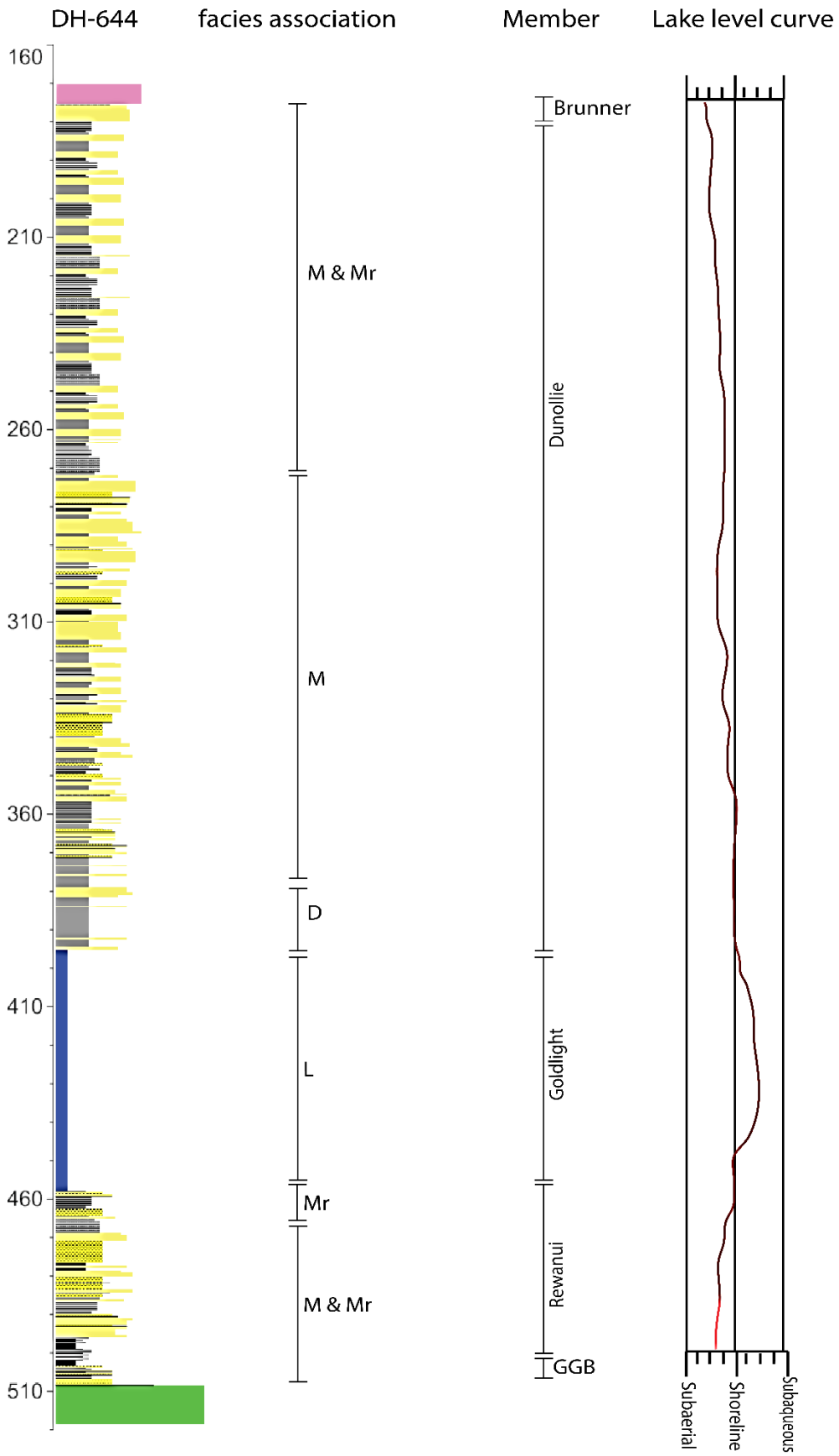
DH-644
facies association
Member
Lake level curve
160
210
260
310
360
410
460
510
M & Mr
M
D
L
Mr
M & Mr
Brunner
Dunollie
Goldlight
Rewanui
GGB
Subaerial
Shoreline
Subaqueous

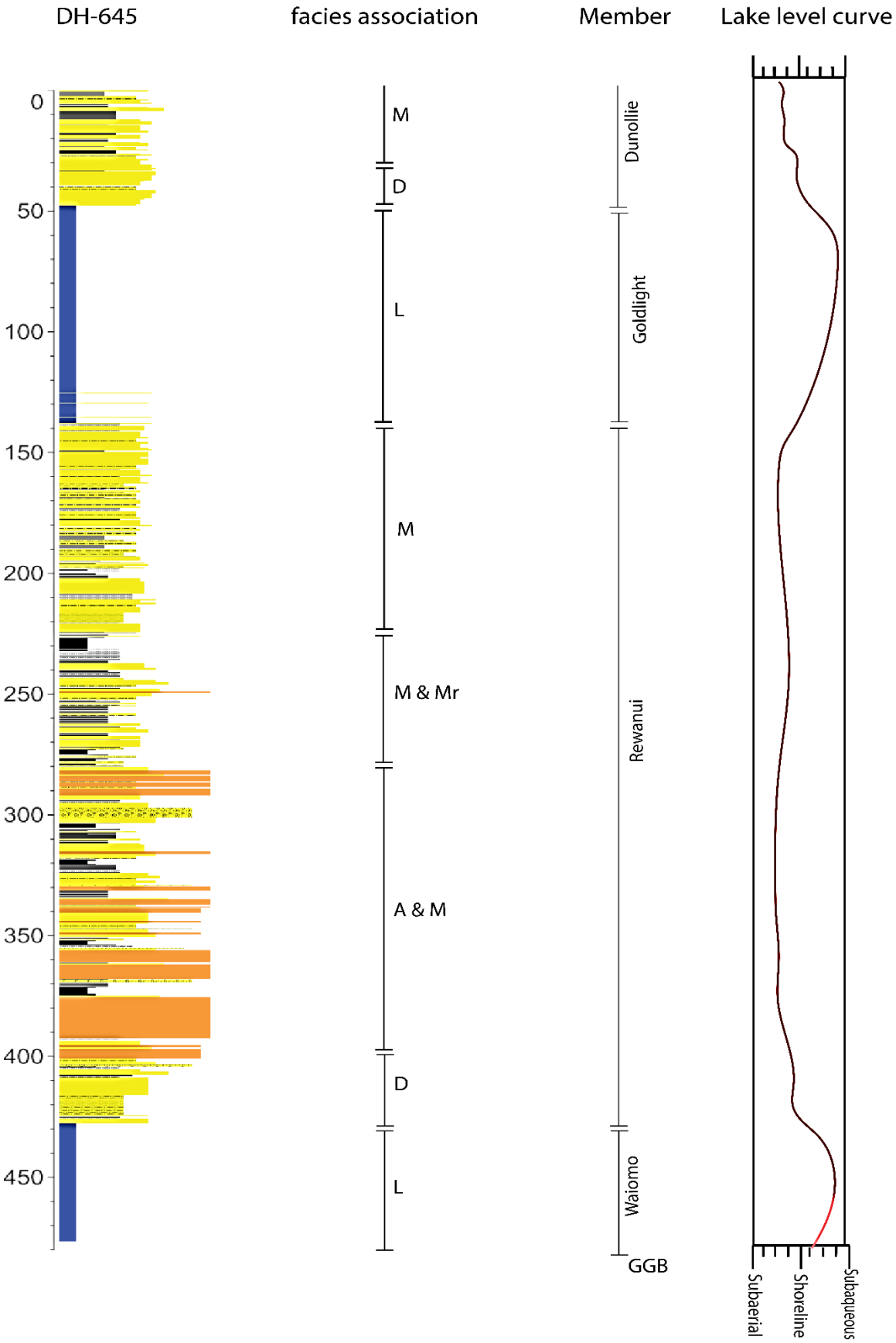
DH-645
facies association
Member
Lake level curve
0
50
100
150
200
250
300
350
400
450
M
D
L
M
M & Mr
A & M
D
L
Dunollie
Goldlight
Rewanui
Waiomo
GGB
Subaerial
Shoreline
Subaqueous

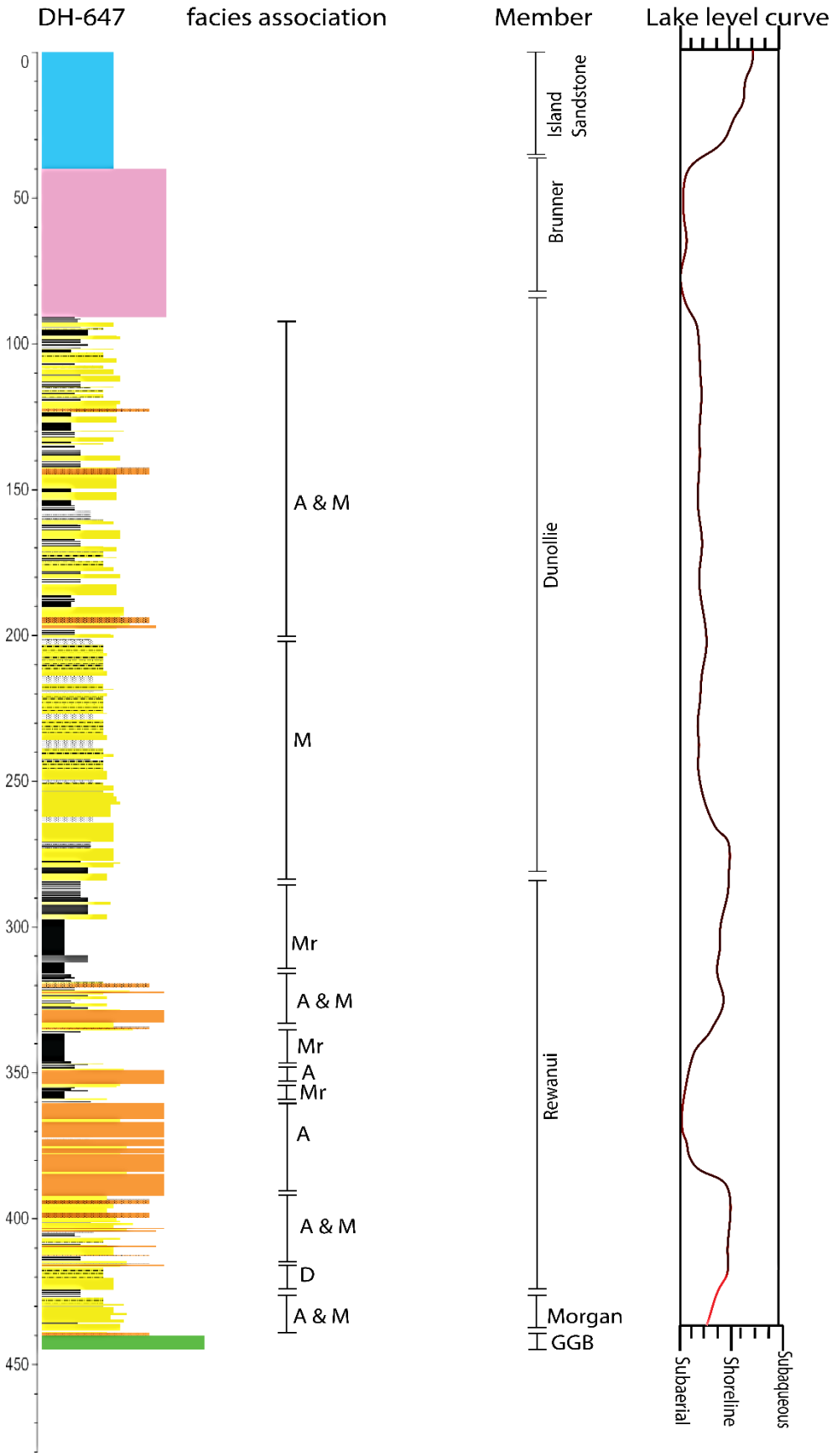
DH-647
facies association
Member
Lake level curve
0
50
100
150
200
250
300
350
400
450
A & M
M
Mr
A & M
Mr
A
Mr
A
A & M
D
A & M
Island Sandstone
Brunner
Dunollie
Rewanui
Morgan
GGB
Subaerial
Shoreline
Subaqueous

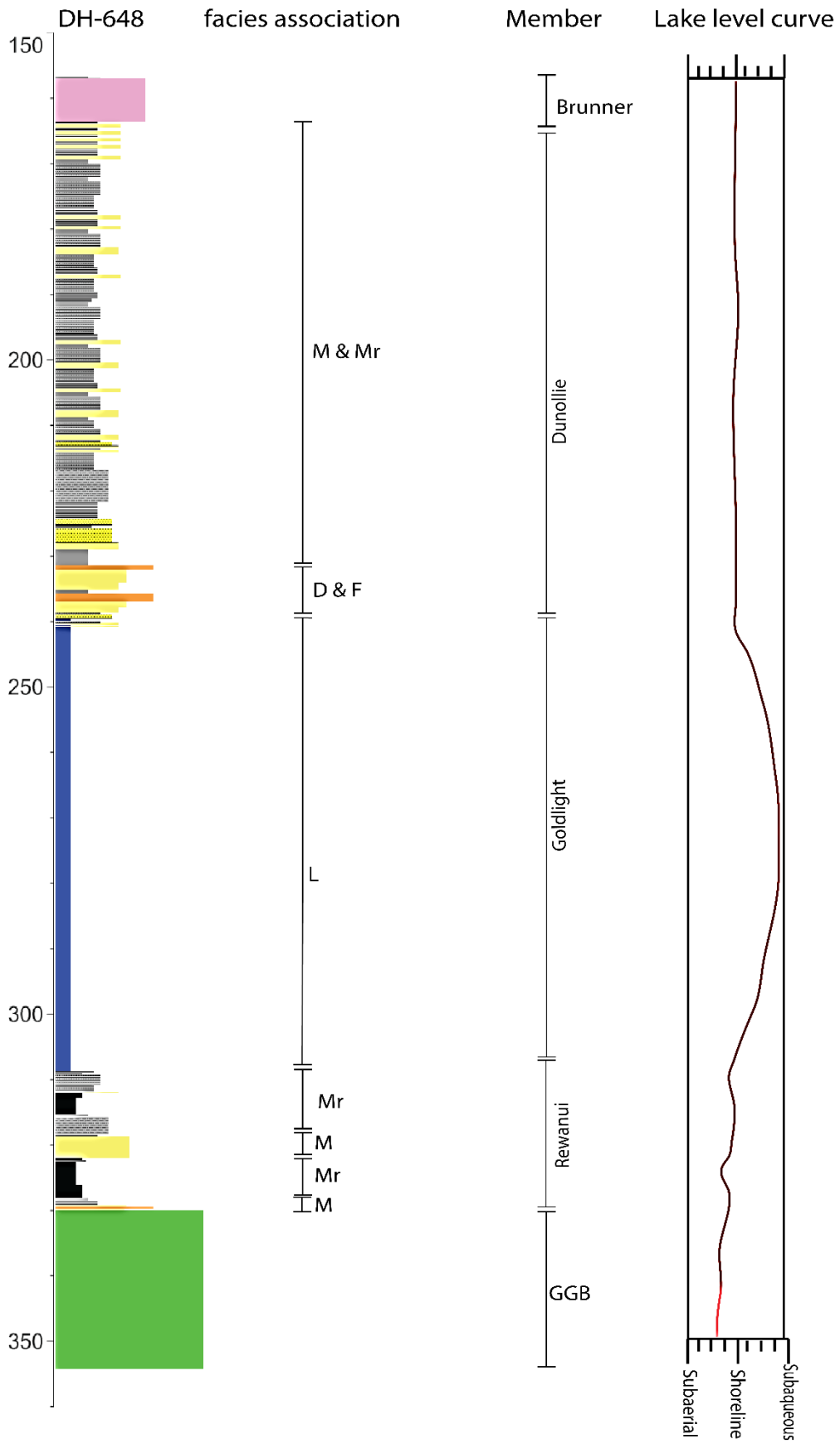
DH-648
facies association
Member
Lake level curve
150
200
250
300
350
M & Mr
D & F
L
Mr
M
Mr
M
Brunner
Dunollie
Goldlight
Rewanui
GGB
Subaerial
Shoreline
Subaqueous

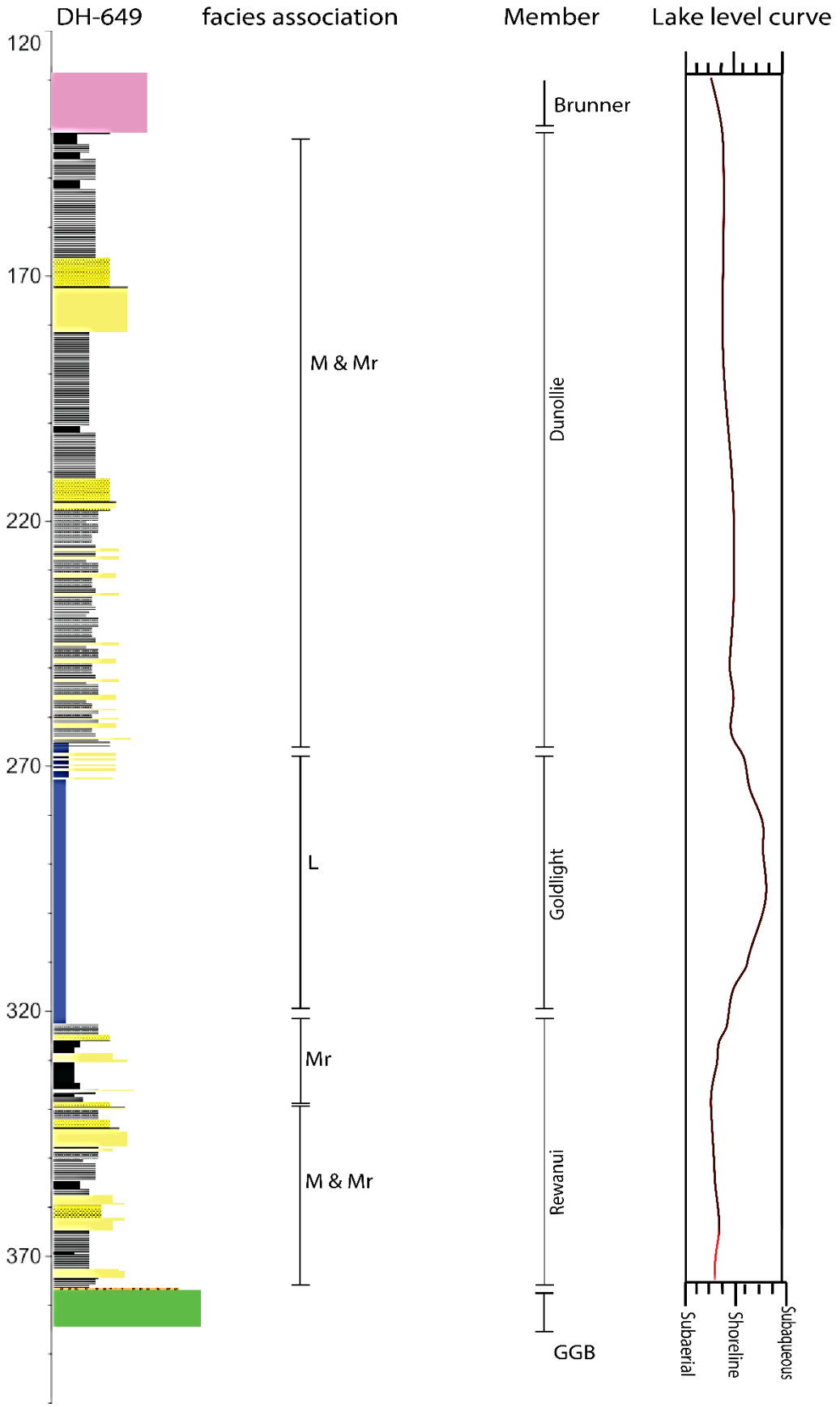
DH-649
facies association
Member
Lake level curve
120
170
220
270
320
370
M & Mr
L
Mr
M & Mr
Brunner
Dunollie
Goldlight
Rewanui
GGB
Subaerial
Shoreline
Subaqueous

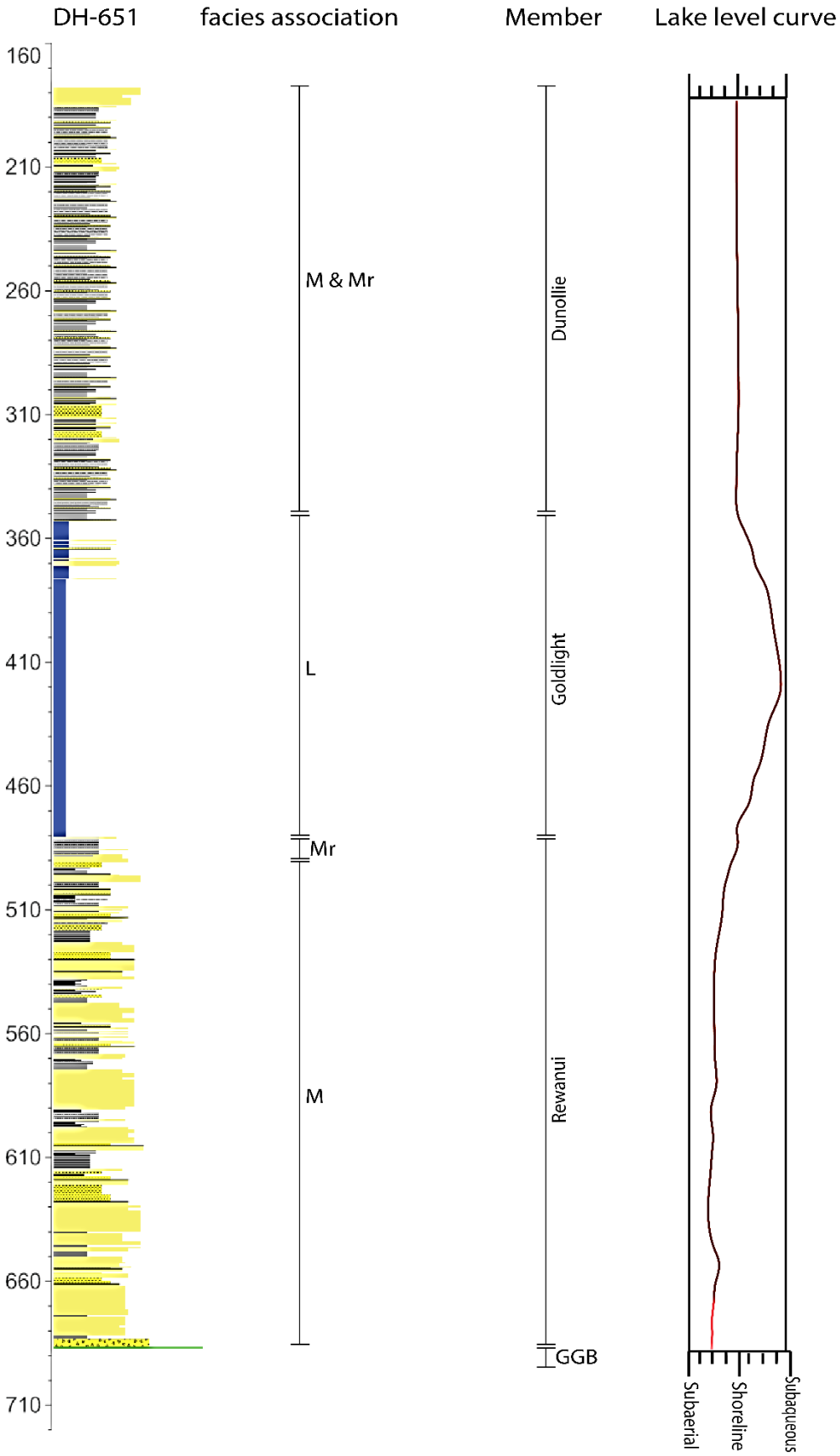
DH-651
facies association
Member
Lake level curve
160
210
260
310
360
410
460
510
560
610
660
710
M & Mr
L
Mr
M
Dunollie
Goldlight
Rewanui
GGB
Subaerial
Shoreline
Subaqueous

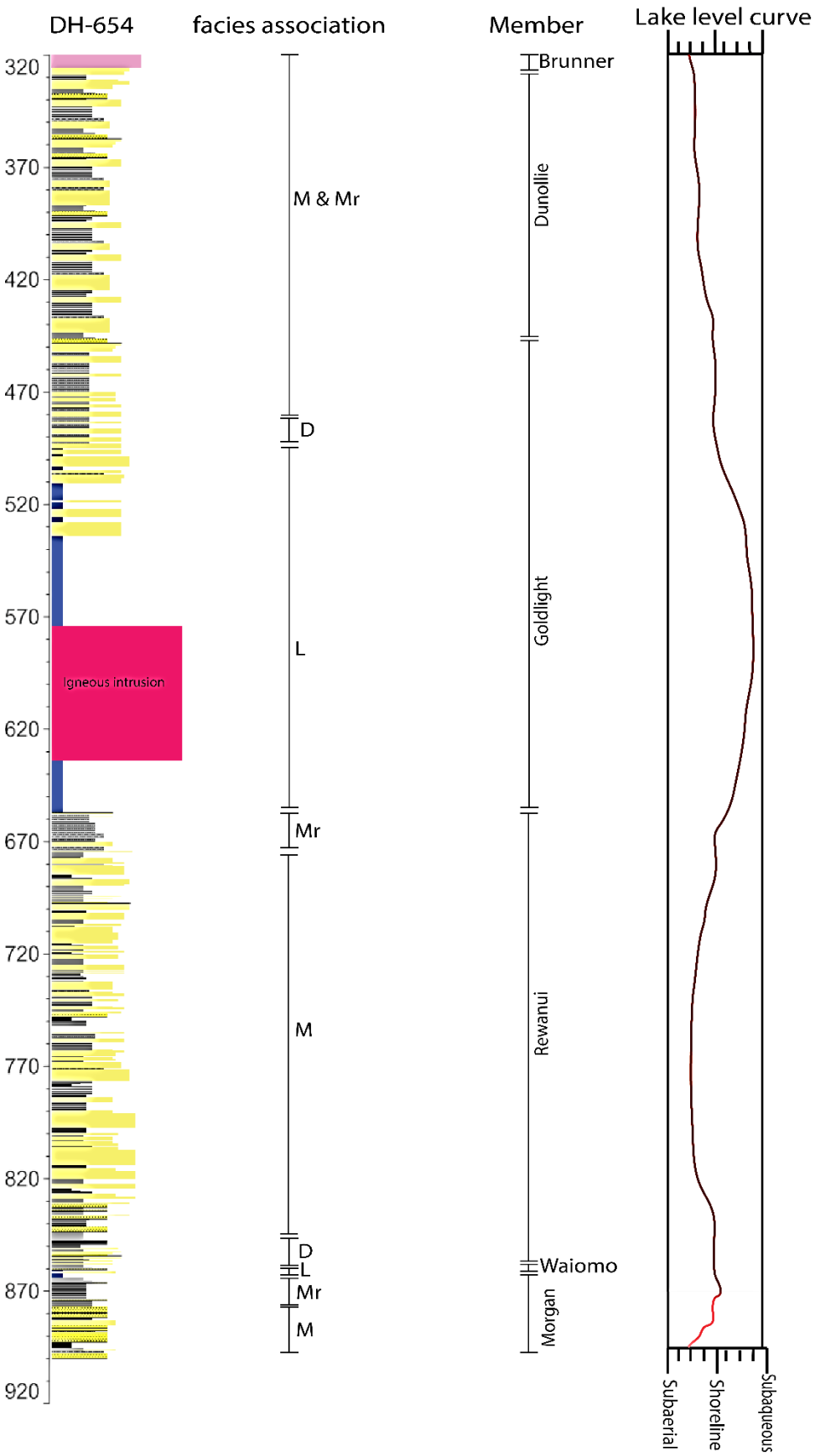
DH-654
facies association
Member
Lake level curve
320
370
420
470
520
570
620
670
720
770
820
870
920
Igneous intrusion
M & Mr
D
L
Mr
M
D
L
Mr
M
Brunner
Dunollie
Goldlight
Rewanui
Waiomo
Morgan
Subaerial
Shoreline
Subaqueous

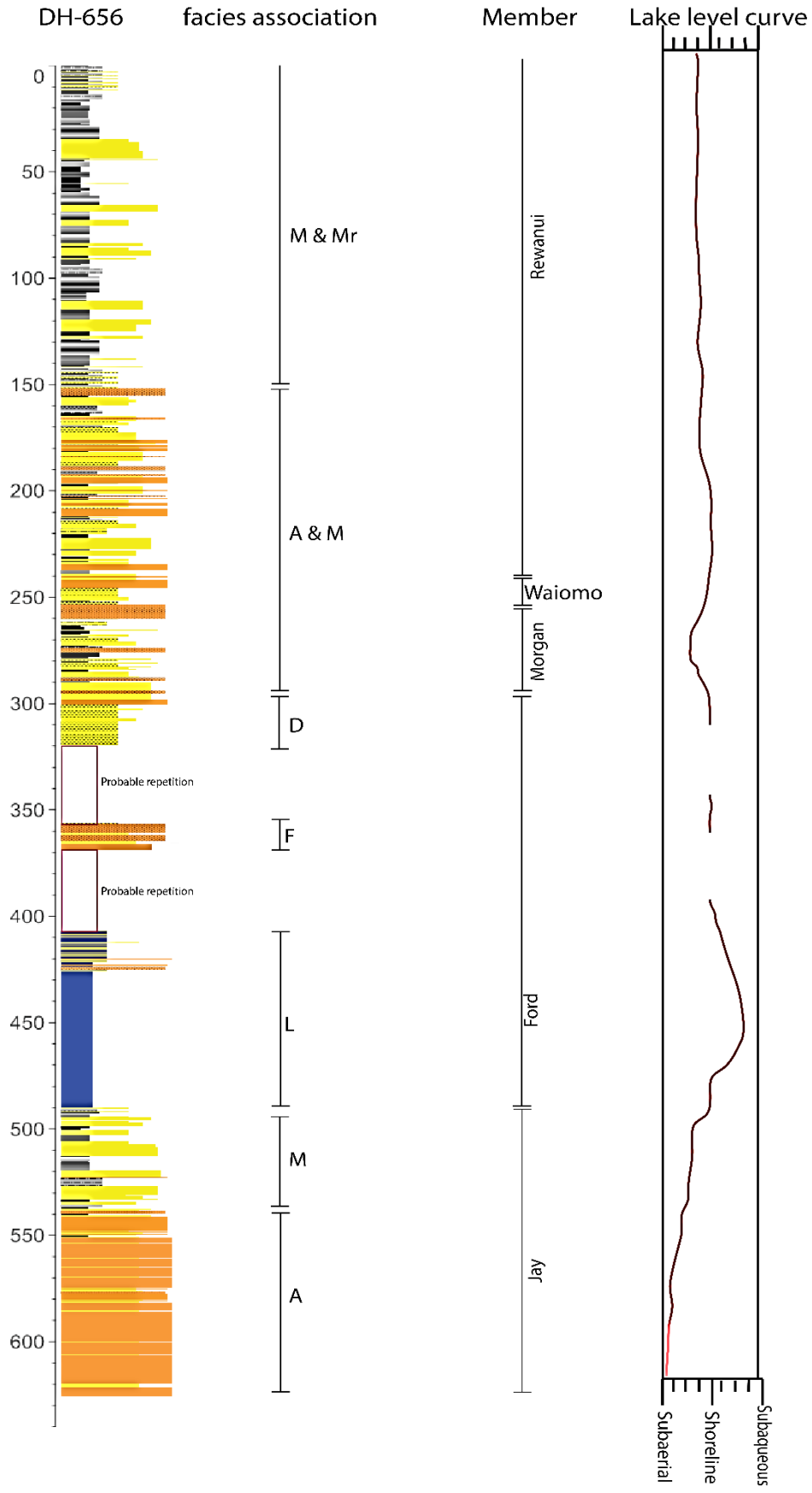
DH-656
facies association
Member
Lake level curve
0
50
100
150
200
250
300
350
400
450
500
550
600
Probable repetition
Probable repetition
M & Mr
A & M
D
F
L
M
A
Rewanui
Waiomo
Morgan
Ford
Jay
Subaerial
Shoreline
Subaqueous

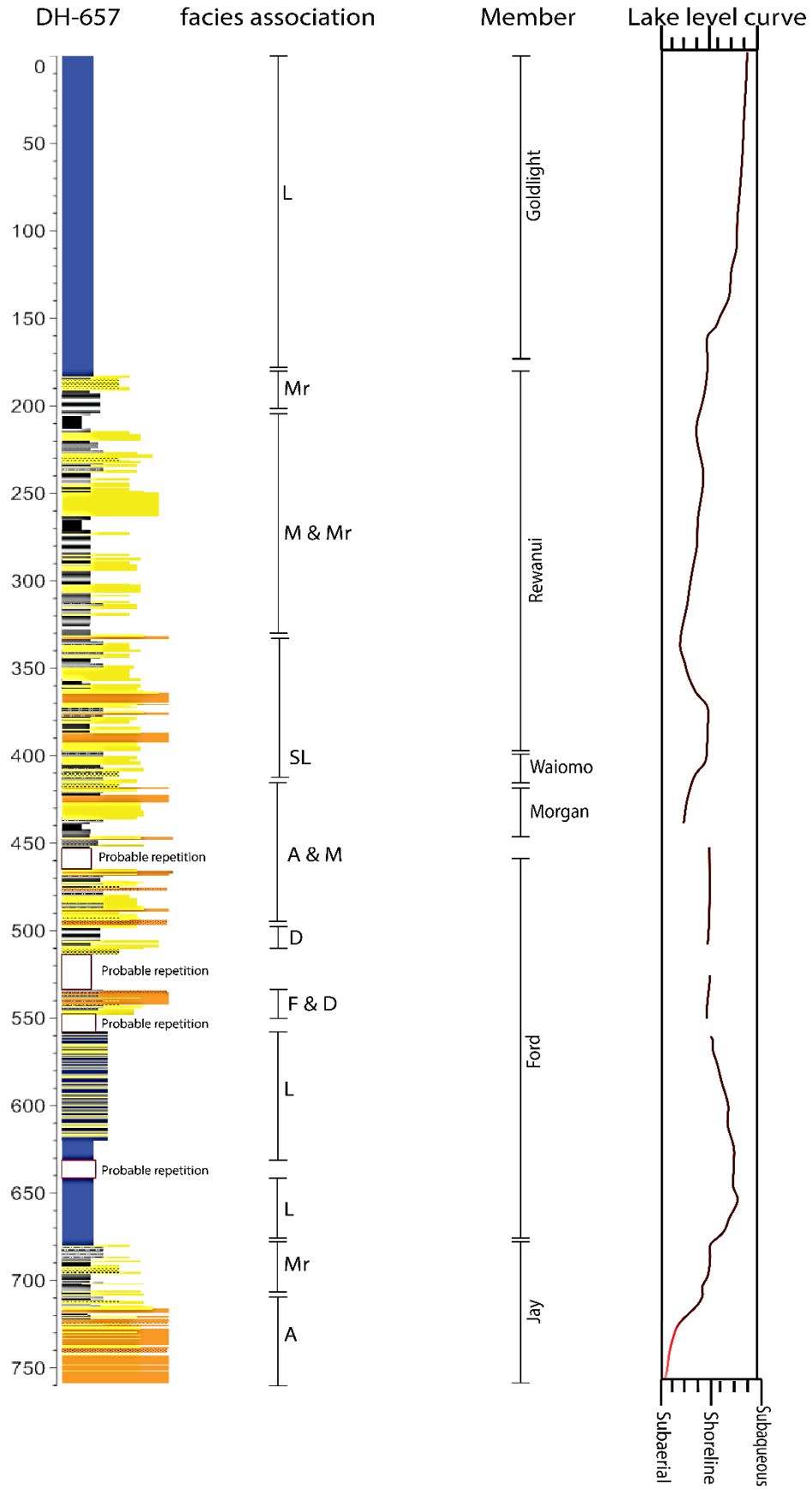
DH-657
facies association
Member
Lake level curve
0
50
100
150
200
250
300
350
400
450
500
550
600
650
700
750
Probable repetition
Probable repetition
Probable repetition
Probable repetition
L
Mr
M & Mr
SL
A & M
D
F & D
L
L
Mr
A
Goldlight
Rewanui
Waiomo
Morgan
Ford
Jay
Subaerial
Shoreline
Subaqueous

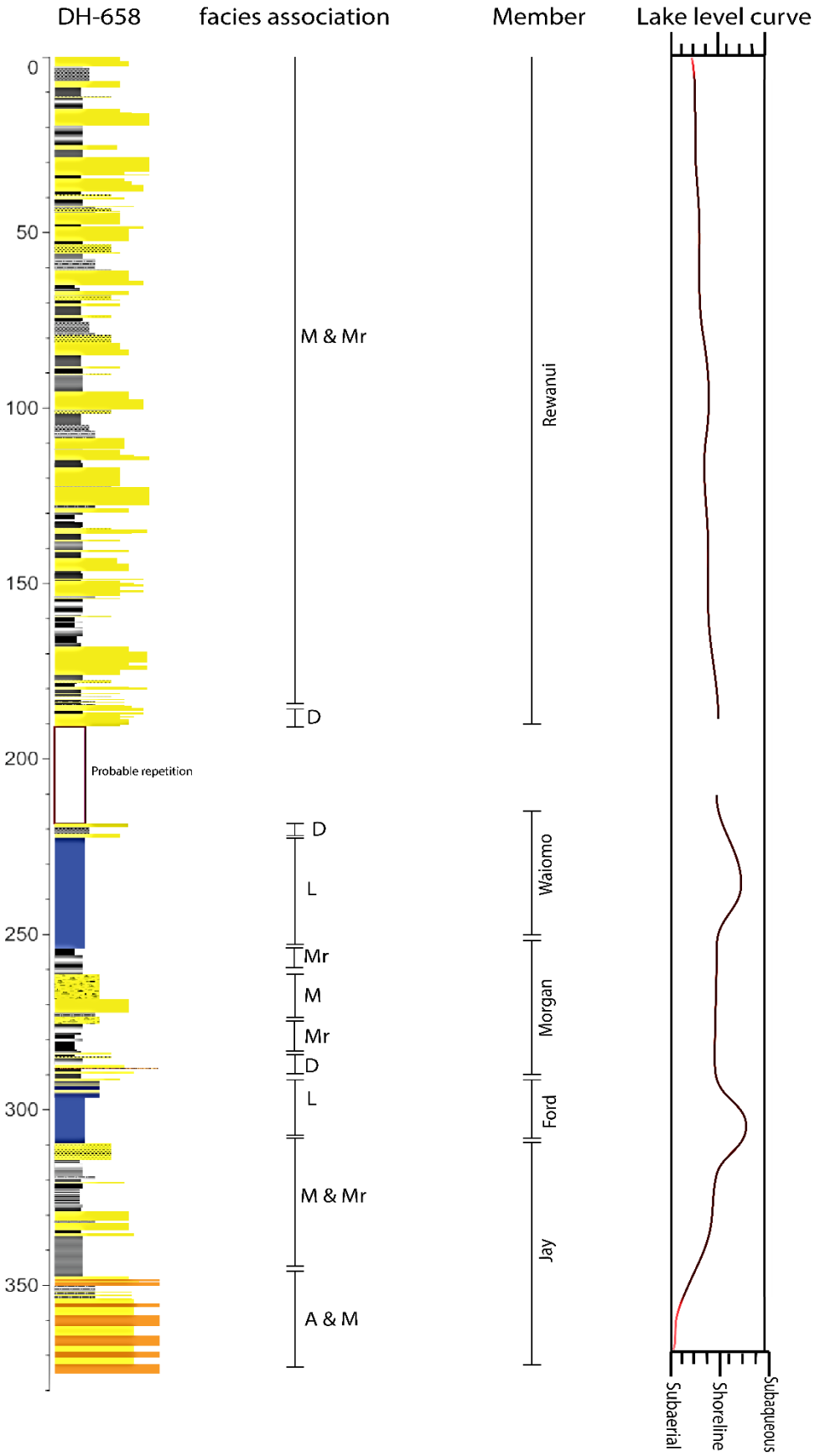
DH-658
facies association
Member
Lake level curve
0
50
100
150
200
250
300
350
Probable repetition
M & Mr
D
D
L
Mr
M
Mr
D
L
M & Mr
A & M
Rewanui
Waiomo
Morgan
Ford
Jay
Subaerial
Shoreline
Subaqueous

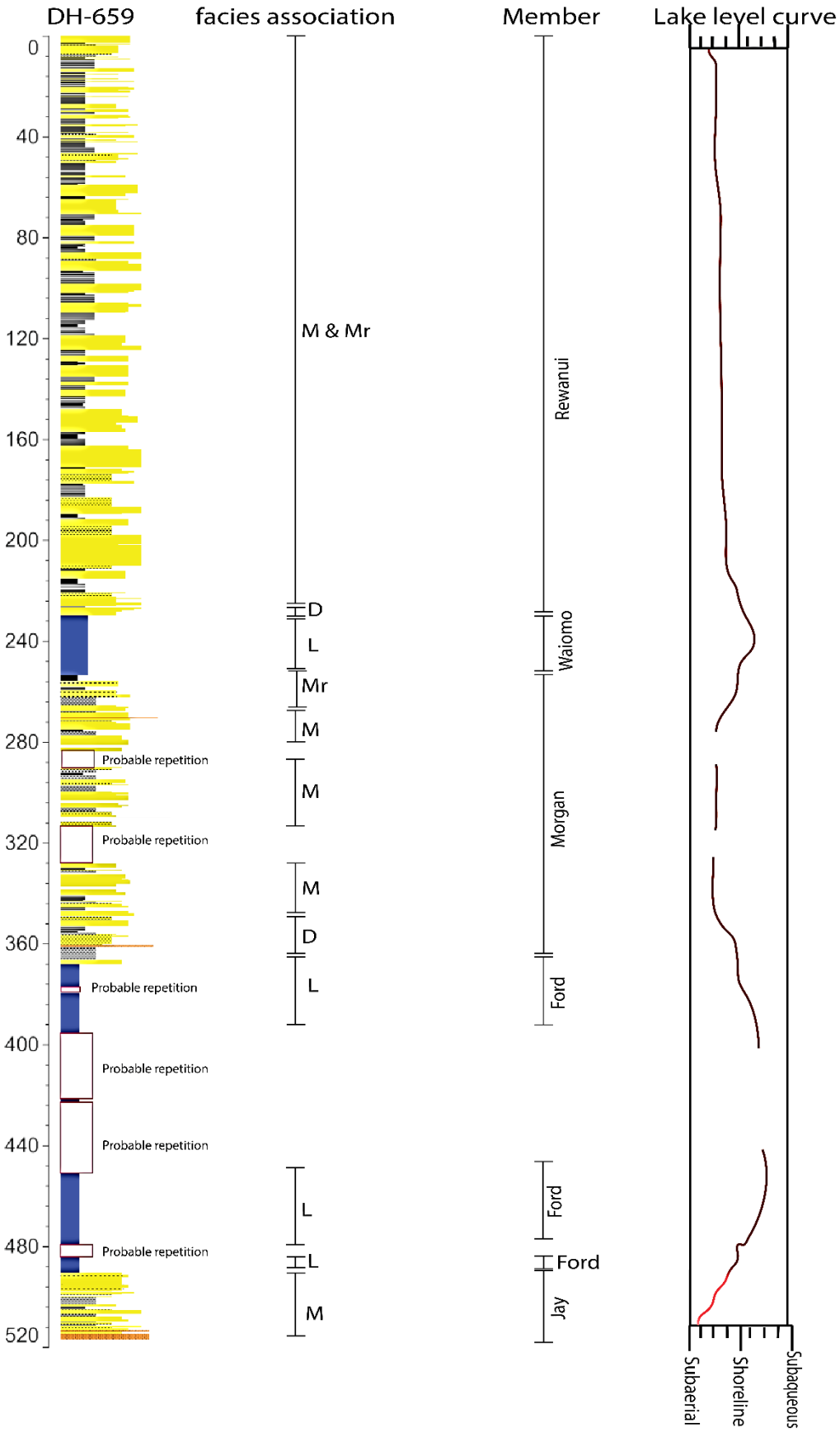
DH-659
facies association
Member
Lake level curve
0
40
80
120
160
200
240
280
320
360
400
440
480
520
Probable repetition
Probable repetition
Probable repetition
Probable repetition
Probable repetition
Probable repetition
M & Mr
D
L
Mr
M
M
M
D
L
L
L
M
Rewanui
Waiomo
Morgan
Ford
Ford
Ford
Jay
Subaerial
Shoreline
Subaqueous

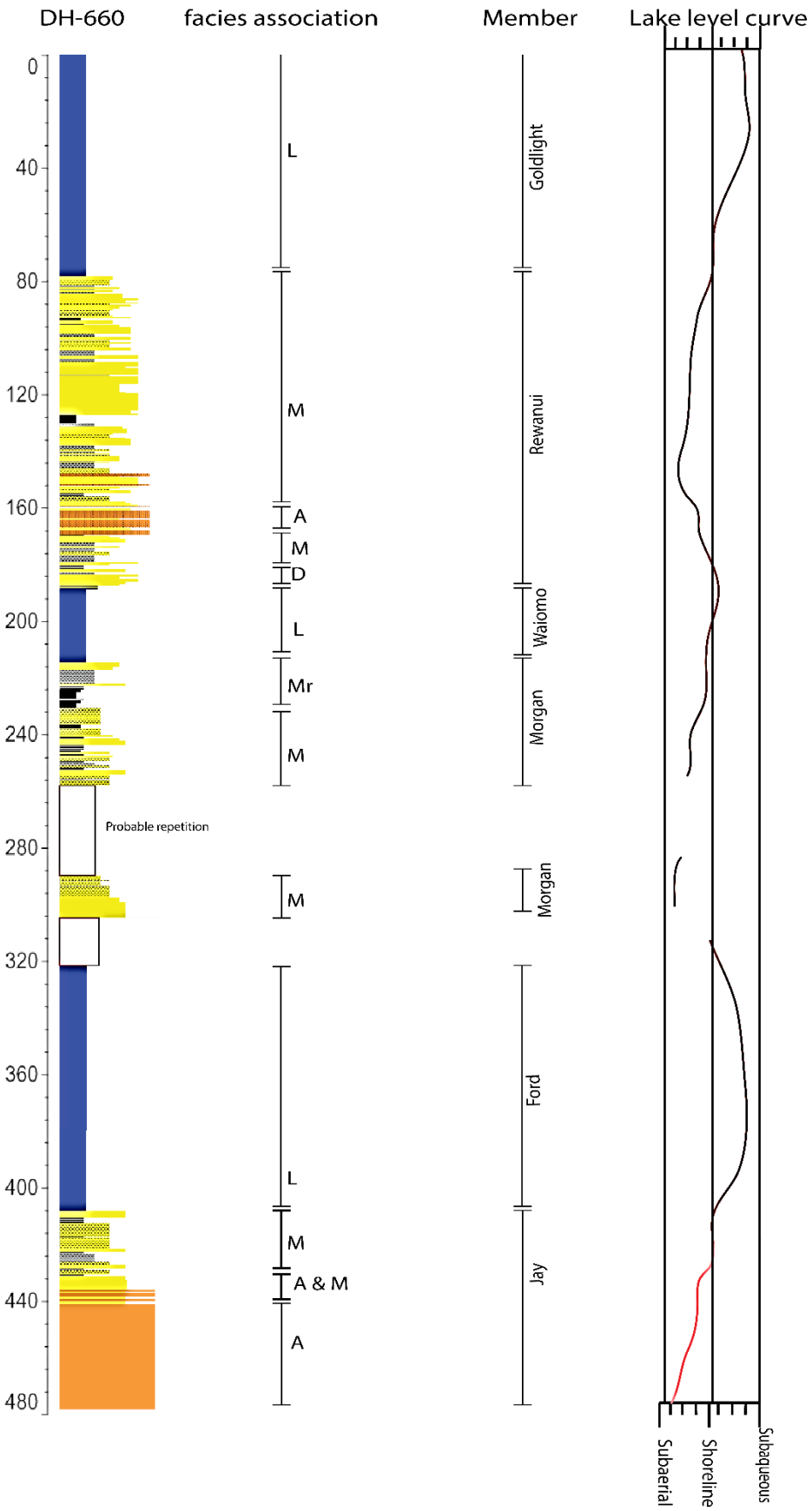
DH-660
facies association
Member
Lake level curve
0
40
80
120
160
200
240
280
320
360
400
440
480
Probable repetition
L
M
A
M
D
L
Mr
M
M
L
M
A & M
A
Goldlight
Rewanui
Waiomo
Morgan
Morgan
Ford
Jay
Subaerial
Shoreline
Subaqueous

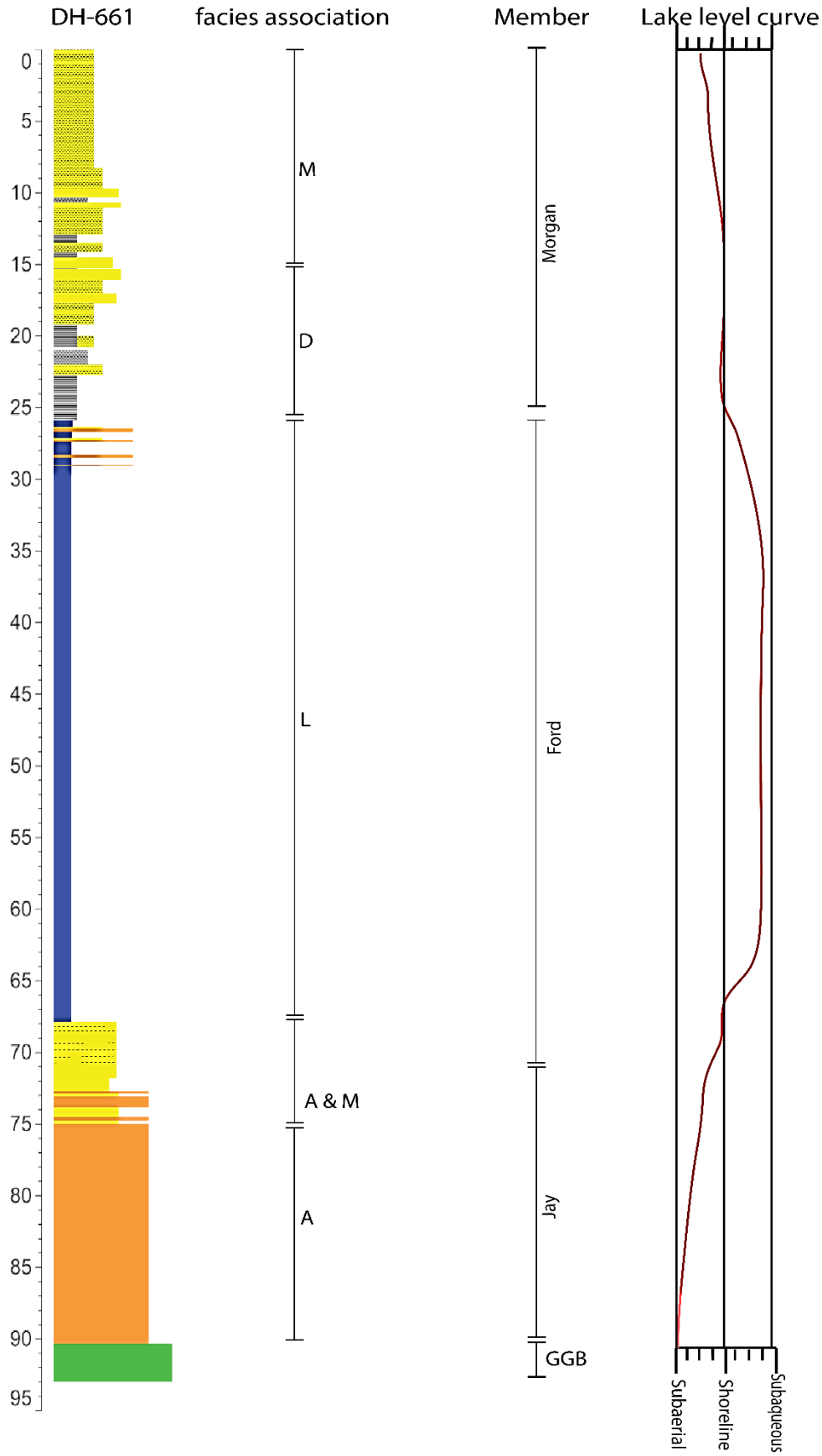
DH-661
facies association
Member
Lake level curve
0
5
10
15
20
25
30
35
40
45
50
55
60
65
70
75
80
85
90
95
M
D
L
A & M
A
Morgan
Ford
Jay
GGB
Subaerial
Shoreline
Subaqueous

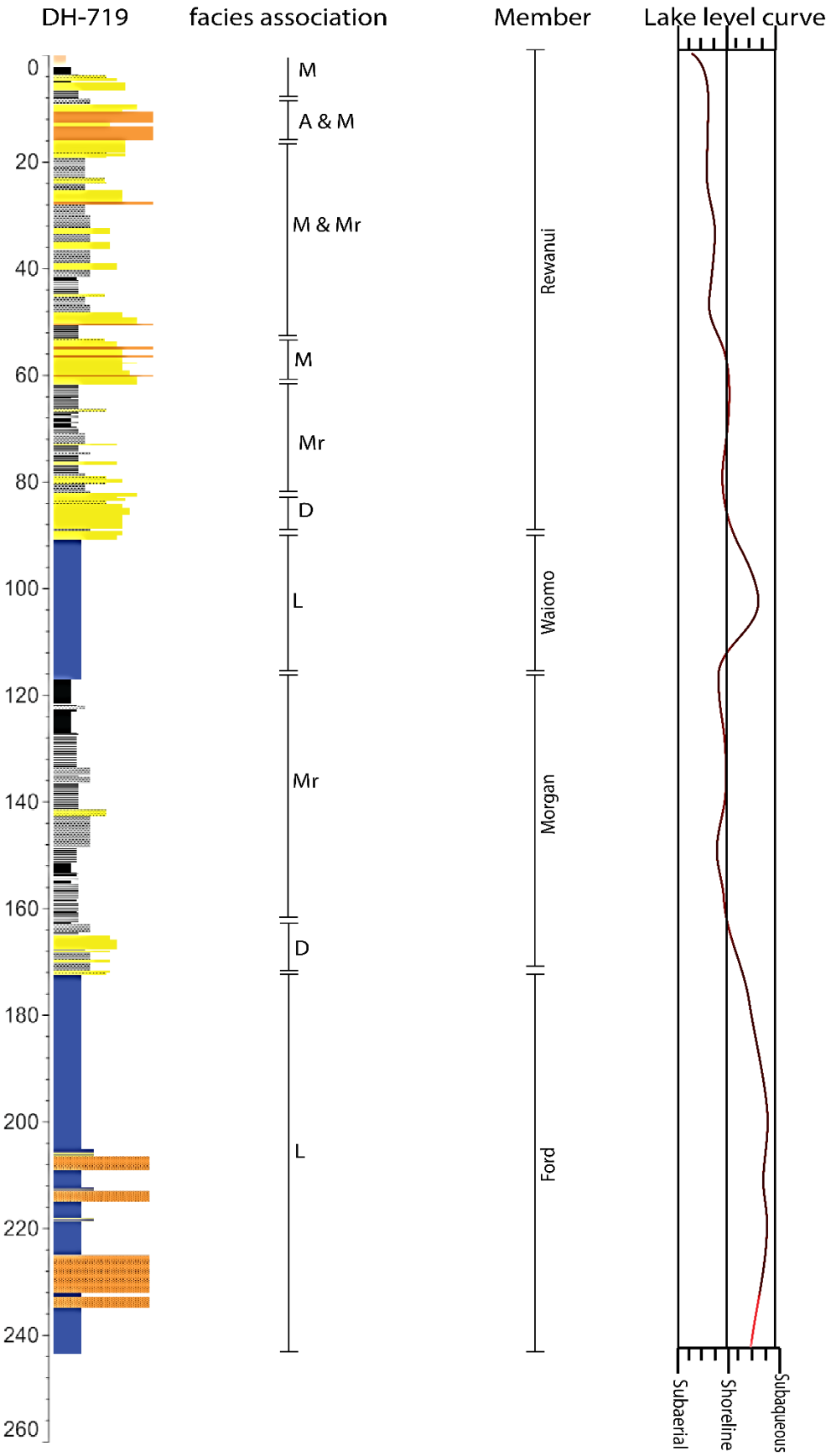
DH-719
facies association
Member
Lake level curve
0
20
40
60
80
100
120
140
160
180
200
220
240
260
M
A & M
M & Mr
M
Mr
D
L
Mr
D
L
Rewanui
Waiomo
Morgan
Ford
Subaerial
Shoreline
Subaqueous

# Appendix 3: Thickness data of the lacustrine mudstones and conglomerates

Coordinate Projection: World Geodetic System (WGS 84)

Thicknesses are measured in meter

| Lacustrine facies thickness of the Ford Member | | | | |
|---|---|---|---|---|
| **Latitude** | **Longitude** | **Massive mudstone facies** | **Sandy turbidite facies** | **Drill hole** |
| -42.36679 | 171.341406 | 21 | 0 | 595 |
| -42.364047 | 171.33916 | 22 | 0 | 596 |
| -42.351376 | 171.26799 | 0 | 0 | 619 |
| -42.39919 | 171.333108 | 5 | 1 | 620 |
| -42.339841 | 171.270823 | 0 | 0 | 621 |
| -42.35843 | 171.256541 | 0 | 0 | 622 |
| -42.385381 | 171.278497 | 0 | 0 | 623 |
| -42.373862 | 171.281852 | 0 | 0 | 624 |
| -42.39855 | 171.317856 | 0 | 0 | 625 |
| -42.370897 | 171.246405 | 0 | 0 | 626 |
| -42.418123 | 171.300242 | 0 | 0 | 627 |
| -42.392834 | 171.264189 | 0 | 0 | 628 |
| -42.393712 | 171.300168 | 0 | 0 | 630 |
| -42.367032 | 171.285646 | 0 | 0 | 631 |
| -42.366582 | 171.295833 | 0 | 0 | 632 |
| -42.381339 | 171.245103 | 0 | 0 | 633 |
| -42.341364 | 171.260914 | 0 | 0 | 634 |
| -42.35863 | 171.274308 | 0 | 0 | 635 |
| -42.382328 | 171.257815 | 0 | 0 | 636 |
| -42.363878 | 171.247234 | 0 | 0 | 637 |
| -42.381752 | 171.270182 | 0 | 0 | 638 |
| -42.349765 | 171.258009 | 0 | 0 | 639 |
| -42.379016 | 171.278552 | 0 | 0 | 640 |
| -42.358563 | 171.265156 | 0 | 0 | 641 |
| -42.372947 | 171.258441 | 0 | 0 | 642 |
| -42.373182 | 171.271464 | 0 | 0 | 643 |
| -42.392937 | 171.251554 | 0 | 0 | 644 |
| -42.365655 | 171.274429 | 0 | 0 | 645 |
| -42.389491 | 171.255197 | 0 | 0 | 646 |
| -42.36439 | 171.260016 | 0 | 0 | 647 |
| -42.385746 | 171.247699 | 0 | 0 | 648 |
| -42.397401 | 171.262531 | 0 | 0 | 649 |
| -42.38187 | 171.252035 | 0 | 0 | 650 |
| -42.404889 | 171.282465 | 0 | 0 | 651 |
| -42.42215 | 171.278914 | 0 | 0 | 654 |
| -42.345604 | 171.302475 | 64 | 15 | 656 |
| -42.354044 | 171.299708 | 50 | 32 | 657 |

| Lacustrine facies thickness of the Ford Member | | | | |
|---|---|---|---|---|
| **Latitude** | **Longitude** | **Massive mudstone facies** | **Sandy turbidite facies** | **Drill hole** |
| -42.342585 | 171.322182 | 18 | 6 | 658 |
| -42.356844 | 171.340384 | 23 | 0 | 659 |
| -42.345308 | 171.338361 | 47 | 12 | 660 |
| -42.338511 | 171.355714 | 38 | 5 | 661 |
| -42.350486 | 171.303167 | 55 | 0 | 662 |
| -42.357701 | 171.29979 | 40 | 10 | 664 |
| -42.347197 | 171.306012 | 60 | 0 | 665 |
| -42.353487 | 171.303389 | 52 | 0 | 666 |
| -42.355303 | 171.348267 | 23 | 0 | 668 |
| -42.344751 | 171.296005 | 0 | 0 | 690 |
| -42.378004 | 171.25711 | 0 | 0 | 696 |
| -42.386154 | 171.262493 | 0 | 0 | 698 |
| -42.386154 | 171.262493 | 0 | 0 | 699 |
| -42.342328 | 171.328549 | 16 | 3 | 719 |
| -42.357788 | 171.354489 | 21 | 0 | 720 |
| -42.357788 | 171.354489 | 19 | 0 | 730 |
| -42.38574 | 171.340812 | 25 | 0 | 732 |
| -42.383769 | 171.326623 | 19 | 0 | 734 |
| -42.36799 | 171.331635 | 23 | 0 | 736 |
| -42.366226 | 171.306819 | 19 | 10 | 925 |
| -42.386612 | 171.291694 | 0 | 0 | 933 |
| -42.386857 | 171.29536 | 0 | 0 | 1011 |
| -42.382515 | 171.309954 | 41 | 6 | 1012 |
| -42.352756 | 171.33243 | 25 | 0 | 1369 |
| -42.339841 | 171.306819 | 72 | 0 | 1400 |
| -42.341364 | 171.307256 | 69 | 0 | 1401 |
| -42.337214 | 171.35255 | 55 | 7 | 1424 |
| -42.347169 | 171.354657 | 29 | 0 | 1431 |
| -42.3219 | -171.2703664 | 0 | 0 | Twelve Mile Beach |

| Lacustrine facies thickness of the Waiomo Member | | | | |
|---|---|---|---|---|
| **Latitude** | **Longitude** | **Massive mudstone facies** | **Sandy turbidite facies** | **Drill hole** |
| -42.36679 | 171.341406 | 27 | 0 | 595 |
| -42.364047 | 171.33916 | 23 | 0 | 596 |
| -42.351376 | 171.26799 | 57 | 8 | 619 |
| -42.39919 | 171.333108 | 32 | 0 | 620 |
| -42.339841 | 171.270823 | 31 | 0 | 621 |
| -42.35843 | 171.256541 | 0 | 0 | 622 |
| -42.385381 | 171.278497 | 0 | 0 | 623 |
| -42.373862 | 171.281852 | 18 | 29 | 624 |
| -42.39855 | 171.317856 | 22 | 0 | 625 |
| -42.370897 | 171.246405 | 0 | 0 | 626 |
| -42.418123 | 171.300242 | 0 | 0 | 627 |
| -42.392834 | 171.264189 | 0 | 0 | 628 |
| -42.393712 | 171.300168 | 20 | 5 | 630 |
| -42.367032 | 171.285646 | 32 | 25 | 631 |
| -42.366582 | 171.295833 | 22 | 28 | 632 |
| -42.381339 | 171.245103 | 0 | 0 | 633 |
| -42.341364 | 171.260914 | 0 | 0 | 634 |
| -42.35863 | 171.274308 | 55 | 32 | 635 |
| -42.382328 | 171.257815 | 0 | 0 | 636 |
| -42.363878 | 171.247234 | 0 | 0 | 637 |
| -42.381752 | 171.270182 | 0 | 0 | 638 |
| -42.349765 | 171.258009 | 0 | 0 | 639 |
| -42.379016 | 171.278552 | 0 | 29 | 640 |
| -42.358563 | 171.265156 | 25 | 15 | 641 |
| -42.372947 | 171.258441 | 0 | 0 | 642 |
| -42.373182 | 171.271464 | 0 | 0 | 643 |
| -42.392937 | 171.251554 | 0 | 0 | 644 |
| -42.365655 | 171.274429 | 52 | 12 | 645 |
| -42.389491 | 171.255197 | 0 | 0 | 646 |
| -42.36439 | 171.260016 | 0 | 0 | 647 |
| -42.385746 | 171.247699 | 0 | 0 | 648 |
| -42.397401 | 171.262531 | 0 | 0 | 649 |
| -42.38187 | 171.252035 | 0 | 0 | 650 |
| -42.404889 | 171.282465 | 0 | 0 | 651 |
| -42.42215 | 171.278914 | 0 | 14 | 654 |
| -42.345604 | 171.302475 | 0 | 0 | 656 |
| -42.354044 | 171.299708 | 0 | 0 | 657 |

| Lacustrine facies thickness of the Waiomo Member | | | | |
|---|---|---|---|---|
| **Latitude** | **Longitude** | **Massive mudstone facies** | **Sandy turbidite facies** | **Drill hole** |
| -42.342585 | 171.322182 | 20 | 0 | 658 |
| -42.356844 | 171.340384 | 23 | 0 | 659 |
| -42.345308 | 171.338361 | 27 | 0 | 660 |
| -42.338511 | 171.355714 | 32 | 0 | 661 |
| -42.350486 | 171.303167 | 16 | 5 | 662 |
| -42.357701 | 171.29979 | 14 | 6 | 664 |
| -42.347197 | 171.306012 | 15 | 8 | 665 |
| -42.353487 | 171.303389 | 16 | 8 | 666 |
| -42.355303 | 171.348267 | 36 | 0 | 668 |
| -42.344751 | 171.296005 | 0 | 0 | 690 |
| -42.378004 | 171.25711 | 0 | 0 | 696 |
| -42.386154 | 171.262493 | 0 | 0 | 698 |
| -42.386154 | 171.262493 | 0 | 0 | 699 |
| -42.342328 | 171.328549 | 27 | 0 | 719 |
| -42.357788 | 171.354489 | 35 | 0 | 720 |
| -42.357788 | 171.354489 | 28 | 0 | 730 |
| -42.38574 | 171.340812 | 27 | 0 | 732 |
| -42.383769 | 171.326623 | 27 | 0 | 734 |
| -42.36799 | 171.331635 | 23 | | 736 |
| -42.366226 | 171.306819 | 27 | 0 | 925 |
| -42.386612 | 171.291694 | 0 | 14 | 933 |
| -42.386857 | 171.29536 | 11 | 4 | 1011 |
| -42.382515 | 171.309954 | 27 | 0 | 1012 |
| -42.352756 | 171.33243 | 19 | 0 | 1369 |
| -42.339841 | 171.306819 | 18 | 0 | 1400 |
| -42.341364 | 171.307256 | 19 | 0 | 1401 |
| -42.347169 | 171.354657 | 31 | 0 | 1431 |
| -42.3219 | -171.2703664 | 15 | 10 | Twelve Mile Beach |

| Lacustrine facies thickness of the Goldlight Member | | | | |
|---|---|---|---|---|
| **Latitude** | **Longitude** | **Massive mudstone facies** | **Sandy turbidite facies** | **Drill hole** |
| -42.36679 | 171.341406 | 121 | 0 | 595 |
| -42.36405 | 171.33916 | 125 | 0 | 596 |
| -42.35138 | 171.26799 | 0 | 8 | 619 |
| -42.39919 | 171.333108 | 140 | 0 | 620 |
| -42.33984 | 171.270823 | 0 | 6 | 621 |
| -42.35843 | 171.256541 | 0 | 0 | 622 |
| -42.38538 | 171.278497 | 39+ | unknown | 623 |
| -42.37386 | 171.281852 | 53+ | unknown | 624 |
| -42.39855 | 171.317856 | 102 | 0 | 625 |
| -42.3709 | 171.246405 | 18 | 7 | 626 |
| -42.41812 | 171.300242 | 96 | 13 | 627 |
| -42.39283 | 171.264189 | 75 | 15 | 628 |
| -42.39371 | 171.300168 | 110.2 | 0 | 630 |
| -42.36703 | 171.285646 | 61 | 17 | 631 |
| -42.36658 | 171.295833 | 57 | 20 | 632 |
| -42.38134 | 171.245103 | 67 | 27 | 633 |
| -42.34136 | 171.260914 | 0 | 0 | 634 |
| -42.35863 | 171.274308 | 80 | 9 | 635 |
| -42.38233 | 171.257815 | 110 | 3 | 636 |
| -42.36388 | 171.247234 | 0 | 0 | 637 |
| -42.38175 | 171.270182 | 118 | 17 | 638 |
| -42.34977 | 171.258009 | 0 | 0 | 639 |
| -42.37902 | 171.278552 | 72 | 15 | 640 |
| -42.35856 | 171.265156 | 0 | 19 | 641 |
| -42.37295 | 171.258441 | 91 | 0 | 642 |
| -42.37318 | 171.271464 | 85 | 0 | 643 |
| -42.39294 | 171.251554 | 63 | 14 | 644 |
| -42.36566 | 171.274429 | 70 | 17 | 645 |
| -42.38949 | 171.255197 | 78 | 20 | 646 |
| -42.36439 | 171.260016 | 0 | 13 | 647 |
| -42.38575 | 171.247699 | 68 | 10 | 648 |
| -42.3974 | 171.262531 | 58 | 9 | 649 |
| -42.38187 | 171.252035 | 75 | 4 | 650 |
| -42.40489 | 171.282465 | 100 | 13 | 651 |
| -42.38347 | 171.236627 | 47 | 9 | 653 |
| -42.42215 | 171.278914 | 101 | 14 | 654 |
| -42415585 | 171.261149 | 107 | 24 | 655 |

| Lacustrine facies thickness of the Goldlight Member | | | | |
|---|---|---|---|---|
| **Latitude** | **Longitude** | **Massive mudstone facies** | **Sandy turbidite facies** | **Drill hole** |
| -42.3456 | 171.302475 | 0 (eroded) | unknown | 656 |
| -42.35404 | 171.299708 | 185+ | unknown | 657 |
| -42.34259 | 171.322182 | 0 (eroded) | unknown | 658 |
| -42.35684 | 171.340384 | 137 | 0 | 659 |
| -42.34531 | 171.338361 | 72+ | unknown | 660 |
| -42.33851 | 171.355714 | 0 (eroded) | unknown | 661 |
| -42.35049 | 171.303167 | 121+ | unknown | 662 |
| -42.3577 | 171.29979 | 160+ | unknown | 664 |
| -42.3472 | 171.306012 | 123+ | unknown | 665 |
| -42.35349 | 171.303389 | 146+ | unknown | 666 |
| -42.3553 | 171.348267 | 0 (eroded) | unknown | 668 |
| -42.34475 | 171.296005 | 53+ | unknown | 690 |
| -42.378 | 171.25711 | 109 | 25 | 696 |
| -42.38615 | 171.262493 | 82 | 29 | 698 |
| -42.38615 | 171.262493 | 58.3 | 12 | 699 |
| -42.34233 | 171.328549 | 175.3 | 0 | 719 |
| -42.35779 | 171.354489 | 137 | 0 | 720 |
| -42.35779 | 171.354489 | 142 | 0 | 730 |
| -42.38574 | 171.340812 | 133 | 0 | 732 |
| -42.38377 | 171.326623 | 138 | 0 | 734 |
| -42.35435 | 171.279476 | 109 | 0 | 735 |
| -42.36799 | 171.331635 | 86+ | unknown | 736 |
| -42.36623 | 171.306819 | 170 | 0 | 925 |
| -42.38661 | 171.291694 | 121 | 0 | 933 |
| -42.38686 | 171.29536 | 121 | 0 | 1011 |
| -42.38252 | 171.309954 | 55+ | unknown | 1012 |
| -42.35276 | 171.33243 | 169 | 0 | 1369 |
| -42.33984 | 171.306819 | 0 (eroded) | unknown | 1400 |
| -42.34136 | 171.307256 | 0 (eroded) | unknown | 1401 |
| -42.33721 | 171.35255 | 0 (eroded) | unknown | 1424 |
| -42.34717 | 171.354657 | 0 (eroded) | unknown | 1431 |
| -42.3219 | -171.2703664 | 0 | 3 | Twelve Mile Beach |

| Jay-Ford conglomerate thickness | | | |
|---|---|---|---|
| **Latitude** | **Longitude** | **Conglomerate thickness** | **Drill hole** |
| -42.383716 | 171.303635 | 25.7 | 226 |
| -42.377932 | 171.311224 | 7+ | 241 |
| -42.375761 | 171.310506 | 1.4 | 246 |
| -42.351376 | 171.26799 | 0 | 619 |
| -42.39919 | 171.333108 | 6+ | 620 |
| -42.339841 | 171.270823 | 0 | 621 |
| -42.35843 | 171.256541 | 0 | 622 |
| -42.373862 | 171.281852 | 0 | 624 |
| -42.39855 | 171.317856 | 0 | 625 |
| -42.370897 | 171.246405 | 0 | 626 |
| -42.418123 | 171.300242 | 0 | 627 |
| -42.392834 | 171.264189 | 0 | 628 |
| -42.393712 | 171.300168 | 0 | 630 |
| -42.367032 | 171.285646 | 0 | 631 |
| -42.366582 | 171.295833 | 0 | 632 |
| -42.381339 | 171.245103 | 0 | 633 |
| -42.341364 | 171.260914 | 0 | 634 |
| -42.35863 | 171.274308 | 0 | 635 |
| -42.382328 | 171.257815 | 0 | 636 |
| -42.363878 | 171.247234 | 0 | 637 |
| -42.381752 | 171.270182 | 0 | 638 |
| -42.349765 | 171.258009 | 0 | 639 |
| -42.379016 | 171.278552 | 0 | 640 |
| -42.358563 | 171.265156 | 0 | 641 |
| -42.372947 | 171.258441 | 0 | 642 |
| -42.373182 | 171.271464 | 0 | 643 |
| -42.392937 | 171.251554 | 0 | 644 |
| -42.365655 | 171.274429 | 0 | 645 |
| -42.389491 | 171.255197 | 0 | 646 |
| -42.36439 | 171.260016 | 0 | 647 |
| -42.385746 | 171.247699 | 0 | 648 |
| -42.397401 | 171.262531 | 0 | 649 |
| -42.38187 | 171.252035 | 0 | 650 |
| -42.345604 | 171.302475 | 76+ | 656 |
| -42.354044 | 171.299708 | 26+ | 657 |
| -42.342585 | 171.322182 | 17.2+ | 658 |
| -42.345308 | 171.338361 | 38+ | 660 |
| -42.338511 | 171.355714 | 17+ | 661 |
| -42.3457 | 171.264203 | 0 | 710 |

| Jay-Ford conglomerate thickness | | | |
|---|---|---|---|
| **Latitude** | **Longitude** | **Conglomerate thickness** | **Drill hole** |
| -42.370333 | 171.268253 | 0 | 787 |
| -42.380684 | 171.272786 | 0 | 833 |
| -42.386612 | 171.291694 | 0 | 933 |
| -42.386857 | 171.29536 | 0 | 1011 |
| -42.382515 | 171.309954 | 0 | 1012 |
| -42.339841 | 171.306819 | 110+ | 1400 |
| -42.337214 | 171.35255 | 17+ | 1424 |
| -42.3219 | -171.2703664 | 0 | Twelve Mile Beach |

| Morgan-Waiomo conglomerate thickness | | | |
|---|---|---|---|
| **Latitude** | **Longitude** | **Conglomerate thickness** | **Drill hole** |
| -42.36679 | 171.34141 | 0 | 595 |
| -42.364047 | 171.33916 | 0 | 596 |
| -42.351376 | 171.26799 | 17.7 | 619 |
| -42.39919 | 171.33311 | 0 | 620 |
| -42.339841 | 171.27082 | 10+ | 621 |
| -42.35843 | 171.25654 | 0 | 622 |
| -42.373862 | 171.28185 | 0 | 624 |
| -42.39855 | 171.31786 | 0 | 625 |
| -42.370897 | 171.24641 | 0 | 626 |
| -42.418123 | 171.30024 | 0 | 627 |
| -42.392834 | 171.26419 | 0 | 628 |
| -42.393712 | 171.30017 | 0 | 630 |
| -42.367032 | 171.28565 | 17+ | 631 |
| -42.366582 | 171.29583 | 0 | 632 |
| -42.381339 | 171.2451 | 0 | 633 |
| -42.341364 | 171.26091 | 15+ | 634 |
| -42.35863 | 171.27431 | 0 | 635 |
| -42.382328 | 171.25782 | 0 | 636 |
| -42.363878 | 171.24723 | 0 | 637 |
| -42.381752 | 171.27018 | 0 | 638 |
| -42.349765 | 171.25801 | 0 | 639 |
| -42.379016 | 171.27855 | 0 | 640 |
| -42.358563 | 171.26516 | 0 | 641 |
| -42.372947 | 171.25844 | 0 | 642 |
| -42.373182 | 171.27146 | 0 | 643 |
| -42.392937 | 171.25155 | 0 | 644 |
| -42.365655 | 171.27443 | 0 | 644 |
| -42.389491 | 171.2552 | 0 | 646 |
| -42.36439 | 171.26002 | 1.3 | 647 |
| -42.385746 | 171.2477 | 0 | 648 |
| -42.397401 | 171.26253 | 0 | 649 |
| -42.38187 | 171.25204 | 0 | 650 |
| -42.345604 | 171.30248 | 11 | 656 |
| -42.354044 | 171.29971 | 9 | 657 |
| -42.342585 | 171.32218 | 0 | 658 |
| -42.356844 | 171.34038 | 0 | 659 |
| -42.345308 | 171.33836 | 0 | 660 |
| -42.338511 | 171.35571 | 0 | 661 |
| -42.355303 | 171.34827 | 1.52 | 668 |

| Morgan-Waiomo conglomerate thickness | | | |
|---|---|---|---|
| **Latitude** | **Longitude** | **Conglomerate thickness** | **Drill hole** |
| -42.373028 | 171.265482 | 0 | 703 |
| -42.368414 | 171.264675 | 0 | 704 |
| -42.375796 | 171.268125 | 0 | 706 |
| -42.342328 | 171.328549 | 0 | 719 |
| -42.357788 | 171.35449 | 0 | 720 |
| -42.357788 | 171.35449 | 0 | 730 |
| -42.38574 | 171.34081 | 0 | 732 |
| -42.383769 | 171.32662 | 0 | 734 |
| -42.36799 | 171.33164 | 0 | 736 |
| -42.380684 | 171.27279 | 0 | 833 |
| -42.349513 | 171.34086 | 0 | 874 |
| -42.366226 | 171.30682 | 0 | 925 |
| -42.386612 | 171.29169 | 0 | 933 |
| -42.386857 | 171.29536 | 0 | 1011 |
| -42.382515 | 171.30995 | 0 | 1012 |
| -42.352756 | 171.33243 | 0 | 1369 |
| -42.339841 | 171.30682 | 6 | 1400 |
| -42.337214 | 171.35255 | 0 | 1424 |
| -42.347169 | 171.35466 | 0 | 1431 |
| -42.3219 | -171.27037 | 28 | Twelve Mile Beach |

| Rewanui-Goldlight conglomerate thickness | | | |
|---|---|---|---|
| **Latitude** | **Longitude** | **Conglomerate thickness** | **Drill hole** |
| -42.351376 | 171.26799 | 50 | 619 |
| -42.39919 | 171.333108 | 0 | 620 |
| -42.339841 | 171.270823 | 99.7 | 621 |
| -42.35843 | 171.256541 | 24 | 622 |
| -42.373862 | 171.281852 | 0 | 624 |
| -42.39855 | 171.317856 | 0 | 625 |
| -42.370897 | 171.246405 | 17 | 626 |
| -42.418123 | 171.300242 | 0 | 627 |
| -42.392834 | 171.264189 | 0 | 628 |
| -42.393712 | 171.300168 | 0 | 630 |
| -42.367032 | 171.285646 | 16 | 631 |
| -42.366582 | 171.295833 | 14 | 632 |
| -42.381339 | 171.245103 | 0 | 633 |
| -42.341364 | 171.260914 | 130 | 634 |
| -42.35863 | 171.274308 | 43.6 | 635 |
| -42.382328 | 171.257815 | 0 | 636 |
| -42.363878 | 171.247234 | 64 | 637 |
| -42.381752 | 171.270182 | 0 | 638 |
| -42.349765 | 171.258009 | 110 | 639 |
| -42.379016 | 171.278552 | 1 | 640 |
| -42.358563 | 171.265156 | 82 | 641 |
| -42.372947 | 171.258441 | 29 | 642 |
| -42.373182 | 171.271464 | 1 | 643 |
| -42.392937 | 171.251554 | 0 | 644 |
| -42.365655 | 171.274429 | 58 | 645 |
| -42.389491 | 171.255197 | 0 | 646 |
| -42.36439 | 171.260016 | 44 | 647 |
| -42.385746 | 171.247699 | 0 | 648 |
| -42.397401 | 171.262531 | 0 | 649 |
| -42.38187 | 171.252035 | 0 | 650 |
| -42.345604 | 171.302475 | 25 | 656 |
| -42.354044 | 171.299708 | 17 | 657 |
| -42.342585 | 171.322182 | 0 | 658 |
| -42.356844 | 171.340384 | 0 | 659 |
| -42.345308 | 171.338361 | 5 | 660 |
| -42.338511 | 171.355714 | 0 | 661 |
| -42.355303 | 171.348267 | 0 | 668 |
| -42.378004 | 171.25711 | 8.4 | 696 |
| 276475.65 | 694863.42 | 1 | 697 |

| Rewanui-Goldlight conglomerate thickness | | | |
|---|---|---|---|
| **Latitude** | **Longitude** | **Conglomerate thickness** | **Drill hole** |
| -42.386154 | 171.262493 | 0 | 698 |
| -42.386154 | 171.262493 | 3.2 | 699 |
| -42.376388 | 171.273294 | 13.5 | 700 |
| -42.368969 | 171.278599 | 9.3 | 701 |
| -42.367497 | 171.253045 | 16.72 | 702 |
| -42.373028 | 171.265482 | 18 | 703 |
| -42.368414 | 171.264675 | 12.5 | 704 |
| -42.376052 | 171.259545 | 20.3 | 705 |
| -42.375796 | 171.268125 | 12.73 | 706 |
| -42.363476 | 171.267909 | 35 | 707 |
| -42.355018 | 171.271822 | 53.26 | 708 |
| -42.353778 | 171.261393 | 50 | 709 |
| -42.3457 | 171.264203 | 99.5 | 710 |
| -42.375389 | 171.255082 | 8.14 | 711 |
| -42.342328 | 171.328549 | 0 | 719 |
| -42.339841 | 171.306819 | 19 | 1400 |
| -42.3219 | -171.2703664 | 200 | Twelve Mile Beach |

| Dunollie conglomerate thickness | | | |
|---|---|---|---|
| **Latitude** | **Longitude** | **Conglomerate thickness** | **Drill hole** |
| -42.351376 | 171.26799 | 4 | 619 |
| -42.39919 | 171.333108 | 0 | 620 |
| -42.339841 | 171.270823 | 17 | 621 |
| -42.35843 | 171.256541 | 13 | 622 |
| -42.39855 | 171.317856 | 0 | 625 |
| -42.370897 | 171.246405 | 0 | 626 |
| -42.418123 | 171.300242 | 0 | 627 |
| -42.392834 | 171.264189 | 0 | 628 |
| -42.367032 | 171.285646 | 0 | 631 |
| -42.366582 | 171.295833 | 0 | 632 |
| -42.381339 | 171.245103 | 3 | 633 |
| -42.341364 | 171.260914 | 119+ | 634 |
| -42.35863 | 171.274308 | 0 | 635 |
| -42.382328 | 171.257815 | 0 | 636 |
| -42.363878 | 171.247234 | 100 | 637 |
| -42.349765 | 171.258009 | 110 | 639 |
| -42.372947 | 171.258441 | 0 | 642 |
| -42.373182 | 171.271464 | 0 | 643 |
| -42.392937 | 171.251554 | 0 | 644 |
| -42.389491 | 171.255197 | 0 | 646 |
| -42.36439 | 171.260016 | 0 | 647 |
| -42.385746 | 171.247699 | 0 | 648 |
| -42.397401 | 171.262531 | 0 | 649 |
| -42.38187 | 171.252035 | 0 | 650 |
| -42.378004 | 171.25711 | 0 | 696 |
| 276475.65 | 694863.42 | 0 | 697 |
| -42.386154 | 171.262493 | 0 | 698 |
| -42.386154 | 171.262493 | 0 | 699 |
| -42.376388 | 171.273294 | 0 | 700 |
| -42.368969 | 171.278599 | 0 | 701 |
| -42.367497 | 171.253045 | 18 | 702 |
| -42.373028 | 171.265482 | 0 | 703 |
| -42.368414 | 171.264675 | 0 | 704 |
| -42.376052 | 171.259545 | 0 | 705 |
| -42.375796 | 171.268125 | 0 | 706 |
| -42.363476 | 171.267909 | 0 | 707 |
| -42.355018 | 171.271822 | 0 | 708 |
| -42.353778 | 171.261393 | 0 | 709 |
| -42.3457 | 171.264203 | 73.63 | 710 |

| Dunollie conglomerate thickness | | | |
|---|---|---|---|
| **Latitude** | **Longitude** | **Conglomerate thickness** | **Drill hole** |
| -42.375389 | 171.255082 | 0 | 711 |
| -42.3219 | -171.2703664 | 32 | Twelve Mile Beach |

# Appendix 4: Geochemical data of the lacustrine mudstones

Samples are collected from drill cores at the Featherston Core Storage near Wellington and Twelve Mile Beach outcrop.

Source rock geochemistry of the Ford Member

| Sample | | | Lithofacies name | Member | Source Rock Analysis | | | | | | | | | |
|---|---|---|---|---|---|---|---|---|---|---|---|---|---|---|
| Number | ID | Depth | | | Weight (mg) | S1 (mg HC/g rock) | S2 (mg HC/g rock) | Tmax (°C) | tTemp (°C) | S3 (mg $CO_2$/g rock) | TOC (wt. %) | HI (mg HC/g TOC) | OI (mg $CO_2$/g TOC) | PI |
| 1 | 656-40 | 656/428.30 | Lacustrine mudstones with minor thin sandstones | Ford | 73.4 | 0.28 | 2.61 | 426.3 | 486.8 | 1.19 | 1.30 | 200 | 91 | 0.10 |
| 2 | 656-39 | 656/429.90 | Lacustrine massive mudstone facies | Ford | 76.4 | 0.41 | 3.69 | 427.6 | 485.7 | 0.48 | 1.39 | 265 | 34 | 0.10 |
| 3 | 656-38 | 656/431.75 | Lacustrine massive mudstone facies | Ford | 75.5 | 0.54 | 4.48 | 428.8 | 481.0 | 0.39 | 1.64 | 274 | 24 | 0.11 |
| 4 | 656-37 | 656/433.24 | Lacustrine massive mudstone facies | Ford | 78.5 | 0.48 | 6.06 | 430.8 | 481.2 | 0.22 | 1.66 | 365 | 13 | 0.07 |
| 5 | 656-36 | 656/435.0 | Lacustrine massive mudstone facies | Ford | 76.6 | 0.37 | 3.27 | 431.0 | 484.7 | 0.58 | 1.48 | 220 | 39 | 0.10 |

**Source rock geochemistry of the Ford Member**

| | | | | | | | | | | | | | | |
|---|---|---|---|---|---|---|---|---|---|---|---|---|---|---|
| 6 | 656-35 | 656/436.81 | Lacustrine massive mudstone facies | Ford | 78.0 | 0.45 | 3.56 | 432.6 | 486.6 | 1.59 | 1.54 | 232 | 104 | 0.11 |
| 7 | 656-34 | 656/438.48 | Lacustrine massive mudstone facies | Ford | 78.2 | 0.57 | 6.61 | 433.8 | 484.7 | 0.80 | 2.04 | 324 | 39 | 0.08 |
| 8 | 656-33 | 656/440.28 | Lacustrine massive mudstone facies | Ford | 74.6 | 0.58 | 9.94 | 435.6 | 479.2 | 0.21 | 2.20 | 453 | 9 | 0.06 |
| 9 | 656-32 | 656/442.10 | Lacustrine massive mudstone facies | Ford | 75.4 | 0.63 | 8.45 | 435.8 | 480.1 | 0.62 | 2.13 | 396 | 29 | 0.07 |
| 10 | 656-31 | 656/443.87 | Lacustrine mudstones with minor thin sandstones | Ford | 74.7 | 0.78 | 12.04 | 436.1 | 475.8 | 0.59 | 2.63 | 457 | 22 | 0.06 |
| 11 | 656-30 | 656/447.65 | Lacustrine mudstones with minor thin sandstones | Ford | 74.2 | 0.09 | 0.79 | 436.3 | 474.6 | 1.56 | 0.71 | 111 | 219 | 0.10 |

**Source rock geochemistry of the Ford Member**

| | | | | | | | | | | | | | | |
|---|---|---|---|---|---|---|---|---|---|---|---|---|---|---|
| 12 | 656-29 | 656/45 0.90 | Lacustrine massive mudstone facies | Ford | 78.8 | 0.44 | 3.63 | 436.8 | 477.6 | 0.64 | 1.65 | 220 | 39 | 0.11 |
| 13 | 656-15 | 656/45 1.43 | Lacustrine massive mudstone facies | Ford | 75.2 | 0.52 | 6.11 | 438.4 | 478.0 | 0.60 | 2.03 | 300 | 30 | 0.08 |
| 14 | 656-14 | 656/45 2.20 | Lacustrine massive mudstone facies | Ford | 78.3 | 0.50 | 5.05 | 438.6 | 480.7 | 0.93 | 1.74 | 290 | 53 | 0.09 |
| 15 | 656-11 | 656/45 3.47 | Lacustrine massive mudstone facies | Ford | 77.1 | 0.38 | 2.67 | 439.0 | 472.8 | 1.23 | 1.19 | 224 | 103 | 0.13 |
| 16 | 656-12 | 656/45 4.40 | Lacustrine massive mudstone facies | Ford | 72.8 | 0.92 | 11.27 | 440.0 | 474.8 | 0.47 | 2.62 | 430 | 18 | 0.08 |
| 17 | 656-13 | 656/45 5.70 | Lacustrine massive mudstone facies | Ford | 73.6 | 0.46 | 3.31 | 440.1 | 484.8 | 1.58 | 1.53 | 216 | 103 | 0.12 |

**Source rock geochemistry of the Ford Member**

| | | | | | | | | | | | | | | |
|---|---|---|---|---|---|---|---|---|---|---|---|---|---|---|
| 18 | 656-10 | 656/457.20 | Lacustrine massive mudstone facies | Ford | 76.3 | 0.58 | 5.86 | 440.2 | 479.1 | 0.42 | 1.70 | 346 | 25 | 0.09 |
| 19 | 656-9 | 656/458.20 | Lacustrine massive mudstone facies | Ford | 77.1 | 0.49 | 3.93 | 440.9 | 481.5 | 0.69 | 1.55 | 254 | 44 | 0.11 |
| 20 | 656-1 | 656/459.38 | Lacustrine massive mudstone facies | Ford | 71.4 | 1.56 | 16.26 | 441.1 | 475.3 | 0.30 | 3.37 | 482 | 9 | 0.09 |
| 21 | 656-2 | 656/460.50 | Lacustrine massive mudstone facies | Ford | 75.0 | 0.40 | 2.56 | 441.7 | 485.0 | 1.40 | 1.38 | 186 | 101 | 0.14 |
| 22 | 656-3 | 656/461.70 | Lacustrine massive mudstone facies | Ford | 76.3 | 0.74 | 5.12 | 441.7 | 485.3 | 1.41 | 2.02 | 254 | 70 | 0.13 |
| 23 | 656_461-8 | 656/461.8 | Lacustrine mudstones with minor thin sandstones | Ford | 78.8 | 1.49 | 25.08 | 441.9 | 480.9 | 0.75 | 4.54 | 552 | 16 | 0.06 |

**Source rock geochemistry of the Ford Member**

| | | | | | | | | | | | | | | |
|---|---|---|---|---|---|---|---|---|---|---|---|---|---|---|
| 24 | 656-4 | 656/463.45 | Lacustrine massive mudstone facies | Ford | 78.1 | 1.08 | 21.08 | 441.9 | 479.0 | 0.34 | 3.80 | 554 | 9 | 0.05 |
| 25 | 656-5 | 656/463.90 | Lacustrine massive mudstone facies | Ford | 79.7 | 0.64 | 8.16 | 442.0 | 489.5 | 0.50 | 2.32 | 352 | 22 | 0.07 |
| 26 | 656-6 | 656/466.65 | Lacustrine massive mudstone facies | Ford | 73.2 | 0.60 | 3.83 | 442.2 | 486.7 | 1.19 | 1.64 | 233 | 72 | 0.14 |
| 27 | 656-8 | 656/467.90 | Lacustrine massive mudstone facies | Ford | 72.9 | 0.81 | 4.94 | 442.3 | 488.8 | 0.60 | 2.01 | 246 | 30 | 0.14 |
| 28 | 656-16 | 656/469.60 | Lacustrine massive mudstone facies | Ford | 72.8 | 0.91 | 7.29 | 442.5 | 471.6 | 0.61 | 2.31 | 315 | 26 | 0.11 |
| 29 | 656-7 | 656/471.10 | Lacustrine massive mudstone facies | Ford | 75.1 | 0.82 | 5.34 | 445.1 | 489.4 | 0.98 | 1.99 | 269 | 49 | 0.13 |

**Source rock geochemistry of the Ford Member**

| | | | | | | | | | | | | | | |
|---|---|---|---|---|---|---|---|---|---|---|---|---|---|---|
| 30 | 656-17 | 656/471.80 | Lacustrine mudstones with minor thin sandstones | Ford | 71.2 | 0.62 | 3.86 | 445.1 | 479.9 | 0.64 | 1.62 | 239 | 39 | 0.14 |
| 31 | 656-18 | 656/473.46 | Lacustrine massive mudstone facies | Ford | 72.4 | 0.53 | 4.30 | 445.3 | 484.8 | 0.69 | 1.62 | 265 | 42 | 0.11 |
| 32 | 656-19 | 656/475.24 | Lacustrine massive mudstone facies | Ford | 72.7 | 1.28 | 20.73 | 445.3 | 477.4 | 0.32 | 3.79 | 546 | 8 | 0.06 |
| 33 | 656-20 | 656/477.08 | Lacustrine massive mudstone facies | Ford | 75.2 | 0.81 | 7.38 | 445.5 | 465.3 | 0.53 | 2.44 | 302 | 22 | 0.10 |
| 34 | 656-21 | 656/478.90 | Lacustrine massive mudstone facies | Ford | 72.1 | 0.97 | 6.00 | 445.7 | 467.8 | 0.91 | 2.51 | 239 | 36 | 0.14 |
| 35 | 656-22 | 656/481.10 | Lacustrine massive mudstone facies | Ford | 73.5 | 0.64 | 6.37 | 445.7 | 470.0 | 0.49 | 2.14 | 298 | 23 | 0.09 |

**Source rock geochemistry of the Ford Member**

| | | | | | | | | | | | | | | |
|---|---|---|---|---|---|---|---|---|---|---|---|---|---|---|
| 36 | 656-23 | 656/483.10 | Lacustrine massive mudstone facies | Ford | 74.1 | 0.57 | 3.83 | 445.8 | 484.1 | 1.20 | 1.89 | 203 | 63 | 0.13 |
| 37 | 656-24 | 656/484.80 | Lacustrine massive mudstone facies | Ford | 79.1 | 0.78 | 6.46 | 445.8 | 466.6 | 0.42 | 2.21 | 292 | 19 | 0.11 |
| 38 | 656-27 | 656/486.67 | Lacustrine massive mudstone facies | Ford | 75.6 | 0.50 | 3.21 | 446.0 | 484.3 | 1.47 | 1.72 | 186 | 85 | 0.14 |
| 39 | 656-25 | 656/489.0 | Lacustrine massive mudstone facies | Ford | 71.9 | 0.63 | 4.59 | 446.3 | 480.9 | 0.56 | 2.08 | 220 | 27 | 0.12 |
| 40 | 656-26 | 656/490.50 | Lacustrine massive mudstone facies | Ford | 74.3 | 0.69 | 6.89 | 446.7 | 475.1 | 0.20 | 2.39 | 288 | 9 | 0.09 |
| 41 | 656-28 | 656/492.15 | Lacustrine massive mudstone facies | Ford | 74.5 | 0.55 | 4.27 | 447.6 | 469.8 | 0.27 | 2.04 | 210 | 13 | 0.11 |

**Source rock geochemistry of the Ford Member**

| | | | | | | | | | | | | | | |
|---|---|---|---|---|---|---|---|---|---|---|---|---|---|---|
| 42 | 658_303 | 658/303 | Lacustrine massive mudstone facies | Ford | 79.4 | 0.15 | 5.24 | 447.7 | 495.1 | 1.58 | 2.56 | 204 | 62 | 0.03 |
| 43 | 658-1 | 658/293.60 | Lacustrine massive mudstone facies | Ford | 75.1 | 0.51 | 3.85 | 447.8 | 484.1 | 1.01 | 2.08 | 185 | 48 | 0.12 |
| 44 | 658-2 | 658/295.44 | Lacustrine massive mudstone facies | Ford | 71.3 | 0.26 | 2.58 | 448.0 | 484.5 | 2.85 | 1.62 | 160 | 176 | 0.09 |
| 45 | 658-3 | 658/296.03 | Lacustrine mudstones with minor thin sandstones | Ford | 73.9 | 0.77 | 8.65 | 448.8 | 484.3 | 0.16 | 3.26 | 266 | 5 | 0.08 |
| 46 | 658-4 | 658/298.15 | Lacustrine massive mudstone facies | Ford | 74.9 | 0.23 | 2.03 | 449.2 | 487.8 | 1.02 | 1.33 | 153 | 77 | 0.10 |
| 47 | 658-5 | 658/301.23 | Lacustrine massive mudstone facies | Ford | 72.7 | 0.39 | 3.45 | 449.3 | 488.3 | 0.65 | 2.03 | 170 | 32 | 0.10 |

**Source rock geochemistry of the Ford Member**

| | | | | | | | | | | | | | | |
|---|---|---|---|---|---|---|---|---|---|---|---|---|---|---|
| 48 | 658-6 | 658/303.03 | Lacustrine massive mudstone facies | Ford | 73.6 | 0.17 | 5.25 | 449.8 | 481.3 | 1.76 | 2.01 | 261 | 87 | 0.03 |
| 49 | 658-7 | 658/305.10 | Lacustrine massive mudstone facies | Ford | 76.0 | 0.21 | 2.22 | 450.4 | 487.0 | 1.39 | 1.40 | 159 | 100 | 0.09 |
| 50 | 658-8 | 658/306.80 | Lacustrine massive mudstone facies | Ford | 79.0 | 0.37 | 6.40 | 450.5 | 488.2 | 0.94 | 2.20 | 291 | 43 | 0.06 |
| 51 | 659_376-4 | 659/376.4 | Lacustrine massive mudstone facies | Ford | 78.2 | 0.50 | 1.28 | 462.4 | 504.7 | 1.87 | 1.43 | 90 | 131 | 0.28 |
| 52 | 659_393 | 659/393 | Lacustrine massive mudstone facies | Ford | 75.2 | 0.59 | 1.16 | 463.3 | 504.4 | 2.29 | 1.37 | 84 | 167 | 0.34 |
| 53 | 660_278-4 | 660/278.4 | Lacustrine massive mudstone facies | Ford | 99.0 | 0.41 | 0.90 | 465.4 | 501.4 | 2.39 | 1.01 | 90 | 237 | 0.31 |

**Source rock geochemistry of the Ford Member**

| | | | | | | | | | | | | | | |
|---|---|---|---|---|---|---|---|---|---|---|---|---|---|---|
| 54 | 660_336-5 | 660/336.5 | Lacustrine massive mudstone facies | Ford | 76.8 | 0.42 | 1.18 | 465.7 | 502.3 | 2.48 | 1.39 | 85 | 179 | 0.26 |
| 55 | 661_30-15 | 661/30.15 | Lacustrine massive mudstone facies | Ford | 77.0 | 0.51 | 0.80 | 471.0 | 510.0 | 1.46 | 1.17 | 68 | 125 | 0.39 |
| 56 | 661_48-8 | 661/48.8 | Lacustrine massive mudstone facies | Ford | 75.3 | 0.53 | 0.85 | 473.7 | 512.7 | 0.90 | 1.21 | 70 | 75 | 0.38 |

**Source rock geochemistry of the Waiomo Member**

| Sample | | | Lithofacies name | Member | Source Rock Analysis | | | | | | | | | |
|---|---|---|---|---|---|---|---|---|---|---|---|---|---|---|
| Number | ID | Depth | | | Weight (mg) | S1 (mg HC/ g rock) | S2 (mg HC/ g rock) | Tmax (°C) | tTemp (°C) | S3 ($mg CO_2$/ g rock) | TOC (wt. %) | HI (mg HC/g TOC) | OI (mg $CO_2$/ g TOC) | PI |
| 1 | 621-22 | 621/359.20 | Lacustrine massive mudstone facies | Waiomo | 78.1 | 0.11 | 7.49 | 430.9 | 469.9 | 0.56 | 1.75 | 428 | 32 | 0.01 |
| 2 | 621-21 | 621/361.0 | Lacustrine Massive mudstone facies | Waiomo | 76.3 | 0.12 | 8.38 | 428.3 | 467.3 | 0.40 | 1.80 | 466 | 22 | 0.01 |
| 3 | 621-20 | 621/362.67 | Lacustrine Mudstones with minor sandstone facies | Waiomo | 80.0 | 0.13 | 8.99 | 424.7 | 463.7 | 1.35 | 2.22 | 406 | 61 | 0.01 |
| 4 | 621-18 | 621/364.10 | Lacustrine massive mudstone facies | Waiomo | 72.2 | 0.08 | 8.59 | 440.9 | 479.9 | 1.72 | 2.07 | 415 | 83 | 0.01 |
| 5 | 621-17 | 621/366.06 | Lacustrine massive mudstone facies | Waiomo | 78.4 | 0.08 | 3.21 | 428.9 | 467.9 | 1.58 | 1.31 | 246 | 121 | 0.02 |
| 6 | 621-15 | 621/368.70 | Lacustrine massive mudstone facies | Waiomo | 74.2 | 0.07 | 5.03 | 434.0 | 473.0 | 0.33 | 1.63 | 308 | 20 | 0.01 |
| 7 | 621-13 | 621/370.15 | Lacustrine massive mudstone facies | Waiomo | 78.6 | 0.07 | 4.58 | 429.2 | 468.2 | 0.41 | 1.66 | 276 | 25 | 0.02 |

| | | | | | | | | | | | | | | |
|---|---|---|---|---|---|---|---|---|---|---|---|---|---|---|
| 8 | 621-12 | 621/371.58 | Lacustrine massive mudstone facies | Waiomo | 73.8 | 0.05 | 2.49 | 434.6 | 473.6 | 1.23 | 1.23 | 203 | 100 | 0.02 |
| 9 | 621-14 | 621/372.35 | Lacustrine massive mudstone facies | Waiomo | 73.1 | 0.10 | 5.31 | 431.8 | 470.8 | 0.32 | 1.68 | 315 | 19 | 0.02 |
| 10 | 621-11 | 621/372.68 | Lacustrine massive mudstone facies | Waiomo | 70.1 | 0.07 | 6.33 | 436.9 | 475.9 | 0.26 | 1.55 | 409 | 17 | 0.01 |
| 11 | 621-10 | 621/374.55 | Lacustrine massive mudstone facies | Waiomo | 78.0 | 0.07 | 5.59 | 438.1 | 477.1 | 0.19 | 1.39 | 403 | 14 | 0.01 |
| 12 | 621-9 | 621/378.70 | Lacustrine massive mudstone facies | Waiomo | 74.5 | 0.05 | 3.87 | 430.0 | 469.0 | 0.58 | 1.31 | 296 | 44 | 0.01 |
| 13 | 621-8 | 621/380.75 | Lacustrine massive mudstone facies | Waiomo | 70.9 | 0.03 | 3.05 | 436.9 | 475.9 | 0.18 | 1.00 | 304 | 18 | 0.01 |
| 14 | 621-7 | 621/381.85 | Lacustrine massive mudstone facies | Waiomo | 80.2 | 0.06 | 4.36 | 431.9 | 470.9 | 0.55 | 1.40 | 312 | 40 | 0.01 |
| 15 | 621-6 | 621/383.75 | Lacustrine massive mudstone facies | Waiomo | 79.6 | 0.05 | 2.36 | 433.0 | 472.0 | 1.78 | 1.16 | 203 | 154 | 0.02 |
| 16 | 621-5 | 621/385.60 | Lacustrine massive mudstone facies | Waiomo | 73.2 | 0.06 | 2.64 | 433.9 | 472.9 | 0.98 | 1.27 | 208 | 77 | 0.02 |

**Source rock geochemistry of the Waiomo Member**

| | | | | | | | | | | | | | | |
|---|---|---|---|---|---|---|---|---|---|---|---|---|---|---|
| 17 | 621-4 | 621/387.66 | Lacustrine massive mudstone facies | Waiomo | 76.1 | 0.06 | 3.18 | 430.2 | 469.2 | 0.27 | 1.32 | 242 | 21 | 0.02 |
| 18 | 624_14 | 624/293.95 | Lacustrine massive mudstone facies | Waiomo | 70.6 | 0.14 | 3.05 | 441 | 480 | 0.66 | 1.08 | 283 | 61 | 0.05 |
| 19 | 624_13 | 624/293.86 | Lacustrine massive mudstone facies | Waiomo | 78.2 | 0.22 | 4.4 | 439 | 478 | 0.41 | 1.28 | 343 | 32 | 0.05 |
| 20 | 624_12 | 624/296.21 | Lacustrine massive mudstone facies | Waiomo | 75.8 | 0.13 | 5.21 | 444 | 483 | 0.6 | 1.48 | 353 | 40 | 0.02 |
| 21 | 624_11 | 624/294.33 | Lacustrine massive mudstone facies | Waiomo | 75.8 | 0.21 | 6.44 | 440 | 479 | 0.46 | 1.57 | 410 | 30 | 0.03 |
| 22 | 624_10 | 624/292.79 | Lacustrine massive mudstone facies | Waiomo | 70.5 | 0.12 | 2.51 | 441 | 480 | 1.04 | 1.09 | 230 | 95 | 0.04 |
| 23 | 624_9 | 624/288.60 | Lacustrine massive mudstone facies | Waiomo | 75.1 | 0.12 | 1.92 | 441 | 480 | 0.78 | 0.91 | 211 | 85 | 0.06 |
| 24 | 624_8 | 624/284.97 | Lacustrine distal turbidite facies | Waiomo | 75.6 | 0.08 | 2.89 | 445 | 484 | 0.91 | 0.97 | 297 | 93 | 0.03 |
| 25 | 630_252-5 | 630/252.5 | Lacustrine massive mudstone facies | Waiomo | 81.5 | 0.60 | 7.52 | 443.2 | 482.2 | 0.48 | 3.02 | 249 | 16 | 0.07 |

| | | | | | | | | | | | | | | |
|---|---|---|---|---|---|---|---|---|---|---|---|---|---|---|
| 26 | 632_587-8 | 632/587.8 | Lacustrine massive mudstone facies | Waiomo | 81.7 | 0.41 | 4.25 | 449.5 | 488.5 | 1.18 | 1.67 | 255 | 71 | 0.09 |
| 27 | 632_606 | 632/606 | Lacustrine massive mudstone facies | Waiomo | 100.0 | 0.65 | 5.16 | 440.4 | 479.4 | 1.26 | 1.77 | 292 | 71 | 0.11 |
| 28 | 635-1 | 635/648.86 | Lacustrine distal turbidite facies | Waiomo | 78.8 | 0.03 | 1.91 | 437.8 | 476.8 | 0.97 | 0.98 | 196 | 100 | 0.02 |
| 29 | 635-2 | 635/651.05 | Lacustrine massive mudstone facies | Waiomo | 79.1 | 0.04 | 1.26 | 435.8 | 474.8 | 1.36 | 0.72 | 176 | 190 | 0.03 |
| 30 | 635-3 | 635/652.79 | Lacustrine massive mudstone facies | Waiomo | 76.7 | 0.04 | 1.61 | 437.0 | 476.0 | 0.60 | 0.86 | 186 | 69 | 0.02 |
| 31 | 635-4 | 635/653.56 | Lacustrine distal turbidite facies | Waiomo | 77.0 | 0.05 | 2.12 | 438.1 | 477.1 | 0.87 | 0.87 | 243 | 100 | 0.02 |
| 32 | 635-5 | 635/655.85 | Lacustrine massive mudstone facies | Waiomo | 73.4 | 0.03 | 2.00 | 440.8 | 479.8 | 0.86 | 0.99 | 202 | 87 | 0.01 |
| 33 | 635-6 | 635/657.20 | Lacustrine massive mudstone facies | Waiomo | 76.0 | 0.09 | 5.59 | 441.1 | 480.1 | 0.16 | 1.39 | 401 | 12 | 0.02 |
| 34 | 635-7 | 635/659.38 | Lacustrine massive mudstone facies | Waiomo | 77.1 | 0.11 | 1.67 | 439.7 | 478.7 | 0.99 | 0.91 | 184 | 109 | 0.06 |

| | | | | | | | | | | | | | | |
|---|---|---|---|---|---|---|---|---|---|---|---|---|---|---|
| 35 | 635-8 | 635/62.70 | Lacustrine massive mudstone facies | Waiomo | 78.9 | 0.07 | 3.46 | 440.6 | 479.6 | 0.35 | 1.15 | 301 | 31 | 0.02 |
| 36 | 635-9 | 635/64.70 | Lacustrine massive mudstone facies | Waiomo | 73.5 | 0.09 | 1.20 | 434.7 | 473.7 | 1.81 | 0.94 | 127 | 192 | 0.07 |
| 37 | 635-10 | 635/66.49 | Lacustrine massive mudstone facies | Waiomo | 74.3 | 0.08 | 1.56 | 437.9 | 476.9 | 2.19 | 1.03 | 152 | 213 | 0.05 |
| 38 | 635-11 | 635/67.89 | Lacustrine massive mudstone facies | Waiomo | 71.4 | 0.06 | 2.96 | 442.4 | 481.4 | 1.52 | 1.24 | 239 | 123 | 0.02 |
| 39 | 635-12 | 635/69.77 | Lacustrine massive mudstone facies | Waiomo | 72.2 | 0.09 | 2.51 | 440.6 | 479.6 | 1.02 | 1.19 | 211 | 85 | 0.03 |
| 40 | 635-13 | 635/71.87 | Lacustrine massive mudstone facies | Waiomo | 76.8 | 0.09 | 5.08 | 442.1 | 481.1 | 0.83 | 1.52 | 334 | 54 | 0.02 |
| 41 | 635-14 | 635/73.71 | Lacustrine massive mudstone facies | Waiomo | 78.0 | 0.16 | 5.56 | 442.7 | 481.7 | 0.99 | 1.69 | 329 | 58 | 0.03 |
| 42 | 635-15 | 635/75.29 | Lacustrine massive mudstone facies | Waiomo | 72.5 | 0.10 | 3.99 | 438.1 | 477.1 | 0.86 | 1.52 | 262 | 56 | 0.02 |
| 43 | 635-16 | 635/77.06 | Lacustrine massive mudstone facies | Waiomo | 78.8 | 0.13 | 2.54 | 438.8 | 477.8 | 1.03 | 1.22 | 209 | 84 | 0.05 |

| | | | | | | | | | | | | | | |
|---|---|---|---|---|---|---|---|---|---|---|---|---|---|---|
| 44 | 635-17 | 635/679.0 | Lacustrine massive mudstone facies | Waiomo | 74.3 | 0.14 | 5.09 | 437.9 | 476.9 | 1.00 | 1.65 | 310 | 61 | 0.03 |
| 45 | 635-18 | 635/680.50 | Lacustrine massive mudstone facies | Waiomo | 72.5 | 0.15 | 6.43 | 435.2 | 474.2 | 0.44 | 1.73 | 372 | 25 | 0.02 |
| 46 | 635-19 | 635/682.10 | Lacustrine massive mudstone facies | Waiomo | 77.7 | 0.14 | 3.24 | 441.3 | 480.3 | 1.35 | 1.40 | 231 | 96 | 0.04 |
| 47 | 635-20 | 635/684.30 | Lacustrine distal turbidite facies | Waiomo | 70.8 | 0.22 | 9.12 | 441.7 | 480.7 | 0.31 | 1.95 | 468 | 16 | 0.02 |
| 48 | 635-21 | 635/685.59 | Lacustrine massive mudstone facies | Waiomo | 74.4 | 0.18 | 7.09 | 439.8 | 478.8 | 0.42 | 1.74 | 408 | 24 | 0.03 |
| 49 | 635-22 | 635/688.10 | Lacustrine massive mudstone facies | Waiomo | 75.5 | 0.26 | 6.63 | 440.5 | 479.5 | 0.47 | 1.72 | 386 | 27 | 0.04 |
| 50 | 635-23 | 635/690.40 | Lacustrine massive mudstone facies | Waiomo | 77.5 | 0.10 | 2.50 | 432.4 | 471.4 | 1.48 | 1.23 | 203 | 120 | 0.04 |
| 51 | 635-24 | 635/692.97 | Lacustrine massive mudstone facies | Waiomo | 73.6 | 0.22 | 7.40 | 436.8 | 475.8 | 0.32 | 1.82 | 407 | 18 | 0.03 |
| 52 | 635-25 | 635/696.27 | Lacustrine massive mudstone facies | Waiomo | 78.6 | 0.12 | 4.13 | 442.3 | 481.3 | 0.43 | 1.73 | 238 | 25 | 0.03 |

**Source rock geochemistry of the Waiomo Member**

| | | | | | | | | | | | | | | |
|---|---|---|---|---|---|---|---|---|---|---|---|---|---|---|
| 53 | 635-26 | 635/699.05 | Lacustrine massive mudstone facies | Waiomo | 71.0 | 0.32 | 13.99 | 437.3 | 476.3 | 0.23 | 2.72 | 514 | 8 | 0.02 |
| 54 | 635-27 | 635/702.76 | Lacustrine massive mudstone facies | Waiomo | 74.0 | 0.16 | 5.18 | 444.8 | 483.8 | 0.79 | 1.85 | 280 | 43 | 0.03 |
| 55 | 635-28 | 635/705.05 | Lacustrine massive mudstone facies | Waiomo | 77.9 | 0.17 | 4.28 | 430.7 | 469.7 | 0.48 | 1.70 | 252 | 28 | 0.04 |
| 56 | 635-29 | 635/708.30 | Lacustrine distal turbidite facies | Waiomo | 79.7 | 0.18 | 4.67 | 430.6 | 469.6 | 0.51 | 1.95 | 239 | 26 | 0.04 |
| 57 | 635-30 | 635/712.02 | Lacustrine massive mudstone facies | Waiomo | 78.5 | 0.17 | 3.76 | 426.3 | 465.3 | 0.33 | 1.57 | 239 | 21 | 0.04 |
| 58 | 654_862-7 | 654/862.7 | Lacustrine massive mudstone facies | Waiomo | 79.8 | 0.93 | 6.63 | 443.6 | 482.6 | 0.71 | 2.62 | 253 | 27 | 0.12 |
| 59 | 659_233 | 659/233 | Lacustrine massive mudstone facies | Waiomo | 78.8 | 0.92 | 3.51 | 467.0 | 506.0 | 1.04 | 3.08 | 114 | 34 | 0.21 |
| 60 | 659_245 | 659/245 | Lacustrine massive mudstone facies | Waiomo | 77.2 | 0.86 | 2.11 | 465.0 | 504.0 | 0.47 | 1.77 | 119 | 27 | 0.29 |
| 61 | 659_249 | 659/249 | Lacustrine massive mudstone facies | Waiomo | 78.7 | 0.52 | 8.31 | 441.1 | 480.1 | 0.53 | 2.65 | 313 | 20 | 0.06 |

**Source rock geochemistry of the Waiomo Member**

| | | | | | | | | | | | | | | |
|---|---|---|---|---|---|---|---|---|---|---|---|---|---|---|
| 62 | 660_192 | 660/192 | Lacustrine massive mudstone facies | Waiomo | 79.2 | 0.59 | 2.55 | 457.5 | 496.5 | 1.95 | 2.12 | 120 | 92 | 0.19 |
| 63 | 660_212-4 | 660/212.4 | Lacustrine massive mudstone facies | Waiomo | 79.9 | 0.64 | 6.51 | 455.1 | 494.1 | 0.30 | 2.78 | 234 | 11 | 0.09 |
| 64 | Twelve Mile Beach/1 | Twelve Mile Beach/1 | Lacustrine massive mudstone facies | Waiomo | 79.5 | 0.01 | 2.43 | 435.5 | 474.5 | 0.21 | 1.18 | 205 | 18 | 0.00 |
| 65 | Twelve Mile Beach/2 | Twelve Mile Beach/2 | Lacustrine massive mudstone facies | Waiomo | 71.3 | 0.01 | 1.50 | 434.1 | 473.1 | 0.39 | 1.12 | 134 | 35 | 0.00 |
| 66 | Twelve Mile Beach/3 | Twelve Mile Beach/3 | Lacustrine massive mudstone facies | Waiomo | 71.6 | 0.00 | 1.45 | 431.9 | 470.9 | 0.18 | 1.10 | 132 | 17 | 0.00 |

**Source rock geochemistry of the Goldlight Member**

| Sample | | | Lithofacies name | Member | Source Rock Analysis | | | | | | | | | |
|---|---|---|---|---|---|---|---|---|---|---|---|---|---|---|
| Number | ID | Depth | | | Weight (mg) | S1 (mg HC/g rock) | S2 (mg HC/g rock) | Tmax (°C) | tTemp (°C) | S3 (mg $CO_2$/g rock) | TOC (wt. %) | HI (mg HC/g TOC) | OI (mg $CO_2$/g TOC) | PI |
| 1 | 628_248 | 628/248 | Lacustrine massive mudstone facies | Goldlight | 83.5 | 0.16 | 3.68 | 429.2 | 468.2 | 2.02 | 2.09 | 176 | 97 | 0.04 |
| 4 | 631_93-6 | 631/93.6 | Lacustrine massive mudstone facies | Goldlight | 82.6 | 0.18 | 3.29 | 433.1 | 472.1 | 1.18 | 1.77 | 185 | 66 | 0.05 |
| 5 | 631_120-1 | 631/120.1 | Lacustrine massive mudstone facies | Goldlight | 80.8 | 0.20 | 4.78 | 433.6 | 472.6 | 1.80 | 2.26 | 211 | 80 | 0.04 |
| 6 | 631b_139-8 | 631/139.8 | Lacustrine massive mudstone facies | Goldlight | 55.1 | 0.25 | 2.66 | 430.8 | 469.8 | 4.37 | 2.01 | 132 | 217 | 0.08 |
| 7 | 632_214-6 | 632/214.6 | Lacustrine massive mudstone facies | Goldlight | 80.5 | 0.36 | 7.49 | 433.6 | 472.6 | 0.81 | 2.66 | 282 | 30 | 0.05 |

**Source rock geochemistry of the Goldlight Member**

| | | | | | | | | | | | | | | |
|---|---|---|---|---|---|---|---|---|---|---|---|---|---|---|
| 8 | 632_235 | 632/235 | Lacustrine massive mudstone facies | Goldlight | 81.0 | 0.30 | 5.16 | 426.8 | 465.8 | 1.57 | 2.42 | 213 | 65 | 0.05 |
| 9 | 632_245 | 632/245 | Lacustrine massive mudstone facies | Goldlight | 79.9 | 0.31 | 7.61 | 436.4 | 475.4 | 0.53 | 2.76 | 275 | 19 | 0.04 |
| 10 | 633_368 | 633/368 | Lacustrine massive mudstone facies | Goldlight | 79.2 | 0.10 | 3.41 | 429.1 | 468.1 | 2.90 | 1.89 | 181 | 154 | 0.03 |
| 11 | 635G-0 | 635/333.68 | Lacustrine massive mudstone facies | Goldlight | 77.2 | 0.03 | 0.82 | 430.8 | 469.8 | 0.42 | 0.85 | 97 | 49 | 0.03 |
| 12 | 635G-1 | 635/335.26 | Lacustrine massive mudstone facies | Goldlight | 74.2 | 0.01 | 1.54 | 431.3 | 470.3 | 0.77 | 1.13 | 136 | 68 | 0.01 |
| 13 | 635G-2 | 635/336.46 | Lacustrine massive mudstone facies | Goldlight | 79.2 | 0.02 | 0.98 | 428.3 | 467.3 | 1.56 | 0.97 | 101 | 161 | 0.02 |

**Source rock geochemistry of the Goldlight Member**

| | | | | | | | | | | | | | | |
|---|---|---|---|---|---|---|---|---|---|---|---|---|---|---|
| 14 | 635G-3 | 635/337.62 | Lacustrine massive mudstone facies | Goldlight | 71.4 | 0.02 | 1.98 | 432.4 | 471.4 | 1.14 | 1.30 | 152 | 88 | 0.01 |
| 15 | 635G-4 | 635/339.28 | Lacustrine massive mudstone facies | Goldlight | 73.7 | 0.04 | 2.67 | 430.7 | 469.7 | 0.95 | 1.58 | 169 | 60 | 0.01 |
| 16 | 635G-5 | 635/339.61 | Lacustrine massive mudstone facies | Goldlight | 77.3 | 0.03 | 2.18 | 432.8 | 471.8 | 0.83 | 1.24 | 176 | 67 | 0.01 |
| 17 | 635G-6 | 635/341.35 | Lacustrine massive mudstone facies | Goldlight | 74.4 | 0.04 | 1.30 | 431.2 | 470.2 | 1.26 | 1.02 | 127 | 123 | 0.03 |
| 18 | 635G-7 | 635/343.14 | Lacustrine massive mudstone facies | Goldlight | 73.9 | 0.02 | 1.21 | 429.2 | 468.2 | 1.18 | 1.05 | 114 | 112 | 0.01 |
| 19 | 635G-8 | 635/344.0 | Lacustrine massive mudstone facies | Goldlight | 73.0 | 0.04 | 1.62 | 432.2 | 471.2 | 1.74 | 1.23 | 132 | 142 | 0.02 |

**Source rock geochemistry of the Goldlight Member**

| | | | | | | | | | | | | | | |
|---|---|---|---|---|---|---|---|---|---|---|---|---|---|---|
| 20 | 635G-9 | 635/34 4.42 | Lacustrine massive mudstone facies | Goldlight | 77.0 | 0.02 | 1.01 | 430.8 | 469.8 | 1.40 | 0.93 | 108 | 150 | 0.02 |
| 21 | 635G-10 | 635/34 5.02 | Lacustrine massive mudstone facies | Goldlight | 79.2 | 0.09 | 3.36 | 428.8 | 467.8 | 1.37 | 1.99 | 169 | 69 | 0.03 |
| 22 | 635G-11 | 635/34 5.82 | Lacustrine massive mudstone facies | Goldlight | 78.5 | 0.05 | 3.17 | 430.7 | 469.7 | 0.49 | 1.59 | 199 | 31 | 0.02 |
| 23 | 635G-12 | 635/34 7.42 | Lacustrine massive mudstone facies | Goldlight | 70.0 | 0.03 | 0.72 | 430.9 | 469.9 | 1.57 | 0.87 | 83 | 180 | 0.04 |
| 24 | 635G-13 | 635/34 8.02 | Lacustrine massive mudstone facies | Goldlight | 70.8 | 0.02 | 0.97 | 429.0 | 468.0 | 1.42 | 1.13 | 85 | 126 | 0.02 |
| 25 | 635G-14 | 635/34 9.72 | Lacustrine massive mudstone facies | Goldlight | 72.9 | 0.04 | 2.84 | 431.3 | 470.3 | 0.54 | 1.62 | 175 | 34 | 0.01 |

**Source rock geochemistry of the Goldlight Member**

| | | | | | | | | | | | | | | |
|---|---|---|---|---|---|---|---|---|---|---|---|---|---|---|
| 26 | 635G-15 | 635/35 0.42 | Lacustrine massive mudstone facies | Goldlight | 75.6 | 0.03 | 0.96 | 429.9 | 468.9 | 0.82 | 0.96 | 100 | 86 | 0.03 |
| 27 | 635G-16 | 635/35 1.18 | Lacustrine massive mudstone facies | Goldlight | 72.6 | 0.03 | 0.85 | 429.8 | 468.8 | 0.92 | 0.91 | 94 | 101 | 0.03 |
| 28 | 635G-17 | 635/35 2.72 | Lacustrine massive mudstone facies | Goldlight | 73.1 | 0.04 | 1.30 | 430.8 | 469.8 | 0.40 | 1.10 | 118 | 37 | 0.03 |
| 29 | 635G-18 | 635/35 3.21 | Lacustrine massive mudstone facies | Goldlight | 78.4 | 0.09 | 1.85 | 430.6 | 469.6 | 0.93 | 1.26 | 147 | 74 | 0.04 |
| 30 | 635G-19 | 635/35 6.18 | Lacustrine massive mudstone facies | Goldlight | 72.3 | 0.05 | 1.35 | 431.7 | 470.7 | 0.74 | 1.03 | 131 | 72 | 0.03 |
| 31 | 635G-20 | 635/36 1.0 | Lacustrine massive mudstone facies | Goldlight | 78.3 | 0.06 | 1.31 | 429.9 | 468.9 | 0.51 | 1.01 | 130 | 51 | 0.04 |

**Source rock geochemistry of the Goldlight Member**

| | | | | | | | | | | | | | | |
|---|---|---|---|---|---|---|---|---|---|---|---|---|---|---|
| 32 | 635G-21 | 635/362.02 | Lacustrine massive mudstone facies | Goldlight | 76.8 | 0.05 | 1.96 | 429.7 | 468.7 | 0.67 | 1.32 | 149 | 51 | 0.02 |
| 33 | 635G-22 | 635/364.0 | Lacustrine massive mudstone facies | Goldlight | 77.2 | 0.03 | 0.98 | 428.5 | 467.5 | 0.47 | 0.92 | 107 | 51 | 0.03 |
| 34 | 635G-23 | 635/366.40 | Lacustrine massive mudstone facies | Goldlight | 74.9 | 0.05 | 1.84 | 431.6 | 470.6 | 0.74 | 1.26 | 147 | 59 | 0.02 |
| 35 | 635G-24 | 635/369.83 | Lacustrine mudstones with minor thin sandstones | Goldlight | 73.0 | 0.01 | 0.27 | 428.2 | 467.2 | 1.28 | 0.38 | 70 | 336 | 0.04 |
| 36 | 635G-25 | 635/375.51 | Lacustrine mudstones with minor thin sandstones | Goldlight | 74.2 | 0.07 | 2.35 | 430.4 | 469.4 | 0.90 | 1.31 | 179 | 68 | 0.03 |
| 37 | 635G-26 | 635/376.80 | Lacustrine massive mudstone facies | Goldlight | 74.9 | 0.05 | 2.34 | 429.6 | 468.6 | 0.51 | 1.21 | 194 | 42 | 0.02 |

**Source rock geochemistry of the Goldlight Member**

| | | | | | | | | | | | | | | |
|---|---|---|---|---|---|---|---|---|---|---|---|---|---|---|
| 38 | 636_195-97 | 636/195.97 | Lacustrine massive mudstone facies | Goldlight | 79.8 | 0.15 | 4.72 | 429.6 | 468.6 | 2.36 | 2.26 | 209 | 104 | 0.03 |
| 39 | 636_249-8 | 636/249.8 | Lacustrine massive mudstone facies | Goldlight | 80.8 | 0.18 | 4.47 | 430.7 | 469.7 | 1.36 | 2.09 | 214 | 65 | 0.04 |
| 40 | 651_470 | 651/470 | Lacustrine massive mudstone facies | Goldlight | 81.9 | 0.30 | 4.76 | 431.9 | 470.9 | 0.99 | 2.23 | 213 | 44 | 0.06 |
| 41 | 654_649-6 | 654/649.6 | Lacustrine massive mudstone facies | Goldlight | 79.9 | 0.31 | 3.94 | 444.0 | 483.0 | 1.43 | 2.30 | 172 | 62 | 0.07 |
| 42 | 660_43-2 | 660/43.2 | Lacustrine massive mudstone facies | Goldlight | 78.7 | 0.67 | 3.85 | 450.1 | 489.1 | 0.46 | 2.38 | 162 | 19 | 0.15 |
| 43 | 660_68 | 660/68 | Lacustrine massive mudstone facies | Goldlight | 76.5 | 0.54 | 3.74 | 451.3 | 490.3 | 1.28 | 2.65 | 141 | 48 | 0.13 |

**Source rock geochemistry of the Goldlight Member**

| | | | | | | | | | | | | | | |
|---|---|---|---|---|---|---|---|---|---|---|---|---|---|---|
| 44 | 660_8-2 | 660/8.2 | Lacustrine massive mudstone facies | Goldlight | 77.8 | 0.51 | 4.39 | 451.0 | 490.0 | 1.01 | 2.74 | 160 | 37 | 0.10 |
| 45 | 662_116-6 | 662/116.6 | Lacustrine massive mudstone facies | Goldlight | 75.2 | 0.29 | 6.54 | 433.9 | 472.9 | 0.51 | 2.69 | 244 | 19 | 0.04 |
| 46 | 662_48-9 | 662/48.9 | Lacustrine massive mudstone facies | Goldlight | 77.0 | 0.29 | 3.96 | 436.6 | 475.6 | 1.62 | 2.30 | 172 | 71 | 0.07 |
| 47 | 664_157-5 | 664/157.5 | Lacustrine massive mudstone facies | Goldlight | 75.1 | 0.29 | 5.49 | 430.3 | 469.3 | 0.89 | 2.58 | 213 | 35 | 0.05 |
| 48 | 664_78-9 | 664/78.9 | Lacustrine massive mudstone facies | Goldlight | 75.7 | 0.40 | 7.35 | 434.6 | 473.6 | 1.24 | 2.93 | 251 | 42 | 0.05 |
| 49 | 665_3-8 | 665/3.8 | Lacustrine massive mudstone facies | Goldlight | 79.8 | 0.27 | 5.26 | 436.6 | 475.6 | 1.34 | 2.95 | 178 | 45 | 0.05 |

**Source rock geochemistry of the Goldlight Member**

| | | | | | | | | | | | | | | |
|---|---|---|---|---|---|---|---|---|---|---|---|---|---|---|
| 50 | 666_144-9 | 666/144.9 | Lacustrine massive mudstone facies | Goldlight | 75.9 | 0.32 | 5.18 | 428.6 | 467.6 | 1.36 | 2.44 | 213 | 56 | 0.06 |
| 51 | 666_9 | 666/9 | Lacustrine massive mudstone facies | Goldlight | 78.3 | 0.23 | 4.51 | 429.9 | 468.9 | 1.25 | 2.25 | 200 | 56 | 0.05 |
| 52 | SMC1 | SMC1 | Lacustrine massive mudstone facies | Goldlight | 74.2 | 0.10 | 2.78 | 424.9 | 463.9 | 0.94 | 2.05 | 136 | 46 | 0.03 |
| 53 | SMC2 | SMC2 | Lacustrine massive mudstone facies | Goldlight | 74.8 | 0.02 | 2.07 | 433.4 | 472.4 | 1.65 | 2.31 | 89 | 71 | 0.01 |
| 54 | SMC3 | SMC3 | Lacustrine massive mudstone facies | Goldlight | 74.7 | 0.08 | 4.02 | 427.5 | 466.5 | 0.38 | 2.86 | 141 | 13 | 0.02 |
| 55 | SMC4 | SMC4 | Lacustrine massive mudstone facies | Goldlight | 73.2 | 0.02 | 2.85 | 430.4 | 469.4 | 0.83 | 2.73 | 104 | 30 | 0.01 |

**Source rock geochemistry of the Goldlight Member**

| | | | | | | | | | | | | | | |
|---|---|---|---|---|---|---|---|---|---|---|---|---|---|---|
| 56 | SMC 5 | SMC5 | Lacustrine massive mudstone facies | Goldlight | 74.5 | 0.07 | 3.04 | 425.9 | 464.9 | 0.58 | 2.63 | 116 | 22 | 0.02 |
| 57 | SMC 6 | SMC6 | Lacustrine massive mudstone facies | Goldlight | 76.5 | 0.09 | 3.10 | 423.8 | 462.8 | 0.53 | 1.95 | 159 | 27 | 0.03 |
| 58 | SMC 7 | SMC7 | Lacustrine massive mudstone facies | Goldlight | 73.2 | 0.13 | 3.90 | 422.2 | 461.2 | 0.51 | 2.13 | 183 | 24 | 0.03 |

**Maceral and vitrinite analysis of Ford and Waiomo members**

| Sample | | | Member | Maceral analysis | | | | Vitrinite reflectance | | | HI |
|---|---|---|---|---|---|---|---|---|---|---|---|
| # | Sampling ID | Sample | | n | Liptnite | Vitrinite | Inertinite | n | %Ro | stdev | (mg HC/g TOC) |
| | | | | | (%) | (%) | (%) | | | | |
| 1 | 621-20 | 621/362.67 | Waiomo | 250 | 52.0 | 28.8 | 19.2 | 48 | 0.45 | 0.06 | 406 |
| 2 | 621-17 | 621/366.06 | Waiomo | 250 | 36.0 | 30.8 | 33.2 | 50 | 0.45 | 0.07 | 246 |
| 3 | 621-15 | 621/368.70 | Waiomo | 250 | 44.8 | 24.8 | 30.4 | 49 | 0.47 | 0.07 | 308 |
| 4 | 621-11 | 621/372.68 | Waiomo | 250 | 42.0 | 30.8 | 27.2 | 47 | 0.43 | 0.08 | 409 |
| 5 | 621-7 | 621/381.85 | Waiomo | 250 | 36.4 | 32.4 | 29.2 | 46 | 0.5 | 0.06 | 312 |
| 6 | 635-11 | 635/667.89 | Waiomo | 250 | 38.8 | 34.0 | 26.4 | 21 | 0.67 | 0.05 | 239 |
| 7 | 635-14 | 635/673.71 | Waiomo | 250 | 46.0 | 33.2 | 19.2 | 47 | 0.61 | 0.10 | 329 |
| 8 | 635-20 | 635/684.30 | Waiomo | 250 | 45.6 | 32.0 | 20.8 | | | | 468 |
| 9 | 635-25 | 635/696.27 | Waiomo | 250 | 33.2 | 37.2 | 28.8 | 36 | 0.51 | 0.08 | 238 |
| 10 | 635-29 | 635/708.30 | Waiomo | 250 | 32.8 | 38.4 | 28.0 | 49 | 0.52 | 0.07 | 239 |
| 11 | 656-1 | 656/459.38 | Ford | 250 | 57.2 | 25.6 | 15.2 | | | | 482 |
| 12 | 656-4 | 656/463.45 | Ford | 250 | 60.4 | 22.0 | 16.0 | 44 | 0.69 | 0.09 | 352 |
| 13 | 656-16 | 656/469.60 | Ford | 250 | 46.0 | 31.6 | 20.0 | 50 | 0.70 | 0.09 | 315 |
| 14 | 656-19 | 656/475.24 | Ford | 250 | 53.2 | 23.2 | 22.4 | 50 | 0.69 | 0.10 | 546 |
| 15 | 656-25 | 656/489.0 | Ford | 250 | 30.0 | 38.0 | 30.8 | 44 | 0.63 | 0.09 | 220 |